Mitochondrial Mechanisms in Autism Spectrum Disorder: Characterising the Neurotoxic Effects of Propionic Acid *In Vitro*

By Caitlyn Mahony

Student Number: MHNCAI001

Supervisor: Dr Colleen O'Ryan

Thesis Presented for the Degree of

DOCTOR OF PHILOSOPHY

in the Department of Molecular and Cell Biology

Faculty of Science

University of Cape Town

February 2025

University of Cape Town

The copyright of this thesis vests in the author. No quotation from it or information derived from it is to be published without full acknowledgement of the source. The thesis is to be used for private study or non-commercial research purposes only.

Published by the University of Cape Town (UCT) in terms of the non-exclusive license granted to UCT by the author.

University of Cape Town

Abstract

Autism Spectrum Disorder (ASD) is a chronic neurodevelopmental condition with a complex molecular aetiology shaped by genetic, epigenetic and environmental factors. The poorly understood nature of ASD aetiology significantly impedes diagnosis and management of the condition, which substantially impairs quality of life. A role for mitochondrial dysfunction in ASD has become increasingly well-recognised, while mitochondria are also emerging as central regulators of neurodevelopment, physiology and function. Moreover, recent work in a South Africa (SA) ASD cohort reported differential DNA methylation (DNAm) signatures converging on mitochondrial metabolism and Propionyl CoA Carboxylase B (PCCB). This project aimed to better characterise the mitochondrial component of ASD aetiology using an *in vitro* system to mechanistically interrogate the molecular signatures found in an understudied SA population.

Building on established preclinical models for both PCCB dysfunction and ASD, Propionic Acid (PPA) was used to recapitulate mitochondrial dysfunction in neuronal-like SH-SY5Y cells. The Thiazolyl Blue Tetrazolium Bromide (MTT), Luminescent ATP Detection and Tetramethylrhodamine, ethyl ester (TMRE) assays revealed a dose- and time-dependent decrease in cell viability from 4 to 72 hours, catalysed by an acute loss of mitochondrial membrane potential at 4 hours. In conjunction, reverse transcription quantitative polymerase chain reaction (RT-qPCR) assays showed an acute and sustained suppression of *PCCB* expression and a systemic dysregulation of the genes that govern mitochondrial metabolism (*PGC1α, c-MYC*), biogenesis (*TFAM, NRF1*), fission (*DRP1*) and fusion (*STOML2, MFN1/2, OPA1*). Confocal microscopy demonstrated associated disruptions to mitochondrial network morphology and integrity, characterised by decreased mitochondrial volume, increased mitochondrial fragmentation and perturbations to mitophagic flux. Finally, live-cell respirometry illustrated functional impairments to metabolic state marked by significant deficits in both oxidative and glycolytic ATP production.

Having effectively recapitulated mitochondrial dysfunction *in vitro,* a model for neurogenesis was developed to examine the interplay between neuronal metabolism and maturation. Phase contrast microscopy, immunocytochemistry and respirometry assays confirmed the efficacy of differentiation, demonstrating successful cell cycle exit, efficient neurite production, elongation and branching, an increased β-III-tubulin (β3T): Nestin (NES) ratio and enhanced mitochondrial capacity. This system was harnessed to characterise PPA-induced disruptions to neurogenesis, demonstrating gross morphological aberrations and significant changes to the composition and connectivity of neuronal networks. Complementary image analysis workflows showed that PPA reduced the length and complexity of neurite processes, disrupted the localisation and expression of cytoskeletal markers and decreased the β3T:NES ratio, indicating substantial impairments to neuronal morphology and maturation.

Lastly, global RNA sequencing was used to characterise the molecular mechanisms that disrupt neuronal maturation under PPA stress, revealing transcriptional signatures of developmental delay and neurotoxicity. PPA upregulated processes involved in pluripotency, proliferation and glycolysis, impaired epigenetic and metabolic reprogramming and inhibited synaptogenesis and neurotransmission. An interplay between stress-responsive, metabolic and neurogenic signalling emerged at the centre of the PPA transcriptome, highlighting reciprocal mechanisms that modulate substrate utilisation, differentiation, synaptogenesis and survival. Moreover, PPA systemically altered convergent mechanisms that shape extracellular matrix dynamics, leading to signatures of neuronal injury, apoptosis and excitotoxicity. Together, transcriptomic profiles reflected impairments to neurogenesis under PPA stress, driven by disruptions to the intrinsic and extrinsic landscapes that shape neuronal cell fate.

This project established an *in vitro* model for neurogenesis and developmental neurotoxicity that lays the groundwork for mechanistic studies on neurodevelopment and disease. The work presented here provides a quantitative assessment of mitochondrial morphology, dynamics and function under PPA stress and is the first study to functionally demonstrate that PPA alters neuronal metabolism and differentiation in the SH-SY5Y model. Moreover, the transcriptional signatures of PPA exposure highlight novel processes that function at the interface between metabolism, neurodevelopment and neurotoxicity. Ultimately, these insights contribute to a mechanistic understanding of the mitochondrial component of ASD aetiology, which could inform the development of novel biomarkers and therapeutic strategies to improve long-term clinical outcomes.

Table of Contents

Title Page ..... **i**
Abstract ..... **ii**
Table of Contents ..... **iv**
Plagiarism Declaration ..... **vii**
Dedication ..... **viii**
Acknowledgements ..... **ix**
Abbreviations ..... **xiii**
Units and Symbols ..... **xx**
List of Figures and Tables ..... **xxi**
Thesis Overview ..... **xxiii**

~ PART I ~

Chapter 1. ..... **1**
The Mitochondrial Hypothesis: Molecular Mechanisms and Clinical Implications **1**
1.1. The Landscape of Molecular Autism Research 1
1.2. From DNA Methylation to Mitochondrial Dysfunction in ASD 5
1.3. Mitochondrial Mechanisms in Neurodevelopment 13
1.4. Beyond Neurogenesis: The Metabolic Nexus of ASD Neurology 22
1.5. Mitochondrial Allostatic Load: A Biopsychosocial Perspective 30
1.6. Summary and Conclusions 35

Chapter 2. ..... **39**
Mitochondrial Dysfunction *In Vitro*: The Propionic Acid Model **39**
2.1. Introduction 39
2.1.1. An *In Vitro* Model to Study Metabolism: The SH-SY5Y System 39
2.1.2. The Metabolic Landscape of SH-SY5Y 40
2.1.3. A Model for Mitochondrial Dysfunction 42
2.2. Methodology 47
2.2.1. Neuronal Cell Culture 47
2.2.2. Characterisation of Cytotoxicity 47
2.2.3. Measurement of Mitochondrial Membrane Potential 48
2.2.4. Examining the Transcriptional Regulation of Mitostasis 50
2.2.5. Evaluating Mitochondrial Content, Connectivity and Turnover 51
2.2.5.1. Mitochondrial DNA Copy Number and Deletions 51
2.2.5.2. Mitochondrial Network Morphology and Mitophagic Flux 52

2.2.6. Live Cell Respirometry to Measure Metabolic Flux 57
2.2.7. Statistical Analysis 59
2.3. Results 59
2.3.1. Cell Viability and Metabolism 59
2.3.2. The Transcriptional Regulation of Mitostasis 63
2.3.3. Mitochondrial Morphology and Turnover 69
2.3.4. Mitochondrial Function and Metabolic State 74
2.4. Discussion 78
2.4.1. Establishing the PPA Model: Profiles of Cytotoxicity and Metabolic Stress 79
2.4.2. Molecular Mechanisms of Mitostasis 81
2.4.3. Functional Evidence of Mitochondrial Remodelling 87
2.4.4. Metabolic Signatures of Energetic Crisis 90
2.5. Summary and Conclusions 99

~ PART II ~

Chapter 3. 101
An *In Vitro* Model for Neurogenesis: The Neurotoxic Effects of Propionic Acid 101
3.1. Introduction 101
3.1.1. Neuronal Differentiation *In Vitro* 101
3.1.2. Neurogenic Signatures of Metabolic Remodelling 105
3.1.3. Confirmation and Characterisation of Neurogenesis 110
3.2. Methodology 111
3.2.1. SH-SY5Y Differentiation 111
3.2.2. Evaluation of Neuronal Morphology and Maturation 113
3.2.2.1. Live Cell Imaging 113
3.2.2.2. Immunocytochemistry 113
3.2.2.3. Metabolic Characterisation 119
3.2.3. Statistical Analysis 119
3.3. Results 120
3.3.1. An *In Vitro* Model for Neurogenesis: Hallmarks of Differentiation 120
3.3.2. Propionic Acid – Induced Developmental Neurotoxicity 129
3.4. Discussion and Conclusions 135

Chapter 4. 140
Transcriptomic Signatures: The Neurotoxic Mechanisms of Propionic Acid 140
4.1. Introduction 140
4.1.1. Experimental Design 140

4.1.2. Analytical Approach 140
4.1.3. Molecular Signatures of Metabolic State 141
4.2. Methodology 144
4.2.1. RNA Collection 144
4.2.2. Library Preparation and Sequencing 145
4.2.3. Quality Control 146
4.2.4. Read Alignment 147
4.2.5. Count Loading, Filtering and Normalisation 147
4.2.6. Assessment of Differential Expression 147
4.2.7. Weighted Gene Correlation Network Analysis (WGCNA) 148
4.2.8. Gene Set Enrichment Analysis (GSEA) 148
4.3. Results 149
4.3.1. Global Disruptions to the Neurogenic Transcriptome 149
4.3.2. Metabolic and Neurotoxic Signatures in the PPA Transcriptome 155
4.3.3. Co-expression Network Analysis: Towards a Mechanistic Framework 161
4.3.4. Ingenuity Pathway Analysis: Upstream Regulators and Downstream Phenotypes 166
4.4. Discussion 174
4.4.1. Transcriptomic Evidence of Epigenetic Reprogramming 176
4.4.2. Intrinsic Signatures of Developmental Delay 181
4.4.3. Integrated Disruptions to Cell Fate and Function 185
4.4.4. The Interface Between Metabolic and Morphological Remodelling 188
4.5. Summary and Conclusions 193

Synthesis, Conclusions & Future Directions 196

~ APPENDICES ~

Appendix 1 204
Appendix 2 206
Appendix 3 211
Appendix 4 219

References 264

Plagiarism Declaration

I, Caitlyn Mahony, declare that this thesis, submitted in fulfilment of the requirements of the degree of Doctor of Philosophy, is my own original work in both concept and execution save for that which has been properly acknowledged or cited. Neither the whole nor any part of this thesis has been, or will be, submitted for any other degree at the University of Cape Town or another university. I have used the Harvard convention for referencing and all figures have been generated using Biorender.com unless otherwise specified. I authorise the University to reproduce for the purpose of research either the whole or any portion of the contents in any manner whatsoever.

Signed by candidate: Date: 03/02/2025

















Dedication

During my first year at university, I found a favourite song
called Bird With a Broken Wing
that taped itself in half-forgotten fragments
to the wall inside my head.

" In this twisted plot I was destined for
I'm an astronaut on the ocean floor
When the curtain falls, I'll be wearing thin
Clawing at the walls as they're closing in

I would run and hide for the afternoon
With the butterfly in the panic room
I never understood until the very end
I still wish I could do it all again

But life demands a final chapter
A story that we all must leave behind
Or a single line, and this is mine
The epilogue of a bird with a broken wing."

This thesis is dedicated to the butterflies
who gave me somewhere to hide
when the world was a panic room
and taught me how to fly
on broken wings.





























Acknowledgements

There are a hundred thousand reasons why this thesis shouldn't have been possible, if not for a hundred thousand miracles that I found along the way. They came with competence, generosity, and compassion in the right people at the right place at the right time, somehow stringing this whole endeavour all the way to the end. In the big grey factory of academia that grinds everything to dust, I encountered kindness, selflessness and patience that almost defies logic. So, I want to say thank you to the miracles, who gave so much more than I could ever have expected and impacted my life in ways they might not even know.

To Tatiana Millard, Ghakiema Salie, Bronwyn Arendze-Bailey, Marilyn Krige, Annestacia Marthinus, Yolande Burrows, Niel Bredekamp, Derick September and Maureen Jacobs who governed the galaxy of MCB, juggling the health and safety rules, the waste disposal systems, the budgeting and administration, autoclaving, equipment servicing and the million other logistical asteroids that threatened to collide at any moment. I cannot comprehend how I would have ever got anything done without you, and I appreciate your work more than you know. To Shakiera Sattar – whose calm presence and kind gaze carried me through honours, who gave me the tissue culture training that would make all of this work possible, who helped us to survive the Great Contamination of 2022, and who has kept cell culture running through a litany of broken hoods, centrifuges, microscopes and incubators. Your patience and capacity to handle so many things so efficiently have been not just a gift, but a necessity to get this project to completion.

Thank you so much to the Hapgood lab, who laid the groundwork for tissue culture in MCB, especially Dr Johnson Mosoko Moliki and Dr Alexis Bick, who helped us to figure out new protocols and equipment and kindly answered the greenest of questions during our first few years in cell culture. Thank you to Keren Cooper and Pei-Yin Liebrich, who trained me on the fluorescent microscope, to Dr Viantha Naidoo, who trained me in confocal microscopy, and Lize Engelbrecht, who did the confocal imaging at the Central Analytical Facility in Stellenbosch. Thank you to the Brombacher lab, who allowed us access to their Seahorse machine, included us in training workshops and gave me lab space to do my experiments - especially Dr Rudranil Hazra, who set up the runs and shared his advice and encouragement during the vast number of months that it took to troubleshoot the assay. And a big thank you to Dr Stuart Meier, who conducted the bioinformatic component of the RNA Seq analysis to make Chapter 4 of this thesis possible.

Then there are the members of lab 405, past and present, who were in the trenches with me. Thank you to Evida and Rachelle, who supervised my honours project and gave their time and experience so generously through hardships that I couldn't have imagined. Thank you to Aqueelah, Talya, Sarah and Gabi who worked with me on different aspects of this project during their honour's degrees over the

years. And a special thank you to Sophia, who has been an example and a mentor to me since the start of this academic journey - amazing, encouraging and inspiring me every day of the six years we have worked together. Thank you for teaching me the fundamentals of qPCR, for helping to source and optimise the primers for all my genes, for organising the RNA Seq experiment with CPGR and for taking on the cohort project that most people would have never even attempted. You seemed like a wizard to me when I was in honours, and I still think that what you have accomplished during your PhD is nothing less than magic. But I have come to appreciate that it is not magic at all - just incredibly hard work, perseverance and courage that comes with an immense cost that you seldom let anyone see. You have so much to offer the world of science, and I will always be grateful for everything you taught me at the bench and beyond.

Thank you to Erin – who is what I consider to be a sort of academic soulmate. Ever since our first year in the lab together, you have masterfully accomplished the things that I have struggled with the most, and finishing this thesis without you would have been like trying to climb a mountain with one leg. Thank you for the work you have done to keep the lab on track – managing budgets, orders, and lists, tracking reagents, supplies and freezer space, helping me to interpret funding application questions and progress reports and getting through (almost) three whole degrees on top of it all. You helped me to turn some of the endless Thought Tsunamis into small things that were tangibly useful in the real world, which is something I never thought they could be. Your steady approach to getting things done always seemed to slow down the whole world and reminded me to breathe, and getting to this point is not something I could have ever even tried if not for the luckiest accident of being your labmate.

A huge thank you to Mignon, who helped me to run the c-MYC, NRF1 and PGC1α PCRs in Chapter 2, worked alongside me to optimise the neurodifferentiation protocols used in Chapter 3, and pulled weekends with me to finish the RNA Seq experiment described in Chapter 4. You truly shared the starkest, grittiest days of this degree with me, giving me hands, eyes and ears to carry the load, witness the journey and listen to the spaghetti scramble of thoughts that sometimes got so tangled. You were someone I felt able to share my whole academic world with, and you made the journey so much less lonely. Thank you for persevering through the Differentiation Depression, for sharpening your pipette on some of the most stubborn primers and being almost as thrilled as I was when something finally worked. You taught me so much about bravery and bridging worlds and you gave me the courage to actually try to write this thing. Whenever I felt the despair creeping in, I imagined telling you about the latest data and just thinking about how excited you would be, helped me to push through the pages.

Thank you to Emma - who spent weeks optimising the PCCB primers, months pioneering the differentiation protocols and years helping me to establish cell banks through import delays, contaminations and (sadly not metaphorical) wildfires. Not to mention an eternity driving me and my cells through stormy Cape Town winters and equally stormy existential crises. Your precision,

perseverance and skill were indispensable to getting this project started, but it was your insight, understanding and compassion that made all the difference in the end. Thank you especially for helping me to keep the anxiety monster at bay – I think you were the only one who really understood that particular hurdle, and just how close I felt to losing everything at times. Your courage in the face of hardship always made me feel less afraid, and your capacity to share the difficult moments with me helped me to feel less alone. I hope you always know how much you inspired me, how much I learned from you and how much of this work would never have been possible without you.

Thank you to Dr Katelyn Cuttler, who appeared like a fairy godmother in the dying days of this degree and helped me to finally turn my cell culture pumpkin into a PhD. In Greek mythology, there is a story about Three Fates who told the future by sharing one eye between them. When you joined the lab in 2023, after years of struggling through tissue culture in the dark, it felt like our Eye had finally arrived. I can't tell you how much I valued your experience, enthusiasm and encouragement, how much of a relief it was to have someone to ask when something wasn't working, or the amount of time you saved me just by sharing a few tricks here and there. Thank you for being interested in every part of the process, for being willing to read all the disparate thoughts I had about everything, and for celebrating even the smallest successes.

To Rebeng – my fellow Weekend Warrior. Thank you for sharing the hours, the tears, the moments of joy when reagents finally arrived, the funding deadlines, the mandatory presentations and the experience of pouring yourself so completely into something that so often lets you down. Watching you wade through absolutely hundreds of mice late into the night is something I think about every time something feels impossible. The sheer will that you have shown throughout your PhD is simply incredible to bear witness to, and the fountain of compassion, humour, kindness and intelligence that you bring into every room is truly a gift to everyone around you.

And of course, thank you to Dr Colleen O' Ryan who has supervised me for the past six years. Thank you for going so many extra miles that they practically became a marathon. Thank you for taking me on in Honours, for letting me stay in Masters, for encouraging me to upgrade to a PhD and for being patient with me as I tried to find my way to the end. From dying NDUF cultures, Covid lockdowns and vehicular collisions to sequential melting freezers, truant ReNcells and endless loadshedding - this degree felt like disaster whack-a-mole at times, and it was only your unflappable ability to keep moving forward that got me to the other side. Thank you for making sure that I didn't get lost in the system, for going out of your way to help me find funding, and for caring about us as people not just as pipette hangers. Thank you for being interested enough to read my chapters just a few months into my degree and for encouraging me to write up papers even though you would need to fork out your own grant money just to publish them (a truly bizarre concept!). Thank you for not limiting me by my weaknesses, for allowing me to explore my interests and for diving with me into the depths of new rabbit holes.

Being able to think, write and explore the field was truly the light at the end of the tunnel that kept me hammering away at the bench, in the endless quest to make my cells turn green. I don't think any other supervisor would have allowed me to figure out this journey in the way that I needed to, or understood why I couldn't just do things in the right order. I don't know yet if this is the finish line we hope it will be, but I do know that getting here has already changed my life and that I owe most of it to you.

To the NRF, UCT and the Science Faculty, thank you so much for funding me during this project. Being funded to do something that gave me so much life was a once-in-a-lifetime opportunity that few people are lucky enough to experience, and one that I will always be incredibly grateful for.

Lastly, I owe a big thank you to the people who got me to the start line in one piece - and held me together all the way through. To my parents – who have always given me more love, support and opportunity than I could ever deserve. Thank you for sharing this convoluted journey with me, for managing the fallout from every failed PCR and for the virtual debriefs with the dogs that got me through each day. To Granny Mary and Grandad Mike – who were the only reason I ever made it to the start of my honour's degree, when I couldn't even think in hours and none of us could have imagined what that would mean six years later. Even from afar, I have felt your faith, love and courage in every miracle I have encountered here – most of them, no doubt, answers to your weekly prayers. To my poor brother, Declan, who ended up being my roommate for the past four years – thank you for bringing family to me. Thank you for dealing with the silence, the sadness and the strangeness that comes with my daily quest for survival and for your gentle introspective presence that makes the world seem kinder. To my sister Sinead – who has always had emotional "spidey senses" far beyond her years and a capacity to turn pain into connection that reaches into the loneliest places. Thank you for loving me and inspiring me across distance and time, and through things that were so difficult to understand. To Carla – who somehow kept me tethered to this degree by a thread woven from last straws, fine lines, frayed ends and sheer willpower. Thank you for supervising so many of the unwritten chapters that went into this thesis, for making all of the written ones possible in the first place, and for helping me learn to laugh again along the way. To Jaqui (and Pax) – thank you for cohabiting my internal world, for holding the things that threatened to break, and for your persistent, and often inconceivable, belief in me. And to Sophie – thank you for reading the roughest drafts of my ongoing thesis on How To Be A Human, for staying when none of it made sense, and for giving me the courage to care.

This thesis was more than a project to me. It was a lifeline that carried me through endings and a journey to rediscovering electricity in things. It was a lesson in running in circles and starting again and plotting a path between beginnings. More than anything, the chance to write this thesis was a gift. Even if I never find something like this again, just knowing it exists is a seed of hope that I will carry with me forever – and with it, an immense gratitude for everyone who made this journey possible.

Abbreviations

4E-BP1	Eukaryotic Translation Initiation Factor 4E Binding Protein 1
5-mTHF	5-Methytetrahydrofolate
AA	Amino Acid
ACAT1	Acetyl-CoA Acetyltransferase 1
ACC	Acetyl CoA Carboxylase
ADHD	Attention Deficit Hyperactivity Disorder
AKT	Protein Kinase B
ALDH6A1	Aldehyde Dehydrogenase 6 Family Member A1
ALS	Amyotrophic Lateral Sclerosis
AMP	Adenosine Monophosphate
AMPK	AMP-Dependent Protein Kinase
ANOVA	Analysis Of Variance
ASCL1	Achaete-Scute Family bhlh Transcription Factor 1
ASD	Autism Spectrum Disorder
ATCC	American Type Culture Collection
ATG5	Autophagy Related 5
ATG7	Autophagy Related 7
ATP	Adenosine Triphosphate
ATRA	All-Trans Retinoic Acid
AURKB	Aurora-B Kinase
β2M	Beta-2-Microglobulin
β3T	Beta-3-Tubulin
BAX	Bcl-2 Associated X-Protein
BCAAs	Branched-Chain Amino Acids
BCKD	Branched-Chain A-Ketoacid Dehydrogenase
BCKDC	Branched-Chain A-Keto Acid Dehydrogenase Complex
BDNF	Brain-Derived Neurotrophic Factor
bHLH	Basic Helix-Loop-Helix
BHMT	Betaine-Homocysteine Methyltransferase
BMP	Bone Morphogenetic Protein
BNIP3	BCL2/Adenovirus E1B 19 kDa Protein-Interacting Protein 3
BP	Base Pair
BSA	Bovine Serum Albumin
BSL2	Biosafety Level 2
Ca^{2+}	Calcium
CaMKII	Calcium/Calmodulin-Dependent Protein Kinase II
cAMP	Cyclic Adenosine Monophosphate
CAMs	Cell Adhesion Molecules
CBS	Cystathionine Beta Synthase
CCCP	Carbonylcyanide-3-Chlorophenylhydrazone
CDKs	Cyclin Dependent Kinases
cDNA	Complementary DNA
c-MYC	Proto-Oncogene C-Myc
CNS	Central Nervous System

CO_2	Carbon Dioxide
CoA	Coenzyme A
CoASH	Coenzyme A with Sulfhydryl Functional Group (or Free CoA)
COMT	Catechol-O-Methyltransferase
COQ	Ubiquinone Biosynthesis O-Methyltransferases
CPGR	Centre For Proteomic and Genomic Research
CPM	Counts Per Million
CPS	Carbamoyl Phosphate Synthetase
CPT	Carnitine Transferase
CPT1	Carnitine Palmitoyltransferase 1
CRCs	Chromatin Remodelling Complexes
CREB	cAMP Response Element-Binding Protein
CREBBP	CREB Binding Protein
CS	Citrate Synthase
CT	Cycling Threshold
CTCF	Corrected Total Cell Fluorescence
CTNF	Corrected Total Neurite Fluorescence
CTNNB1	Beta-Catenin
CYP540	Cytochrome P450
DA	Dopamine
DAMPs	Damage-Associated Molecular Patterns
DAPI	4′,6-Diamidino-2-Phenylindole
DBH	Dopamine Beta-hydroxylase
DE	Differentially Expressed
DEGs	Differentially Expressed Genes
DGE	Differential Gene Expression
DHFR	Dihydrofolate Reductase
DIC	Differential Interference Contrast
DLX1	Distal-Less Homeobox 1
DM	Differential Methylation
DMEM	Dulbecco’s Modified Essential Medium
DMSO	Dimethyl Sulfoxide
DNA	Deoxyribonucleic Acid
DNAm	DNA Methylation
DRP1	Dynamin-Related Protein 1
DSM	Diagnostic And Statistical Manual of Mental Disorders
DSMZ	German Collection of Microorganisms and Cell Cultures
EBSS	Earle's Balanced Salt Solution
ECACC	European Collection of Authenticated Cell Cultures
ECAR	Extracellular Acidification Rate
ECM	Extracellular Matrix
EDTA	Ethylenediaminetetraacetic Acid
EIF	Eukaryotic Translation Initiation Factor
ELS	Early Life Stress
EMEM	Eagle’s Minimum Essential Media
EMT	Epithelial Mesenchymal Transition

ENO2	Enolase 2
EP300	Histone Acetyltransferase P300
ER	Endoplasmic Reticulum
ERKs	Extracellular Signal-Regulated Kinases
ERR	Estrogen-Related Receptor
ETC	Electron Transport Chain
EVs	Extracellular Vesicles
F12	Hams F12 Nutrient Supplement
FA	Fatty Acid
FADH	Flavin Adenine Dinucleotide
FAE	Fatty Acid Elongation
FAO	Fatty Acid Oxidation
FAS	Fatty Acid Synthesis
FBS	Foetal Bovine Serum
FCCP	Carbonyl Cyanide P-Trifluoro-Methoxyphenyl Hydrazone
FFARs	Free Fatty Acid Receptors
FIS1	Mitochondrial Fission Protein 1
FOXO	Forkhead Box O
FZD	Frizzled
GABA	Gamma-Aminobutyric Acid
GAD	Generalised Anxiety Disorder
GAG	Glycosaminoglycan
GATOR1	Gap Activity TOward Rag 1
GCs	Glucocorticoids
GDH	Glutamate Dehydrogenase
GLI1	Glioma-Associated Oncogene 1
GO	Gene Ontology
GPCRs	G-Coupled Protein Receptors
GPs	Glycoproteins
GRs	GC Receptors
GS	Glutamine Synthetase
GSEA	Gene Set Enrichment Analysis
GSH	Glutathione
GSK3β	Glycogen Synthase Kinase-3 Beta
GSS	Glutathione Synthetase
GSSG	Glutathione Disulfide
GTP	Guanosine Triphosphate
HATs	Histone Acetyltransferases
HDACs	Histone Deacetylase
HG	High Glucose
HIF-1α	Hypoxia Inducible Factor-1α
HK2	Hexokinase
HPA	Hypothalamic-Pituitary-Adrenal
HSD	Hydroxysteroid Dehydrogenase
ICC	Immunocytochemistry
IDO1	Indoleamine-Pyrrole 2-3-Dioxygenase

IFN	Interferon
IgG	Immunoglobulin G
IL	Interleukin
IPA	Ingenuity Pathway Analysis
IPCs	Intermediate Precursors
iPSCs	Induced Pluripotent Stem Cells
iTRAQ	Isobaric Tags for Relative and Absolute Quantitation
JaCoP	Just Another Colocalisation Plugin
JMJC	Jumonji-C Domain-Containing
JNK	Jun N-Terminal Kinase
KDMs	Histone Lysine Demethylases
KSR	Ketosteroid Reductase
KYN	Kynurenine
KYNA	Kynurenic Acid
LC3β	Microtubule-Associated Protein Light Chain 3 Beta
LCLs	Lymphoblastoid Cell Lines
LC-MS	Liquid Chromatography Mass Spectrometry
LDHA	Lactate Dehydrogenase
LDs	Lipid Droplets
LIAS	Lipoyl Synthase
MAL	Mitochondrial Allostatic Load
MAMs	Mitochondrial Associated Endoplasmic Reticulum Membranes
MAO	Monoamine Oxidase
MAP2	Microtubule-Associated Protein 2
MAPK	Mitogen-Activated Protein Kinase
MC	Methylcitrate
MCD	Malonyl-CoA Decarboxylase
MCT-1	Monocarboxylate Lactate Transporter 1
MDD	Major Depressive Disorder
MDS	Multi-Dimensional Scaling
MDVs	Mitochondrial Derived Vesicles
MECP2	Methyl CpG Binding Protein-2
MEM	Minimum Essential Medium
MFF	Mitochondrial Fission Factor
MFN1	Mitofusin 1
MHCs	Major Histocompatibility Complexes
MICOS	Mitochondrial Contact Site and Cristae Organising System
MiNA	Mitochondrial Network Analysis
MIP	Maximum Intensity Projection
miRNA	Micro RNAs
MIRO1	Microtubule-Associated Motor Proteins Mitochondrial Rho GTPase 1
MOI	Module Of Interest
mPTP	Membrane Permeability Transition Pore
mRNA	Messenger RNA
MS	Methionine Synthase
mtDNA	Mitochondrial DNA

mtFAS	Mitochondrial Fatty Acid Synthesis
MTHFR	Methylenetetrahydrofolate Reductase
MTIF	Melanocyte Inducing Transcription Factor
mTOR	Mechanistic Target of Rapamycin
mTORC1	Mechanistic Target of Rapamycin Complex 1
MTT	Thiazolyl Blue Tetrazolium Bromide
MZ	Monozygotic
NA	Numerical Aperture
NaCl	Sodium Chloride
NAD +	Nicotinamide Adenine Dinucleotide
NADH	Reduced Nicotinamide Adenine Dinucleotide
NADPH	Nicotinamide Adenine Dinucleotide Phosphate
NAGS	N-Acetyl Glutamate Synthetase
nBAF	Neuronal BAF
NBM	Neurobasal Medium
NCBI	National Centre for Biotechnology Information
ND2	NADH Dehydrogenase 2
NDDs	Neurodevelopmental Disorders
nDNA	Nuclear DNA
NE	Norepinephrine
NEAA	Non-Essential Amino Acids
NES	Nestin
NeuN	Neuronal Nuclei
NF	Neurofibromatosis
Nfe2l2	Nuclear factor erythroid-derived 2-like 2
NGF	Nerve Growth Factor
NICD	Notch Intracellular Domain
NIX	BNIP3-Lik
NMDAR	N-Methyl-D-Aspartate Receptor
NOX	Nicotinamide Adenine Dinucleotide Phosphate Oxidase
NPCs	Neuronal Progenitor Cells
NRFs	Nuclear Respiratory Factors
NSCs	Neuronal Stem Cells
OADH	Oxoadipate Dehydrogenase
OCFAs	Odd-Chain Fatty Acids
OCR	Oxygen Consumption Rate
OMA1	Oma1 Zinc Metallopeptidase
OPA1	Optic Atrophy Protein 1
OXPHOS	Oxidative Phosphorylation
PA	Propionic Acidemia
PANK	Pantothenate Kinase
PARK	Parkin
PBS	Phosphate-Buffered Saline
PC	Propionylcarnitine
PCA	Principal Component Analysis
PCC	Propionyl CoA Carboxylase

PCCA Propionyl CoA Carboxylase Alpha
PCCB Propionyl CoA Carboxylase Beta
PCP Planar Cell Polarity
PCT Propionate-Coa Transferase
PDH Pyruvate Dehydrogenase
PDK Pyruvate Dehydrogenase Kinase
PDL Poly-D-Lysine
PEMT Phosphatidylethanolamine N-Methyltransferase
PEP Phosphoenolpyruvate
PG Proteoglycan
PGC1α Peroxisome Proliferator-Activated Receptor Gamma Coactivator-1 Alpha
PGs Proteoglycans
PI Phosphatidylinositol
PI3K Phosphoinositide-3 Kinase
PINK1 PTEN Homolog-Induced Kinase 1
PK Pyruvate Kinase
PKA Protein Kinase A
PKC Protein Kinase C
PKM2 Pyruvate Kinase Isoform 2
PL Phospholipase
PMT Photomultiplier Tubes
PPA Propionic Acid
PPAR Peroxisome Proliferator-Activated Receptor
PPP Pentose-Phosphate Pathway
PPREs PPAR Responsive Elements
PTEN Phosphatase And Tensin Homolog
PTMs Post-Translational Modifications
PTSD Post-Traumatic Stress Disorder
QC Quality Control
QUIN Quinolinic Acid
RA Retinoic Acid
RAPTOR Regulatory-Associated Protein Of mTOR
RAREs Retinoic Acid Response Elements
RARs Retinoic Acid Receptors
RhoA Ras Homolog Family Member A
RIN RNA Integrity Number
RISC RNA-Induced Silencing Complex
RNA Ribonucleic Acid
RNAseq RNA Sequencing
ROCK Rho-Associated Kinase
ROI Region Of Interest
ROS Reactive Oxygen Species
ROUT Robust Regression and Outlier Removal
rRNA Ribosomal RNA
RT-qPCR Reverse Transcription Quantitative Polymerase Chain Reaction
RXR Retinoid X Receptor

S6K1	P70S6 Kinase
SA	South African
SAH	S-Adenosylhomocysteine (SAH)
SAM	S-Adenosyl-L-Methionine
SAMTOR	S-Adenosylmethionine Sensor Upstream of mTORC1
SCFAs	Short Chain Fatty Acids
SDS	Sodium Dodecyl Sulfate
SERT	Serotonin Transporter
SF	Serum-Free
SIRT	Sirtuin
SMAD3	SMAD Family Member 3
SMRT	Silencing Mediator of Retinoic Acid and Thyroid Hormone Receptor
SNAP25	Synaptosome Associated Protein 25
SNT	Single Neurite Tracer
SREBPs	Sterol Regulatory Binding Proteins
SSA	Sub-Saharan Africa
STAT3	Signal Transducer and Activator of Transcription 3
STOML2	Stomatin-Like Protein 2
SUCL	Succinate CoA Ligase
SYN-1	Synapsin 1
SYP	Synaptophysin
TCA	Tricarboxylic Acid Cycle
TE	Tris-EDTA
TET	Ten–Eleven Translocation
TFAM	Mitochondrial DNA Transcription Factor A
TGF	Transforming Growth Factor
TH	Tyrosine Hydroxylase
THF	Tetrahydrofolate
TMM	Trimmed Mean Of M
TMRE	Tetramethylrhodamine, Ethyl Ester
TRAK	Trafficking Kinesin
TRK	Tyrosine Receptor Kinase
TSC1	Tuberous Sclerosis
ULK1	UNC-51-Like Autophagy-Activating Kinase 1
UPR	Unfolded Protein Response
USA	United States of America
VEGF	Vascular Endothelial Growth Factor
WGCNA	Weighted Gene Co-Expression Network Analysis
XBP1	X-Box-Binding Protein 1
YAP1	Yes1 Associated Transcriptional Regulator
αKDH	Alpha-Ketoglutarate Dehydrogenase
α-KG	Alpha-Ketoglutarate
Wnt	Wingless-Related Integration Site

Units and Symbols

AFU	Arbitrary Fluorescent Units
cm	Centimetre
°C	Degrees Celsius
g	Gram
µL	Microlitre
µM	Micromolar
mg	Milligram
mL	Millilitre
mm	Millimetre
mM	Millimolar
min	Minute
ΔΨm	Mitochondrial Membrane Potential
M	Molar
ng	Nanogram
nm	Nanometre
nM	Nanomolar
pmol	Picomol
RFU	Relative Fluorescence Units
RLU	Relative Luminescent Units
rpm	Revolutions Per Minute
s	Second

List of Figures and Tables

Figure A Thesis Contents and Outline
Figure 1.1 Convergent Molecular Signatures in Autism Spectrum Disorder
Figure 1.2 The Redox/Methylation Hypothesis
Figure 1.3 The SAM Depletion Hypothesis
Figure 1.4 An Overview of Mitochondrial Metabolism
Figure 1.5 An Overview of Mitochondrial Dynamics
Figure 1.6 The Metabolic Shift: Mitochondrial Remodelling During Neurogenesis
Figure 1.7 The Relationship Between Metabolic and Epigenetic Remodelling
Figure 1.8 The Mitochondrial Modulation of Neuroimmune State
Figure 1.9 Neuron-Glia Metabolic Coupling
Figure 1.10 Mitochondrial Mechanisms in ASD Neurochemistry
Figure 1.11 The Interplay Between Metabolic and Stress-Responsive Signalling
Figure 1.12 Contextualising the Mitochondrial Hypothesis
Figure 1.13 Central Research Question, Aims and Objectives
Figure 2.1 Studying Mitostasis *In Vitro*
Figure 2.2 Image Analysis Workflow to Quantify Mitochondrial Content, Morphology Turnover
Figure 2.3 Image Pre-processing Pipeline
Figure 2.4 Quantification of Mitochondrial Content and LC3β Expression
Figure 2.5 Colocalisation Analysis Workflow
Figure 2.6 Propionic Acid-Induced Cytotoxicity in SH-SY5Y Cells
Figure 2.7 A Model for PCCB-Associated Mitochondrial Dysfunction
Figure 2.8 Master Metabolic Regulators Perturbed by Propionic Acid
Figure 2.9 Transcriptional Regulators of Mitogenesis
Figure 2.10 Canonical Regulators of Fusion and Fission
Figure 2.11 Central Regulators of Mitochondrial Morphology and Dynamics
Figure 2.12 Transcriptional Disruptions to Mitostasis Induced by Propionic Acid
Figure 2.13 Decreased Mitochondrial Content Under Propionic Acid Stress
Figure 2.14 Impairments to Mitochondrial Network Integrity in the Propionic Acid Model
Figure 2.15 Remodelling of Mitochondrial Morphology in Response to Propionic Acid
Figure 2.16 Perturbations to Mitophagic Flux Induced by Propionic Acid
Figure 2.17 Impaired ATP Production and Altered Metabolic Phenotype
Figure 2.18 Disruptions to Mitochondrial Metabolism Induced by Propionic Acid
Figure 2.19 End-Point Measures of Mitostasis in the Propionic Acid Model
Figure 2.20 Putative Mechanisms of Transcriptional Remodelling
Figure 2.21 Profiles of Glucose Utilisation Under Propionic Acid Stress
Figure 2.22 The CoA Sequestration Hypothesis
Figure 3.1 The Neurogenic Mechanisms of Retinoic Acid
Figure 3.2 Neurogenic Signalling by Brain-derived Neurotrophic Factor
Table 3.1 Metabolic Remodelling During SH-SY5Y Differentiation
Figure 3.3 A Graphical Summary of Metabolic Remodelling *In Vitro*
Figure 3.4. Differentiation Protocol and Experimental Design
Figure 3.5 An Immunocytochemistry Assay to Measure Nestin and β-3-Tubulin Expression
Table 3.2 Visualisation Conditions for Wide Field Fluorescent Microscopy
Figure 3.6 Image Processing and Analysis Pipeline for Cell Quantification
Figure 3.7 Pre-processing and Image Analysis Pipeline for 20X Images

Figure 3.8 Pre-processing and Image Analysis Pipeline for 60X Stacks
Figure 3.9 Quantification of Neurite Morphology with Automated and Manual Tracing Techniques
Figure 3.10 Inhibition of Cell Proliferation During Differentiation
Figure 3.11 Evaluation of Neurite Morphology in Live Cell Cultures
Figure 3.12 Quantification of Neuronal Maturation and Morphology
Figure 3.13 Automated and Manual Tracing Techniques to Quantify Neurite Morphology
Table 3.3 A Comparison of Auto and Manual Tracing Techniques in 60X Images
Figure 3.14 Automated Quantification of Neurite Morphology in 20X Images
Figure 3.15 Metabolic Profiles of *In Vitro* Neurogenesis
Figure 3.16 Gross Morphological Disruptions Induced by Propionic Acid
Figure 3.17 Morphological Composition of Neurons Under Propionic Acid Stress.
Figure 3.18 Altered Expression and Localisation of Neuronal Markers.
Figure 3.19 Increased Colocalisation of Nestin and β-3-Tubulin with Propionic Acid Exposure.
Figure 3.20 Disruptions to Neurite Elongation and Branching.
Figure 3.21 Morphological Disruptions Validated by Autotracing in Broader Cell Populations
Table 4.1 Molecular Profiles of SH-SY5Y Differentiation
Figure 4.1 Molecular Signatures of Metabolic Remodelling
Figure 4.2 A Two-Pronged Approach to Transcriptomic Analysis
Figure 4.3 MultiQC Report Summarising Quality Control Parameters for all 12 samples
Table 4.2 Pairwise QL F-Tests Conducted for Differential Gene Expression Analysis
Figure 4.4 All Significantly Differentially Expressed Genes Identified In 5 Pairwise QL-F Tests
Figure 4.5 Annotating the Neurogenic Transcriptome
Figure 4.6 Annotating the PPA Transcriptome
Figure 4.7 Cell-fate Regulators Perturbed by Propionic Acid
Figure 4.8 Central Mechanisms of Propionic Acid-Induced Neurotoxicity
Figure 4.9 Metabolic Signatures in the PPA Transcriptome
Figure 4.10 Central Regulators of Metabolic Remodelling
Figure 4.11 Convergent Regulators of Neuronal Metabolism and Maturation
Figure 4.12 Neurotoxic Signatures in the PPA Transcriptome
Figure 4.13 Coregulated Modules Identified By WGCNA
Figure 4.14 Modules of Interest Associated Experimental Conditions
Figure 4.15 Functional Annotations Associated with Modules of Interest
Figure 4.16 Modules of Interest Mapped Across Mechanistic Clusters
Figure 4.17 A Mechanistic Framework for Propionic Acid-Induced Developmental Neurotoxicity
Table 4.3 Functional Signatures of Propionic Acid Exposure From Ingenuity Pathway Analysis
Figure 4.18 Significantly Enriched Pathways Identified with Ingenuity Pathway Analysis
Table 4.4 Significantly Enriched Disease Pathways Associated with Propionic Acid
Figure 4.19 Top Transcriptional Regulators in the PPA Transcriptome
Table 4.5 Top Transcriptional Regulators in The PPA Transcriptome
Figure 4.20 Differentially Expressed Regulators in the PPA Transcriptome
Figure 4.21 Convergent Regulators in the PPA Transcriptome
Figure 4.22 Epigenetic Regulators of Metabolic Remodelling
Figure 4.23 Transcriptional Signatures of Epigenetic Remodelling
Figure 4.24 Intrinsic Signatures of Developmental Delay
Figure 4.25 The Interplay Between Metabolic and Morphological Remodelling
Figure 4.26 Reshaping the Intrinsic and Extrinsic Landscapes of *In Vitro* Neurogenesis
Figure B Main Considerations and Conclusions Emerging from this Thesis

Thesis Overview

Molecular research into Autism Spectrum Disorders (ASD) has evolved rapidly since the turn of the century with the introduction of high-throughput "omics" technologies. Yet, researchers are still grappling with how to translate novel genetic associations into an understanding of ASD aetiology that can be harnessed to improve quality of life. From a mechanistic perspective, mitochondrial processes have emerged as a subject of interest in both molecular autism and neuroscience research. Our research group previously reported differential DNA methylation (DNAm) signatures converging on mitochondrial processes in an understudied South African (SA) ASD cohort (Stathopoulos *et al.,* 2020; Bam *et al.,* 2021). In fact, the mitochondrial component of ASD aetiology has become increasingly well-established over the last decade (Frye *et al.,* 2024). Concurrently, mitochondrial mechanisms have emerged as focal regulators of neurodevelopment, physiology and function that are widely implicated in neurodevelopmental and neurodegenerative disorders (Garone, De Giorgio and Carli, 2024). Moreover, an emerging field known as mitochondrial psychobiology has pioneered the concept of mitochondrial allostatic load (MAL), illustrating how mitochondria mediate interactions between underlying biology and the environment to influence long-term clinical outcomes (Picard, Trumpff and Burelle, 2019).

This thesis examines the role of mitochondrial dysfunction in ASD aetiology, building on the molecular signatures identified in our ASD cohort to develop, and test, a mechanistic hypothesis *in vitro*. This thesis is divided into two parts, tied together by a central research question about the role of mitochondrial dysfunction in neurodevelopment and disease. Part I describes the origins and implications of the mitochondrial dysfunction hypothesis before establishing a neuronal cell model to study mitochondrial dysfunction *in vitro.* In Part II, this model system is harnessed to investigate the relationship between mitochondrial dysfunction and neurogenesis, by developing and characterising a model for mitochondrial-associated neurotoxicity. These primary aims are achieved according to four broad objectives, addressed in Chapters 1 – 4 **(Figure A).**

Chapter 1 introduces the broader landscape of molecular autism research, highlighting pertinent clinical, socio-economic and psychosocial considerations that shape the aims and directions of the field. This chapter collates the existing evidence for mitochondrial mechanisms in ASD, demonstrating how mitochondria shape diverse facets of ASD aetiology that could be targeted to improve quality of life. Chapter 2 establishes an *in vitro* model for mitochondrial dysfunction in neuronal-like SH-SY5Y cells, using Propionic acid (PPA) to recapitulate the mitochondrial signatures associated with Propionyl CoA carboxylase B (PCCB) observed in our ASD cohort. Chapter 3 builds on this work to develop and characterise an *in vitro* model for neuronal differentiation, which is harnessed to study the effect of PPA

on neuronal morphology and maturation. Lastly, Chapter 4 examines the transcriptional signatures that underpin PPA-associated neurotoxicity to better understand the mechanistic relationship between neuronal metabolism and development.

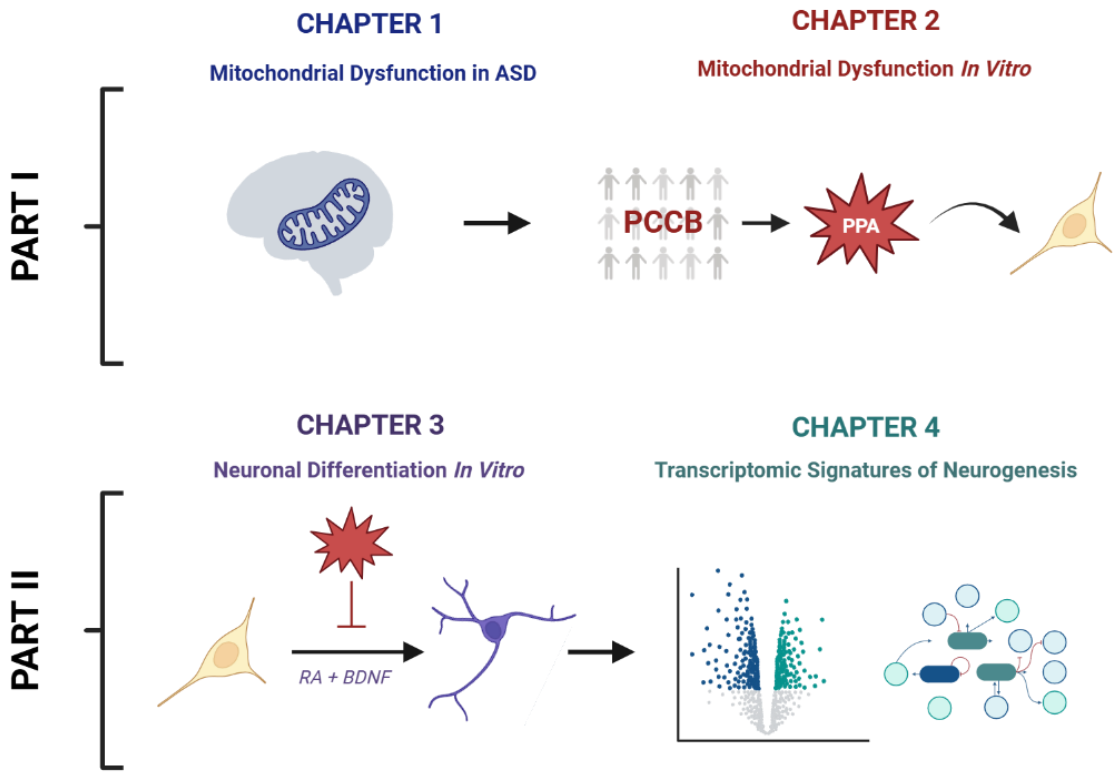


Figure A. Thesis Contents and Outline. Chapter 1 describes how mitochondria influence neurodevelopment, neurophysiology and neurochemistry to shape clinical outcomes in Autism Spectrum Disorder (ASD). Chapter 2 develops an *in vitro* model for mitochondrial dysfunction based on the signatures in a South African ASD Cohort. Chapter 3 establishes an *in vitro* model for neuronal differentiation to study the effect of metabolic stress on neuronal maturation, while Chapter 4 characterises the underlying transcriptional mechanisms that drive this response. This work provides new insight into the mitochondrial mechanisms that govern neurodevelopment and function, contributing to an understanding of the mitochondrial component of ASD aetiology. BDNF – brain-derived neurotrophic factor; PCCB - Propionyl CoA carboxylase B; PPA – propionic acid; RA – retinoic acid.

Ultimately, this thesis expands current characterisations of the PPA model, providing novel insight into mechanisms and manifestations of PPA-induced neurotoxicity. This work establishes an *in vitro* system to serve as a bridge between gene identification and mechanistic translation in the SA context. Moreover, this thesis develops a molecular workflow to characterise different facets of mitochondrial homeostasis *in vitro* and highlights novel considerations for the SH-SY5Y system in neurotoxicology research. Together, this project lays the groundwork for new avenues of research into mitochondrial dysfunction and neurotoxicity that could yield insight into the mitochondrial component of ASD aetiology.

~ PART I ~

Chapter 1.

The Mitochondrial Hypothesis: Molecular Mechanisms and Clinical Implications

1.1. The Landscape of Molecular Autism Research

Autism research spans disparate academic disciplines shaped by intersecting sociological, clinical, and molecular landscapes. Although first described in the scientific literature in 1943, ASD was only included in the Diagnostic and Statistical Manual of Mental Disorders (DSM-III) in 1980 (Rosen, Lord and Volkmar, 2021) and the clinical conceptualisations of autism are still evolving (Whiteley, Carr and Shattock, 2021). Current diagnostic texts define ASD as a lifelong neurodevelopmental condition marked by differences in social communication, interaction and behaviour that are present during early development and significantly impact daily functioning (American Psychiatric Association, 2022). These criteria capture diverse and dynamic presentations that can vary across life-stages and sociocultural contexts (Lombardo and Mandelli, 2022). The phenotypic heterogeneity of ASD is compounded by a range of frequent comorbidities including epilepsy, attention deficit hyperactivity disorder (ADHD), sleep disorders, gastrointestinal problems, intellectual disability, anxiety and depression (Zhang *et al.,* 2019). Similarly, the capacity and motivation to mask ASD-associated traits varies significantly between individuals due to differences in underlying physiology and sociocultural factors that contribute to socialisation (Petrolini, Rodríguez-Armendariz and Vicente, 2023). Accordingly, it remains challenging to effectively operationalise the DSM-V criteria in the form of standardised tools that provide quantitative thresholds for diagnostic classification (Evers *et al.,* 2021).

The molecular aetiology of ASD is equally multi-faceted, with an undisputed but complex genetic component that is influenced by both epigenetic and environmental factors (Choi and An, 2021). The heritability of ASD was first established with the high rates of concordance between monozygotic (MZ) twins. Varying rates of concordance between 60 and 90% have been documented in the literature, but the most recent estimates range between 96 and 99% (Tick *et al.,* 2016; Castelbaum *et al.,* 2019; Masini *et al.,* 2020; Ho *et al.,* 2022). As the throughput, accuracy and scale of molecular ASD research has advanced rapidly over the past two decades, genomic studies have validated the genetic origins of ASD, demonstrating an estimated heritability between 64 and 91% (Yasuda *et al.,* 2022; Ghafouri-Fard *et al.,* 2023; Kereszturi, 2023). This work has revealed a complex genetic architecture defined by significant pleiotropy, extensive locus heterogeneity and common and rare *de novo* mutations with variable penetrance (Havdahl *et al.,* 2021). In fact, no single mutation accounts for more than 1% of ASD cases

(Duffney *et al.,* 2018), while more than 65% of additive heritability cannot be attributed to known genetic variants (Havdahl *et al.,* 2021) and 85% of all ASD cases are idiopathic (Casanova *et al.,* 2020; Stoccoro *et al.,* 2023). Together, the heterogeneity in clinical presentations and genetic aetiology presents considerable challenges to molecular ASD research. Nevertheless, the diverse molecular origins of ASD are thought to converge on common biological processes that could inform novel biomarkers and therapeutic strategies (Murtaza *et al.,* 2022; Pintacuda *et al.,* 2023; Khaliulin, Hamoudi and Amal, 2024).

Despite the exponential increase in molecular ASD research since the start of the genomic revolution, existing research is still largely conducted in the Global North (Bakare *et al.,* 2022). The rich genetic diversity of African populations has the potential to yield novel insight into ASD aetiology, and characterising understudied populations is an emerging priority for the field. However, autism remains poorly studied across Sub-Saharan Africa (SSA) (De Vries, 2016; Franz *et al.,* 2017). We recently conducted a review of molecular ASD research in Africa to quantify and explain this geographical disparity (Frickel *et al.,* 2023). In this review, we report that molecular ASD research across the whole African continent amounts to less than half of the output from the United States of America (USA), with the existing research coming from only seven of 54 African countries. In South Africa (SA), molecular researchers are already constrained by a lack of infrastructure, funding and human resources, but poor access to health care, a shortage of qualified clinicians, a lack of centralised databases, an absence of culturally relevant diagnostic tools and widespread misconceptions about mental conditions further limits the scope of molecular ASD research in this context (Abubakar, Ssewanyana and Newton, 2016; Franz *et al.,* 2017; Bakare *et al.,* 2022; Samadi, 2022).

Yet, these factors alone cannot entirely account for the regional gap in molecular ASD research. A recent evaluation of health science research capacity showed that SA ranked first in Africa with respect to the number of universities, first-author publications, and clinical trials (Wenham *et al.,* 2021). At the same time, SA has produced more than 50% of all ASD research in SSA, with an exponential increase in research output over the last decade (Frickel *et al.,* 2023). Thus, SA has the infrastructure to produce high-quality research in both autism and molecular biology. Yet, we found that only five molecular ASD studies have been conducted in SA populations since 1935. This discrepancy between research capacity and research output appears to be due to a lack of investment among stakeholders in both the molecular and clinical sectors. The disproportionate burden of infectious disease across SSA means that the limited resources available for molecular research are seldom allocated to research on non-communicable diseases (Nyirenda, 2016). Similarly, existing research on neuropsychiatric conditions prioritises studies on diagnosis and intervention rather than an understanding of molecular aetiology (Frickel *et al.,* 2023). While there is a growing awareness of the stark gap in the literature on autism in SSA, resources are not allocated to molecular ASD research due to a perceived lack of translatability in this context.

In fact, the translatability of molecular ASD research is an issue that the field is grappling with internationally. Despite the hundreds of risk genes identified to date, a prevailing challenge of molecular autism research is to *"translate gene discovery into an actionable understanding of ASD physiology"* (Manoli and State, 2021). There is still a significant lag between molecular studies and the development of strategies that tangibly improve people's lives. Indeed, even promising *in vitro* and *in vivo* molecular studies have failed to produce translatable results in clinical trials (Young and Findling, 2015; Jeste and Geschwind, 2016; Loth, Murphy and Spooren, 2016; Vorstman *et al.,* 2017; Sestan and State, 2018; McCracken *et al.,* 2021). This can largely be attributed to the dynamic interplay between genetic, epigenetic and environmental factors that contribute to ASD aetiology. Yet, molecular research may also require a more interdisciplinary approach to produce socially transformative outputs (de Vries, 2023).

In recent years, the evolving sociological landscape of autism research has required clinicians and scientists to reevaluate the aims and directions of the field. Historically, autism research has primarily relied on the medical model of disability, rooted in a pathologisation of external ASD traits (Whiteley, Carr and Shattock, 2021). However, the field is now progressing towards a more comprehensive biopsychosocial disability model (Chown and Beardon, 2017; Doyle, 2020). This model recognises that an individual's experience of disability is influenced by both biological and sociological factors, emphasising that biological *differences* are not necessarily biological *deficits* (Fletcher-Watson *et al.,* 2019). The neurological differences associated with ASD may indeed present challenges to independent functioning; yet an inability to function within a societal framework that accommodates only one neurotype is not itself pathological (Doyle, 2020). On the other hand, everyone has their own individual experience of *intrinsic disability* that causes internal distress irrespective of their sociological context. Considering both perspectives, autism research is shifting its focus to improving quality of life and minimising internal distress, rather than eradicating or correcting external behaviours (Leadbitter *et al.,* 2021).

Still, an over-reliance on the medical model of disability is often unavoidable in molecular research, which requires unambiguous definitions of disease, reductionist animal and cell culture models, and highly specific questions with limited scope. Biomedical research tends to rely on limited measurements of behaviour and functioning, where the efficacy of an intervention is frequently evaluated by a decrease in ASD-associated behaviours. Yet, it is becoming clear that external presentations of ASD do not always correlate with health, well-being or quality of life (Cage and Troxell-Whitman, 2019; Cassidy *et al.,* 2020; Hull, Petrides and Mandy, 2020; Cook *et al.,* 2021). In this context, it is important to acknowledge that molecular ASD research may be rooted in a one-dimensional understanding of autism that could hinder its translatability in a clinical and sociological context.

Nevertheless, molecular research has great potential to inform both pharmacological and psychosocial interventions that could improve quality of life. Insight into the heritability of ASD has already been instrumental in increasing access to early diagnoses and shifting blame away from caregivers or individuals themselves for their differences (Chiapperino and Hens, 2023). Likewise, molecular therapies have been able to effectively treat co-occurring health conditions in syndromic ASDs, improving life expectancy and clinical outcomes (Schubert-Bast *et al.,* 2019). Better characterising molecular ASD aetiology could be essential to improve the resolution, specificity and utility of diagnostic labels, while population-specific biomarkers and pharmacological interventions could make early diagnosis and treatment much more accessible in resource-constrained contexts. In the long term, many areas of society will need to be systemically restructured to better accommodate different neurotypes. However, in a country like SA, where access to basic education and health care remains limited for a majority of the population, children with different needs are still left to fend for themselves. While psychological and sociological interventions are slowly becoming more accessible, there is a need for more targeted pharmacological approaches to alleviate distress for people who are simply not accommodated by the system.

Ultimately, different sectors of autism research have distinct roles, but socially transformative molecular research requires socially responsive practices (de Vries, 2023). An understanding of ASD physiology within a biopsychosocial framework could also provide novel insight into the cellular mechanisms at the interface between environmental stressors and biological processes that determine long-term clinical outcomes. On the one hand, ASD is associated with increased exposure to early life stress (ELS), which not only increases the risk of psychopathology and suicidality (Fogelman and Canli, 2019; LeMoult *et al.,* 2020; Sahle *et al.,* 2021; Su *et al.,* 2022) but it also impairs clinical outcomes in a range of neurodevelopmental, neurodegenerative and neuropsychiatric conditions (Guidi *et al.,* 2021). On the other hand, increasing evidence also suggests an underlying susceptibility to psychopathology mediated by genetic and neurological aspects of ASD aetiology (Muscatello *et al.,* 2020; Unruh, Bodfish and Gotham, 2020; Scarpa *et al.,* 2021; Warrier and Baron-Cohen, 2021). Thus, clinical outcomes in ASD are determined by interactions between ELS and ASD physiology (Singletary, 2015; Scarpa *et al.,* 2021; Makris, Eleftheriades and Pervanidou, 2022). With high rates of poverty, food insecurity, infectious disease, and consequent childhood abuse or neglect across SA, the relationship between genetic aetiology, ELS and pathophysiology has direct implications for the health and well-being of individuals with ASD. Mechanistically understanding this relationship is therefore central to our understanding of the sociological and physiological factors that impact quality of life.

It is within this context that our research group studies the molecular aetiology of ASD in SA populations. We previously conducted the first null-hypothesis-based molecular study in an ASD cohort from SA, revealing DNAm signatures that converged on mitochondrial metabolism (Stathopoulos *et al.,* 2020). Notably, DNAm and mitochondrial dysfunction have separately been implicated in ASD,

and there is now increasing evidence that these processes are mechanistically intertwined. Moreover, mitochondria function as critical regulators of neurodevelopment that shape diverse facets of ASD aetiology. This chapter reviews the relationship between DNAm and mitochondrial dysfunction in ASD, describing the biochemical context that informs the central aims and objectives of this thesis. In doing so, this chapter demonstrates how the molecular signatures in our SA cohort reflect emerging trends in the broader literature, highlighting recent insights implicating mitochondria as central modulators of neuronal maturation, physiology and function that operate at the intersection between biology and the environment. Together, this discussion illustrates how mitochondrial dysfunction contributes to diverse facets of ASD aetiology that are susceptible to ELS, presenting novel therapeutic avenues to improve quality of life.

1.2. From DNA Methylation to Mitochondrial Dysfunction in ASD

The complex heritability of ASD and the varying rates of discordance between MZ twins indicate that autism cannot solely be explained by genetic factors (Wiśniowiecka-Kowalnik and Nowakowska, 2019). Therefore, a role for epigenetic mechanisms in ASD is a focus of ongoing research. The epigenome is shaped by modifications to DNA and histone tails that regulate chromatin architecture (Tremblay and Jiang, 2019). Epigenetic state plays a critical role in embryonic neurogenesis by governing the spatiotemporal patterns of gene expression that determine neuronal identity, development and function (Salinas, Connolly and Song, 2020). Operating at the interface between environmental stressors and transcriptional regulation, epigenetic mechanisms are sensitive to chemical, immunological, endocrinological and psychological insults that are linked to the development of ASD (Kubota and Mochizuki, 2016). Moreover, a recent systematic review demonstrated that almost 20% of ASD candidate genes participate in epigenetic regulation (Duffney *et al.,* 2018), including several genes that are causally implicated in syndromic neurodevelopmental disorders (NDDs) (Rangasamy, D'Mello and Narayanan, 2013). In fact, cumulative evidence has revealed systemic changes to DNAm (Banerjee and Adak, 2021; Sun *et al.,* 2022; Stoccoro *et al.,* 2023), histone acetylation (Sun *et al.,* 2016; Tseng *et al.,* 2022), histone methylation (Shulha *et al.,* 2012) and microRNA (miRNA) (Vasu *et al.,* 2019; Garrido-Torres *et al.,* 2023) profiles in ASD.

DNAm is one of the most well-studied epigenetic mechanisms in ASD because DNAm patterns play a fundamental role in regulating neuronal identity and development during early embryogenesis (Siu and Weksberg, 2017). DNAm modulates gene expression by changing chromatin accessibility, recruiting repressor and enhancer complexes and regulating alternative splicing (Corley *et al.,* 2019). A role for DNAm in ASD is supported by syndromic ASDs underpinned by genomic imprinting disorders, *de novo* mutations in DNAm machinery, loci-specific and global DNAm profiles and the sensitivity of DNAm profiles to environmental risk factors linked to NDDs (Ciernia and LaSalle, 2016; Keil and Lein, 2016; Tremblay and Jiang, 2019). Early studies reported the differential methylation (DM) of

single genes in ASD post-mortem cortex tissue, which correlated with downregulated mRNA and protein expression (Nagarajan *et al.,* 2006; Gregory *et al.,* 2009). Subsequent whole-genome methylation screens in patient-derived lymphoblastoid cell lines (LCLs) and blood samples revealed DM signatures converging on central nervous system (CNS) development and neurological disease (Nguyen *et al.,* 2010; Wong *et al.,* 2014). These findings were ultimately validated with genome-wide DM signatures found across three regions in post-mortem ASD brain tissue (Ladd-Acosta *et al.,* 2014).

Since this seminal work, epigenetic mechanisms in ASD have been widely studied and the role of DNAm in ASD has been extensively reviewed (Ciernia and LaSalle, 2016; Keil and Lein, 2016; Siu and Weksberg, 2017; Waye and Cheng, 2018; Tremblay and Jiang, 2019; Wiśniowiecka-Kowalnik and Nowakowska, 2019; Banerjee and Adak, 2021; Sun *et al.,* 2022; Gholamalizadeh *et al.,* 2024). Recent studies and meta-analyses have found that DNAm signatures consistently converge on mechanisms implicated in ASD aetiology (Andrews *et al.,* 2018; Wong *et al.,* 2019; Bakulski *et al.,* 2021; García-Ortiz *et al.,* 2021; Stoccoro *et al.,* 2023), correlate with differences in cognition, behaviour and neurophysiology (Jia *et al.,* 2019; Massrali *et al.,* 2019; Kraan *et al.,* 2020) and distinguish between ASD endophenotypes (Siu *et al.,* 2019; Lee and Hu, 2020; Hu *et al.,* 2021). Thus, DNAm is a well-established component of ASD aetiology. However, epigenetic mechanisms in ASD remain unexplored in SA populations. We conducted the first whole-genome methylation screen in an SA ASD cohort and identified DM across 898 genes that converged on mitochondrial canonical pathways (Stathopoulos *et al.,* 2020). Subsequent validation studies demonstrated that central genes involved in mitochondrial biogenesis, fission and fusion were DM in ASD, which was associated with altered mitochondrial DNA (mtDNA) copy number and urinary metabolomic profiles (Bam *et al.,* 2021). Together, this data suggests a mitochondrial endophenotype underpinned by DNAm in SA, proposing a role for mitochondrial function in ASD physiology.

It is this hypothesis that informed the direction of my PhD, which evolved from a mechanistic curiosity about the relationship between mitochondrial function and ASD aetiology. In order to establish whether the functional signatures implicated in our cohort were reflected in the broader literature, my project began with a quantitative review of published molecular ASD datasets **(Figure 1.1)** (Mahony and O'Ryan, 2021). Here, 19 transcriptomic, proteomic and DNAm profiles were collated from ASD cohort studies and meta-analyses published between 2016 and 2021. These datasets were inherently and intentionally heterogeneous, derived from different cohorts spanning a wide range of ages and tissue types from both blood and brain samples **(Table S1.1).** This approach aimed to identify common molecular mechanisms that were implicated in our own DNAm data and consistently dysregulated across a range of datasets using diverse molecular techniques in different cohorts, tissue types and developmental stages.

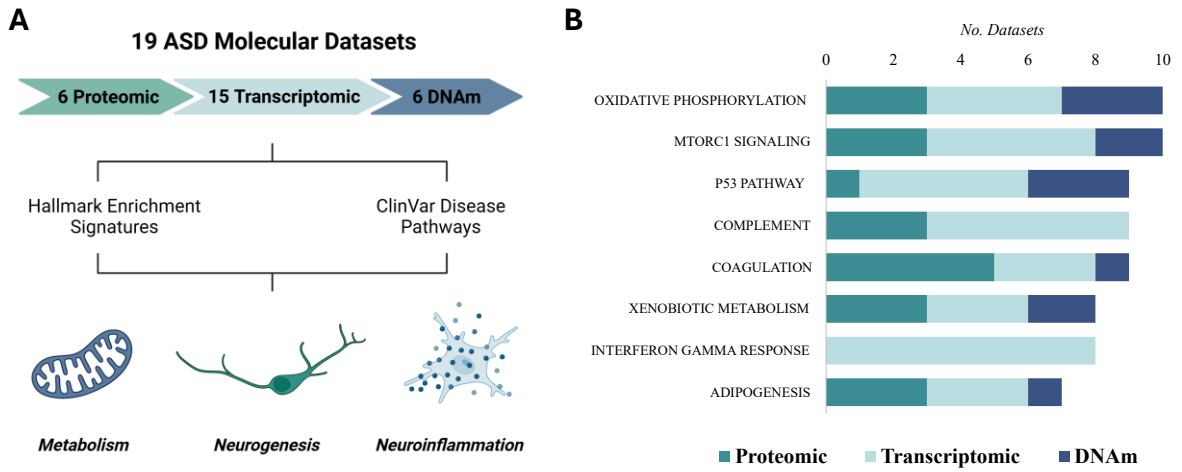


Figure 1.1. Convergent Molecular Signatures in Autism Spectrum Disorder (Taken from Mahony and O'Ryan, 2021)). **A)** Analysis Workflow and Graphical Overview. **B)** Hallmark Canonical Pathways implicated in at least seven independent datasets. Datasets were collated from 19 studies and meta-analyses on Autism Spectrum Disorder (ASD) cohorts published between 2017 and 2021, including six proteomic, eight transcriptomic and six DNA methylation (DNAm) profiles. All gene lists were converted into NCBI Entrez Gene IDs, and each dataset was annotated according to the top 10 significantly enriched Hallmark Canonical pathways. The Hallmark Canonical Pathways that were most consistently enriched across ASD proteomic, transcriptomic and DNA methylation (DNAm) datasets converged on processes involved in mitochondrial metabolism, neurogenesis and neuroinflammation.

Using a quantitative approach to functionally annotate each dataset with standardised enrichment signatures, this work revealed canonical pathways and protein-protein interaction networks that converged on processes involved in proliferation, differentiation, metabolism and inflammation. Of note, mitochondrial oxidative phosphorylation (OXPHOS) was one of the two most consistently dysregulated pathways across all 19 datasets, implicated in brain tissue using all three molecular approaches, and enriched in samples from children ranging from 18 months to 12 years old (Figure S1.1; Table S1.2). Thus, the mitochondrial signature in our cohort was not unique to the SA population, the tissue type or the age range employed in our own study but was reflected in both blood and brain tissue from diverse populations. This analysis emphasised the functional relevance of our DNAm signatures in the developing brain and highlighted mitochondrial metabolism as a convergent mechanism that may be implicated in idiopathic ASD.

In fact, a mitochondrial component in ASD aetiology has become increasingly well-established over the past two decades. A review of clinical data in 1998 first proposed a link between mitochondrial metabolism and autism, reporting consistent evidence for lactic acidosis, plasma carnitine deficiency, impaired neuronal energy production and altered urinary metabolomics (Lombard, 1998). Multiple lines of evidence have since emerged to support this hypothesis, which have been well-described in recent reviews (Siddiqui, Elwell and Johnson, 2016; Griffiths and Levy, 2017; Rose *et al.,* 2018; Castora, 2019; Balachandar *et al.,* 2020; Citrigno *et al.,* 2020; Frye, 2020; Thorsen, 2020; Khaliulin, Hamoudi and Amal, 2024). The prevalence of mitochondrial disorders is significantly higher in individuals with

ASD compared to the general population (Cheng, Rho and Masino, 2017), while both clinical and genetic aspects of ASD aetiology are frequently observed in patients with inherited metabolic disorders (Žigman *et al.,* 2021; Shchelochkov *et al.,* 2024). A recent meta-analysis of ASD-associated biomarkers revealed consistent disruptions to plasma lactate, pyruvate, ATP and acyl-carnitine profiles, altered mtDNA copy number, increased mtDNA mutations and deletions and perturbed electron transport chain (ETC) activity (Frye *et al.,* 2024). Independent studies have also demonstrated altered mitochondrial morphology, dynamics and bioenergetics (Pecorelli *et al.,* 2020; Frye *et al.,* 2021; Hassan *et al.,* 2021), impaired mitochondrial quality control (Ebrahimi-Fakhari *et al.,* 2016; Wang *et al.,* 2021) and transcriptomic (Ginsberg *et al.,* 2012; Zeidán-Chuliá *et al.,* 2014; Forés-Martos *et al.,* 2019; Aldosary *et al.,* 2020), proteomic (Abraham, Szoko and Natowicz, 2019; Shen, Feng, *et al.,* 2019; Shen, Zhao, *et al.,* 2019; Cicaloni *et al.,* 2020; Yao *et al.,* 2021), epigenomic (Stathopoulos *et al.,* 2020; Bam *et al.,* 2021; Hu *et al.,* 2021) and metabolomic (Glinton and Elsea, 2019; Gevi, Belardo and Zolla, 2020; Ristori *et al.,* 2020; Smith *et al.,* 2020; L. Wang *et al.,* 2021; Korteling *et al.,* 2022; Piras *et al.,* 2022; Smith and Donley, 2022; Un *et al.,* 2022) signatures converging on mitochondrial processes in ASD. Moreover, there is consistent evidence for increased oxidative stress in ASD, which is both a cause and consequence of mitochondrial dysfunction (Bjørklund *et al.,* 2020; Hu *et al.,* 2020; Manivasagam *et al.,* 2020; Pangrazzi, Balasco and Bozzi, 2020; Thorsen, 2020; Chen *et al.,* 2021). Thus, ongoing research is exploring the utility of existing and novel therapeutics to target mitochondrial mechanisms in ASD (Frye, 2020; Nabi *et al.,* 2022; Indika *et al.,* 2023; Varma, Bhandari and Kuhad, 2024).

As a source of the substrates and cofactors that drive epigenetic modifications, mitochondria are established regulators of epigenetic state (Matilainen, Quirós and Auwerx, 2017; Wiese and Bannister, 2020; Meiliana, Dewi and Wijaya, 2021; Zhu, Li and Tian, 2022) and this relationship plays an essential role in neurodevelopment (Sánchez-Ramírez *et al.,* 2024), neurodegeneration (Coppedè, 2021, 2024; Xu *et al.,* 2021) and disease (Gao *et al.,* 2018; Chakraborty and Mukherjee, 2024). In particular, Lopes, (2020) described the intricate relationship between DNAm and mitochondrial metabolism mediated by: i) the methylation of nuclear-encoded mitochondrial genes; ii) nuclear-encoded methyltransferases and demethylases that regulate mtDNA methylation; iii) mtDNA retrograde signalling that alters nuclear DNAm and iv) mitochondrial-derived metabolites that regulate DNAm machinery. Here, the S-adenosyl-L-methionine (SAM) produced by one-carbon (1C) metabolism provides the methyl groups used by histone and DNA methyltransferases, which are modulated by the energy-sensitive AMP-dependent protein kinase (AMPK), while histone and DNA demethylases are regulated by the alpha-ketoglutarate (α-KG), fumarate, succinate and nicotinamide adenine dinucleotide (NAD+) generated by OXPHOS (Zhu, Li and Tian, 2022). Indeed, *in vitro* and *in vivo* models have verified the coupling between mitochondrial metabolism and nuclear DNAm, demonstrating that DNAm profiles are altered by mitochondrial inhibitors and different mtDNA haplotypes (Bellizzi *et al.,* 2012; Scola *et al.,* 2014; Atilano *et al.,* 2015; Lozoya *et al.,* 2018; Cortés-Pereira *et al.,* 2019; Kopinski *et al.,* 2019).

The multifaceted relationship between DNAm and mitochondrial function remains understudied in ASD. Nevertheless, a mechanistic link between the epigenetic and metabolic facets of ASD aetiology has long been considered through the lens of the redox/methylation hypothesis. Proposed by Deth *et al.,* (2008) and more recently reviewed by Bjørklund *et al.,* (2021), the redox/methylation hypothesis suggests a relationship between oxidative stress and altered methylation capacity mediated by 1C metabolism **(Figure 1.2).** In brief, 1C metabolism is an integrated system comprised of the folate, methionine cycle and transulfuration cycles, coupling folate-dependent methionine synthesis to the glutathione (GSH/GSSG) antioxidant system via the homocysteine recycling pathway. Consequently, DNAm is sensitive to disruptions to folate, homocysteine or glutathione cycling and this relationship is widely documented in ASD. Genetic variants involved in folate metabolism and transport have been implicated in ASD (Frye, Slattery and Quadros, 2017; Razi *et al.,* 2020; Tisato *et al.,* 2021), while cerebral folate deficiency is linked to an increased risk of NDDs (Lintas, 2019). Indeed, systematic reviews have found that folic acid supplementation improves neurodevelopmental outcomes and mitigates oxidative stress, altered DNAm capacity and core ASD symptoms (Hoxha *et al.,* 2021; Rossignol and Frye, 2021a; Sampaio *et al.,* 2021; Chen *et al.,* 2023). Likewise, significant differences in plasma homocysteine, methionine, cysteine and glutathione profiles have been reported in systematic reviews of clinical ASD data (Frustaci *et al.,* 2012; Bjørklund *et al.,* 2020; Chen *et al.,* 2021; Gulati *et al.,* 2024; Polat *et al.,* 2024), while a relationship between 1C metabolism and DNAm has been established in both clinical (James *et al.,* 2004, 2009; Melnyk *et al.,* 2012; Shpyleva *et al.,* 2014) and preclinical studies (Kloypan *et al.,* 2015; Singhal *et al.,* 2015; Wei *et al.,* 2016). To date, the redox/methylation hypothesis has highlighted several novel ASD biomarkers (Khemakhem *et al.,* 2017; Ristori *et al.,* 2020; Smith *et al.,* 2020) and targeted therapies that have been shown to improve mitochondrial function, redox homeostasis and clinical outcomes (Delhey *et al.,* 2017; Citrigno *et al.,* 2020; Rossignol and Frye, 2021a).

Importantly, emerging evidence suggests that the mechanistic relationship between epigenetic and metabolic mechanisms in ASD aetiology extends beyond the redox/methylation hypothesis. Indika *et al.,* (2021) recently proposed a more direct relationship between DNAm and mitochondrial metabolism in ASD underpinned by SAM depletion. These authors noted a decrease in methionine, SAM and the SAM/SAH ratio that was consistently linked to ASD across independent studies and meta-analyses, an observation that has since been validated in more recent systematic reviews (Polat *et al.,* 2024). Moreover, SAM supplementation has been shown to mitigate ASD-associated behaviours in preclinical models (Ornoy *et al.,* 2019, 2023; Weinstein-Fudim *et al.,* 2019, 2020) and a range of clinical studies have explored SAM as a therapeutic target in neurodevelopmental and psychiatric disorders (Gao *et al.,* 2018; Curpan, Luca and Ciobica, 2021; Rossignol and Frye, 2021b; Frye *et al.,* 2023).

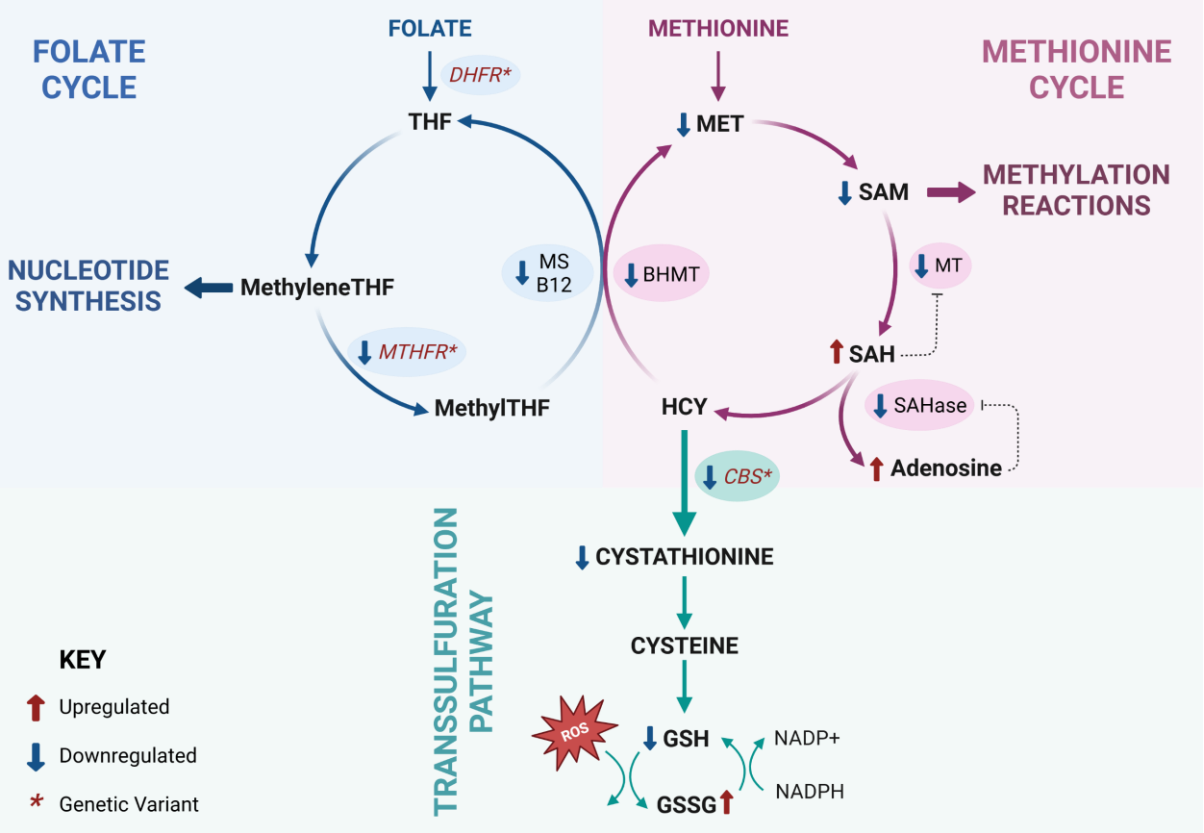


Figure 1.2. The Redox/Methylation Hypothesis. Disruptions to one carbon (1C) metabolism in Autism Spectrum Disorder (ASD) are depicted showing convergent changes to metabolites and enzymes in the folate, methionine and glutathione pathways reported by recent systematic reviews (Indika *et al*., 2021; Tisato *et al*. 2021). In the folate cycle, dietary folate is reduced by dihydrofolate reductase (DHFR) to form tetrahydrofolate (THF). THF enters the methionine cycle as 5,10-methyleneTHF, which is reduced by methylenetetrahydrofolate reductase (MTHFR) to produce 5-methytetrahydrofolate (5-mTHF). 5-THF donates a methyl group to homocysteine (Hcy) in a reaction catalysed by methionine synthase (MS) and betaine-homocysteine methyltransferase (BHMT) to produce methionine, which ultimately forms the methyl donor S-adenosylmethionine (SAM) that is used for methylation reactions. Methionine is recycled via the conversion of SAM to S- adenosylhomocysteine (SAH), which is used to produced adenine by SAHase. Hcy can also be metabolised by cystathionine beta synthase (CBS) to enter the transsulfuration pathway as cysteine. Cysteine is then incorporated into glutathione (GSH), which is an essential antioxidant enzyme responsible for metabolising reactive oxygen species (ROS) generated by mitochondrial respiration. To maintain the cellular redox equilibrium, glutathione disulfide (GSSG) is reduced back to GSH at the expense of NADPH, thereby forming a redox cycle.

The SAM depletion hypothesis considers the integrated processes that couple 1C metabolism to mitochondrial homeostasis beyond their shared reliance on oxidative state **(Figure 1.3).** Methionine directly contributes to tricarboxylic acid cycle (TCA) anaplerosis via the methylmalonyl pathway and indirectly governs mitochondrial metabolism by regulating the mechanistic target of rapamycin complex 1 (mTORC1). The mTOR signalling pathway is a focal regulator of proliferation, differentiation, metabolism and survival that is widely implicated in neurodevelopmental and neurodegenerative disease (Licausi and Hartman, 2018). Several well-studied genes implicated in syndromic ASD converge on disruptions to mTOR signalling, including tuberous sclerosis complexes (TSC1/2), neurofibromatosis (NF) and phosphatase and tensin homolog (PTEN) (Selamet and Usta,

2023). *In vivo* models have shown that disrupting mTOR signalling during neurodevelopment impairs synaptogenesis and synaptic pruning leading to cortical malformations, seizures, hyperactivity and differences in sensory processing, cognition and social interactions (Thomas *et al.,* 2023). Indeed, both preclinical and clinical studies demonstrate hyperactive mTOR signalling in ASD that can be targeted to mitigate ASD-associated behaviours (Winden, Ebrahimi-Fakhari and Sahin, 2018; Thomas *et al.,* 2023). Therefore, mTOR is proposed to be a convergent mechanism in idiopathic ASD that serves as a promising target for novel therapeutic strategies (Ganesan *et al.,* 2019; Sharma and Mehan, 2021). Notably, mTOR is a master regulator of mitochondrial metabolism that is broadly regulated by metabolic state (Szwed, Kim and Jacinto, 2021) and is directly modulated by methionine availability via the SAM Sensor Upstream of MTORC1/Gap Activity TOward Rags 1 (SAMTOR/ GATOR1) pathway (Gu *et al.,* 2017). Thus, SAM depletion and mTOR signalling are convergent signatures in ASD pathophysiology that function at the interface between metabolic and epigenetic state.

In fact, SAM coordinates diverse metabolic processes that are critical for mitochondrial homeostasis. As the obligatory methyl donor for methylation reactions, SAM modulates the activity of an array of mitochondrial enzymes that govern mitochondrial dynamics, structure and function - including Lipoyl synthase (LIAS), ubiquinone biosynthesis O-methyltransferases (COQ3 and COQ5) and Phosphatidylethanolamine N-methyltransferase (PEMT) (Dieckmann, 2024). LIAS facilitates the synthesis of lipoate which is a focal regulator of bioenergetic and redox homeostasis that has been shown to modulate mitochondrial biogenesis, integrity and dynamics (Dieter, Esselun and Eckert, 2022; Longhitano *et al.,* 2023; Yu *et al.,* 2023) while decreasing oxidative stress, inflammation and neurotoxicity (Lv *et al.,* 2022; Zhang *et al.,* 2022; Superti and Russo, 2024). Lipoate functions as a cofactor required by four mitochondrial dehydrogenase complexes involved in TCA metabolism and anaplerosis; namely, pyruvate dehydrogenase (PDH), α-ketoglutarate dehydrogenase (αKDH), branched-chain α-ketoacid dehydrogenase (BCKD) and 2-oxoadipate dehydrogenase (OADH) (Monné *et al.,* 2022). Together, these complexes facilitate the oxidation of acetyl CoA, branched-chain amino acids (BCAAs), lysine and tryptophan coupled to NAD+ cycling, which is an essential regulator of oxidative and metabolic state (Xie *et al.,* 2020). On the other hand, COQ produces the ubiquinone that forms part of the mitochondrial ETC (Monné *et al.,* 2022), while PEMT governs the balance between phosphatidylethanolamine and phosphatidylcholine in the mitochondrial membrane (Li *et al.,* 2023). Consequently, methionine supplementation has been shown to promote TCA cycle flux and mitochondrial respiration, improve mitochondrial membrane fluidity and attenuate oxidative and metabolic stress *in vitro* (Tripodi *et al.,* 2018; Catanesi *et al.,* 2021; Goicoechea *et al.,* 2024).

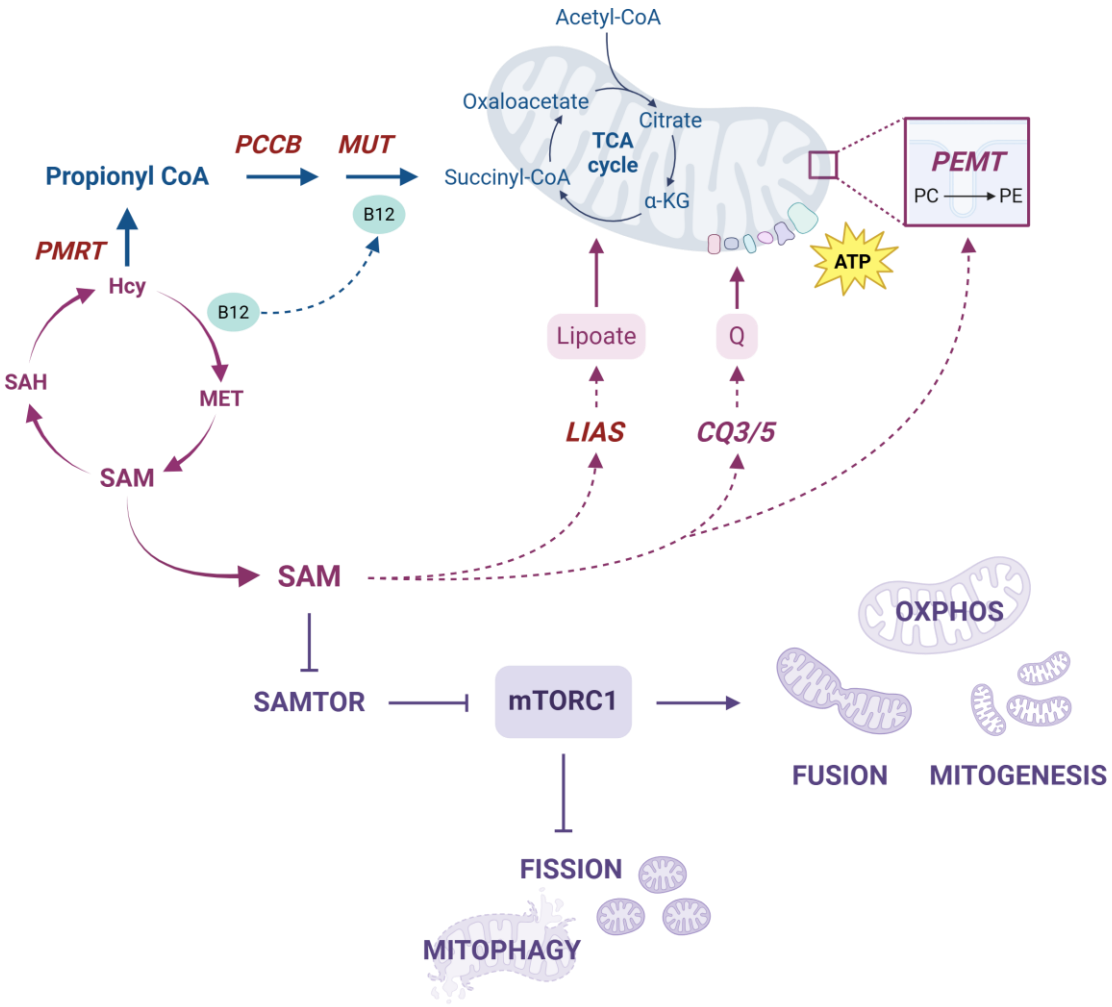


Figure 1.3. The SAM Depletion Hypothesis. The methionine cycle shapes mitochondrial structure, metabolism and function. Methionine is shunted into the TCA cycle via the methylmalonyl pathway (blue) or used to produce SAM in the methionine cycle (pink). SAM directly regulates mTORC1 (purple), a master metabolic regulator, via SAMTOR. SAM is also used as a cofactor for several mitochondrial enzymes required for mitostasis: Lipoyl synthase (LIAS), which synthesises TCA cycle dehydrogenases, ubiquinone biosynthesis O-methyltransferases (COQ3 and COQ5) which produce the ubiquinone in the ETC and Phosphatidylethanolamine N-methyltransferase (PEMT) which controls the composition of the mitochondrial membrane. Genes highlighted in red were differentially methylated in our ASD cohort. ETC – Electron Transport Chain; Hcy – homocysteine; MET – methionine; mTORC1 - Mechanistic Target Of Rapamycin Kinase; MUT – Methylmalonyl-CoA Mutase; SAH - S- adenosylhomocysteine; SAM - S-adenosylmethionine; TCA- Tricarboxylic Acid; PCCB – Propionyl CoA Carboxylase B; PRMT - Protein Arginine N-methyltransferase 1.

Together, the integrated pathways that drive OXPHOS and 1C metabolism reveal a mechanistic relationship between methylation capacity and mitochondrial function that bridges separate molecular signatures implicated in ASD. Interestingly, the methylmalonyl pathway was implicated across three of the nine significantly enriched canonical pathways in our SA ASD cohort, as well as several SAM-dependent processes involved in acyl metabolism, lipoate salvage and ETC function. Thus, a relationship between methionine cycling and mitochondrial metabolism may contribute to the metabolic phenotype observed in our ASD cohort. Notably, the biochemical signature that underpins this

relationship has significant implications for the regulation of neurodevelopment, physiology and function. Mitochondrial dysfunction is associated with impaired OXPHOS, reduced ATP synthesis and a consequent energy deficit, which has been well-described in the context of both metabolic disease and neuropathology. However, mitochondria are also implicated in diverse biological processes, ranging from Ca2+ buffering, redox balance and apoptosis to gene expression, hormone synthesis, immune signalling and neurotransmission (Picard, Wallace and Burelle, 2016). As the mitochondrial component of ASD aetiology has become increasingly recognised, mitochondria are also emerging as central regulators of neuronal development and function that shape diverse aspects of ASD physiology.

1.3. Mitochondrial Mechanisms in Neurodevelopment

During neurodevelopment, pluripotent neuronal stem cells (NSCs) differentiate into mature neurons and glial cells in response to tightly regulated spatiotemporal cues that shape neuronal architecture (Beckervordersandforth, 2017). Symmetric cell division facilitates NSC self-renewal, while asymmetric division gives rise to intermediate precursors (IPCs) that migrate to the outer layer of the ventricular zone before undergoing differentiation (Belmonte-Mateos and Pujades, 2022). During early embryogenesis, IPCs undergo neurogenesis to produce mature neurons, while mature glial cells are generated through gliogenesis during late pre-natal and early post-natal development (Sheloukhova and Watanabe, 2024). A tight balance between NSC quiescence, activation, proliferation, migration and differentiation governs neurophysiology and function from embryonic development to adulthood (Scandella *et al.,* 2023). Notably, neurodifferentiation is characterised by a distinct remodelling of mitochondrial metabolism and dynamics that functions as a fundamental regulator of stem cell fate (Maffezzini *et al.,* 2020; Brunetti *et al.,* 2021; Iwata and Vanderhaeghen, 2021; Landry and Huang, 2021; Coelho *et al.,* 2022; Ozgen *et al.,* 2022; Bonzano *et al.,* 2024; Garone, De Giorgio and Carli, 2024).

Metabolic state is shaped by interdependent processes that govern mitochondrial metabolism and dynamics. On the one hand, different profiles of substrate utilisation regulate the balance between anabolic and catabolic metabolism that modulates energy production and biosynthesis **(Figure 1.4).** Undifferentiated NSCs largely rely on aerobic glycolysis to produce the metabolic intermediates that drive rapid cell growth and proliferation (Maffezzini *et al.,* 2020). Glycolysis produces energy more quickly, but less efficiently than OXPHOS (Iwata and Vanderhaeghen, 2021); thus, NSCs also rely on fatty acid oxidation (FAO) to meet their energy demands (Sánchez-Ramírez *et al.,* 2024). On the other hand, post-mitotic differentiating neurons exhibit high rates of mitochondrial respiration to fuel the energy-demanding processes required for neurite outgrowth, axonal transport and synaptic signalling (Iwata and Vanderhaeghen, 2021). Concurrently, fatty acid metabolism shifts away from FAO towards *de novo* lipogenesis, to facilitate the synthesis of membrane lipids required for synaptogenesis, synaptic vesicle cycling and myelination (Maffezzini *et al.,* 2020).

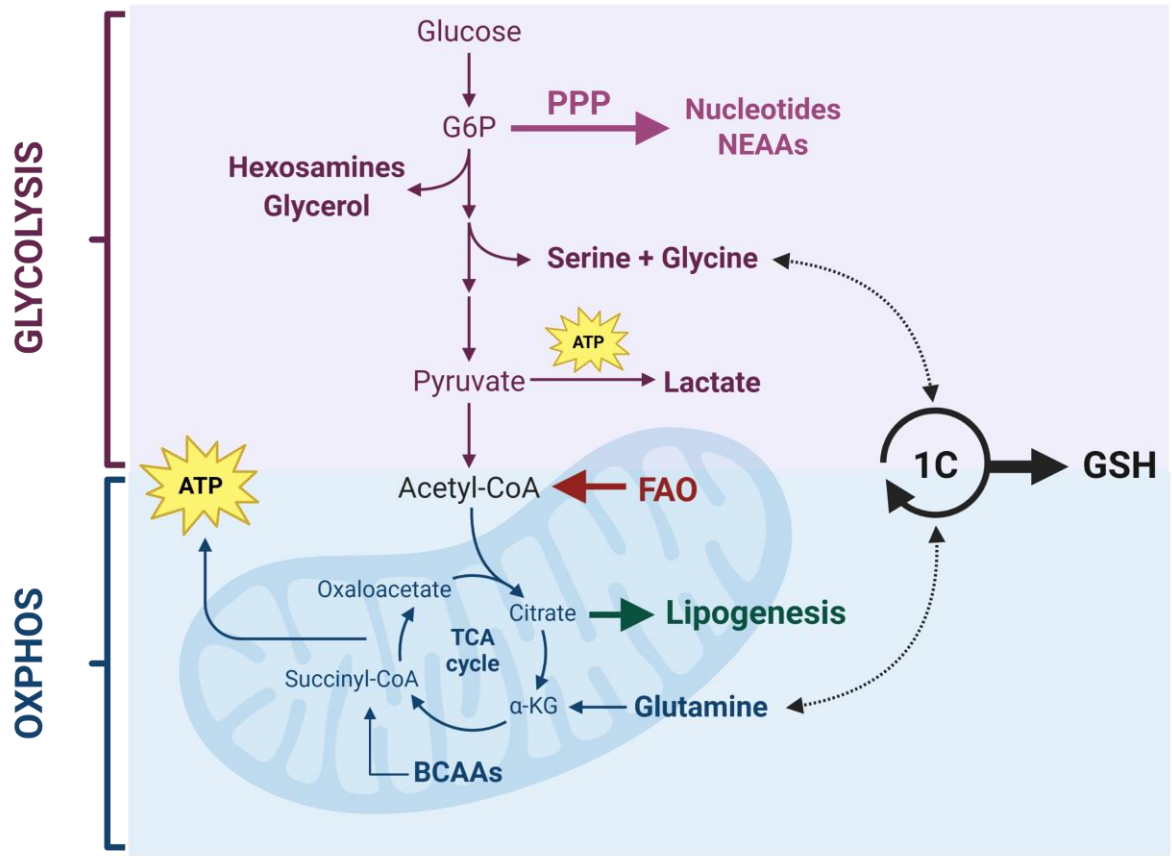


Figure 1.4. An Overview of Mitochondrial Metabolism. Glucose that is imported into the cytosol is metabolised by aerobic glycolysis (purple) to produce i) nucleotides or non-essential amino acids (NEAAs) in the pentose-phosphate pathway (PPP); ii) hexosamines and glycerol, used to synthesise glycoconjugates; iii) serine and glycine, used for one-carbon (1C) metabolism and glutathione (GSH) synthesis; or iv) proteins, collagen, bile salts, purines and porphyrins. The pyruvate derived from glycolysis can either be converted to lactate in a reaction that produces 8 ATP molecules per mol of glucose or imported into the mitochondria as acetyl CoA to fuel oxidative phosphorylation (OXPHOS) (blue). The reducing equivalents generated in the TCA cycle drive electron transport chain (ETC) activity, producing 32 ATP molecules per mol of glucose. In addition to glucose, lipids can provide acetyl CoA via fatty acid oxidation (FAO), while glutamine and branched chain amino acids (BCAAs) can be incorporated into the TCA cycle via glutaminolysis or the methylmalonyl pathway respectively. Citrate can be exported from the mitochondria to fuel lipogenesis while glutamate is incorporated into 1C metabolism as a substrate for GSH synthesis.

Current evidence suggests that metabolic remodelling during neurogenesis is driven by a marked downregulation of canonical glycolytic genes including the c-MYC proto-oncogene (c-MYC), hexokinase (HK2), lactate dehydrogenase (LDHA) and pyruvate kinase isoform 2 (PKM2) (Khacho and Slack, 2018). Simultaneously, an increase in mtDNA copy number, mitochondrial mass, mitochondrial membrane potential, mitochondrial gene expression and ETC activity is mediated by an upregulation of peroxisome proliferator-activated receptor gamma coactivator 1-alpha (PGC1α), estrogen-related receptor gamma (ERRγ) and mitochondrial transcription factor A (TFAM) which function as master transcriptional regulators of mitochondrial metabolism, biogenesis and redox homeostasis (Zheng *et al.,* 2016). Importantly, attenuating this metabolic shift by upregulating aerobic

glycolysis, inhibiting mitochondrial respiration or disrupting mitochondrial biogenesis, translation, dynamics or mtDNA integrity has been shown to significantly impede neuronal differentiation and survival (Zheng *et al.,* 2016; Arrázola *et al.,* 2018; Khacho and Slack, 2018; Baum and Gama, 2021).

Similarly, the remodelling of lipid metabolism plays a defining role in regulating cell fate transitions. Although the brain predominantly primarily relies on glucose as an energy source, fatty acids are critical for NSC maintenance, proliferation, migration and differentiation (Ito *et al.,* 2016; Iwata and Vanderhaeghen, 2021), while cholesterol, phospholipids and sphingolipids sustain neuronal integrity, plasticity and signalling (Sánchez-Ramírez *et al.,* 2024). Neuronal lipid homeostasis is maintained by PPARα and γ, which function as master regulators of fatty acid uptake, transport, storage and turnover (M. D'Angelo et al. 2018). During development, the balance between FAO and lipogenesis is determined by carnitine palmitoyltransferase 1 (CPT1α), which imports fatty acids into the mitochondrial matrix, and malonyl CoA, which functions as a substrate for lipogenesis and an endogenous inhibitor of FAO (Fadó, Rodríguez-Rodríguez and Casals, 2021). In NSCs, the high AMP: ATP ratio maintained by glycolysis inhibits lipogenesis via AMPK, which decreases intracellular malonyl CoA by inhibiting acetyl-CoA carboxylase (ACC) and activating malonyl-CoA decarboxylase (MCD) (Foster, 2012). As neurons differentiate, an increase in oxidative ATP production coincides with a decrease in CPT1α expression, leading to an increase in malonyl CoA synthesis and a decrease in mitochondrial fatty acid import (Knobloch *et al.,* 2017). Inhibiting FAO has been shown to attenuate NSC self-renewal (Ito *et al.,* 2016; Knobloch *et al.,* 2017), while genetically disrupting lipogenesis impairs neuronal differentiation, memory and cognition (Knobloch *et al.,* 2013; Di Giacomo *et al.,* 2017; Bowers *et al.,* 2020). Thus, the shift in glucose metabolism is intrinsically tied to the reprogramming of fatty acid utilisation during neurodevelopment, and both are essential to modulate NSC self-renewal and differentiation.

As mitochondrial respiration is upregulated to meet higher energy demands, an increase in the production of reactive oxygen species (ROS) necessitates a remodelling of mitochondrial dynamics to cope with metabolic and oxidative stress (Martorana *et al.,* 2018). Mitochondrial dynamics refers to the integrated processes that maintain mitochondrial homeostasis (or *mitostasis*) by modulating mitochondrial abundance, localisation, ultrastructure, interconnectivity and turnover **(Figure 1.5)** (Quintana-Cabrera and Scorrano, 2023). The molecular regulation of mitostasis is multidimensional and complex, with new facets still emerging in ongoing research. Still, the major players that govern mitochondrial integrity are well-characterised, with the current state of the field comprehensively reviewed elsewhere (Giacomello *et al.,* 2020; Iwata, Casimir and Vanderhaeghen, 2020; Cardanho-Ramos and Morais, 2021; Campos, Bozi and Ferreira, 2022; Choubey, Zeb and Kaasik, 2022; Coelho *et al.,* 2022; Chen, Zhao and Li, 2023; Quintana-Cabrera and Scorrano, 2023; Ul Fatima and Ananthanarayanan, 2023; Kondadi and Reichert, 2024; Lacombe and Scorrano, 2024; Wang *et al.,* 2024; Zimmermann *et al.,* 2024).

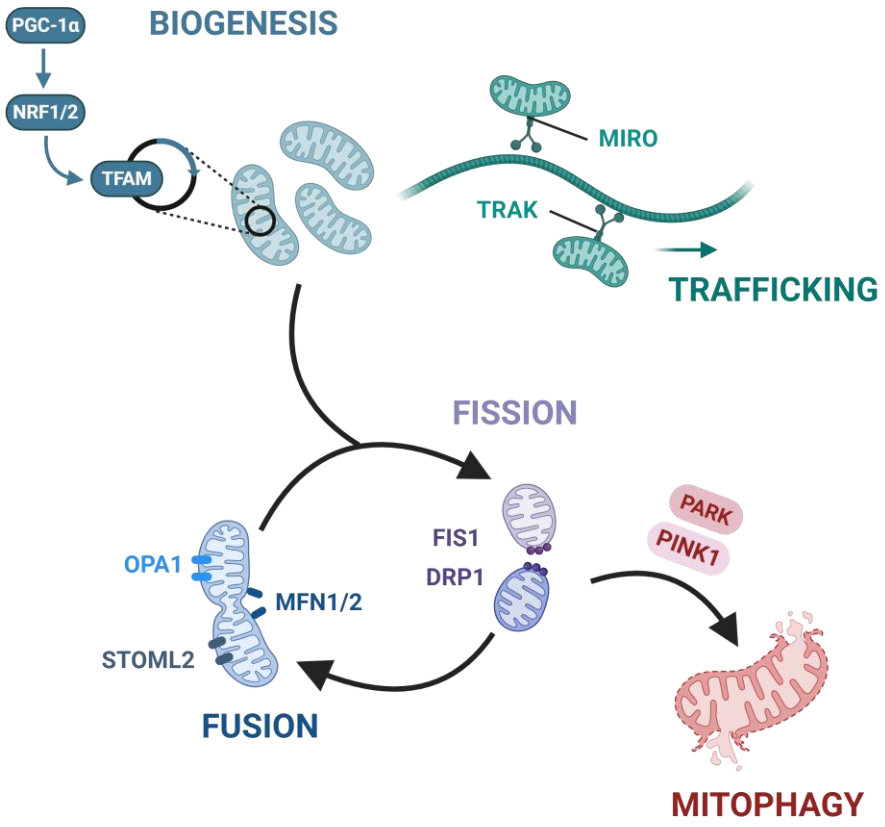


Figure 1.5. An Overview of Mitochondrial Dynamics. Mitochondrial biogenesis drives mitochondrial DNA replication and translation via peroxisome proliferator-activated receptor gamma coactivator 1-alpha (PGC1α), nuclear respiratory factors (NRF1/2) and mtDNA transcription factor A (TFAM). Mitochondrial fission and fusion maintain mitochondrial function and ultrastructure via the coordinated actions of mitofusin 1/2 (MFN1/2), optic atrophy protein 1 (OPA1), Stomatin-like protein 2 (STOML2), dynamin-related protein 1 (DRP1) and mitochondrial fission protein 1 (FIS1). Mitophagy degrades damaged mitochondria tagged by phosphatase and tensin homolog-induced kinase 1 (PINK1) and Parkin (PARK) while trafficking kinesin (TRAK) and mitochondrial rho (MIRO) adaptor proteins transport mitochondria along microtubules in the intracellular cytoskeleton.

Mitochondrial biogenesis (or *mitogenesis*) is governed by PGC1α, a master regulator of mitostasis, and nuclear factor erythroid-derived 2-like 2 (Nfe2l2), a redox-sensitive transcription factor that modulates oxidative state (Cherry and Piantadosi, 2015). Following transcriptional activation by PGC1α or Nfe2l2, nuclear respiratory factors (NRFs) facilitate mtDNA replication by upregulating the expression of mtDNA transcription factors (Chen *et al.,* 2022). Fusion and fission are orchestrated by canonical dynamin-related GTPases mitofusin 1/2 (MFN1/2), optic atrophy protein 1 (OPA1), dynamin-related protein 1 (DRP1) and mitochondrial fission protein 1 (FIS1) in cooperation with accessory proteins at the inner and outer mitochondrial membranes (Quintana-Cabrera and Scorrano, 2023). Mitochondrial ultrastructure is determined by the structure, complexity and density of the cristae (Pernas and Scorrano, 2016), governed by interactions between OPA1, Stomatin-like protein 2 (STOML2) and the mitochondrial contact site and cristae organising system (MICOS) complex at the inner mitochondrial membrane (Hu *et al.,* 2021; Kondadi and Reichert, 2024). Mitochondrial trafficking is facilitated by

microtubule-anchored kinesins and dynein motors linked to mitochondria via trafficking kinesin (TRAK) and mitochondrial rho (MIRO) adaptor proteins (Chen, Zhao and Li, 2023), while mitophagy is mediated by interactions between PTEN homolog-induced kinase 1 (PINK1), Parkin and autophagic machinery (Lacombe and Scorrano, 2024). Together, a tight balance between each branch of mitostasis is a prerequisite for neuronal metabolism, development and survival.

Mitochondrial dynamics are tightly coupled to stem cell fate, with separate roles played by mitochondrial biogenesis, fission, fusion and mitophagy during different phases of development (Khacho and Slack, 2018). As NSCs develop into mature neurons, they acquire a highly polarised morphology with functionally and physiologically distinct sub-cellular domains (Papageorgiou and Filiou, 2024). Thus, a remodelling of mitochondrial dynamics is crucial to meet local energy demands in growth cones, axonal branches, dendritic arbours and synaptic terminals (Goglia *et al.,* 2024). The transition from NSC self-renewal to differentiation is triggered by mitochondrial fission and clearance, which eliminates exhausted mitochondria, promotes mitochondrial motility and facilitates efficient mitochondrial turnover (Arrázola *et al.,* 2018). As a result, the mitochondrial network is redistributed across distal regions of neuronal axons, growth cones and synapses where local energy production and Ca^{2+} buffering are most critical (Goglia *et al.,* 2024). The sub-cellular localisation of mitochondria orchestrates neuronal polarisation and synaptogenesis by driving axon formation, axon branching and dendritic arborisation (Beckervordersandforth, 2017). At the same time, an increase in local biogenesis, fission and fusion enables rapid changes to mitochondrial capacity in response to dynamic developmental conditions (Han *et al.,* 2021).

When neurons become terminally differentiated, these dynamic mitochondrial pools are replaced by organised mitochondrial networks with complex, interconnected branches (Alberti *et al.,* 2022). Stable mitochondrial populations are established at synaptic terminals and mitochondrial ultrastructure matures, with well-defined, complex cristae that enhance metabolic capacity by increasing the surface area available for ETC activity and facilitating the formation of respiratory super-complexes and intracistal compartments in the mitochondrial matrix (Baum and Gama, 2021). Importantly, this shift in mitochondrial dynamics is intrinsically linked to metabolic state (Wai and Langer, 2016; Zimmermann *et al.,* 2024) and disrupting mitochondrial remodelling has profound implications for neuronal metabolism and differentiation. Knockdown studies have shown that promoting fusion in NSCs leads to self-renewal, while inducing fission triggers differentiation (Khacho and Slack, 2018). On the other hand, inhibiting fusion, fission or mitophagy impairs neurite outgrowth, axon branching, synaptic vesicle cycling and neurotransmission (Vantaggiato *et al.,* 2019; Baum and Gama, 2021). Thus, current evidence suggests a synergistic reprogramming of glucose and lipid metabolism underpinned by a remodelling of mitochondrial dynamics that drives neuronal maturation **(Figure 1.6).**

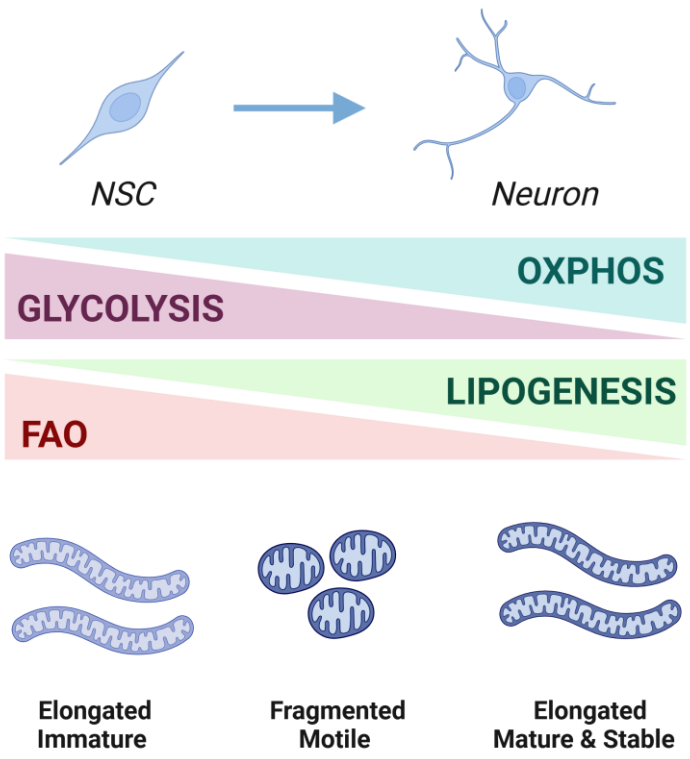


Figure 1.6. The Metabolic Shift: Mitochondrial Remodelling During Neurogenesis. Neurodifferentiation is driven by a remodelling of mitochondrial metabolism and dynamics. As neurons mature, glucose metabolism shifts from glycolysis to oxidative phosphorylation (OXPHOS), while lipid metabolism switches from fatty acid oxidation (FAO) towards lipogenesis. Neuronal commitment is marked by increased mitochondrial fragmentation, motility and turnover as high rates of mitochondrial fission, trafficking, mitophagy and biogenesis facilitate rapid mitochondrial remodelling across nascent synapses. Upon terminal differentiation, mitochondrial pools stabilise, and mitochondrial ultrastructure matures, while fusion drives the formation of elongated and interconnected mitochondrial networks.

The relationship between neuronal metabolism and differentiation is multifaceted, involving mitochondria-to-nucleus retrograde signalling and biochemical crosstalk between the canonical pathways that govern development and mitostasis. Section **1.2** highlighted that mitochondrial metabolism influences epigenetic state, while Sánchez-Ramírez *et al.,* (2024) recently described the tight coupling between metabolic and epigenetic remodelling that drives neurogenesis **(Figure 1.7)**. Oxidative respiration supplies acetyl CoA to histone acetyltransferases (HATs) that activate neuron-specific genes, while the NAD^+ required for OXPHOS, glycolysis and FAO also drives the activity of Sirtuin (SIRT) histone deacetylase (HDACs). The acyl CoA/CoA and NAD^+/NADH ratios that are broadly modulated by metabolic state shape the histone acetylation profiles that determine NSC fate. Likewise, the intracellular pools of αKG, succinate and fumarate modulate DNAm patterns by regulating Jumonji-C domain-containing (JMJC) histone demethylases and Tet DNA demethylases (Garone, De Giorgio and Carli, 2024). Notably, both preclinical and epidemiological studies have shown that DNAm is altered by disruptions to 1C metabolism during development (Lin *et al.,* 2014; Yu *et al.,* 2014; Kühnen *et al.,* 2016; Rabaneda *et al.,* 2016; Fawal *et al.,* 2018; Wang *et al.,* 2022), while SAM, SAH and methionine levels influence NSC fate by remodelling DNAm *in vitro* (Shyh-Chang *et al.,* 2013; Shiraki *et al.,* 2014; Sperber *et al.,* 2015; Desai *et al.,* 2019). Thus, the redox/methylation hypothesis in ASD has important implications for the relationship between epigenetic and metabolic state during neurodevelopment.

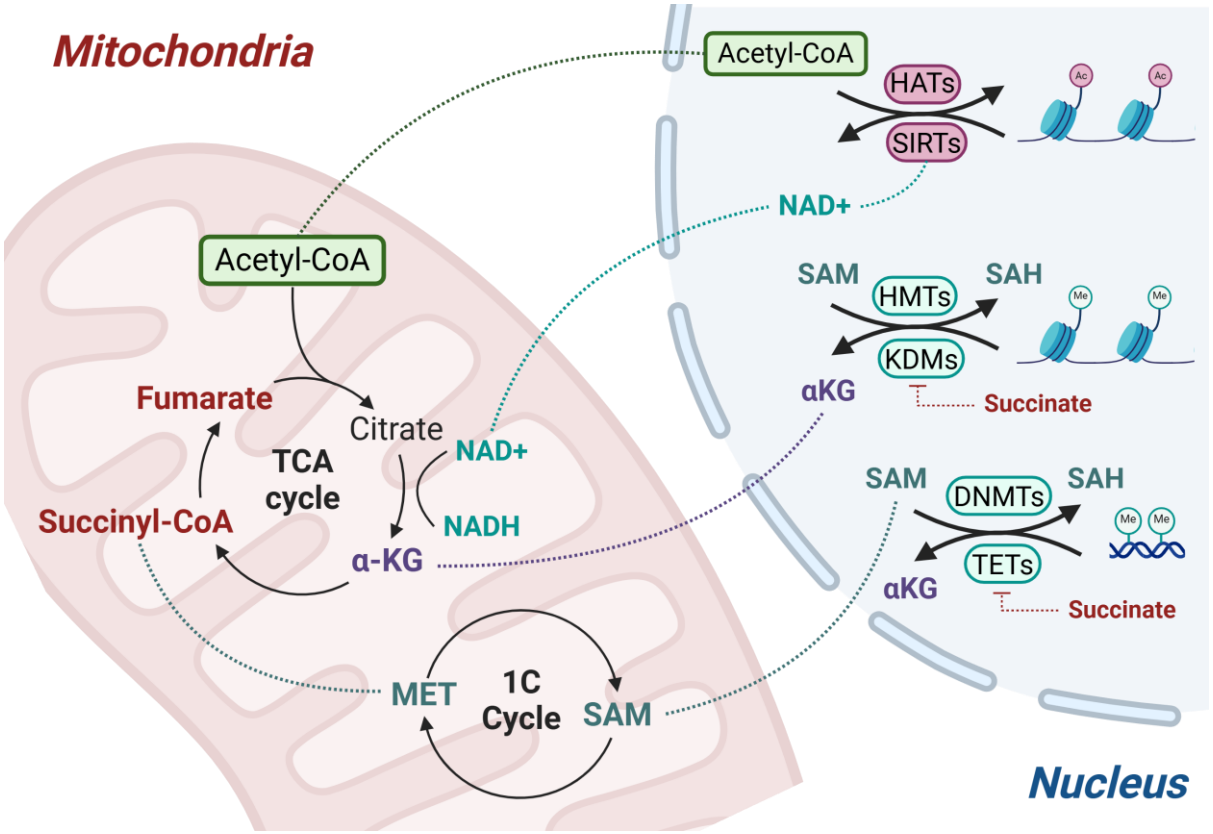


Figure 1.7. The Relationship Between Metabolic and Epigenetic Remodelling (inspired by Matilainen, Quirós and Auwerx, 2017)**.** The acetyl CoA that fuels the TCA cycle is used as a cofactor for histone acetyltransferases (HATs), while sirtuin histone deacetylases rely on the nicotinamide adenine dinucleotide (NAD^+) derived from oxidative phosphorylation. Alpha-ketoglutarate (αKG) removes DNA methylation marks by activating Ten–eleven translocation (TET) demethylases while succinate and fumarate competitively inhibit TETs and Histone lysine demethylases (KDMs). Lastly, the S-Adenosyl methionine (SAM) produced in one carbon metabolism is a cofactor for histone and DNA methyltransferases.

As well as directly regulating the expression of neurogenic genes via epigenetic remodelling, mitochondria also modulate the upstream signalling cascades that shape the neurogenic transcriptome. The Wnt and Notch pathways are the two major pathways involved in cell fate determination that function synergistically to modulate neuronal differentiation and patterning (Bejoy *et al.,* 2020). Notch signalling is mediated by interactions between cognate transmembrane receptors on neighbouring cells, triggering the cleavage and nuclear translocation of the Notch intracellular domain (NICD) to promote the expression of bHLH transcription factors that maintain pluripotency (Lampada and Taylor, 2023). Canonical WNT/β-catenin signalling is activated by secreted glycoprotein ligands that bind to transmembrane Frizzled (FZD) receptors, leading to the inhibition of the Glycogen synthase kinase-3 beta (GSK3β) complex which allows for the β-catenin-dependent activation of Wnt target genes involved in NSC proliferation and lineage commitment (Liu *et al.,* 2022). On the other hand, non-canonical Wnt signalling is mediated via the Jun N-terminal kinase (JNK), Rho-associated kinase (ROCK), phospholipase C (PLC), phosphoinositide-3 kinase (PI3K) and protein kinase C (PKC)

cascades that modulate cytoskeletal remodelling, synaptogenesis and survival (Bengoa-Vergniory and Kypta, 2015; Konopelski Snavely *et al.,* 2023). Both the Notch and Wnt pathways interact with the mTOR cascade that regulates cell growth, pluripotency and morphogenesis in concert with TGF-β, Hedgehog (Shh) and Hippo signalling, forming an integrated regulatory network that shapes neuronal identity, morphology and function (Hurlbut *et al.,* 2007; Boksha *et al.,* 2021).

Increasing evidence suggests that these pathways are sensitive to biochemical markers of metabolic and oxidative state and directly influence the transcriptional mechanisms that govern mitostasis. Firstly, the interplay between mitochondrial dynamics and Notch signalling plays an instrumental role in neuronal lineage commitment. In undifferentiated stem cells, Notch signalling promotes glycolytic metabolism through interactions with forkhead box protein O1 (FOXO1), which regulates the expression of rate-limiting enzymes in canonical glycolysis (Hwang, Tang and Paik, 2021). Concurrently, canonical Notch signalling inhibits the expression of both PPARγ and PGC1α, decreases mitochondrial content and reduces ETC activity (Bi and Kuang, 2015; Huang *et al.,* 2023; Tien *et al.,* 2023) while limiting mitochondrial ROS and maintaining mitochondrial integrity via interactions with PINK1 and Bcl-2 Associated X-protein (BAX) (Kasahara and Scorrano, 2014). The mitochondrial fragmentation that triggers neuronal differentiation is accompanied by an upregulation of mitochondrial-derived ROS, which inhibits Notch signalling via Nfe2l2 (Khacho *et al.,* 2016). Here, oxidative stress triggers the nuclear translocation of Nfe2l2, which upregulates the transcription of the Notch inhibitor Botch (Khacho and Slack, 2018). At the same time, the enhanced ETC activity increases the NAD^+/ NADH ratio, culminating in the activation of SIRT1, which represses canonical Notch signalling as part of a polycomb repressive complex (Yu *et al.,* 2024). Targeted disruptions to mitochondrial dynamics have been shown to modulate the Notch pathway via Ca^{2+} / calcineurin signalling (Kasahara and Scorrano, 2014), while several studies have demonstrated changes to Notch signalling in response to specific metabolic substrates, mtDNA mutations and ETC inhibitors (Wakabayashi *et al.,* 2014; Rodrigues *et al.,* 2020; Winanto *et al.,* 2020; Tay, Chia and Ong, 2021). Together, this illustrates a tight coupling between Notch signalling and metabolic remodelling that governs stem cell fate.

Likewise, an interdependent relationship between Wnt signalling and metabolic state is critical to regulate NSC metabolism, proliferation and differentiation. Canonical Wnt signalling promotes glycolysis by upregulating c-MYC, LDHA, monocarboxylate lactate transporter 1 (MCT-1), hypoxia-inducible factor-1α (HIF-1α) and pyruvate dehydrogenase kinase (PDK), shunting pyruvate towards lactate production rather than OXPHOS (Vallée, Lecarpentier and Vallée, 2021). At the same time, an antagonistic relationship between Wnt/β-catenin and PPARγ governs glycolysis, OXPHOS, mitochondrial biogenesis, lipid metabolism and redox homeostasis (Corona and Duchen, 2016). Indeed, Wnt signalling has been shown to modulate at least 150 genes involved in mitochondrial function (Garone, De Giorgio and Carli, 2024). Both Wnt/β-catenin and Wnt/ Ca^{2+} signalling regulate mitochondrial biogenesis, dynamics and morphology (Arrázola, Silva-Alvarez and Inestrosa, 2015;

Singh *et al.,* 2018; Mishra *et al.,* 2019); and conversely, disruptions to mitochondrial metabolism, dynamics and redox homeostasis have been shown to alter Wnt signalling *in vitro* (Bernkopf and Behrens, 2018; Zhang *et al.,* 2019, 2022; Delgado-Deida, Alula and Theiss, 2020; Cui *et al.,* 2021).

Impairments to mitochondrial ATP production can promote Wnt/ β-catenin signalling via the AMPK-dependent phosphorylation of β-catenin (Zhang *et al.,* 2019); however, mitochondrial dysfunction can also inhibit Wnt signalling by inducing endoplasmic reticulum (ER) stress (Garone, De Giorgio and Carli, 2024). Mitochondrial-derived ROS has been shown to activate Wnt signalling via interactions with the Dishevelled and Nucleoredoxin complex (Delgado-Deida, Alula and Theiss, 2020) while mitochondrial dynamics modulates β-catenin degradation via the Ca^{2+} / calmodulin-dependent protein kinase II (CaMKII) cascade (Bernkopf and Behrens, 2018; Cui *et al.,* 2021). The coupling between Wnt/β-catenin and mitostasis has been demonstrated in several preclinical models using targeted gene knockdowns, ETC inhibitors or mitochondrial transplantation (Bernkopf and Behrens, 2018; Singh *et al.,* 2018; Zhang *et al.,* 2019, 2022) and this relationship has been found to play an integral role in determining NSC fate (Rharass *et al.,* 2014).

Lastly, increasing evidence demonstrates a reciprocal interplay between Wnt and mTOR signalling that orchestrates metabolic reprogramming during differentiation (Garone, De Giorgio and Carli, 2024). On the one hand, GSK3β cooperates with AMPK to inhibit mTORC1 by phosphorylating TSC2 in response to energetic stress; however, GSK3β has also been shown to promote mTOR signalling by targeting p70S6 kinase (S6K1), eukaryotic translation initiation factor 4E binding protein 1 (4E-BP1) and the regulatory-associated protein of mTOR (RAPTOR) (Papadopoli, Pollak and Topisirovic, 2021). On the other hand, the PI3K/AKT cascade that activates mTORC1 also inhibits GSK3β, while mTOR directly impedes GSK3β-dependent transcription by preventing its nuclear translocation (Bautista *et al.,* 2018). Notably, section **1.2.** introduced the mTOR pathway as a master metabolic regulator that is centrally implicated in ASD aetiology. During neurogenesis, the PI3K/AKT cascade plays a fundamental role in driving the mitochondrial metabolic shift by activating mTOR and upregulating cAMP response element binding protein (CREB), which increases the expression of PGC1α to promote mitochondrial biogenesis and function (Agostini *et al.,* 2016; Beckervordersandforth, 2017). Conversely, mTOR signalling is regulated by AMPK, cAMP, αKG and acetyl CoA, and is thus tightly coupled to metabolic state (Szwed, Kim and Jacinto, 2021). Critically, interactions between Wnt and mTOR signalling have been shown to drive cortical neurogenesis *in vitro* (López-Tobón *et al.,* 2019) while Wnt/mTOR crosstalk is linked to the behavioural, neurophysiological and cognitive disruptions observed in ASD murine models (Qin, Dai and Yin, 2016). Thus, Wnt and mTOR signalling function as synergistic regulators of metabolism and development that connect the mitochondrial and neurological components of ASD aetiology.

Notably, cumulative genetic and preclinical data demonstrates a consistent role for Wnt signalling in ASD (Caracci, Avila and De Ferrari, 2016; Kwan, Unda and Singh, 2016; Mulligan and Cheyette, 2016; Bae and Hong, 2018; Iakoucheva, Muotri and Sebat, 2019; Vallée, Vallée and Lecarpentier, 2019; Caracci *et al.,* 2021; Elgamal *et al.,* 2023). In fact, a recent systematic review highlights a relationship between Wnt signalling, glycolysis, and oxidative stress in ASD murine models (Bou Najm, Alame and Takash Chamoun, 2024). Likewise, preclinical models for ASD consistently report hallmarks of constitutive Notch signalling which can be targeted to mitigate ASD-associated behaviours (Li *et al.,* 2023; Zhang, Wang, Li, Deng and Shen, 2023; Zhang, Wang, Li, Deng, He, *et al.,* 2023; Deng *et al.,* 2024). Thus, Wnt, Notch and mTOR signalling serve as convergent mechanisms involved in neuronal metabolism and maturation with direct relevance for ASD aetiology.

Together, this discussion illustrates a central role for mitochondria in the regulation of neuronal differentiation through interactions with neurogenic signalling pathways that are separately implicated in ASD neurology. Considering the cumulative evidence for mitochondrial dysfunction in ASD, disruptions to metabolic reprogramming that interfere with neuronal maturation may contribute to the neurodevelopmental and neurophysiological hallmarks of ASD that alter cognition and behaviour. This is the mechanistic hypothesis that has shaped this thesis and its primary objectives. However, the relevance of mitochondrial function to ASD aetiology extends far beyond the context of embryonic neurogenesis. In fact, mitochondria continuously shape the interactions within and between heterogenous cell populations in the brain that regulate neuronal plasticity, neurophysiology and behaviour throughout post-natal development and adulthood.

1.4. Beyond Neurogenesis: The Metabolic Nexus of ASD Neurology

Neuronal differentiation is just one aspect of neurodevelopment that is modulated by interactions between diverse cell types in the developing brain. Glial cells are non-excitable cells in the CNS that are critical for neuronal metabolism, structure, plasticity and function with diverse roles in immunoregulation, neuroprotection, blood-brain barrier formation, redox homeostasis and neurotransmission (Sheloukhova and Watanabe, 2024). Glial cells comprise both macroglia (astrocytes and oligodendrocytes derived from NSCs during late embryogenesis) and microglia (the resident immune cells in the CNS derived from macrophage progenitors in the yolk sac) (Revuelta *et al.,* 2020; Pérez-Rodríguez, Blanco-Luquin and Mendioroz, 2021). Glial phenotypes are dynamic, shift in response to different stimuli and can be either neurotoxic or neuroprotective (Afridi *et al.,* 2020). Gliosis describes a pathogenic consequence of impaired glial homeostasis, marked by an over-proliferation of reactive glia and chronic neuroinflammation (Sofroniew, 2020). Markedly, gliosis has been described as a universal hallmark of neuropathology (Verkhratsky, Rodríguez and Parpura, 2013) that is widely documented in both mitochondrial disease (Lake *et al.,* 2015; Sherry, Lee and Choi, 2015; McAvoy and

Kawamata, 2019; Hanaford and Johnson, 2022; Aguilar *et al.,* 2024) and ASD (Petrelli, Pucci and Bezzi, 2016; Gładysz, Krzywdzińska and Hozyasz, 2018; Mekori-Domachevsky, Segal-Gavish and Gross, 2019; Liao, Liu, *et al.,* 2020; Liao, Yang, *et al.,* 2020; Revuelta *et al.,* 2020; Savino *et al.,* 2020; Usui, Kobayashi and Shimada, 2023). Indeed, post-mortem studies have demonstrated an upregulation of microglial-specific genes (Edmonson, Ziats and Rennert, 2014), increased microglial density (Morgan *et al.,* 2010; Tetreault *et al.,* 2012), excessive microglial activation (Vargas *et al.,* 2005; Suzuki *et al.,* 2013) and disruptions to microglial morphology and organisation in ASD brain tissue (Liao, Yang, *et al.,* 2020; Fetit *et al.,* 2021) while innate immune activation is a well-established component of ASD aetiology (Hughes, Moreno and Ashwood, 2023; Aytulun and Ünal, 2024; Vacharasin *et al.,* 2024).

Notably, distinct metabolic signatures underpin the dynamic glial phenotypes that shape neuronal circuitry (Afridi *et al.,* 2020). Microglia are the only glial cells present in the early embryonic brain (Schafer *et al.,* 2012) that are continuously remodelled during neurodevelopment to regulate NSC self-renewal, migration and differentiation, synaptogenesis and synaptic pruning (Savino *et al.,* 2020; Pérez-Rodríguez, Blanco-Luquin and Mendioroz, 2021). This necessitates a careful balance between the resting and reactive microglial phenotypes which is primarily governed by the classical complement system (Magdalon *et al.,* 2020). However, mitochondrial metabolism also modulates microglial activation via both extrinsic and intrinsic mechanisms **(Figure 1.8).** Mitochondrial dysfunction in surrounding brain tissue leads to the release of damage-associated molecular patterns (DAMPs) that bind to microglial receptors and induce pro-inflammatory signalling (Castora, 2019). Conversely, microglial activation is intrinsically coupled to metabolic reprogramming (Lauro and Limatola, 2020).

Resting microglia rely primarily on OXPHOS, while the shift toward the inflammatory M1 phenotype is driven by a decrease in mitochondrial respiration and an upregulation of glycolysis (Harry *et al.,* 2020). Concurrently, microglial activation is marked by a switch from FAO to fatty acid synthesis (FAS) that remodels TCA cycle flux and ETC activity (Loving and Bruce, 2020). In fact, recent work has demonstrated that mitochondrial metabolism directly regulates microglial activation while mitochondrial dysfunction has profound implications for microglial inflammatory state (Bernier, York and MacVicar, 2020; Fairley, Wong and Barron, 2021). *In vitro* studies have shown that microglial activation is induced by ETC inhibition and mitochondrial fragmentation, while this response could be mitigated by targeting mitochondrial fission, membrane potential, or ROS (Park *et al.,* 2013; Ye *et al.,* 2016; Lauro and Limatola, 2020; Mora-Romero *et al.,* 2024). At the same time, mitochondrial dysfunction inhibits the transition to the anti-inflammatory M2 phenotype, exacerbating neuroinflammation and oxidative stress (Ferger *et al.,* 2010; Tang and Le, 2016). Conversely, different cytokine stimuli are known to alter microglial metabolic state. Inflammatory stimuli were found to induce a metabolic switch from OXPHOS to glycolysis in microglia *in vitro*, marked by increased lactate production and decreased mitochondrial activity, oxygen consumption and ATP production (Voloboueva *et al.,* 2013; Gimeno-Bayón *et al.,* 2014; Lively and Schlichter, 2018). This metabolic shift

correlates with increased production of proinflammatory cytokines and nitric oxide (Freemerman *et al.,* 2014; Lively and Schlichter, 2018), demonstrating a proinflammatory feedback loop driven by metabolic reprogramming.

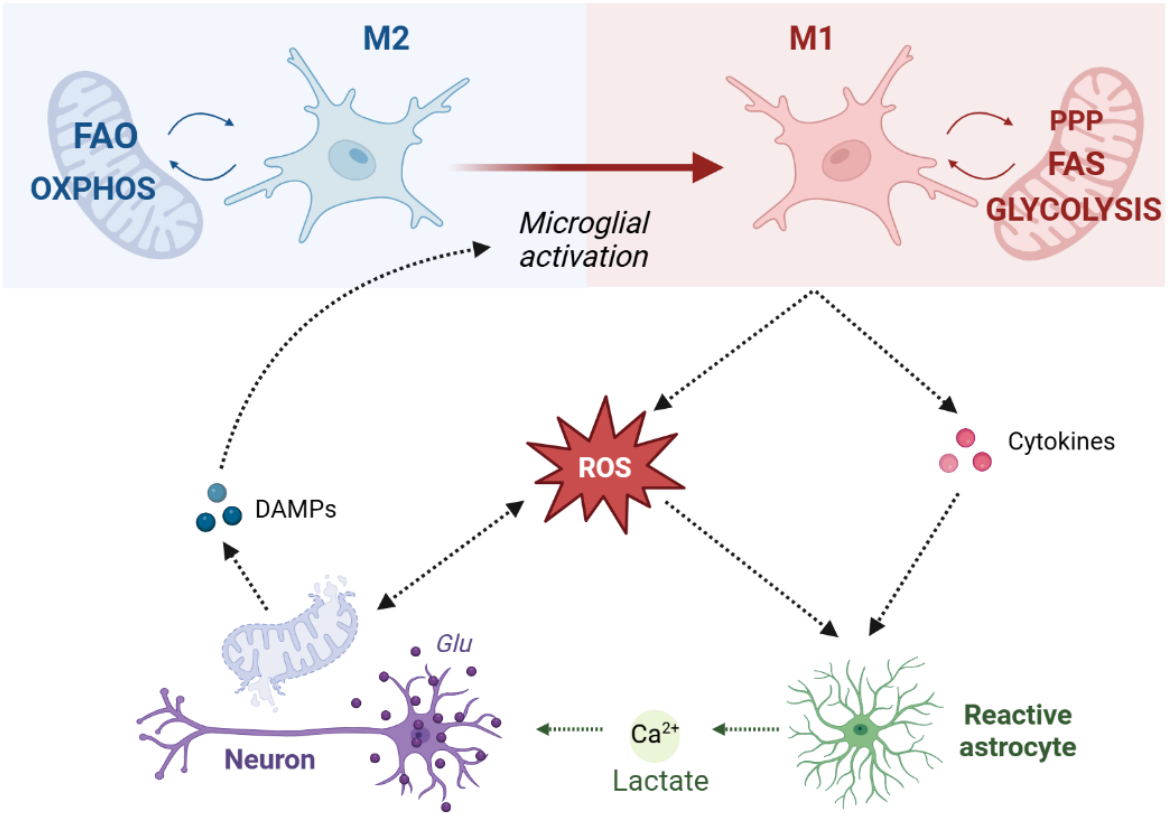


Figure 1.8. The Mitochondrial Modulation of Neuroimmune State (Taken and adapted from Mahony and O'Ryan, (2022)). Neuroimmune homeostasis is maintained by a tightly regulated interplay between dynamic glial phenotypes. Microglial activation toward a pro-inflammatory state is driven by intrinsic metabolic reprogramming away from oxidative phosphorylation (OXPHOS) and fatty acid oxidation (FAO) toward glycolysis, fatty acid synthesis (FAS) and the pentose phosphate pathway (PPP). Conversely, microglial metabolic profile directly influences inflammatory state. Activated microglia release pro-inflammatory cytokines and ROS, which in turn activates neighbouring astrocytes and induces mitochondrial dysfunction in neurons. Reactive astrocytes release lactate and Ca^{2+}, which upregulates glutamatergic neurotransmission and culminates in an excitotoxic loop that drives further inflammation and oxidative stress. Damaged mitochondria in neurons induce the release of damage-associated molecular patterns (DAMPs), upregulating pro-inflammatory signalling in microglia.

The reciprocal relationship between microglial metabolism and activation has significant consequences for NSC fate. Both metabolic (Fasano *et al.,* 2009; Liu *et al.,* 2009; Chatoo *et al.,* 2010; Wang *et al.,* 2013) and oxidative (Hou *et al.,* 2012; Huang, Zou and Corniola, 2012; Prozorovski *et al.,* 2015) stress have been found to promote gliogenesis at the expense of neurogenesis *in vitro*. Likewise, pathological microglial activation has been shown to enhance NSC proliferation and gliogenesis while inhibiting neuronal differentiation and survival (Sato, 2015; Zhang, Zhang and You, 2018; Araki, Ikegaya and Koyama, 2021; Pérez-Rodríguez, Blanco-Luquin and Mendioroz, 2021). By shifting NSC fate towards

gliogenesis and inducing microglial activation, mitochondrial dysfunction could significantly influence the composition, connectivity and plasticity of neural networks. Indeed, disruptions to microglial metabolism lead to synaptic pruning deficits, excitotoxicity and neurodegeneration with implications for neurophysiology, cognition and behaviour (Araki, Ikegaya and Koyama, 2021; Yang *et al.,* 2021; Cantando *et al.,* 2024). Notably, aberrant microglial activation is thought to contribute to the increased dendritic spine density, cortical hyperconnectivity, excitation/inhibition (E/I) imbalance and resultant behavioural phenotypes in ASD (Cowan, Petri and Jr., 2018; Zengeler and Lukens, 2021; Luo and Wang, 2024). Moreover, both clinical and preclinical studies have revealed a role for mTOR (Johnson *et al.,* 2013; Wen *et al.,* 2013; Sarn *et al.,* 2020; Cantando *et al.,* 2024) and Wnt (Scuderi *et al.,* 2014; Xu *et al.,* 2015; Lee *et al.,* 2019) signalling in the relationship between mitochondrial dysfunction and astrogliosis, which emphasises the convergence between the metabolic and neuroimmune mechanisms that govern neurogenesis in ASD.

Beyond embryogenesis, interactions between mitochondria, microglia and macroglia continuously modulate neuronal activity, structure and function. Astrocytes and oligodendrocytes provide neurons with trophic, metabolic and structural support that is essential for neuronal viability, and these functions are closely coupled to glial metabolism (Sheloukhova and Watanabe, 2024). Unlike resting microglia, astrocytes and oligodendrocytes rely primarily on glycolysis, and both provide axons with glycolytic intermediates to support neuronal energy production (Mayorga-Weber, Rivera and Castro, 2022). Astrocytes are immensely energetic cells marked by high rates of glucose consumption, glycolytic and mitochondrial respiration, and an enhanced resistance to oxidative stress that allows them to effectively metabolise fatty acids (Maly, Morales and Pletnikov, 2021). Oligodendrocytes exhibit a comparatively greater degree of oxidative reliance to sustain the energy-demanding process of myelin synthesis but lack the antioxidant capacity of astrocytes, which limits their capacity for FAO (Meyer and Rinholm, 2021). As a result, both neurons and oligodendrocytes rely on substrates derived from astrocytic metabolism through neuron-glia metabolic coupling **(Figure 1.9).**

Neurons rely on glial glycolysis for metabolic intermediates, antioxidant enzymes and neurotransmitter precursors – including lactate, alanine, glutathione, glycine and serine (Afridi *et al.,* 2020). Moreover, astrocytic fatty acid metabolism functions as an essential buffer against nutrient depletion or lactic acidosis and provides substrates for the lipids that comprise neuronal membranes and synaptic vesicles (Barber and Raben, 2019). As neuronal energy supplies are depleted with chronic stimulation, peroxidated fatty acids are shuttled from neurons to astrocytes, where they are either stored as lipid droplets or oxidised to produce acetyl CoA, NADH, FADH or ketones to fuel neuronal respiration (Rose *et al.,* 2017). Concurrently, redox homeostasis is maintained by a reciprocal relationship between neuronal oxidative state and astrocytic glutathione synthesis. Oxidative stress upregulates astrocytic glycolysis to increase the supply of cysteine, glutamate and y-glutamatylcysteine for GSH biosynthesis in neighbouring neurons (Vicente-Gutierrez *et al.,* 2019). Meanwhile, mitochondrial respiration in

astrocytes is reduced as glutamate is shunted away from TCA anaplerosis towards GSH synthesis. As such, astrocyte metabolism is tightly coupled to neuronal activity. Glutamatergic signalling promotes glycolysis via the induction of Ca^{2+} signalling cascades in astrocytes, while glial-derived lactate potentiates glutamatergic signalling in neurons in a process called gliotransmission (Mosienko, Teschemacher and Kasparov, 2015). Although glial cells lack excitable membranes, astrocytes can excite neurons by releasing gliotransmitters like lactate, ATP, glutamate or D-serine in response to intracellular ionic signals, and this process is modulated by metabolic state (Calì *et al.,* 2024). Thus, an interplay between metabolism, glutamate signalling and gliotransmission shapes the coordinated functions of neurons and astrocytes that maintain energy homeostasis in the brain.

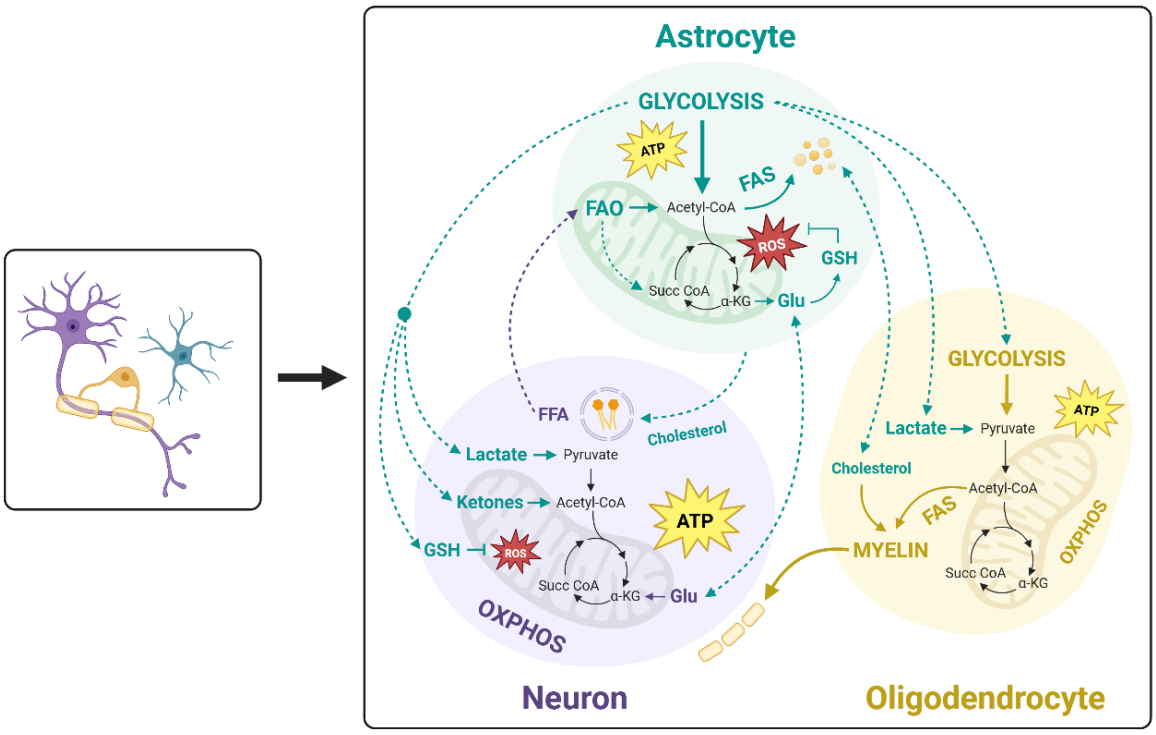


Figure 1.9. Neuron-Glia Metabolic Coupling. Astrocytes are highly glycolytic cells with an enhanced resistance to reactive oxygen species (ROS) that allows for efficient fatty acid oxidation (FAO). Astrocytic glycolysis supplies both neurons and oligodendrocytes with metabolic intermediates to fuel oxidative phosphorylation (OXPHOS) and antioxidants such as glutathione (GSH) and its precursors (serine and glycine) to mitigate oxidative stress. Fatty acid precursors exported from astrocytes facilitate the synthesis of neuronal membranes and synaptic vesicles as well as the myelin in oligodendrocytes that maintains neuronal integrity. Free fatty acids in neurons are shuttled back to astrocytes where they are stored in lipid droplets (LDs) or oxidised to fuel mitochondrial respiration.

Likewise, metabolic coupling between astrocytes, oligodendrocytes and microglia is essential for neuronal integrity and survival. Oligodendrocytes rely on astrocytes to supply lactate and creatine for energy during active myelination, as well as the cholesterol that comprises 70% of the myelin sheath (Meyer and Rinholm, 2021). Cholesterol synthesised in astrocytes is also essential for microglial survival and phagocytotic activity (Loving and Bruce, 2020). Conversely, the metabolic reprogramming

that underpins microglial activation facilitates myelin degradation and turnover, while both astrocytes and microglia play an essential role in cholesterol clearance and recycling (Chausse, Kakimoto and Kann, 2021). Consequently, mitochondrial function is essential to modulate myelin synthesis, turnover and degradation. Metabolic stress not only impedes the myelinating capacity of oligodendrocytes but also promotes the glycolytic shift that drives microglial activation and phagocytosis. As such, mitochondrial dysfunction is linked to demyelination, which is widely observed in neurodegeneration and neuropathology (Campbell, Licht-Mayer and Mahad, 2019). In fact, aberrant myelination is a hallmark of ASD neurophysiology that is thought to contribute to the associated disruptions to neural connectivity, synaptic plasticity and signalling (Graciarena *et al.,* 2019; Khanbabaei *et al.,* 2019; Lee *et al.,* 2019; Galvez-Contreras *et al.,* 2020; Chen *et al.,* 2022; Khelfaoui, Ibaceta-Gonzalez and Angulo, 2024).

This discussion illustrates how mitochondrial metabolism coordinates the interactions between neurons and glia that shape neurodevelopment, physiology and function. Importantly, these interactions are dependent on neuroinflammatory state. Like microglia, astrocytes shift towards a distinct reactive phenotype under inflammatory conditions in a process called reactive astrogliosis, and this has profound consequences for neuron-glia metabolic coupling (Liddelow, Marsh and Stevens, 2020). Reactive astrogliosis is marked by an upregulation of glycolysis with a loss of mitochondrial membrane potential, reduced mitochondrial respiration, increased mitochondrial fragmentation and elevated ROS (Rahman and Suk, 2020). Conversely, mitochondrial dysfunction has been shown to induce reactive astrogliosis *in vitro* (Astakhova *et al.,* 2019; Fiebig *et al.,* 2019) while either inhibiting mitochondrial fission (Joshi et al. 2019) or promoting mitochondrial respiration (Martínez-Palma *et al.,* 2019) attenuated this response. This relationship underpins the self-sustaining and self-amplifying "auto-toxic loop" that exacerbates pathogenic signalling between microglia and astrocytes in the context of mitochondrial dysfunction or oxidative stress (Bantle *et al.,* 2021). Metabolic stress in microglia induces a shift towards glycolysis, consequent microglial activation, and the release of ROS and inflammatory cytokines that promote reactive astrogliosis. In turn, reactive astroglia undergo metabolic remodelling marked by increased glycolysis, mitochondrial fragmentation and oxidative stress, which potentiates glutamatergic signalling and microglial activation in a positive feedback loop.

This highlights a mechanistic relationship between neuroinflammation and neurotransmission underpinned by mitochondrial metabolism. In fact, central facets of ASD neurochemistry are directly modulated by mitochondrial function. ASD is characterised by an E/I imbalance (Marotta *et al.,* 2020; Hollestein *et al.,* 2023) and disruptions to glutamatergic, serotonergic and dopaminergic signalling (Zheng *et al.,* 2016; Montanari *et al*., 2022; Esposito *et al.,* 2024; Wegiel *et al.,* 2024; Blum *et al.,* 2024; Havranek, Bacova and Bakos, 2024; Martin *et al.,* 2024). Importantly, this neurochemical landscape underpins distinct behavioural, emotional and cognitive features of the ASD phenotype; glutamatergic excitotoxicity is thought to contribute to anxiety, perseveration, motor stereotypies, language processing

delays and cognitive deficits (Kawada, Kuramoto and Mimori, 2020); serotonin signalling is linked to altered social memory, facial recognition, emotional regulation and communication (Rodnyy *et al.,* 2024) and dopamine signalling is associated with disruptions to sleep, mood and attention (Pavăl, 2023).

Interestingly, neurotransmitter synthesis is tied to mitochondrial metabolism, while neuron-glia metabolic coupling directly facilitates neurotransmitter signalling and recycling **(Figure 1.10).** Numerous reviews have comprehensively described the relationship between mitochondrial metabolism and glutamatergic (Mira and Cerpa, 2020; Andersen *et al.,* 2021; Cavalcanti-de-Albuquerque *et al.,* 2021), serotonergic (Gardner and Boles, 2011; Fanibunda *et al.,* 2019; Yabut *et al.,* 2019; Tian, Du and Guo, 2023) and dopaminergic (Burbulla *et al.,* 2017; Ben-Shachar, 2020) neurotransmission, although this relationship remains understudied in ASD. At the centre of neuron-glia metabolic coupling, glutamate signalling modulates metabolic and redox homeostasis as a substrate for both OXPHOS and GSH synthesis in neurons and astrocytes (Andersen *et al.,* 2021). Thus, glutamate-glutamine cycling is regulated by mitochondrial TCA cycle flux as well as intracellular redox homeostasis (Sedlak *et al.,* 2019). Mitochondrial dysfunction can contribute to glutamatergic excitotoxicity by diverting glutamate away from GSH synthesis and inhibiting the energy-dependent glutamate import that removes excess glutamate from the synaptic cleft. Concurrently, the relationship between glial metabolism and reactive astrogliosis leads to the release of inflammatory cytokines, ROS and gliotransmitters that potentiate neuronal excitability while broadly disrupting the Ca^{2+} signalling cascades that facilitate intracellular responses to neurotransmitter signalling.

Likewise, dopamine signalling is coupled to mitochondrial function via a reciprocal interplay between dopamine autooxidation and oxidative state. In fact, dopamine directly inhibits the mitochondrial ETC, while oxidative dopamine metabolites contribute to oxidative stress, mitochondrial membrane depolarisation, decreased ETC activity and impaired energy production (Ben-Shachar, 2017; 2020). On the other hand, dopamine is a precursor required to produce norepinephrine (NE) which protects mitochondrial function by preventing membrane depolarisation and has both anti-inflammatory and antioxidant properties (Wong *et al.,* 2020). Similarly, serotonin, melatonin, and kynurenine (KYN) metabolites are modulated by a relationship between mitochondrial function and tryptophan metabolism (Michelhaugh, Guastella and Mittal, 2015). Serotonin not only promotes mitochondrial biogenesis, oxidative capacity and ATP synthesis (Weng *et al.,* 2015, 2016; Scholpa *et al.,* 2018; Fanibunda *et al.,* 2019) but also facilitates the synthesis of melatonin, which is critical for bioenergetic, redox and immune homeostasis (Molina-Carballo, Jerez-Calero and Muñoz-Hoyos, 2020). Notably, melatonin also governs the balance between the serotonin and KYN branches of tryptophan metabolism by regulating the rate-limiting enzymes involved in serotonin synthesis and turnover (Li *et al.,* 2017).

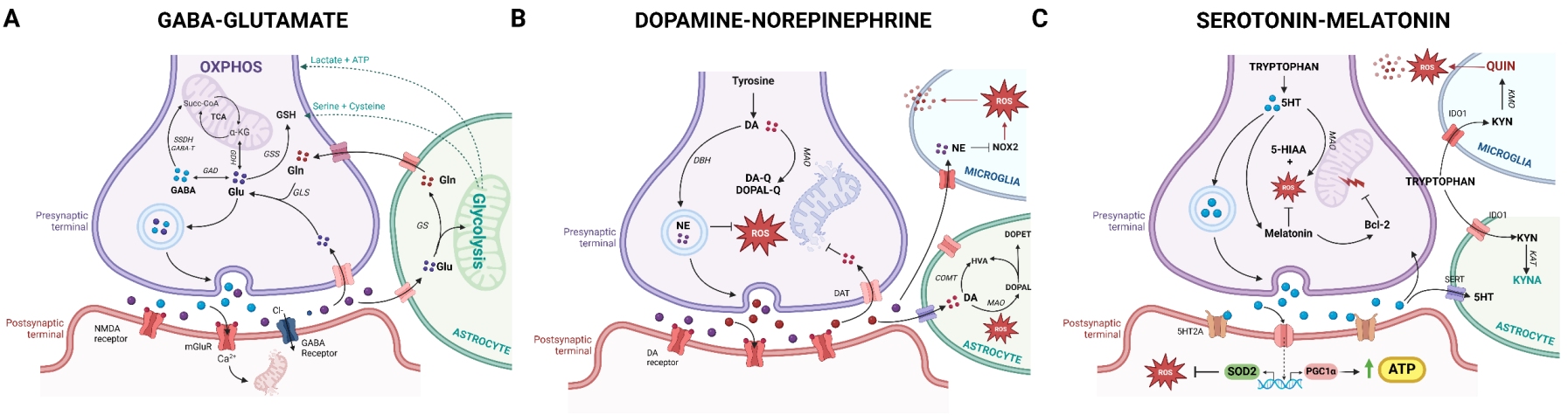


Figure 1.10. Mitochondrial Mechanisms in ASD Neurochemistry (Taken from Mahony and O'Ryan, (2022)). **A)** Glutamine (Gln) and Glutamate (Glu) are synthesised in the mitochondria of glutamatergic neurons and glial cells. Glu is directly integrated into the TCA cycle via GDH, converted into GABA via GAD, shunted into the transulfuration pathway via GSS, or released from the presynaptic compartment of glutamatergic neurons. A small percentage of Glu in the synaptic cleft is taken up by post-synaptic glutamate receptors, triggering the Ca^{2+}-dependent signalling cascades that facilitate neurotransmission. Chronic glutamatergic activation leads to an influx of Ca^{2+} and mitochondrial dysfunction in post-synaptic neurons. The majority of presynaptically-released Glu diffuses out of the synaptic cleft and is taken up by glial cells where it is either integrated into the TCA cycle or converted to Gln by GS. **B)** In dopaminergic neurons, dopamine (DA) is either deaminated by MAO or auto-oxidised by mitochondrial-derived ROS to produce quinones that lead to oxidative stress, mtDNA damage and mitochondrial deficits. DA can also enter the mitochondria to directly inhibit the ETC. Upon neuronal excitation, DA is released into the synaptic cleft and reimported into presynaptic neurons or taken up by surrounding glial cells where it is degraded by COMT or MAO. DA can also be metabolised by DBH in synaptic vesicles to generate NE which exerts antioxidant effects via the inhibition of NOX signalling in microglia. **C)** Serotonin (5-HT) is produced from tryptophan via MAO in serotonergic neurons while melatonin is produced from 5-HT in pinealocytes. 5-HT upregulates mitochondrial biogenesis, oxidative capacity and ATP synthesis and decreases oxidative stress while melatonin mitigates against mitochondrial membrane permeabilisation by activating Bcl-2. Once released, 5-HT can be taken up by either presynaptic neurons or glial cells via 5-HT transporters and broken down by MAO. In glial cells, tryptophan is oxidised via the KYN pathway. Astrocytes produce the neuroprotective metabolite KYNA while microglia generate the neurotoxic metabolite QUIN. Microglial immune activation in response to pro-inflammatory stimuli upregulates the expression of IDO1 to facilitate tryptophan transport into the cell, which both decreases local tryptophan availability and increases the production of QUIN in microglia. Bcl2 - B-cell lymphoma 2; COMT - catechol-Omethyltransferase; DBH - DA betahydroxylase; ETC - electron transport chain; GABA - Gamma-aminobutyric acid; GAD - glutamate decarboxylase; GDH - glutamate dehydrogenase; GSH - glutathione; GS - glutamine synthetase; GSS - glutathione synthetase; IDO1- Indoleamine-pyrrole 2-3-dioxygenase; KYN - kynurenine; KYNA - kynurenic acid; MAO - monoamine oxidase; mtDNA - mitochondrial DNA; NE - norepinephrine; NOX - Nicotinamide adenine dinucleotide phosphate oxidase; QUIN - quinolinic acid; ROS - reactive oxygen species. * *While specific neuronal subtypes express subsets of the enzymes involved in the metabolism of each neurotransmitter, all pathways are depicted in one diagram for the sake of simplicity.*

Interestingly, the KYN pathway functions at the interface between metabolism, neuroendocrinology and neuroinflammation. The quinolinic acid (QUIN) branch of KYN metabolism is coupled to *de novo* NAD^+ synthesis, which is critical to modulate both metabolic and oxidative state (Xie *et al.,* 2020). Mitochondrial dysfunction shifts the KYN pathway toward QUIN production by increasing the demand for NAD^+; conversely, QUIN contributes to mitochondrial dysfunction by increasing cytoplasmic Ca^{2+} concentration and superoxide production in microglia (Castro-Portuguez and Sutphin, 2020). A consequent shift toward a pathogenic microglial phenotype upregulates tryptophan import, decreasing local tryptophan availability for serotonin synthesis and further increasing the rate of QUIN production (Savino *et al.,* 2020). Moreover, QUIN promotes excitotoxicity by upregulating glutamatergic neurotransmission and inhibiting glutamate uptake from the synaptic cleft (Notarangelo and Pocivavsek, 2017). Together, this discussion illustrates that mitochondrial metabolism modulates the glutamatergic, dopaminergic and serotonergic neurotransmitter systems that contribute to gliosis, excitotoxicity and neuroinflammation. Thus, mitochondrial dysfunction shapes the neurochemical landscape that governs cognition, emotional regulation and behaviour, illustrating a convergence between molecular signatures and clinical presentations in ASD aetiology.

1.5. Mitochondrial Allostatic Load: A Biopsychosocial Perspective

The literature reviewed in this chapter has demonstrated growing evidence for mitochondrial dysfunction in ASD that is supported by an emerging role for mitochondria in ASD neurology. Interestingly, the mitochondrial aspect of ASD aetiology could also yield insight into the neurological and psychosocial mechanisms that influence long-term clinical outcomes. ASD is associated with a high prevalence of comorbid psychopathologies that substantially impair functioning and decrease quality of life – including generalised anxiety disorder (GAD), major depressive disorder (MDD), post-traumatic stress disorder (PTSD) and suicidal ideation (Etyemez *et al.,* 2020; Smith and White, 2020; Oakley, Loth and Murphy, 2021). Of note, children with ASD are six times more likely to reach clinically significant thresholds for measures of depression (Muscatello *et al.,* 2020), while rates of suicide risk, suicide attempts, and mortality by suicide are more than doubled across the lifespan (Cassidy *et al.,* 2014; Costa, Loor and Steffgen, 2020; Howe *et al.,* 2020; Kõlves *et al.,* 2021; Oakley, Loth and Murphy, 2021). This phenomenon remains largely uncharacterized, but emerging evidence suggests a role for both environmental and biological susceptibility factors.

It is widely acknowledged that interactions between genetic and environmental factors contribute to ASD aetiology, though this relationship is complex and poorly understood (Xavier Santos, Rasga and Moura Vicente, 200AD; Kubota and Mochizuki, 2016; Sealey *et al.,* 2016; Cheroni, Caporale and Testa, 2020; Khogeer *et al.,* 2022). In particular, environmental insults experienced during critical periods of neurodevelopment can profoundly impact the neuroimmune, neuroendocrine and neurochemical landscapes of the developing brain (Fogelman and Canli, 2019). This phenomenon is defined as ELS,

which refers to "*environmental events or chronic conditions that objectively threaten the physical and/or psychological wellbeing of an individual*" during the post-natal and adolescent periods marked by significant neuroplasticity (Sheth, McGlade and Yurgelun-Todd, 2017). Several forms of ELS have been characterised in the literature, ranging from poverty, neglect, abuse, or violence to food insecurity, immunological insults, natural disasters and systemic racism (Jones, Merrick and Houry, 2020). Importantly, researchers have noted a distinction between good, tolerable, and toxic stress that differentially induce adaptation, resilience or pathology. Here, the defining feature of toxic stress is "*a lack of internal resources or external support systems, resulting in chronic physiological dysregulation*" (Picard *et al.,* 2018).

There is substantial evidence from both epidemiological and preclinical studies that toxic stress increases the risk of psychopathology and suicidality (Sheth, McGlade and Yurgelun-Todd, 2017; Malinovskaya *et al.,* 2018; Fogelman and Canli, 2019; Lähdepuro *et al.,* 2019; Targum and Nemeroff, 2019; LeMoult *et al.,* 2020; Sahle *et al.,* 2021; Su *et al.,* 2022) as well as cancer, autoimmune, cardiac and neurodegenerative disease (Guidi *et al.,* 2021). Importantly, an increased exposure to ELS is well-documented in ASD (Schroeder *et al.,* 2014; Griffiths *et al.,* 2019; Kuenzel *et al.,* 2021; Trundle *et al.,* 2022), while lifetime stress exposure has been linked to suicidality in ASD (Moseley *et al.,* 2024). In fact, recent work has defined distinct internal experiences that precipitate psychopathology in ASD – namely, social camouflaging and autistic burnout - that closely reflect the established definitions for toxic stress (Mahony and O'Ryan, 2022). Moreover, several authors have proposed an underlying susceptibility to ELS mediated by molecular and neurological aspects of ASD aetiology (Singletary, 2015; Cheroni, Caporale and Testa, 2020; Scarpa *et al.,* 2021; Makris, Eleftheriades and Pervanidou, 2022). Thus, interactions between ELS and ASD aetiology may be centrally involved in determining clinical outcomes.

The pathological responses to ELS are thought to be mediated by allostatic load, which describes the physiological consequences of chronic stress on the metabolic, endocrine and immune systems required for homeostasis (Picard and McEwen, 2018a). Notably, a growing body of work suggests that the molecular components of allostatic load are modulated by mitochondrial metabolism (Picard *et al.,* 2015; Juster *et al.,* 2016; Hoffmann and Spengler, 2018; Picard and McEwen, 2018b, 2018a; Ridout, Khan and Ridout, 2018; Picard, Trumpff and Burelle, 2019; Daniels, Olsen and Tyrka, 2020; Allen, Caruncho and Kalynchuk, 2021; Zitkovsky, Daniels and Tyrka, 2021; Mposhi and Turner, 2023; Liu *et al.,* 2024). As I recently reviewed in more detail (Mahony and O'Ryan, 2022), both *in vivo* models and epidemiological studies have shown markers of mitochondrial dysfunction associated with ELS exposure, while experimentally disrupting mitochondrial function has been shown to alter the pathophysiological consequences of chronic stress. On the other hand, mitochondrial dysfunction is separately implicated in the pathogenesis of neuropsychiatric disorders, including MDD, GAD and suicidality (Ben-Shachar and Ene, 2018; Kim *et al.,* 2019; Giménez-Palomo *et al.,* 2021; Klein *et al.,*

2021; Ni, Ma and Chung, 2022). In fact, an emerging field characterised as "mitochondrial psychobiology" is exploring the utility of targeting mitochondrial mechanisms to treat neurodevelopmental, neuropsychiatric and neurodegenerative conditions (Picard, Trumpff and Burelle, 2019). Thus, mitochondrial dysfunction emerges as a convergent signature in ELS, ASD and psychopathology that could serve as a therapeutic target to mitigate negative neuropsychiatric outcomes.

Mitochondrial allostatic load (MAL) is defined as the adaptive changes to mitochondrial morphology, dynamics, and function that modulate the response to chronic stress (Picard and McEwen, 2018a). The relationship between MAL and ELS is governed by the Hypothalamic-Pituitary-Adrenal (HPA) axis that coordinates the molecular stress response (Makris *et al.,* 2021). Children are particularly vulnerable to HPA disruption during early childhood and adolescence, which are periods marked by higher HPA axis plasticity; thus, HPA signalling is a key mediator of pathological responses to ELS (Sheth, McGlade and Yurgelun-Todd, 2017; Agorastos *et al.,* 2019). In fact, a recent systematic review has demonstrated an established role for HPA axis dysregulation in mood disorders, suicidal behaviour, and the relationship between ELS and major depression (Ceruso *et al.,* 2020). Notably, a bidirectional relationship between mitochondrial metabolism and stress-responsive signalling has emerged, mediated by both genomic and non-genomic mechanisms that have been comprehensively described **(Figure 1.11)** (Picard and McEwen, 2018a; Ridout, Khan and Ridout, 2018; Lapp, Bartlett and Hunter, 2019; de Guia, 2020; Jaszczyk and Juszczak, 2021; Kokkinopoulou and Moutsatsou, 2021; Melchinger and Garcia, 2023; Bhattacharya *et al.,* 2024).

The HPA axis initiates stress-responsive signalling via glucocorticoids (GCs) like cortisol and corticosterone that act on GC receptors (GRs) to regulate genes involved in neurogenesis, neuroplasticity, and neurotransmission (Finsterwald and Alberini, 2014). The cytochrome P450 enzymes that drive GC synthesis are coupled to mitochondrial redox homeostasis (Prasad *et al.,* 2014); and conversely, GC signalling modulates mitochondrial integrity, activity, ROS production and Ca^{2+} buffering (Du *et al.,* 2009; Tome *et al.,* 2012; Picard, Juster and McEwen, 2014; He *et al.,* 2017; Choi *et al.,* 2021). Moreover, GCs affect the availability and turnover of key energetic substrates in the brain, including pyruvate, glucose, lactate and ketone bodies which regulate mitochondrial OXPHOS, glycolysis and FAO, respectively (Jaszczyk and Juszczak, 2021). GCs also modulate mitochondrial dynamics by regulating the expression of relevant genes via GC response elements in both nuclear and mtDNA (Lee *et al.,* 2013; Lapp, Bartlett and Hunter, 2019; Kokkinopoulou and Moutsatsou, 2021). Indeed, GCs suppress the expression of the genes involved in mitochondrial fusion, trafficking and clearance (Choi and Han, 2021) and upregulate central transcriptional regulators of mitogenesis (Lee *et al.,* 2013; Ridout, Khan and Ridout, 2018; Dempster *et al.,* 2021). Accordingly, animal models have shown that both chronic stress and corticosterone treatment increase mtDNA copy number (Cai *et al.,* 2015) and conversely, that mtDNA genetic variants can alter corticosterone production and HPA

signalling (Gimsa *et al.,* 2009; Picard *et al.,* 2015). Together, this illustrates an interdependent relationship between the metabolic and neuroendocrine components of allostasis.

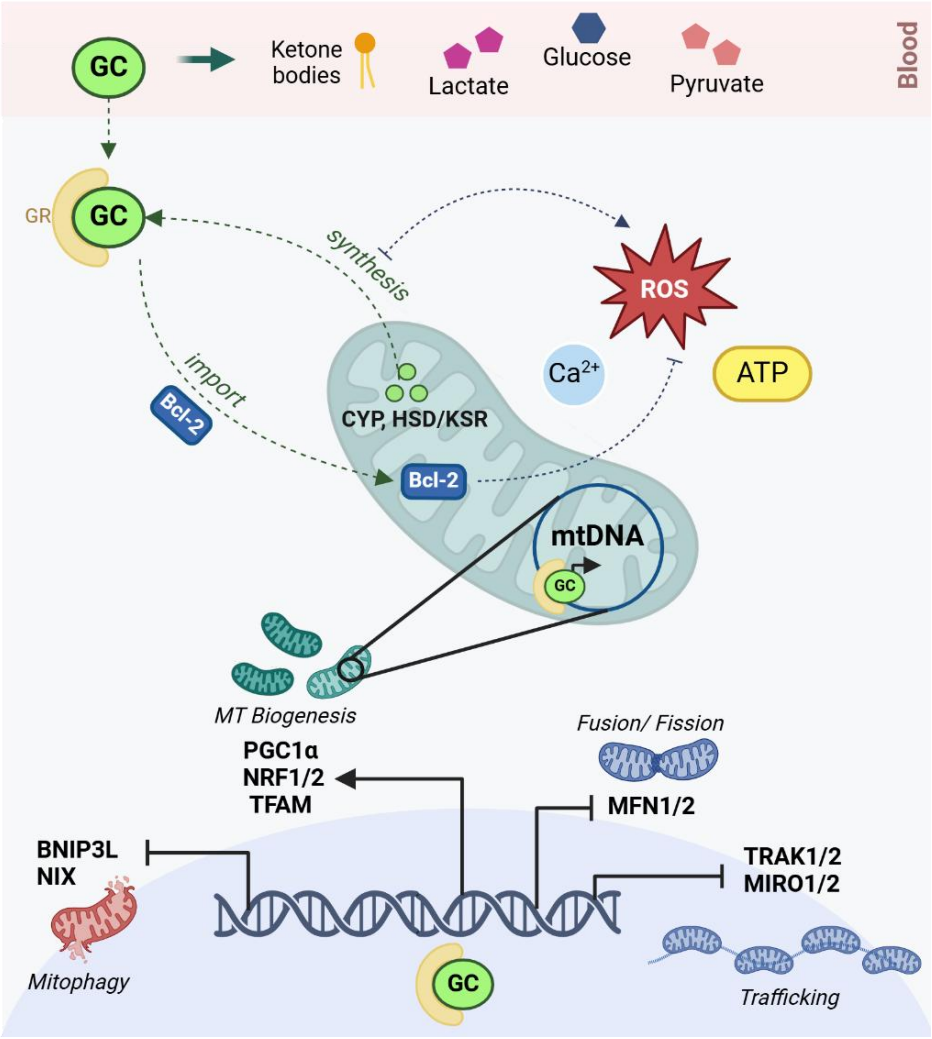


Figure 1.11. The Interplay Between Metabolic and Stress-Responsive Signalling (Taken from Mahony and O'Ryan, (2022)). Chronic stress activates the Hypothalamic-Pituitary-Adrenal (HPA) axis, leading to the release of glucocorticoids (GCs) that diffuse through the blood-brain barrier to activate glucocorticoid receptors (GRs) Rs in neurons. GCs alter circulating levels of key energetic substrates including ketone bodies, glucose, lactate and pyruvate, which modulate mitochondrial fatty acid oxidation, glycolysis and oxidative phosphorylation. Activated GRs act via B-cell lymphoma 2 (Bcl-2) and other non-genomic mechanisms to modulate membrane potential, Ca^{2+} buffering, ATP production and redox homeostasis in the mitochondria. Activated GRs also bind to glucocorticoid response elements in both nuclear and mitochondrial DNA to moderate the transcription of key genes involved in the regulation of mitochondrial trafficking (TRAK1/2, MIRO1/2), morphology (MFN1/2), biogenesis (PGC1α, TFAM, NRF1/2) and mitophagy (BNIP3, NIX). Conversely, mitochondria are responsible for the synthesis of GCs via the cytochrome P450 (CYP540) and hydroxysteroid dehydrogenase/ketosteroid reductase (HSD/KSR) enzymes. GC synthesis increases mitochondrial reactive oxygen species (ROS), and conversely, oxidative stress is known to inhibit steroidogenesis. BNIP3 - Bcl2 interacting protein 3; MFN1/2 - mitofusin 1 and 2; MIRO1/2 - mitochondrial Rho GTPase; NIX - BNIP3-like; NRF1/2 - nuclear respiratory factors 1/2; PGC1α - peroxisome proliferator-activated receptor gamma coactivator-1 alpha; TFAM - mitochondrial transcription factor A; TRAK1/2 - Trafficking Kinesin Protein 1/2.

The neuroimmune system is the second established component of allostatic load that works in concert with HPA neuroendocrine signalling to modulate the stress response. Neuroimmune dysregulation is widely documented in stress-related (Fogelman and Canli, 2019; Dutcher *et al.,* 2020; Brown, Worrell and Pariante, 2021) and neuropsychiatric (Furtado and Katzman, 2015; Lurie, 2018; Troubat *et al.,* 2021) disorders, while a reciprocal relationship between inflammation and HPA signalling has been well-described in the context of psychopathology (Pace and Miller, 2009; Beurel, Toups and Nemeroff, 2020; Nettis and Pariante, 2020; Sugama and Kakinuma, 2020; Silva *et al.,* 2021; Troubat *et al.,* 2021). Notably, **Section 1.4** emphasised that neuroinflammation is an established component of ASD aetiology that is tightly coupled to metabolic state. Given that HPA signalling regulates mitochondrial function, and that mitochondria are central to immune modulation, it has been proposed that HPA-immune interactions could be mediated by mitochondrial mechanisms (Kasahara and Inoue, 2015; Picard and McEwen, 2018; Mocayar Marón *et al.,* 2019). Indeed, mitochondria directly govern the NFκB and inflammasome pathways at the interface between neuroendocrine and neuroimmune signalling (Boeck *et al.,* 2016). Congruent with this, recent data demonstrate that ELS simultaneously impairs mitochondrial function and increases neuroinflammation in animal models (González-Pardo *et al.,* 2020) while clinical studies report a significant correlation between mitochondrial respiration and pro-inflammatory signalling in response to ELS (Boeck *et al.,* 2016).

Importantly, MAL also functions as a mechanistic link between the neuroendocrine and neurochemical landscapes that drive psychopathology in response to ELS. As described in section **1.4**, the relationship between mitochondrial dysfunction and ASD neurochemistry influences cognition and behaviour via glutamatergic, serotonergic and dopaminergic signalling. This neurochemical signature is not only associated with core facets of ASD aetiology but also has direct functional implications for stress-related psychopathology. Preclinical studies have shown that chronic stress disrupts glutamate (Ohta *et al.,* 2020; Deutschmann, Kirkland and Briand, 2021; Hyer *et al.,* 2021; Xu *et al.,* 2021), serotonin (Wang *et al.,* 2022) and dopamine (Majcher-Maślanka *et al.,* 2017; Bonapersona, Joëls and Sarabdjitsingh, 2018; Catale *et al.,* 2022) signalling, leading to increased anxiety-like behaviours and impairments in social recognition, social interest and cognitive flexibility. These data are supported by human cohort studies showing that ELS impairs dopaminergic responses to psychosocial stress (Pruessner *et al.,* 2004; Oswald *et al.,* 2014), and alters glutamate/glutamine cycling (Averill *et al.,* 2020) and serotonin transporter binding (Underwood *et al.,* 2018) in patients with MDD.

Notably, interactions between HPA signalling and neurotransmission play a central role in modulating suicide risk after ELS exposure (Berardelli *et al.,* 2020). Glutamate is involved in both driving HPA responses and limiting HPA overactivation (Evanson and Herman, 2015; Mathew and Joy, 2019) while GC signalling is modulates the plasticity and excitability of glutamatergic synapses (Gulyaeva, 2021). Serotonergic neurotransmission excites hypothalamic neurons in the amygdala (Troubat *et al.,* 2021) and acts as an important regulator of GR signalling in the pre-frontal cortex after exposure to acute

stress (Sbrini *et al.,* 2020). On the other hand, an inverse relationship between corticosteroids and serotonin receptor binding densities mediates suicidality following ELS (Pompili *et al.,* 2010). Finally, GCs also activate the mesolimbic dopamine pathway (DeRosse and Barber, 2021) by upregulating the rate-limiting step of dopamine synthesis, downregulating dopamine degradation, clearance and synaptic uptake, or by acting directly on GRs in dopamine-receptive (Lopez and Flagel, 2020). Thus, the interplay between mitochondrial dysfunction and HPA dysregulation directly shapes the neurochemical signatures that precipitate psychopathology in response to chronic stress (Berardelli *et al.,* 2020).

This discussion illustrates that mitochondria not only govern neurodevelopment, physiology and function, but may also modulate the allostatic mechanisms that lead to psychopathology. Importantly, this may highlight a novel molecular susceptibility to ELS that has been overlooked in the context of ASD. Given the high prevalence of both ELS and psychopathology in ASD, a role for HPA signalling in ASD has been widely studied. Despite substantial evidence for global disruptions to cortisol signalling (Corbett and Schupp, 2014; Corbett and Simon, 2014; Taylor and Corbett, 2014; Tordjman *et al.,* 2014; Tomarken, Han and Corbett, 2015; Edmiston, Blain and Corbett, 2017; Alagendran *et al.,* 2019; Hadwin *et al.,* 2019; Makris *et al.,* 2021), HPA hyperactivation (Tordjman *et al.,* 2014; Tomarken, Han and Corbett, 2015; Ogawa *et al.,* 2017; Muscatello and Corbett, 2018) and increased stress reactivity (Spratt *et al.,* 2012; Alagendran *et al.,* 2019) in ASD, current findings lack intra- and inter-individual reproducibility, while numerous studies report no significant differences in cortisol levels, rhythms, variability or responsivity (Sharpley *et al.,* 2017; Alagendran *et al.,* 2019; Hadwin *et al.,* 2019). The existing literature suggests some role for HPA signalling in ASD; however, the relationship between HPA axis signalling and psychopathology is likely mediated by pleiotropic mechanisms (Muscatello *et al.,* 2020). In this context, the mitochondrial component of ASD aetiology may function as a novel molecular susceptibility to HPA dysregulation that increases the risk of psychopathology. Thus, better understanding the relationship between mitochondrial dysfunction, MAL and HPA signalling could yield insight into neuropsychiatric comorbidities in ASD that impact quality of life.

1.6. Summary and Conclusions

This chapter introduced and contextualised the mitochondrial hypothesis, illustrating how mitochondrial mechanisms could yield insight into molecular, clinical and neurological components of ASD aetiology that influence clinical outcomes **(Figure 1.12).** Molecular ASD research is shaped by a complex landscape spanning diverse academic disciplines and sociocultural contexts. The clinical conceptualisations of ASD are still evolving, while its diverse presentations are underpinned by a multifaceted molecular aetiology that remains poorly understood. These factors present considerable challenges to the field of molecular ASD research, which is grappling with a need to improve its translatability. Increasingly, researchers are recognising a need for a more biopsychosocial framework to understand the interactions between biological and environmental factors that influence clinical

outcomes. This is highly relevant in SA, where poor access to health care limits diagnosis and intervention while exposure to ELS is widespread due to high rates of poverty, infectious disease and institutionalised inequality. Yet, ASD remains significantly understudied in SA populations. Better characterising ASD in genetically diverse African populations could yield novel insight into ASD aetiology and contribute to the development of population-specific biomarkers to improve the accessibility of diagnosis and intervention. In this context, our research group has explored DNAm signatures in a novel SA ASD cohort, revealing a dysregulation of mitochondrial metabolism associated with ASD.

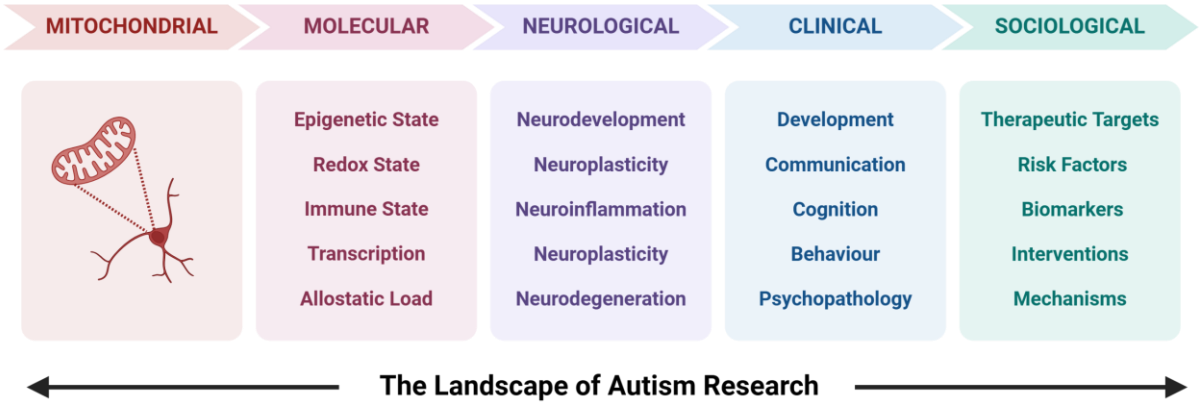


Figure 1.12. Contextualising the Mitochondrial Hypothesis. The mitochondrial component of autism spectrum disorder (ASD) has implications for the molecular, neurological, clinical and sociological landscapes that shape ASD research. This chapter has described the evidence for mitochondrial dysfunction in ASD, focussing on the relationship between mitochondrial metabolism and neurogenesis that informs the central aims and objectives of this research project. Beyond neurogenesis, mitochondria modulate epigenetic, redox and immune homeostasis with functional implications for transcriptional regulation and allostatic load. Mitostasis influences ASD neurology by modulating aspects of neurodevelopment, physiology and function that underpin clinical hallmarks of ASD. Moreover, as regulators of the neuroendocrine and neuroimmune components of allostasis, mitochondria mediate the interactions between environmental and biological factors that determine long-term clinical outcomes in ASD. Better characterising the mitochondrial component of ASD could help to identify environmental risk factors and psychosocial interventions and aid the development of diagnostic biomarkers and novel therapeutics to improve quality of life.

This thesis builds on the molecular signatures implicated in our SA cohort to examine underlying mechanisms that contribute to ASD. This chapter reviewed the cumulative evidence for DNAm and mitochondrial dysfunction in ASD, highlighting the interplay between epigenetic and mitochondrial mechanisms as an interesting target for future research in this context. As the mitochondrial component in ASD has become increasingly well-established, mitochondria have also emerged as central regulators of neurodevelopment, physiology and function. Neurogenesis relies on metabolic reprogramming that upregulates oxidative respiration by remodelling profiles of substrate utilisation and mitochondrial dynamics. Moreover, disruptions to mitochondrial metabolism, morphology or connectivity profoundly

influence neuronal differentiation and NSC fate, while metabolic state is tightly coupled to the epigenetic remodelling that shapes the neurogenic transcriptome. Mitochondria also modulate the balance between resting and reactive microglia that shape neural circuitry during embryonic neurogenesis, facilitate post-natal synaptic pruning and govern neuroimmune homeostasis throughout adulthood. In fact, metabolic coupling underpins the relationship between neurons, astrocytes and oligodendrocytes that controls neuronal activity, integrity and function. This interplay drives a pathogenic feedback loop between mitochondrial dysfunction, oxidative stress, reactive gliosis and glutamatergic excitotoxicity that is widely implicated in neuropsychiatric and neurodegenerative disorders. Moreover, mitochondrial metabolism in neurons and glia modulates the synthesis, release, reuptake and recycling of neurotransmitters that shape neurochemistry, cognition and behaviour in ASD, demonstrating how mitochondria contribute to clinical ASD presentations.

Lastly, this chapter highlights that the mitochondrial mechanisms implicated in ASD are emerging as central regulators of pathological stress responses that contribute to psychopathology, suicidality and other pathophysiological outcomes. ASD is not only associated with increased ELS and psychosocial stress, but recent characterisations of internal autistic experiences have highlighted chronic and distinct forms of stress in ASD that often go unrecognised. A growing body of work on MAL has described how mitochondria orchestrate both the neuroimmune and neuroendocrine components of allostasis. As such, mitochondria may be centrally involved in mediating the adaptive and toxic responses to ELS that influence clinical outcomes. In fact, mitochondrial psychobiology is exploring how mitochondria can be targeted to develop novel therapies to mitigate psychopathology and other pathological stress responses. This emphasises that mitochondria function at the interface between biological and sociological factors that determine quality of life, and present novel therapeutic targets to improve long-term clinical outcomes.

Better characterising the relationship between mitochondrial dysfunction and neurodevelopment could yield insight into both neurological and molecular aspects of ASD aetiology that influence neuropsychiatric outcomes in this context. Accordingly, this thesis aims to investigate how mitochondrial dysfunction impacts neuronal viability, metabolism, morphology and maturation by addressing the specific objectives outlined in **Figure 1.13.** This work develops an *in vitro* system to characterise mitochondrial mechanisms in ASD and provides novel insight into the relationship between neuronal metabolism and development. Ultimately, this lays the groundwork for future studies to characterise new genes identified in our ASD cohort, yield mechanistic insight into ASD aetiology or explore targeted mitochondrial therapeutics to improve quality of life.

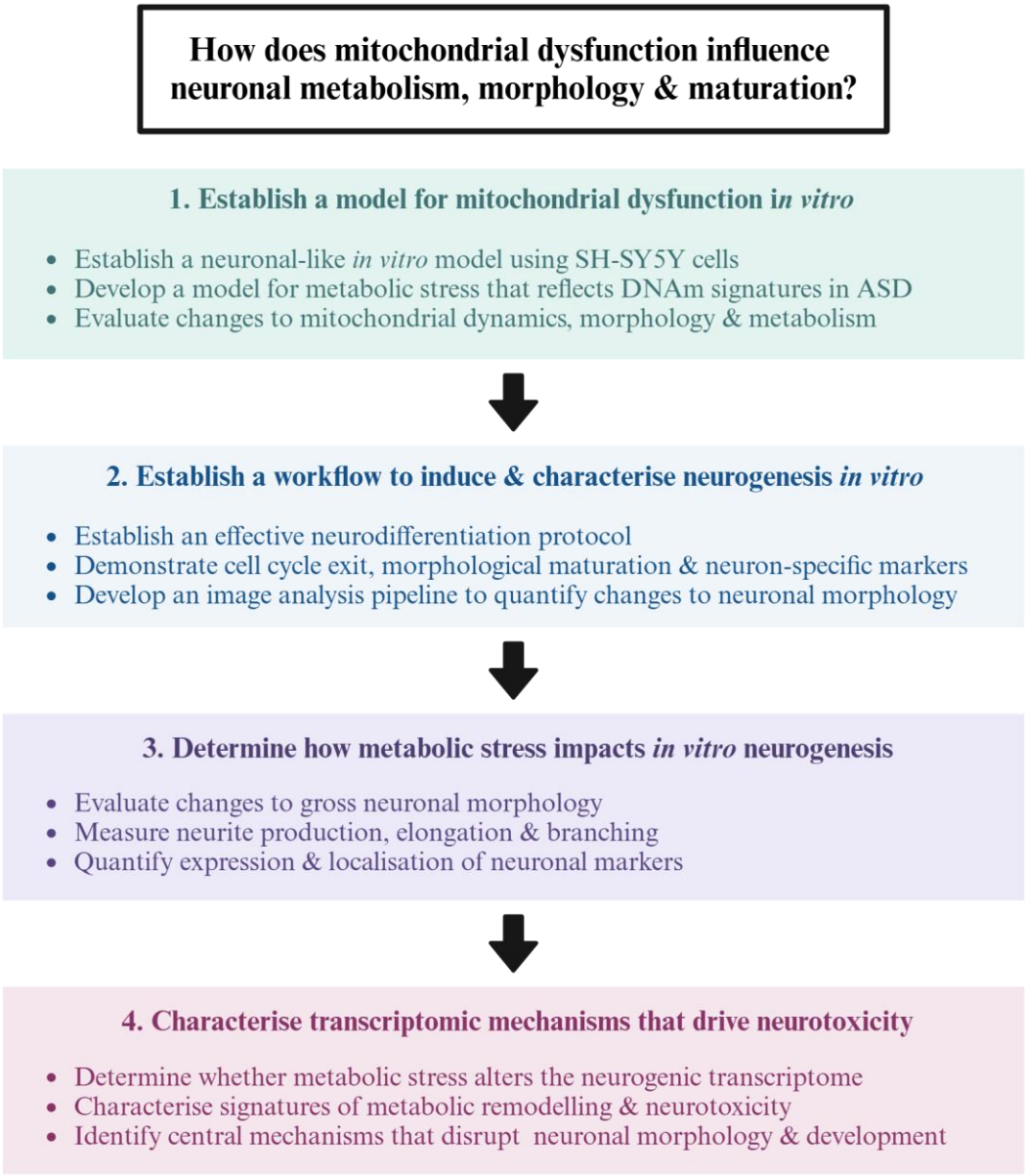


Figure 1.13. Specific Research Question, Aims and Objectives. This thesis examines how mitochondrial dysfunction impacts neuronal metabolism, morphology and maturation using an *in vitro* system to achieve four aims: 1) establish and characterise a model for mitochondrial dysfunction *in vitro*; 2) establish an *in vitro* model for neurogenesis; 3) examine whether mitochondrial dysfunction alters *in vitro* neurogenesis and 4) characterise the underlying transcriptional mechanisms that mediate this response.

Chapter 2.

Mitochondrial Dysfunction *In Vitro*: The Propionic Acid Model

2.1. Introduction

Chapter 1 reviewed an intricate relationship between metabolism and neurogenesis that may yield insight into the mitochondrial component of ASD aetiology. However, this discussion also highlighted some of the challenges involved in translating molecular signatures into a mechanistic understanding of ASD. In SA, these challenges are compounded by socioeconomic factors that significantly impede the recruitment and phenotyping of the well-powered, finely characterised cohorts that are needed for large-scale molecular studies. Yet, the phenotypic heterogeneity and aetiological complexity of ASD can confound even sufficiently powered molecular studies. Moreover, brain tissue remains notoriously inaccessible – particularly during pre- and post-natal neurodevelopment - and the functional consequences of molecular disruptions are cell-type and life-stage specific. In this context, *in vitro* systems have emerged as useful reductionist models in which to study specific aspects of neuronal development, physiology and function. In resource-constrained contexts, a combined top-down and bottom-up approach that employs both small-scale cohort studies and mechanistic *in vitro* approaches could not only maximise translatability but also facilitate the development of molecular neuroscience infrastructure. Therefore, this chapter aims to establish an *in vitro* system that can be used to ask targeted mechanistic questions and build local ASD research capacity.

2.1.1. An In Vitro Model to Study Metabolism: The SH-SY5Y System

The SH-SY5Y cell line is widely used as a cost-effective "workhorse" cell line to study neurodevelopment and disease (Lopez-Suarez *et al.,* 2022). SH-SY5Y cells are thrice-subcloned immortalised derivatives of the parental SK-N-SH cell line that was originally established from human neuroblastoma tissue (Feles et al. 2022). SH-SY5Y cells are comprised of distinct subtypes that reflect the neuroblast-like (N) and epithelial-like (S) phenotypes in the parental SK-N-SH line (Kovalevich, Santerre and Langford, 2021). N-type cells are immature neuronal progenitor cells (NPCs) while S-type cells reflect multipotent precursors to non-neuronal cells in the neural crest (Bell *et al.,* 2013). Despite this inherent heterogeneity, N-type cells comprise ~80% of SH-SY5Y cultures *in vitro* (Bell *et al.,* 2013) and several reviews have recently described the features that make this system particularly suitable for the study of neuropsychiatric disorders (ÖZ, 2019; Ducray *et al.,* 2020; Alrashidi, Eaton and Heales, 2021; Bayeva, Coll and Piskareva, 2021; Bell and Zempel, 2021; Campos, Bozi and Ferreira, 2022; Ioghen, Ceafalan and Popescu, 2023). As well as its reproducibility, capacity for rapid expansion and cost-effective maintenance, the SH-SY5Y cell line can be differentiated into homogenous N-type

derivatives that display phenotypic and molecular hallmarks of primary neurons (Simões *et al.,* 2022). This system can be used to examine the mechanisms that drive neurogenesis, which is particularly relevant for the study of NDDs. Moreover, the genetic (Krishna *et al.,* 2014), transcriptomic (Nishida *et al.,* 2008; Beveridge *et al.,* 2009; Korecka *et al.,* 2013; Chiocchetti *et al.,* 2016; Pezzini *et al.,* 2017; Mercatelli *et al.,* 2021) and proteomic (Murillo *et al.,* 2017; Zhang, Gygi and Paulo, 2021; Barth *et al.,* 2022; Pandey *et al.,* 2022) profiles of the SH-SY5Y cell line have been comprehensively evaluated, providing a well-characterised molecular landscape in which to study neuropathological mechanisms.

There are clear limitations to the translatability of *in vitro* studies for *in vivo* and clinical applications, yet a pervasive challenge in molecular research is the need to balance feasibility with translatability. The very features that make the SH-SY5Y system much more accessible – its immortalised nature, its capacity for proliferation and long-term storage, and its flexibility in the face of varied culture conditions – are also those that diverge most significantly from the primary neuronal phenotype it is intended to model. More biologically accurate models such as human-derived neuronal stem cells (NSCs), primary neurons, brain-tissue biopsies or 3D organoid systems are also much more time- and cost-intensive, require specialised infrastructure and come with complex ethical considerations with respect to their origins. Therefore, this chapter established standard cell culture operating procedures within the scope of the SH-SY5Y system as a prerequisite for the more refined models employed in subsequent chapters and beyond the scope of this thesis. The primary research aim of this project was to examine the relationship between mitochondrial dysfunction and neurogenesis. Therefore, the scope of this study was to i) establish a model for mitochondrial dysfunction, ii) establish a model for *in vitro* neurogenesis and iii) explore how mitochondrial metabolism modulates neurogenesis *in vitro.* Chapter 2 addresses the first of these objectives, harnessing the flexible, efficient and cost-effective nature of the undifferentiated phenotype to characterise different facets of mitostasis. Here, this model system was intentionally designed to maximise its translatability and lay the groundwork to establish a suitable model for neurogenesis in Chapter 3.

2.1.2. The Metabolic Landscape of SH-SY5Y

The utility of any model system lies in its capacity to ask specific mechanistic questions in a highly controlled environment. Thus, the environment itself should be carefully considered with the nature of the research question in mind. Here, the SH-SY5Y cell line is used to investigate the metabolic regulation of neurogenesis based on the mechanistic hypothesis derived from molecular ASD signatures. Therefore, it is important to consider the variables that influence the utility of the SH-SY5Y cell line to study neurogenesis. The culturing, differentiation and pathological relevance of the SH-SY5Y cell line has been widely reviewed (Pahlman *et al.,* 1990; Feng, Wang and Sheng, 2006; Xie, Hu and Li, 2010; Kovalevich and Langford, 2013; Xicoy, Wieringa and Martens, 2017; O'Neill Sarah, Irani Julia, Fodjo Siewe Nelson Joseph, Nono Denis, Abbo Catherine, Sato Yasuaki, Mugarura Augustine,

Dolo Housseini, Ronse Maya, 2019; Campos Cogo *et al.,* 2020; Ducray *et al.,* 2020; Bayeva, Coll and Piskareva, 2021; Ioghen, Ceafalan and Popescu, 2023). Yet, Feles *et al.,* (2022) noted an absence of standardised parameters for SH-SY5Y subculturing, which are critical for robust and reproducible protocols for neuronal differentiation. Similarly, Xicoy, Wieringa and Martens, (2017) highlighted that recommendations on basic subculture vary even between different cell-line suppliers.

Recent systematic reviews of the SH-SY5Y cell line have described seven different media formulations with divergent nutrient profiles (Xicoy, Wieringa and Martens, 2017; Lopez-Suarez *et al.,* 2022). The most frequently used formulation (in 67-69% of studies) is either Dulbecco's Modified Essential Medium (DMEM) or DMEM with Ham's F12, which is the most cost-effective method for large-scale expansion of the cell line. Indeed, many studies describe DMEM: F12 as the *de facto* method for SH-SY5Y subculture (Xie, Hu and Li, 2010; Kovalevich and Langford, 2013; Smerker, 2014; Sakagami *et al.,* 2017; Mohammed Izham *et al.,* 2018; ÖZ, 2019; Feles *et al.,* 2022; Kaya *et al.,* 2024; Kronenberger *et al.,* 2024). However, numerous cell line suppliers recommend the use of minimum essential medium (MEM) or MEM: F12, including the American Type Culture Collection (ATCC), the European Collection of Authenticated Cell Cultures (ECCAC) and the German Collection of Microorganisms and Cell Cultures (DSMZ) (Xicoy, Wieringa and Martens, 2017). Of the most frequently reported formulations in the literature, there are marked differences with respect to the concentrations of glucose, glutamine, glutathione, sodium pyruvate, sodium bicarbonate, AAs, vitamins and inorganic salts. As either direct substrates or essential cofactors in different metabolic pathways, the balance between these components is central to the determination of basal metabolic state. Therefore, media composition is an integral consideration for the use of the SH-SY5Y cell line to study metabolic mechanisms in neuropathology.

Yet, the relationship between growth media and SH-SY5Y metabolism remains poorly recognised. Previous authors have noted the general significance of media composition for SH-SY5Y metabolism, differentiation and function (Xicoy, Wieringa and Martens, 2017; Mohammed Izham *et al.,* 2018; Simões *et al.,* 2021) and several studies have sought to optimise subculture conditions to promote SH-SY5Y proliferation (Buttiglione *et al.,* 2007; Sakagami *et al.,* 2017; Mohammed Izham *et al.,* 2018; Kaya *et al.,* 2024). However, the parameters that facilitate rapid cell growth are unlikely to best recapitulate the post-mitotic neuronal phenotype. The oncogenic origins of the SH-SY5Y cell line are fundamental to its capacity for cell line expansion but also contribute to a metabolic state reminiscent of the "Warburg Effect" that is a characteristic of tumour tissue (Gogvadze, Zhivotovsky and Orrenius, 2010). Consequently, the SH-SY5Y model displays a predominantly glycolytic metabolic profile, particularly under high-glucose conditions, which contrasts the oxidative reliance of primary neurons. Manipulating the availability of glucose, growth factors or micronutrients may shift SH-SY5Y metabolism towards oxidative rather than glycolytic metabolism (Swerdlow *et al.,* 2013; Wilkins *et al.,* 2016; Xie, 2018; Kronenberger *et al.,* 2024). However, few studies have explored the implications of

media composition for the context-specific relevance of the SH-SY5Y cell line as a model for neurogenesis.

To identify the optimal conditions to study neuronal metabolism, it is necessary to consider the extent to which SH-SY5Y metabolism reflects or diverges from the *in vivo* neuronal phenotype. Several studies have compared the metabolic profile of the SH-SY5Y cell line against glioblastoma, neuroblastoma, NSCs or primary neuronal cultures. In the undifferentiated state, SH-SY5Y cells display an oxidative capacity that reflects non-neuronal cancer-derived cell lines (Kim *et al.,* 2015; Prado *et al.,* 2015) but is considerably lower than primary neuronal cultures (Sotolongo, Ghiso and Rostagno, 2020). Conversely, basal glycolysis is markedly reduced in undifferentiated SH-SY5Y cells compared to either hepatocellular carcinoma or glioblastoma lines (Kim *et al.,* 2015; Prado *et al.,* 2015). This indicates a greater degree of oxidative reliance than non-neuronal cell lines even if oxidative capacity is more limited than in mature neurons. However, unlike the intrinsic oxidative reliance exhibited by primary neurons, undifferentiated SH-SY5Y cells display an "opportunistic" metabolic profile that shifts with nutrient availability (Xun *et al.,* 2012) and a reciprocal relationship between oxidative and glycolytic metabolism (Swerdlow *et al.,* 2013) that allows them to compensate for mitochondrial dysfunction by upregulating glycolytic flux (Farina *et al.,* 2018; Bovio *et al.,* 2021; Yang *et al.,* 2021). In fact, SH-SY5Y cells display a capacity for glycolytic compensation in the absence of mitochondrial respiration that is sufficient for cell viability (Lu *et al.,* 2013; Xiao *et al.,* 2019) which starkly contrasts the mitochondrial dependence of mature neurons.

Interestingly, mitochondrial reliance can be promoted by replacing glucose with alternative carbon sources (Naia *et al.,* 2021), while serum depletion decreases the glycolytic reliance of SH-SY5Y cells (Kronenberger *et al.,* 2024). Thus, low-glucose media with glutamine supplementation and serum depletion should be used to model oxidative reliance in the SH-SY5Y system. Here, glucose will be depleted rather than replaced because i) glucose is a primary energy source in the brain and ii) this study aims to evaluate both oxidative and glycolytic metabolism. Hence, this chapter establishes the SH-SY5Y system using DMEM: F12 for cell-line expansion and cell bank maintenance, while cells are weaned onto EMEM: F12 with 5mM Glucose, 2mM L-Glutamine and 1% non-essential amino acids (NEAAs) according to the protocol described by (Shipley, Mangold and Szpara, 2016) at least one passage prior to all experiments, employing a 24-hour FBS depletion before treatments.

2.1.3. A Model for Mitochondrial Dysfunction

This chapter aims to establish an *in vitro* model for mitochondrial dysfunction based on the DNAm patterns identified in our ASD cohort. Chapter 1 introduced the methylmalonyl pathway as a point of convergence between mitochondrial metabolism and DNAm that shapes both metabolic and epigenetic remodelling during neurodevelopment. Notably, this pathway comprised three of the eight mitochondrial pathways that were differentially regulated in our ASD cohort. Among the significantly

DM genes was PCCB, one of two subunits comprising a central enzyme in the methylmalonyl pathway involved in the conversion of propionyl CoA to succinyl CoA during TCA cycle anaplerosis (Wongkittichote, Ah Mew and Chapman, 2017). Our research group previously demonstrated the DM of PCCB using three independent methods – namely, the Illumina 450K Array, targeted next-generation bisulphite sequencing and pyrosequencing – and urinary metabolomic profiles revealed a significant dysregulation of metabolites directly associated with PCCB activity in our ASD cohort (Stathopoulos *et al.,* 2020). Moreover, a recent analysis of genomic, epigenomic and transcriptomic ASD datasets identified PCCB as one of 16 genes modulated by ASD-associated regulatory regions in both foetal and adult cortex tissue (Golovina et al. 2021). Therefore, this chapter establishes a model for mitochondrial dysfunction that recapitulates the dysregulation of PCCB *in vitro.*

Genetic mutations in PCCB are causally implicated in Propionic Acidemia (PA), a primary metabolic disease characterised by an accumulation of propionyl CoA that results from a PCC deficiency (Wongkittichote, Ah Mew and Chapman, 2017). *In vivo,* up to 50% of propionyl CoA is derived from BCAAs, while 30% comes from odd chain fatty acids (OCFAs) and cholesterol and 20% is produced by intestinal microbiota (Chandler *et al.,* 2011). At physiological levels, propionyl CoA is metabolised by PCC to produce succinyl-CoA, which is either oxidised in the TCA or used to fuel gluconeogenesis (Wilson *et al.,* 2017). However, at pathophysiological levels, toxic propionyl derivatives are known to cause lactic acidosis, hyperammonaemia, muscle weakness, cardiomyopathy and CNS dysfunction (Marchuk *et al.,* 2023). Interestingly, the neurological symptoms associated with PA are also widely observed in ASD, including cognitive deficits, seizures, dystonia, developmental delay and language impediments, and a relationship between PA and ASD has been demonstrated in the clinical literature (Witters *et al.,* 2016; de la Bâtie *et al.,* 2018; Shchelochkov *et al.,* 2024). Moreover, both PA and ASD manifest with immunological and gastrointestinal abnormalities, oxidative stress, mitochondrial dysfunction and decreased serum free carnitine, which is depleted by the conversion of propionyl CoA into propionyl-carnitine esters (Roginski *et al.,* 2020; Frye *et al.,* 2024). Therefore, establishing a model to study the relationship between PCCB-associated mitochondrial dysfunction and neurodevelopment could not only yield insight into the mitochondrial component of ASD aetiology, but also contribute to an understanding of the clinical convergence of PA and ASD more broadly.

Several preclinical models have been established to study PA pathophysiology, each best suited to address different aspects of the disease phenotype. Targeted genetic disruptions are ideal for the study of specific genotype-phenotype associations, but *in vivo* and patient-derived models are limited with respect to species- and cell-specific mechanisms. Genetic knockout models of PCC deficiency are constrained by neonatal fatality *in vivo*, while even hypomorphic murine models only partially recapitulate disease physiology, particularly given species-specific differences in the metabolism of PCC substrates and the expression, regulation and activity of the PCC enzyme itself (Collado *et al.,* 2020). Patient-derived cell lines are useful species-specific alternatives, but these have historically been

restricted by the accessibility of relevant tissue. Most studies have resorted to patient-derived fibroblasts, which typically display low levels of PCC substrates, while hepatocytes have been used to model a more metabolically active tissue with a higher energy demand (Chapman *et al.,* 2016; Collado *et al.,* 2020). However, small patient populations, high rates of post-natal mortality and ethical considerations associated with brain tissue biopsies create significant barriers to the study of neuronal-specific mechanisms in patient-derived primary cell lines.

As such, propionic acid (PPA) is widely used as an alternative model for PA pathophysiology. *In vitro,* PPA is metabolised to propionyl CoA via propionate-CoA transferase (PCT), which reflects the accumulation of propionyl derivatives induced by PCC deficiency (Frye *et al.,* 2015). Notably, several lines of evidence suggest a central role for PPA derivatives in PA pathophysiology: i) PPA readily crosses the gut-blood, blood-brain, and placental barriers (Joon, Kumar and Parle, 2023); ii) PA patients develop normally *in utero*, likely due to the activity of maternal PCC; iii) PA symptoms are managed primarily by reducing propionate load and iv) liver transplants can improve clinical outcomes but fail to negate pathology due to the sustained elevation of propionyl metabolites (Park *et al.,* 2020). Moreover, a growing body of literature demonstrates that PPA administration recapitulates metabolic, neurological, immunological and behavioural aspects of PA aetiology. Studies in patient-derived cell lines and *in vivo* models for PCC deficiency illustrate impairments to TCA metabolism, ETC activity and mitochondrial function, as well as mtDNA depletion, altered mitochondrial morphology, impaired glucose, AA and lipid metabolism and increased oxidative stress (Anzmann *et al.,* 2019; Wajner, Vargas and Amaral, 2020; Marchuk *et al.,* 2023). Similarly, PPA has been shown to disrupt TCA cycle flux, impair fatty acid and glucose oxidation, and increase intracellular lactate, ROS and apoptosis (Khalil *et al.,* 2015; Wang *et al.,* 2018; Roginski *et al.,* 2020).

In addition, both clinical and preclinical studies suggest a link between PPA and ASD aetiology. Clinical data demonstrates significant changes to the composition of gut microbiota associated with PPA production in ASD, which is considered a promising therapeutic target to mitigate ASD-associated behaviours (Liu *et al.,* 2019; Ho *et al.,* 2020; Iglesias–vázquez *et al.,* 2020; Lin *et al.,* 2022; Prosperi *et al.,* 2022; Lagod and Naser, 2023). Moreover, *in vivo* studies have shown that PPA consistently induces neurophysiological and behavioural aspects of ASD aetiology, to the extent that PPA has become a well-established preclinical model for ASD. Pioneered by MacFabe *et al.,* (2007), the PPA murine ASD model is associated with impaired cognition, memory, sociability and motor function as well as increased hyperactivity, stereotypy, perseveration, anxiety and seizures (El-Ansary, Bacha and Kotb, 2012; Shultz and Macfabe, 2014; Joon, Kumar and Parle, 2023). Concurrently, PPA has been found to disrupt gross neuronal morphology, neuronal organisation, dendritic spine maintenance, neurotransmission, synaptic gap junction signalling, neuroimmune state and redox homeostasis (Nankova *et al.,* 2014; Choi *et al.,* 2018, 2020; Sylla *et al.,* 2020; Khera *et al.,* 2022; Joon, Kumar and Parle, 2023).

However, researchers have yet to fully elucidate the mechanisms that mediate the neurotoxic effects of PPA, particularly as it pertains to the regulation of neurodevelopment. *In vitro* studies have facilitated more targeted questions in neuronal models (Nankova *et al.,* 2014; Abdelli, Samsam and Naser, 2019; Choi *et al.,* 2020), including a small but growing body of work in the SH-SY5Y cell line (El Ansary, Abu Shmais and Al Dbass, 2013; Hu *et al.,* 2018; Kim *et al.,* 2019; Filippone *et al.,* 2020; Jung *et al.,* 2020). Previous studies have established that PPA exerts concentration-dependent effects on the metabolism and viability of SH-SY5Y cells, showing neuroprotective effects at low doses (0.1-10uM) (Hu *et al.,* 2018; Filippone *et al.,* 2020) while inducing mitochondrial dysfunction-driven apoptosis from 1-10mM (El Ansary, Abu Shmais and Al Dbass, 2013; Kim *et al.,* 2019; Jung *et al.,* 2020). Still, the relationship between mitochondrial dynamics, metabolism and function remains uncharacterised in this context. Chapter 1 emphasised that mitochondria are constantly adapting to intracellular demands as a balance between biogenesis, fission, fusion and mitophagy maintains a dynamic state of homeostasis (Wai and Langer, 2016). Yet, most experimental techniques rely on intrinsically reductionist end-point measurements of mitochondrial function that seldom reflect the multifaceted nature of upstream processes. As such, a multipronged approach using several complementary techniques is recommended for the study of mitostasis *in vitro* (Patergnani *et al.,* 2021).

This chapter establishes a model for PCCB-associated mitochondrial dysfunction using PPA in undifferentiated SH-SY5Y cells. This is achieved according to three primary objectives, namely to; i) successfully establish the PPA model in the SH-SY5Y system; ii) address existing gaps in the literature pertaining to the effect of PPA on metabolic state and iii) interrogate specific aspects of mitostasis with relevance for the metabolic regulation of neurogenesis. To this end, a range of techniques are employed to characterise dose- and time-dependent effects on several interdependent facets of mitochondrial function **(Figure 2.1).** This work characterises how PPA influences the transcriptional, morphological and metabolic mechanisms that govern mitostasis in neuronal-like cells. Together, this chapter contributes to current understandings of SH-SY5Y metabolism, informs future studies on the neuropathology of PA in the SH-SY5Y cell line, and lays the foundation for studies on the relationship between metabolism and neurogenesis in subsequent chapters.

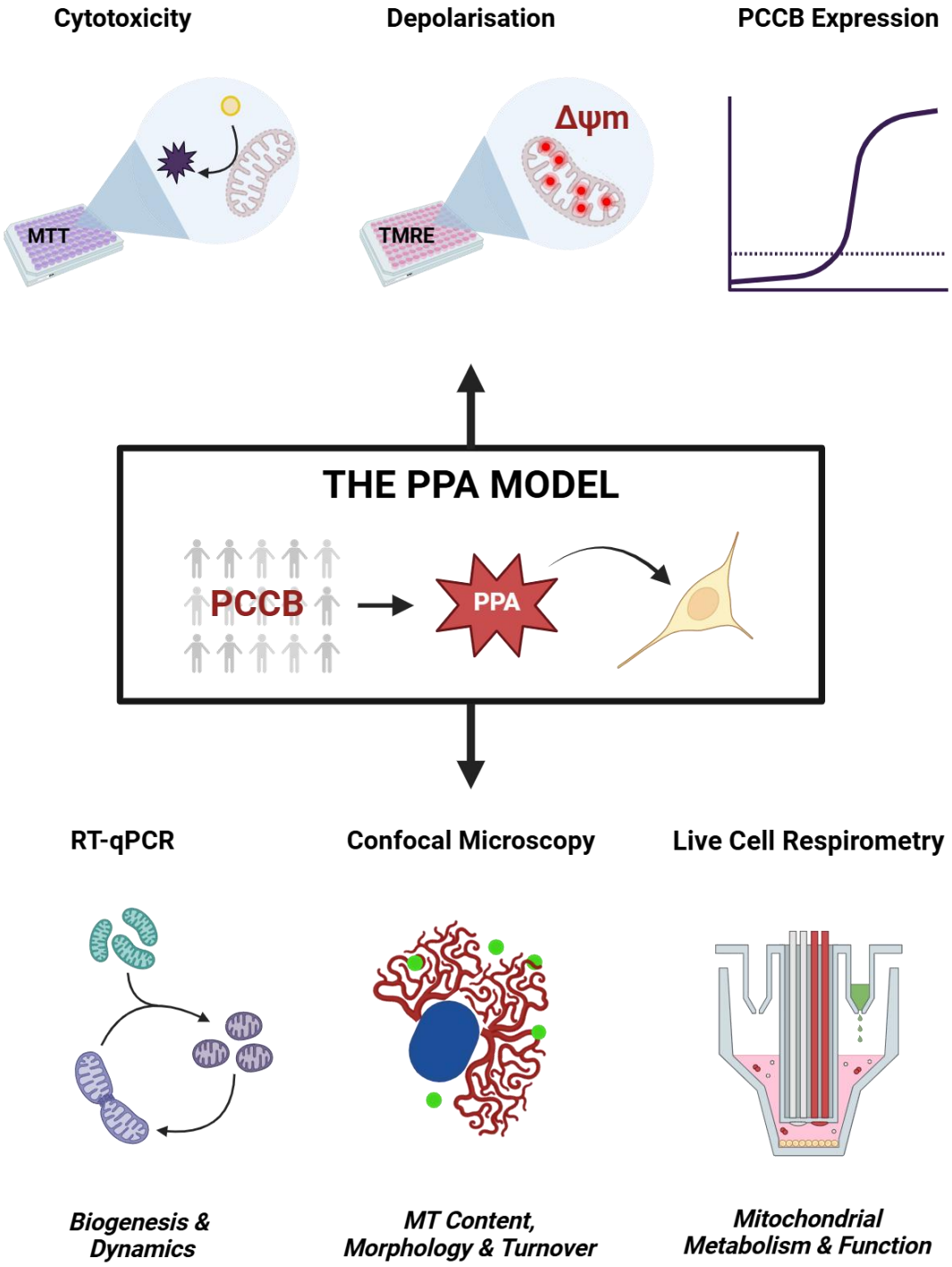


Figure 2.1. Studying Mitostasis *In Vitro*. A model for mitochondrial dysfunction was established in SH-SY5Y cells using propionic acid (PPA) to recapitulate the differential methylation of Propionyl CoA carboxylase B (PCCB) in an Autism Spectrum Disorder cohort. Windows of cytotoxicity associated with PCCB-dependent mitochondrial dysfunction were established using cell viability and mitochondrial membrane potential (ΔΨm) assays in conjunction with reverse transcription quantitative polymerase chain reactions (RT-qPCRs). This model was used to measure the transcriptional dysregulation of central genes involved in mitochondrial biogenesis and dynamics, which were functionally validated using confocal microscopy to quantify mitochondrial content, morphology and mitophagic flux. Downstream changes to metabolic state were determined using Seahorse live cell respirometry assays to measure oxidative and glycolytic ATP production. MTT - Thiazolyl Blue Tetrazolium Bromide; TMRE - tetramethylrhodamine, ethyl ester.

2.2. Methodology

2.2.1. Neuronal Cell Culture

The SH-SY5Y cell line (ECACC, 94030304-1VL) was obtained from Sigma-Aldrich at p12 and a cell bank of <33 vials between p14-p19 was established using the protocol recommended by the manufacturer. For cell-line maintenance and sub-culturing, cells were grown in a 1:1 ratio of DMEM (Thermo Fisher Scientific, 41965039) and Hams F12 (Thermo Fisher Scientific, 11765054) with 1% Penicillin-Streptomycin (Thermo Fisher Scientific, 15140122), and 15% Foetal Bovine Serum (FBS) (Thermo Fisher Scientific, 10493106) at 5% CO2 and 37°C in a NUAIRE 4750E incubator (serial #N162864042114). Cells were sub-cultured at 85-95% confluency at a 1:5 ratio using 0.05% Trypsin-EDTA (Sigma Aldrich, T3924-100ML) followed by a three-minute centrifugation at 1000 rpm (Hermile Z446 centrifuge, serial # 79A2000009). Cells from p14-p19 were cryopreserved in 1mL complete DMEM, 5% Dimethyl Sulfoxide (DMSO) at -80°C at a concentration of approximately 1 x 10^6 cells/mL. Since high passage numbers are known to increase the S-type: N-type ratio in the SH-SY5Y line, all cells used for subsequent experiments were between p19-22 and were adapted to Eagle's Minimum Essential Media (EMEM) (Thermo Fisher Scientific, BoC 1-31S01-I): F12 at a 1:1 ratio to Ham's F12 with 1% PS, 15% FBS, 1% non-essential amino acids (NEAA) (Inqaba Biotechnical Industries, SC 0823) and 200mM L-glutamine (Inqaba Biotechnical Industries, BoC 5-10K00-H) at least one passage before seeding. Propionic Acid (PPA) was administered in the form of sodium propionate (C3H5NaO2, CAS # 137-40-6) (Sigma-Aldrich, P5436-100G) by dissolving 0.096g in 10mL pre-warmed sterile MilliQ water to form a 1M stock solution which was filtered through a 0.22mm filter and stored at 4°C for no longer than four weeks before use. All tissue culture workflows were conducted in a sterile Biosafety Level 2 laboratory equipped with an ESCO Biosafety Cabinet, Model AC2-451.

2.2.2. Characterisation of Cytotoxicity

To characterise the profiles of cytotoxicity associated with PPA in the SH-SY5Y cell line, Thiazolyl Blue Tetrazolium Bromide (MTT) (Sigma-Aldrich, M5655-500MG) was used to measure total cellular reduction potential under a range of different treatment conditions. An initial series of experiments in DMEM: F12 explored broad windows of cytotoxicity from 1 – 500mM PPA over 30 minutes to two hours. Having established an acutely cytotoxic effect at supraphysiological concentrations, the effect of a 24-hour exposure to pathological concentrations from 3-5mM was investigated using both MTT reduction and ATP production to assess cell viability. Finally, treatment concentrations in complete EMEM: F12 were further titrated between 3-10mM over 4-72 hours after a 24-hour FBS depletion. These concentrations were informed by previous studies in SH-SY5Y cells (Afaf, Ghada and Abeer,

2013; Hu *et al.,* 2018; Kim *et al.,* 2019; Filippone *et al.,* 2020; Jung *et al.,* 2020) as well as plasma concentrations of PPA reported in PA that can reach up to 5mM (Roginski *et al.,* 2020).

In order to employ the MTT assay as a measure of cell viability, the influence of seeding density, MTT concentrations, incubation times and cell proliferation was considered in line with the recommendations made by Ghasemi et al. (2021). Cells were seeded in clear 96-well plates (Sigma-Aldrich, M0812-100EA) at 5 x 10^5 per well in 200uL per well. After an overnight incubation in complete EMEM: F12, cells underwent 24 hours of FBS depletion before treatment. On the day of the assay, cell media was replaced with 0.5mg/mL MTT diluted in serum-free media from a stock solution of 5mg/mL in MilliQ water. After a two-hour incubation in the dark at 5% CO2 and 37°C, the MTT solution was carefully removed and 100uL of DMSO was used to dissolve the formazan crystals in each well. After shaking the plate for 10 minutes, the absorbance was measured at 570nm using an absorbance spectrophotometer microplate reader (Thermo Fisher Scientific, Multiskan™ GO, Serial number:110000010644). Each treatment was administered in triplicate, and each well was corrected against the average absorbance of DMSO-blanks. Relative cell viability was calculated as the average blank-corrected absorbance of all three triplicates normalised to the average of untreated controls.

Since MTT assays can be confounded by metabolic, redox and proliferative state, preliminary MTT assays were cross-checked using ATP production as a reflection of cell viability. For ATP assays, cells were seeded at 2.4 x 10^6 per well in white 96-well plates (BioSmart Scientific, #30196), allowed to adhere for 24 hours and treated with PPA for 24 hours. ATP concentrations were evaluated using the Luminescent ATP Detection Assay Kit (Biocom Africa, AB113849) according to the manufacturer's instructions. Briefly, cells were lysed using 50µL detergent and 50µL substrate solution per well and luminescence was read on the GloMax Luminometer (Promega, E5311), data was normalised against media-only blanks and standard curves in triplicate were used to convert relative luminescent units (RLU) to total ATP (µM) per well. Changes to cell viability and morphology were also cross-referenced by visualising live cells after 24, 48 and 72 hours of PPA exposure, using an Olympus CKX41 Inverted Microscope equipped with an NA0.30 Condenser Lens, CAch N 10X PhP and LCAch N 20X Ph1 objectives and a 6V 30W Lamphouse. Images were captured using Olympus Stream Start 2.5 build 24576 software in conjunction with a 0.5X camera adaptor.

2.2.3. Measurement of Mitochondrial Membrane Potential

To determine whether changes in cell viability were associated with mitochondrial dysfunction, mitochondrial membrane potential (ΔΨm) was measured in response to acute (four-hour) PPA treatment using the tetramethylrhodamine, ethyl ester (TMRE) assay (Thermo Fischer Scientific, T669). TMRE is a fluorescent cationic dye that diffuses through cell membranes due to its lipophilic nature and is hydrolysed to tetramethylrhodamine which accumulates in the negatively charged mitochondrial matrix in a manner that is proportional to ΔΨm (Connolly *et al.,* 2017). TMRE fluorescent signal can be

quantified using confocal microscopy, flow cytometry or fluorescence-based microplate assays. Live-cell confocal microscopy is the most sensitive technique to quantify TMRE signal at low concentrations; however, accurate quantification requires strictly matched periods of dye loading and light exposure between samples, which presents significant logistical challenges (Perry *et al.,* 2011). This approach is also more costly, time-intensive, and requires access to BSL2 facilities equipped with a high-resolution confocal imaging unit. In the absence of the required infrastructure, and with the aim of characterising a population-level dose-dependent response across a range of PPA concentrations, a microplate-based TMRE assay was optimised as a higher-throughput alternative.

Irrespective of the method of signal quantification, the relationship between fluorescent signal and ΔΨm depends on the experimental design and the concentration of TMRE used. Here, TMRE was added to cells after exposure to the relevant treatment, and fluorescence was measured as a single end-point marker of ΔΨm which typically necessitates the use of non-quenching dye concentrations between 1 and 30nM (Perry *et al.,* 2011). On the other hand, the manufacturers of microplate-based TMRE assay kits recommend concentrations ranging from 200 to 1000nM depending on the cell line used (Abcam 2016) and studies in SH-SY5Y cells routinely use TMRE at 100 – 1000nM in the same experimental paradigm (Dai *et al.,* 2015a, 2015; Waseem *et al.,* 2017; Tan, Zakharova and An, 2021; Zandona *et al.,* 2021; Vulin *et al.,* 2022). With reference to the aforementioned literature, both quenching and non-quenching concentrations from 30-500nM were tested in both negative (untreated) and positive (treated with the mitochondrial membrane decoupler carbonylcyanide-p-trifluoromethoxyphenylhydrazone or FCCP) controls. The upper limit of concentrations was determined in order to avoid the cytotoxic potential of TMRE at concentrations of 1000nM and higher (Perry *et al.,* 2011). In addition, different seeding densities, incubation periods and staining solutions were tested to identify the most reproducible conditions that accurately revealed a significant decrease in membrane potential in samples treated with 10-50μM FCCP for two or 24 hours **(Figure S2.1).** The positive control was chosen as the concentration at which cell viability was maintained while TMRE fluorescence was significantly decreased.

After optimisation of all relevant parameters, cells were seeded in clear 96-well plates at 5 x 10^4 per well in full EMEM: F12, allowing for one empty well between each sample to minimise signal cross-talk. After a 24-hour incubation and a 24-hour FBS depletion, cells were treated in triplicate with 0, 3, 5, and 10mM PPA for 4 hours or 25μM FCCP for two hours, both in serum-free EMEM. Subsequently, cells were incubated in 250nM TMRE for 20 minutes at 37°C, followed by a rinse with 0.2% bovine serum albumin (BSA, Inqaba Biotechnical Industries, GLS GE1877-50G) in 1X phosphate-buffered saline (PBS, pH 7.4). 100μL 0.2% BSA was added to each well, including blanks, before fluorescence was measured on a GloMax-Multi Detection System (Model E7801, Anatech, 2014, Serial number:518130957) using the green fluorescent filter (Ex 525, Em 580~640nm). Each sample was rinsed once with 1X PBS before being lysed in 50μL 250mM Tris/ 0.1% Triton X-100 for 20 minutes at room temperature. Subsequently, lysates were diluted 1:2 to reach a final concentration of 0.05%

Triton-X 100 before being transferred in duplicate to a fresh 96 well plate. 150µL of Bradford reagent (Lasec Pty, BBRD5000201) was added to each well, and samples were mixed and incubated for 5 minutes. Absorbance at 595nM was measured on the Multiskan™ GO microplate reader, and protein concentrations were calculated from blank-corrected absorbance values according to a standard curve that was run in triplicate with each assay. For the sake of quality control and reproducibility, biological repeats were retained if total RFU and protein concentrations among technical replicates varied by less than 10%. Blank-correct TMRE fluorescence was normalised to protein concentration per well and membrane potential was calculated relative to untreated controls as per the equation described by the manufacturer, where $\%\text{TMRE signal} = \frac{(Sample - Blank)}{Untreated\ Control - Blank}\ x\ 100$.

2.2.4. Examining the Transcriptional Regulation of Mitostasis

To characterise the dynamic transcriptional responses to PPA, quantitative reverse transcription polymerase chain reaction (RT-qPCR) assays were used to study eleven genes involved in mitochondrial metabolism and dynamics. First, PCCB expression was measured to determine whether the PPA model recapitulated a dysregulation of PCCB *in vitro*. Subsequently, mRNA expression was measured for central genes involved in crosstalk between neuronal metabolism and maturation (*c-MYC, PGC1α*), mitochondrial biogenesis (*NRF1, Nfe2l2, TFAM*), fission (*DRP1*) or fusion (*MFN1, MFN2, STOML2, OPA1*). SH-SY5Y cells were seeded in 6-well plates at 3 x 10^5 per well in complete EMEM: F12 and allowed to adhere for 24 hours. The next day, cells were subject to 24 hours of FBS depletion before a series of 72-hour, 24-hour and four-hour treatments at 0,3,5 and 10mM PPA. RNA was extracted using the Quick-RNA™ Miniprep (Inqaba Biotechnical Industries, ZR R1055) according to the manufacturer's instructions with minor modifications. Briefly, cells were washed once with 1X PBS before 300µL lysis buffer was added to each well. After 1 minute of scraping, the cells were transferred to an Eppendorf and RNA was extracted in accordance with the prescribed protocol. RNA was eluted in 25µL DNAse/RNAse-free water and quantified using a NanoDrop ND-1000 UV-Vis Spectrophotometer (Inqaba Biotechnical Industries, Model ND1000, Serial number:2511) before storage at -80°C until further analysis.

All RNA samples used for RT-qPCR analysis had a concentration ≥ 95ng/µL and A260:280 / 260:230 ratios between 1.8-2.2. The cDNA synthesis was performed using the Tetro™ cDNA Synthesis Kit (Celtic Molecular Diagnostics, BIO-65043) according to the manufacturer's instructions. A total of 700ng of RNA was added to each reaction, along with 0.5µL of oligoDT and 0.5µL Random Hexamer primers in a total of 20µL/reaction. cDNA was stored at -80°C for no longer than 7 days before use. RT-qPCR assays were run using a Rotor-Gene Q6-plex (QIAGEN RG, Serial Number: R0618110) in 10µL reactions comprising of 5µL Luna Universal qPCR Master Mix (Inqaba Biotechnical Industries, NEB M3003L) and gene-specific quantities of cDNA and primers made up in sterile MilliQ water. The primers supplied by Inqaba Biotechnical Industries are detailed in **Table S2.1** along with the relevant

master mix and cycling conditions for each gene. Samples from between three and five biological repeats as well as standard curves were run in triplicate, and data was analysed using Rotor-Gene Q Software 2.3.5. All qPCR runs had efficiencies between 0.8-1.2 and R values between 0.90-1.2 respectively and the standard deviation between technical replicates was < 0.3. Relative expression was calculated using the delta delta Ct method where fold change in expression = $2^{-\Delta\Delta Ct}$ (Livak and Schmittgen 2001).

2.2.5. Evaluating Mitochondrial Content, Connectivity and Turnover

2.2.5.1. Mitochondrial DNA Copy Number and Deletions

Transcriptional disruptions to mitostasis can influence both the abundance and integrity of mtDNA (Sabouny and Shutt, 2021). Notably, changes to mtDNA copy number and deletions have been reported in a range of neuropsychiatric and neurodegenerative diseases (Tyrka *et al.,* 2016; Chung *et al.,* 2019; Czarny *et al.,* 2020), including ASD (Giulivi *et al.,* 2010; Gu *et al.,* 2013; Napoli, Wong and Giulivi, 2013; Chen *et al.,* 2015; Golzio and Katsanis, 2016; Yoo, Park and Kim, 2017; Varga *et al.,* 2018; J. I. Kim *et al.,* 2019; S. Liu *et al.,* 2021; Al-Kafaji *et al.,* 2023). Accordingly, mtDNA copy number and deletions are widely used as markers of mitochondrial function in both clinical (Castellani *et al.,* 2020; Li *et al.,* 2022) and preclinical (Rothfuss, Gasser and Patenge, 2010; Al-Kafaji and Golbahar, 2013; Burgueño *et al.,* 2013; Masser *et al.,* 2016; C. Liu *et al.,* 2019; S. A. Kim *et al.,* 2019; H. Wang *et al.,* 2021; Jang, Lee and Kim, 2021; Wasner *et al.,* 2022) studies.

Here, qPCR of the mitochondrial NADH dehydrogenase genes (ND1 and ND4) and the nuclear reference gene β2M was used to measure mtDNA copy number and deletions. Prior to treatment, cells were seeded at a density of 5 x 10^5 cells per well in sterile 6-well plates (Thermo Fischer Scientific, 140675) in complete EMEM: F12 for 24 hours. Following an additional 24-hour FBS-depletion, cells were treated with 0, 3, 5, and 10mM PPA in serum-free media for 72 hours. On the day of extraction, cells were washed once with 1X PBS before 300µL lysis buffer (Saline/EDTA; 10mM EDTA, 40mM NaCl, pH8) was added to each well and samples were incubated for 10 minutes at 37°C. Each well was scraped for one minute using sterile cell scrapers (Biosmart Scientific, 90021) before cells were transferred to a clean Eppendorf and lysed with 10% SDS and 20mg/ml Proteinase K at 56°C for 2 hours. Proteins were removed with 6M NaCl at room temperature for one hour and samples were centrifuged at 10 000 rpm (Eppendorf – Netheler – Hinz 5426 centrifuge, Serial number 542601273) for 10 minutes at room temperature. The supernatants were transferred to a fresh Eppendorf and the centrifugation step was repeated before samples were mixed with 1mL isopropanol and incubated overnight at -20°C. Subsequently, samples were centrifuged at 10 000 rpm for 20 minutes before the pellet was washed with 70% ethanol and centrifuged for 20 minutes at 10 000 rpm. After pellets were air-dried for 1 hour, DNA was eluted in 20µL TE buffer (10mM Tris; 1mM EDTA; pH8) and samples

were quantified using a NanoDrop ND-1000 UV-Vis Spectrophotometer (Inqaba Biotechnical Industries, Model ND1000, Serial number:2511) and stored at -20°C until subsequent analysis.

All samples with A260:280 and 260:230 ratios between 1.8-2.2 and 1.5-2.1 respectively were diluted in MilliQ water to 45ng/µL before downstream qPCR assays were run using a Rotor-Gene Q 6-plex (QIAGEN RG, Serial Number: R0618110) in 10µL reactions comprising of 5µL Luna Universal qPCR Master Mix (Inqaba Biotechnical Industries, NEB M3003L) and gene-specific quantities of DNA and primers made up in sterile MilliQ water. The primers for ND1, ND4 and β2M (Inqaba Biotechnical Industries) are detailed in **Table S2.1** along with the relevant master mix and cycling conditions for each gene. Samples from five biological repeats and standard curves were run in triplicate, and data was analysed using Rotor-Gene Q Software 2.3.5. All qPCR runs had efficiencies between 1.09-1.2 and R values between 0.98-1.2 respectively and the standard deviation between technical replicates was < 0.3. Mitochondrial copy numbers and deletions were quantified according to the protocol described by Quiros et al. (2017) using the $2^{-\Delta\Delta Ct}$ method where mtDNA copy number is calculated using ΔCt = Ct (MT-ND1) - Ct (β2M) and mtDNA deletions are calculated using ΔCt = Ct (MT-ND4) - Ct (MT-ND1).

2.2.5.2. Mitochondrial Network Morphology and Mitophagic Flux

Importantly, changes to mtDNA copy number may not reflect differences in biogenesis, but rather disruptions to mitochondrial turnover and clearance. Therefore, fluorescent probes in conjunction with confocal microscopy can be used to quantify mitochondrial volume. Here, visualisation techniques were used to examine mitochondrial network morphology and connectivity, while a multiplex immunocytochemistry assay was designed to quantify mitochondrial turnover (Redmann *et al.,* 2018). Microtubule-associated protein light chain 3 Beta (LC3β) functions at the intersection of autophagic and mitophagic flux as an essential component of the mature autophagosomes that degrade damaged mitochondria (Ashrafi and Schwarz, 2012). The colocalisation of LC3β puncta with fluorescently labelled mitochondria is an established method to assess mitophagy *in vitro* that has been widely employed in the SH-SY5Y cell line (Dagda *et al.,* 2009; Dai *et al.,* 2015; Dagda and Rice, 2017; Redmann *et al.,* 2018; Lawana *et al.,* 2020; Choi and Han, 2021; Patergnani *et al.,* 2021). Since mitochondrial membrane depolarisation specifically induces mitophagy without perturbing other aspects of autophagic flux (Ashrafi and Schwarz, 2012), FCCP or CCCP is used as a positive control in this context (Gómez-Sánchez *et al.,* 2014; Parganlija *et al.,* 2014; Berezhnov *et al.,* 2016).

Sample Preparation: SH-SY5Y cells were seeded in EMEM: F12 15% FBS at 1.5 x 10^5 per well on 12 x 0.16mm glass coverslips (Lasec SA, GLAS2C29M12RND) in 24 well plates. After allowing the cells to adhere for 24 hours, cells were exposed to a 24-hour FBS depletion before 72-hour and 24-hour 5mM PPA treatments were administered in serum-free media. On the day of staining, positive controls were treated with 25uM FCCP for 2 hours before all samples were stained with 300nM MitoTracker™ Red

CMXRos Dye (Thermo Fisher Scientific, M7512) for 30 minutes in the dark at 37°C. Subsequently, cells were rinsed twice with 1X PBS and fixed with 4% formaldehyde at room temperature for 20 minutes. After rinsing with 1X PBS to remove the fixative, samples were permeabilised with 0.5% Triton-X 100 for 20 minutes and blocked with 3% BSA for one hour at 4°C. Samples were then incubated overnight with monoclonal mouse IgG anti-human LC3β antibody (Thermo Fischer Scientific, MA5-31541) at a dilution of 1:200 in 0.3% BSA at 4°C. The next day, cells were rinsed twice with 1X PBS, followed by three five-minute washes and a 90-minute incubation with 1:1000 Goat anti-Mouse IgG Alexa Fluor Plus 488 (Thermo Fischer Scientific, A32723) in 1X PBS at 4°C. The wash step was repeated before each sample was stained with 250nM Dapi (Biocom Africa, 422801) for 10 minutes. After two rinses and three washes in 1X PBS, each sample was mounted using 7µL of Antifade Mountant (Thermo Fischer Scientific, S36972) and allowed to dry at room temperature for 2 hours before being stored in the dark at 4°C until imaging.

Samples were transported to the Central Analytical Facility (Stellenbosch University, Cape Town, SA) where they were imaged using a Carl Zeiss LSM780 AxioObserver Confocal Microscope equipped with Elyra PS1 super-resolution technology and Zen 2012 Software. After evaluating negative controls to ensure an absence of crosstalk between fluorescent spectra and non-specific binding of secondary antibodies (Figure S2.2), each region of interest (ROI) was visualised using the LCI Plan-Achromat 63X oil DIC M27 objective with an effective numerical aperture (NA) of 1.4. MitoTracker CMX was excited with a 561nm laser at 10% intensity and detected at 566-683nm at a gain of 750. The LC3 channel was excited with the Argon multiline laser 25mW at 488 nm and 2% intensity and detected at 499-552nm at a gain of 750. Lastly, Dapi was excited with the Diode 405nm CW/PS laser at 10% intensity and detected at 410-496nm at a gain of 800. All channels were detected using a GaAsP 32+2 PMT detector. Z stacks were captured as a series of 0.36µM slices using unidirectional line sequential scanning. A total of five ROIs were captured per sample, comprising at least 46 and up to 86 cells per condition for a total of 288 cells from three independent biological repeats.

Image Analysis: Image analysis was conducted in Fiji ImageJ according to the workflow depicted in **Figure 2.2.** OME Z stacks were converted into 8-bit .tif files and a maximum intensity projection (MIP) of all three channels was used to identify individual ROIs each containing one well-segmented cell. Each channel was separated and pre-processed independently using an optimised pre-processing protocol shown in **Figure 2.3.** First, the background was subtracted using a rolling ball of 10 pixels before the Iterative Deconvolve plugin was used to perform 10 rounds of deconvolution on each channel. Stacks were despeckled and smoothed before the unsharp mask filter was used with a radius = 1 and mask = 0.80 to improve signal: noise ratios. Processed images were thresholded using the Li thresholding algorithm and subsequently filtered to remove any particles less than 0.06µM.

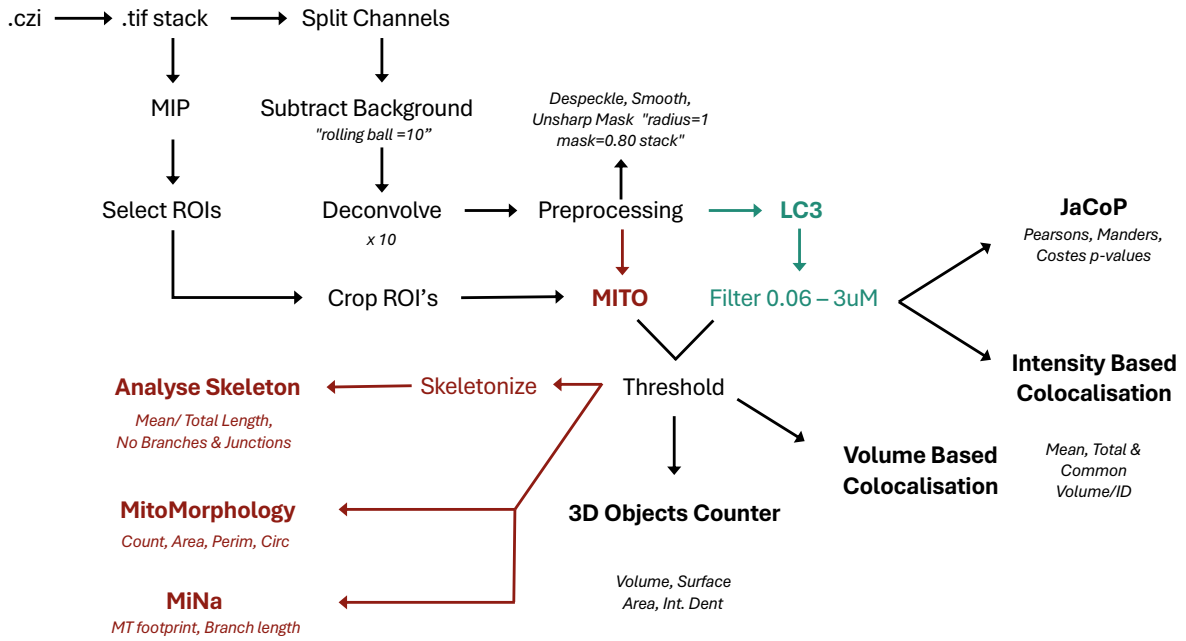


Figure 2.2. Image Analysis Workflow to Quantify Mitochondrial Content, Morphology and Turnover. Z-stacks were saved as .czi files and converted into .tif stacks before a composite maximum intensity projection (MIP) was generated to select and crop regions of interest (ROIs) each containing one well-segmented cell. Each .tif stack was divided into separate ROIs before channels were split, background was subtracted (rolling ball = 10 pixels) and the iterative deconvolve plugin was used to perform 10 rounds of deconvolution. Stacks were subject to a preprocessing protocol during which stacks were despeckled, smoothed and enhanced using an unsharp mask where the radius was set to 1 and the mask was weighted to 0.90. The MitoTracker channel (MITO) was thresholded and the filtered mask was skeletonised to measure branch length, branches and junctions. The thresholded mask was also analysed using the MitoMorphology and Mitochondrial Network Analysis (MiNA) plugins to evaluate mitochondrial count, area, perimeter, circularity and footprint. Both the grayscale and thresholded masks were used to measure mitochondrial volume, surface area and integrated density using the 3D Objects Counter plugin. Pre-processed LC3 stacks were filtered using a threshold of 0.06uM before thresholding, and the 3D Objects counter was used to measure total LC3 volume and integrated density. Colocalisation between MitoTracker and LC3 was measured using both volume-based and intensity-based colocalisation to calculate the ratio of common volume to total volume per channel, while the Just Another Colocalisation Plugin (JaCoP) was used to calculate the Pearsons, Mandes and Costes coefficients for colocalisation.

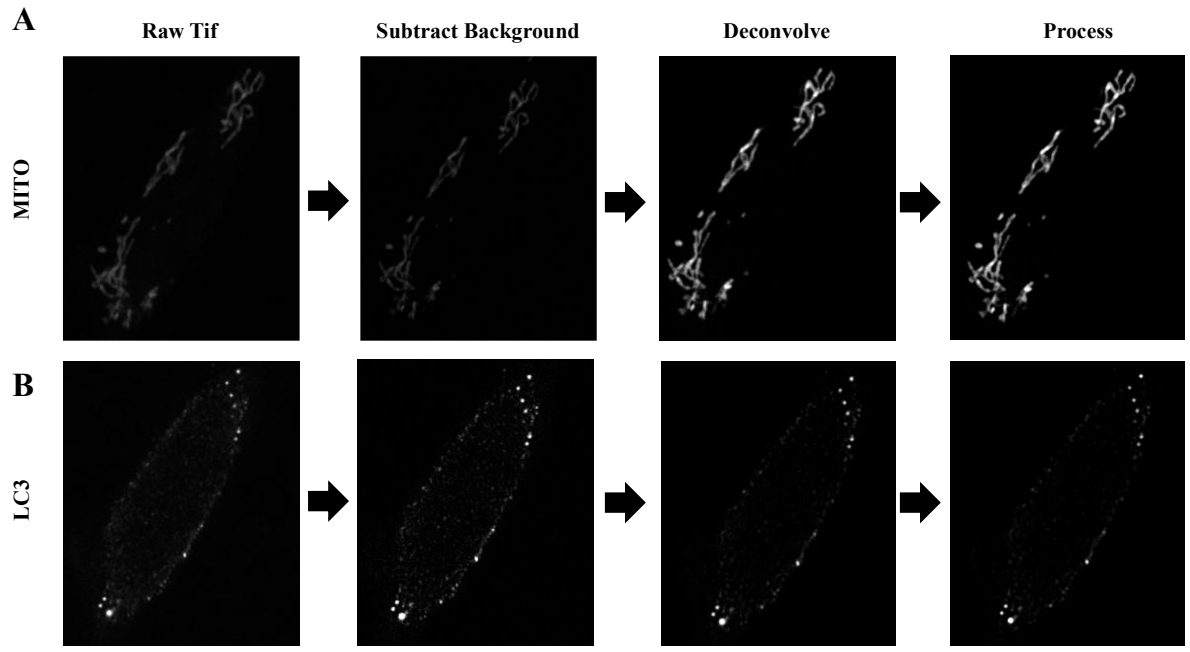


Figure 2.3. Image Pre-processing Pipeline. Representative slices of showing **A)** MitoTracker (MITO) and **B)** LC3β signal in raw .tif stacks, after subtracting background (rolling ball = 10 pixels), following 10 rounds of deconvolution using the Iterative Deconvolve plugin and after a pre-processing protocol employing despeckling, smoothing and enhancing with an unsharp mask.

A two-pronged approach was used to quantify mitochondrial content, morphology and connectivity based on the protocol described by Chaudhry, Shi and Luciani, (2020). This approach quantifies parameters related to mitochondrial size, shape and network complexity in both 2D slices and 3D stacks **(Figure 2.4A).** Thresholded 2D slices were examined using the "analyse particles" command to measure area, perimeter and circularity as well as the Mitochondrial Morphology macro developed by Dagda *et al.,* (2009) for a more comprehensive assessment of mitochondrial shape. Binarised slices were skeletonised and the "skeletonise 2D/3D" command was used to quantify and measure branches and junctions in the mitochondrial network. Similarly, 3D stacks were used to calculate an object map using the "3D object counter", followed by the "particle analyser 3D" command on the greyscale image to calculate volume, integrated density, surface area and sphericity. 3D skeletons were analysed from thresholded masks using the Mitochondrial Network Analysis (MiNA) plugin developed by (Valente et al. 2017). LC3 volume and expression were evaluated using the 3D particle analyser as described above, setting the minimum puncta volume to 10 voxels in line with the parameters used by Stauffer et al, (2018) (**Figure 2.4B).**

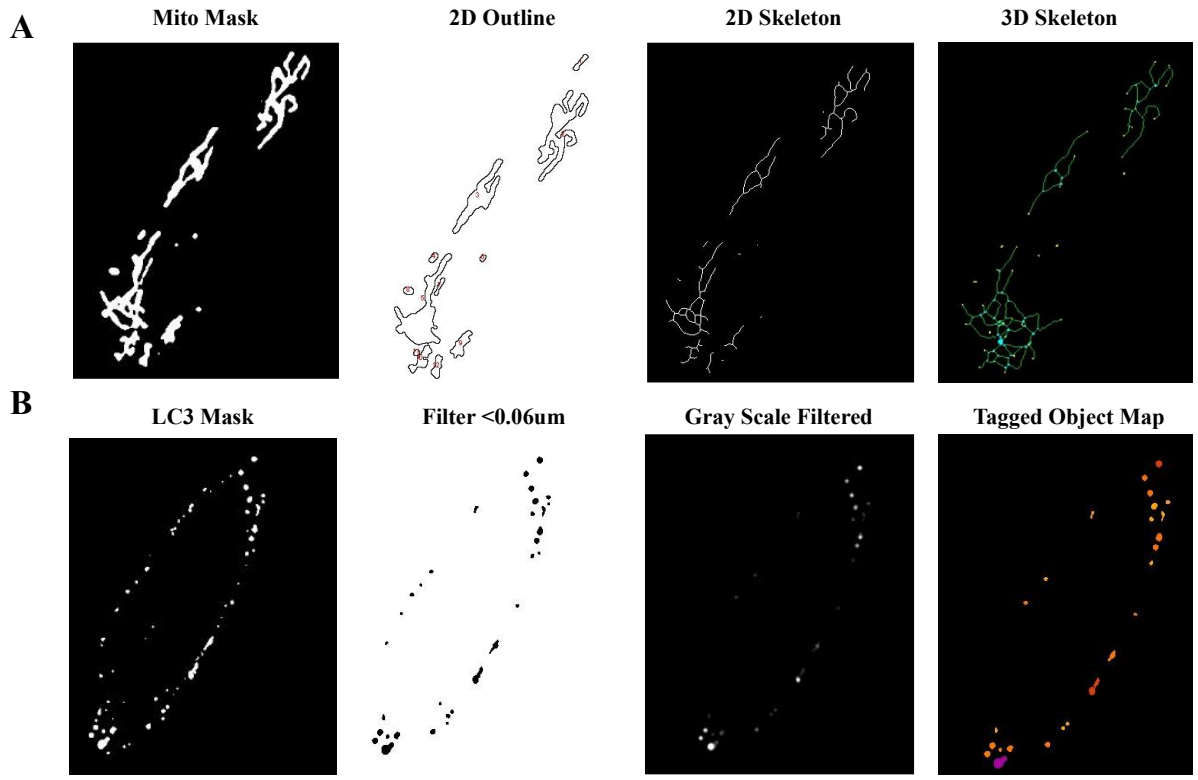


Figure 2.4. Quantification of Mitochondrial Content and LC3β Expression. A) Analysis of Mitochondrial Content and Morphology. Binarised masks were used to generate 2D outlines, 2D Skeletons and 3D skeletons using the MitoMorphology, Analyse Skeleton and Mitochondrial Network Analysis (MiNA) plugins respectively. **B)** Analysis of LC3β Volume. Binarised Masks were filtered to remove particles smaller than 0.06uM and volume was measured using the 3D objects counter plugin.

Subsequently, colocalisation of LC3 and MitoTracker was measured using both volume-based and intensity-based colocalisation approaches with two different macros to ensure that the results were internally consistent. First, the ImageJ JaCoP plugin (Bolte and Cordelières, 2006) was used to calculate Pearsons, M1 and M2 colocalisation coefficients using Costes thresholding. Secondly, the macro developed by Cordelières and Zhang, (2020) for 3D quantitative colocalisation analysis was adapted to calculate volume-based and intensity-based colocalisation coefficients **(Figure 2.5).**

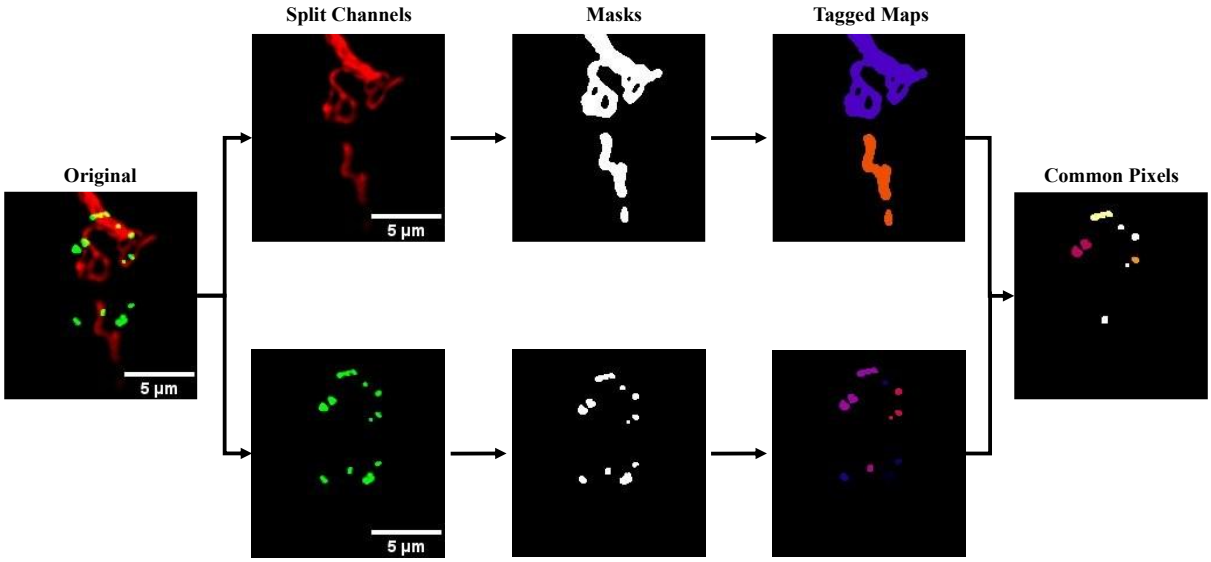


Figure 2.5. Colocalisation Analysis Workflow (Based on Cordelières & Zhang, (2020)). Original .tif stacks from each channel were converted into binarised masks that were used to generate a common mask containing only areas of colocalisation. The common pixels mask was overlayed with tagged object maps for each channel to calculate the volume and integrated density for all objects relative to common objects.

2.2.6. Live Cell Respirometry to Measure Metabolic Flux

Changes to gene transcription and mitochondrial morphology may suggest disruptions to mitostasis, but do not provide measures of end-point metabolic state. Several metabolic parameters can be quantified to examine the relationship between ATP production, glycolysis and oxidative respiration – such as the levels of ATP, lactate, TCA cycle intermediates or the activity of different enzymes associated with distinct metabolic pathways. These methods are well-suited to a targeted examination of pathways of interest but are limited with respect to a more comprehensive characterisation of metabolic state. For example, metabolite analysis using LC-MS provides a static measurement at one point in time, while radiolabelling of specific substrates is both time- and cost-intensive (Radogna *et al.,* 2021). Conversely, luminescence- or absorbance-based assays that facilitate real-time analysis of enzymatic activity are low-throughput and expensive, allowing for the study of only one variable at a time (Johnson *et al.,* 2022).

The gold-standard method to measure cellular bioenergetics is live-cell respirometry using Seahorse technology to assess both oxidative and glycolytic metabolism. Using standardised assays developed by the manufacturers, this approach quantifies dynamic changes to metabolic flux in response to targeted disruptions, facilitating a comprehensive assessment of both basal metabolism and compensatory metabolic capacity. The disadvantage of live-cell respirometry is that it requires specialised technology, reagents and training which limits its accessibility. Although a 96-well Seahorse instrument was inaccessible, the Brombacher lab at UCT's Institute for Infectious Disease generously allowed me to use their recently acquired Seahorse XFp instrument. The Seahorse XFp employs 6-well

pairwise experiments between one case and one control in triplicate. Budgetary constraints allowed for one set of 12 plates to be used for cell characterisation, assay optimisation and experimental runs, which necessitated careful experimental design. However, the XFp miniplate creates a much smaller microchamber in which changes to oxygen consumption and proton efflux are measured, leading to improved sensitivity (Agilent Technologies 2021).

First, a series of cell characterisation experiments was carried out to establish the seeding density and cycling conditions at which oxygen consumption (OCR), extracellular acidification rate (ECAR) and minimum oxygen levels were within the parameters recommended by the manufacturers **(Table S2.2; Figure S2.3A, B).** Subsequently, titration experiments were conducted to identify the FCCP concentration at which maximal respiration is induced **(Figure S2.3C).** Optimised experimental conditions were used to first broadly characterise PPA-induced metabolic shifts using ATP Rate Assays, while subsequent MitoStress tests were conducted to examine different aspects of mitochondrial function. In each case, SH-SY5Y cells were seeded in 6-well plates at a density of 3 x 10^5 cells/mL in 2mL complete EMEM: F12 and allowed to adhere for 24 hours. The next day, media was replaced with serum-free EMEM: F12 for 24 hours before cells were treated with 5mM PPA in serum-free EMEM: F12 72 hours before the assay. The day before the assay, both treated and untreated cells were seeded in poly-D-lysine (PDL) coated XFp 6-well miniplates (Chemetrix, 103721-100) at 30 000 cells per well in 30µL of serum-free EMEM: F12 with or without 5mM PPA. After allowing cells to rest at room temperature for 30 minutes, each well was supplemented with an additional 50µL per well, moats were hydrated with sterile MilliQ water, and plates were incubated overnight at 5% CO2 37°C. The next day, media was replaced by 180µL per well of Seahorse XF DMEM (Chemetrix, 103575-100) supplemented with 200mM glutamine (103579-100), 100mM pyruvate (103578-100) and 100mM glucose (103577-100), all at pH 7.4. Seahorse cartridges, having been incubated in MilliQ water at 37°C overnight, were hydrated with pre-warmed calibrant and both XFp miniplates and cartridges were incubated in a non-CO_2 37°C incubator for 60 minutes before the assay. Cartridges were loaded according to the protocols detailed by the manufacturers and calibrated for 15 minutes while cell media was replaced with fresh XFp DMEM before being transferred to the Seahorse XF HS Mini Bioanalyser (Brombacher Research Group, Institute of Infectious Diseases, University of Cape Town).

ATP rate assays were conducted using the Seahorse XFp Real-Time ATP Rate Assay Kits (Chemetrix, 103591-100) according to the protocol detailed in **Table S2.3.** Briefly, the assay comprised three cycles of three measurements each at basal respiration, after the addition of 1.5µM oligomycin and finally after the addition of 0.5µM Rotenone/Antimycin A (Rot/AA). MitoStress Tests were performed as described above, with the exception of a 1.5µM FCCP (Biocom Africa, AB12008) treatment before the addition of Rot/AA **(Table S2.4).** Subsequently, protein normalisation was carried out using the Bradford assay described in **2.2.4**. Data was analysed using the Seahorse Analytics online platform, ensuring that each

run passed quality control checks related to basal respiration, pH, and oxygen availability for the duration of the assay.

2.2.7. Statistical Analysis

Data were analysed in GraphPad Prism v10.0.2 (San Diego, California USA). For confocal microscopy data, outliers were removed with the Robust regression and Outlier removal (ROUT) approach using the standard Q coefficient of 1%. All data were tested for normality using the Shapiro-Wilks Test before being evaluated for significance. All datasets comprising three or more conditions were analysed with one-way ANOVAs (parametric) or Kruskal-Wallis (non-parametric) tests and post-hoc Dunnet's multiple comparisons tests were conducted to evaluate significance while MitoStress Tests were analysed using two-tailed paired T-tests. P-values are annotated on the graphs as follows: *p<0.05, **p<0.01, ***p<0.001, and ****p<0.0001.

2.3. Results

2.3.1. Cell Viability and Metabolism

Mechanistic studies of metabolism generally rely on end-point measurements of mitochondrial function, but mitostasis is an intrinsically dynamic process. Although models of acute mitochondrial dysfunction (i.e., ETC inhibitors or mitochondrial membrane uncouplers) might be suitable to study primary mitochondrial diseases, a different approach is required to study disorders marked by subtle and systemic disruptions to mitostasis. To identify treatment conditions that could capture responses ranging from mitochondrial compensation to mitochondrial dysfunction, PPA doses and incubation periods were titrated in serial cell viability assays. The first aim of this chapter was to recapitulate the published model of PPA stress in SH-SY5Y cells. As such, initial experiments aimed to identify broad windows of cytotoxicity in DMEM: F12 to reflect the conditions most commonly reported in the literature.

Initial MTT assays conducted in DMEM found that acute (two-hour) PPA stress decreased MTT reduction to ~58% of untreated controls, while chronic (24-hour) treatment decreased MTT reduction to 82% and 67% at 3 and 5mM respectively **(Figure S2.4A).** Although the MTT assay is widely used to measure cell viability, this assay more strictly reflects cellular reduction potential, which can be confounded by metabolic, redox and proliferative state (Ghasemi *et al.,* 2021). In line with the approach employed by Kim *et al.,* (2019), the cytotoxicity profiles generated from the MTT assay were cross-referenced using intracellular ATP production as an alternative assessment of cell viability. ATP concentrations were significantly decreased to 85% of untreated controls after 24 hours at 5mM PPA **(Figure S2.4B, C).** However, this response was smaller in magnitude than detected using the MTT

assay, and ATP levels showed no changes at lower PPA doses. These results are consistent with previous studies in SH-SY5Y cells (El Ansary, Abu Shmais and Al Dbass, 2013; Kim *et al.,* 2019) and reveal a consistency between the MTT and ATP assays at higher PPA doses.

Since the MTT assay detected significant changes in viability at lower concentrations, subsequent experiments in EMEM: F12 used the MTT assay to establish the lower boundary of doses that did not compromise cell viability or reduction potential. Time course experiments were conducted to evaluate the effect of PPA on the viability, health and morphology of SH-SY5Y cells over 4, 24 and 72 hours, using a 2-hour treatment of 100μM FCCP as a positive control for cell death **(Figure 2.6A).** No significant changes in cell viability were detected from 4-24 hours, while 72 hours at 5 and 10mM decreased MTT reduction to 64% and 27% of healthy controls respectively. While these cytotoxicity profiles differ from the responses in DMEM: F12, this data is consistent with previous studies in EMEM: F12 that found no significant changes to SH-SY5Y cell viability after 24 hours up to10mM PPA (Filippone *et al.,* 2020). Thus, the cytotoxicity profiles of PPA in both DMEM and EMEM: F12 successfully recapitulate the responses reported in the literature.

Moreover, cell morphology was distinctly altered in a dose- and time-dependent manner that appeared to pre-empt significant cytotoxicity **(Figure 2.6B).** While control cells maintained in serum-free EMEM: F12 displayed a rounded tear-drop morphology, PPA induced a thickening and curving of cell bodies at low doses, while cells became elongated and spindle-shaped at higher doses. There was a noticeable accumulation of floating dead cells in cultures treated for 72 hours, which reflects the decrease in cell viability detected using the MTT assay. Moreover, cells treated with 5-10mM show a marked elongated morphology from 24 hours, preceding significant changes in viability. Cumulatively, the data suggests that PPA treatments less than 4 hours do not impact cell viability at any concentration, while doses <3mM retain viability and morphology until ~ 48 hours. From 5-10mM, morphological changes are detected from 24 hours and significant cytotoxicity is demonstrated at 72 hours. Together, these data suggest dose-dependent changes to cell viability under PPA stress, establishing windows of cytotoxicity for the SH-SY5Y system using EMEM: F12 to promote oxidative reliance.

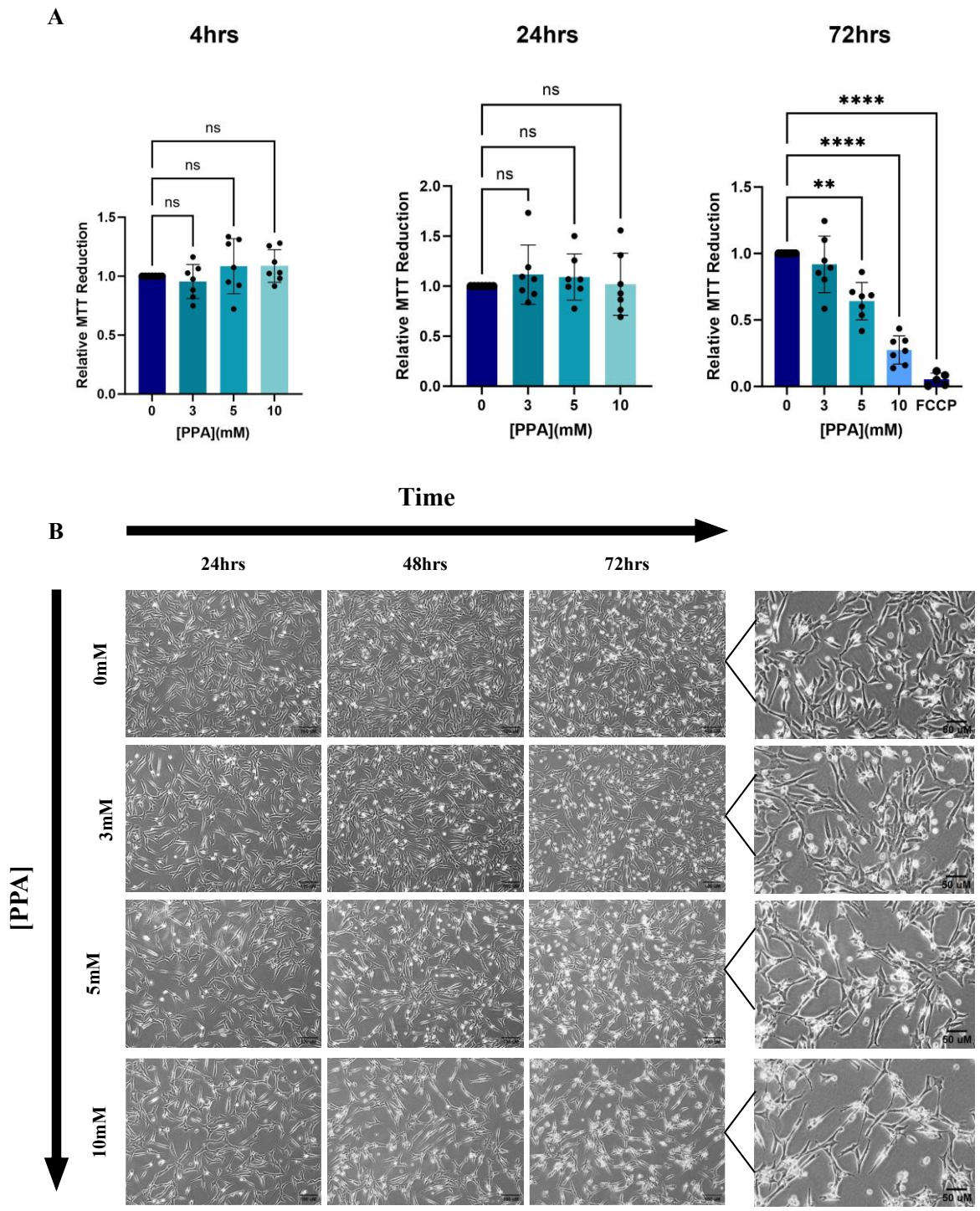


Figure 2.6. Propionic Acid-Induced Cytotoxicity in SH-SY5Y Cells. Undifferentiated SH-SY5Y cells were exposed to propionic acid (PPA) in EMEM: F12 for 4, 24 and 72 hours followed by MTT assays to establish windows of cytotoxicity. **A)** MTT assays revealed a time- and dose-dependent decrease in cell viability in response to 3-10mM PPA or 2 hours of 100µM FCCP as a positive control (n=7) where data represent mean and standard deviation. All experiments were conducted in triplicate and cell viability was calculated as the average blank-corrected absorbance of all three triplicates normalised to the average of untreated controls. Data were tested for normality using the Shapiro-Wilks test before significance was determined using one-way ANOVAs and Dunnet's Post-Hoc Comparisons where *p<0.05, **p<0.01, ***p<0.001, and ****p<0.0001. **B)** Morphological changes in undifferentiated SH-SY5Y cells exposed to PPA for 24, 48 and 72 hours were visualised using a light microscope at 20X magnification, revealing decreased cell density and elongated cell bodies with prolonged PPA exposure.

However, the nature of PPA-associated cytotoxicity cannot be inferred from MTT and ATP assays. More targeted approaches were required to evaluate whether PPA could be further explored as a model for PCCB-associated metabolic stress. Here, EMEM: F12 was employed as basal growth media for all subsequent studies using the approach described in **2.1.2**. One of the earliest signs of mitochondrial dysfunction *in vitro* is a loss of ΔΨm (Gorospe *et al.,* 2023), which is widely assessed using cationic fluorophores such as TMRE that load specifically in polarised mitochondria (Perry *et al.,* 2011). Using the ΔΨm uncoupler FCCP as a positive control, relative TMRE intensity showed a dose-dependent decrease after acute (four-hour) PPA treatment, with 10mM PPA reducing ΔΨm by 26% compared to untreated controls **(Figure 2.7A).** Notably, this effect is equivalent to the 23% decrease observed after two hours at 25μM FCCP and consistent with the decreased ΔΨm previously reported in SH-SY5Y cells exposed to PPA (Kim *et al.,* 2019).

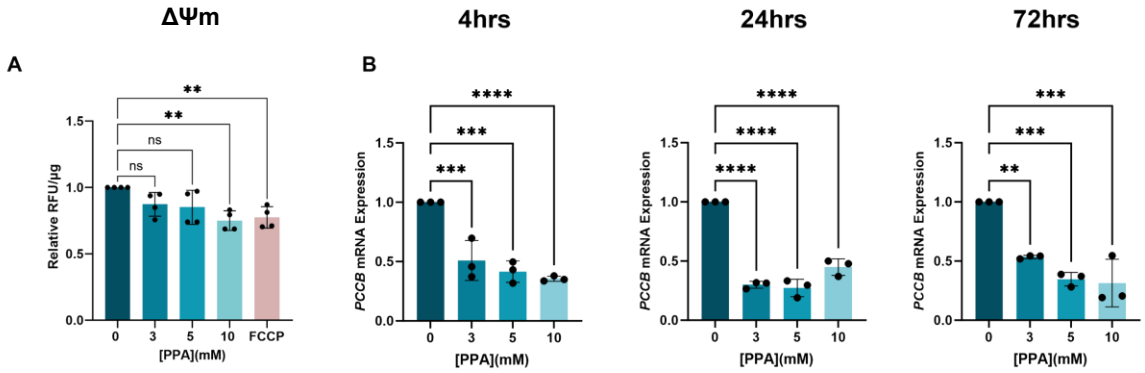


Figure 2.7. A Model for PCCB-Associated Mitochondrial Dysfunction. A) Acute exposure to PPA decreases mitochondrial membrane potential. Data represent relative TMRE fluorescence calculated from RFU/ug of protein according to the calculation described by the manufacturer where % ΔΨm = (treatment – blank) / (untreated control – blank). **B)** Propionyl CoA Carboxylase B (PCCB) mRNA expression measured by Reverse Transcription Quantitative Polymerase Chain Reaction (RT-qPCR) relative to β2M demonstrates an inhibition of PCCB transcription under PPA exposure. Data represent the fold-change in expression relative to untreated controls according to the ΔΔCT method ($2^{-\Delta\Delta CT}$). Each assay was performed in triplicate, data were tested for normality using the Shapiro-Wilks test before significance was established using one-way ANOVAs with Dunnet's multiple comparisons where **p<0.01, ***p<0.001, and ****p<0.0001.

While PPA is commonly used as a model for PA, the relationship between PPA and the regulation, expression and activity of the PCC enzyme itself remains poorly characterised. Here, the transcriptional profile of *PCCB* was measured to assess some degree of dysregulation to metabolic flux. In contrast to the profiles of cytotoxicity observed in Figure 2.7, PCCB expression was acutely inhibited under PPA stress, in a manner that appears neither dose- nor time-dependent **(Figure 2.7B).** Regardless of time or concentration, *PCCB* expression was reduced between 55-73% in response to PPA, reflecting an immediate and sustained disruption to the transcriptional regulation of metabolic flux. While the implications of *PCCB* transcription for PCC activity are unclear, the fact that PPA suppresses *PCCB* transcription in SH-SY5Y cells is a novel, and interesting, observation in this context that may reflect

a broad dysregulation of TCA cycle flux. Moreover, the decrease in *PCCB* expression at 4 hours coinciding with a loss of ΔΨm supports the utility of the PPA model to further study mitochondrial dysfunction associated with PCCB dysregulation *in vitro.*

Having established that acute PPA exposure induces a decrease in ΔΨm that compromises cell viability, specific aspects of mitochondrial function and homeostasis were examined using a three-pronged approach. First, PPA-induced disruptions to central transcriptional regulators of mitochondrial metabolism and dynamics were evaluated across a window of treatment conditions ranging from those with no effect on cell viability to those associated with significant cytotoxicity. Secondly, mitochondrial content, morphology and turnover were explored using mtDNA copy number and deletions in conjunction with confocal microscopy to visualise mitochondrial networks and autophagosomes. Lastly, metabolic state was assessed using live-cell respirometry to measure oxidative and glycolytic flux.

2.3.2. The Transcriptional Regulation of Mitostasis

To examine the relationship between PPA exposure and the transcriptional regulation of mitostasis, ten genes involved in mitochondrial metabolism (*PGC1α, c-MYC)*, biogenesis (*TFAM, NRF1* and *Nfe2l2),* fusion (*MFN1, MFN2, OPA1, STOML2*) and fission (*DRP1*) were evaluated across four PPA doses and three time points. These genes included four genes that were significantly DM in our ASD cohort - *PGC1α, DRP1, MFN2, STOML2* (Stathopoulos *et al.,* 2020; Bam *et al.,* 2021), and several transcription factors involved in cross-talk between metabolism and neurogenesis, including *c-MYC, TFAM, NRF1* and *Nfe2l2* (Zheng *et al.,* 2016; Beckervordersandforth, 2017; Cai *et al.,* 2021; Iwata and Vanderhaeghen, 2021). As master transcriptional regulators of mitochondrial metabolism and biogenesis, both *c-MYC* and *PGC1α* play an essential role in metabolic remodelling during neurodevelopment (Zheng *et al.,* 2016). Here, PPA induced a clear dose- and time-dependent decrease in *c-MYC* expression, with a 50% decrease in expression after 4 hours at 10mM that amounted to a 96% reduction after 72 hours **(Figure 2.8A).** *PGC1α* displayed a more complex transcriptional profile, with a consistent but highly variable increase in expression from 4-72 hours at higher PPA doses **(Figure 2.8B).**

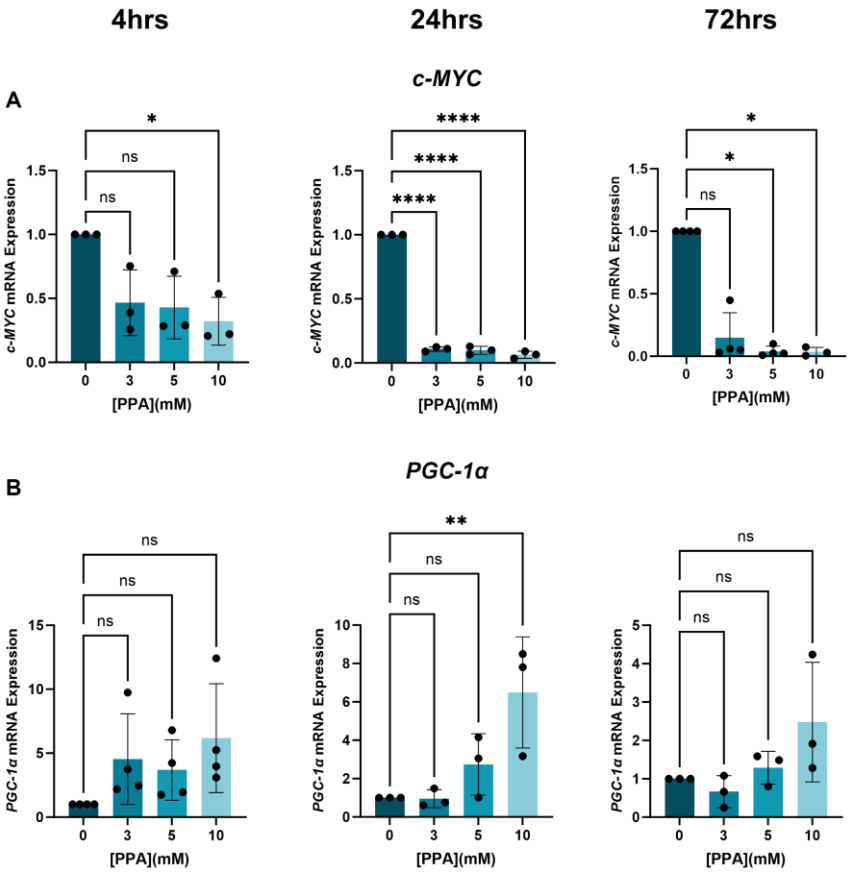


Figure 2.8. Master Metabolic Regulators Perturbed by Propionic Acid. Reverse Transcription Quantitative Polymerase Chain Reaction (RT-qPCR) was used to measure mRNA expression of **A)** c-MYC relative to β2M and **B)** PGC1α relative to 18S. Data represent the fold-change in expression relative to untreated controls according to the ΔΔCT method ($2^{-\Delta\Delta CT}$). Each assay was performed in triplicate, data were tested for normality using the Shapiro-Wilks test before significance was determined using one-way ANOVAs with Dunnet's multiple comparisons or Kruskal-Wallis test with Dunn's Post-Hoc Comparisons where *p<0.05, **p<0.01, ***p<0.001, and ****p<0.0001. c-MYC - c-MYC protooncogene; PGC1α - Peroxisome Proliferator-Activated Receptor Gamma Coactivator-1 Alpha.

Mitogenesis is essential for the maintenance of metabolic capacity under stress and serves as a compensatory mechanism to mitigate mitochondrial dysfunction (Al-Kafaji and Golbahar, 2013; Masser *et al.,* 2016; Zeng *et al.,* 2019). Canonically, mitochondrial biogenesis is mediated by the TFAM-NRF1 cascade that functions downstream of either PGC1α or Nfe2l2 in response to metabolic or oxidative stress (Jornayvaz and Shulman, 2010). However, this cascade can also be modulated by c-MYC, which functions as an independent regulator of mitochondrial transcription, translation and complex assembly (Morrish and Hockenbery, 2014). Here, the transcriptional profiles of *TFAM, NRF1* and *Nfe2l2* were characterised to further explore the regulation of mitogenesis in response to PPA **(Figure 2.9).** After 24 hours of PPA stress, a decreasing trend in expression was observed for all three transcriptional regulators, though *Nfe2l2* expression was not significantly impacted. Both *TFAM* and *NRF1* displayed a time-dependent response, where mRNA levels decreased by 60-70% after 24 hours at 10mM, reaching 75-82% inhibition by 72 hours.

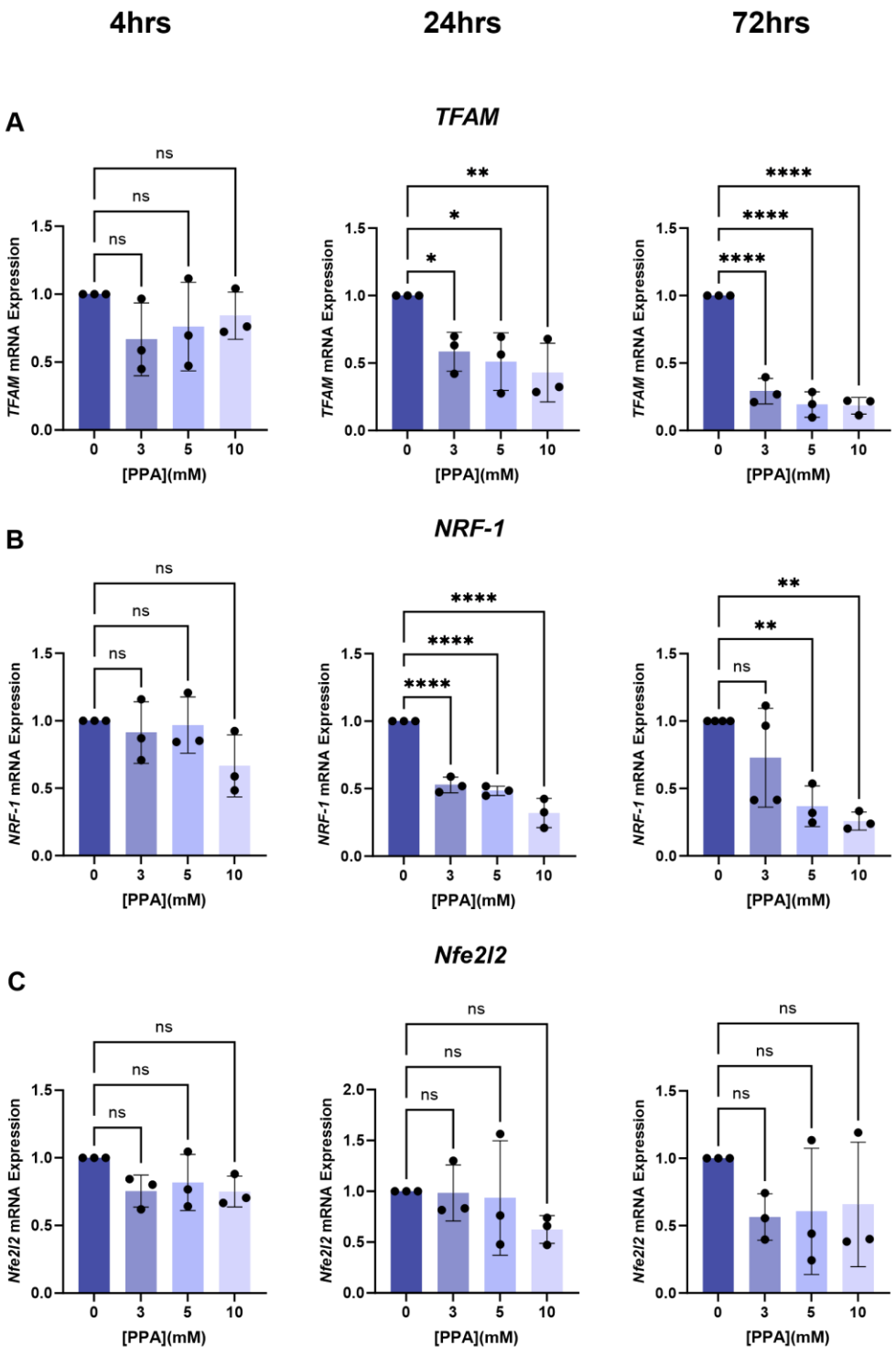


Figure 2.9. **Transcriptional Regulators of Mitogenesis.** Reverse Transcription Quantitative Polymerase Chain Reaction (RT-qPCR) was used to measure mRNA expression of **A)** TFAM, **B)** NRF1 and **C)** Nfe2l2 relative to β2M. Data represent the fold-change in expression relative to untreated controls according to the ΔΔCT method ($2^{-\Delta\Delta CT}$). Each assay was performed in triplicate, data were tested for normality using the Shapiro-Wilks test and significance was established using one-way ANOVAs or Kruskal-Wallis test with Dunn's Post-Hoc Comparisons with Dunnet's multiple comparisons where *p<0.05, **p<0.01, ***p<0.001, and ****p<0.0001. TFAM - Mitochondrial DNA Transcription Factor A; NRF1 - Nuclear Respiratory Factor 1; Nfe2l2 - Nuclear factor erythroid-derived 2-like 2.

Like mitogenesis, the dynamic remodelling of mitochondrial morphology and interconnectivity is an essential component of mitostasis. Under stress, fusion serves as a form of complementation by integrating dysfunctional mitochondrial components into functioning organelles, while fission facilitates the removal and clearance of damaged units in the mitochondrial network (Youle and Van Der Bliek, 2012). Mitochondrial network integrity is maintained by fission and fusion events driven by interactions between STOML2 and the dynamin-related GTPases MFN1, MFN2, OPA1 and DRP1 (van der Bliek, Shen and Kawajiri, 2013). Here, PPA-induced disruptions to mitochondrial dynamics were investigated via the transcriptional profiles of central regulators involved in mitochondrial fission, fusion and ultrastructure **(Figures 2.10** and **2.11).** The expression of *MFN1/2, DRP1, OPA1* and *STOML2* was significantly attenuated under PPA stress, though each gene displayed distinct patterns of expression over time. *MFN1* levels were not significantly disrupted until 72 hours, at which point a 50-60% decrease in expression was observed irrespective of PPA concentration **(Figure 2.10A).** *MFN2* expression was significantly decreased by 24 hours, but 72 hours was required for a dose-dependent effect to emerge, where expression was decreased by 50% at 3mM and ~70% from 5-10mM **(Figure 2.10B).** In contrast, *DRP1* expression exhibited a dose- and time-dependent decrease from 24 hours, where the 50% reduction at 10mM progressed to 60% after 72 hours **(Figure 2.10C).** Interestingly, both *OPA1* and *STOML2* showed similar patterns of expression, marked by a small but significant 30-40% decrease in expression after 4 hours, dropping further by 24 hours to a 70-75% reduction that was maintained through 72 hours **(Figure 2.11).** However, while *OPA1* levels were equivalent between different PPA concentrations, the expression of *STOML2* was modulated in a dose-dependent manner.

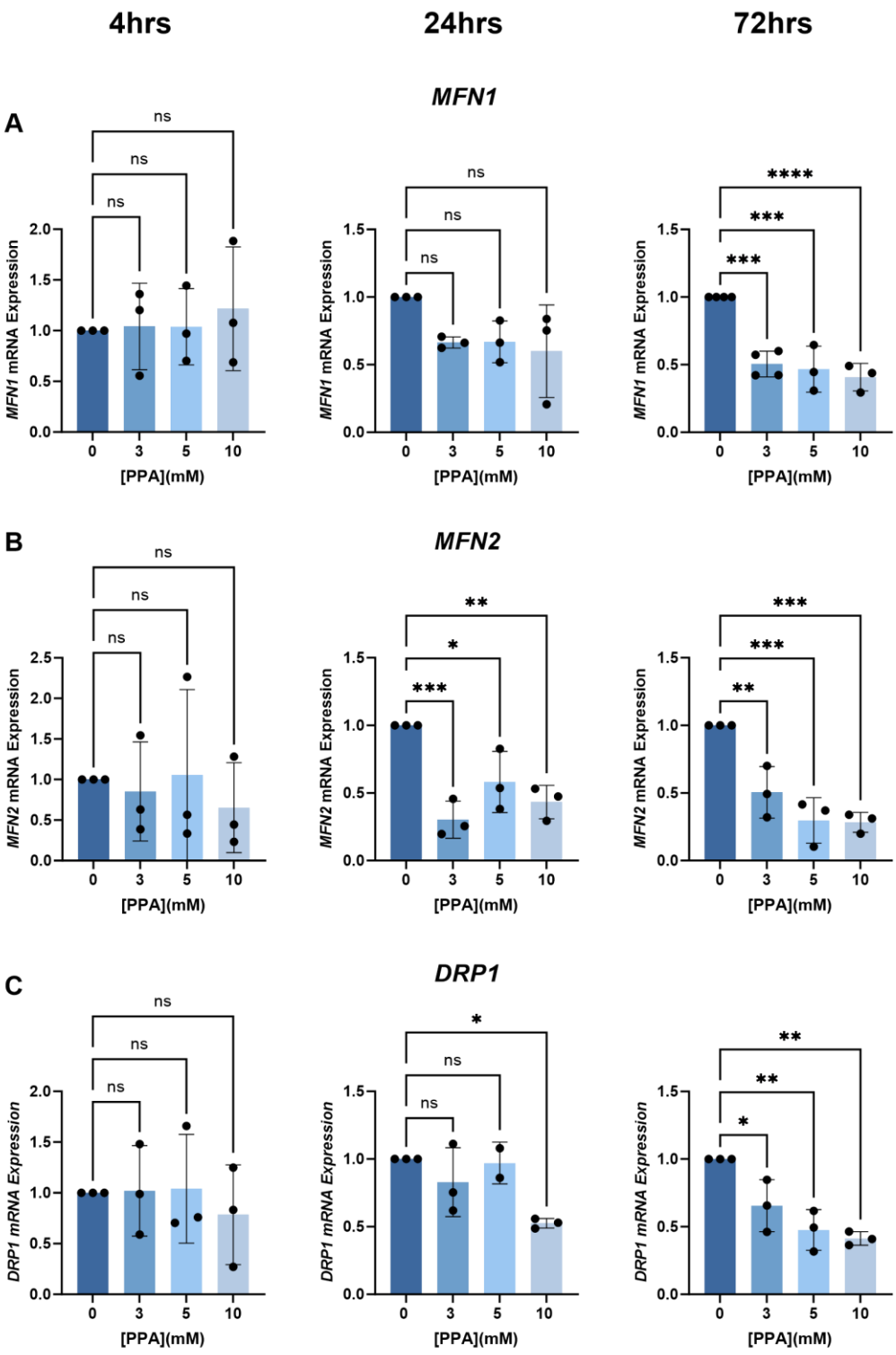


Figure 2.10. Canonical Regulators of Fusion and Fission. Reverse Transcription Quantitative Polymerase Chain Reaction (RT-qPCR) was used to measure mRNA expression of **A)** MFN1, **B)** MFN2 and **C)** DRP1 relative to β2M. Data represent the fold-change in expression relative to untreated controls according to the ΔΔCT method ($2^{-\Delta\Delta CT}$). Each assay was performed in triplicate, data were tested for normality using the Shapiro-Wilks test and significance was established using one-way ANOVAs with Dunnet's multiple comparisons or Kruskal-Wallis test with Dunn's Post-Hoc Comparisons where *p<0.05, **p<0.01, ***p<0.001, and ****p<0.0001. DRP1 - Dynamin-Related Protein 1; MFN1/2 – Mitofusin 1/2.

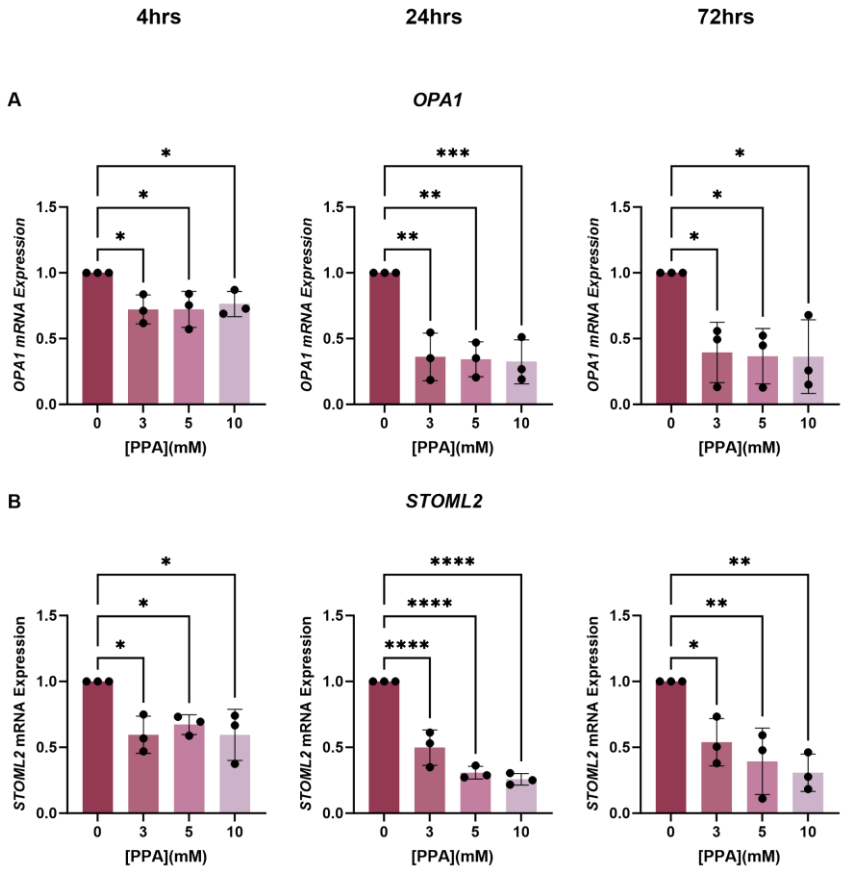


Figure 2.11. Central Modulators of Mitochondrial Morphology and Dynamics. Reverse Transcription Quantitative Polymerase Chain Reaction (RT-qPCR) was used to measure mRNA expression of **A)** OPA1 and **B)** STOML2 relative to β2M. Data represent the fold-change in expression relative to untreated controls according to the ΔΔCT method ($2^{-\Delta\Delta CT}$). Each assay was performed in triplicate, data were tested for normality using the Shapiro-Wilks test and significance was established using one-way ANOVAs with Dunnet's multiple comparisons or Kruskal-Wallis test with Dunn's Post-Hoc Comparisons where *p<0.05, **p<0.01, ***p<0.001, and ****p<0.0001. OPA1 - Optic Atrophy 1; STOML2 - Stomatin-Like Protein 2.

Of the eleven mitochondrial genes investigated here, three distinct transcriptional profiles emerged **(Figure 2.12).** *PGC1α* was the only gene to demonstrate significant upregulation in response to PPA, and while transcription levels vary, a consistent pattern of acute upregulation that is attenuated over time was observed at all PPA concentrations, where both the degree of initial upregulation and the subsequent rate of downregulation was dose-dependent **(Figure 2.12B).** In contrast, the other 10 genes of interest examined here were transcriptionally downregulated by PPA, although there is a separation between four early-responders and six late-responders **(Figure 2.12C-E).** *c-MYC* and *PCCB* showed the greatest degree of initial downregulation, but while *PCCB* expression stabilised after 24 hours, *c-MYC* was attenuated further with time. Like *PCCB, OPA1* and *STOML2* were acutely and significantly downregulated by hours, reaching a maximum level of 60% downregulation by 24 hours that was sustained to 72 hours. On the other hand, *TFAM, NRF1, MFN1/2* and *DRP1* displayed a more time-dependent response that took effect only after at least 24 hours of PPA exposure. While *TFAM, NRF1*

and *MFN1/2* were downregulated by 24 hours, *NRF1* expression appeared to stabilise at this point while *TFAM* and *MFN1/2* were further attenuated in a time-dependent manner. *DRP1* expression was less susceptible to PPA stress, only showing significant signs of inhibition after 72 hours of exposure, while *Nfe2l2* expression displayed more minor fluctuations at all time points.

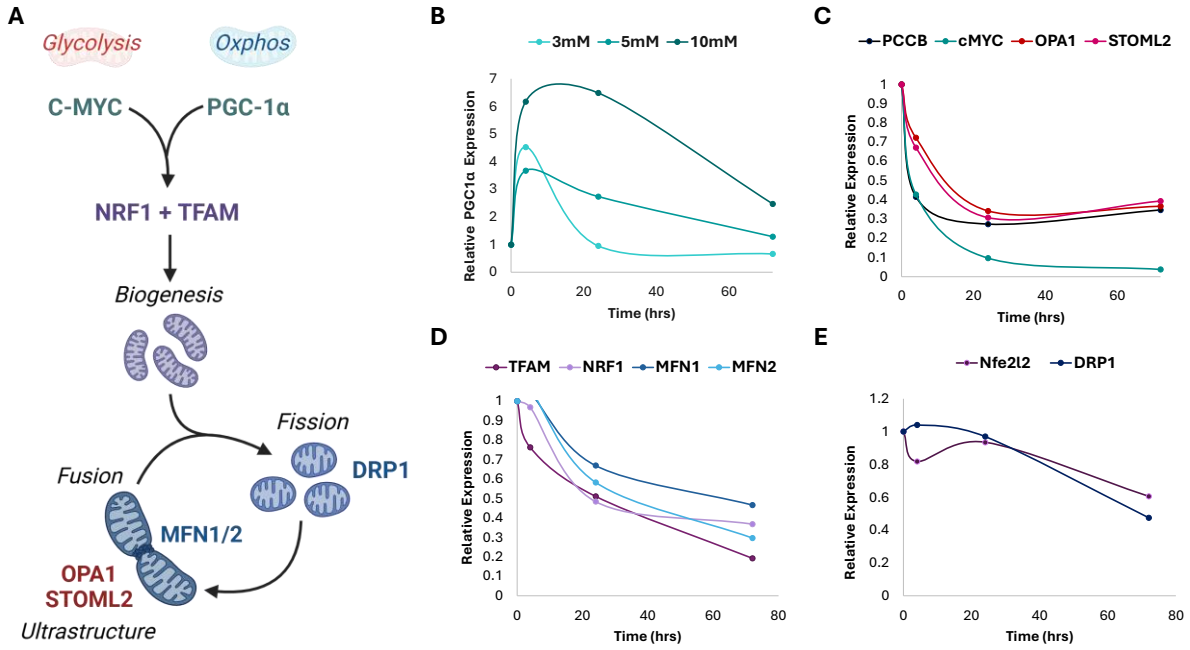


Figure 2.12. Transcriptional Disruptions to Mitostasis Induced by Propionic Acid. A) Transcriptional disruptions induced by Propionic Acid (PPA) stress converge on a dysregulation of mitochondrial biogenesis, dynamics and metabolism. **B)** PGC1α expression over time at 3, 5 and 10mM PPA. **C)** Early, **D)** Medium and **E)** Late responders show distinct patterns of downregulation over time at 5mM PPA. c-MYC – c-MYC protooncogene; DRP1 - Dynamin-Related Protein 1; MFN1/2 – Mitofusin 1/2; NRF1 – Nuclear Respiratory Factor 1; Nfe2l2 - Nuclear factor erythroid-derived 2-like 2; OPA1 – Optic Atrophy 1; PGC1α - Peroxisome Proliferator-Activated Receptor Gamma Coactivator-1 Alpha; STOML2 – Stomatin-like Protein 2; TFAM – Mitochondrial DNA Transcription Factor A.

Importantly, the transcriptional profiles of individual genes may not reflect acute changes to specific mitochondrial processes. Fission, fusion or biogenesis may be induced as an acute response to metabolic stress by activating or recruiting existing transcripts and proteins. Still, maintaining the pool of mRNA transcripts can be considered a prerequisite for the subsequent levels of regulation that shape mitochondrial dynamics. Thus, the data presented here may suggest that chronic PPA exposure depletes the mRNA levels of critical genes that maintain mitostasis, which could have implications for mitochondrial morphology, dynamics and metabolism.

2.3.3. Mitochondrial Morphology and Turnover

To examine whether transcriptional changes were associated with downstream disruptions to mitostasis, complementary RT-qPCR and immunocytochemistry assays were used to evaluate mitochondrial

content, morphology and turnover. The treatment conditions used for these experiments were based on the transcriptional profiles in section **2.2.2.** and a range of preliminary experiments that found no changes to mtDNA copy number after 24 and 48 hours of PPA stress (data not shown). After 72 hours at 3-10mM, neither mtDNA copy number nor the ND4:ND1 ratio used to assess mtDNA deletions was altered in response to PPA **(Figure S2.5).** However, confocal microscopy revealed subtle disturbances to mitochondrial content over time. Although 10mM PPA had the most substantial effect on both transcriptomic profiles and cell viability, 5mM was chosen to study a more intermediate response from 24-72 hours, with the aim of capturing different responses that occur both before and after significant cytotoxicity is observed. Quantifying mitochondrial content using two independent image analysis workflows showed that mitochondrial mass was retained until 24 hours under 5mM PPA stress, while mitochondrial volume, fluorescent signal, area, and mitochondrial footprint were decreased by 20-27% after 72 hours **(Figure 2.13).**

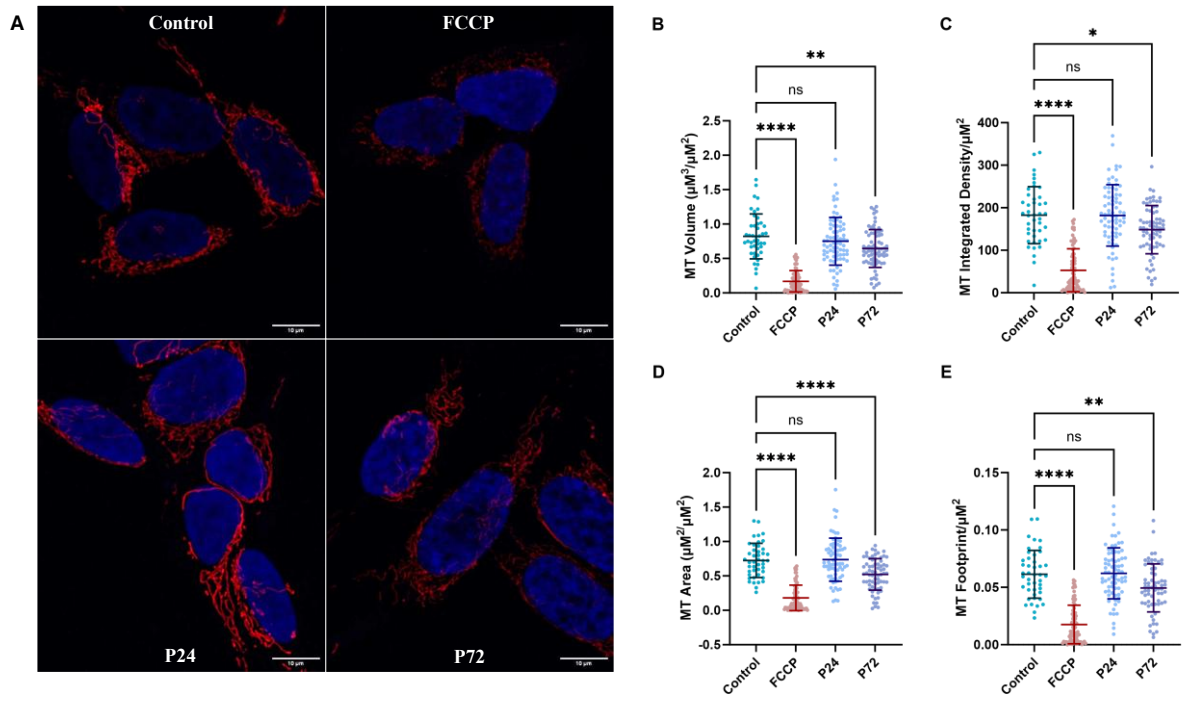


Figure 2.13. Decreased Mitochondrial Content Under Propionic Acid Stress. A) Representative maximum intensity projections of SH-SY5Y cells at 63X magnification after exposure to 25µM FCCP for 2 hours or 5mM PPA for 24 – 72 hours. Cells were stained with 300nM MitoTracker CMX Ros and visualised with a Zeiss LSM780 Confocal Microscope, using the 63X oil DIC M27 objective and a 561nm laser. Mitochondrial content was quantified according to **B)** Mitochondrial Volume; **C)** Integrated Density; **D)** Mitochondrial Area and **E)** Mitochondrial Footprint per cell normalised to total cell surface area. Data represent 288 cells with 46-86 cells per treatment condition from three independent biological repeats. Data was filtered using the ROUT method to identify outliers before being tested for normality using the Shapiro-Wilks test. Significance was evaluated using Kruskal-Wallis test with Dunn's Post-Hoc Comparisons where *p<0.05, **p<0.01, ***p<0.001, and ****p<0.0001.

A similar trend was observed using both 2D and 3D approaches to examine mitochondrial network morphology, where network connectivity was maintained at 24 hours, but signs of network fragmentation emerged after 72 hours (Figure 2.14A). Although the total length of the mitochondrial network remained unchanged, mean branch length decreased by 26% while the average density of junctions and triple branch points increased by 2- and 2.5-fold respectively **(Figure 2.14B-E).** It is worth noting that similar, though non-significant increases were observed in other measures of network fragmentation, including the number of total branches, quadruple branches and network trees, which increased by an average of 12, 50 and 27% respectively **(Figure S2.6A-C).** This is also consistent with the analysis conducted using the Mito Morphology macro, which suggested a significant 20-22% decrease in average mitochondrial area and perimeter after 72 hours **(Figure 2.15 A-C).** Moreover, the area: perimeter ratio, which serves as a measure of interconnectivity, was significantly reduced by 15% under the same conditions **(Figure 2.15D).** However, total mitochondrial count remained unchanged despite the decrease in average and total mitochondrial volume **(Figure S2.6D).**

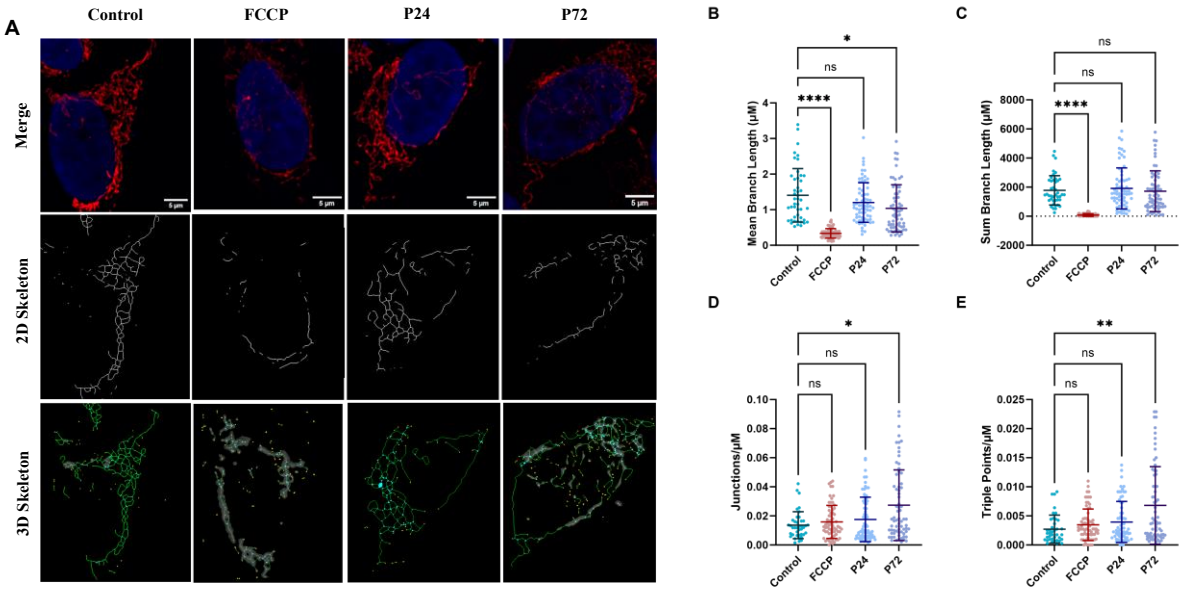


Figure 2.14. Impairments to Mitochondrial Network Integrity in the Propionic Acid Model. A) Representative maximum intensity projections of mitochondrial networks stained with MitoTracker CMX Ros, as well as the 2D and 3D network skeletons derived from binarised 8-bit masks. Changes in network morphology were quantified by measuring **B)** Mean branch length, **C)** Total network length, **D)** the density of junctions and **E)** the density of triple branch points across the mitochondrial network. Data represent 288 cells with 46-86 cells per treatment condition from three independent biological repeats. Data was filtered using the ROUT method to identify outliers before being tested for normality using the Shapiro Wilks test. Significance was evaluated using Kruskal-Wallis test with Dunn's Post-Hoc Comparisons where *p<0.05, **p<0.01, ***p<0.001, and ****p<0.0001.

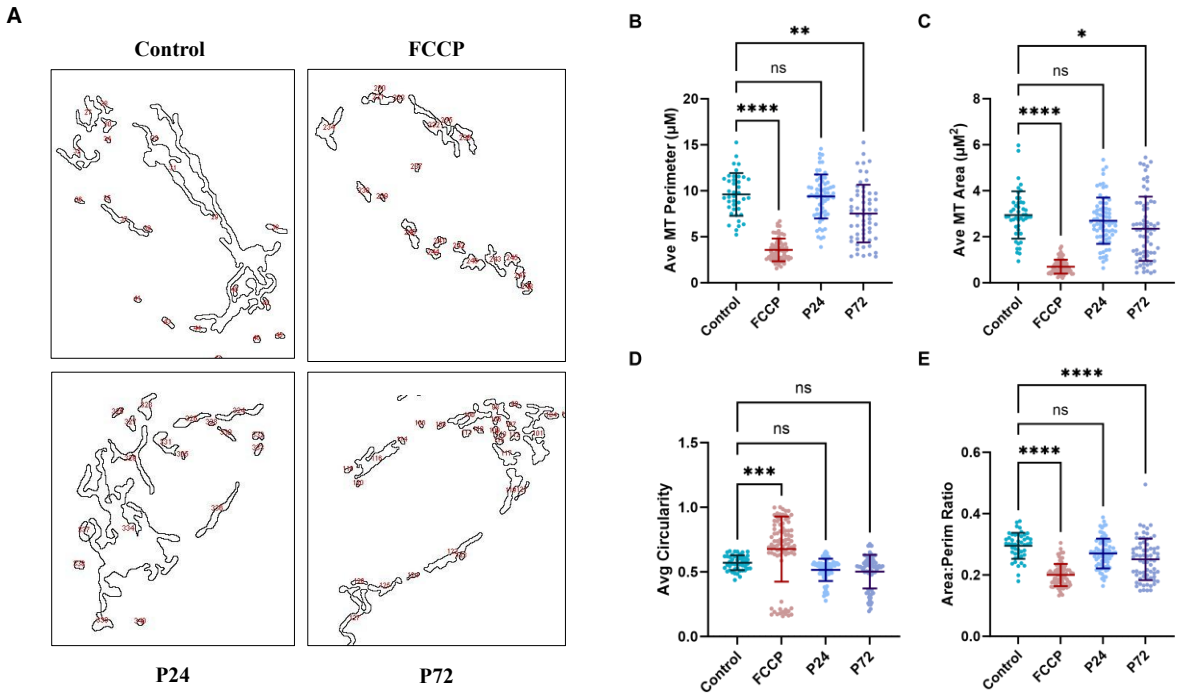


Figure 2.15. The Remodelling of Mitochondrial Morphology in Response to Propionic Acid. A) Representative masks generated from the MitoMorphology macro showing binary outlines of mitochondrial networks in 2D slices. Mitochondrial particles were characterised according to **B)** Perimeter, **C)** Area, **D)** Circularity and **E)** Area: Perimeter ratio normalised to circularity to account for mitochondrial swelling. Data represent 288 cells with 46-86 cells per treatment condition from three independent biological repeats. Data was filtered using the ROUT method to identify outliers before being tested for normality using the Shapiro Wilks test. Significance was evaluated using Kruskal-Wallis test with Dunn's Post-Hoc Comparisons where *p<0.05, **p<0.01, ***p<0.001, and ****p<0.0001.

Importantly, the approaches used to assess mitochondrial content and network morphology were validated with the FCCP positive control, which was characterised by a profound 76-80% decrease in mitochondrial content **(Figure 2.13),** a fragmented mitochondrial network marked by a 76% decrease in mean branch length **(Figure 2.14),** a 52% decrease in mitochondria count **(Figure S2.6D),** a 76 and 62% decrease in average mitochondria area and perimeter and a concurrent 18% increase in circularity **(Figure 2.15).** In comparison, the response induced by PPA indicated a subtle remodelling of mitochondrial dynamics that sustained mitostasis to a point and better retained mitochondrial content even as the balance between stress and compensation was disrupted.

The mechanisms that drive mitochondrial remodelling under PPA stress cannot be determined based on mitochondrial network morphology alone. However, the decrease in mitochondrial size, branch length and network connectivity in the absence of significant changes to mtDNA copy number or mitochondrial count may indicate a role for mitophagic clearance. Here, mitophagy was examined using LC3β to evaluate the degree of colocalisation between autophagosomes and the mitochondrial network. An analysis of total LC3β expression showed a decrease in the number, volume and fluorescent intensity of LC3β puncta in cells exposed to both FCCP and PPA **(Figure S2.7).** Importantly, while LC3β is often

used as a starting point, it cannot be used to infer overall autophagic flux in the absence of other parameters such as LC3α, p62, or autolysosome inhibitors. The data presented here demonstrate only that the balance between autophagosome formation and clearance appears to be altered relative to untreated controls, which contextualises subsequent analyses of mitophagic flux.

Unlike total LC3β expression, LC3β localisation can be used to more specifically evaluate the targeting of active autophagosomes. Three different methods used to quantify colocalisation between MitoTracker Red and LC3β puncta suggested that PPA significantly altered mitophagic flux over time. Both volume- and intensity-based approaches showed a significant increase in the LC3β colocalisation ratio at 24 hours, which represents the fraction of total LC3β colocalised with MitoTracker Red **(Figure 2.16A, B).** The Pearson's coefficient, which represents the degree of correlation between the intensity of two fluorescent signals, was also significantly increased at the same conditions, as was the LC3β Manders coefficient, which denotes the degree of co-occurrence between two signals **(Figure 2.16C).** Interestingly, the mitochondrial colocalisation ratio was not substantially altered at 24 hours **(Figure S2.8A-C)** which illustrates that the proportion of the mitochondrial network undergoing mitophagy remains unchanged. Similarly, the total volume of colocalisation per cell was unperturbed at these conditions **(Figure S2.8D).** Together, this data illustrates a subtle and dynamic remodelling of mitochondrial content, network morphology and mitophagic flux that points to an imbalance in mitostasis under PPA stress. What remains uncertain is whether this state of imbalance is one that retains function through mitochondrial remodelling, or whether these perturbations have functional implications for mitochondrial metabolism.

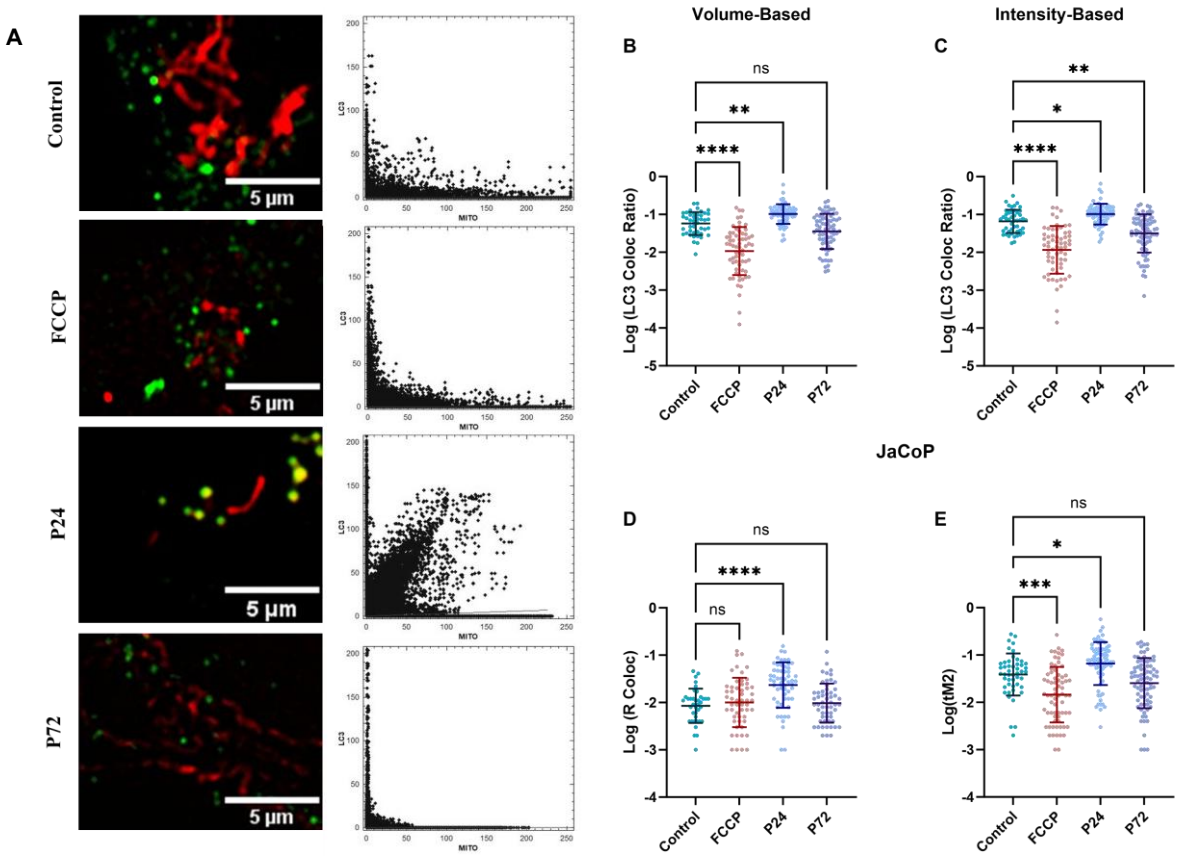


Figure 2.16. Perturbations to Mitophagic Flux Induced by Propionic Acid. A) Representative regions from 2D slices where yellow structures depict colocalisation of LC3 puncta (green) and MitoTracker-stained mitochondrial networks (red) and the associated cytofluorograms from the cells of interest. **B)** Volume-based and **C)** Intensity-based colocalisation coefficients measured as the colocalisation ratio across LC3 puncta. **D)** Pearson's and **E)** Manders coefficients calculated from the JaCoP ImageJ plugin. Data represent 288 cells with 46-86 cells per treatment condition from three independent biological repeats. Data was log-normalised and filtered using the ROUT method to identify outliers before being tested for normality using the Shapiro Wilks test. Significance was evaluated using Kruskal-Wallis test with Dunn's Post-Hoc Comparisons where *p<0.05, **p<0.01, ***p<0.001, and ****p<0.0001.

2.3.4. Mitochondrial Function and Metabolic State

The data presented thus far suggest that PPA disrupts the transcriptional and morphological mechanisms that govern mitostasis. However, the fundamental mechanism by which mitochondrial dysfunction is thought to dysregulate neurodevelopment is by changing endpoint metabolism and bioenergetic state. Here, live-cell respirometry using Seahorse technology was used to examine PPA-induced disruptions to mitochondrial energy production and metabolic state. The manufacturers of Seahorse technology suggest that metabolism should be studied using a top-down approach, where initial assays are designed to characterise broad changes to metabolic flux and to inform subsequent more targeted assays to interrogate specific pathways. The ATP rate assay characterises broad energy metabolic phenotypes and identifies whether subsequent assays should focus on oxidative or glycolytic metabolism.

Based on the mitochondrial network remodelling observed in section **2.4.3**, a 72-hour exposure to 5mM PPA was chosen to explore whether the changes to mitochondrial morphology and content were associated with disruptions to mitochondrial metabolism and function. Given resource constraints, coupled with previous studies that relied on the improved sensitivity of the XFp to quantify metabolic changes with one biological repeat (Pandey *et al.,* 2022), the ATP rate assay was performed once in triplicate as a preliminary investigation of metabolic state. Relative to untreated controls, PPA-treated cells displayed a 60-62% reduction in OCR under both basal and stressed conditions **(Figure 2.17A-C).** Similarly, both basal and stressed ECAR were markedly reduced (between 70-77%) with PPA exposure **(Figure 2.17D-F).** While the addition of mitochondrial inhibitors decreased OCR by ~ 55% in both cases, ECAR was increased 1.8- and 1.4-fold in controls and PPA-treated samples respectively, reflecting a shift towards glycolysis to compensate for the lower rate of oxidative energy production. However, this compensatory capacity was attenuated by 40% in PPA-treated samples. As a result, PPA exposure was associated with a distinctly quiescent metabolic phenotype, characterised by reduced energy consumption **(Figure 2.17G)** and more than a 60% drop in the rate of ATP production (Figure 2.17H). Here, oxidative ATP production was decreased by 40% with PPA exposure, while glycolytic energy production was reduced by 86%. Consequently, while ATP production was 90% oxidative in controls, this actually increased to 96% in PPA-treated samples, due to the profound decrease in glycolytic metabolism.

Notably, both treated and untreated samples displayed a substantially higher rate of oxidative rather than glycolytic ATP production, with a mitochondrial reliance above 90% in both cases. This reflects the degree of oxidative reliance previously reported in primary neurons and glucose-deprived SH-SY5Y cells (Wilkins *et al.,* 2016; Naia *et al.,* 2021), although SH-SY5Y cells grown in high-glucose, FBS-rich medium typically display a preference for glycolysis over oxidative metabolism (Kronenberger *et al.,* 2024). The protocol used here employed a lower glucose concentration in combination with serum depletion and glutamine supplementation, which likely enhanced mitochondrial dependence in the undifferentiated state. Nevertheless, the data in **Figure 2.17** shows that untreated cells still display a capacity to upregulate glycolysis in response to mitochondrial inhibition. In this context, it is noteworthy that glycolytic metabolism was suppressed by PPA despite the concurrent drop in oxidative respiration. In contrast to the targeted mitochondrial dysfunction induced by ETC inhibitors, this suggests a distinct feature of PPA-induced metabolic stress that attenuates the capacity for glycolytic compensation in SH-SY5Y cells. Nevertheless, the fact that both treated and untreated samples displayed an oxidative reliance above 90% suggested that the disruptions to oxidative metabolism would have more profound implications for neuronal function and differentiation. Therefore, subsequent experiments employed MitoStress tests to explore specific aspects of mitochondrial function under PPA stress.

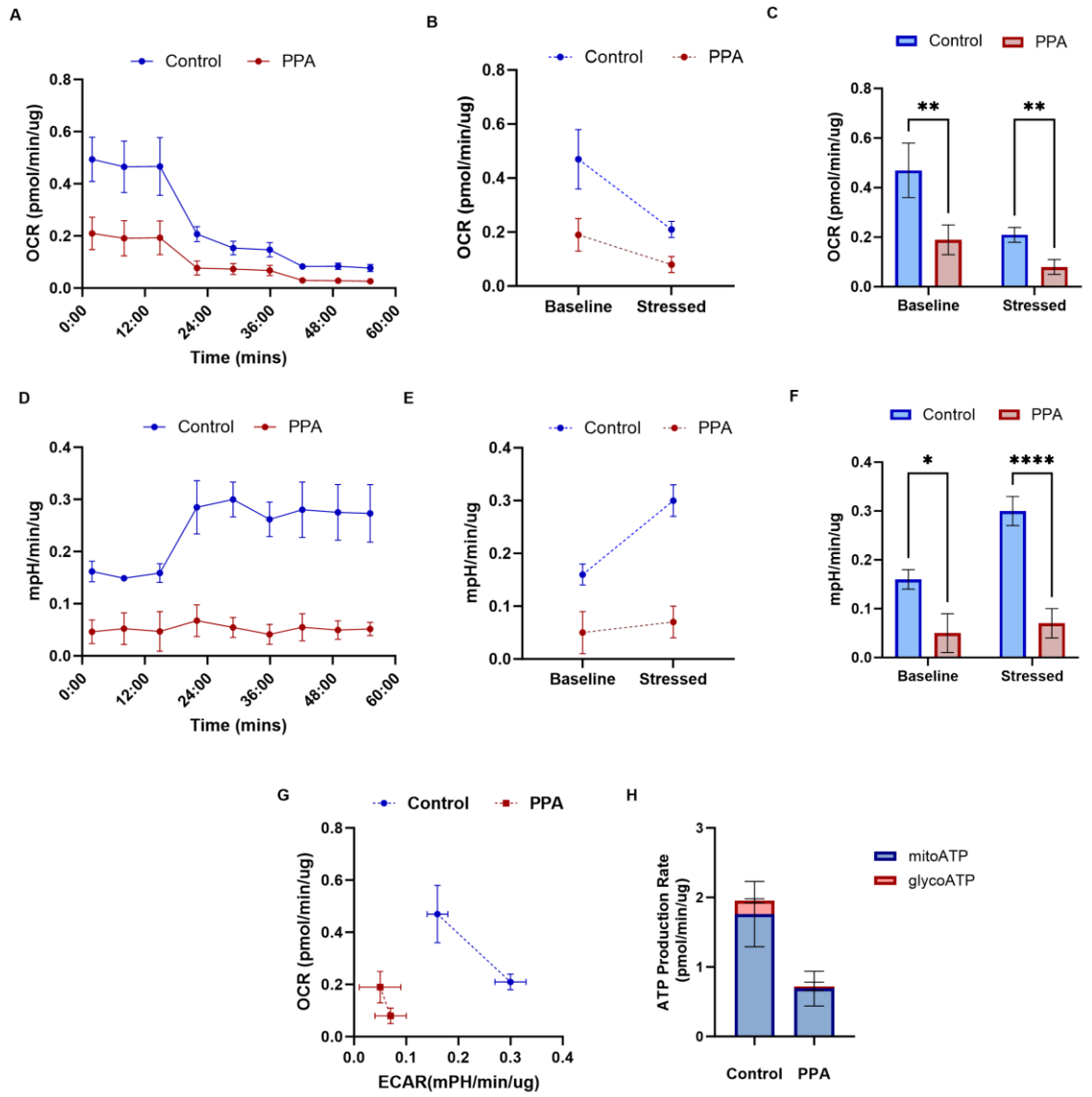


Figure 2.17. Impaired ATP Production and Altered Metabolic Phenotype. The ATP Rate Assay was used to quantify total, mitochondrial and glycolytic ATP production in SH-SY5Y cells after 72 hours at 5mM PPA. Data represent oxygen consumption rate (OCR) **(A-C)**, extracellular acidification rate (ECAR) **(D-F)**, and metabolic phenotype **(G, H)** measured over the duration of the assay. Here, baseline refers to basal metabolic state while stressed refers to metabolic state after the addition of Oligomycin and Rot/AA. Data represent triplicates from one biological repeat where significant differences were measured with two-way ANOVAs and Tukey's Post Hoc Comparisons; *p<0.05, **p<0.01, ***p<0.001, and ****p<0.0001.

The MitoStress test uses sequential injections of targeted mitochondrial ETC inhibitors to measure basal, spare and maximal respiratory capacity. First, oligomycin is injected to inhibit ATP synthase which blocks ATP-linked oxygen consumption. The mitochondrial membrane uncoupler FCCP is added to promote maximal respiration, which allows for an assessment of spare respiratory capacity - defined as the ability of the cell to respond to increased energy demand. Lastly, rotenone and antimycin A are injected to simultaneously inhibit ETC complex 1 and 3, which allows for the quantification of oxygen consumption derived from non-mitochondrial processes, such as cytoplasmic or peroxisomal oxidation

reactions driven by cyclo-oxygenases, cytochrome P450s or NADPH oxidases (Agilent Technologies, 2021). Due to the pairwise nature of the 6-well XFp assay, paired T-tests were employed to assess significant changes across four biological repeats, each conducted in triplicate. In line with the results from the ATP rate assay, 72 hours of 5mM PPA significantly decreased basal OCR and ECAR by 41 and 45% respectively **(Figure 2.18A-C).** Non-mitochondrial OCR was reduced by 51%, while maximal and spare respiratory capacity were decreased by 47 and 57% respectively **(Figure 2.18D-F).** The metabolic potential, defined as the range in OCR and ECAR measured over the duration of the assay was significantly reduced by 48 and 67% percent respectively **(Figure 2.18G).**

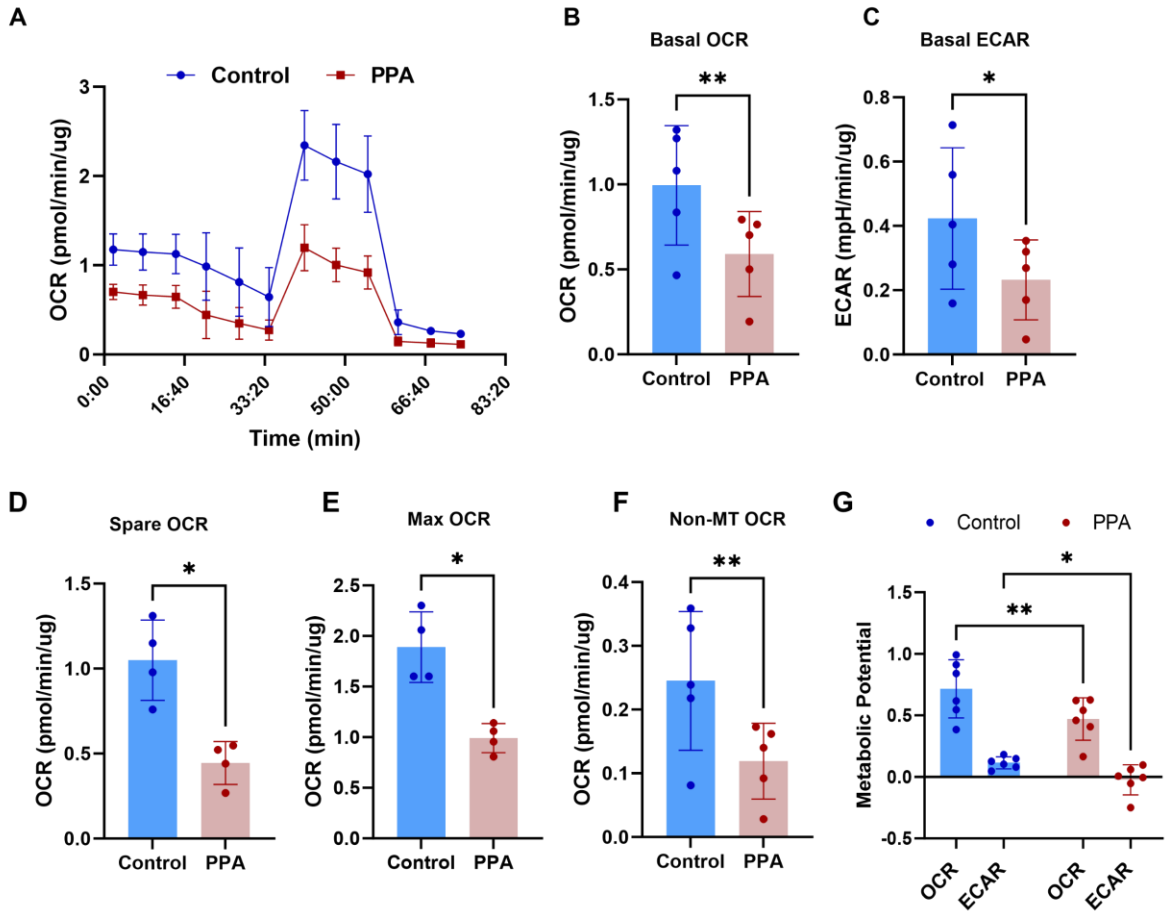


Figure 2.18. Disruptions to Mitochondrial Metabolism Induced by Propionic Acid. Undifferentiated SH-SY5Y cells were exposed to 5mM PPA for 72 hours before MitoStress Tests were employed to assess mitochondrial metabolism. **A)** Oxygen consumption rate over the duration of the MitoStress test. **B)** Basal oxygen consumption rate (OCR) and **C)** Basal extracellular acidification rate (ECAR) measured after three cycles of mixing and measuring. **D)** Spare respiratory capacity measured as the difference between maximal respiration and basal respiration. **E)** Maximal OCR calculated as the average of three consecutive cycles after the addition of 1.5uM FCCP. F) Non-mitochondrial OCR measured after the addition of Rot/AA. **G)** Metabolic potential represents the range in OCR and ECAR measured over the duration of the assay. Data represent the mean and standard deviation from four independent biological repeats, analysed using paired two-tailed T-tests; *p<0.05, **p<0.01, ***p<0.001, and ****p<0.0001.

This data shows that PPA-induced disruptions to both the transcriptional and morphological remodelling of mitochondrial dynamics culminated in substantial metabolic deficits. As well as a significant decrease in oxidative energy production, PPA induces a more substantial reduction in both maximal and spare capacity, with an attenuation of the capacity for glycolytic compensation. It is worth noting that these energetic deficits are observed in cells that are neither proliferating nor differentiating and thus have a relatively low energy demand compared to proliferative NSCs, differentiating progenitors or mature neurons *in vivo*. Thus, the relative metabolic deficit induced by PPA may depend on the experimental context. Nevertheless, these data demonstrate that PPA substantially decreases not only basal mitochondrial respiration but also the capacity to respond to an increased energy demand via either oxidative or glycolytic metabolism, which has profound implications for the energy-reliant process of neuronal differentiation.

2.4. Discussion

This chapter established an *in vitro* model for mitochondrial dysfunction in undifferentiated SH-SY5Y cells to recapitulate the signatures associated with mitochondrial dysfunction in our ASD cohort. Building on an established biochemical model for PCC dysfunction, this study evaluated the dynamic changes to mitochondrial homeostasis and function in SH-SY5Y cells exposed to PPA **(Figure 2.19).** PPA induced dose- and time-dependent effects on cell viability and metabolism catalysed by a loss of mitochondrial membrane potential at 4 hours, changes to cell morphology from 24 hours, and cumulative disruptions to mitostasis that culminated in significant cell death by 72 hours. Concurrently, there was an acute and sustained decrease in *PCCB* expression and a systemic dysregulation of the transcriptional mechanisms that govern mitogenesis, fission and fusion. These disruptions were reflected by changes to mitochondrial network morphology and dynamics characterised by decreased mitochondrial volume, increased mitochondrial fragmentation and perturbations to mitophagic flux. Finally, live-cell respirometry showed that PPA suppressed mitochondrial respiration, depleted spare respiratory capacity and inhibited glycolysis, leading to a significantly reduced ATP production rate and a quiescent energetic profile.

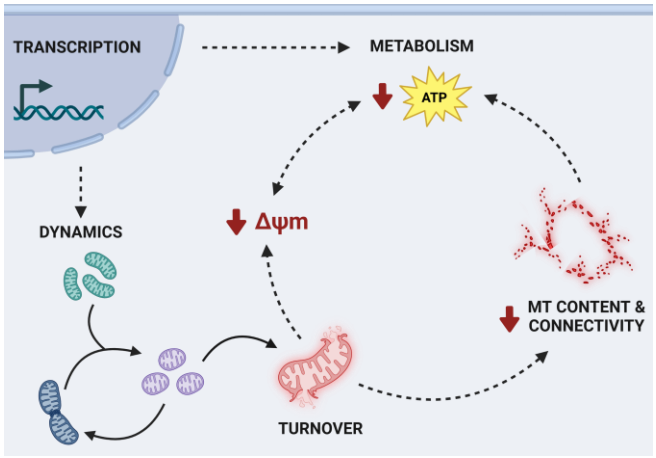


Figure 2.19. End-Point Measures of Mitostasis in the Propionic Acid Model. SH-SY5Y cells exposed to Propionic Acid (PPA) exhibited disruptions to transcriptional, morphological and metabolic mechanisms that maintain mitostasis. PPA altered the expression of 11 central regulators of mitochondrial metabolism, biogenesis, fission and fusion, reduced mitochondrial content and connectivity, altered mitophagic flux, decreased both mitochondrial membrane potential (ΔΨm) and impaired oxidative and glycolytic ATP production.

Collectively, this work demonstrates that PPA alters mitochondrial content, morphology and metabolism with functional implications for neuronal viability and energetic state. The discussion that follows considers these data in the broader context of the PPA model, highlighting the underlying mechanisms that may lead to mitochondrial dysfunction and the functional implications for neurodevelopment. Together, the interdependent mechanisms that are modulated by PPA in its capacity as a substrate, a toxin and a signalling molecule have profound consequences for the mitochondrial regulation of neurogenesis and may yield novel insight into the aetiology of ASD.

2.4.1. Establishing the PPA Model: Profiles of Cytotoxicity and Metabolic Stress

This study employed a top-down approach, using progressively more sensitive techniques to characterise PPA-induced mitochondrial dysfunction. First, the PPA model was established by defining broad windows of cytotoxicity, metabolic stress and *PCCB* dysregulation. After titrating PPA concentrations based on profiles of acute cytotoxicity, both MTT and ATP assays revealed significant cell death after 24 hours at 5mM PPA in DMEM: F12. This is congruent with previous SH-SY5Y studies in DMEM: F12 that reported cytotoxic effects at 1, 5 and 10mM PPA after 24 (El Ansary, Abu Shmais and Al Dbass, 2013; Kim *et al.,* 2019), 48 and 72 hours (Jung *et al.,* 2020). Here, a discrepancy between the MTT and ATP assays emerged, where the MTT assay appeared to detect significant changes in cell viability at lower doses. This discrepancy could be attributed to differences in the sensitivity of each assay, or to the different intracellular parameters used by each assay to assess cell viability. It is possible that total cellular reduction potential is more sensitive to mild changes to metabolic state, while total ATP levels are only depleted once the degree of mitochondrial dysfunction is sufficient to significantly impair energy production. Interestingly, this is consistent with the results previously reported by Kim *et al.,* (2019), where significant cytotoxicity was detected at lower doses (1mM) with the MTT assay, while ATP concentrations only reflected significant cell death from 5mM. Together, this suggests that the MTT assay may be better suited to detect the lower threshold of treatment that does not impair mitochondrial function.

Thus, the MTT assay was used to characterise the cytotoxicity of PPA in the context of oxidative reliance, using EMEM: F12 with serum depletion and glutamine supplementation. Here, a dose-dependent effect on cell viability emerged only after 72 hours of PPA exposure. While fewer studies have examined PPA stress in EMEM: F12, this data is congruent with previous work in this system that showed no significant changes to SH-SY5Y cell viability after 24 hours at 5-10mM PPA (Filippone *et al.,* 2020). This highlights an interesting divergence from the results observed in the DMEM: F12 model which may be due to differences in basal metabolic state. Direct comparisons between cell viability using both media formulations would be needed to validate this hypothesis, particularly given the variable nature of the MTT assay itself across experimental systems. Nevertheless, this discrepancy underlines a need to consider how basal metabolic state influences studies of mitochondrial dysfunction

in the SH-SY5Y model, highlighting diverse effects of metabolic stress that warrant further investigation. Here, the cytotoxic profiles of PPA in EMEM: F12 highlighted a period from 24 to 72 hours at 5mM PPA that captured the earliest shift from mitochondrial compensation to dysfunction and cell death. Accordingly, this window was used to inform subsequent studies of mitochondrial morphology and metabolism. Notably, 5mM reflects the highest concentrations of plasma PPA reported in the clinical literature (Roginski *et al.,* 2020), while PPA concentrations above 5mM have been shown to induce cell death in HT22 hippocampal neuronal cells after 48 hours (Jeon *et al.,* 2022), which emphasises the physiological relevance of this model.

To determine whether the cytotoxic effects of PPA were associated with disruptions to mitochondrial function, acute changes to ΔΨm were evaluated using TMRE. Here, an acute loss of ΔΨm was induced by 10mM PPA, reflecting the results published by Kim *et al.,* (2019) after 4 hours at 5-10mM. In fact, mitochondrial depolarisation has been reported in other *in vitro* models of PPA accumulation (Roginski *et al.,* 2020) as well as *in vivo* models for PCC deficiency (Chapman *et al.,* 2018). A loss of ΔΨm is known to induce mitophagy via the mitochondrial membrane permeability transition pore (mPTP), ultimately culminating in apoptotic cell death (Ashrafi and Schwarz, 2012). Indeed, several studies have demonstrated that PPA-induced cytotoxicity is mediated by apoptosis in both *in vivo* (Alfawaz et al. 2022; A. K. El-Ansary, Bacha, and Kotb 2012; Alhusaini et al. 2022) and *in vitro* (Tang *et al.,* 2011; Filippone *et al.,* 2022) and models, including the SH-SY5Y cell line (El Ansary, Abu Shmais and Al Dbass, 2013). In this chapter, the decreased ΔΨm at 4 hours and the reduced cell viability observed by 72 hours is consistent with mPTP-mediated apoptotic cell death associated with mitochondrial dysfunction. Ongoing work in our lab aims to validate the mitochondrial membrane depolarisation observed here using more sensitive live-cell confocal microscopy techniques across a broader range of conditions. Moreover, targeted assays to distinguish between apoptotic and necrotic cell death would be needed to establish a direct relationship between mitochondrial membrane depolarisation and cell death induced by PPA. Here, ΔΨm was used only as a preliminary measure of mitochondrial dysfunction that confirms previous reports in the PPA model before progressing towards more targeted investigations of metabolic state.

The *in vitro* model established in this chapter aimed to recapitulate the signatures of PCCB dysfunction observed in our ASD cohort. Therefore, *PCCB* expression was measured to evaluate whether the disruptions to cell viability and metabolism induced by PPA were associated with changes to metabolic flux. After 4 hours, PPA immediately reduced *PCCB* expression by up to 55%, which was sustained throughout the 72-hour exposure. This reveals a novel relationship between PPA exposure and *PCCB* expression that remains understudied in the PPA model. Importantly, the correlation between mRNA transcription, protein expression and enzyme activity is complex. Studies have found that PCCB protein levels are better predicted by *PCCA*, rather than *PCCB*, mRNA expression, as the PCCB monomer is stabilised in complex with PCCA (Jiang *et al.,* 2020; Spangsberg Petersen *et al.,* 2024). Moreover, both

PCCA and PCCB proteins are post-translationally cleaved by mitochondrial matrix proteases, and the function of the PCC enzyme is biotin-dependent (Wongkittichote, Ah Mew and Chapman, 2017). Therefore, a comprehensive assessment of the transcription, translation, modification and localisation of the PCCA and PCCB subunits would be needed to demonstrate an undisputed relationship between PPA and PCC function. Here, the administration of PPA reflects a biochemical consequence of PCC dysfunction regardless of its effect on PCC expression and activity. Nevertheless, it is worth noting that *in vitro* studies have revealed an essential role for PCCB as a chaperonin during PCC complex assembly (Kelson, Ohura and Kraus, 1996; Muro *et al.,* 2001; Pérez-Cerdá *et al.,* 2003) while data from PA patient fibroblasts demonstrated a correlation between *PCCB* mRNA and PCC function (Jiang *et al.,* 2020). Therefore, the data presented here suggest a level of transcriptional dysregulation that recapitulates the DM of PCCB observed in our ASD cohort *in vitro* and proposes a relationship between PPA and *PCCB* expression that should be examined in future studies. Altogether, this work demonstrates evidence for cytotoxicity and mitochondrial dysfunction under PPA stress that recapitulates published aspects of the PPA model, establishes the validity of this experimental system and informs subsequent measures of mitostasis *in vitro.*

2.4.2. Molecular Mechanisms of Mitostasis

While several studies have shown impairments to mitochondrial function under PPA stress in the SH-SY5Y system (El Ansary, Abu Shmais and Al Dbass, 2013; Kim *et al.,* 2019; Jung *et al.,* 2020), the molecular mechanisms that drive these disruptions remain poorly understood. This chapter evaluated the transcriptional profiles of ten mitochondrial genes involved in four central aspects of mitostasis across twelve conditions. Cumulative evidence has revealed a critical role for both PGC1α and c-MYC in metabolic remodelling during neurodevelopment (Zheng *et al.,* 2016; Beckervordersandforth, 2017; Di Giacomo *et al.,* 2017; Shyh-Chang and Ng, 2017; Garone, De Giorgio and Carli, 2024; Sánchez-Ramírez *et al.,* 2024). Likewise, loss-of-function studies have found that OPA1, MFN1/2 and DRP1 are essential for NSC, self-renewal, neurogenesis and neuronal function (Chen *et al.,* 2003; Ishihara *et al.,* 2009; Wakabayashi *et al.,* 2009; Bradshaw *et al.,* 2016; Khacho *et al.,* 2016), while PGC1α, STOML2, MFN2 and DRP1 were found to be DM in our ASD cohort (Stathopoulos *et al.,* 2020; Bam *et al.,* 2021). Thus, better understanding how these genes respond to metabolic stress could yield insight into mitochondrial mechanisms that are critical for neuronal maturation.

Of the ten genes evaluated here, eight genes were significantly downregulated by PPA, though each displayed distinct transcriptional profiles over time. Of these, *c-MYC* was the most substantially downregulated gene across all twelve conditions, reaching more than 90% inhibition by 72 hours. Markedly, *c-MYC* modulates the transcription of 599 mitochondrial genes required for mitochondrial biosynthesis, assembly and function (Morrish and Hockenbery, 2014) and a reciprocal relationship between c-MYC and mitochondrial dysfunction is well-documented in the literature. Graves *et al.,*

(2012) showed that c-MYC knockdown decreased mitochondrial content, polarisation, size, cristae complexity and connectivity, impaired oxidative and glycolytic metabolism and altered the expression of key fission and fusion proteins including OPA1, MFN1, MFN2 and DRP1. Similarly, several studies have shown that suppressing c-MYC decreased the expression of its targets *TFAM* and *NRF1*, leading to impaired mitochondrial respiration and increased oxidative stress (Gleyzer and Scarpulla, 2016; Kunkel, Chaturvedi and Tyagi, 2016; Cigliano *et al.,* 2017; Zarrabi *et al.,* 2017). Conversely, metabolic stress has been found to decrease c-MYC expression in SH-SY5Y cells (Conn *et al.,* 2003). In fact, the downregulation of c-MYC induced by metabolic stress was found to promote mitochondrial fission and apoptosis (Wang *et al.,* 2018), while inhibiting c-MYC was sufficient to attenuate stress-induced apoptosis *in vitro* (Guzenko *et al.,* 2024). Importantly, the relationship between c-MYC, metabolic state and mitochondrial dynamics plays a regulatory role in cell fate, NSC activation and neuronal differentiation (Zheng *et al.,* 2016; Prieto *et al.,* 2018; Cai *et al.,* 2021), and this is reflected in the SH-SY5Y model (Sakuma *et al.,* 2024). Thus, an attenuation of c-MYC expression is both a known cause and consequence of mitochondrial dysfunction that has profound implications for mitochondrial morphology, dynamics and metabolism during neurogenesis.

Interestingly, the decrease in *c-MYC* expression was reflected by a significant downregulation of both *TFAM* and *NRF1* from 24 – 72 hours of PPA stress, which suggests convergent disruptions to transcriptional regulators of mitogenesis. The early suppression of c-MYC that precedes significant disruptions to *TFAM* and *NRF1* may reflect the role played by c-MYC as an upstream transcriptional regulator. Notably, PPA was previously shown to decrease *TFAM* mRNA expression after 4 hours in SH-SY5Y cells (Kim *et al.,* 2019), while studies in colorectal carcinoma found that both *TFAM* and *NRF1* were downregulated with long-term PPA exposure (Tang *et al.,* 2011). Notably, Kim *et al.,* (2019) found that TFAM protein expression increased under the same conditions, while Tang *et al.,* (2011) revealed a pattern of acute upregulation followed by transcriptional inhibition over time. On the other hand, PPA has been shown to increase mitochondrial biogenesis by upregulating *TFAM* or *NRF1* expression in several *in vivo* and *in vitro* systems (Kim *et al.,* 2019; Ribeiro *et al.,* 2020; Jiao *et al.,* 2021; Wang *et al.,* 2022, 2023). Thus, the transcriptional mechanisms that mediate PPA-induced disruptions to mitogenesis appear to be complex, dynamic and context-dependent and may not always reflect downstream changes to protein expression and function.

This was exemplified by the transcriptional response of *PGC1α*, which contradicted the patterns of downregulation displayed by the other genes of interest. Rather, *PGC1α* displayed varying patterns of upregulation under PPA stress, with evidence for significant dysregulation at 24 hours. This is consistent with previous studies in SH-SY5Y cells, which reported a 7.5-fold increase in PGC1α mRNA and protein expression after 4 hours at 5mM PPA (Kim *et al.,* 2019). Similarly, 2-4mM PPA upregulated PGC1α transcription in bovine enterocytes (Zhan *et al.,* 2020) and increased mRNA and protein expression in bovine- (Wang *et al.,* 2022), and human-derived hepatocytes (Wang *et al.,* 2023).

Interestingly, *PGC1α* expression was also increased 1.5-fold in PCCB-/- iPSC-derived cardiomyocytes compared to the isogenic control (Álvarez *et al.,* 2023). As an energy-sensitive regulator of mitostasis, *PGC1α* responds to ATP depletion, redox state or intracellular Ca^{2+} flux via the AMPK, cAMP, NAD^{+}/SIRT1, or CaMK pathways respectively (Cardanho-Ramos and Morais, 2021). Thus, the variability in *PGC1α* expression under PPA stress may be due to complex and interdependent mechanisms that govern *PGC1α* expression in response to metabolic and oxidative state. The increase in *PGC1α* expression observed here, while highly variable, reflects previous models of PPA stress and PCCB dysfunction and may suggest disruptions to energy-sensitive signalling pathways that modulate transcription.

Notably, PGC1α has been shown to modulate the transcription and activity of MFN1/2, DRP1 and OPA1 (Chen *et al.,* 2022), thereby coupling the regulation of mitochondrial biogenesis, fission and fusion. While metabolic stress has been shown to disrupt *OPA1, MFN1/2* and *DRP1* transcription in SH-SY5Y cells (Zhu, Li and Lu, 2014; Zhou *et al.,* 2018; Ge *et al.,* 2024), the genes involved in mitochondrial dynamics remain uncharacterised in the PPA model. Here, transcriptional signatures revealed a coordinated downregulation of fusion and fission machinery in response to PPA. *OPA1* and *STOML2* were the most significantly impacted by PPA stress, displaying convergent transcriptional profiles marked by a 70% decrease in expression by 24 hours at 10mM. Interestingly, OPA1 and STOML2 interact directly to remodel mitochondrial ultrastructure by facilitating the assembly of respiratory super-complexes in the mitochondrial membrane (Mitsopoulos *et al.,* 2015; Hu *et al.,* 2021; von der Malsburg *et al.,* 2023). In this context, it is worth noting recent work in our lab that revealed significant disruptions to mitochondrial morphology and ultrastructure under PPA stress (Buchanan *et al.,* 2023), which is supported by similar findings from independent studies in SH-SY5Y cells (Kim *et al.,* 2019; Jung *et al.,* 2020) and PA-derived hepatocytes (Schumann *et al.,* 2021). The transcriptional inhibition of *OPA1* and *STOML2* observed here may propose a mechanism that precedes downstream disruptions to mitochondrial ultrastructure, which could significantly influence mitochondrial integrity and respiratory capacity under stress.

In fact, STOML2 also modulates mitochondrial biogenesis, fission, fusion and mitophagy via interactions with cardiolipins and prohibitins (Christie *et al.,* 2011), MFN2 (Hájek, Chomyn and Attardi, 2007), PINK1 and PARK (Zheng *et al.,* 2021; Fan *et al.,* 2022; Qin *et al.,* 2022; Zanon *et al.,* 2024) respectively. As such, STOML2 coordinates diverse aspects of mitostasis that govern mitochondrial abundance, connectivity and turnover. Yet, STOML2 remains relatively understudied compared to the canonical GTPases involved in mitochondrial dynamics. Importantly, STOML2 was the most significantly DM gene in our ASD cohort (Stathopoulos *et al.,* 2020) that was subsequently validated using targeted next-generation bisulphite sequencing (Bam *et al.,* 2021). Likewise, MFN2 and DRP1 were both DM in our ASD cohort and transcriptionally suppressed by PPA *in vitro.* MFN2 is an essential component of the mitochondrial-associated endoplasmic reticulum membranes (MAMs) that govern

Ca^{2+} and redox homeostasis, autophagic flux and the stress response (Luan *et al.,* 2021), while DRP1-dependent fission is not only crucial to sustain mtDNA copy number, mitochondrial respiration, and ATP production, but also serves as a protective buffer to prevent mPTP-induced apoptosis (Ikeda *et al.,* 2015). Thus, further characterising the expression, activity and function of STOML2, MFN2 and DRP1 under PPA stress could yield novel insights into the mitochondrial mechanisms that contribute to ASD aetiology. Indeed, Chapter 1 described the dynamic remodelling of mitochondrial networks that drives neurogenesis, emphasising that disruptions to mitochondrial dynamics could have functional implications for neurodevelopment.

Collectively, the transcriptional profiles of PPA exposure demonstrate an erosion of the adaptive capacity maintained by fission and fusion to mitigate mitochondrial dysfunction under stress. However, further work will be required to identify the mechanisms of transcriptional regulation that alter gene expression under PPA stress – and to characterise downstream changes to protein translation, modification and activity that directly alter mitochondrial function. There are several possible mechanisms that could be involved in transcriptional remodelling in the PPA model **(Figure 2.20).** On the one hand, PPA can indirectly modulate transcription factors that respond to biochemical markers of metabolic state, such as AMP or NAD^+. Of note, AMPK negatively modulates *c-MYC* mRNA stability (Dong *et al.,* 2020), while upregulating the expression of PGC1α (Wang *et al.,* 2023) in response to metabolic stress. Therefore, the transcriptional profiles induced by PPA may be mediated by the AMPK cascade that is triggered by an energetic deficit. On the other hand, PPA directly activates free fatty acid receptors (FFARs) and the PPAR family of nuclear receptors (Falomir-Lockhart *et al.,* 2019), which each control a range of transcription factors involved in proliferation, metabolism and differentiation (Di Giacomo *et al.,* 2017; Ang *et al.,* 2018).

The FFARs are G-coupled protein receptors (GPCRs) in the plasma membrane that modulate transcription by activating downstream cAMP- protein kinase A (PKA) or phospholipase C (PLC) signalling cascades (Ang *et al.,* 2018). PPA is known to activate two FFARs *in vivo* (FFAR2 and FFAR3) (Lee, Kim and Han, 2024), both of which are expressed in neurons (Colina, Puhl and Ikeda, 2018; Falomir-Lockhart *et al.,* 2019) and the SK-N-SH system (Razazan *et al.,* 2021). In fact, SCFAs have been shown to activate both FFAR2 and FFAR3 signalling in SH-SY5Y cells (Getachew *et al.,* 2020; Razazan *et al.,* 2021; Saikachain *et al.,* 2023). Notably, the p38 MAPK cascade activated downstream of FFAR2 promotes PGC1α transcription, stability and activity (Fernandez-Marcos and Auwerx, 2011) and has been shown to inhibit *c-MYC* mRNA expression in SH-SY5Y cells (He *et al.,* 2023), which reflects the transcriptional profiles induced by PPA stress. This is thought to be mediated by the p38-dependent inhibition of GSK3β, which controls PGC1α stability, localisation and activity and functions as an upstream activator of *c-MYC* transcription (Martin *et al.,* 2018; Theeuwes *et al.,* 2020). Interestingly, the antagonistic relationship between GSK3β and PGC1α plays an important role in driving NSC differentiation and metabolic remodelling (A Vallée et al. 2018), while Wnt / c-MYC

signalling has been shown to modulate mitostasis (Wang *et al.,* 2018) and neurogenesis (Tsai *et al.,* 2023; Özar *et al.,* 2024) in the SH-SY5Y model. Thus, PPA-induced disruptions to *c-MYC* and *PGC1α* expression may be driven by FFAR signalling that could disrupt the interplay between neuronal metabolism and maturation by interfering with Wnt signalling during development.

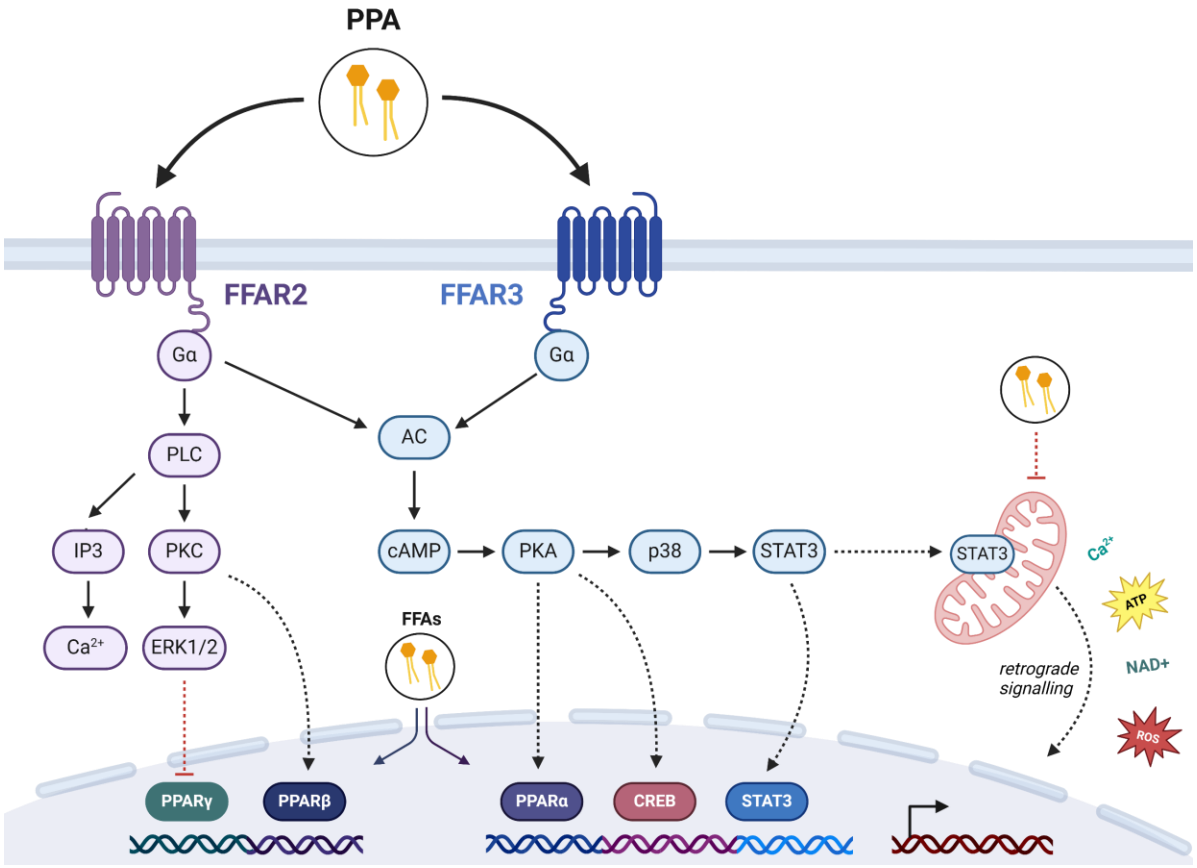


Figure 2.20. Putative Mechanisms of Transcriptional Remodelling. Propionic Acid (PPA) acts as a ligand for free fatty acid receptors 2 and 3 (FFAR2 and 3) which modulate transcription via the cAMP-protein kinase A (PKA) and phospholipase c (PLC) signalling cascades. The p38 MAPK cascade activated downstream of PKA signalling regulates the phosphorylation of signal transducer and activator of transcription 3 (STAT3), which modulates the expression of both nuclear and mitochondrial genes. PPA can also directly activate peroxisome proliferator-activated receptors (PPARs) that form heterodimeric complexes to regulate the expression of genes involved in survival, proliferation, metabolism and differentiation. Finally, PPA modulates biochemical markers of metabolic and oxidative state that control central transcriptional regulators of mitostasis.

The p38 MAPK pathway also regulates the downstream phosphorylation of STAT3, which has been shown to mediate PPA-induced toxicity in a range of *in vitro* (Park *et al.,* 2020; Bilotta *et al.,* 2021; Han *et al.,* 2024) and *in vivo* studies (Zhao *et al.,* 2018; Khera *et al.,* 2022). Notably, STAT3 not only modulates the transcription of a range of nuclear-encoded genes involved in metabolism, redox homeostasis, proliferation and neurogenesis, but can also bind directly to mtDNA, where it associates with TFAM to direct the expression of mitochondrial transcripts (Macias *et al.,* 2014; Su *et al.,* 2020). In particular, *in vitro* studies have shown that STAT3 regulates the expression of *c-MYC* (Tolomeo and

Cascio, 2021), *PGC1α, NRF1* (Macias et al. 2014), *OPA1* (Nan *et al.,* 2017; Chang *et al.,* 2023; Ge *et al.,* 2024) and *DRP1* (Fix *et al.,* 2019; Zhang *et al.,* 2024). Interestingly, STAT3 is also among the top 10 transcription factor binding sites in the PCCB promoter, while STOML2 has been shown to regulate STAT3 phosphorylation (Qu *et al.,* 2019; Liu *et al.,* 2020). Thus, the similar transcriptional profiles of PCCB, STOML2 and OPA1 may be governed by STAT3-dependent mechanisms. Together, disruptions to STAT3 activity driven by FFAR signalling may propose a convergent mechanism that drives transcriptional remodelling in the PPA model.

Unlike the membrane-bound FFARs, the PPARs are ligand-activated transcription factors that, when bound by fatty acids, form heterodimeric complexes that bind directly to PPAR Responsive Elements (PPREs) in the genome (Falomir-Lockhart *et al.,* 2019). In this way, PPARs serve as central regulators of energy homeostasis that drive metabolic remodelling during neurodevelopment (Di Giacomo *et al.,* 2017). Notably, the upregulation of PGC1α in PCCB-/- cardiomyocytes was accompanied by a significant increase in PPARγ expression (Álvarez *et al.,* 2023), while PPA has been shown to selectively upregulate PPARγ *in vitro* (Filippone *et al.,* 2022). This suggests that the positive feedback loop between PPARγ and PGC1α may play a role in regulating PGC1α expression under PPA stress. Indeed, PPA has been found to disrupt the expression of both PPARα and PPARγ in several *in vitro* models (Higashimura *et al.,* 2015; May and Den Hartigh, 2021; Filippone *et al.,* 2022; Wang *et al.,* 2022; Chen *et al.,* 2024) while pharmacologically rescuing PPARα/γ activity has been shown to attenuate the pathophysiology of PPA *in vivo* (Mirza and Sharma, 2018; Khera *et al.,* 2022). Previous studies have demonstrated that both PPARα and PPARγ modulate mitogenesis, mitophagy, mitochondrial dysfunction and oxidative stress in SH-SY5Y cells (Miglio, Rosa, *et al.,* 2009; Bell *et al.,* 2013; Chiang *et al.,* 2013; Minghetti *et al.,* 2014; Ko *et al.,* 2016; Vella *et al.,* 2016; Lee *et al.,* 2019; Szychowski and Skóra, 2023). Moreover, the role of PPARs in regulating both neurogenesis and metabolism in the SH-SY5Y system is well established (Di Loreto *et al.,* 2007; Miglio, Rattazzi, *et al.,* 2009; D'Angelo *et al.,* 2011; Avci *et al.,* 2013) and SCFAs, including PPA, have been shown to govern neuronal metabolism and development by regulating PPAR signalling *in vivo* (Sanz-Martos *et al.,* 2022; Yu *et al.,* 2024). Thus, PPARs are PPA-responsive transcription factors that could be centrally involved in the relationship between mitochondrial dysfunction and neurotoxicity. Accordingly, both FFARs and PPARs emerge as relevant targets for future research into the mechanisms of transcriptional regulation under PPA stress.

Importantly, all of the genes studied here are also subject to complex post-transcriptional and post-translational regulatory mechanisms that determine their expression, localisation and function. For example, c-MYC translation, protein stability and function is modulated by p53 and FOXO signalling, the stress-responsive EIF-ATF axis, and post-translational O-GlcNAcylation, acetylation or methylation (Sabnis, Somasagara and Bunting, 2017; Dong *et al.,* 2020; Guzenko *et al.,* 2024). PGC1α activity is regulated by phosphorylation, methylation, acetylation, O-GlcNAcylation and ubiquitination

(Fernandez-Marcos and Auwerx, 2011; Luo *et al.,* 2019; Miller, Clark and Anderson, 2019), while TFAM is regulated by phosphorylation, acetylation or ubiquitination that mediates TFAM-mtDNA interactions and turnover (Picca and Lezza, 2015). As a highly labile protein subject to continuous ubiquitination and proteasomal degradation, Nfe2l2 is regulated primarily at the protein level, which may explain the less acute transcriptional response observed under PPA exposure (Meiliana, Dewi and Wijaya, 2021).

Similarly, the activity and function of proteins involved in mitochondrial dynamics relies on post-translational modifications (PTMs) that drive their recruitment and tethering to the mitochondrial membrane. Both MFN1 and 2 are regulated by phosphorylation and ubiquitination, while DRP1 is subject to SUMOylation, phosphorylation and O-GlcNAcylation, which facilitates the assembly of DRP1 complexes that interact with adaptor proteins to drive mitochondrial fission (Adaniya *et al.,* 2019). OPA1-mediated fusion relies on the ratio between the long (L) and short (S) OPA1 isoforms, which is partly modulated by STOML2 (Hu *et al.,* 2021), while OPA1 activity is regulated by acetylation and O-GlcNAcylation (Meiliana, Dewi and Wijaya, 2021). STOML2 activity is known to be regulated by post-translational phosphorylation, glycosylation and ubiquitination, while protein-protein interactions between all of these key regulators also mediate their functions (Adaniya *et al.,* 2019). As such, future work will be needed to examine how PPA changes protein expression, activity and function to establish a mechanistic relationship between the transcriptional disruptions observed here and downstream changes to mitochondrial function. Nevertheless, this data does reflect a systemic dysregulation of genes required for mitostasis, which provides novel insight into the molecular signatures involved in PPA-associated metabolic stress.

2.4.3. Functional Evidence of Mitochondrial Remodelling

This study evaluated several different endpoints of mitostasis to evaluate whether transcriptional disruptions were associated with impairments to mitochondrial function. Here, confocal microscopy demonstrated that PPA perturbed mitochondrial integrity as cells progressed from mitochondrial compensation to cell death. Although mitochondrial network morphology remained intact until 24 hours of PPA stress, mitochondrial fragmentation was evident after 72 hours, illustrated by a significant decrease in mitochondrial content, size, area, perimeter and volume. Concurrently, PPA impaired mitochondrial network connectivity, reflected by a decrease in average branch length, an increase in the density of branch points and a reduced area: perimeter ratio. Notably, this fragmented network morphology is characteristic of cells derived from PA patients (Schumann *et al.,* 2021) and reflects previous studies of PPA administration *in vitro* (Wei *et al.,* 2024). However, unlike the global degradation of the mitochondrial network induced by FCCP, PPA significantly reduced total mitochondrial content and average mitochondrial size without a concurrent decrease in either mtDNA copy number or mitochondrial count.

A decrease in mitochondrial size can reflect an increase in fission, a decrease in fusion or an increase in mitogenesis to generate small nascent mitochondria. Yet, an increase in mitochondrial count would result from any of these mechanisms in isolation. The mitochondrial remodelling observed here is more likely due to a net imbalance in mitostasis resulting from disruptions to several processes simultaneously. Indeed, recent work in our lab showed that PPA significantly altered the frequency of both fission and fusion events after 24 hours in a dose-dependent manner (Buchanan *et al.,* 2023). However, the mechanisms that alter mitochondrial network integrity under PPA stress remain under investigation. Recent studies have shown that toxic propionyl derivatives disrupt mitochondrial morphology by inhibiting the MICOS complex (Zhou *et al.,* 2022), modulating mitochondria-endoplasmic reticulum (ER) contacts (Brondani *et al.,* 2023) or increasing DRP1 protein expression and oligomerisation (Park *et al.,* 2015; Okada *et al.,* 2021). The transcriptional profiles associated with PPA exposure presented in **2.4.2.** also revealed an acute downregulation of transcripts required for fusion, which may contribute to an imbalance in mitochondrial dynamics. Ultimately, future work will be needed to better characterise the disruptions to mitochondrial dynamics that remodel mitochondrial networks under PPA stress.

Still, the fact that mitochondrial count remains unchanged despite the decrease in mitochondrial size, branch length, and network connectivity may suggest a role for mitophagic clearance. Here, LC3β was used to measure the colocalisation between autophagosomes and mitochondrial networks to evaluate whether PPA alters mitophagic flux. Importantly, LC3β is detected upon the formation of mature autophagosomes but not after their subsequent degradation in autolysosomes. As such, a decrease in total LC3β expression at a single time point may reflect an inhibition of autophagosome formation or an upregulation of autophagic degradation. Here, total LC3β expressed was reduced in FCCP-treated positive controls which contradicts the expected response to ΔΨm depolarisation. However, the reduced LC3β expression in conjunction with the significantly decreased mitochondrial content suggests that active mitophagy likely occurred before samples were fixed and stained, at which point most active autophagosomes had been degraded along with a substantial fraction of the mitochondrial network. Since nutrient starvation is known to induce autophagy *in vitro* (Orhon and Reggiori, 2017), it is also possible that the use of serum depletion to reduce glycolytic reliance also influenced measures of autophagic flux in this study.

While samples exposed to PPA displayed a similar decrease in total LC3β, it is unclear whether this reflects a suppression or upregulation of autophagy. The existing literature shows that PPA consistently perturbs autophagic flux *in vitro*, but the nature of this dysregulation appears to be highly context-specific. For example, PPA upregulates autophagy in cancer-derived, bovine and murine cell models (Tang *et al.,* 2011; Iannucci *et al.,* 2016; Gao *et al.,* 2021; Pham *et al.,* 2021; Filippone *et al.,* 2022; Jia *et al.,* 2022; Ma and Wang, 2022) and upregulates autophagosome formation but impairs autophagic degradation in hippocampal neurons (Choi *et al.,* 2020; Jeon *et al.,* 2022). While future work will

establish global changes to autophagic flux, this study focused on LC3β localisation to assess mitophagic control under PPA stress. Here, the LC3β colocalisation ratio was significantly increased after 24 hours of PPA exposure but decreased by 72 hours, while the mitochondrial colocalisation ratio remained unchanged at these conditions.

Considering the decrease in total LC3β expression, this data may indicate that PPA does not alter global autophagic flux, but rather that the existing autophagic capacity is preferentially harnessed for mitophagic control. This appears to precede significant changes to mitochondrial content or connectivity, as the highest degree of LC3β-MitoTracker colocalisation was observed under conditions at which mitochondrial mass and network morphology remained largely unperturbed. On the other hand, severe stress induced by either FCCP or PPA appeared to decrease active mitophagy below homeostatic levels. This decrease in mitophagy occurs after the mitochondrial network has been largely degraded during FCCP exposure, while a similar downregulation of mitophagic flux under PPA stress occurred when a substantial fraction of mitochondrial volume was still retained. This could suggest that both the upregulation and subsequent downregulation of mitophagic flux serve a compensatory purpose that facilitates cell survival under prolonged PPA stress.

Indeed, an increase in mitophagy was previously observed after 24 hours at 1-2mM PPA in SH-SY5Y cells using correlative light and transmission microscopy (Jung *et al.,* 2020). Interestingly, these authors showed that 72 hours at 1mM PPA increased the number of autophagosomes, autolysosomes and LC3 puncta without altering total LC3 expression. Thus, the total autophagic and mitophagic activity observed at 5mM does not negate differential effects at earlier time points or lower doses and may suggest that, like the FCCP control, active autophagosomes were most prevalent under PPA stress before cells were visualised. Several studies have also proposed a role for autophagy as a protective mechanism to mitigate PPA- induced apoptosis *in vitro* (Tang *et al.,* 2011; Iannucci *et al.,* 2016; Gao *et al.,* 2021; Pham *et al.,* 2021; Filippone *et al.,* 2022; Jia *et al.,* 2022; Ma and Wang, 2022), while studies in neuronal-like cell lines illustrate impairments to autophagic flux with prolonged PPA exposure (Choi *et al.,* 2020; Jung *et al.,* 2020; Jeon *et al.,* 2022) and PA-derived cell lines demonstrate decreased mitophagic flux despite high rates of autophagy (Schumann *et al.,* 2021).

This discrepancy might be explained by a preferential reliance on micromitophagy in highly oxidative cells (Choubey, Zeb and Kaasik, 2022). Unlike macromitophagy, which is governed by the autophagic machinery, micromitophagy is a more targeted process that minimises the cost to mitochondrial capacity (Roberts et al. 2016). Micromitophagy can also serve as a compensatory mechanism to maintain mitostasis under conditions that impair autophagic flux (Ma, Han and Zhan, 2024). Rather than degrading whole organelles via autophagosomes, micromitophagy removes damaged mitochondrial contents via small mitochondrial-derived vesicles (MDVs) (Choubey, Zeb and Kaasik, 2022). This mechanism can be triggered by a loss of $\Delta\Psi m$ or oxidative stress, leading to an accumulation of

damaged proteins at the mitochondrial membrane, which is distorted as its components become oxidised (Choubey, Zeb and Kaasik, 2022). Subsequently, MDVs are formed from the outer mitochondrial membrane in a process mediated by PINK1 and PARKIN and then sequestered directly into endolysosomes through the coordinated function of MIRO1 and DRP1(Ma, Han and Zhan, 2024). Notably, this chapter showed that PPA induced mitochondrial depolarisation, impaired ATP production and decreased mitochondrial volume without evidence of increased LC3β puncta formation or total mitophagic activity. Moreover, PPA-exposed cells displayed an oxidative reliance above 90% and PPA has previously been found to impair autophagic flux in neurons (Choi *et al.,* 2020; Jeon *et al.,* 2022). Thus, micromitophagy may be employed as a mechanism of mitochondrial quality control under PPA stress that contributes to the subtle decrease in mitochondrial content without significantly upregulating autophagosome formation.

Collectively, the data presented here reveal novel insights into the remodelling of mitochondrial dynamics under PPA stress, suggesting changes to mitochondrial volume, connectivity, integrity and turnover. Future work will be needed to identify the molecular mechanisms that remodel mitochondrial networks under PPA stress. This discussion has considered several mechanisms that could inform the direction of future studies. The current literature highlights the MICOS complex, DRP1, MFN2 and OPA1 as potential drivers of mitochondrial dynamics under PPA stress, while PINK1, PARKIN, DRP1 and MIRO1 may be involved in modulating mitophagic flux. It will be important to clarify the effect of PPA on autophagy, macromitophagy and micromitophagy in future studies in order to understand neuron-specific responses to PPA. Here, the differential effects of glycolytic and oxidative reliance in the presence and absence of serum depletion could provide insight into the variable relationship between PPA and autophagy reported in the current literature. Still, the work presented here effectively demonstrates significant changes to mitochondrial network integrity that supports the transcriptional dysregulation of mitostasis under PPA stress and indicates functional implications for mitochondrial metabolism.

2.4.4. Metabolic Signatures of Energetic Crisis

This chapter ultimately aimed to establish a model for mitochondrial dysfunction that altered end-point metabolic state, so that subsequent chapters could examine the downstream consequences for neurogenesis. Having characterised dynamic changes to cell viability, transcription, and mitochondrial morphology, live-cell respirometry was employed to evaluate mitochondrial metabolism under chronic PPA stress. Here, 72 hours at 5mM PPA significantly suppressed mitochondrial respiration, depleted spare respiratory capacity and inhibited both basal and compensatory glycolysis. As a result, PPA decreased total ATP synthesis by more than 60% while basal, spare, maximal and non-mitochondrial respiration were all impaired by at least 40%. This not only demonstrates significant impairments to mitochondrial energy production but suggests systemic disruptions to metabolic state. Indeed, the

biochemical landscape associated with PPA exposure reshapes both anabolic and catabolic metabolism via coordinated disruptions to OXPHOS, glycolysis, gluconeogenesis and glutaminolysis **(Figure 2.21).** These metabolic deficits can be attributed to the overproduction of propionyl CoA and its derivatives. *In vitro,* PPA is converted to propionyl CoA, which is an endogenous metabolite produced by either aldehyde dehydrogenase 6 family member A1 (ALDH6A1), acetyl-CoA acetyltransferase 1 (ACAT1) or branched-chain α-keto acid dehydrogenase complex (or BCKDC) during the catabolism of valine, thymine, isoleucine, methionine, threonine or cholesterol (Sun *et al.,* 2023). As a precursor to succinyl CoA, propionyl CoA can be used to fuel either OXPHOS or gluconeogenesis, but it can also react with oxaloacetate, carnitine, glycine or reactive nitrogen species to produce methylcitrate (MC), propionylcarnitine (PC), propionylglycine (PG) or 3-hydroxypropionate respectively (Abily-Donval *et al.,* 2017).

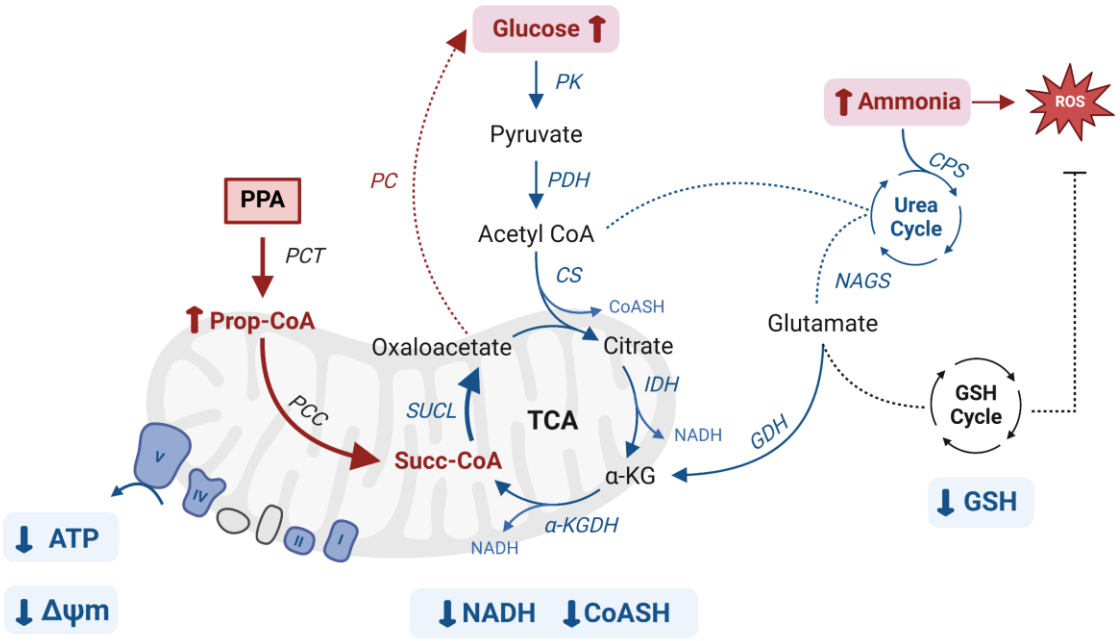


Figure 2.21. Profiles of Glucose Utilisation Under Propionic Acid Stress. Propionic Acid (PPA) is metabolised by propionate-CoA transferase (PCT) to produce Propionyl CoA (Prop-CoA), which is in turn metabolised by Propionyl CoA Carboxylase (PCC) to produce Succinyl CoA (Succ-CoA). Prop-CoA directly inhibits including pyruvate dehydrogenase (PDH), alpha-ketoglutarate dehydrogenase (αKGDH) and succinate CoA ligase (SUCL) in the TCA cycle as well as electron transport chain (ETC) complexes I, II, IV and V. Succ-CoA inhibits citrate synthase (CS) and αKGDH which limits the production of NADH and CoASH needed for oxidative phosphorylation. The increased CoA: CoASH ratio inhibits glycolysis via pyruvate kinase (PK) but upregulates pyruvate carboxylase (PC) and other gluconeogenic enzymes. PPA dysregulates glutamate metabolism by inhibiting glutamate dehydrogenase (GDH) in glutaminolysis, αKGDH in TCA anaplerosis, N-acetyl glutamate synthetase (NAGS) and carbamoyl phosphate synthetase (CPS) in the urea cycle and sequestering glutamate in propionylglutamate. In turn, disruptions to glycolytic and glutamate metabolism perturb the synthesis of glutathione (GSH) which modulates redox homeostasis. Together, disruptions to the TCA cycle, glycolysis, the urea cycle and one carbon metabolism inhibit ATP synthesis, impair mitochondrial membrane potential, erode metabolic flexibility and contribute to hyperammonaemia, oxidative stress and excitotoxicity.

At pathological levels, each of these byproducts can disrupt OXPHOS via both direct and indirect mechanisms. Propionyl CoA directly inhibits several TCA cycle enzymes, including PDH, alpha-ketoglutarate dehydrogenase (αKGDH) and succinate CoA ligase (SUCL), leading to decreased pyruvate, αKG and succinate oxidation, reduced ETC activity and diminished ATP and GTP production (Wongkittichote, Ah Mew and Chapman, 2017). Similarly, PPA has been shown to inhibit the ETC Complexes I, II, IV and V in both patient-derived cell lines and murine models (Collado *et al.,* 2020; Mehan *et al.,* 2020; Park *et al.,* 2020). Concurrently, propionyl CoA inhibits N-acetyl glutamate synthetase (NAGS) and carbamoyl phosphate synthetase (CPS) in the urea cycle (Stern and Wilcox, 1994), which leads to hyperammonaemia, TCA dysregulation, impaired mitochondrial respiration and oxidative stress (Angelova *et al.,* 2022). As propionyl CoA accumulates, there is also an increase in the production of succinyl CoA, which enhances flux through the latter half of the TCA cycle. However, succinyl CoA inhibits both citrate synthase (CS), which is coupled to the conversion of acetyl CoA to CoA, and αKGDH which converts NAD^+ to NADH (Frye *et al.,* 2015). Similarly, the conversion of propionyl CoA to MC disrupts TCA cycle flux via the inhibitory effect of MC on CS (Sun *et al.,* 2023). Thus, pathophysiological levels of propionyl CoA slow pyruvate oxidation and mitochondrial respiration while "short-circuiting" the early TCA steps that produce both the free CoA (CoASH) required by PDH and αKGDH, and the NADH used for ETC-coupled ATP synthesis.

At the same time, the influx of succinyl CoA leads to an accumulation of oxaloacetate, which functions as a gluconeogenic substrate (Wang *et al.,* 2023). Concurrently, the elevated acyl CoA: CoASH ratio inhibits the terminal stage of glycolysis mediated by pyruvate kinase (PK) (Weber, Lea and Stamm, 1967) while upregulating pyruvate carboxylase (PC) at the start of gluconeogenesis (Chen and Park, 2022). In fact, PPA has been found to upregulate several gluconeogenic enzymes, including fructose 1,6-bisphosphatase, phosphoenolpyruvate carboxykinase, and glucose-6-phosphatase in animal models (Zhan *et al.,* 2020; Wang *et al.,* 2023), leading to hyperglycaemia in both preclinical (Perry *et al.,* 2016; Tirosh *et al.,* 2019; Xu *et al.,* 2022) and clinical studies (Tirosh *et al.,* 2019; Adler *et al.,* 2021). In this way, PPA shifts glucose metabolism towards gluconeogenesis rather than glycolysis, which decreases the production and oxidation of pyruvate as an energy source.

This is consistent with the suppression of glycolysis induced by PPA in SH-SY5Y cells and may explain the synergistic inhibition of both glycolytic and oxidative ATP production in this context. Indeed, the decrease in NADH production and CS activity under PPA stress has been shown to collapse the $\Delta\Psi m$ via the mPTP (Roginski *et al.,* 2020) and inhibit both oxidative and glycolytic metabolism *in vitro* (Sun *et al.,* 2023), which reflects the metabolic deficits observed in SH-SY5Y cells exposed to PPA. Notably, this contrasts the reciprocal relationship between glycolytic and oxidative metabolism usually observed in SH-SY5Y cells (Swerdlow *et al.,* 2013; Farina *et al.,* 2018; Bovio *et al.,* 2021; Yang *et al.,* 2021) and profoundly impacts the capacity to compensate for metabolic stress. While neurons rely primarily on mitochondrial respiration for energy, glycolysis provides essential intermediates for oxidative

metabolism (Li *et al.,* 2023). In fact, studies in SH-SY5Y cells reported that an upregulation of glycolysis fuels the increased mitochondrial capacity that drives neurogenesis (Xun *et al.,* 2012; Li *et al.,* 2020) while inhibiting glycolysis was found to impair the differentiation of primary cortical neurons *in vitro* (Agostini *et al.,* 2016). Indeed, *in vivo* studies revealed an essential role for glycolysis in the dynamic and cell-type specific adaptions to metabolic stress in the brain (Wolfe *et al.,* 2024) while attenuating neuronal glycolysis decreased synaptic ATP production leading to neurophysiological and cognitive deficits (Li *et al.,* 2023). Importantly, glycolytic intermediates also fuel the anabolic pathways that produce the proteins, lipids and nucleotides required for synaptic development, plasticity and signalling (Zhang *et al.,* 2021). Thus, PPA-induced disruptions to glycolytic flux may not only impact metabolic state, but also have profound consequences for neurophysiology and function.

In neurons, the pyruvate derived from glycolysis is supplemented with the αKG derived from glutaminolysis to sustain the high rates of OXPHOS. Glutaminolysis is critical for the maintenance of *metabolic flexibility*, defined as the capacity for a cell to derive energy from different substrates in response to different environmental conditions (Virmani and Cirulli, 2022). This is not only a vital compensatory response required to adapt to forms of metabolic stress, but also one of the defining features of NSCs that facilitates neuronal maturation (Xun *et al.,* 2012). Glutaminolysis has been shown to play a central role in upregulating mitochondrial capacity in NPCs (Gkini and Namba, 2023), SH-SY5Y cells (Lezi and Swerdlow, 2016) and primary neurons (Agostini *et al.,* 2016), while glutamate supplementation was found to promote neuronal differentiation by enhancing oxidative respiration in hippocampal neurons (D'Andrea *et al.,* 2024). Notably, propionyl CoA disrupts glutamate cycling by i) decreasing the activity of PK which facilitates the synthesis of glutamate from glucose, ii) increasing the production of MC which inhibits the glutamate dehydrogenase (GDH) that drives glutaminolysis, iii) directly inhibiting the activity of αKGDH, which integrates glutamate into the TCA cycle via anaplerosis, iv) inhibiting both NAGS and CPS, which incorporate glutamine into the urea cycle and v) sequestering free glutamate in the form of propionylglutamate (Wang *et al.,* 2018; Marchuk, Wang, Ladd, Chen and G. F. Zhang, 2023). This is particularly relevant for the SH-SY5Y model established in this chapter, which favoured glutamine over glucose as a carbon source to recapitulate the oxidative reliance of neurons *in vivo*. Here, the inhibition of glutamate-driven anaplerosis likely limited its utility as an energy source in PPA-exposed cells, contributing to the observed reduction in oxygen consumption and ATP production.

Importantly, glutamate is also centrally involved in the regulation of neurodevelopment, neurotransmission, and neuroplasticity (Nisar *et al.,* 2022). In fact, a dysregulation of glutamatergic signalling due to TCA cycle dysfunction is implicated as a fundamental mechanism in PPA-associated neuropathology (Wongkittichote, Ah Mew and Chapman, 2017). *In vitro* studies have shown that PCCB deficiency alters GABA/glutamate cycling by disrupting TCA metabolism in human forebrain organoids (Zhang *et al.,* 2023). Moreover, *in vivo* models show that PPA consistently promotes

glutamatergic excitotoxicity (El-Ansary *et al.,* 2018; Al-Suwailem *et al.,* 2019; Alfawaz *et al.,* 2022), which is a hallmark of ASD aetiology associated with anxiety, perseveration, seizures and motor stereotypies (Nisar *et al.,* 2022). Glutamate also serves as an essential substrate for GSH synthesis, which is critical for neuronal redox homeostasis as one of the most abundant thiols in the brain (Pradhan *et al.,* 2020; Aoyama, 2021; Iskusnykh, Zakharova and Pathak, 2022). Intracellular pools of GSH are modulated by the rate of GSH oxidation, the availability of glycolytic intermediates and the recycling of glycine and cysteine through one carbon metabolism (Aoyama, 2021). PPA not only upregulates GSH oxidation due to the increased NAD^+: NADH ratio, but also suppresses glycolytic flux and perturbs the turnover of GSH precursors in the methionine and folate cycles. As a result, GSH deficiency is widely reported in the PPA murine model for ASD (MacFabe *et al.,* 2007; Shultz *et al.,* 2008; El-Ansary, Bacha and Kotb, 2012; Shultz and Macfabe, 2014; Al-Daihan and Shafi Bhat, 2015; Khalil *et al.,* 2015; Mirza and Sharma, 2019; Alfawaz *et al.,* 2022). Collectively, the separate mechanisms that inhibit both glycolysis and glutaminolysis under PPA stress not only effectively eliminate the capacity for metabolic flexibility, but also deplete crucial substrates needed to synthesise dendritic extensions, synaptic vesicles, neurotransmitters and antioxidants.

As well as systemic disruptions to glucose utilisation, the energetic deficits induced by PPA may be attributed to a dysregulation of CoA homeostasis **(Figure 2.22).** Plasma CoASH deficiency is frequently reported in PA (Virmani and Cirulli, 2022; Marchuk, Wang, Ladd, Chen and G.-F. Zhang, 2023), while PPA administration decreases CoASH *in vitro* (Wilson *et al.,* 2017; Wang *et al.,* 2018). In fact, upregulating CoASH biosynthesis was able to alleviate the metabolic deficits associated with PCC dysfunction *in vivo* (Subramanian *et al.,* 2021, 2023). Notably, acyl CoA metabolism operates as a regulatory switch that balances energy production with biosynthesis in response to energetic state (Shi and Tu, 2015). Acetyl CoA functions at the intersection between anabolic and catabolic metabolism by regulating glycolysis, gluconeogenesis, OXPHOS and the balance between FAO and FAS (Czumaj *et al.,* 2020). Likewise, CoASH is an essential cofactor involved in OXPHOS, AA and lipid metabolism (Czumaj *et al.,* 2020) that serves as a carrier for activated acyl groups required for energy production, lipid synthesis, detoxification, protein acetylation and transcriptional regulation (Grevengoed, Klett and Coleman, 2014). Thus, CoA sequestration may play a central role in PA pathophysiology.

Both propionyl and succinyl CoA broadly disrupt mitochondrial CoA metabolism by directly sequestering CoASH, inhibiting CoASH synthesis and dysregulating the mechanisms that maintain CoA homeostasis (Steinberg and Rucker, 2005; Gout, 2018). CoASH biosynthesis is driven by pantothenate kinase (PANK) in a reaction that consumes both cysteine and ATP (Czumaj *et al.,* 2020). The suppression of glycolysis induced by PPA depletes intracellular pools of both cysteine and ATP, while propionyl CoA directly inhibits PANK (Halvorsen and Skrede, 1982) which is also subject to feedback inhibition by the acyl CoA: CoASH ratio that is disrupted by PPA (Steinberg and Rucker, 2005; Gout, 2018). Concurrently, PPA broadly perturbs the balance between fatty acyl import, export

and sequestration in the mitochondrial matrix (Fadó, Rodríguez-Rodríguez and Casals, 2021). On the one hand, propionyl CoA directly inhibits ACC, which drives the rate-limiting reaction of lipogenesis, while upregulating the mitochondrial import of fatty acyl CoAs (He *et al.,* 2021). This exacerbates the mitochondrial acyl imbalance that is partly responsible for the energy deficit induced by PPA (Geoghegan *et al.,* 2017) and depletes the cytosolic malonyl CoA required for neuronal lipogenesis (Tracey et al. 2018). On the other hand, PPA directly sequesters free carnitine, which facilitates both the import and export of acyl CoAs across the mitochondrial membrane as well as the release of CoASH in the mitochondrial matrix (Ferreira and McKenna, 2017). In fact, carnitine is crucial for the maintenance of metabolic flexibility and plays an essential role in antioxidant defence, detoxification and neuroprotection (Ferreira and McKenna, 2017; Maldonado, Vázquez and Fagiolino, 2020). Thus, diverse disruptions to CoA metabolism under PPA stress exacerbate its inhibitory effect on TCA flux, further erode metabolic flexibility and deplete fatty acid substrates that are critical for neurodevelopment, physiology and function.

Interestingly, the CoA sequestration hypothesis metabolism may reveal a mechanistic relationship between the metabolic, transcriptional and morphological impairments to mitostasis observed in the PPA model. As cofactors for acetyltransferases that modify histones and proteins, acyl CoA metabolism broadly modulates the expression and function of mitochondrial genes. Histone acetylation is determined by nucleocytosolic acyl CoA concentrations and PPA has previously been shown to increase histone acetylation *in vitro* (Kiefer, Beyer-Sehlmeyer and Pool-Zobel, 2006; Nguyen *et al.,* 2007) by increasing acyl CoAs, inhibiting HDACs (Silva *et al.,* 2018) and activating HATs (Thomas and Denu, 2021). Recent studies have found that acetyltransferases can also mediate a process called propionylation, during which propionyl groups are added directly to histones (Park *et al.,* 2020). Indeed, increased histone propionylation has been observed in PA and as a consequence of PPA administration in preclinical studies (Lagerwaard *et al.,* 2021; Park *et al.,* 2023). While the context-specific implications of histone propionylation are under investigation, histone propionylation has been characterised as a mark of active chromatin (Taudt *et al.,* 2017) with key roles in protein turnover, mitochondrial function, differentiation and cell fate (Trefely *et al.,* 2020; Lagerwaard *et al.,* 2021). Acetylation also modulates gene expression by activating transcription factors and thousands of proteins involved in metabolism – including several genes of interest examined in this chapter, such as c-MYC, PGC1α, TFAM and OPA1 - and levels of protein acetylation are linked to acyl CoA availability (Shi and Tu, 2015). In addition, CoA binds directly to cysteine residues in more than 500 metabolic proteins, which serves as a protective mechanism in response to metabolic or oxidative stress (Filonenko and Gout, 2023). Therefore, disruptions to the propionyl, acyl and CoASH pools in the nucleus, cytosol and mitochondria can broadly alter the regulation of gene expression and protein activity with implications for mitochondrial function and dynamics under stress.

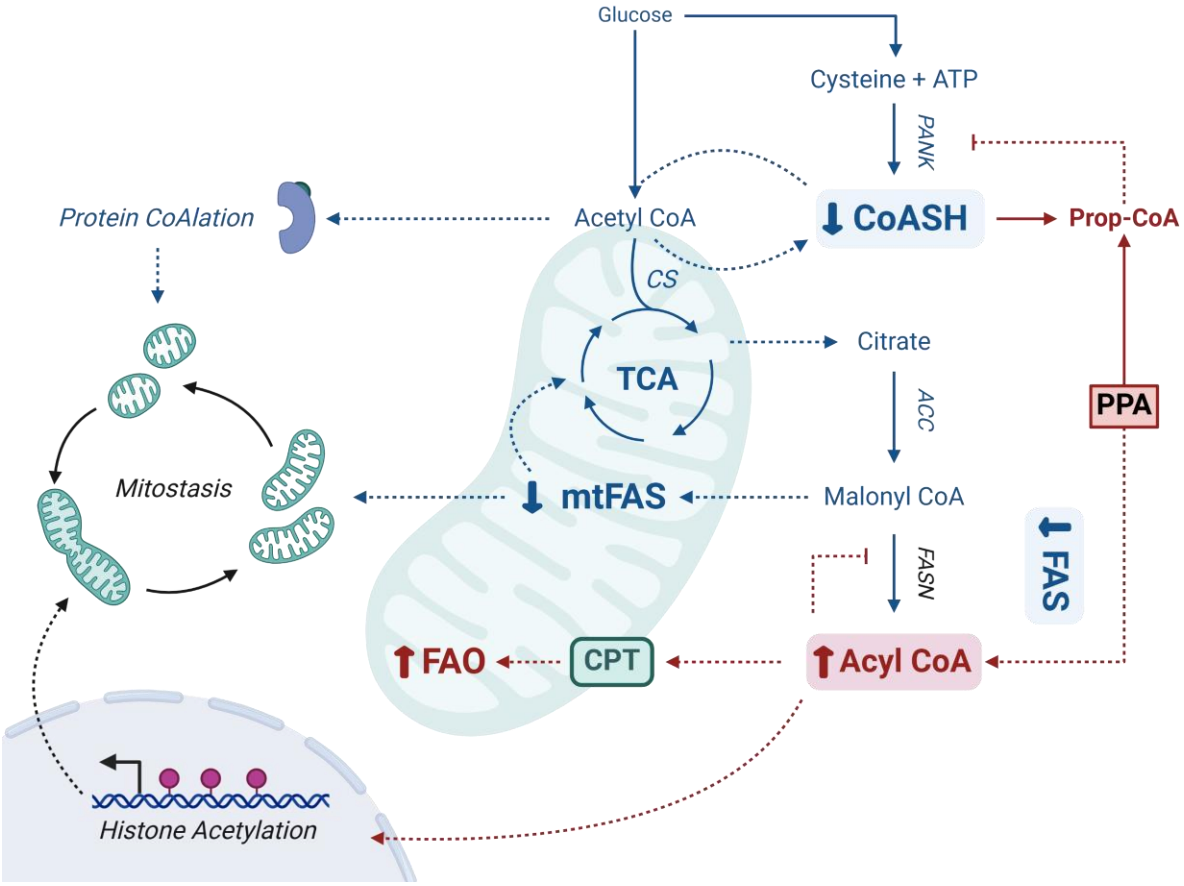


Figure 2.22. The CoA Sequestration Hypothesis. Propionic Acid (PPA) sequesters CoASH as Propionyl CoA (Prop-CoA), which directly inhibits pantothenate kinase (PANK) while preventing the release of CoASH coupled to citrate synthase (CS) activity. Disruptions to glycolysis also impair CoASH synthesis by depleting intracellular cysteine and ATP. Prop-CoA inhibits acetyl CoA carboxylase (ACC), limiting the synthesis of malonyl CoA, which is required for mitochondrial fatty acid synthesis (mtFAS). mtFAS is required to produce lipoic acid, acyl carrier proteins and mitochondrial membrane phospholipids; thus, disruptions to mtFAS impair mitochondrial respiration, biogenesis and electron transport chain (ETC) assembly, decrease mitochondrial volume and perturb mitochondrial membrane composition, which is coupled to mitochondrial membrane potential (ΔΨm), dynamics, morphology and function. Concurrently, the accumulation of Acyl CoAs inhibits Fatty Acid Synthetase (FAS) while upregulating the activity of the carnitine transferase (CPT) that imports fatty acyls into the mitochondrial matrix. This depletes the free carnitine required for mitochondrial acyl buffering, promotes fatty acid oxidation (FAO) and exacerbates the acyl imbalance that inhibits mitochondrial respiration. A dysregulation of nucleocytosolic acyl CoAs impacts the global histone acetylation profiles that regulate gene expression while CoAlation modulates the activity of proteins involved in mitochondrial metabolism and dynamics. Thus, impairments to the CoASH: Acyl CoA ratio could influence both transcriptional and post-transcriptional mechanisms that govern mitochondrial metabolism, morphology and dynamics.

In addition, CoA metabolism functions as a bridge between metabolism and mitostasis that couples metabolic state to mitochondrial dynamics. The energetic deficit induced by PPA decreases the synthesis of malonyl CoA, which is the obligatory substrate required for mitochondrial fatty acid synthesis (mtFAS) (He *et al.,* 2021). mtFAS is a process distinct from cytosolic FAS that produces essential metabolic cofactors, ETC complexes and mitochondrial membrane phospholipids in the mitochondrial matrix (Nowinski *et al.,* 2020). Notably, deficits in mtFAS have been shown to inhibit mitochondrial

biogenesis (Kursu *et al.,* 2013), decrease mitochondrial volume, and disrupt ETC assembly (Nowinski *et al.,* 2020). Importantly, mtFAS also modulates the composition of the mitochondrial membrane, which is known to influence mitochondrial morphology and ultrastructure (Guler *et al.,* 2008). Perturbations to mitochondrial membrane composition can promote fission by destabilising membrane lipid bilayers and depleting the substrates for the mitochondrial phospholipases that catalyse fusion (Wai and Langer, 2016). The density and distribution of cardiolipin, phosphatidylethanolamine and phosphatidylcholine in the inner mitochondrial membrane has also been shown to influence the formation, organisation and morphology of mitochondrial cristae, which in turn governs fission and fusion events across the mitochondrial network (Ikon and Ryan, 2017; Venkatraman *et al.,* 2023). This highlights the possibility that the disruptions to mitochondrial content and connectivity induced by PPA may be underpinned by changes to CoA metabolism and mtFAS. In particular, the decrease in mitochondrial volume without significant changes to mtDNA copy number is consistent with an inhibition of mtFAS, which would impact mitochondrial biosynthesis more than mtDNA replication. Moreover, the mitochondrial fragmentation induced by PPA is consistent with disruptions to mitochondrial dynamics resulting from changes to mitochondrial membrane composition, which could also drive the disruptions to mitochondrial morphology and ultrastructure previously reported in the PPA model (Kim *et al.,* 2019; Jung *et al.,* 2020; Buchanan *et al.,* 2023).

On the other hand, the mitochondrial remodelling induced by PPA can also be explained by a broader relationship between mitochondrial morphology and metabolic state. Different profiles of substrate utilisation are associated with distinct changes to mitochondrial morphology, and a reciprocal relationship between metabolic state and mitochondrial dynamics is well-documented (Wai and Langer, 2016). Pérez-Hernández *et al.,* (2022) found that some TCA metabolites induce mitochondrial fusion while others, including succinate and SCFAs, induce mitochondrial fission. Similarly, D'Andrea *et al.,* (2024) showed that inhibiting pyruvate and glutamate import differentially impacts mitochondrial elongation and network complexity in neurons. Moreover, Toleikis *et al.,* (2020) showed that levels of FAO modulate the size of the cristae, the intermembrane space and the mitochondrial matrix, while Ngo *et al.,* (2023) reported a reciprocal relationship between FAO and mitochondrial fragmentation. Here, mitochondrial fragmentation was found to be a cause and consequence of increased FAO by shifting the balance between fatty-acyl CoA import and export. In this context, the mitochondrial fragmentation observed in PPA-exposed SH-SY5Y cells reflects the response associated with increased FAO (Ngo *et al.,* 2023), elevated intracellular succinate (Pérez-Hernández *et al.,* 2022) and impaired glutamate metabolism (D'Andrea *et al.,* 2024) *in vitro*. Thus, the metabolic signature of PPA exposure is consistent with the observed changes to mitochondrial size, shape, ultrastructure and network integrity, proposing a role for metabolic remodelling in PPA-induced disruptions to mitochondrial morphology.

The molecular players that mediate the relationship between mitochondrial metabolism and morphology remain under investigation. However, a loss of ΔΨm associated with TCA inhibition is

known to induce mitochondrial fragmentation by activating both DRP1 (Jones *et al.,* 2017) and the OMA1 metalloprotease that mediates L-OPA1 cleavage (Morciano *et al.,* 2021). Alternatively, L-OPA1 cleavage by the AAA protease YME1L is thought to be modulated by mitochondrial OXPHOS and energetic state (Wai and Langer, 2016), while fatty acid overload is known to trigger the ubiquitin-dependent degradation of MFN2 (Hu *et al.,* 2024). Indeed, a decrease in MFN2 expression was found to mediate fatty acid-induced mitochondrial fragmentation in both *in vitro* (Hu *et al.,* 2024) and *in vivo* (Schneeberger *et al.,* 2013) studies. There is also evidence to suggest that substrate utilisation profiles are associated with the differential regulation of MFN1 (Zhang *et al.,* 2019) and STOML2 (Zhang *et al.,* 2021). Thus, a reciprocal relationship between transcriptional, morphological and metabolic remodelling could connect the diverse disruptions to mitostasis under PPA stress.

The metabolic profile of PPA exposure may also yield insight into the associated changes to mitochondrial turnover and mitophagic flux. Section **2.4.2** described how AMPK functions as an upstream regulator of both c-MYC and PGC1α that is activated by an energetic deficit. In fact, AMPK serves as a focal regulator of mitochondrial biogenesis, dynamics and clearance (Herzig and Shaw, 2017) that triggers autophagy by inhibiting the mTOR and UNC-51-like autophagy-activating kinase 1 (ULK1). AMPK also promotes mitophagy by directly recruiting autophagosomal complexes to the mitochondrial membrane (Liang et al. 2015) and phosphorylating both the mitochondrial fission factor (MFF) that recruits DRP1 to the mitochondria and PINK1 (Zimmermann *et al.,* 2024). Thus, AMPK could drive disruptions both autophagic and mitophagic flux in response to the decreased ATP production rate induced by PPA. Indeed, several *in vitro* studies have shown that PPA upregulates autophagy in an AMPK-dependent manner (Tang *et al.,* 2011; Iannucci *et al.,* 2016; Gao *et al.,* 2021; Pham *et al.,* 2021). On the other hand, a drop in intracellular levels of αKG due to a suppression of glutaminolysis can activate autophagy by inhibiting the RAG GTPase upstream of mTORC1 (Zimmermann *et al.,* 2024). Moreover, the decrease in both CoASH and NADH that results from PPA-mediated TCA inhibition has implications for autophagic flux. As a substrate for the EP300 acetylase that inhibits LC3 and ATG7, a depletion of acetyl CoA is known to trigger autophagy *in vitro* (L. Shi and Tu 2015). Similarly, an increase in NAD^+ has been shown to increase mitophagy *in vitro*, mediated by the activation of sirtuin deacetylases that target autophagy-related proteins (ATGs) and LC3 (Zimmermann *et al.,* 2024). Therefore, the bioenergetic consequences of PPA exposure could broadly modulate autophagic flux via upstream AMPK-mTOR signalling and by directly influencing the PTMs that activate autophagic proteins.

Collectively, this discussion proposes a mechanistic convergence between the disruptions to mitochondrial bioenergetics, connectivity and morphology under PPA stress. The TCA inhibition induced by PPA may increase intracellular succinate, AMP and NAD^+ while depleting αKG, CoASH and acetyl CoA – all of which are metabolic signatures associated with mitochondrial fragmentation and mitophagic clearance. The activation of AMPK could disrupt the integrated regulation of

mitogenesis, autophagy and mitophagy, while the decrease in ΔΨm may trigger fission and mitophagy mediated by DRP1, OMA1 and PINK1 respectively. Similarly, the shift in lipid utilisation that promotes FAO at the expense of lipogenesis could promote mitochondrial fragmentation by downregulating MFN2. Moreover, the depletion of malonyl CoA profoundly alters the regulatory feedback loop that couples metabolic state with mitogenesis, which has implications for TCA metabolism, mitochondrial biosynthesis, and the interdependent relationship between mitochondrial ultrastructure and network connectivity. Like metabolic flexibility, the dynamic remodelling of the mitochondrial network and cristae ultrastructure is essential to drive cellular adaptions under stress. The disruptions to substrate utilisation and mtFAS induced by PPA could ultimately erode this adaptive capacity and hinder both the metabolic and morphological mechanisms that remodel mitostasis during neurodevelopment and beyond.

2.5. Summary and Conclusions

This chapter studied PPA-induced mitochondrial dysfunction in the context of oxidative reliance using undifferentiated SH-SY5Y cells exposed to glucose- and FBS- depletion. An acute loss of ΔΨm, disruptions to gross cellular morphology and dose-dependent cytotoxicity suggested mPTP-mediated apoptosis that was consistent with previous characterisations of the PPA model in SH-SY5Y cells. This chapter revealed novel disruptions to gene expression, mitochondrial network morphology and metabolism that suggested systemic impairments to mitostasis under PPA stress. The data revealed a depletion of mRNA transcripts required for the adaptive remodelling of mitostasis via biogenesis, fission and fusion, which was associated with impaired mitochondrial content, connectivity and turnover. Consequently, PPA substantially inhibited mitochondrial respiration, eroded spare respiratory capacity, decreased metabolic flexibility and reduced glycolytic and oxidative ATP production. At a biochemical level, this is consistent with the disruptions to TCA metabolism, glycolysis, gluconeogenesis and CoASH recycling that have been previously reported in the PPA model. An emerging relationship between metabolic state, transcriptional regulation, mitochondrial dynamics and mitophagic flux highlights a mechanistic convergence between the functional consequences of PPA exposure for mitostasis. Moreover, the implications for substrate utilisation, redox homeostasis, neurodevelopment and neurotransmission highlight potential consequences for neuronal metabolism, survival and differentiation under PPA stress.

The data presented here act as a springboard for numerous future studies beyond the scope of this thesis. Further work should be conducted to characterise the relationship between gene transcription and protein expression, localisation and function, and to examine the molecular players that drive disruptions to mitochondrial content and connectivity. Moreover, a targeted study of mitophagic and autophagic flux could be used to clarify the time-dependent and context-specific mechanisms that may perturb mitochondrial turnover in this system. Building on the live-cell respirometry presented here, it

may be useful to study different aspects of metabolic state and substrate utilisation over different time points. Further exploring the relationship between p38 MAPK and STAT3 signalling could contribute to an understanding of PPA-induced transcriptional remodelling, while the mechanistic link between CoA metabolism and mtFAS could yield insight into the changes to mitochondrial content and connectivity.

Nevertheless, this is the first study to report PPA-induced changes to SH-SY5Y metabolic state using gold-standard live-cell respirometry, and provides the first quantitative assessment of mitochondrial morphology, dynamics and function in the context of oxidative reliance. The data presented here clearly demonstrate integrated impairments to mitostasis reflected at the level of transcription, morphology and metabolism – each of which is critical for neuronal development and function. Accordingly, this work effectively establishes a model for mitochondrial dysfunction in undifferentiated neuronal-like cells as a prerequisite for subsequent investigations into the metabolic mechanisms that govern neurogenesis. Ultimately, this chapter identifies central mechanisms that may be associated with PPA-induced neurotoxicity, emphasising potential consequences for energy production, redox homeostasis and neuronal development that highlight several novel targets for future research in the PPA model.

~ PART II ~

Chapter 3.

An *In Vitro* Model for Neurogenesis: The Neurotoxic Effects of Propionic Acid

3.1. Introduction

Chapter 2 established a model for metabolic stress that perturbed mitochondrial dynamics, morphology and function in undifferentiated SH-SY5Y cells. Importantly, Chapter 1 highlighted that disruptions to mitostasis not only inhibit neuronal maturation but may also disrupt the composition, connectivity and architecture of neuronal networks. In fact, Kim *et al.,* (2019) showed that PPA perturbs neurogenic signalling pathways in undifferentiated SH-SY5Y cells, which could have functional implications for neurodevelopment. However, undifferentiated NPCs and mature neurons differ substantially with respect to their bioenergetic state and susceptibility to metabolic and oxidative stress (Xie, Hu and Li, 2010; Forster *et al.,* 2016). Consequently, different stages of neuronal development may be associated with divergent responses to PPA, which limits the translatability of findings in undifferentiated cells to more mature neuronal populations.

Yet, none of the previous studies that have characterised PPA-induced mitochondrial dysfunction in the SH-SY5Y system have used differentiated cells, or explored how PPA might alter the process and endpoints of neurogenesis. Building on the model developed in Part I, Part II of this thesis examined the relationship between PPA-induced mitochondrial dysfunction and neurodevelopment *in vitro* to address three main objectives. First, a differentiation protocol was developed to successfully recapitulate the morphological, molecular and metabolic features of mature neurons in the SH-SY5Y system. Subsequently, this system was used to examine how PPA-induced mitochondrial dysfunction influences neuronal morphology and maturation. Lastly, global RNA sequencing (RNAseq) was employed to characterise the transcriptional mechanisms that drive PPA-induced disruptions to neurogenesis *in vitro*. Chapter 3 addresses the first two of these objectives, establishing a model for PPA-induced neurotoxicity that expands current characterisations of the PPA model and lays the groundwork for mechanistic studies on neurodevelopment and neuropathology.

3.1.1. Neuronal Differentiation In Vitro

The SH-SY5Y cell line is an inherently heterogeneous system comprised of at least two subtypes that model different lineages in the neural crest (N. Bell *et al.,* 2013). SH-SY5Y differentiation protocols are designed to produce a homogenous population of neuronal cells by inhibiting the proliferation of S-

type cells and driving N-type cells towards a mature neuronal phenotype. As a model for *in vivo* neurodevelopment, the SH-SY5Y system is most suitable for the study of neuronal differentiation, elongation and connectivity (Feles *et al.,* 2022) which is driven by interactions between endogenously expressed cytoskeletal and extracellular matrix (ECM) proteins (Hynds and Snow, 2001). Nevertheless, separate studies have also demonstrated the formation of synaptic connections with polarised axons and dendrites (Hromadkova *et al.,* 2020), the production and recycling of synaptic vesicles (Sarkanen *et al.,* 2007; Teppola *et al.,* 2016; Martin, Gandawijaya and Oguro-Ando, 2022), the expression of neurotransmitter channels and receptors (Korecka *et al.,* 2013; Martin, Gandawijaya and Oguro-Ando, 2022; Singh, Somvanshi and Kumar, 2022) and a distinct remodelling of electrophysiology and elasticity (Teppola *et al.,* 2016; Şahin *et al.,* 2021) during SH-SY5Y differentiation.

Just as the undifferentiated phenotype can vary under specific culture conditions, there are numerous differentiation protocols reported in the literature that differentially influence the terminal neuronal phenotype (Kovalevich, Santerre and Langford, 2021). The SH-SY5Y cell line can be driven towards a mature dopaminergic, adrenergic, glutamatergic or cholinergic phenotype using a number of neurogenic agents, each of which can be administered at different concentrations, over different time periods and in combination with different nutrient supplementation or serum depletion protocols. The differentiation protocols most frequently reported in the literature employ retinoic acid (RA), phorbol esters, dibutyryl-cAMP, staurosporine, bone morphogenetic protein (BMP) or neurotrophins like nerve growth factor (NGF) or brain-derived neurotrophic factor (BDNF) (Xie, Hu and Li, 2010; Xicoy, Wieringa and Martens, 2017; Kovalevich, Santerre and Langford, 2021; dos Santos, Gomes and Costa, 2023; Hoffmann *et al.,* 2023; Ioghen, Ceafalan and Popescu, 2023; Langerscheidt, Bell-Simons and Zempel, 2024).

Of these, RA is most commonly used, usually at a concentration of 5-10 μM for at least 3–5 days (Xicoy, Wieringa and Martens, 2017; Kovalevich, Santerre and Langford, 2021). The neurogenic effects of RA are canonically mediated by retinoic X receptors (RXRs) that form heterodimers with retinoic acid receptors (RARs) and PPARs to activate transcription from both RA response elements (RAREs) and PPREs in the genome (Xie, Hu and Li, 2010). In addition, RARs and RXRs modulate WNT/β-catenin, mTORC1 and Transforming Growth Factor-β (TGF-β) signalling via protein-protein interactions in the cytoplasm (Piazza, Carlone and Spencer, 2024). In this way, both canonical and non-canonical RA signalling drives neuronal maturation by initiating cell cycle exit, neurite production and the expression of neuronal-specific genes (Bayeva, Coll and Piskareva, 2021) **(Figure 3.1).** Notably, RA is critical for *in vivo* embryonic development (Berenguer *et al.,* 2022), and disruptions to retinol metabolism, biosynthesis and signalling have been implicated in ASD and other NDDs (Baranova *et al.,* 2021; Upadhyay *et al.,* 2021). Thus, RA drives neuronal maturation via signalling pathways that recapitulate relevant mechanisms associated with neurodevelopment *in vivo.*

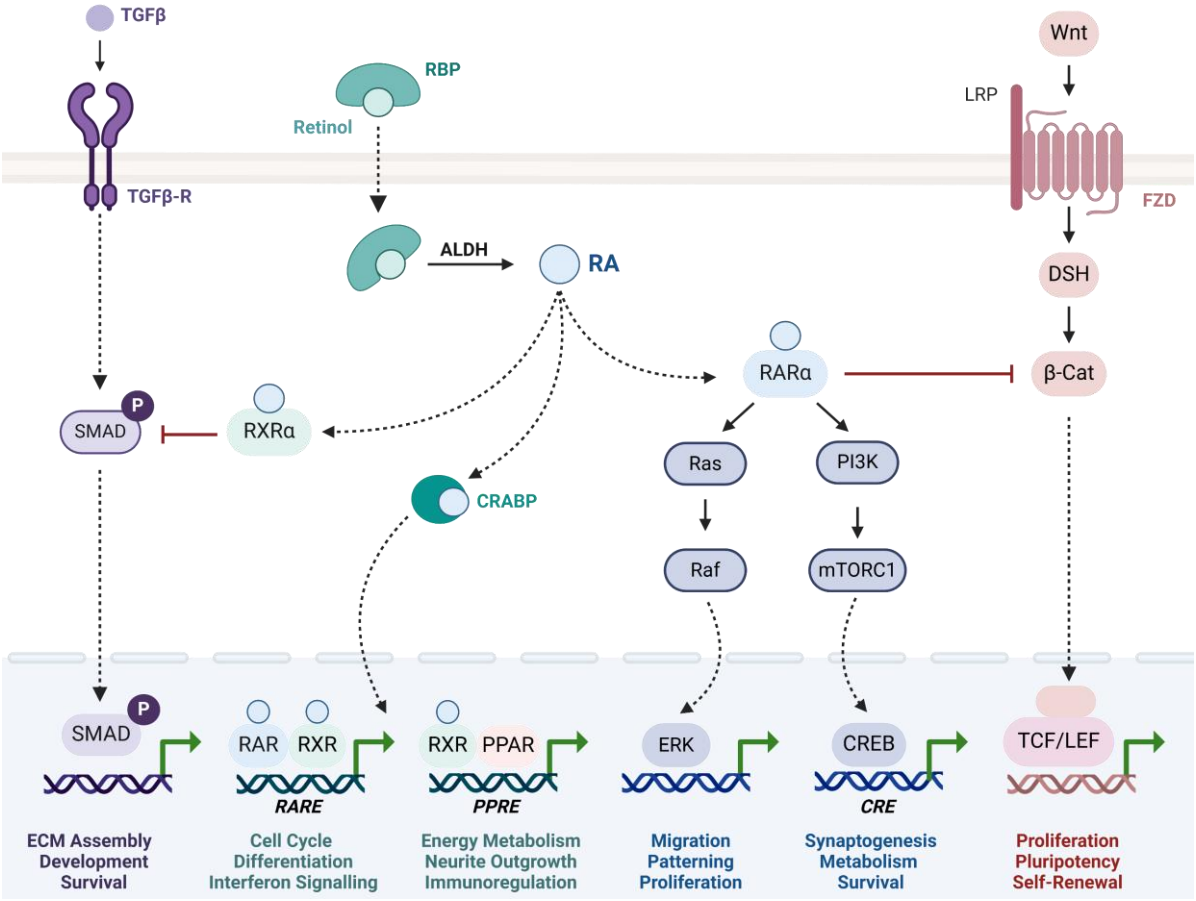


Figure 3.1. The Neurogenic Mechanisms of Retinoic Acid. Retinol is transported into cells via retinoid binding proteins (RBPs), where it is converted into Retinoic Acid by aldehyde dehydrogenases (ALDH), bound by cellular retinoic acid-binding protein (CRABP) in the cytoplasm and transported to the nucleus. Nuclear RA activates retinoid X receptors (RXRs) and RA receptors (RARs), which form heterodimers that drive transcription from RA response elements (RAREs) to regulate genes involved in growth, differentiation and interferon signalling. Activated RXRs can also dimerise with peroxisome proliferator activated receptors (PPARs) bound by fatty acids to promote transcription from PPREs, thereby regulating genes involved in proliferation and energy metabolism. RA also mediates non-genomic effects by binding to RARs or RXRs in the cytoplasm. Cytoplasmic RARα upregulates mechanistic target of rapamycin (mTOR) signalling by activating phosphoinositide 3 kinase (PI3K), which promotes mitochondrial metabolism, lipid synthesis, neuronal migration, neurite branching and cytoskeletal remodelling. RARα also inhibits the canonical Wnt/β-catenin pathway by sequestering free β-catenin. On the other hand, RXRα inhibits TGF-β signalling by preventing the nuclear translocation of phosphorylated SMAD transcription factors.

Yet, SH-SY5Y differentiation by RA alone has an efficiency of only ~20% (Yang *et al.,* 2016) and tends to yield heterogeneous populations of both S- and N-type cells (Xie, Hu and Li, 2010). *In vivo*, the development of mature neuronal networks is driven by neurotrophins like BDNF, which acts via the tropomyosin-related kinase β (TRKβ) receptor to facilitate synaptogenesis via downstream phospholipase-Cγ (PLCγ), PI3K/mTOR, Rho-associated protein kinase (ROCK) and Ras/Raf cascades (Yang *et al.,* 2016; Ghani *et al.,* 2024) (**Figure 3.2).** Once activated by extracellular BDNF at the plasma membrane, TRKβ receptors promote the endogenous expression of BDNF via the mTOR/CREB axis, producing a BDNF precursor (pro-BDNF) that independently activates PI3K, NFκβ and JNK signalling via the p75 neurotrophic receptor (p75NTR) / sortilin complex (Wang and Tian, 2021). Together, BDNF

governs both extrinsic and intrinsic mechanisms that control neuronal proliferation, metabolism and survival as well as synaptic development, plasticity and signalling (Kowiański *et al.,* 2017).

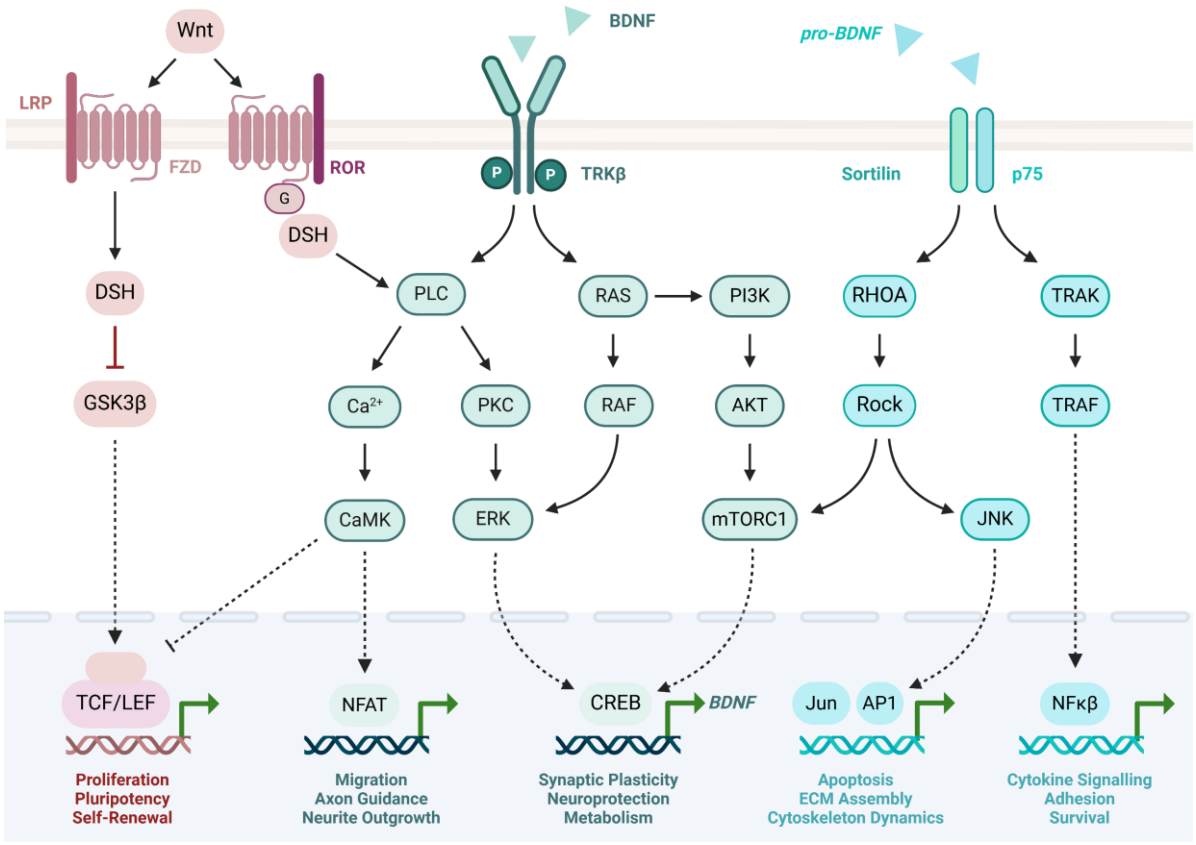


Figure 3.2. Neurogenic Signalling by Brain-derived Neurotrophic Factor. Brain-derived neurotrophic factor (BDNF) activates tropomyosin-related kinase β (TRKβ), which triggers downstream phospholipase-Cγ (PLCγ), PI3K/mTOR, Rho-associated protein kinase (ROCK) and Ras/Raf cascades required to regulate neuronal survival, growth cone development, actin dynamics, neurite branching and mitochondrial function. The mTOR pathway activated by BDNF promotes BDNF transcription via cAMP response element binding protein (CREB), which produces a BDNF precursor (pro-BDNF) that is cleaved to form the mature BDNF protein. Pro-BDNF binds to the p75 neurotrophic receptor (p75NTR)/sortilin complex, which triggers Rho, Jun-related Kinase (JNK) and Nuclear Factor Kabba B (NFκβ) signalling to modulate growth cone dynamics, neuronal survival and apoptosis.

Accordingly, disruptions to BDNF expression, localisation, trafficking and function are widely implicated in neurodevelopmental and neuropsychiatric disorders (Wang, Kavalali and Monteggia, 2022), including ASD (Liu *et al.,* 2021; Nangdev *et al.,* 2024). Importantly, SH-SY5Y cells express the TRKβ receptor in response to RA exposure *in vitro*, and sequential treatment with RA and BDNF has been found to decrease proliferation, increase the rate of neurite production, elongation and branching, promote synapse development, polarisation and signalling and inhibit the accumulation of S-type cells over time (Encinas *et al.,* 2000; Shipley, Mangold and Szpara, 2016; Yang *et al.,* 2016; Hromadkova *et al.,* 2020; Dravid, Raos and Svirskis, 2021; dos Santos, Gomes and Costa, 2023). Thus, protocols using both RA and BDNF are recommended to more accurately study the morphological remodelling that defines neurogenesis *in vitro.*

Like every aspect of an *in vitro* system, the optimal differentiation protocol should be designed with the specific research question in mind. Here, the SH-SY5Y system will be used to examine crosstalk between underlying mechanisms that modulate neurogenesis. Thus, it is critical to consider the extent to which the morphological remodelling induced by different neurogenic agents is reflected in underlying molecular and metabolic signatures. Several studies have characterised the transcriptional programmes that are differentially modulated by RA and RA-BDNF during SH-SY5Y differentiation. Nishida *et al.,* (2008) found that BDNF activated a neurogenic programme that was suppressed with RA treatment alone, while Goldie, Barnett and Cairns, (2014) revealed that BDNF uniquely regulated genes involved in neuronal differentiation, axonogenesis and synaptic signalling. Interestingly, this response was associated with an upregulation of neuron-specific miRNAs and miRNA biogenesis machinery, which is known to play a critical role in synaptic development and plasticity by modulating temporospatial patterns of protein synthesis. Indeed, Jauhari *et al.,* (2017) showed that miRNA-dependent post-transcriptional regulation was essential for SH-SY5Y differentiation, which is marked by profound shifts in miRNA expression profiles (Beveridge *et al.,* 2009; Das and Bhattacharyya, 2014; Watanabe, Yamaji and Ohtsuki, 2018). Thus, BDNF specifically drives transcriptional and post-transcriptional programmes that are critical for neurogenesis in the SH-SY5Y system.

Notably, Chiocchetti *et al.,* (2016) found that the biological relevance of RA-BDNF-driven neurogenesis also depends on the administration protocol. A sequential (sRA-BDNF) protocol has typically been used for SH-SY5Y differentiation since a landmark study by Encinas *et al.,* (2000) showed that the BDNF receptor is most highly expressed after 5 days of RA administration. However, given the central role played by BDNF during early neurodevelopment *in vivo,* Chiocchetti *et al.,* (2016) explored a protocol using continuous (cRA-BDNF) exposure similar to the methods often used to differentiate neuronal stem cells (NSCs) and induced pluripotent stem cells (iPSCs). Compared to both RA and sRA-BDNF treatment, the transcriptomic signature induced by cRA-BDNF was most reminiscent of mature cortical neurons *in vivo.* Moreover, this protocol recapitulated the early induction of ASD-associated risk genes during *in vivo* neurodevelopment as well as signatures associated with glutamatergic and GABAergic signalling, which are highly pertinent to ASD aetiology. As such, the cRA-BDNF protocol has since been employed in several studies using the SH-SY5Y system to study neurodevelopmental mechanisms in ASD (Haslinger *et al.,* 2018; Unsicker *et al.,* 2021; Bamford *et al.,* 2024).

3.1.2. Neurogenic Signatures of Metabolic Remodelling

In order to study the relationship between metabolism and neurodevelopment, it is also critical to establish a differentiation protocol that recapitulates the metabolic remodelling associated with neurogenesis *in vivo.* Independent studies have shown that differentiation reshapes mitochondrial metabolism, dynamics, morphology and localisation in SH-SY5Y cells (Schneider *et al.,* 2011; Xun *et*

al., 2012; Forster *et al.,* 2016; Li *et al.,* 2020; Naia *et al.,* 2021; Pandey *et al.,* 2022; D'Aloia *et al.,* 2024; Matrella *et al.,* 2024). However, the mechanisms that mediate metabolic remodelling in this system are still not fully elucidated. While some studies have reported an increase in mitochondrial biogenesis during differentiation (Pandey *et al.,* 2022; D'Aloia *et al.,* 2024; Matrella *et al.,* 2024), others have found no change in mitochondrial content even as oxidative capacity increased (Schneider *et al.,* 2011; Xun *et al.,* 2012; Li *et al.,* 2020; Naia *et al.,* 2021). Several authors have proposed that metabolic remodelling is driven by changes to substrate utilisation or ETC composition, control and function (Schneider *et al.,* 2011; Xun *et al.,* 2012). More recently, Matrella *et al.,* (2024) demonstrated that changes to mitochondrial membrane composition increased mitochondrial capacity via the formation of respiratory supercomplexes while D'Aloia *et al.,* (2024) revealed an increase in the connectivity and complexity of mitochondrial networks. Still, these changes remain poorly understood with respect to their precise nature and underlying mechanisms.

Indeed, while the differential effects of neurogenic agents on SH-SY5Y morphology, neuronal lineage, electrophysiology, signalling and susceptibility to neurotoxic compounds are well-established, the nature and degree of metabolic remodelling associated with each protocol remains uncharacterised (Pahlman *et al.,* 1990; Feng, Wang and Sheng, 2006; Filograna *et al.,* 2015; Serdar *et al.,* 2018; Campos Cogo *et al.,* 2020; Ducray *et al.,* 2020; Hromadkova *et al.,* 2020; Bayeva, Coll and Piskareva, 2021; Kovalevich, Santerre and Langford, 2021; Şahin *et al.,* 2021; Ioghen, Ceafalan and Popescu, 2023). Alrashidi, Eaton and Heales, (2021) noted the relevance of metabolic state for the study of mitochondrial-related neuropathologies in the SH-SY5Y system, while Simões *et al.,* (2021) highlighted a need to consider how different protocols uniquely modulate mitochondrial content, distribution and bioenergetics. Yet, no studies have compared different neurogenic agents with respect to their capacity to reshape metabolism *in vitro*. Moreover, it is unclear whether the phenotypic markers typically used to verify neuronal differentiation reflect an underlying shift in metabolic state.

Given that this study focussed on metabolic mechanisms in neurogenesis, the metabolic phenotype associated with SH-SY5Y differentiation was evaluated with reference to publicly available respirometric datasets. As the most direct method to measure metabolic state, live-cell respirometry data was obtained from the Agilent Life Science Publication Database (https://www.agilent.com/search/?N=4294836537), which collates and categorises publications that reference or cite Agilent Seahorse technology. Although this database is not exhaustive, it does provide a representative snapshot of existing research that could aid in study design. Filtering for "Seahorse XF Technology" and the SH-SY5Y cell line identified 76 unique studies, of which more than 75% used undifferentiated cells in isolation, 24% used differentiated cells and only five (~6.5%) compared metabolic profiles before and after differentiation. Four additional comparative studies were sourced from PubMed, Google Scholar and EBSCO host. Of the nine available studies that quantified metabolic shifts during SH-SY5Y differentiation, each used different approaches to model and confirm

differentiation, and each reported slightly different metabolic profiles associated with neurogenesis **(Table 3.1).** All nine studies employed RA to induce differentiation, of which seven used RA-only, two used sRA-BDNF and two used alternative approaches.

Table 3.1. Metabolic Remodelling During SH-SY5Y Differentiation. Data summarise the nine studies that quantified metabolic state in undifferentiated and differentiated SH-SY5Y cells detailing the basal media, neurogenic agents, neurogenic markers and metabolic profiles reported in each case. RA – retinoic acid, BDNF-brain-derived neurotrophic factor, SF – serum free OCR – oxygen consumption rate, ECAR- extracellular acidification rate, HG – high glucose (10-25mM), LG – low glucose (0-10mM), 10P – 10mM Pyruvate, 2dFU - 2-deoxy-5-fluorouridine, ns – non-significant.

	Reference	**Neurogenic Protocol**	**Neuronal Marker**	**Metabolic Profile**
Day 1	(von Niederhäusern *et al.,* 2019)	24 hrs 10 µM RA, 5% FBS, DMEM GlutaMAX™ +/- HG	TH, CHT1	HG - ns increase in basal/ max OCR LG – decreased OCR
	(Xun *et al.,* 2012)	24 hrs 10um RA, 10% FBS, MEM/EBSS & Ham's F-12	Morphology	6-fold increase in basal & max OCR; increase in max ECAR
Day 5	(Li *et al.,* 2020)	5 days 10 µM RA, 10% FBS, DMEM/F12	Morphology	Increase in basal & max OCR & ECAR
	(Schneider *et al.,* 2011)	5 days 10 µM ATRA, 1% FBS, DMEM	MAP2	Same basal/ATP-linked OCR but increased max & spare capacity; decreased basal but increased max ECAR
Day 6-7	(Ducray *et al.,* 2017)	6 days 10 µM RA, 5-1%FBS, DMEM HG	MAP-2, β-3-tubulin	Decreased basal & max OCR & ECAR
	(Matrella *et al.,* 2024)	5 days 10 µM RA, 1% FBS; 2 days + 10 µM 2dFU in DMEM HG + 2 mM L-Glutamine	β-3-tubulin, MAP2, TH, ENO2	Higher basal, max & spare OCR, same basal but increased max & spare ECAR
Day 8	(Pandey *et al.,* 2022)	5 days 10 µM RA low FBS; 3 days + 100ng/ml BDNF SF EMEM: F12 + NEAA	β-3-tubulin, SYN-1, SYP, NF-M, NES	Increase in basal, max, ATP-linked & spare OCR; ns decrease in basal & max ECAR
	(Naia *et al.,* 2021)	5 days 10 µM RA 10% FBS; 3 days + 25ng/ml BDNF SF in DMEM +/- HG or 10mM Pyruvate	MAP2, SNAP25	HG - ns decrease in basal & max OCR, ns increase in ATP-linked OCR. 10P - significantly increased max & ATP – linked OCR
Day 20 - 40	(D'Aloia *et al.,* 2024)	7 days 10 µM RA, 13-33 days + 10ng/mL NGF + 10ng/mL NRG + 24nM VitD3 in Optimem 2 mM glutamine	NeuN, PSD95, SYN-1, SYP	Same basal but increased max & spare OCR

Chapter 2 established that undifferentiated SH-SY5Y cells exhibit an opportunistic metabolic profile with a lower oxidative capacity and a higher glycolytic dependence compared to primary neurons. The data presented in Table 3.1 demonstrate a distinct metabolic shift during differentiation that increases mitochondrial capacity; eight of nine studies reported a significant increase in basal, spare or maximal oxidative respiration as early as 24 hours and up to 40 days into differentiation. Yet ATP-linked respiration remained lower than in primary cortical neurons (Naia *et al.,* 2021) while glycolytic capacity was still higher than in differentiated NSCs (Li *et al.,* 2020). In fact, of the six studies that examined both oxidative and glycolytic respiration during neurogenesis, four (80%) showed an upregulation of glycolytic activity or capacity in differentiated cells, while only one study demonstrated an increased mitochondrial capacity with a reduced glycolytic reliance **(Figure 3.3).** Moreover, the shift in both basal and spare mitochondrial capacity varied substantially across all nine studies.

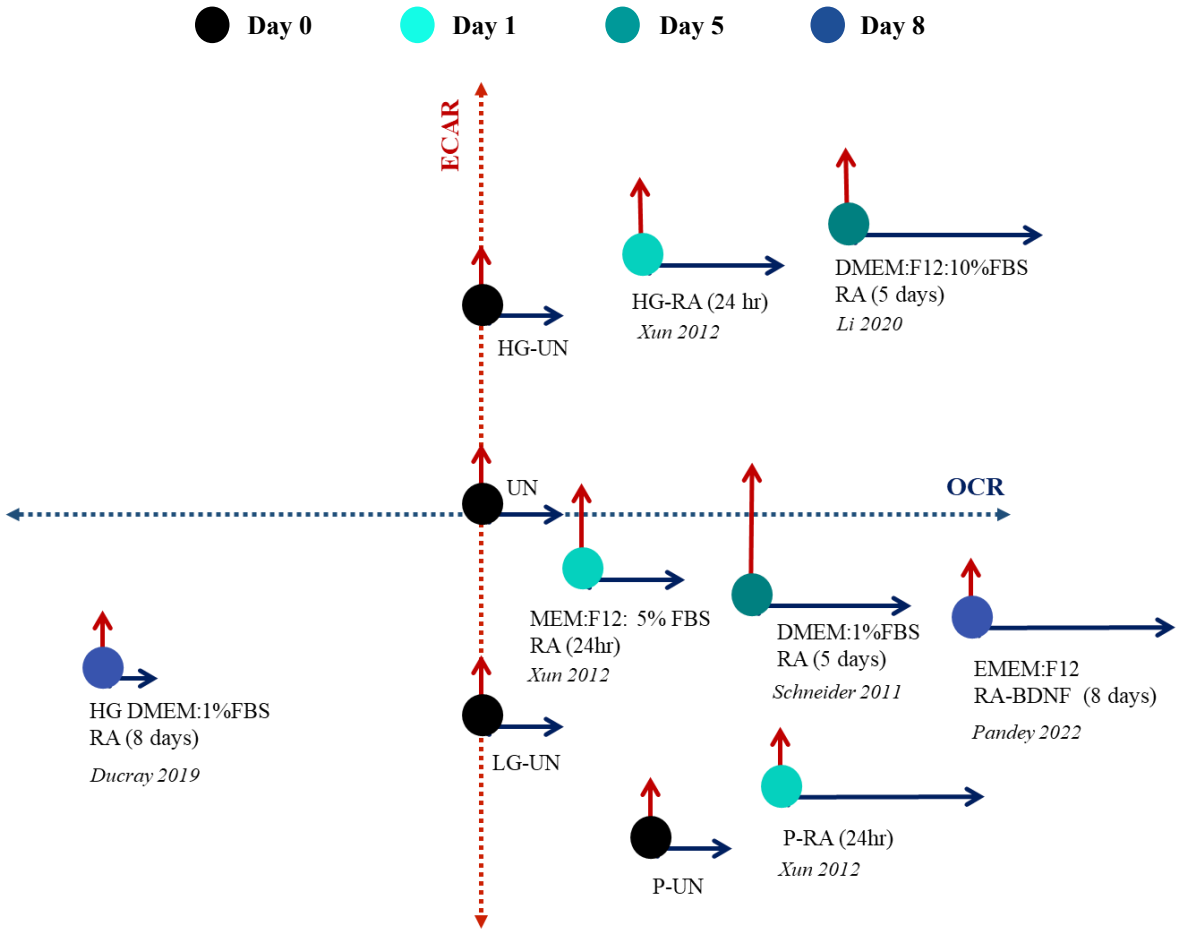


Figure 3.3. A Graphical Summary of Metabolic Remodelling *In Vitro*. Data summarise the findings from six studies of SH-SY5Y differentiation that measured both extracellular acidification rate (ECAR) and oxygen consumption rate (OCR). The metabolic profile associated with each differentiation protocol is depicted relative to undifferentiated controls where data points represent basal OCR (x – axis) and ECAR (y -axis) colour coded by day of differentiated; black = day 0 (undifferentiated controls), light turquoise = day 1, green = day 5, blue = day 8 of differentiation. In each case, maximal OCR/ECAR are depicted as blue and red arrows. BDNF = brain derived neurotrophic factor; HG – high glucose; LG – low glucose; P- pyruvate as only carbon source; RA = retinoic acid; UN - Undifferentiated Controls.

Together, existing respirometric profiles from SH-SY5Y differentiation highlight several relevant considerations for *in vitro* studies of neurogenesis. Firstly, each of the protocols in Table 3.1. were validated with established markers for differentiation, yet each produced markedly different metabolic profiles. Indeed, Li *et al.,* (2020) found that neither glycolytic nor mitochondrial inhibitors perturbed neurite production, elongation or connectivity in differentiated SH-SY5Y cultures, while Naia *et al.,* (2021) showed that different carbon sources profoundly impacted SH-SY5Y metabolism but had no effect on neuronal morphology or the expression of neuronal markers. Thus, morphological and biochemical markers of neurogenesis may not always reflect a mature metabolic state in the SH-SY5Y system. Secondly, the diverse metabolic profiles depicted in Figure 3.3. underline the need to consider how different protocols may impact neuronal metabolism *in vitro.*

There are three primary variables that appear to influence metabolic remodelling in the SH-SY5Y system: i) nutrient and serum supplementation, ii) length of differentiation and iii) neurogenic agent/s. All of the studies that used high glucose DMEM (10 - 25mM) failed to significantly increase basal oxidative metabolism regardless of the differentiation protocol used (Ducray *et al.,* 2017; von Niederhäusern *et al.,* 2019; Naia *et al.,* 2021), while studies in EMEM showed an increase in basal, spare and maximal respiratory capacity (Xun *et al.,* 2012; Pandey *et al.,* 2022). Total glucose deprivation decreased metabolic activity (von Niederhäusern *et al.,* 2019) while pyruvate or glutamine supplementation increased oxidative reliance (Naia *et al.,* 2021; Matrella *et al.,* 2024). Similarly, serum depletion appeared to reduce glycolytic dependence (Schneider *et al.,* 2011; Pandey *et al.,* 2022; Matrella *et al.,* 2024), which is consistent with observations in undifferentiated cells (Kronenberger *et al.,* 2024). Moreover, the trend across all nine studies suggests that metabolic capacity increases over time, which is in line with the findings reported by Schneider *et al.,* (2011) and D'Aloia *et al.,* (2024). Although differences in medium composition, Seahorse technology and serum depletion protocols preclude an objective comparison between neurogenic agents, the capacity for longer periods of differentiation facilitated by BDNF may promote a more distinct metabolic shift in the terminal neuronal phenotype (Naia *et al.,* 2021; Pandey *et al.,* 2022; D'Aloia *et al.,* 2024). Indeed, BDNF has been shown to enhance mitochondrial respiration, ATP synthesis, biogenesis, fusion and trafficking in developing neurons (Cardanho-Ramos and Morais, 2021).

Although the metabolic state associated with SH-SY5Y differentiation appears to be highly context-specific, these data can be understood with reference to the emergent and non-emergent properties of SH-SY5Y metabolism that should inform *in vitro* studies for neurogenesis (Schneider *et al.,* 2011; Xun *et al.,* 2012). Cumulative data shows that SH-SY5Y differentiation is characterised by an increasingly oxidative bioenergetic state driven by a shift in metabolic *profile* (the ratio of ATP derived from OCR vs ECAR) and spare bioenergetic *capacity* (maximal – basal respiration) rather than absolute metabolic *activity* (net OCR or ECAR). In other words, while most studies report an upregulation of both oxidative and glycolytic activity, an oxidative metabolic profile emerges because mitochondrial respiration is

consistently upregulated to a greater extent. Indeed, the oxidative profile associated with differentiation is defined as an emergent property of SH-SY5Y cells that does not depend on nutrient composition (Xun *et al.,* 2012). Here, it is the increase in spare mitochondrial capacity rather than basal mitochondrial activity that drives differentiation (Schneider *et al.,* 2011). On the other hand, oxidative and glycolytic activity are non-emergent properties, in that they can be influenced by different carbon sources (Xun *et al.,* 2012). This may explain the reduced glycolytic reliance induced by glucose depletion and pyruvate or glutamate supplementation. Importantly, Figures 3.1 and 3.2 highlight that RA and BDNF directly modulate signalling pathways that govern metabolic state – including the PPAR, CREB, Wnt and mTOR cascades. Thus, while differentiation drives an intrinsically oxidative profile that mirrors neurogenesis *in vivo,* both media composition and neurogenic agents may differentially influence metabolic remodelling in the SH-SY5Y system.

Together, this analysis reveals a distinct oxidative shift during SH-SY5Y differentiation that reflects *in vivo* neurodevelopment. Nevertheless, media composition is essential to modulate glycolytic reliance during SH-SY5Y differentiation to better reflect the *in vivo* neuronal phenotype. Based on respirometric profiles, the protocol employed by Pandey *et al.,* (2022) is the most suitable to drive an increase in oxidative metabolism while decreasing glycolytic reliance. In fact, Pandey *et al.,* (2022) demonstrated a convergence between proteomic and respirometric profiles in the same system. Therefore, the nutrient supplementation, serum depletion and neurogenic agents employed by Pandey *et al.,* (2022) will be used to establish an *in vitro* model for neurogenesis in this chapter. However, given the insights from Chiocchetti *et al.,* (2016) regarding the biological and pathological relevance of the SH-SY5Y system, the model established here will employ the cRA-BDNF method of administration rather than the serial treatment that is typically used in this context. Ultimately, this discussion illustrates the context-specific relevance of the SH-SY5Y system to study metabolic mechanisms in neurodevelopment and informs a suitable protocol to model neurogenesis *in vitro.*

3.1.3. Confirmation and Characterisation of Neurogenesis

Chapter 2 emphasised that *in vitro* models should be tightly controlled, well-characterised and reproducible to maximise the utility of such inherently reductionist systems. To this end, an *in vitro* model for neurogenesis should include i) a standardised differentiation protocol that is validated with ii) appropriate undifferentiated controls and iii) suitable neurogenic markers to verify the emergence of a mature neuronal phenotype. Here, a differentiation protocol was designed with reference to the aforementioned literature in order to recapitulate relevant features of neurogenesis associated with both metabolism and ASD aetiology. There are two types of undifferentiated controls commonly employed in this context, almost always in isolation: proliferative controls grown overnight with FBS supplementation or quiescent controls maintained over the duration of differentiation in serum-free media. However, each control may be best suited to capture different features of neurogenesis. Here,

both controls are used to establish a suitable model for neurogenesis while proliferative controls are used to quantify morphological and molecular markers of differentiation.

The protocol established here was verified using well-validated markers of the differentiated neuronal phenotype. In the undifferentiated state, SH-SY5Y cells are highly proliferative with non-polarised cell bodies, few elongated processes, and biochemical markers of immature neurons (Xie, Hu and Li, 2010). For example, Nestin (NES) is a cytoskeletal protein highly expressed in NSCs that modulates NSC self-renewal, proliferation and migration (Bernal and Arranz, 2018). Conversely, the differentiated state is defined by cell cycle exit, shrunken cell bodies, complex and interconnected processes and mature neuronal markers (Riegerová *et al.,* 2021). The production, elongation and branching of mature neurites is driven by a downregulation of NES, which remodels axonal growth cone dynamics (Bott *et al.,* 2019). Concurrently, the neuron-specific protein β-3-Tubulin (β3T) is upregulated to modulate neuronal migration, axon guidance and synaptogenesis (Singh and Tsai, 2010). As such, the expression of NES and β3T is widely used to supplement measures of cell division and neurite complexity to verify differentiation in the SH-SY5Y system (Bayeva, Coll and Piskareva, 2021; Kovalevich, Santerre and Langford, 2021).

A variety of methods have been used for this purpose, including immunocytochemistry (ICC), western blots or quantitative polymerase chain reaction (qPCR) (Xie, Hu and Li, 2010). Of these, ICC is considered a more reliable method to examine population-wide changes in expression and localisation that also provides insight into the morphology and connectivity of neuronal networks (Xicoy, Wieringa and Martens, 2017). Therefore, the system established here is validated with a multiplex ICC assay designed to quantify NES and β3T expression, using Dapi to monitor relative rates of proliferation and phase-contrast microscopy to visualise interconnected neuronal networks in live cell cultures. Together, this workflow quantifies morphological and biochemical features of mature neurons in the SH-SY5Y system that can be used to characterise PPA-induced disruptions to neurogenesis.

3.2. Methodology

3.2.1. SH-SY5Y Differentiation

The procedures described by Chiocchetti *et al.,* (2016) and Pandey *et al.,* (2022) were used as a starting point for the differentiation protocol developed here, with several parameters that were further optimised in our system – namely, seeding density, serum-depletion and the length of the differentiation period. A series of initial experiments found that seeding density played a critical role in determining neuronal viability, maturation and connectivity; overly confluent cultures were marked by stunted neurites and increased NES expression after differentiation while sparsely seeded cultures were prone to cell death after 4-6 days. Cultures were disposed to over-proliferate in 5-10% FBS but failed to

remain viable in serum-free medium, while fully developed neuronal networks began to shrink and aggregate beyond 9 days in culture. Having determined the optimal conditions to balance confluency, viability and maturation, the protocol used for subsequent differentiation experiments was as follows: SH-SY5Y cells were seeded in 6 well plates at a density of 7.5 x 10^4 cells per well in complete EMEM: F12, allowed to rest at room temperature for 30 minutes to ensure homogeneous cell plating and left to adhere for 24 hours. The next day, media was replaced with differentiation media, comprising EMEM: F12, 1% FBS, 1% P/S, 1% NEAAs, 200mM L-Glutamine with 10µM retinoic acid (RA) (Sigma-Aldrich, R2625-100MG) and 50ng/ml BDNF (Thermo Fisher Scientific, 10908010). Cells were incubated in the dark at 5% CO_2 37°C for a further eight days, replacing media with fresh differentiation media every two days.

In order to i) verify the efficacy of the differentiation protocol described above and subsequently ii) evaluate the effect of PPA on neurogenesis, differentiation experiments were designed to include four experimental groups **(Figure 3.4).** Day 1 undifferentiated controls (C1) were maintained overnight in full EMEM with 15% FBS, day 9 negative controls were maintained at 1% FBS for nine days without the addition of neurogenic agents (C9) while day 9 neurons were differentiated as described above (D9). For samples exposed to PPA during differentiation (DP), 5mM PPA was administered with the differentiation media 24 hours after seeding and every two days until day nine.

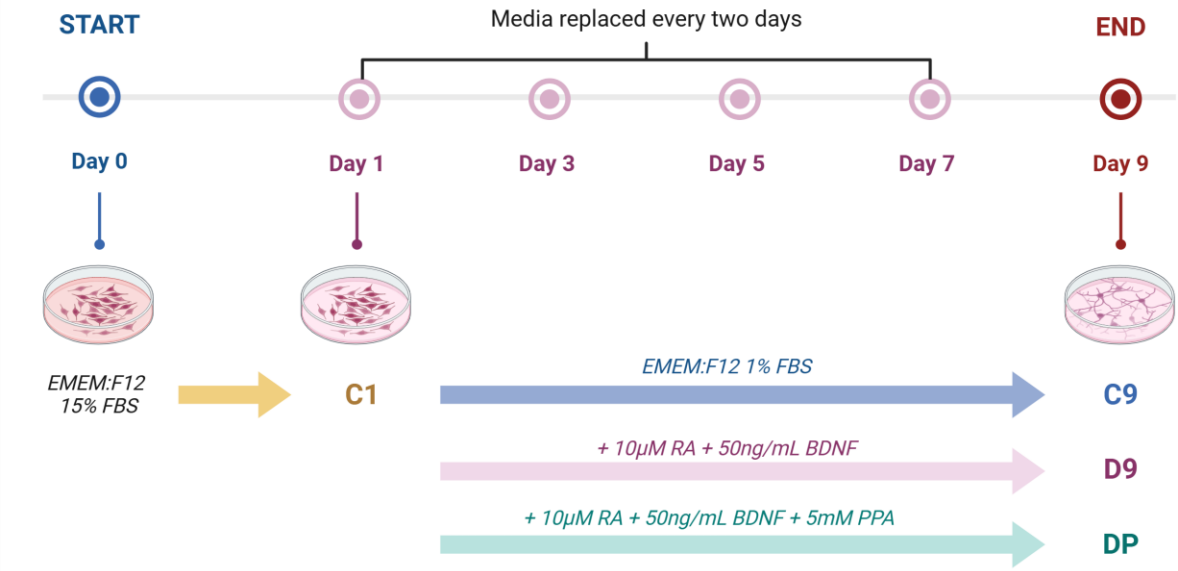


Figure 3.4. Differentiation Protocol and Experimental Design. On Day 0, SH-SY5Y cells were seeded in 6 well plates at 7.5 x 10^4 cells per well in complete EMEM: F12 with 15% FBS and allowed to adhere for 24 hours (C1). From day 1, media was replaced EMEM: F12, 1% FBS (C9) with 10µM retinoic acid (RA) and 50ng/ml BDNF (D9) and 5mM Propionic Acid (PPA) (DP), refreshing media every 2 days until the endpoint of differentiation at day 9.

3.2.2. Evaluation of Neuronal Morphology and Maturation

3.2.2.1. Live Cell Imaging

To evaluate the efficacy of the differentiation protocol established above, several neuronal features were examined using a combination of phase-contrast microscopy and ICC. Initial optimisation experiments showed that the integrity of the neuronal network was largely retained after fixation and allowed for the assessment of β3T and NES expression and localisation **(Figure S3.1).** However, to account for the possible effects of fixation on neurite morphology, phase-contrast microscopy was used to visualise live cells alongside the fluorescent microscopy employed to quantify neuronal markers in fixed samples. On day 0, SH-SY5Y cells were seeded in 6-well plates on 12 x 0.16 mm glass coverslips at a density of 7.5 x 10^4 per well. After 24 hours, media was removed and replaced with either 1% FBS EMEM (negative controls) or differentiation media and differentiated for a further 8 days. On day 9, live cells were visualised using a Nikon Ti-E inverted microscope equipped with a CHGFIE Intensilight mercury-fiber illuminator and NIS-Elements AR imaging software v5.21.01 (Department of Molecular and Cell Biology, University of Cape Town). Cells were viewed under a phase-contrast filter using a 20X S Plan Flour objective (NA = 0.45) and images were captured with a Nikon D200 DS-Fi2 colour camera. At least three ROIs were captured per sample and images were saved as 24-bit .tif files prior to analysis in Fiji/ImageJ.

3.2.2.2. Immunocytochemistry

A multiplex immunocytochemistry (ICC) assay was designed to measure β3T and NES expression as depicted in **Figure 3.5.** Both primary and secondary antibodies were titrated to identify optimal concentrations and incubation periods at which signal: noise ratios were minimised and subsequently checked for specificity of binding and cross-reactivity **(Figure S3.2).** On day 9, samples were fixed, permeabilised and blocked according to the protocol detailed in **2.2.6.** and then incubated overnight with monoclonal rabbit IgG anti-human Nestin (Thermo Fischer Scientific, MA5-32272) and monoclonal mouse IgG2a anti-human B-3-Tubulin (Thermo Fischer Scientific, MA1-118) at a dilution of 1:300 and 1:500 in 0.3% BSA respectively. Subsequently, cells were rinsed twice with 1X PBS, followed by three five-minute 1X PBS washes and a 90-minute incubation with 2:1000 Goat anti-Rabbit IgG Alexa Fluor 594 (Thermo Fischer Scientific, R37117) and 1:1000 Goat anti-Mouse IgG Alexa Fluor Plus 488 (Thermo Fischer Scientific, A32723) in 1X PBS at 4°C. The wash step was repeated before each sample was stained with 250nM Dapi (Biocom Africa, 422801) for 10 minutes. After two rinses and three washes in 1X PBS, each sample was mounted using 7µL of Antifade Mountant (Thermo Fischer Scientific, S36972) and allowed to dry at room temperature for 2 hours before being stored in the dark at 4°C until imaging.

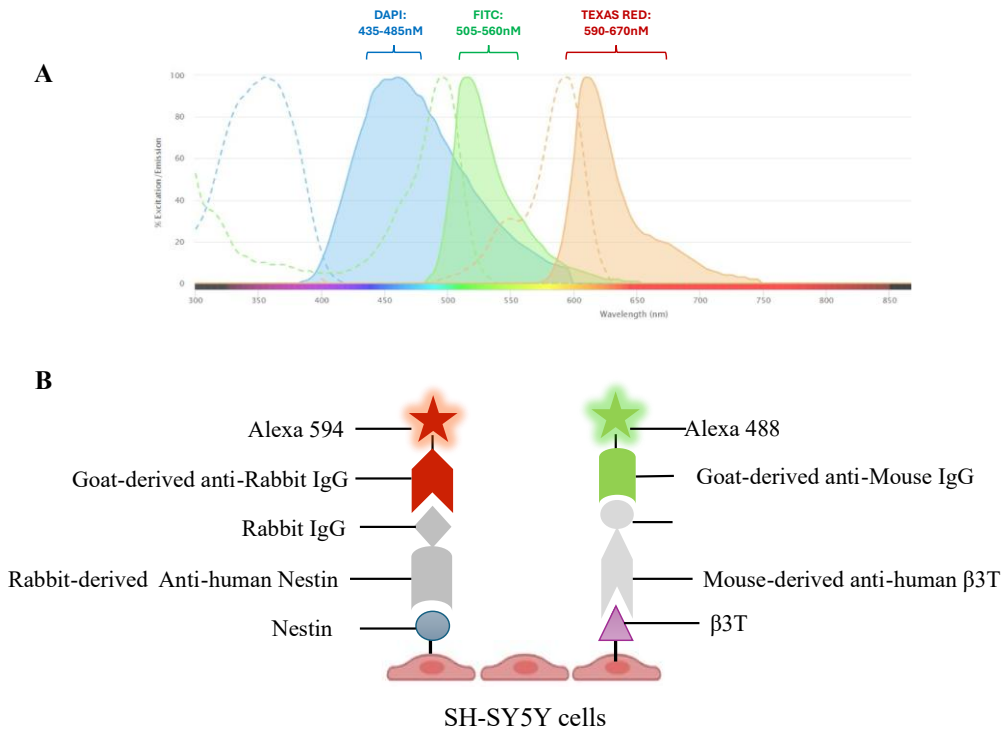


Figure 3.5. A Multiplex Immunocytochemistry Assay to Measure Nestin and β-3-Tubulin Expression. A) Excitation and emission spectra for Dapi (blue), Alexa-488 (green) and Alexa-594 (red) demonstrate clear separation between excitation spectra and distinct emission peaks that correspond to the windows of detection for the corresponding Dapi, FITC and Texas Red filters. **B)** Primary monoclonal antibodies for the human Nestin and β-3-Tubulin proteins (β3T) derived from rabbit and goat respectively are detected with anti-rabbit Alexa-594 and anti-goat Alexa-488, both with an IgG immunogenicity.

Coverslips were imaged using the aforementioned Nikon C-HGFIE inverted microscope with either a 10X Plan Flour PH1 (NA=0.3), a 20X S Plan Flour (NA=0.45) or the Apo TIRF 60X oil DIC objective (NA=1.49). Based on recommendations from Dravid *et al.,* (2021) each sample was visualised across eight - twelve ROIs at 10X, 20X and 60X magnification, where 10X images were used to measure cell proliferation, 20X images were used to quantify fluorescent intensity and 60X images were used primarily to measure neurite morphology. Dapi staining was visualised using the Chroma DAPI Filter Set #49000 (Ex/Em = 320-380nm/ 435-485nm), β3T expression was visualised with Chroma FITC/Alexa 488 Filter Set #49011 (Ex/Em = 460-500nm/505-560nm) and Nestin was visualised using the Chroma Texas Red Filter Set #49008 (Ex/Em = 540-580nm/ 590-670nm) at standard conditions detailed in **Table 3.2.** 10X and 20X images were captured on a single plane using the DS-Fi2 colour camera and saved as 24-bit. tifs, while 60X samples were captured as a series of 0.2uM slices and saved as .ND2 Z stacks prior to analysis.

Table 3.2. Visualisation Conditions for Wide Field Fluorescent Microscopy.

Objective	Dapi	β3T (Alexa-488)	Nestin (Alexa-594)
10X Plan Flour PH1 (NA=0.3)	1x Analogue Gain 1s Exposure	-	-
20X S Plan Flour (NA=0.45)	1x Analogue Gain 600ms Exposure	1x Analogue Gain 1s Exposure	1x Analogue Gain 1.5s Exposure
Apo TIRF 60X oil DIC objective (NA=1.49)	1x Analogue Gain 150ms Exposure	1x Analogue Gain 500ms Exposure	1x Analogue Gain 700ms Exposure

3.2.2.3. Image Analysis

Phase-contrast images of live cells were used to establish broad changes to neuronal morphology in line with those expected during differentiation. Images were converted to 8-bit. tifs and the Neuron J plugin (Meijering *et al.,* 2004) was used to manually trace and classify neurites. A neurite was defined as any extension beyond the perimeter of the cell body. Primary neurites were defined as those directly connected to the cell body, while secondary neurites were connected to cell bodies only via an independent neuronal extension. Tracings were saved as .ndf files and used to measure the number of neurites, total, mean and maximal neurite length, and number of secondary neurites as a proxy for neurite branching.

Fluorescent images were used to quantitatively examine cell proliferation, neurite morphology, and the expression and localisation of neuronal markers. To measure relative rates of cell division, Dapi images were pre-processed and analysed using the protocol depicted in **Figure 3.6.** Images and stacks were converted to 8-bit. tifs before background was subtracted using the rolling ball algorithm (where rolling ball = 50 pixels for 10X and 20X images, and 100 pixels for 60X stacks). 60X stacks were also subject to four rounds of iterative deconvolution before maximum intensity projections were generated for downstream analysis. Images and MIPs were smoothed, enhanced (saturated pixels = 90%) and despeckled before the separate nuclei macro (Baeker, 2013) was adapted to create an indexed mask of segregated nuclei. Briefly, images were scaled using bilinear interpolation and binarised using the Huang thresholding algorithm before watershedding. Subsequently, the analyse particles command was used to count nuclei in binarised masks, based on size > 100 pixels and circularity > 0.3. The number of nuclei in each image was used both as a measure of cell proliferation between samples and for the subsequent normalisation of β3T and Nestin expression.

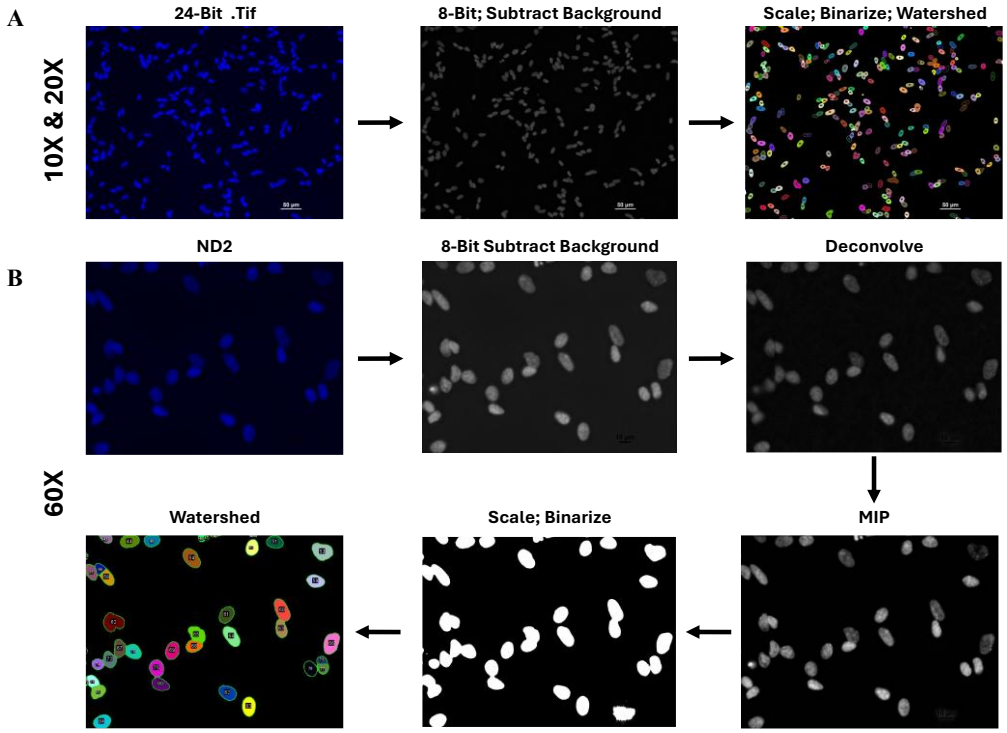


Figure 3.6. Image Processing and Analysis Pipeline for Cell Quantification. A) 24-bit .tif images captured at 10X and 20X magnification were converted to 8-bit. tifs before background was subtracted using a rolling ball = 50 pixels. Images were smoothed, despeckled and scaled using bilinear interpolation before binarisation using the Huang autothresholding algorithm. Nuclei were separated using watershedding and the analyse particle command was used to count the number of individual nuclei with a minimum size of 100 pixels and a minimum circularity of 0.3. B). ND2 Z-stacks were converted to 8-bit .tifs and background was subtracted using a rolling ball = 100 pixels. Four rounds of deconvolution were conducted using the Iterative Deconvolve 3D plugin and a maximum intensity projection (MIP) was generated using the Z-project tool in Image J. MIPs were scaled, binarised, watershed and quantified using the pipeline described for 10X and 20X images.

The expression of β3T and Nestin was quantified using the protocol summarised in **Figures 3.7** and **3.8.** After converting images and stacks to 8-bit tifs, background was subtracted using a rolling ball = 50 pixels for 20X images and 100 pixels for 60X stacks. 60X stacks were subject to four (β3T) or six (NES) rounds of iterative deconvolution using the Iterative Deconvolve 3D ImageJ plugin before MIPs were generated for subsequent analysis. β3T and NES greyscale images were subsequently used to define ROIs localised to either neurites or cell soma. β3T images and MIPs were enhanced (saturated pixels=90%) and sharpened before binary masks were generated using the Huang thresholding algorithm. Binarised masks were used to define ROIs encompassing total cell area. A Gaussian Blur Filter (sigma radius = 4) was applied to non-binarised enhanced images before convolution with a 5x5 kernel was used to extract neurite outlines. Following binarisation using Default thresholding, the convolved masks were used to define ROIs specifically localised to cell neurites. Greyscale NES images were binarised using the Huang thresholding algorithm and used to define ROIs localised to cell soma. Unenhanced greyscale images were used to measure β3T and NES area and integrated density in 1) total cell area, defined by the ROIs generated from binarised β3T masks, ii) neurites, defined by the ROIs generated from convolved β3T masks and iii) cell bodies, defined by ROIs generated from

binarised NES masks. Background fluorescence was calculated from an average of five representative background ROIs in each image and fluorescent intensity was calculated as Integrated Density – (Fluorescence Area X Mean Background Fluorescence) normalised to Dapi count (Teppola *et al.,* 2016).B3T and NES colocalisation was evaluated across 20X and 60X greyscale images using the Colocalisation Threshold plugin in Image J, where the ROI was defined by the mask derived from the β3T channel and zero-zero pixels were excluded from analysis.

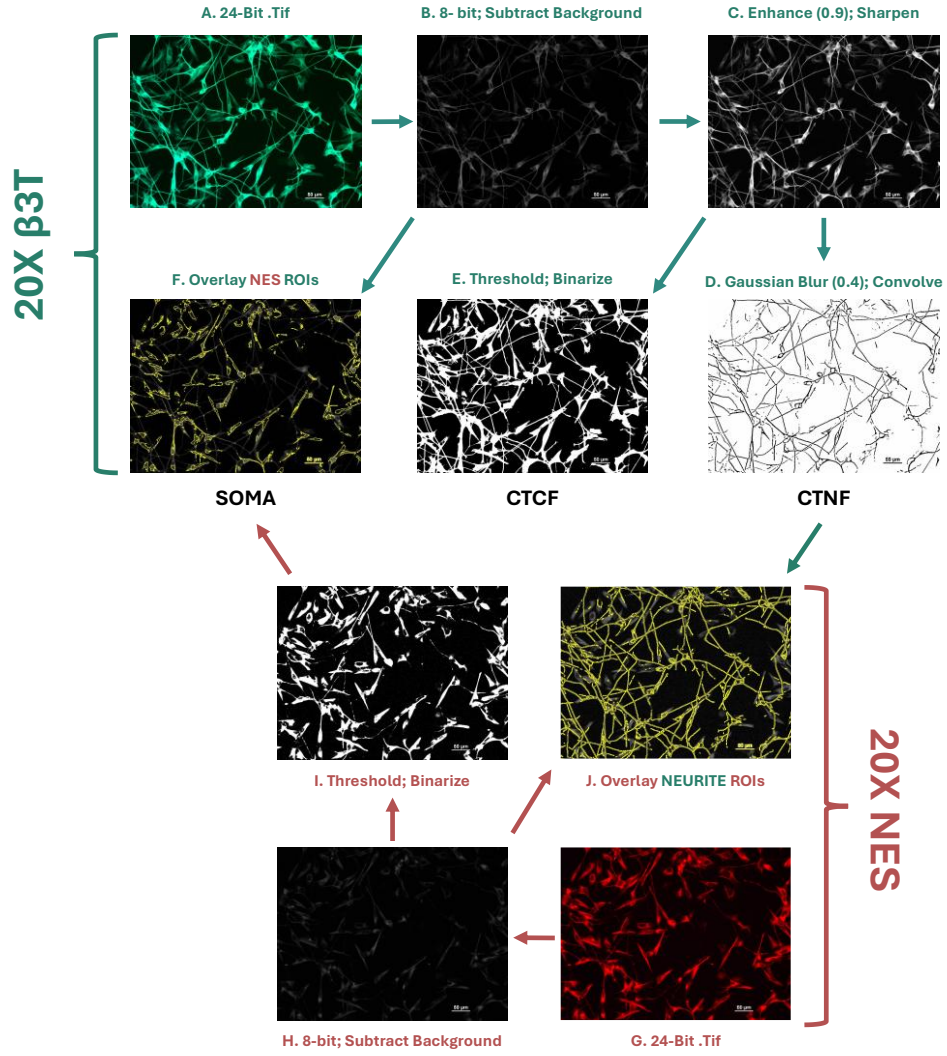


Figure 3.7. Pre-processing and Image Analysis Pipeline for 20X Images. 24-bit. tifs of β-3-Tubulin (β3T) and Nestin (NES) captured with the FITC **(A)** or Texas Red **(G)** filters were converted to 8-bit. tifs and background was subtracted using a rolling ball of 50 pixels **(B,H).** β3T images were enhanced (setting saturated pixels to 90%) and sharpened before the Gaussian Blur Filter (sigma radius = 4) was applied and convolution with a 5x5 kernel was used to extract neurite outlines (D) to calculate corrected total Neurite Fluorescence (CTNF). Enhanced β3T and greyscale NES images were binarised using the Huang autothresholding algorithm **(E, I)** to generate a mask for corrected total cell fluorescence (CTCF). The NES mask was overlayed on grayscale β3T and NES images to measure the area and integrated density of the cell soma **(F)** while the neurite outlines were used to measure the area and integrated density of neurites **(J).** Background fluorescence was calculated from an average of five representative background regions of interest in each image and fluorescent intensity in total cell area, cell neurites and cell soma was calculated as Integrated Density – (Fluorescence Area X Mean Background Fluorescence) normalised to Dapi count.

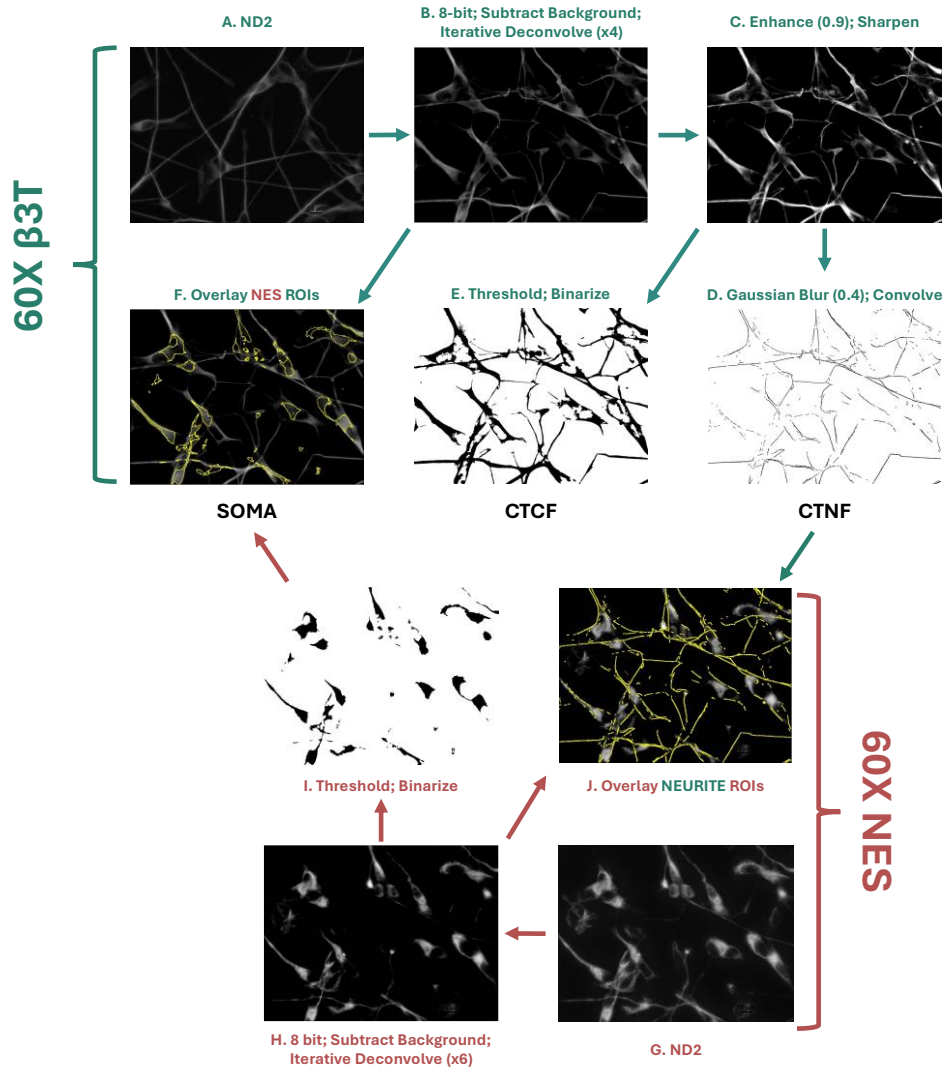


Figure 3.8. Pre-processing and Image Analysis Pipeline for 60X Stacks. ND2 Z-stacks of 0.2 µM slices captured at 60X **(A,G)** were converted to 8-bit .tifs and background was subtracted using a rolling ball of 100 pixels before four **(B)** or six **(H)** rounds of deconvolution were performed using the Iterative Deconvolve 3D plugin in Image J. Maximum intensity projections (MIPs) were generated using the Z-project tool and β3T MIPs were enhanced (setting saturated pixels to 90%) and sharpened before the Gaussian Blur Filter (sigma radius = 4) was applied and convolution with a 5x5 kernel was used to extract neurite outlines **(D).** Enhanced β3T and greyscale NES MIPs were binarised using the Huang autothresholding algorithm **(E, I).** The NES mask was overlayed on grayscale β3T and NES images to measure the area of the cell soma **(F)** while the neurite outlines were used to measure the area of neurites **(J).** Background fluorescence was calculated from an average of five representative background regions of interest in each image and fluorescent intensity in total cell area, cell neurites and cell soma was calculated as Integrated Density – (Fluorescence Area X Mean Background Fluorescence) normalised to Dapi count.

β3T images were also used to quantitatively assess neurite production, elongation and morphology with a combination of manual and automated neurite tracing techniques **(Figure 3.9).** The Single Neurite Tracer (SNT) plugin (Longair, Baker and Armstrong, 2011) was used to generate automated tracings from convolved β3T 20X and 60X masks. The parameters for automated tracing were optimised for maximum coverage of the neuronal network that minimised false connections and filtered out small components, where length > 10µM for 20X images and > 20µM for 60X images, and maximum

connection distance was < 5µM for both datasets. Automated tracing was prone to overestimate neurite length in undifferentiated cells and falsely identify neurite branches in differentiated samples. Therefore, 60X convolved masks were manually traced with SNT to supplement the data generated from automated tracings. Both datasets were saved as .traces files, and subsequently analysed to quantify the number of paths per cell, mean, maximum and total path length, the mean and total number of branches per path and the mean path complexity.

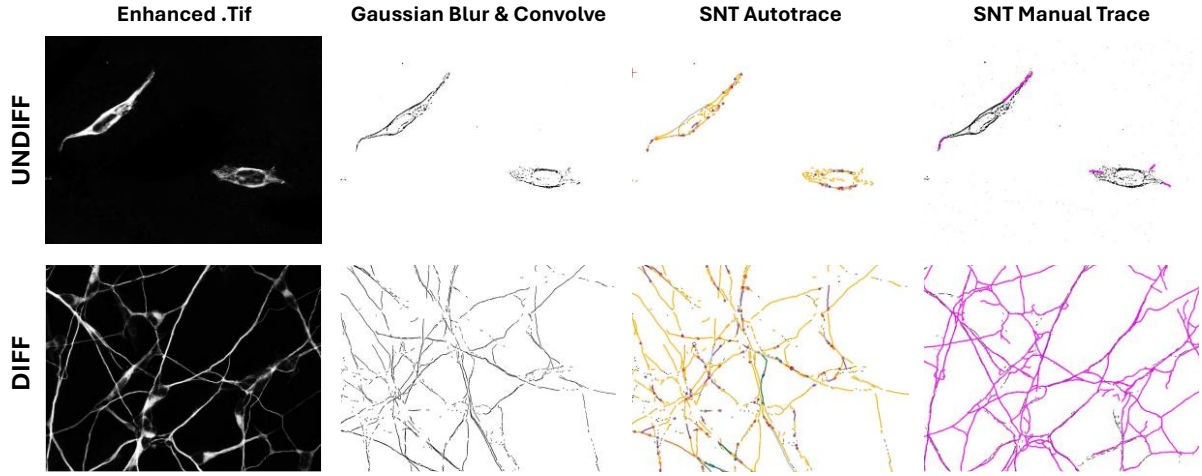


Figure 3.9. Quantification of Neurite Morphology with Automated and Manual Tracing Techniques. The Single Neurite Tracer (SNT) plugin was used to trace binarised convolved masks of β-3-Tubulin-stained neurites using automated tracing (where minimum length = 10µM for 20X images and 20µM for 60X images and maximum connection distance = 5µM) and manual tracing techniques.

3.2.2.3. Metabolic Characterisation

To confirm that neuronal differentiation induced a metabolic shift, live-cell respirometry was used to assess basal and spare metabolic capacity in undifferentiated cells grown overnight in 15% FBS and differentiated cells after nine days of 1% FBS + 10µM RA + 50ng/mL BDNF administration. On day 9 of differentiation, cells were seeded in PDL-coated XFp 6-well miniplates at 30 000 cells per well and incubated overnight at 5% CO2 37°C. PDL plates and cartridges were prepared and loaded as described in **2.2.7** before being transferred to the Seahorse XF HS Mini Bioanalyser (Brombacher Research Group, Institute of Infectious Diseases, University of Cape Town). Basal metabolic rate was evaluated over three time points, followed by three measurements after injections of 1.5µM oligomycin and 1.5µM FCCP respectively. Subsequently, protein normalisation was carried out using the Bradford assay and data was analysed using the Seahorse Analytics online platform.

3.2.3. Statistical Analysis

All microscopy data were analysed in GraphPad Prism v10.0.2 (San Diego, California USA). Outliers were removed with the Robust regression and Outlier removal (ROUT) approach using the standard Q

coefficient of 1%. Date were tested for normality using the Shapiro-Wilks Test before being analysed with either unpaired two-tailed T-tests, one-way ANOVAs (parametric) or Kruskal-Wallis (non-parametric) tests and post-hoc Dunnet's multiple comparisons tests to evaluate significance. P-values are annotated on the graphs as follows: *p<0.05, **p<0.01, ***p<0.001, and ****p<0.0001.

3.3. Results

3.3.1. An In Vitro Model for Neurogenesis: Hallmarks of Differentiation

Efficient differentiation in the SH-SY5Y cell line is marked by an attenuation of cell proliferation, the production of elongated processes, a decrease in the expression of the stem-cell marker NES, and an increase in the expression of β3T (Lopes *et al.,* 2010; Xicoy, Wieringa and Martens, 2017; Kovalevich, Santerre and Langford, 2021). Here, each of these parameters were evaluated to establish and confirm an efficient model for *in vitro* neurogenesis. Firstly, cell proliferation was examined using Dapi to quantify the number of cells in culture after i) 24 hours in full EMEM: F12; ii) 9 days in serum-depleted media or iii) 9 days in differentiation media. Cells were counted across 12-24 regions of interest (ROIs) at both 10X and 20X magnification for each condition. The 10X images captured broad population-wide trends while the 20X images facilitated more accurate nuclei segmentation during image analysis. Both 10X and 20X images showed that cell number increased in both day 9 samples relative to day 1 controls, but that the differentiation protocol substantially inhibited cell growth compared to day 9 controls maintained in serum-depleted medium **(Figure 3.10).** Here, the rate of cell proliferation was 3-3.5 times higher in day 9 controls than in differentiated samples. Together, this indicates effective cell cycle exit during differentiation, which is both a hallmark of, and prerequisite for, *in vitro* neurogenesis.

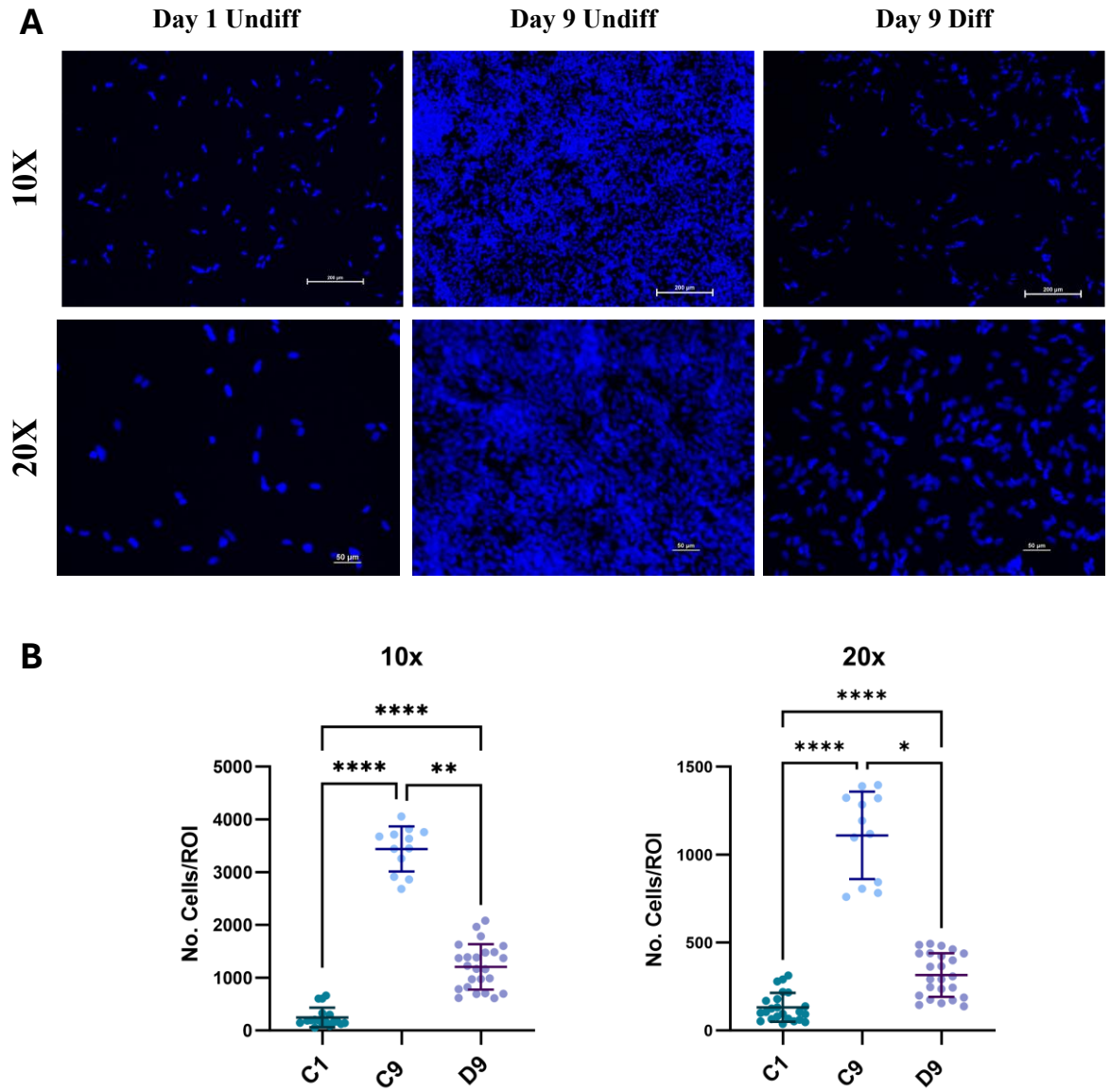


Figure 3.10. Inhibition of Cell Proliferation During Differentiation. SH-SY5Y cells were seeded in 6 well plates in full EMEM: F12 at 7.5x 10^4/ well and allowed to proliferate for 24 hours (C1) before being switched to 1% FBS (C9) or 1% FBS + 10µM RA and 50ng/mL BDNF (D9) for 9 days. Cell populations were fixed, permeabilised and stained with 250nM Dapi for 10 minutes before being visualised with a Nikon Ti-E inverted microscope equipped with a CHGFIE Intensilight mercury-fibre illuminator, a Nikon D200 DS-Fi2 colour camera and a DAPI Filter Set #49000 (Ex/Em = 320-380nm/ 435-485nm). Cell populations were captured across 12-24 ROIs per condition from three independent biological repeats with both a 10X Plan Flour PH1 (NA=0.3) and a 20X S Plan Flour (NA=0.45) objective**. A)** Representative images of cell populations at 10X and 20X magnification, scale bars = 200µM and 50µM respectively**. B)** Quantification of cell number per ROI under each condition measured using Fiji/Image J. Data represent mean and standard deviation and significance was determined using a Kruskal Wallis Test with Dunn's Post-Hoc Multiple Comparisons where *p<0.05, **p<0.01, ***p<0.001, and ****p<0.0001.

Before proceeding with a more comprehensive analysis of neuronal complexity and maturation, a preliminary characterisation of neurite morphology was conducted using phase contrast images of live-cell cultures. Although this approach fails to account for cell number per ROI, it does provide

preliminary insight into the morphological remodelling induced under different conditions that informed downstream experiments. This analysis revealed that both serum-depletion and differentiation significantly increased the production and elongation of neurite processes **(Figure 3.11).**

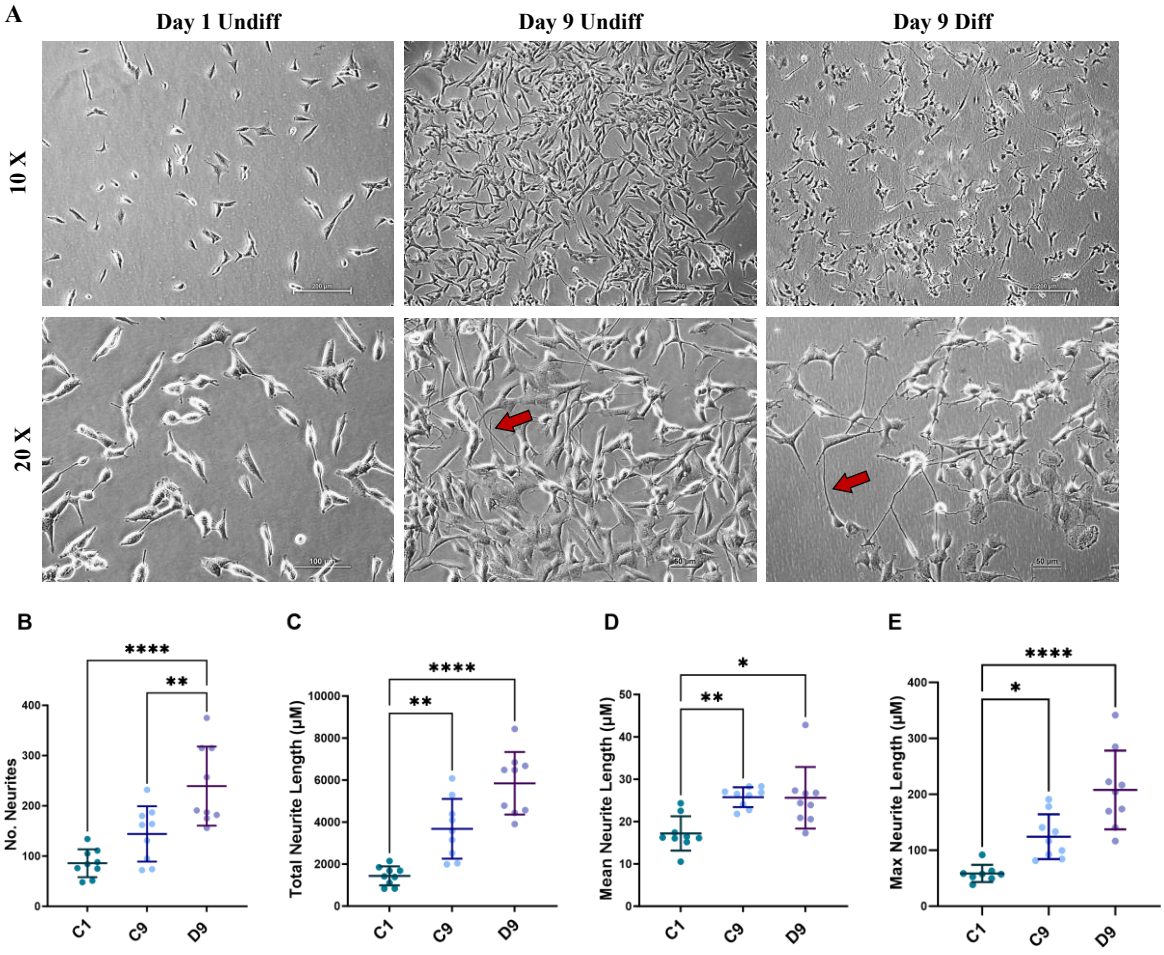


Figure 3.11. Evaluation of Neurite Morphology in Live Cell Cultures. SH-SY5Y cells were seeded in 6 well plates in EMEM: F12 15% FBS and allowed to proliferate for 24 hours (C1) before being switched to 1% FBS (C9) or 1% FBS + 10µM RA and 50ng/mL BDNF (D9) for 9 days. Cell populations were visualised with a Nikon Ti-E inverted microscope equipped with a CHGFIE Intensilight mercury-fiber illuminator and a Nikon D200 DS-Fi2 colour camera. Cell populations were captured across 9 ROIs per condition from three independent biological repeats with a 20X S Plan Flour (NA=0.45) objective and neurite morphology was evaluated using manual tracing in Neuron J. **A)** Representative Phase Contrast Images of SH-SY5Y cells at 10X and 20X magnification, scale bars = 200µM and 50µM respectively, where neurite processes are highlighted by red arrows. **B)** Total Number of Neurites, **C)** Total Neurite Length, **D)** Mean Neurite Length and **E)** Maximum Neurite Length per ROI under each condition. Data represent mean and standard deviation and significance was determined using either one-way ANOVAs or Kruskal Wallis Tests with Dunn's Post-Hoc Multiple Comparisons where *p<0.05, **p<0.01, ***p<0.001, and ****p<0.0001.

Relative to day 1 controls, the mean neurite length was increased by 1.5-fold in both FBS-depleted controls and differentiated samples. However, while differentiation increased the total number and length of neurites by 2.8 and 4-fold respectively, these parameters were only increased 1.7- and 2.6-fold

with FBS depletion. This suggests that serum depletion may contribute to the emergence of neuronal features during differentiation but verifies the neurogenic effect of RA-BDNF administration *in vitro*. This data also shows that serum-depletion more strictly isolates signatures associated solely with neurogenic agents; however proliferative controls better reflect the morphological characteristics of immature NPCs. Moreover, the highly confluent nature of day 9 controls confounds automated image analysis techniques required for the quantification of neurite complexity and the expression of neuronal markers **(Figure S3.3).** Together, this demonstrated evidence of neurite production and elongation during differentiation and suggested that day 1 controls were better suited for subsequent analyses of maturation and morphology.

The expression and localisation of NES and β3T were used to quantitatively evaluate neuronal maturation and morphology using ICC. Both NES and β3T are cytoskeletal proteins that primarily maintain cell structure and stability, but these two proteins also modulate cell division, neuronal migration, axon guidance and synaptogenesis (Singh and Tsai, 2010; Bernal and Arranz, 2018). NES is highly expressed in the cell body of NPCs and absent in mature neurites (Bott *et al.,* 2019) while β3T is specifically expressed in mature neurons as an essential component of the axon cytoskeleton (Sánchez-Mendoza *et al.,* 2017). Here, differentiation significantly altered the expression of NES and β3T in both the soma and neurites compared to undifferentiated controls **(Figure 3.12).** On average, differentiation decreased the size of the soma by 12% and increased the total neurite area by 21%, leading to a 34% increase in the neurite: soma area ratio per cell **(Figure 3.12B-D).** Both NES and β3T displayed a marked intracellular gradient, where expression was 1.6- and 2.6-fold higher in the cell soma than in the neurite processes **(Figure S3.4).** This gradient was amplified in differentiated cells, where cell bodies expressed NES and β3T at levels 2.4- and 3.2- times greater than in neurite extensions. This reflects the 3-fold difference in β3T expression between cell bodies and neurites previously reported (Dravid *et al.,* 2021); one of the features of the SH-SY5Y line that makes it amenable to quantitative image analysis (Pani *et al.,* 2014).

Interestingly, total β3T expression per cell was 0.2-fold higher in day 1 controls compared to differentiated cells **(Figure 3.12E).** On the other hand, both 20X and 60X images showed that NES expression was reduced by at least 50% during differentiation **(Figure 3.12E),** particularly in neurite extensions, where NES was downregulated by 63 -70% **(Figure S3.5A).** Due to the dynamic nature of NES and β3T expression during different stages of differentiation, an increase in β3T area along with the presence of β3T+/ NES- neurite processes is often used to verify neuronal differentiation (Simões *et al.,* 2021). Here, differentiation significantly increased the ratio of β3T: NES expression by up to 2.15-fold in neurite extensions **(Figure 3.12G; Figure S3.5C)** and significantly decreased β3T and NES colocalisation, demonstrated by a 0.73-fold decrease in the Pearsons colocalisation coefficient and a 0.51- and 0.62-fold decrease in the Manders coefficients **(Figure 3.12H-J).** Together, this demonstrates that differentiation significantly increases β3T+ area, decreases the size of cell soma, downregulates

total NES expression and remodels the cytoskeletal network to facilitate the production and elongation of neurite processes. Moreover, while signal quantification was conducted primarily in 20X images, it is worth noting that the significant trends were recapitulated in the 60X ROIs **(Figure S3.6).**

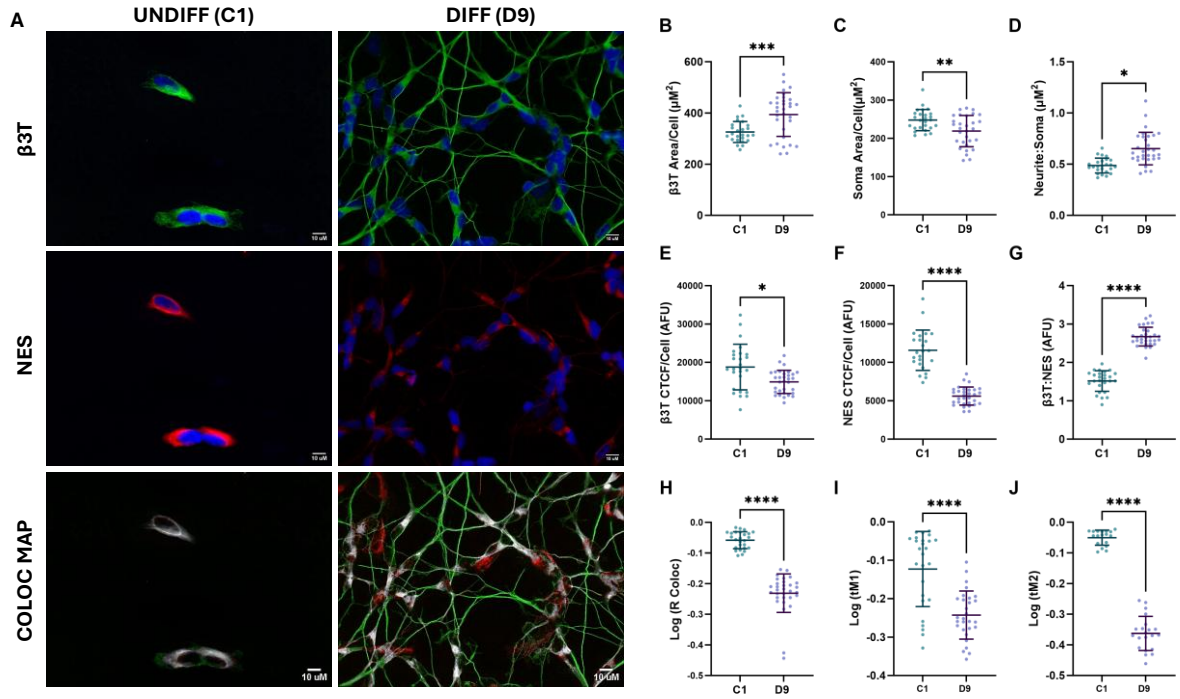


Figure 3.12. Quantification of Neuronal Maturation and Morphology. A multiplex immunocytochemistry assay was used to visualise Nestin (NES) and β-3-tubulin (β3T) expression in undifferentiated (C1) and differentiated SH-SY5Y cells after nine days of RA-BDNF treatment (D9). Samples from three independent biological repeats were imaged across 25-35 ROIs per condition using a Nikon C-HGFIE inverted microscope with both a 20X S Plan Flour (NA=0.45) and an Apo TIRF 60X oil DIC objective (NA=1.49) equipped with a DS-Fi2 colour camera. **A)** Representative maximum intensity projections generated from 60X Z-stacks showing the expression and localisation of β3T and NES in undifferentiated and differentiated cells. Colocalisation maps generated using the Colocalisation Threshold plugin indicate areas of colocalisation in grey, β3T localisation in green and NES localisation in red, scale bar = 10μM. **B)** β3T + area per cell. **C)** Soma area per cell. **D)** Neurite: Soma area ratio. **E)** Total β3T and **F)** Total NES expression per cell calculated as corrected total cell fluorescence (CTCF) = Integrated Density – (Fluorescence Area X Mean Background Fluorescence) normalised to Dapi count. **G)** Ratio of β3T:NES signal per cell. **H)** Log-normalised Pearson's (R) and **I,J)** Manders (tM1/2)colocalisation coefficients calculated with the Colocalisation Threshold plugin in Image J, where tM1 represents the fraction of β3T + area occupied by NES and tM2 represents the fraction of NES + area occupied by β3T. Data represent mean and standard deviation, and significance was evaluated using either one-way ANOVAs or Kruskal Wallis Tests with Dunn's Post-Hoc Multiple Comparisons where *p<0.05, **p<0.01, ***p<0.001, and ****p<0.0001.

The presence of β3T-positive neurite extensions also allows for a quantitative evaluation of neuronal network complexity and connectivity. Binary fluorescent images can be used in combination with automated tracing techniques to allow for high-throughput and objective measurements of neurite length and branching. This is particularly important for neuronal networks that can be highly heterogeneous, emphasising a need to capture bigger cell populations for a representative sample. However, autotracing doesn't always distinguish between cell outlines, fibrous filaments in the soma,

and tubular neuronal extensions and is prone to record single branched processes as separate paths. Manual tracing can facilitate more accurate measures of neurite production and elongation, but is slow, laborious and subject to researcher bias that can confound the reliability of the data. Here, complementary automated and manual tracing techniques were implemented to cross-check the data generated using each approach and enable an analysis of the broader populations captured in 20X images.

First, 60X images were analysed using both manual and autotracing tracing in SNT path **(Figure 3.13A).** Manual tracing recorded a significant increase in the total number of neurites, the number of neurites per cell, mean neurite length, the number and density of branches and the mean complexity per path **(Figure 3.13B-H).** Autotracing parameters were optimised to limit the identification of false neurites in undifferentiated controls while retaining sufficient coverage of the neuronal network in differentiated cells. Compared to manual tracing, the optimised autotracing protocols tended to overestimate the length and number of neurites in NPCs while underestimating total neurite length in differentiated neurons and incorrectly capturing the number of separate paths and branch points. As a result, autotracing found no significant differences in the total number of neurites, branches or neurite length per cell **(Figure S3.7).** Nevertheless, autotracing did reveal a significant increase in the mean path length and complexity, the maximum path length and the total number and length of neurites per ROI **(Figure 3.13I-O).**

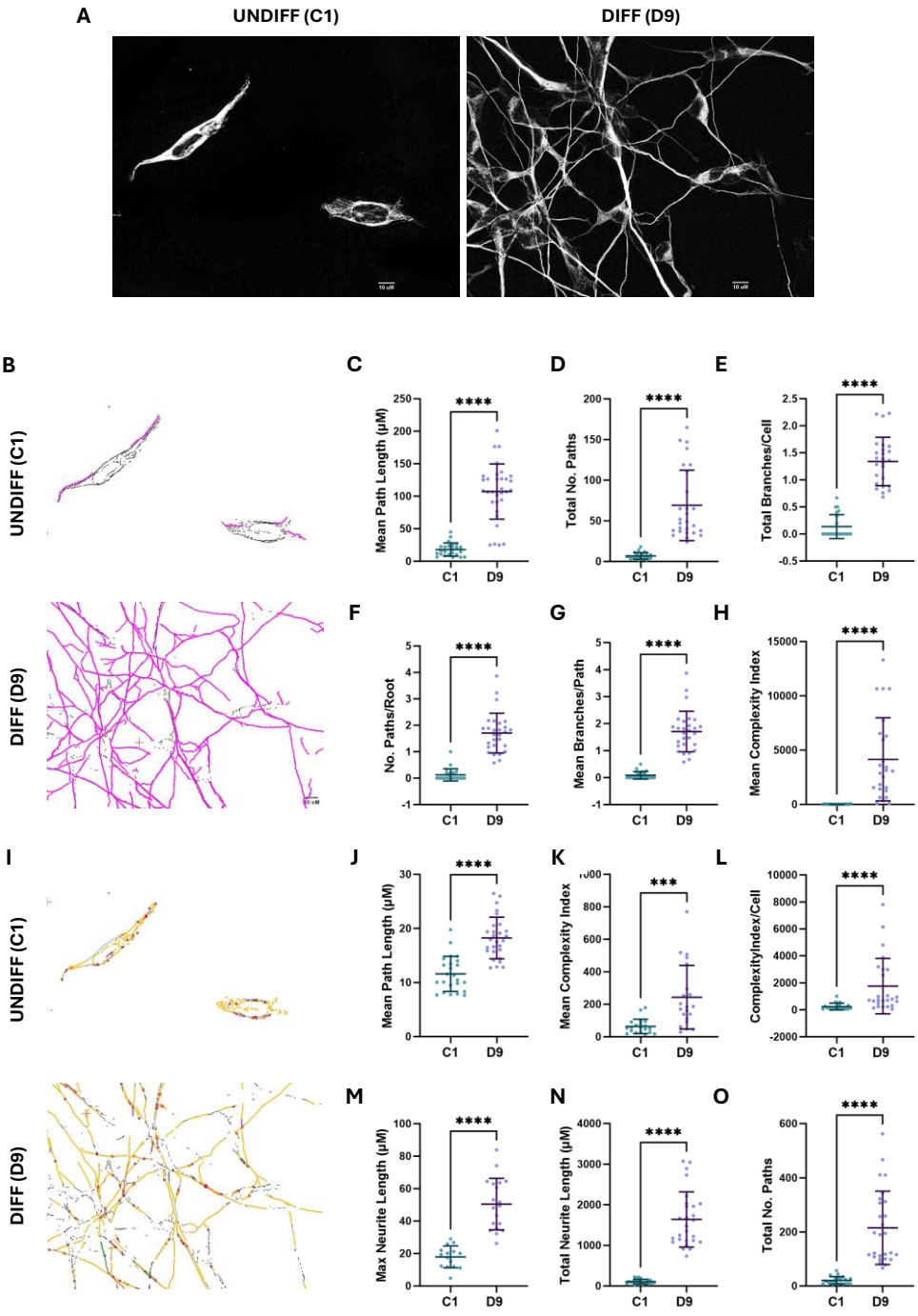


Figure 3.13. Automated and Manual Tracing Techniques to Quantify Neurite Morphology. Maximum intensity projections derived from 60X β3T Z-stacks were subject to preprocessing, Gaussian convolution and thresholding to generate binary masks of neurite outlines. Binary masks were traced with the Single Neurite Tracer (SNT) Image J plugin using both automated and manual tracing techniques. **A)** Greyscale maximum intensity projections showing β3T expression in undifferentiated and differentiated SH-SY5Y cells, scale bar =10µM. **B)** Manual tracings in SNT were used to measure **C)** mean path length, **D)** total number of paths per ROI, **E)** total number of branches per cell, **F)** total number of paths per cell, **G)** mean number of branches per path and **H)** mean complexity index per path. **I)** Neurite tracing generated from binary neurite outlines with automated tracing in SNT. Automated tracings were used to measure **J)** mean path length, **K)** mean complexity per path, **L)** total complexity per cell, **M)** maximum path length, **N)** total path length per ROI and **O)** total number of paths per ROI. Data represent mean and standard deviation across 24-27 ROIs per condition from three biological repeats, where significance was evaluated using either one-way ANOVAs or Kruskal Wallis Tests with Dunn's Post-Hoc Multiple Comparisons where *p<0.05, **p<0.01, ***p<0.001, and ****p<0.0001.

Table 3.3 summarises the pertinent values recorded using each tracing technique for both undifferentiated and differentiated cells. The comparison between manual tracing and autotracing indicates that autotracing overestimates the total number of paths and underestimates mean path length in both populations, while total path length, branching and complexity are overestimated in controls and underestimated in differentiated cells. While only manual tracing detects an increase in mean path length and branching in the neural network, both techniques illustrate an increase in the number of paths, total path length and mean path complexity with differentiation. Therefore, these parameters were evaluated in autotraced 20X images to validate the differences in neurite morphology across a broader sample.

Table 3.3. A Comparison of Auto and Manual Tracing Techniques in 60X Images. Data represent means across 24-27 ROIs from three independent repeats. The fold difference represents the ratio between the result generated using autotracing relative to manual tracing techniques, blue = FC < 1; red = FC > 1. Parameters that show the same trend during differentiation using both techniques are highlighted in green.

Parameter	Undifferentiated			Differentiated		
	Manual	Auto	Fold Difference	Manual	Auto	Fold Difference
Total No. Paths	6.74	20.77	**3.08**	**68.96**	**213.81**	**3.11**
Total Path Length (µM)	89.50	107.31	**1.2**	**2203.62**	**1637.36**	0.74
Path Length/ Cell (µM)	36.55	53.05	**1.45**	**81.88**	58.69	0.72
Mean Path Length (µM)	17.94	11.60	0.65	**107.16**	18.25	0.17
No. Branches/Cell	0.14	5.47	**39.07**	**1.34**	3.03	**3.01**
No. Branches/Path	0.09	1.33	**13.78**	**1.71**	1.22	0.71
Mean Complexity Index	18.02	68.83	**3.82**	**4153.73**	**243.32**	0.06

In the 20X images, autotracing detected a significant increase in the number of neurites and branch points, mean, maximum and total neurite length and mean path complexity **(Figure 3.14).** This reflects the trends detected by both auto and manual tracing in 60X images and demonstrates a convergence between three different datasets that illustrate a quantitative increase in neurite elongation, complexity and connectivity during differentiation. With the significant changes to cytoskeletal composition demonstrated in Figure 3.14, this data effectively reflects a mature neuronal phenotype compared to undifferentiated cells and establishes a workflow to quantitatively characterise disruptions to neuron morphology and maturation in this system.

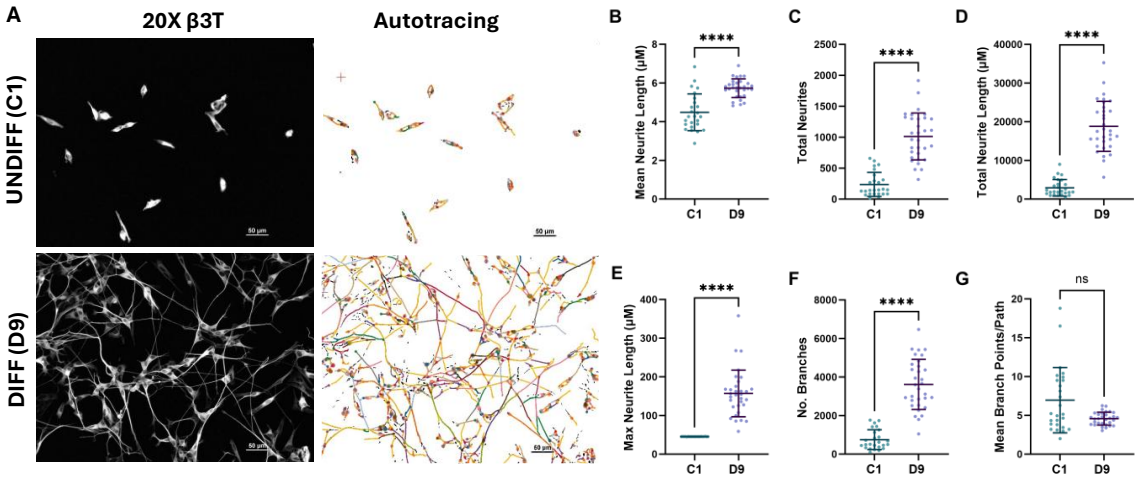


Figure 3.14. Automated Quantification of Neurite Morphology in 20X Images. Greyscale images showing β3T-stained neurons at 20X magnification were subject to preprocessing, Gaussian convolution and thresholding to generate binary masks of neurite outlines, which were autotraced using the Single Neurite Tracer (SNT) Image J plugin. **A)** Representative images of undifferentiated and differentiated SH-SY5Y cells, scale bar =50μM. Automated tracings were used to measure **B)** mean path length, **C)** total number of paths per ROI, **D)** total path length, **E)** maximum path length, **F)** total number of branches per ROI and **G)** mean branch points per path using SNT. Data represent mean and standard deviation across 26-36 ROIs per condition from three biological repeats, where significance was evaluated using either one-way ANOVAs or Kruskal Wallis Tests with Dunn's Post-Hoc Multiple Comparisons where *p<0.05, **p<0.01, ***p<0.001, and ****p<0.0001.

Before using this system to study mitochondrial mechanisms in neurogenesis, metabolic remodelling was verified with a cell characterisation respirometry assay. While basal OCR increased only slightly during differentiation (from 0.67 to 0.76 pmol/min/μg), maximal OCR increased by 83% (from 1.3 to 2.4 pmol/min/μg) and spare capacity increased by 97% (from 0.87 to 1.72 pmol/min/μg) **(Figure 3.15A; Figure S3.8A, B).** On the other hand, both basal and compensatory ECAR remained unchanged **(Figure 3.15B; Figure S3.8C, D).** Although both undifferentiated and differentiated cells displayed an aerobic energetic phenotype under basal conditions, differentiation increased spare oxidative capacity and reduced glycolytic compensation under stress **(Figure 3.15C).** Although this data is limited to one biological repeat, this trend recapitulates the increased oxidative capacity and decreased glycolytic reliance demonstrated by Pandey *et al.,* (2022) and reflects the emergence of an oxidative profile with increased bioenergetic capacity that mediates neurogenesis *in vivo.* Thus, the protocol established here not only reshapes neuronal morphology but also remodels neuronal metabolism in line with the mature neuronal phenotype, illustrating its utility to examine the interplay between neuronal metabolism and maturation *in vitro.*

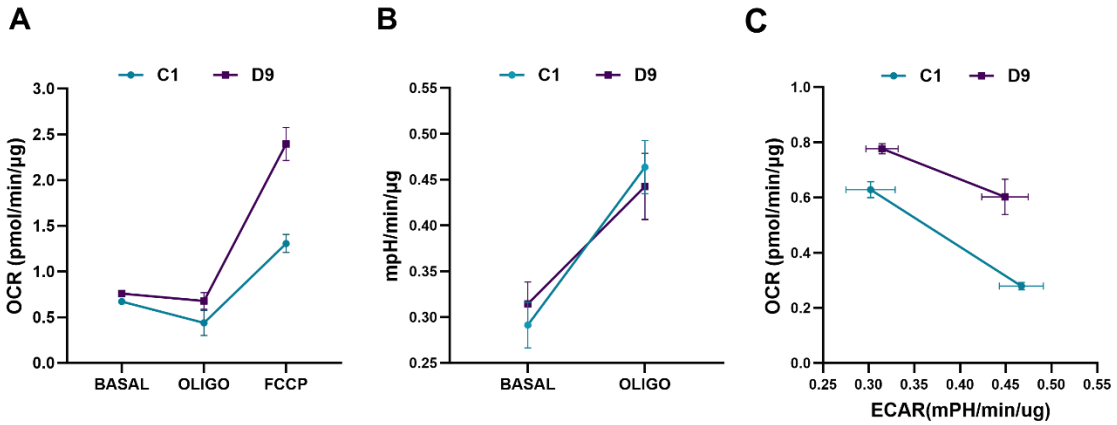


Figure 3.15. Metabolic Profiles of *In vitro* Neurogenesis. Undifferentiated SH-SY5Y cells in 15% FBS (C1) and differentiated cells subject to nine days at 1% FBS + 10µM RA and 50ng/mL BDNF (D9) were seeded in 6-well PDL coated XFp miniplates and assessed using the XFp Bioanalyser to evaluate **A)** oxygen consumption rate (OCR) and **B)** extracellular acidification rate (ECAR) at basal conditions, following 1.5µM oligomycin (OLIGO) and following 1.5µM FCCP injection. **C)** Metabolic phenotype under basal and stressed conditions in undifferentiated and differentiated cells. Data points represent the mean of three measurements under each condition, across three to six replicates from one biological repeat.

3.3.2. Propionic Acid – Induced Developmental Neurotoxicity

Building on the model for PPA-induced mitochondrial dysfunction established in Chapter 2, the workflow established in **3.3.1** was used to characterise a model for PPA-induced neurotoxicity. PPA did not significantly change total cell count over the course of differentiation, though a slight decrease in cell number was apparent relative to differentiated controls **(Figure S3.9).** On the other hand, neuronal morphology was markedly perturbed under PPA treatment **(Figure 3.16).** While differentiated controls displayed increasingly small and rounded soma during differentiation, cells exposed to PPA exhibited large, flat cell bodies with flat, feathery extensions. Instead of long, thin and branched neurites, cells differentiated with PPA grew stunted, thick and linear processes that failed to form a connected neural network. These observations were supported by quantitative measures of neurite morphology using manual tracing of live cell cultures, which showed a 20% decrease in neurite length **(Figure 3.16B)** and a 40% decrease in neurite production **(Figure 3.16C, D).** Moreover, while differentiation increased the number of secondary neurites by 12-fold from day 1, PPA decreased neurite branching by close to 50% **(Figure 3.16E).**

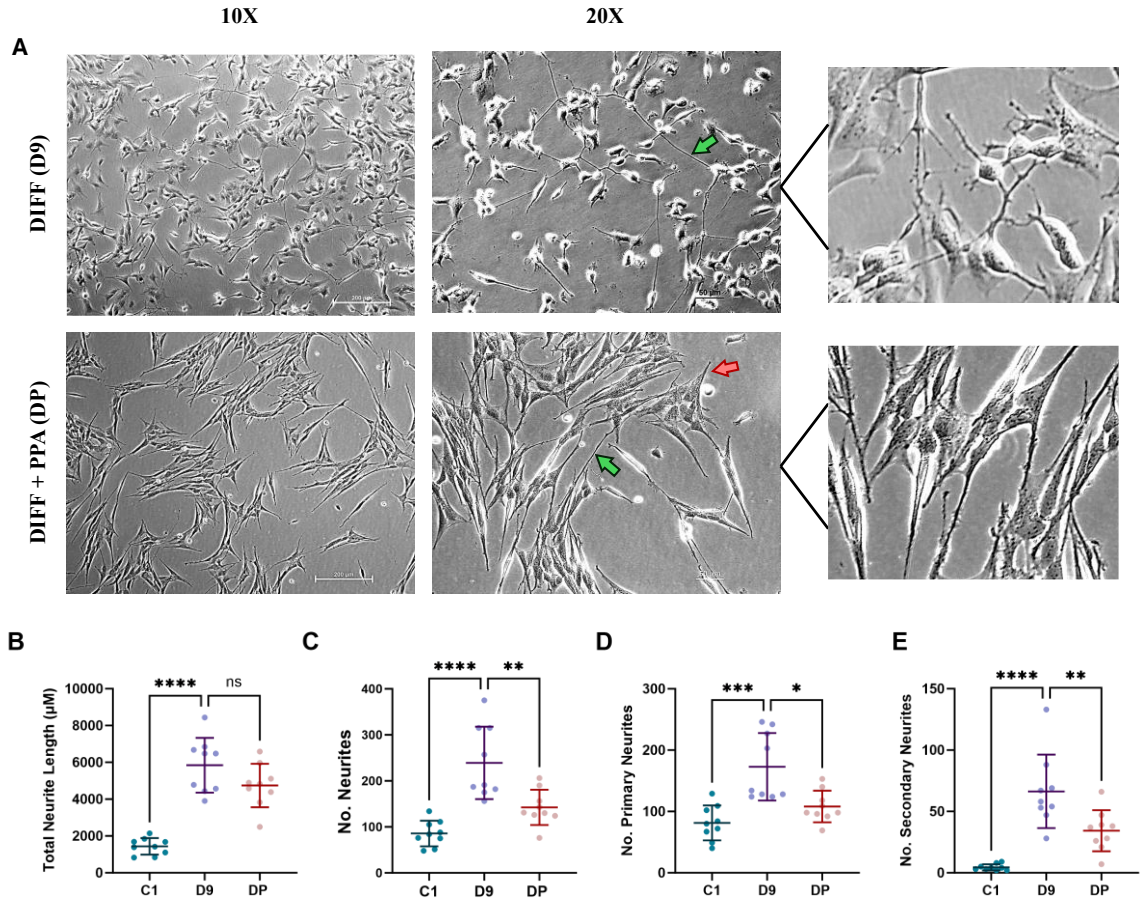


Figure 3.16. Gross Morphological Disruptions Induced by Propionic Acid. SH-SY5Y cells were differentiated with 10µM RA and 50ng/mL BDNF for nine days in the absence (D9) or presence (DP) of 5mM propionic acid (PPA). **A)** Representative phase contrast images of live cell cultures at 10X and 20X magnification, scale bar = 200µM and 50µM respectively. Green arrows highlight tubular neurite extensions and red arrows denote non-tubular processes. Manual tracing in Neuron J was used to measure **B)** Total Neurite Length, **C)** Total Number of Neurite, **D)** Number of Primary Neurites and **E)** Number of Secondary Neurites under each condition. Data represent mean and standard deviation from 9 ROIs across three biological repeats, and significance was determined using either one-way ANOVAs or Kruskal Wallis Tests with Dunn's Post-Hoc Multiple Comparisons where *p<0.05, **p<0.01, ***p<0.001, and ****p<0.0001.

Examining the patterns of NES and β3T expression further consolidated changes to neuronal morphology **(Figure 3.17).** PPA increased the size of NES+ soma by 3.3-fold **(Figure 3.17B)** with a notable absence of NES - neurite extensions. Interestingly, this occurred in conjunction with a 2.8-fold increase in β3T area **(Figure 3.17C),** which largely comprised thick, flat and fibrous expansions rather than tubular neurite-like processes. Moreover, PPA reduced the neurite: soma area ratio by 64% **(Figure 3.17D),** indicating a clear shift in the morphological composition of neuronal populations.

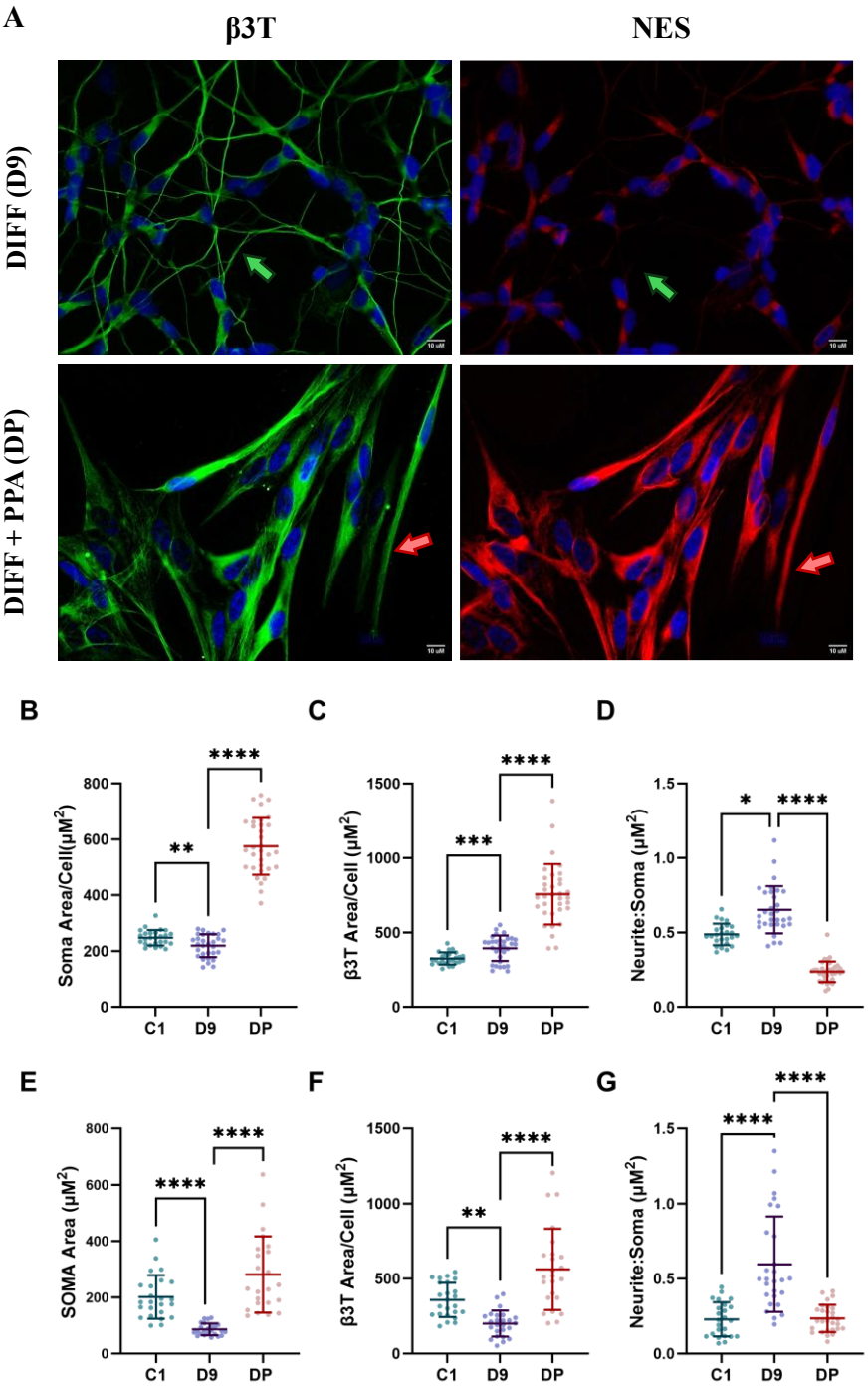


Figure 3.17. Morphological Composition of Neurons Under Propionic Acid Stress. SH-SY5Y cells were differentiated with 10μM RA and 50ng/mL BDNF for nine days in the absence (D9) or presence (DP) of 5mM propionic acid (PPA) before immunocytochemistry was used to evaluate Nestin (NES) and β-3-tubulin (β3T) expression under each condition. **A)** Representative maximum intensity projections at 60X magnification showing the expression and localisation of NES and β3T, scale bar = 10μM. Green arrows highlight tubular NES negative neurite processes while red arrows indicate non-tubular NES positive cellular expansions that emerge under PPA stress. The area of NES + soma, β3T + neurons and the ratio of the neurite: soma area per cell were measured across 32-35 ROIs per condition at 20X magnification **(B-D)** and 20-25 ROIs per condition at 60X magnification **(E-G)**, each from three independent biological repeats. Data represent mean and standard deviation, and significance was determined using either one-way ANOVAs or Kruskal Wallis Tests with Dunn's Post-Hoc Multiple Comparisons where *p<0.05, **p<0.01, ***p<0.001, and ****p<0.0001.

PPA also significantly altered the expression and localisation of neuronal markers during differentiation **(Figure 3.18A; Figure S3.10).** The expression of NES was increased between 2.2 and 2.9-fold in both soma and neurites, while β3T expression was increased by 1.7-fold in the cell body but remained unchanged in neurite extensions **(Figure 3.18 B-D).** Consequently, PPA decreased the β3T: NES ratio by 41% and 55% in the soma and neurites respectively, suggesting an inhibition of neuronal maturation. Indeed, PPA eroded the expression gradient that separates β3T and NES localisation during differentiation, exemplified by a 2.6-, 1.6 and 2.5-fold increase in the Pearsons and Manders colocalisation ratios **(Figure 3.19).**

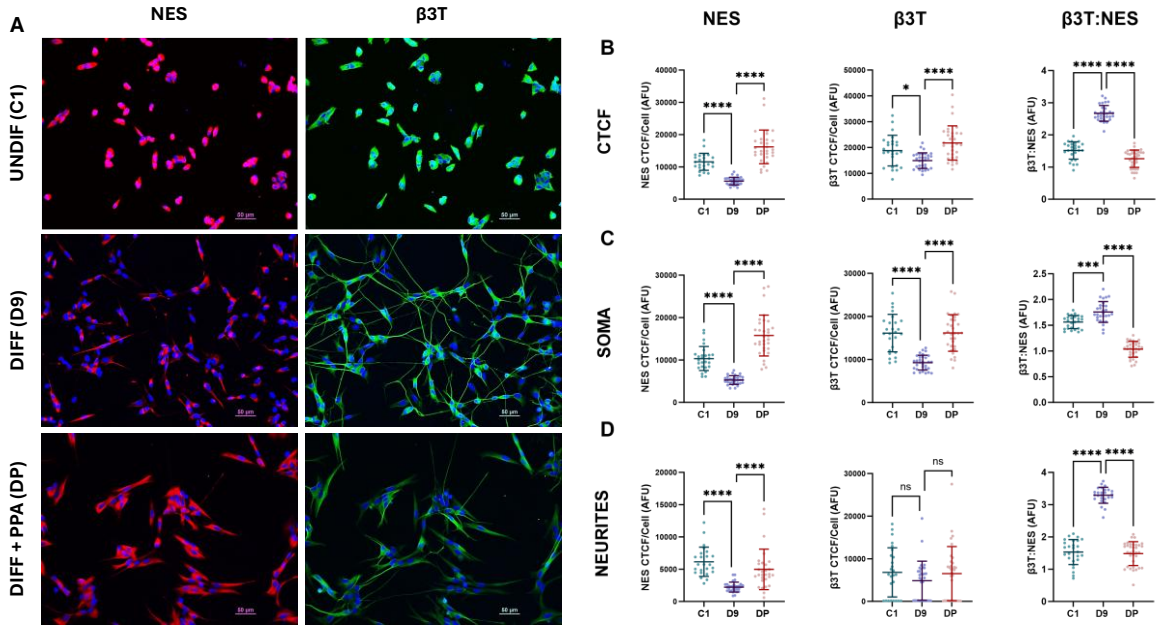


Figure 3.18. Altered Expression and Localisation of Neuronal Markers. Nestin (NES) and β-3-tubulin (β3T) expression was evaluated in SH-SY5Y cells differentiated with 10μM RA and 50ng/mL BDNF for nine days in the absence (D9) or presence (DP) of 5mM propionic acid (PPA). **A)** Representative images of NES and β3T expression visualised at 20X magnification using immunocytochemistry, scale bar = 50μM. The corrected total cell fluorescence (CTCF) method was used to measure total NES and β3T expression per cell in **B)** Total Cell Area, **C)** Cell Soma and **D)** Neurite Extensions where CTCF = Integrated Density – (Fluorescence Area X Mean Background Fluorescence) normalised to Dapi count. Data represent mean and standard deviation across 32-35 ROIs at 20X magnification from three independent biological repeats, and significance was determined using either one-way ANOVAs or Kruskal Wallis Tests with Dunn's Post-Hoc Multiple Comparisons where *p<0.05, **p<0.01, ***p<0.001, and ****p<0.0001.

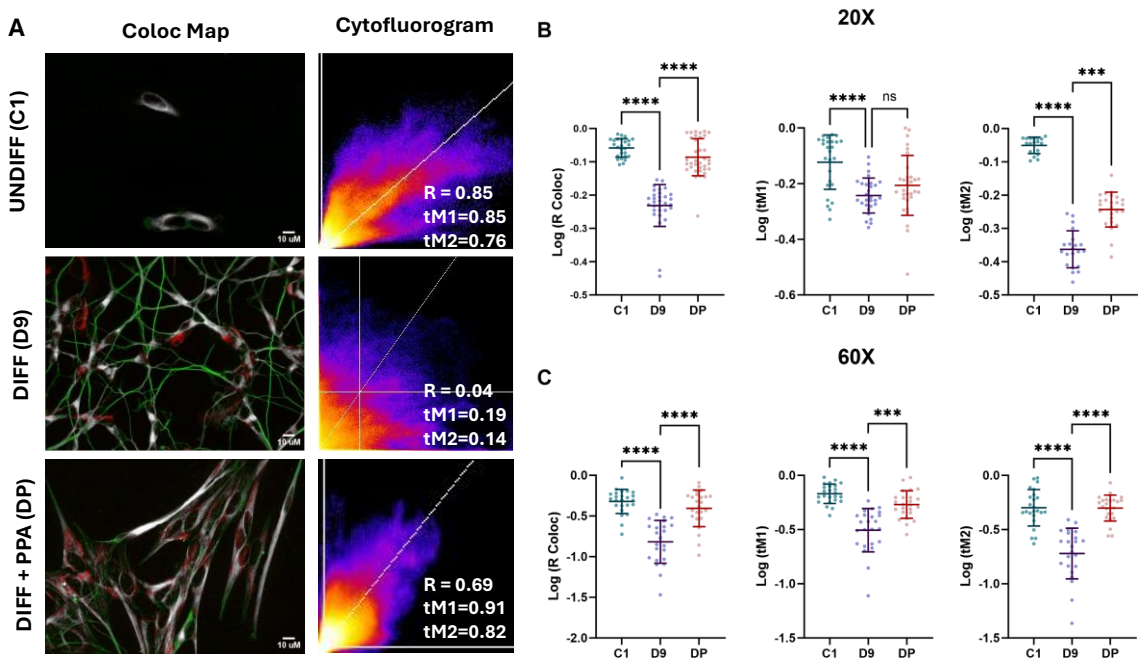


Figure 3.19. Increased Colocalisation of Nestin and β-3-Tubulin with Propionic Acid Exposure. Nestin (NES) and β-3-tubulin (β3T) localisation was evaluated in SH-SY5Y cells differentiated with 10μM RA and 50ng/mL BDNF for nine days in the absence (D9) or presence (DP) of 5mM propionic acid (PPA). **A)** Representative colocalisation maps, cytofluorograms and corresponding colocalisation coefficients derived from the Colocalisation Threshold plugin in Image J, scale bar = 10μM. Areas of colocalisation are depicted in grey, β3T localisation in green and NES localisation in red. Pearson (R) and Manders (tM1/2) coefficients were calculated for 32-35 ROIs per condition at 20X magnification **(B)** and 20-25 ROIs per condition at 60X magnification **(C)**, each from three independent biological repeats, where tM1 represents the fraction of β3T area occupied by NES and tM2 represents the fraction of NES area occupied by β3T. Data represent means and standard deviations for log-normalised coefficients and significance was determined using either one-way ANOVAs or Kruskal Wallis Tests with Dunn's Post-Hoc Multiple Comparisons where *p<0.05, **p<0.01, ***p<0.001, and ****p<0.0001.

Subsequently, the tracing techniques described in **3.3.1** were used to evaluate whether these morphological disruptions influenced the formation of neuronal networks. Again, both techniques were used to examine populations captured in 60X images and these trends were validated in autotraced 20X images. Manual tracing showed that PPA reduced the total number of neurites, total neurite length and mean neurite length by 69%, 58% and 42% respectively **(Figure 3.20B-E),** decreased the number and density of branches by 47% and 75% **(Figure 3.20F, G)** and reduced mean path complexity by more than 95% **(Figure 3.20H, I).** Of the parameters that distinguished undifferentiated and differentiated cells using autotracing, PPA significantly decreased the total number of paths and branches per ROI as well as the total and mean path length **(Figure 3.20J-M).** These trends were supported by data from 20X images, which revealed a significant decrease in mean, maximum and total neurite length, as well as the number of neurites and branches under PPA stress **(Figure 3.21).** This is consistent with the morphological changes that were visually observed during PPA exposure and demonstrate a quantitative decrease in the production, elongation and connectivity of neurites in this context.

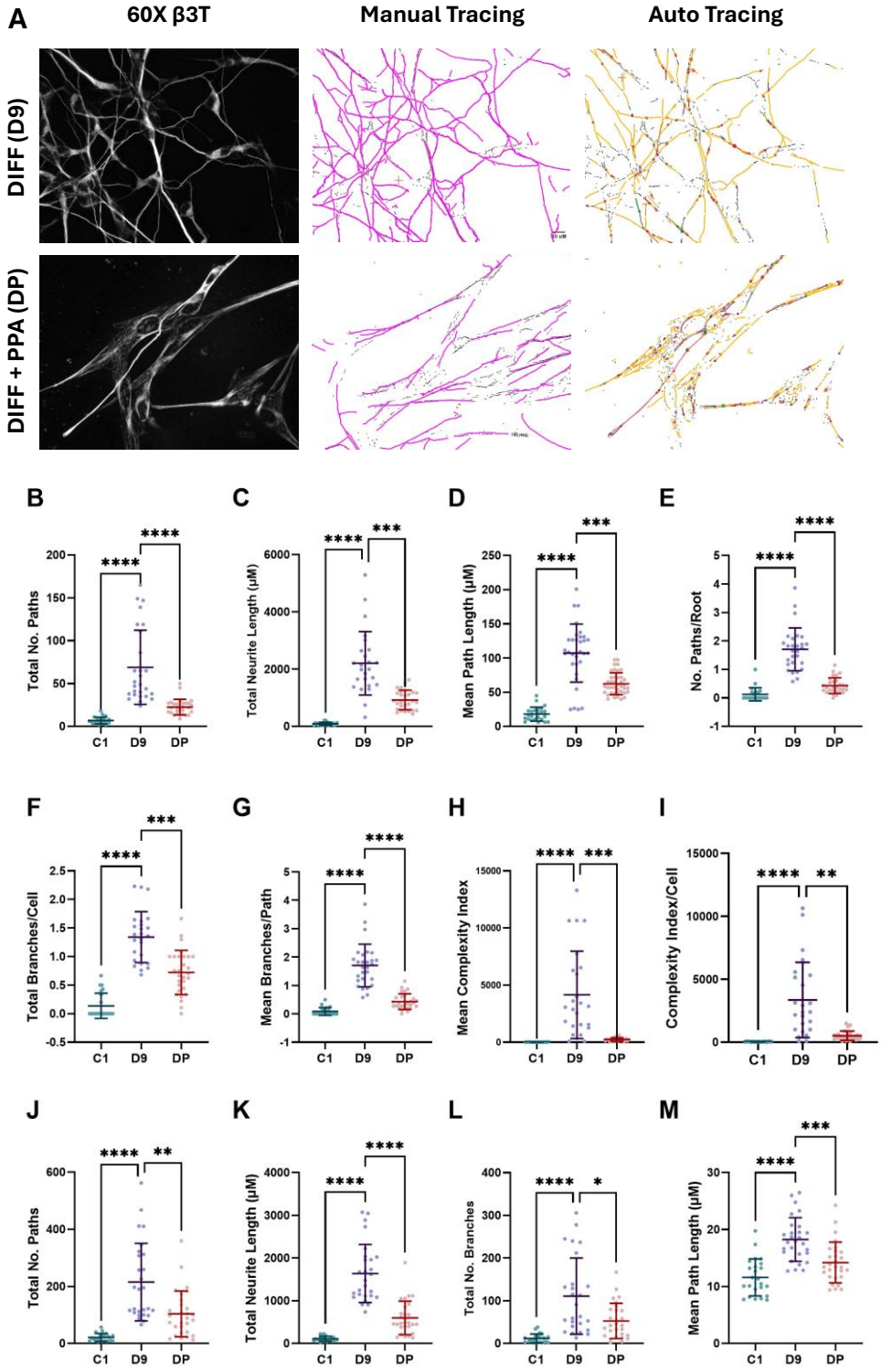


Figure 3.20. Disruptions to Neurite Elongation and Branching. Single Neurite Tracer (SNT) was used to trace binary convolved masks of β3T+ neurites after nine days of differentiation with 10μM RA and 50ng/mL BDNF in the absence (D9) or presence (DP) of 5mM propionic acid (PPA). **A)** Representative maximum intensity projections of β3T stained neuronal populations at 60X magnification and the associated tracing generated using manual and automated tracing techniques. Quantitative measures of neurite production, elongation and connectivity were captured from 20-25 ROIs per condition at 60X magnification across three biological repeats using SNT to analyse manual tracings **(B – I)** and autotracings **(J-M).** Data represent means and standard deviations, and significance was determined using either one-way ANOVAs or Kruskal Wallis Tests with Dunn's Post-Hoc Multiple Comparisons where *p<0.05, **p<0.01, ***p<0.001, and ****p<0.0001.

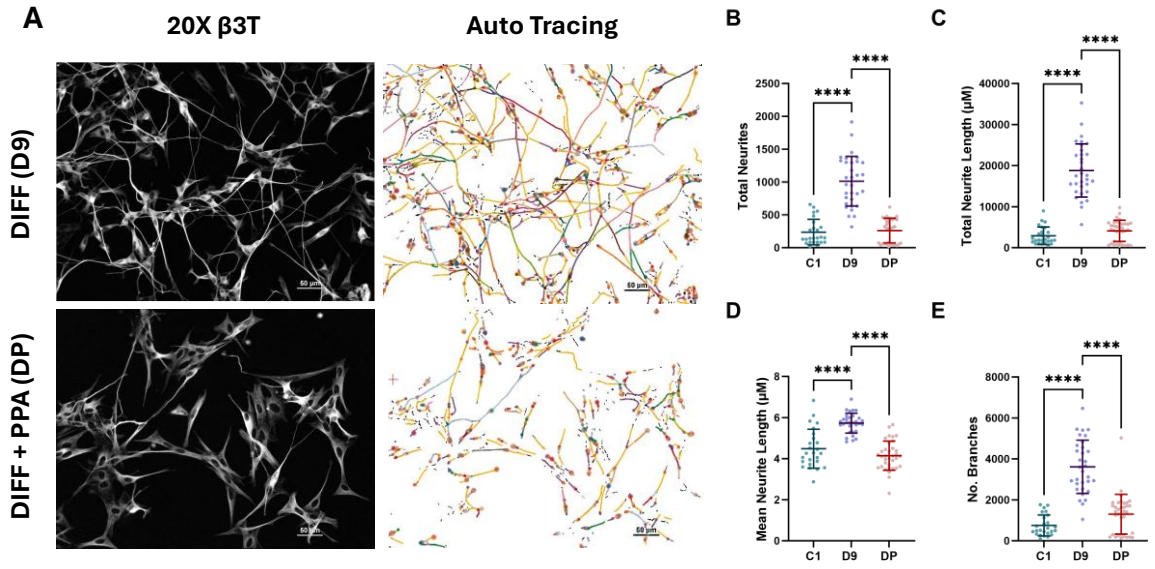


Figure 3.21. Morphological Disruptions Validated by Autotracing In Broader Cell Populations. SH-SY5Y cells differentiated for nine days with 10μM RA and 50ng/mL BDNF in the absence (D9) or presence (DP) of 5mM propionic acid (PPA) were visualised at 20X magnification and Single Neurite Tracer (SNT) was used to autotrace binary convolved masks of β3T+ neurites. **A)** Representative 20X images of β3T stained neuronal populations and the associated autotracing generated with SNT, scale bar = 50μM. Quantitative measures of neurite production **(B),** elongation **(C, D)** and complexity **(E)** were captured from 32-35 ROIs per condition across three biological repeats. Data represent means and standard deviations, and significance was determined using either one-way ANOVAs or Kruskal Wallis Tests with Dunn's Post-Hoc Multiple Comparisons where *p<0.05, **p<0.01, ***p<0.001, and ****p<0.0001.

3.4. Discussion

This chapter established a cell model to study neurogenesis using the SH-SY5Y system, successfully developing a workflow to induce, confirm and characterise neuronal differentiation *in vitro*. The existing literature describing the SH-SY5Y model acknowledges the heterogeneity of the terminal neuronal phenotype depending on the specific differentiation protocol employed. Previous studies have demonstrated that RA combined with BDNF efficiently drives cell cycle exit and morphological remodelling that reflects *in vivo* neurogenesis (Encinas *et al.,* 2000; Shipley, Mangold and Szpara, 2016; Yang *et al.,* 2016; Hromadkova *et al.,* 2020; Dravid, Raos and Svirskis, 2021; dos Santos, Gomes and Costa, 2023). Moreover, cotreatment with RA and BDNF drives transcriptional and post-transcriptional mechanisms required for SH-SY5Y differentiation that reflect *in vivo* neurogenesis and recapitulate relevant signatures involved in ASD aetiology (Nishida *et al.,* 2008; Goldie, Barnett and Cairns, 2014; Chiocchetti *et al.,* 2016). However, the protocols best suited to model the metabolic shift associated with *in vivo* neurogenesis remain uncharacterised. This chapter evaluated available respirometric data from the SH-SY5Y cell line to identify a differentiation protocol that recapitulates the metabolic remodelling required for neuronal maturation. This data highlighted a need to consider basal growth medium, serum depletion and neurogenic agents to promote the emergent oxidative profile

of differentiated SH-SY5Y cells while mitigating the inherent glycolytic reliance that diverges from the *in vivo* neuronal phenotype. Considering both molecular and metabolic signatures associated with SH-SY5Y differentiation, the findings reported by Pandey et al. (2022) and Chiocchetti et al. (2016) were used to design a nine-day RA and BDNF administration protocol in low-serum EMEM: F12 to model *in vitro* neurogenesis.

Using phase contrast microscopy, ICC and live-cell respirometry, this chapter demonstrated efficient cell cycle exit, neurite production, elongation and branching and a metabolic shift that increased oxidative capacity without upregulating glycolytic activity during *in vitro* neurogenesis. An evaluation of total cell counts in undifferentiated and differentiated cultures showed that neurogenesis decreased cell proliferation by more than three-fold compared to serum-depleted controls. This not only demonstrated successful cell cycle exit but also ensured an appropriate cell density to allow for the formation, identification, visualisation and segmentation of neurite processes *in vitro,* which is a prerequisite for quantitative assessments of neuronal maturation and morphology (Dravid *et al.,* 2021). A morphological analysis of live cell cultures showed that differentiation increased neurite production and elongation by more than 1.3-fold compared to serum-depletion alone. Interestingly, neurogenic features also emerged in serum-depleted controls, which reflects previous reports that FBS-depletion upregulates the expression of neuronal markers and promotes neurite production, elongation and branching in SH-SY5Y cells ((Thomson *et al.,* 2022). This data suggested that serum-depleted controls could be important for the isolation of neurogenic signatures in subsequent mechanistic studies of neuronal differentiation. However, this also reflected a clear divergence from the undifferentiated phenotype that could confound morphological analyses of neuronal differentiation. Accordingly, day 1 undifferentiated controls were used for subsequent measures of neuronal morphology and maturation using ICC.

Congruent with documented features of the SH-SY5Y cell line, differentiation was associated with a decrease in the size of cell soma with a concurrent increase in total neurite area (Dwane, Durack and Kiely, 2013) and a marked intracellular gradient in the expression of cytoskeletal proteins (Dravid *et al.,* 2021). Here, levels of both NES and β3T expression were more than two times higher in cell soma than in neurite extensions. Although β3T expression remained largely unchanged during differentiation, total NES expression was decreased by up to 50%, leading to a two-fold increase in the β3T: NES expression ratio. A decrease in NES and an increase in β3T expression are widely accepted markers of neuronal differentiation (Kovalevich, Santerre and Langford, 2021). However, while several studies (Murillo *et al.,* 2017; Serdar *et al.,* 2020; Unsicker *et al.,* 2021) report that β3T is upregulated during SH-SY5Y differentiation, others have shown no changes to total β3T expression measured by qPCR (Simões *et al.,* 2021), ICC and western blot (Pezzini *et al.,* 2017). Likewise, although the data presented here are consistent with the 50-55% decrease in NES previously demonstrated by flow cytometry (Graham and Train, 2017) and western blot (Lopes *et al.,* 2010; Unsicker *et al.,* 2021), SH-SY5Y

differentiation has also been shown to increase or maintain NES expression (Forster *et al.,* 2016; Pezzini *et al.,* 2017; Simões *et al.,* 2021; Barth *et al.,* 2022).

Importantly, both NES and β3T exhibit dynamic expression profiles over the course of neurodevelopment, and this may explain the discrepancies in the literature. For example, NES expression may increase during early phases of neurogenesis (Jin *et al.,* 2009), while β3T can be expressed in NPCs prior to the terminal mitotic division that initiates neurogenesis and increases during early synaptogenesis (Singh and Tsai, 2010; Duly *et al.,* 2022). Moreover, β3T expression varies with neuronal activity and is differentially expressed in N- and S-type SH-SY5Y cells (Bell *et al.,* 2013). Thus, the change in NES and β3T expression in differentiated cultures depends on the relative proportion of N- and S-type cells in undifferentiated controls and the specific stage of maturation at which measurements are taken. Given that the β3T signal is markedly higher in cell bodies relative to neurites, the slight decrease in β3T expression per cell observed here may also be due to the reduced fraction of cell area comprised by the soma in differentiated samples.

Given these considerations, future studies could explore alternative neuronal proteins to verify neuronal maturation *in vitro.* Nevertheless, the data presented here reveal a significant decrease in NES expression, an increase in the β3T:NES ratio and a shift in cell morphology that is consistent with a mature neuronal phenotype. Indeed, the localisation of NES and β3T diverged significantly with the emergence β3T+/ NES- neuronal processes, exemplified by the decrease in the Pearson and Manders colocalisation ratios. In addition, quantitative assessments reveal unequivocal changes to neurite morphology with a significant increase in neurite length, number and complexity using both auto and manual tracing techniques. Importantly, this morphological remodelling was underpinned by a distinct metabolic shift that increased oxidative capacity while decreasing glycolytic reliance. Thus, the differentiation protocol employed here induced morphological, molecular and metabolic features of neurogenesis that are consistent with previous studies in the SH-SY5Y cell line and reflect hallmarks of neuronal maturation *in vivo.* Moreover, this work developed an automated image analysis pipeline to quantify the expression and localisation of neuronal markers as well as the size and complexity of neuronal networks. Together, this establishes a suitable system to study neurogenesis *in vitro*, which could facilitate diverse avenues of future research into the molecular aetiology of ASD.

Here, this system was harnessed to evaluate the neurotoxic effects of PPA, building on the model for mitochondrial dysfunction established in Chapter 2. Although PPA did not appear to significantly alter cell count during differentiation, it is important to note that the method used here cannot distinguish between the relative rates of cell division and cell death that modulate cell density. Thus, disruptions to either cannot be ruled out. In fact, preclinical studies have shown that PPA promotes the proliferation and self-renewal of human NSCs (Abdelli, Samsam and Naser, 2019; Lagod, Abdelli and Naser, 2024), impairs neuronal viability (Ju *et al.,* 2023) and upregulates markers of apoptotic cell death (El-Ansary,

Al-Daihan and El-Gezeery, 2011; Khera *et al.,* 2022; Sharma, Bhalla and Mehan, 2022). Thus, future work should aim to establish whether PPA alters *in vitro* markers associated with cell proliferation, senescence or cell death to clarify the effect of PPA on cell division and viability.

However, PPA exposure during neurogenesis significantly perturbed gross neuronal morphology, because tubular neuronal extensions were replaced by enlarged cell soma and feathery extensions of the cell body. Moreover, PPA profoundly altered the expression and localisation of cytoskeletal proteins, leading to an increase in NES expression, an absence of NES – neurite processes and a significantly reduced β3T: NES ratio. In addition, PPA impaired the formation and connectivity of neuronal networks, illustrated by a significant decrease in the number, length and complexity of neurite processes. Although no previous studies have investigated how PPA influences neurodifferentiation in the SH-SY5Y cell line, these observations are consistent with other preclinical studies of PPA-associated neurotoxicity. The available literature suggests that PPA concentrations up to 300μM may mediate a neuroprotective effect in the context of neuronal injury (Hu *et al.,* 2018; Ostendorf *et al.,* 2020; Gisevius *et al.,* 2024), while doses above 1mM consistently impair neuronal viability, maturation and function. Significant neurophysiological impairments are observed in PPA murine models, including gross morphological aberrations, changes to synaptic ultrastructure, disruptions to neuronal organisation, as well as evidence of neuronal injury and cortical atrophy (Sharma, Rahi and Mehan, 2019; Lobzhanidze *et al.,* 2020; Rahi *et al.,* 2021; Baser, Kesli and Ates, 2023; Zhvania *et al.,* 2024). Similarly, *in vitro* studies have shown that PPA decreased dendritic spine density (Choi *et al.,* 2020), impaired neurite production (Ju *et al.,* 2023), reduced neurite outgrowth and decreased the expression of neuronal markers (Abdelli, Samsam and Naser, 2019).

It is unclear whether these morphological alterations are associated with, or mechanistically driven by, changes to metabolic flux. However, recent studies in SH-SY5Y cells demonstrated significant impairments to both mitochondrial respiration and neuronal maturation in response to methylmalonic acid, which closely reflects the biochemical signature of PPA exposure (Da Costa *et al.,* 2021). Accordingly, future work will investigate how PPA impacts neuronal metabolism and mitochondrial function during *in vitro* neurogenesis. Moreover, it will be useful to determine whether the morphological disruptions induced by PPA are associated with changes to metabolic state, mitochondrial dynamics, or mitochondrial content, morphology, and connectivity. In particular, time-course experiments would yield novel insight into the dynamic changes to mitostasis and metabolic flux during differentiation and in response to PPA.

In addition, the mechanisms that underpin PPA-induced neurotoxicity remain unclear. Some evidence suggests that PPA impairs neurite outgrowth by disrupting autophagic flux (Choi *et al.,* 2020), while other studies have revealed a role for FFAR signalling mediated by FFAR3 (Abdelli, Samsam and Naser, 2019; Lagod, Abdelli and Naser, 2024). Notably, this work demonstrates a significant shift towards

gliogenesis that leads to neuroinflammation and gliosis, proposing convergent disruptions to neurodevelopment, neurophysiology and neuroimmune state in the PPA model. Therefore, ongoing work in our research group is evaluating how PPA influences neurodifferentiation and gliogenesis in a multipotent cell model, which will facilitate a more comprehensive assessment of the interactions between neurons, oligodendrocytes and astrocytes that modulate neuronal structure and function. Nevertheless, this is the first study to functionally demonstrate that metabolic stress induced by PPA alters neurogenesis in SH-SY5Y cells, establishing and characterising a model for PPA-induced neurotoxicity. In doing so, this chapter lays the groundwork for mechanistic studies into the relationship between mitochondrial dysfunction and neurodevelopment, and how it might be exploited to mitigate neuropathology.

Chapter 4.

Transcriptomic Signatures: The Neurotoxic Mechanisms of Propionic Acid

4.1. Introduction

While Chapter 3 revealed marked impairments to neurogenesis under PPA stress, the mechanisms that drive this response remain unclear. Notably, Chapter 2 demonstrated transcriptional disruptions to central regulators of mitostasis under PPA stress, while Kim *et al.,* (2019) previously showed that PPA perturbed the expression of neurogenic genes in undifferentiated SH-SY5Y cells. More recently, Da Costa *et al.,* (2021) found that methylmalonic acid, the metabolite produced directly upstream from PPA, alters both the metabolism and maturation of SH-SY5Y cells, but the mechanisms that drive this response remain unexplored. Therefore, Chapter 4 employed global RNA-Seq to investigate whether PPA disrupts the transcriptional crosstalk that governs neuronal metabolism and maturation.

4.1.1. Experimental Design

Given the breadth and depth of any -omics dataset, the analytical scope should be defined at the outset. The transcriptomic analysis presented in this chapter was informed by i) the experimental design used, ii) the primary research aims and iii) the nature of the molecular dataset in question. This chapter was designed to characterise the transcriptomic signatures associated with the end-point disruptions to neuronal morphology and maturation observed in Chapter 3. Therefore, the transcriptional profiles of neurons exposed to PPA during differentiation (DP) were compared to day 1 undifferentiated controls grown in 15% FBS (C1), day 9 negative controls maintained in 1% FBS without RA or BDNF (C9) and day 9 positive controls differentiated with RA and BDNF (D9). This approach allowed for the isolation of five distinct transcriptomic signatures associated with i) serum depletion; ii) the neurogenic programme driven by RA and BDNF; iii) differentiation induced by serum depletion and neurogenic agents; iv) the neurogenic programme under PPA stress and v) PPA exposure alone. Together, all five transcriptomic signatures were used to characterise the neurotoxic mechanisms that disrupt neurogenesis under PPA stress.

4.1.2. Analytical Approach

In this chapter, transcriptomic profiles were examined through an exploratory lens intended to identify the broad mechanistic relationships that drive PPA-induced neurotoxicity *in vitro.* This was achieved using a stepwise approach informed by three primary objectives: i) validate PPA-induced disruptions to neuronal metabolism, maturation and morphology; ii) identify central mechanisms by which PPA disrupts neurogenesis and iii) better characterise the relationship between metabolism and neurodevelopment. Here, global expression profiles were analysed in a two-pronged approach that

integrated both targeted and untargeted analyses to balance scope with specificity **(Figure 4.1).** In this way, transcriptional signatures were used to ask targeted questions and test specific hypotheses without foreclosing on novel biological processes and mechanistic relationships that may arise from the data itself.

First, pairwise differential gene expression (DGE) analysis examined whether PPA significantly altered the neurogenic transcriptome and identified defining features across different transcriptional landscapes. Secondly, targeted overlays were conducted to identify metabolic and neurotoxic signatures in the PPA transcriptome with reference to previous transcriptomic datasets in the SH-SY5Y model. Subsequently, weighted gene co-expression network analysis (WGCNA) was used to explore the mechanistic relationships between significantly enriched functional signatures in the PPA transcriptome. Lastly, Ingenuity Pathway Analysis (IPA) was employed to identify upstream signalling pathways, downstream disease phenotypes and convergent regulatory hubs that govern neurodevelopment, physiology and function. Together, this workflow revealed functional signatures associated with PPA-induced disruptions to neurogenesis and highlighted central regulators of neurodevelopment, metabolism and neurotoxicity that shape the PPA transcriptome.

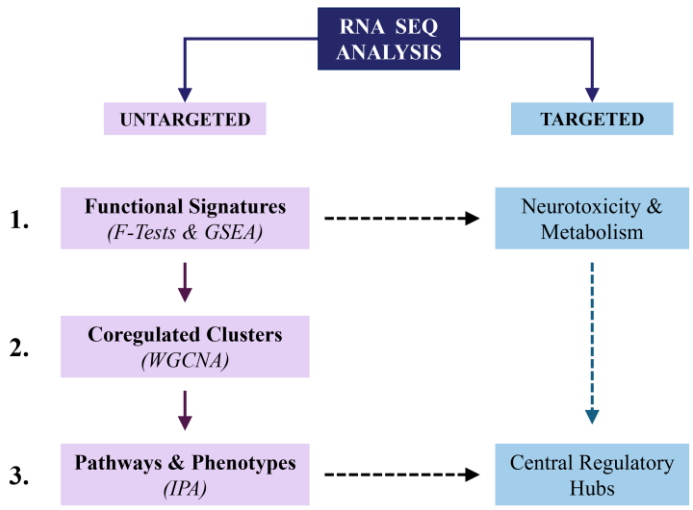


Figure 4.1. A Two-Pronged Approach to Transcriptomic Analysis. Significantly differentially expressed genes (DEGs) were identified using edgeR's quasi-likelihood (QL) pipeline with Benjamini Hochberg correction. Transcriptomic signatures were functionally annotated using gene set enrichment analysis (GSEA), while targeted overlays were conducted to characterise metabolic and neurotoxic hubs with reference to prior studies in the SH-SY5Y model. Weighted gene co-expression network analysis (WGCNA) revealed coregulated mechanistic clusters and Ingenuity Pathway Analysis (IPA) highlighted signalling pathways, disease phenotypes and regulatory networks.

4.1.3. Molecular Signatures of Metabolic State

Importantly, any transcriptomic study should also consider the context-specific utility of transcriptomic data to understand underlying molecular mechanisms. In this study, transcriptomic analysis provides a useful tool to interrogate regulatory crosstalk between metabolism and neurogenesis, in that it captures interdependent signatures of dysregulation across a broad range of genes and pathways. However, transcriptional profiles at a single endpoint of differentiation may not reflect directional changes to protein function, activity or metabolic flux. Therefore, a transcriptomic approach to study metabolic remodelling should consider the extent to which metabolic activity is reflected in underlying molecular

signatures. To this end, nine publicly available molecular profiles of SH-SY5Y differentiation were collated and annotated to characterise the molecular landscape that shapes metabolic state **(Table 4.1)**.

Table 4.1. Molecular Profiles of SH-SY5Y Differentiation. Data provide a summary of eight molecular studies of SH-SY5Y differentiation, detailing the molecular technique and the differentiated protocol used, the experimental design and the molecular dataset(s) that was collated from each study. RA – retinoic acid, BDNF-brain-derived neurotrophic factor, FBS – foetal bovine serum; SF – serum free, DMEM – Dulbecco's Modified Essential Medium; NBM – neurobasal medium.

	Reference	Molecular Approach	Differentiation Protocol	Experimental Design	Dataset Used
Transcriptome	(Nishida *et al.,* 2008)[1]	Affymetrix Human Genome Microarray	5 days 10μM RA 15% FBS; 3 days + 50 ng/ml BDNF in SF DMEM: F12	Extracted RNA on day 0, after 5 days RA and 8 days sRA-BDNF	RA: 113 up / 194 downregulated genes; BDNF: 219 up / 105 downregulated genes (FDR < 0.05)
	(Beveridge *et al.,* 2009) [2]	Illumina HumanRef-8-V2 BeadChip	6 days 10μM ATRA + 50 ng/ml BDNF in DMEM 1% FBS	Extracted RNA at day 0 and 6.	2946 up / 3001 downregulated genes (FDR < 0.05)
	(Chiocchetti *et al.,* 2016) [3]	Illumina HumanHT-12 v4 Expression BeadChip	11 days 10μM RA, 2mM cAMP, 50 ng/ml BDNF in NBM + B27	Extracted RNA at 0, 1, 3, 5, 7, 9 and 11 days *in vitro*	2217 up / 2074 downregulated genes on day 11 (FDR<0.05)
	(Pezzini *et al.,* 2017) [4]	Illumina HiSeq 1000	6 days 10μM RA 5% FBS in DMEM; 3 days 50 ng/ml BDNF, 2mM cAMP in NBM + B27	Extracted RNA at day 0 and day 9	1989 transcripts with |log2(FC)| ≥1; FDR ≤ 0.05
Proteome	(Barth *et al.,* 2022) [5]	Label-Free Quantitative LC–MS/MS	6 days 10μM RA 2.5% FBS in MEM	Extracted protein on day 0 and 6	114 up /160 downregulated proteins (logFC > |0.3|; q<0.05)
	(Leung *et al.,* 2024) [6]	LC-MS/MS w/ phosphopeptide enrichment	5 days 8uM RA 10% FBS in DMEM	Extracted proteins on day 0 and 5	599 up / 713 downregulated proteins (FDR<0.05)
	(Murillo *et al.,* 2017) [7]	iTRAQ-based quantitation via LC–MS/MS w/ phosphopeptide enrichment	5 days 10uM RA 15% FBS; 10 days 50ng/ml BDNF SF DMEM: F12	Proteins extracted on day 0 and 15	366 proteins with logFC ≥ 1.5 or ≤ 0.67; p < 0.05
	(Pandey *et al.,* 2022) [8]	Label-Free Quantitative LC-MS/MS	5 days 10μM RA with reducing serum; 3 days 100 ng/ml BDNF SF MEM: F12	Extracted protein at day 0 and 8	215 up / 163 downregulated proteins (FC > 2; p < 0.05)

Subsequently, the molecular datasets detailed in Table 4.1 were subject to gene set enrichment analysis (GSEA) to identify significantly enriched Hallmark metabolic pathways among up- and down-regulated genes **(Figure 4.2A).** To get a more detailed view of specific signatures associated with mitostasis and

substrate utilisation, each dataset was overlayed with non-redundant composite gene lists derived from Reactome, Go and Hallmark pathways representing processes involved in mitochondrial, glucose, AA and lipid metabolism **(Table S4.2).** The global expression profiles associated with each pathway **(Figure S4.1**) were used to calculate a net perturbation score (NPS) for each dataset **(Figure S4.2, Figure 4.1B, C**) which reflects whether each metabolic pathway is relatively more enriched among up- or down-regulated genes.

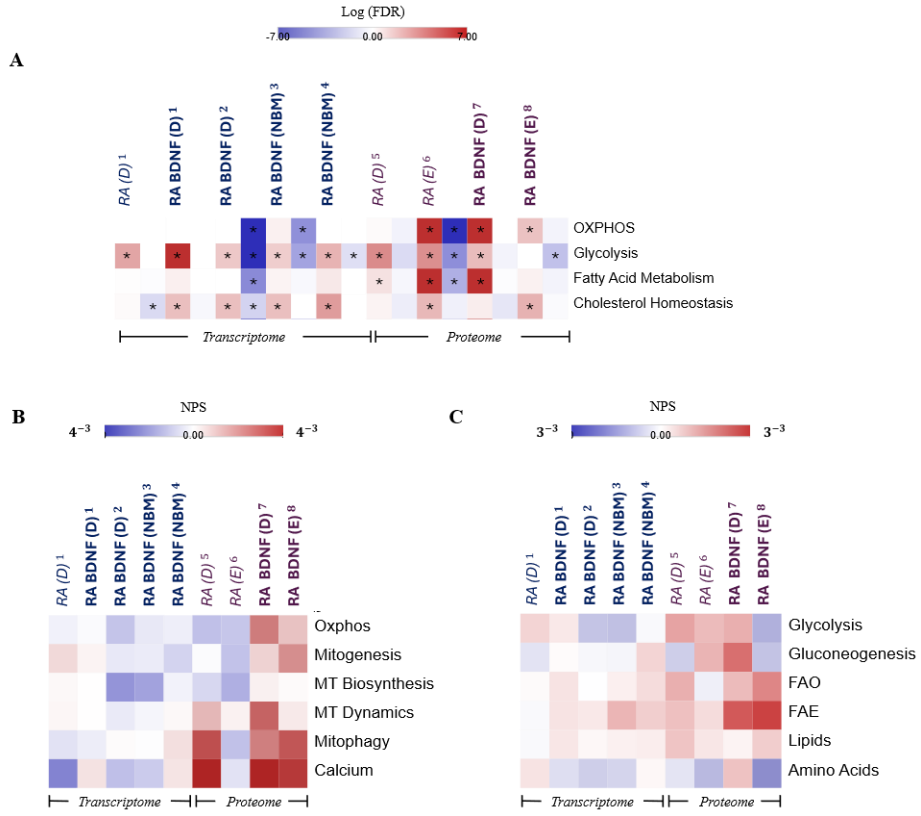


Figure 4.1. Molecular Signatures of Metabolic Remodelling. **A)** Significantly enriched hallmark metabolic pathways among downregulated (blue) and upregulated (red) genes in each dataset (1-8) listed in Table 4.1, where * = $p < 0.05$. Net Perturbation Scores (NPS) for manually curated gene sets involved in **B)** mitostasis and **C)** substrate utilisation where $NPS = \frac{(Fraction\ of\ Upregulated\ Genes\ per\ Pathway)}{Total\ No.of\ Upregulated\ Genes\ per\ Dataset)} - \frac{(Fraction\ of\ Downregulated\ Genes\ per\ Pathway)}{Total\ No.of\ Downregulated\ Genes\ per\ Dataset)}$. Transcriptomic datasets are depicted in blue, proteomic datasets are shown in purple, RA only datasets are in italics and RA+BDNF are in bold. D - DMEM; E - EMEM; FAE - fatty acid elongation; FAO - fatty acid oxidation; MT - mitochondrial; OXPHOS - oxidative phosphorylation. Note: the NPS should not be considered as an absolute measure of pathway activity but rather as a way to summarise relative expression data across different molecular datasets.

Together, the enrichment and perturbation scores associated with mitostasis and substrate utilisation propose an interesting divergence between molecular and respirometric profiles of metabolic remodelling in the SH-SY5Y system. Unlike the consistent oxidative shift observed in respirometric data, none of the published transcriptomic datasets reflect a significant upregulation of oxidative metabolism during neurodifferentiation. In fact, OXPHOS is significantly enriched among

downregulated genes in two transcriptomic datasets, while perturbation scores reveal a net downregulation of OXPHOS across all five transcriptomic datasets. Of these, three also indicate a decrease in mitogenesis and mitochondrial gene expression, translation and biosynthesis. Conversely, proteomic signatures of mitostasis and substrate utilisation are consistent with respirometric profiles of SH-SY5Y differentiation on several levels. Three of the four proteomic datasets reflect an enrichment of OXPHOS among upregulated genes, though only the two studies that used BDNF reflect a net upregulation of OXPHOS and mitogenesis. Studies using either EMEM or BDNF reflected an upregulation of genes involved in mitochondrial dynamics, turnover and Ca^{2+} buffering. Both proteomic studies in DMEM showed an increase in glycolysis and gluconeogenesis, while only the protocol using EMEM in combination with BDNF reflected an upregulation of OXPHOS with a downregulation of glycolysis on a molecular level. Thus, proteomic signatures appear to reflect the emergent and non-emergent features of metabolic remodelling that were evident in respirometric profiles of SH-SY5Y differentiation.

The trend observed across all nine published datasets suggests that signatures associated with mitochondrial metabolism are more consistently observed on the proteomic rather than transcriptomic levels in the SH-SY5Y system. Interestingly, the length of neuronal axons means that local protein synthesis is essential to meet the dynamic energy demands of distal synapses (Cardanho-Ramos and Morais, 2021). Moreover, mitochondrial translation in axonal growth cones is thought to facilitate the energy production necessary for neuronal elongation (Duarte, Ciampi and Duarte, 2023). Thus, it is possible that local translation plays a similar role in driving mitochondrial metabolism during differentiation, which may explain the discrepancy between mRNA and protein levels of mitochondrial genes. However, broad changes to substrate utilisation can still be detected in transcriptomic data. In particular, both transcriptomic and proteomic datasets reveal a consistent enrichment of glycolysis among differentially expressed genes (DEGs), suggesting a tight regulation of glucose utilisation during neurogenesis. Moreover, pathways involved in lipid metabolism display a consistent signature of upregulation across both transcriptomic and proteomic datasets, particularly those involved in cholesterol homeostasis and lipogenesis. Collectively, this discussion emphasises that different molecular techniques may capture distinct aspects of metabolic remodelling in the SH-SY5Y system and establishes a cell-type specific “molecular dictionary” to interpret metabolic signatures in transcriptomic data.

4.2. Methodology

4.2.1. RNA Collection

RNA was extracted from 24 SH-SY5Y cell culture samples, comprising four experimental conditions in duplicate: Day 1 undifferentiated control cells were grown overnight in full EMEM as described in

2.2.1; Day 9 control cells were maintained in EMEM at 1% FBS; Day 9 differentiated cells were differentiated into a neurons using the protocol described in **3.2.1** while DP cells were differentiated according to the same protocol in the presence of 5mM PPA. For all day 9 samples, media and relevant treatments were administered every 48 hours. RNA was extracted using the Zymo Quick-RNA™ Miniprep Kit (ZR R1055, Zymo Research) according to the manufacturer's instructions with the following modifications: 300 µl of RNA lysis buffer was added to each well in a 6-well plate before scrapping for 1 minute with cell scrapers. RNA was eluted in a total volume of 25 µl DNase/RNase-free water by centrifuging at 16 000 rpm for 1 minute (Eppendorf – Netheler – Hinz 5426 centrifuge, Serial number 542601273). Initial quality control was performed using the NanoDrop ND-1000 UV-Vis Spectrophotometer to select samples with an A260/280 ratio between 1.8-2.0 and an A260/230 ratio between 1.5-2.2. Selected samples were subsequently analysed on the Qubit® 4 Fluorometer using the fluorescent-based Qubit RNA High-Sensitivity (HS) Assy Kit (Thermo Fisher Scientific) and total RNA of the final samples was determined using the QuantiFluor® RNA System Kit on the GloMax-Multi Detection fluorometric system (Promega). RNA ScreenTape Analysis was performed on the Agilent TapeStation 4200 with the RNA Screen Tape System Kit (Agilent) and all of the final RNA samples used for sequencing had an RNA Integrity Number (RIN) >9 **(Table S4.2.).**

4.2.2. Library Preparation and Sequencing

RNA samples were sent to the Centre for Proteomic and Genomic Research (CPGR), Cape Town, South Africa for library preparation and sequencing. Sequencing libraries were prepared from 500 ng of each RNA sample using the Illumina Stranded Total RNA Prep with Ribo-Zero Plus kit according to the manufacturer's instructions. As total cellular RNA comprises up to 90% rRNA, ribosomal RNA depletion was employed to increase the sensitivity to transcriptomic reads. Although polyA selection is recommended for higher exonic coverage in clinical settings, rRNA depletion captures more unique transcriptomic features because it is able to capture non-poly (A)-tailed RNA, pre-processed RNA, small tRNAs, siRNA, snRNA, microRNAs and fragmented mRNAs (Zhao *et al.,* 2018). The IDT for Illumina RNA UD Indexes Ligation Set A kit was used for indexing. Individual library concentrations ranged from 7.9 ng/µl to 156.9 ng/µl as determined using the QuantiFluor® RNA System Assay Kit (Promega), while the average fragment size ranged from 358 bp to 398 bp. The individual libraries were pooled together at a concentration of 1 nM of each sample. qPCR quantification was carried out using the sparQ Universal Library Quantification Kit for Illumina (QuantaBio) according to the manufacturer's instructions. The final pool concentration was 0.321 ng/µl as determined by the Qubit 1X dsDNA HS Assay and 2.6nM measured by qPCR, with an average fragment size of 360 bp as determined by the Agilent TapeStation HS D1000 Assay **(Table S4.3).** The pooled libraries were diluted to 0.5 nM for a final loading concentration of 100 pM on the NovaSeq 6000 before denaturing, diluting, and sequencing. Libraries were sequenced on the Illumina NovaSeq 6000 sequencing system, using the

Illumina NovaSeq 6000 SP Reagent Kit v1.5 (200 cycles). The run yielded a Q30 above the 85% recommended by Illumina, with 83.5% of reads passing filtering.

4.2.3. Quality Control

FASTQ files were pretrimmed to remove adaptor sequences using bbdduk.sh from the BBTools suite (sourceforge.net/projects/bbmap/) before being uploaded to Illumina's Basespace Sequencing Hub. Reads were subjected to quality control using FastQC v0.12.1 (https://www.bioinformatics.babraham.ac.uk/projects/fastqc/) and MultiQC v1.10.1 (Ewels *et al.,* 2016) (https://doi.org/10.1093/bioinformatics/btw354). A total of 905 million reads were detected across 12 samples, with an average of 18.8 million reads (ranging between 12.9- 57.9 million reads) per sample **(Table S4.4).** FastQC analysis confirmed less than 0.5% adaptor contamination in the trimmed sequences **(Figure S4.3A).** Across all samples, both the mean Phred score (mean quality value across each base position in the read) and the per sequence quality score were above 30 **(Figure S4.3B, C).** The average and median read lengths were 67 and 68 bps respectively for all samples, with all sequences lying between 35-68bps and more than 98% of sequences above 60bps, 97% above 65 bps and 87% above 67bps in length **(Figure S4.3D).** Finally, all samples showed a less than 0.25% per base N content, meaning that at any given base, less than 1% were not assigned any base call **(Figure S4.3E).** All samples were flagged for non-uniform per-base sequence content, high sequence duplication levels and overrepresented sequences **(Figure S4.3F, G, H).** However, these parameters are designed to ensure high quality whole-genome DNA sequences and are less suitable when evaluating RNA read quality. This is because RNA Seq libraries are expected to have non-uniform base distribution over the first 10-15 nucleotides per read, while the GC content and levels of sequence duplication will reflect true differences in differential expression between transcripts in each library. Therefore, FastQC showed that all sequences were of sufficient quality and length, with no adaptor contamination and valid base calls for downstream analysis **(Figure 4.3).**

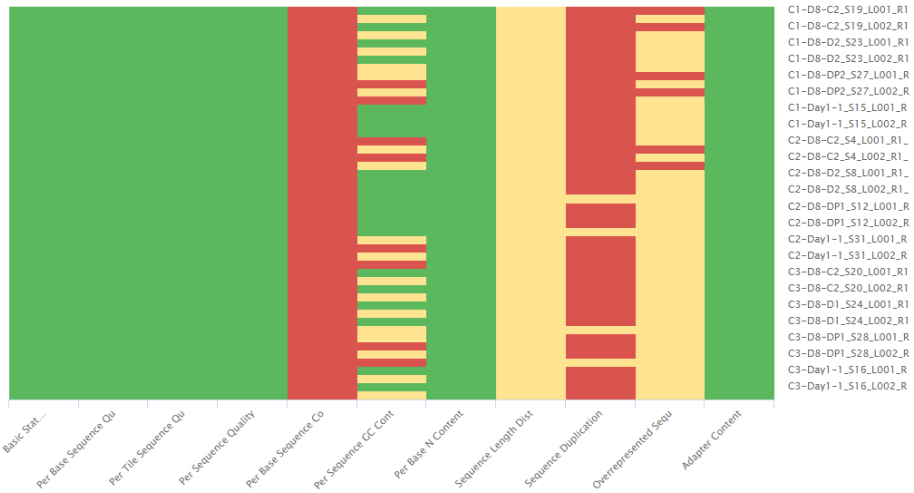


Figure 4.3. MultiQC Report Summarising Quality Control Parameters for all 12 samples.

4.2.4. Read Alignment

The pipeline for read alignment, mapping and quantification (up to **4.2.6**) was developed and performed by a collaborating bioinformatician, Dr Stuart Meier, at the UCT Lung Institute. Briefly, reads were mapped to Ensembl v109 based on the Genome Reference Consortium Human Build 38 GRCh38.p14 using the Spliced Transcripts Alignment to a Reference software (STAR v 2.7.11a) (https://github.com/alexdobin/STAR) (Dobin *et al.,* 2013). On average, 84.81% of reads per sample were uniquely mapped to exactly one genomic locus, with an average read length of 134bp. 15.15% of reads were unmapped, comprising 6.57% of reads that were too short to map, 8.21% that mapped to multiple (less than 10) loci and 0.23% that mapped to too many (more than 10) loci (**Table S4.5; Figure S4.4).** Of the uniquely mapped reads, 69.86% mapped to annotated genomic features, 5.5% mapped to ambiguous features and 24.59% did not map to features. A total of 67710 unique Ensembl genes were detected across all samples, and of these, 35298 were matched to corresponding ENTREZ gene IDs.

4.2.5. Count Loading, Filtering and Normalisation

DGE analysis was performed using edgeR's quasi-likelihood (QL) pipeline (Chen, Lun and Smyth, 2016) to quantify and statistically evaluate gene- level differences in expression. This pipeline was selected given that it was designed for studies that include multiple treatment factors with small numbers of biological replicates. The estimated counts, abundances and effective transcript lengths were imported into R with tximport package. For gene-level differential expression analysis, gene counts were defined as reads that overlap any exon of a given gene. Raw gene counts were scaled by the number of reads per sample to generate counts per million (CPM) values and gene libraries were filtered based on a minimum CPM of 0.8 in at least 3 of 12 samples using the dmFilter function. Normalisation by trimmed mean of M (TMM) values was performed on the filtered datasets to correct for sequencing depth and compositional bias between libraries, where effective library sizes were calculated by multiplying the original library sizes by the normalisation factors (**Figure S4.5)**. TMM does not employ gene-length correction since gene-length is consistent between samples; thus, this method is used for differential expression analysis rather than absolute quantification. A total of 14555 unique Entrez IDs were assigned CPM values ranging between 0 – 22864.37 and CPMs were log-transformed before being assessed for differential expression between conditions.

4.2.6. Assessment of Differential Expression

The QL pipeline includes a precision estimation step to account for gene-specific variation that arises from both biological and technical sources. With small sample sizes between 3-6 replicates, estimates of variation can be unreliable. To improve these estimates, information can be shared across genes that show the same patterns of expression, since genes with similar levels of expression are likely to show

similar levels of dispersion. Here, the dispersion for each gene was calculated using maximum likelihood estimation based on expression level. The quarter-root QL dispersion was plotted against the average abundance of each gene and shrinkage was employed to squeeze raw QL dispersion estimates towards a global trend to reduce the uncertainty of the estimates and decrease detection of false positives. Lastly, differential expression was assessed using QL F-tests and multiple testing correction was performed using the Benjamini-Hochberg method. Statistically significant differences in expression were defined by FDR<0.05.

4.2.7. Weighted Gene Correlation Network Analysis (WGCNA)

To identify modules of co-regulated genes, the WGCNA R package (Langfelder and Horvath, 2008) was implemented in line with the soft-thresholding approach developed by (Zhang and Horvath, 2005). A scale-free topology model fit was calculated for the expression matrix of all log-normalised CPMs and a soft threshold of 10 was selected to filter out noise and balance independence with connectivity; where the mean and median connectivity were 283 and 233 respectively **(Table S4.6; Figure S4.6).** After merging similar modules using a dissimilarity threshold of 0.25, 22 modules were identified, and a correlation matrix was constructed to evaluate the association of each module with different experimental conditions. Modules of Interest (MOIs) were selected for further investigation and functional annotation.

4.2.8. Gene Set Enrichment Analysis (GSEA)

Significantly differentially expressed genes (DEGs) and MOIs were subject to functional annotation using a multi-pronged GSEA approach. Several curated gene sets are commonly used to functionally annotate transcriptomic data – including gene ontologies, canonical pathways and gene-phenotype associations. Since this study was designed to explore the relationship between underlying mechanisms, gene sets were annotated according to significantly enriched GO Biological Processes, Reactome and MSigDB Hallmark Canonical Pathways using the open access tools Enrichr (https://maayanlab.cloud/Enrichr/) (Kuleshov *et al.*, 2016) and ExpressAnalyst (https://www.expressanalyst.ca/) (Ewald *et al.*, 2023). The background used in all enrichment tests was the total library of expressed genes that passed the filter for DGE analysis. The genes that were dysregulated by PPA were further examined using a trial version of Ingenuity Pathway Analysis (IPA) (QIAGEN Inc., https://www.qiagenbioinformatics.com/products/ingenuity-pathway-analysis).

4.3. Results

4.3.1. Global Disruptions to the Neurogenic Transcriptome

Following the RNA sequencing pipeline described in **4.2**, hierarchical clustering and principal component analysis (PCA) were performed to evaluate the internal consistency of the experimental system. Hierarchical clustering demonstrated consistent grouping among biological replicates within experimental conditions, with a clear distinction between undifferentiated and differentiated samples **(Figure S4.7A).** Likewise, PCA identified two top components capturing 58% of the variance that separated undifferentiated from differentiated samples **(Figure S4.7B, C)**, while component 3 – accounting for 13% of the variance – showed a clear separation among all four groups **(Figure S4.7D).** Together, this illustrates a distinct transcriptomic signature associated with *in vitro* neurogenesis that seemed to be significantly altered by PPA exposure. Five pairwise QL F-tests were conducted on log-normalised CPM values, with the aim of isolating five unique transcriptomic signatures **(Table 4.2; Figure 4.4A).** In total, 9605 unique genes were found to be significantly DE between at least two conditions **(Figure 4.4, B, Figure S4.8)**. Subsequently, specific overlays were used to isolate signatures associated with FBS depletion **(Figure 4.4C),** RA-BDNF **(Figure 4.4D)** and PPA **(Figure 4.4E, F).**

Table 4.2. Pairwise QL F-Tests Conducted for Differential Gene Expression Analysis. Data show the number of differentially expressed genes identified in five pairwise comparisons. C1 = day 1 undifferentiated controls in 15% FBS; C9 = day 9 controls maintained at 1% FBS; D9 = day 9 neurons differentiated with RA+BDNF; DP = day 9 neurons differentiated with 5mM PPA. BDNF – Brain-derived neurotrophic factor; FBS – foetal bovine serum; RA – retinoic acid; PPA – propionic acid.

Transcriptomic Signature	**C9 vs C1** *FBS Depletion*	**D9 vs C1** *Neurogenesis*	**D9 vs C9** *RA-BDNF*	**DP vs C9** *Diff + PPA*	**DP vs D9** *PPA*
Down	1464	3165	2892	3236	1531
Up	1261	2659	2402	3017	1230
TOTAL	**2725**	**5824**	**5294**	**6253**	**2761**

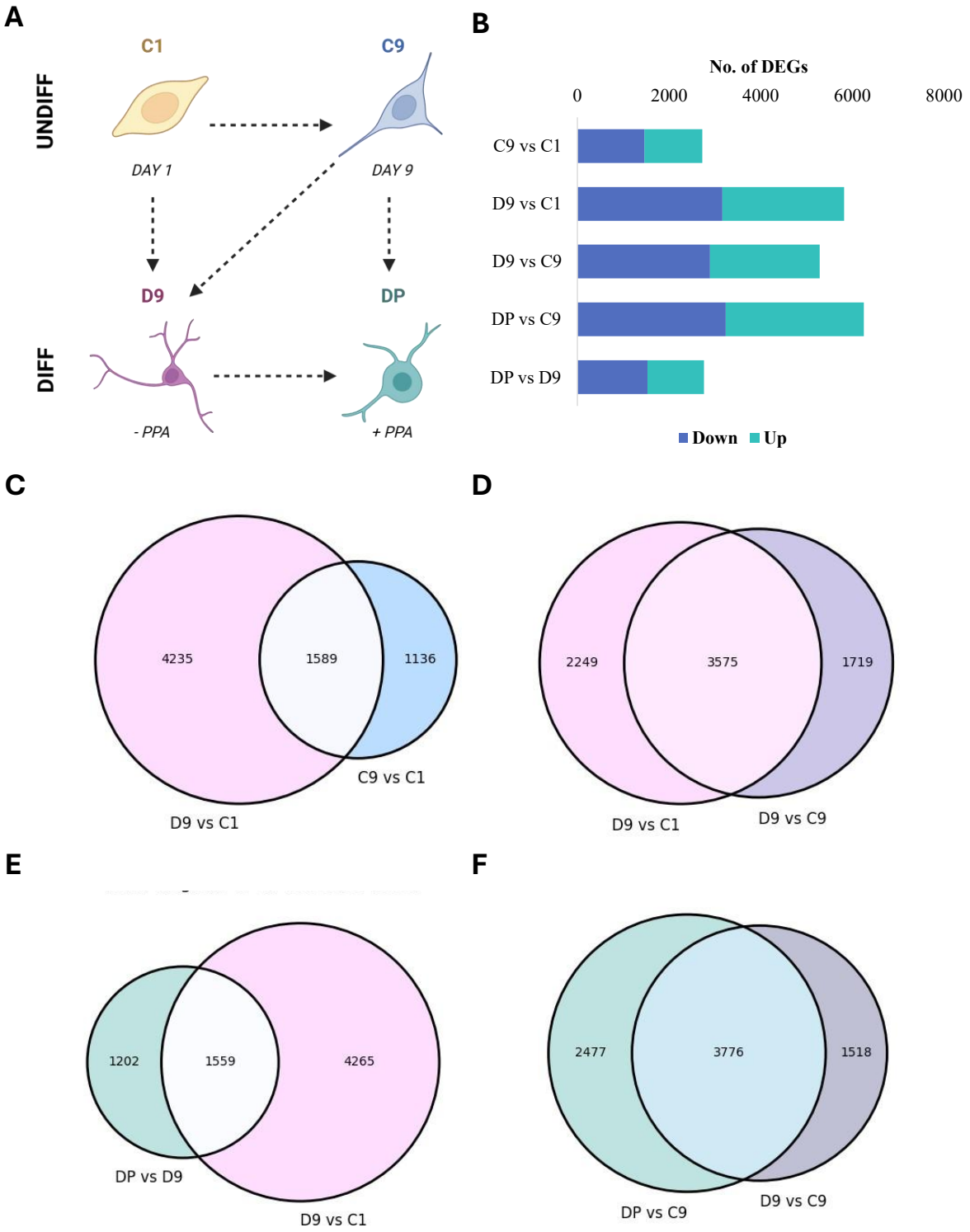


Figure 4.4. All Significantly Differentially Expressed Genes Identified In 5 Pairwise QL-F Tests. A) Graphical Depiction of all four treatment conditions. **B)** Overview of the differentially expressed genes (DEGs) identified in each pairwise comparison. Venn Diagrams depict the overlap between the DEGs between **A)** C9 and D9 relative to C1; **D)** D9 relative to C1 and C9; **E)** D9 relative to C1 and D9 and **F)** D9 and DP relative to C9. C1 = undifferentiated controls grown in 15% FBS; C9 = day 9 negative controls maintained at 1% FBS without RA or BDNF; D9 = day 9 positive controls differentiated with RA and BDNF and DP = day 9 neurons differentiated in the presence of 5mM Propionic Acid.

A total of 2725 genes were DE in response to 9 days of serum depletion without RA-BDNF treatment, indicating a clear shift away from the undifferentiated phenotype. This was driven by a decrease in cell proliferation and migration with an upregulation of the unfolded protein response (UPR), translation and neurotransmission **(Figure 4.5A; Table S4.7).** Markedly, FBS-depletion alone altered 1589 DEGs that were also DE during differentiation **(Figure 4.4C)** of which 84% were DE in the same direction. This highlighted a neurogenic signature associated with serum depletion that inhibited cell division, proliferation and glycolysis and upregulated synapse organisation and signalling **(Table S4.8).** On the other hand, the 1136 genes altered by FBS-depletion that were not perturbed during differentiation revealed neurotoxic mechanisms that inhibited neuronal migration, ECM remodelling, and cytokine signalling while promoting p53 signalling, the cellular response to starvation, AA deficiency and the UPR (**Table S4.9).**

Compared to serum depletion alone, RA-BDNF treatment induced close to double the number of DEGs relative to day 1 controls (~5000). Of these, a majority (3575) were significantly DE relative to both day 1 and day 9 controls **(Figure 4.4D),** highlighting a subset of genes induced specifically by RA+BDNF exposure. These genes converged on a downregulation of cell proliferation and metabolism with an upregulation of CNS development, synapse assembly and signalling, ECM organisation, axon guidance and neurite outgrowth **(Figure 4.5B-D; Table S4.10).** Interestingly, the distinction between day 1 and day 9 controls differentially influenced the isolation of neurogenic signatures **(Table S4.11).** Day 1 controls captured the inhibition of cell division and metabolism, while day 9 controls more clearly revealed an upregulation of ECM assembly, CNS development and neurogenic signalling driven by RA (RA, Interferon, Wnt) and BDNF (NFκβ, cytokine, JAK/STAT, RAS, TGF-β). Thus, both controls can be used in an informed manner to yield specific insights into different aspects of neurogenesis in the SH-SY5Y model.

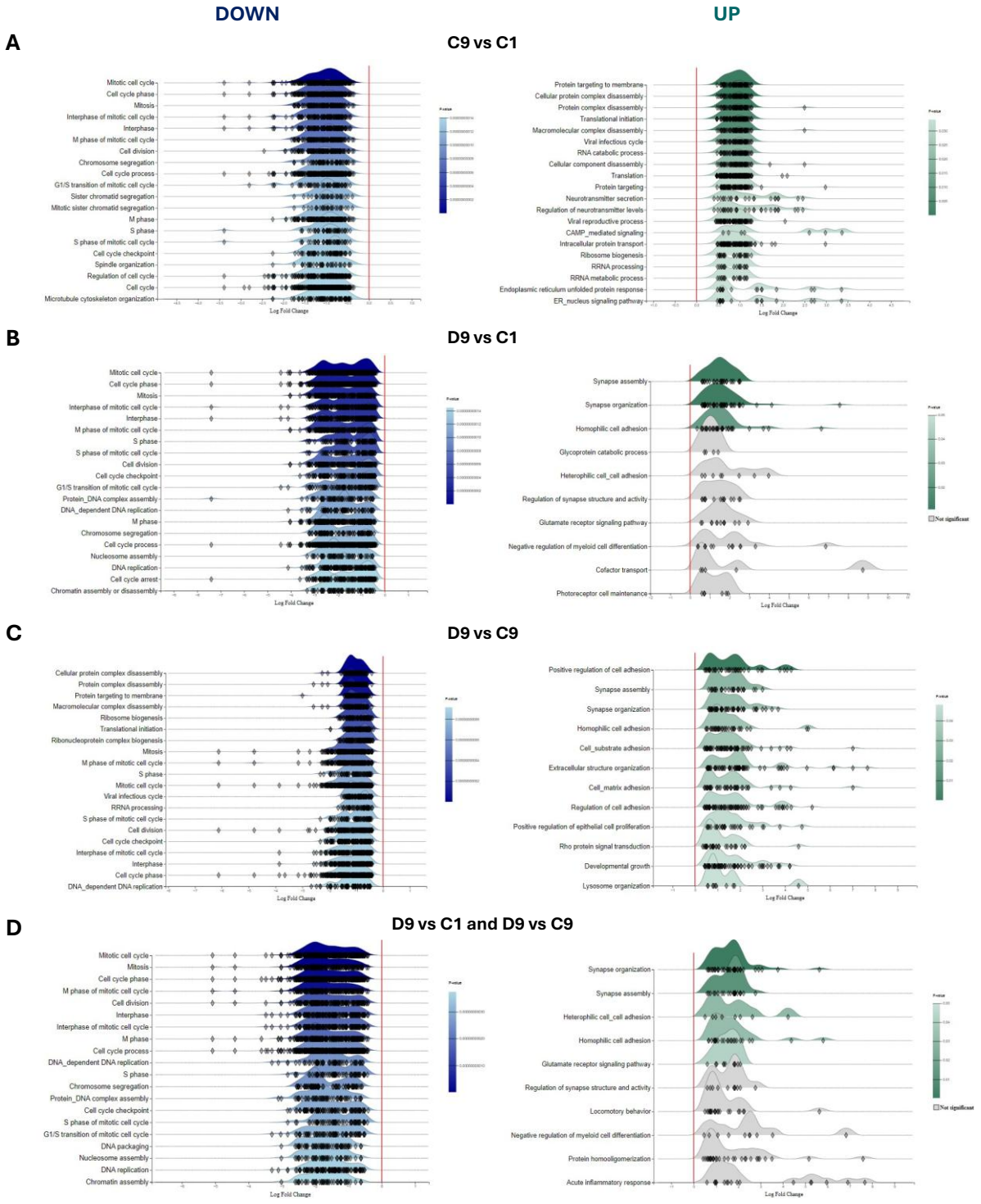


Figure 4.5. Annotating the Neurogenic Transcriptome. Data represent ridgeline plots showing the log fold change in expression for all differentially expressed genes in the top 20 enriched GO Biological Pathways among significantly up and downregulated genes between **A)** Day 9 FBS-depleted controls (C9) relative to day 1 proliferative controls (C1), **B)** Day 9 differentiated neurons (D9) relative to C1, **C)** D9 relative to C9 and **D)** D9 relative to both C1 and 9.

Relative to differentiated controls, PPA significantly perturbed 2761 genes that upregulated processes involved in proliferation, glycolysis, glycoconjugate metabolism, ECM remodelling, axon guidance, wound healing and inflammation **(Figure 4.6A; Table S4.12).** On the other hand, PPA suppressed

synapse assembly, organisation and signalling, cholesterol synthesis and transport and the epigenetic regulation of gene expression**.** Notably, PPA upregulated 705 genes that were downregulated during differentiation and downregulated 587 genes that were upregulated during differentiation **(Figure 4.4E).** Thus, at least 46% of PPA-induced transcriptional changes were directly counter-productive to the emergence of a mature neuronal phenotype. Moreover, PPA suppressed or reversed more than 30% of the transcriptional programme that distinguished between undifferentiated and differentiated controls **(Figure 4.4F).** Together, this response showed that PPA impairs the neurogenic programme by disrupting cell cycle exit, synaptogenesis and synaptic signalling **(Figure 4.6B, C).**

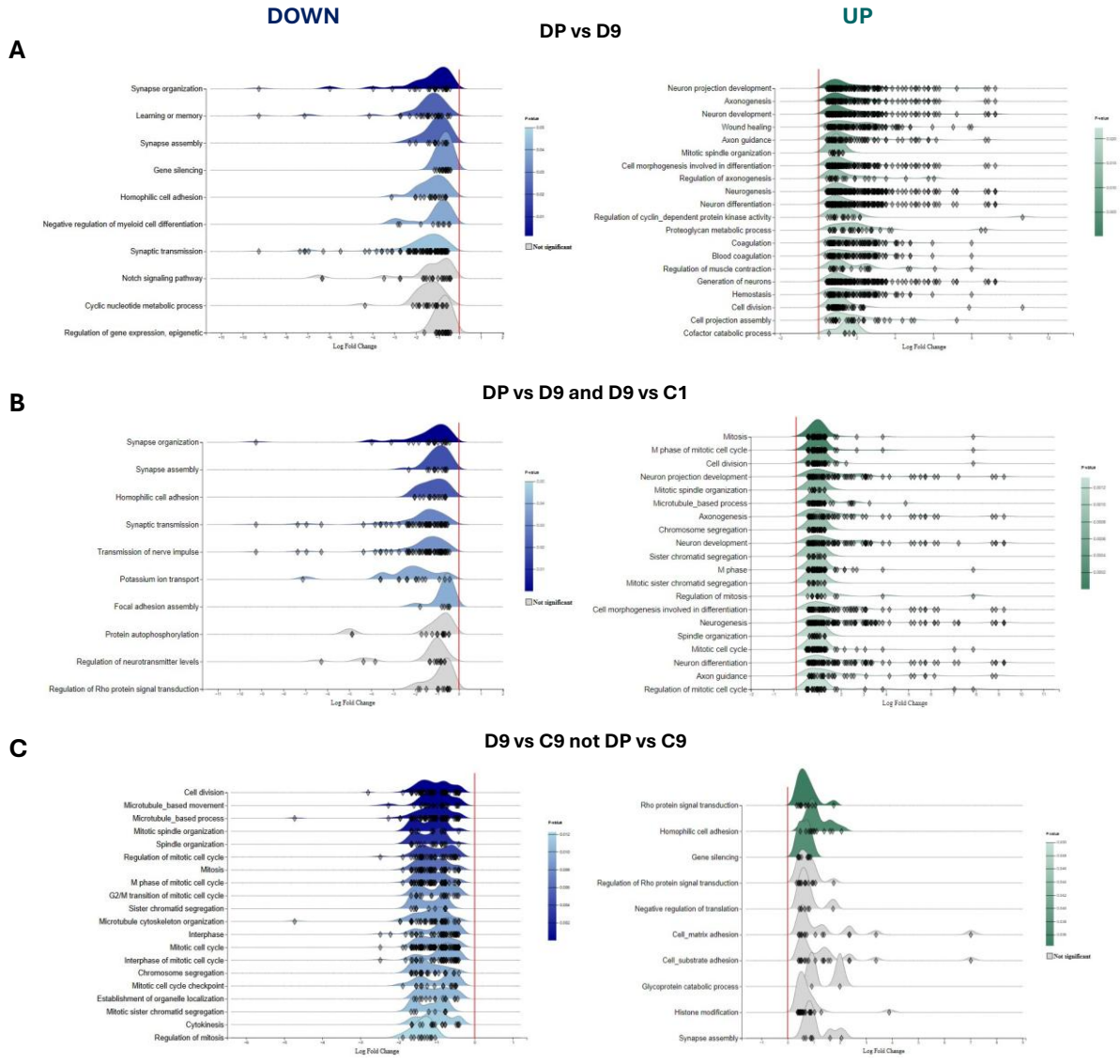


Figure 4.7. Annotating the PPA Transcriptome. Data represent ridgeline plots showing the log fold change in expression for all differentially expressed genes in the top 20 enriched GO Biological Pathways among **A)** Significantly up and downregulated genes between PPA-exposed neurons (DP) relative to day 9 differentiated controls (D9), **B)** the 705 genes that were upregulated by PPA but downregulated during differentiation relative to day 1 undifferentiated controls (C1) and the 587 genes that were downregulated by PPA but upregulated during differentiation and **C)** the 1518 genes that were differentially expressed during differentiation but not PPA treated neurons relative to day 9 undifferentiated controls (C9).

Comparing the DEGs identified across all five pairwise comparisons highlighted 204 genes that were DE across all four treatment conditions **(Figure 4.7A),** revealing a group of central cell fate regulators that are perturbed by PPA. These genes converged on the regulation of proliferation, differentiation and neurite development **(Figure 4.7B),** including processes involved in ECM organisation, axon guidance and inflammation, as well as Notch, NFκβ and GPCR signalling **(Table S4.13).** A transcription factor regulatory network comprising all 204 shared genes identified the top ten hub genes with the greatest betweenness centrality **(Figure 4.7C, D)**, including canonical effectors of the Notch (*HES1*), Shh (*TBX3*) and TGF-β (*SMAD3*) pathways, key regulators of VEGF and semaphorin *(PLXNA2, NRP1*) signalling, and central coordinators of neuronal metabolism (*FOXO3)*, survival *(ERK3, KLF6)* and differentiation *(POU3F2)* **(Table S4.14).** Thus, PPA appears to alter NPC fate by disrupting a hub of neurogenic genes that govern proliferation, metabolism, ECM assembly and synaptogenesis.

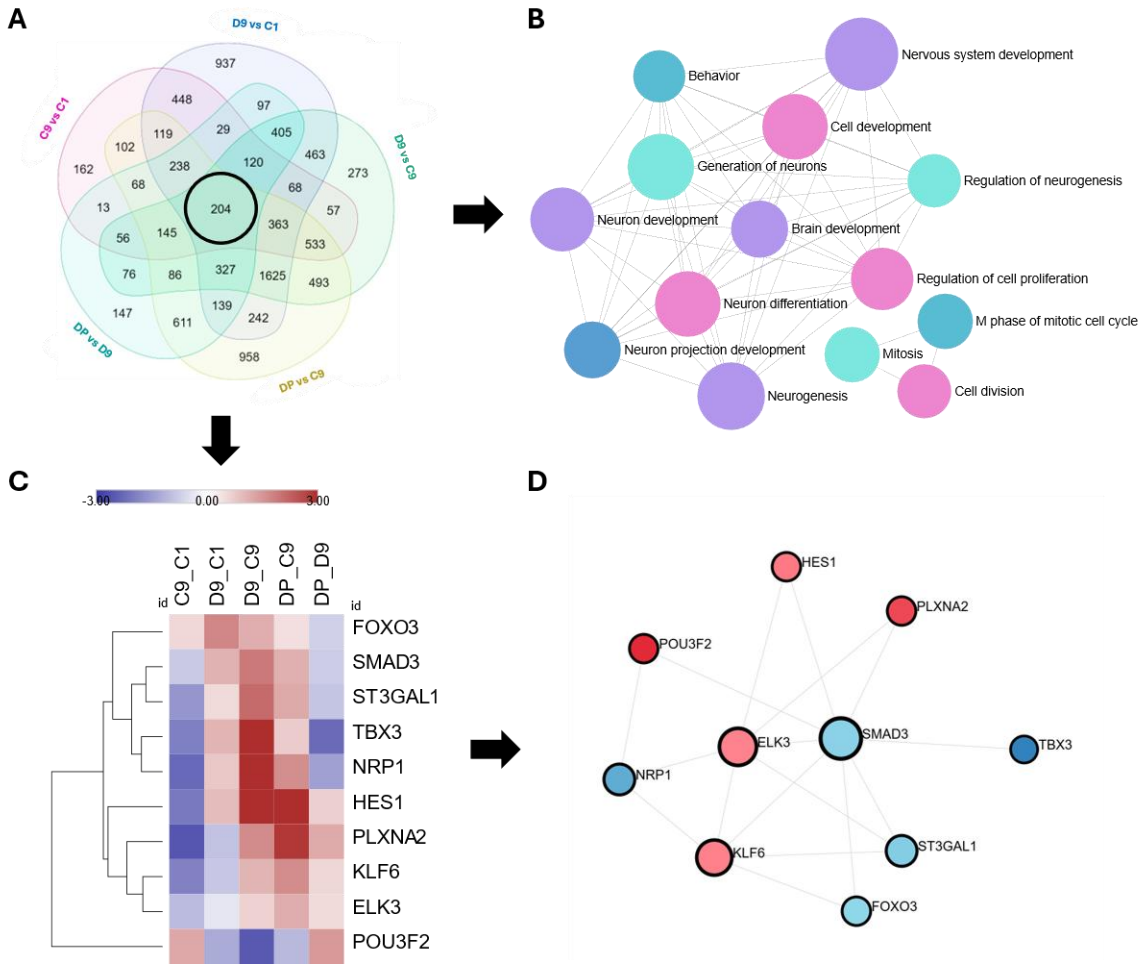


Figure 4.7. Cell-fate Regulators Perturbed by Propionic Acid. A) Venn diagram highlighting the 204 genes that are differentially expressed between conditions in all 5 pairwise comparisons. **B)** Global Enrich Net of top 15 GO Biological Process in the 204 shared genes. **C)** Log Fold Change values for the top ten hub genes in the Chea3 transcription factor- gene regulatory network for all 204 genes. **D)** Chea3 transcription factor- gene regulatory network for ten hub genes where node sizes depict the betweenness centrality for each gene and node colours represent log fold change in expression in neurons exposed to propionic acid (DP) relative to differentiated controls (D9).

Collectively, this preliminary analysis reveals transcriptomic landmarks associated with serum depletion, neurogenesis and the response to PPA *in vitro* **(Figure 4.8).** Both serum depletion and RA-BDNF induced cell cycle exit, synapse assembly and neurotransmission but neurotoxic mechanisms associated with starvation, senescence and the UPR emerged in the absence of neurogenic agents. PPA impaired the neurogenic programme by inhibiting epigenetic regulation, cell cycle exit, neurite development and neurotransmitter signalling while disrupting glycoconjugate and cholesterol metabolism, ECM remodelling and axon guidance. A central hub of cell fate regulators implicated Notch, TGF-β and Shh signalling as focal mechanisms that drive PPA-induced disruptions to neurogenesis. Moreover, PPA upregulated signatures of glycolysis, inflammation and injury, all of which are implicated in neuropathology. Together, the transcriptional response to PPA suggests marked perturbations to the epigenetic, metabolic and morphological remodelling that governs neurodevelopment and function.

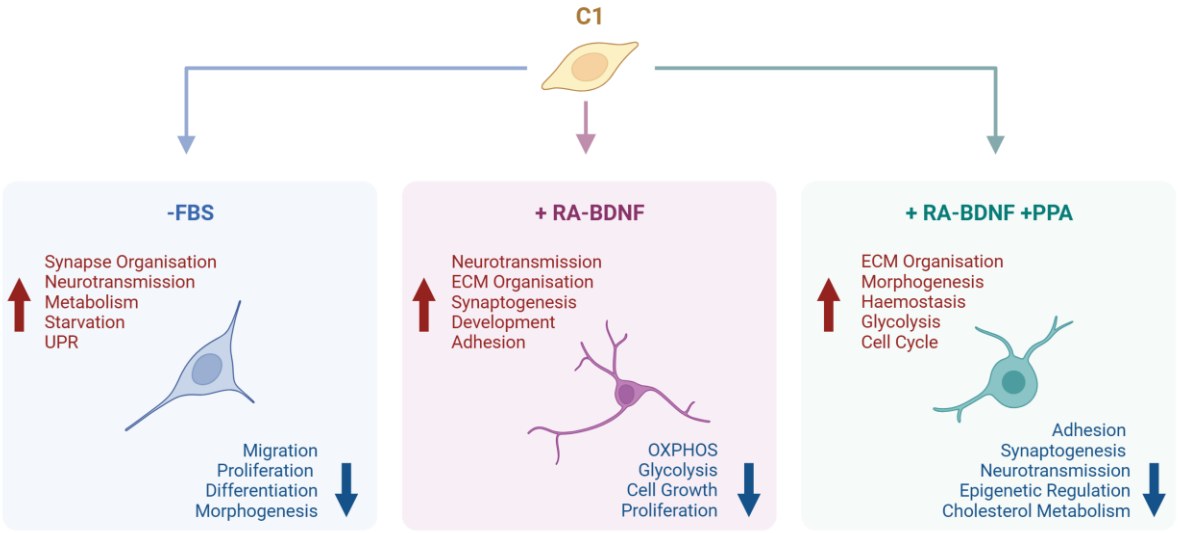


Figure 4.8. Central Mechanisms of Propionic Acid-Induced Neurotoxicity. A graphical summary of the upregulated (red) and downregulated (blue) processes associated with FBS-depletion, neurogenesis and Propionic Acid (PPA). BDNF – Brain Derived Neurotrophic Factor; ECM – extracellular matrix; FBS – Foetal Bovine Serum; OXPHOS – Oxidative Phosphorylation; RA – Retinoic Acid; UPR -Unfolded Protein Response.

4.3.2. Metabolic and Neurotoxic Signatures in the PPA Transcriptome

Preliminary functional annotations demonstrated that PPA upregulated the turnover of ECM glycoconjugates and suppressed cholesterol synthesis and transport. Thus, the PPA transcriptome reflects a dysregulation of processes involved in both glucose and lipid metabolism that may contribute to PPA-associated neurotoxicity. Here, a more targeted analysis of the PPA transcriptome aimed to better characterise the relationship between metabolic remodelling and neurotoxicity under PPA stress. Firstly, the transcriptomic datasets derived from pairwise DEG analysis were overlayed with the non-redundant

metabolic pathways detailed in **Table S4.1.** Subsequently, the metabolic signature associated with each condition was characterised using the workflow described in **4.1.3 (Figure 4.9).**

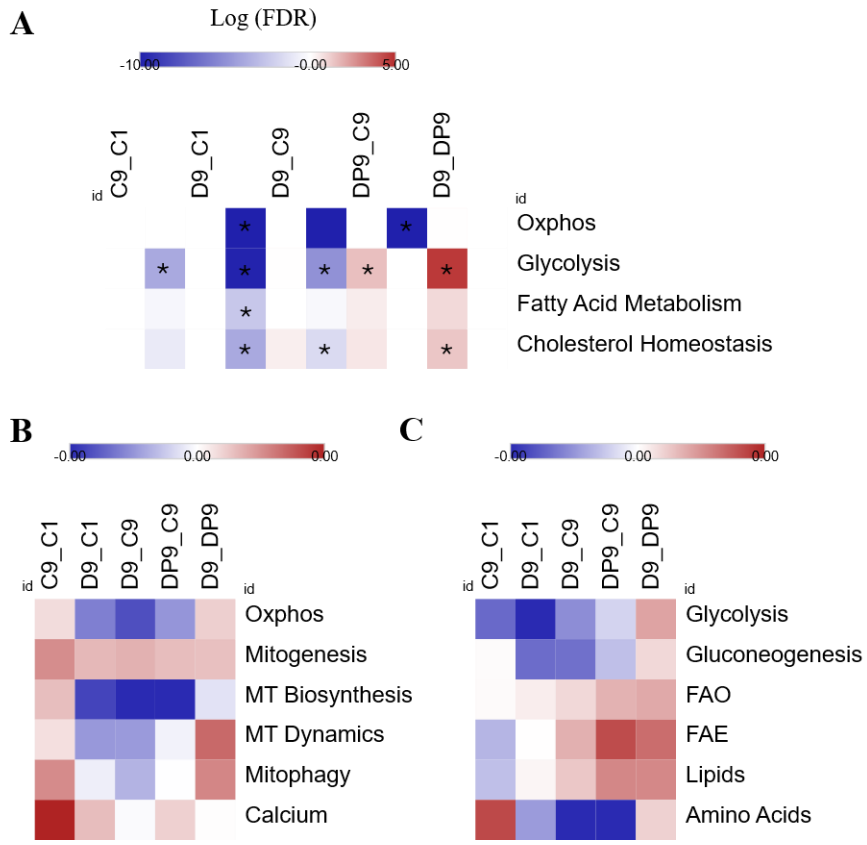


Figure 4.9. Metabolic Signatures in the PPA Transcriptome. A) Significantly enriched hallmark metabolic pathways among significantly downregulated (blue) and upregulated (red) genes identified in each pairwise comparison, where * = $p < 0.05$. Net Perturbation Scores (NPS) for manually curated gene sets involved in **B)** mitostasis and **C)** substrate utilisation. OXPHOS = oxidative phosphorylation; MT = mitochondrial; FAO = fatty acid oxidation; FAE = fatty acid elongation; $NPS = \frac{(No.\ of\ upregulated\ genes) - (No.of\ downregulated\ genes)}{Total\ No.of\ Differentially\ Expressed\ Genes\ per\ dataset)}$.

In line with previous studies in the SH-SY5Y system, the neurogenic transcriptome reflected a downregulation of mitochondrial, glucose and AA metabolism, with a net upregulation of genes involved in fatty acid metabolism and lipogenesis**.** This data is consistent with a metabolic shift away from cell growth and proliferation, towards the synthesis of substrates needed for ECM formation, synaptogenesis and neurotransmission. However, PPA significantly altered the expression of 215 canonical metabolic genes **(Figure S4.9),** and reshaped transcriptional signatures of metabolic state. As well as significantly upregulating glycolysis **(Figure 4.9A),** PPA increased the expression of genes involved in OXPHOS, mitochondrial dynamics, gluconeogenesis and AA metabolism **(Figure 4.9 B, C),** which reflects the signature associated with serum-depleted controls. Moreover, PPA significantly altered the expression of genes involved in lipid homeostasis, biosynthesis and degradation. Although transcriptomic profiles may not reflect real-time metabolic activity, this data does reflect a deviation from the metabolic signature associated with *in vitro* neurogenesis.

In fact, interrogating the most significant DEGs identified in each metabolic pathway revealed perturbations to central regulators of mitostasis under PPA stress **(Figure 4.10A, Table S4.15).** PPA significantly disrupted a total of 66 mitochondrial genes **(Figure 4.10B)** that converged on mitochondrial metabolism, organisation and trafficking **(Figure 4.10C).** Here, PPA upregulated genes involved in mitophagy and glycolysis and altered several regulators of mitochondrial fission, fusion, morphology and Ca^{2+} buffering. PPA also perturbed the synthesis, degradation and transport of AAs, where the most significant disruptions to AA metabolism converged on pathways converged on the synthesis of dopamine, epinephrine and norepinephrine, GABA/glutamate cycling and nitric oxide signalling **(Figure 4.10D).** On the other hand, the remodelling of lipid metabolism was associated with a dysregulation of the synthesis, turnover and signalling of sterols, phospholipids, glycolipids and sphingolipids that form neuronal membranes and synaptic vesicles **(Figure 4.10E).**

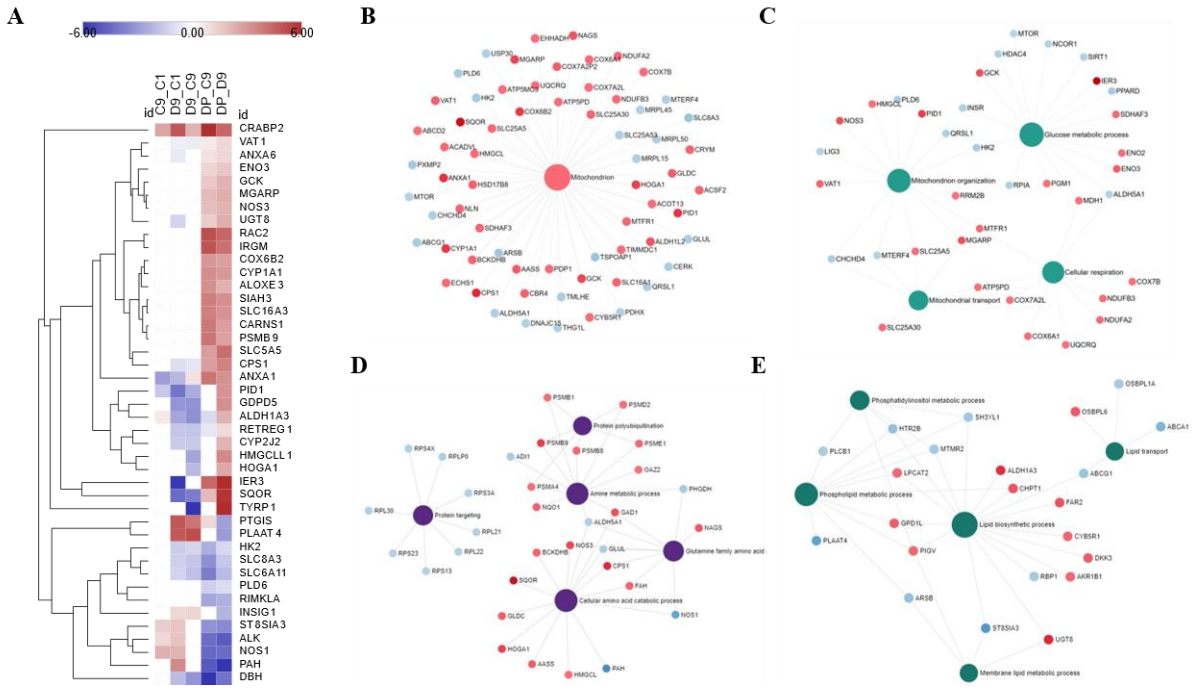


Figure 4.10. Central Regulators of Metabolic Remodelling. A) Log fold change values for the 43 metabolic genes that were most substantially transcriptionally dysregulated by Propionic Acid (|LogFC| > 1). Enrich Nets depict differentially expressed genes that **A)** localise to the mitochondrion or have central roles in **B)** mitostasis, **C)** lipid metabolism and D) amino acid metabolism.

Cumulatively, this data reveals disruptions to all of the primary metabolic pathways that control the turnover of substrates needed for energy production and biosynthesis in differentiating neurons. Moreover, this analysis illustrates a remodelling of metabolic flux that may not only impact bioenergetic state, but also has specific implications for neuronal morphology, maturation and function. In fact, cross-referencing the metabolic signatures in Figure 4.10 with the hub of 204 cell fate regulators identified in Figure 4.7 highlighted 14 genes that function at the interface between neuronal metabolism and maturation **(Figure 4.11; Table S4.16).** Here, *FOXO3* emerged as a canonical regulator of

mitostasis, redox homeostasis, autophagy and survival that significantly influences neuronal cell fate. Other metabolic genes that were DE across all four treatment conditions included those involved in glycosylation (*ST3GAL1*), RA signalling (*ALDH1A3, CRABP2*) and lipid homeostasis, transport and signalling (*ABCG1, ABCA1, PLD1, CNR1, ANXA1*), including three high ranking ASD risk genes listed in the SFARI database (*ALDH1A3, ANXA1, CNR1).* Together, this work highlights PPA-induced disruptions to metabolic state that significantly influence neuronal cell fate by interfering with RA signalling, ECM assembly, cytoskeletal remodelling and synaptic signalling.

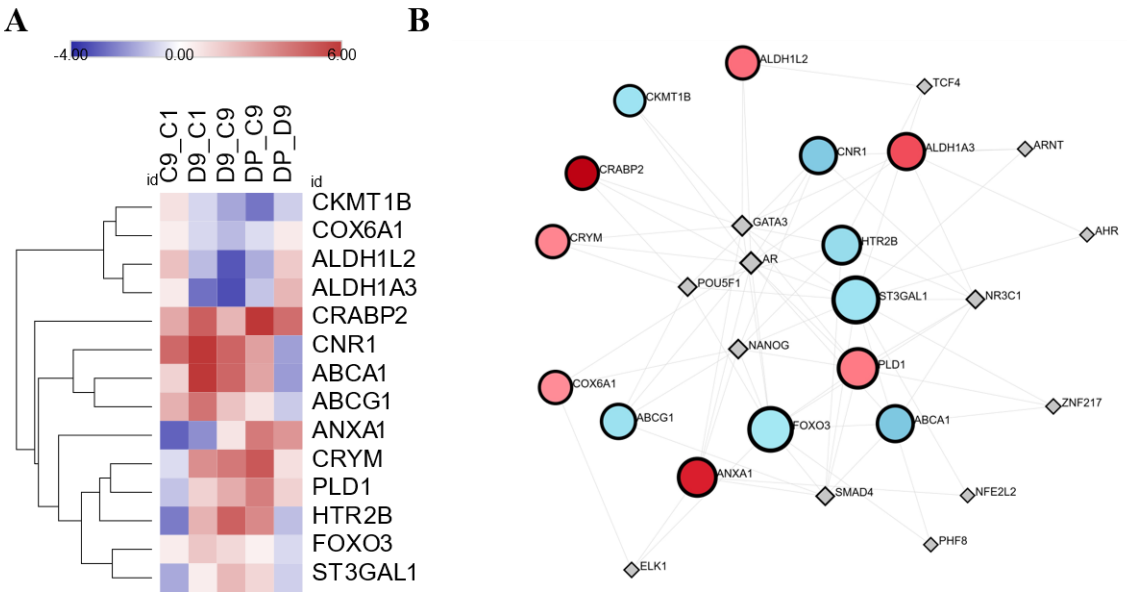


Figure 4.11. Convergent Regulators of Neuronal Metabolism and Maturation. A) Log Fold Change values for the 14 metabolic genes that were differentially expressed across all five pairwise comparisons**. B)** Chea3 transcription factor- gene regulatory network for all 14 metabolic hub genes where node sizes depict the betweenness centrality for each gene and node colours represent the log fold change in expression in neurons exposed to propionic acid (DP) relative to differentiated controls (D9).

Functionally significant impairments to the neurogenic transcriptome were further evaluated with reference to previous transcriptomic studies in the SH-SY5Y model. Firstly, the neurogenic transcriptome generated in **4.3.1** was compared to the transcriptomic dataset published by Chiocchetti *et al.,* (2016). This analysis highlighted 2018 genes that were associated with neurodifferentiation in both studies **(Figure S4.10A),** demonstrating an inhibition of cell proliferation with an upregulation of synapse assembly, development and neurotransmission **(Figure S4.10B).** Of these, PPA reversed the neurogenic profile of 650 genes **(Figure 4.23A)** including 55 central cell fate regulators converging on regulatory hubs governed by *SMAD3* and *FOXO3* **(Figure 4.12B, C; Table S4.17).** Together, this reveals a neurotoxic signature that upregulates cell cycle progression and inhibits development, patterning, morphogenesis and differentiation under PPA stress **(Figure S4.10C).**

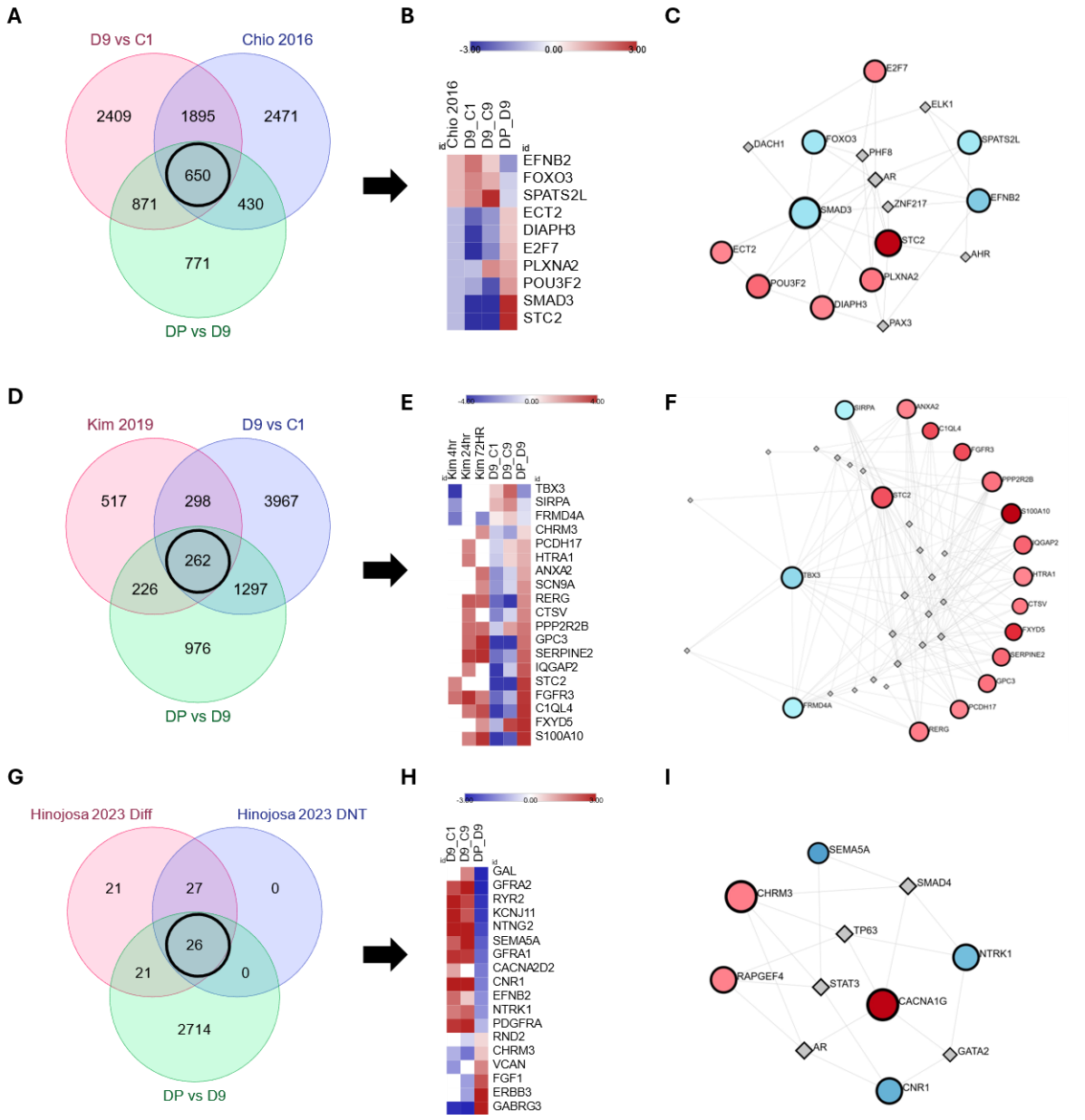


Figure 4.12. Neurotoxic Signatures in the PPA Transcriptome. A) Venn diagram depicting the common differentially expressed genes (DEGs) in the neurogenic transcriptome (D9 vs C1), previous transcriptomic profiles of SH-SY5Y differentiation (Chiocchetti *et al*, 2016), and neurons exposed to Propionic Acid (PPA) (DP vs D9). **B, C)** The top ten hub genes among the 55 central cell fate regulators that were validated in the Chiocchetti transcriptome and perturbed by PPA. **D)** Venn diagram depicting the common DEGs in the neurogenic transcriptome (D9 vs C1), the PPA transcriptome (DP vs D9) and the DEGs in undifferentiated SH-SY5Y cells exposed to PPA for 4 – 72 hours (Kim *et al.,* 2019). **E, F)** The 17 central cell fate regulators that were DE in response to both acute (Kim *et al.,* 2019) and chronic PPA exposure. **G)** Venn diagram showing the common genes in the PPA transcriptome and the mRNA markers for differentiation and developmental neurotoxicity (DNT) in the SH-SY5Y model reported by Hinojosa *et al.,* (2023). **H, I)** The 14 markers for DNT that were significantly disrupted by PPA. **F)** The 6 DNT markers perturbed by PPA that were implicated as high-ranking SFARI risk genes. All Chea3 networks are constructed as concentric networks around the DEG with the greatest betweenness centrality; node sizes depict the betweenness centrality for each gene and node colours represent log fold change in expression in DP relative to D9.

Secondly, the PPA transcriptome was compared to gene expression profiles associated with acute PPA exposure in undifferentiated SH-SY5Y cells (Kim *et al.,* 2019), highlighting 422 genes that were dysregulated in both datasets **(Figure 4.12D).** This analysis revealed an acute response to PPA that reversed the transcriptional profile of 282 neurogenic genes, leading to an upregulation of glycolysis, wound healing and cell growth while inhibiting transcriptional regulation, CNS development and morphogenesis **(Table S4.18; Figure S4.11).** Here, a shared regulatory hub emerged converging on *TBX3*, a central regulator of neurodevelopment that governs TGF-β and Shh signalling. Moreover, the Kim transcriptome revealed acute disruptions to 19 central cell fate regulators involved in Notch (*GDPD5*), Wnt (*GPC3*), Shh (*TBX3*) and TGF-β signalling (*HTRA1*), as well as essential modulators of proliferation, neurite outgrowth and synaptic signalling **(Table S4.19).** This data validates the neurotoxic signatures associated with PPA and suggests an acute transcriptional dysregulation that could impair cell cycle exit and neuronal lineage commitment during early development.

In fact, the PPA transcriptome reflects hallmarks of developmental neurotoxicity in the SH-SY5Y system. Using gold-standard positive controls for neurotoxicity, Hinojosa *et al.,* (2023) recently identified 94 mRNA markers associated with differentiation and 53 markers for neurotoxicity in the SH-SY5Y model. Here, PPA impaired the neurogenic profiles of 21 markers of differentiation **(Table S4.20)** including 14 markers of neurotoxicity **(Figure 4.12G, H).** These included six high-ranking ASD risk genes involved in synapse assembly, organisation and signalling **(Figure 4.12I),** comprising three of the five most consistent neurotoxic markers described by Hinojosa *et al.,* (2023) (*CNR1, SEMA5A, NTRK1*) and three central cell fate regulators identified in this study (*RAPGEF2, CHRM3, CACNA1G*). Thus, the PPA transcriptome reflects cell-type specific mRNA signatures of neurotoxicity that point to mechanisms involved in ASD and neuropathology.

This analysis supplements preliminary annotations of the PPA transcriptome, demonstrating signatures of metabolic remodelling that contribute to cell-line-specific markers of neurotoxicity. PPA significantly altered the expression of 215 canonical metabolic genes, leading to a remodelling of substrate utilisation and mitochondrial dynamics. The most significant DE metabolic genes converged on the synthesis, transport and turnover of glycoconjugates, membrane lipids and neurotransmitters required for ECM assembly, synaptogenesis and synaptic signalling. Moreover, 14 metabolic genes implicated as central cell fate regulators suggest a focal role for RA signalling, cholesterol homeostasis, cytoskeletal remodelling and glycosylation in the neurotoxic response to PPA. Indeed, PPA was shown to alter the neurogenic signatures that have been validated in previous SH-SY5Y datasets, while inducing mRNA markers of neurotoxicity in the SH-SY5Y system. The transcriptomic data reported by Kim *et al.,* (2019) validated signatures associated with proliferation, glycolysis and neuronal injury as well as impairments to epigenetic regulation and CNS development. In particular, the Chiocchetti and Kim transcriptomes highlight a central role for *SMAD3, FOXO3* and *TBX3* in the neurotoxic response to PPA, while an acute dysregulation of Wnt, Shh and Notch signalling suggests functional implications

for the regulation of cell fate during early neurodevelopment. Together, this discussion demonstrates significant disruptions to the processes that shape neuronal metabolism and maturation under PPA stress which reflects the impairments to metabolism and neurogenesis presented in Chapters 2 and 3. Moreover, this work reveals focal molecular hubs at the interface between neuronal metabolism and maturation, highlighting novel target genes for future studies into PPA-induced neurotoxicity.

4.3.3. Co-expression Network Analysis: Towards a Mechanistic Framework

Thus far, both untargeted and targeted approaches have implicated central mechanisms that modulate neurogenesis, metabolism and cytotoxicity in the PPA transcriptome. However, the real utility of transcriptomic data is the ability to progress beyond the identification of relevant biological processes, towards an understanding of how these processes are linked through underlying mechanisms. Here, WGCNA was employed to identify networks of coregulated genes that perturbed neuronal development *in vitro*. Using the log-normalised CPMs for all mapped genes retained after filtering, WGCNA identified 22 modules of coregulated genes **(Figure 4.13).**

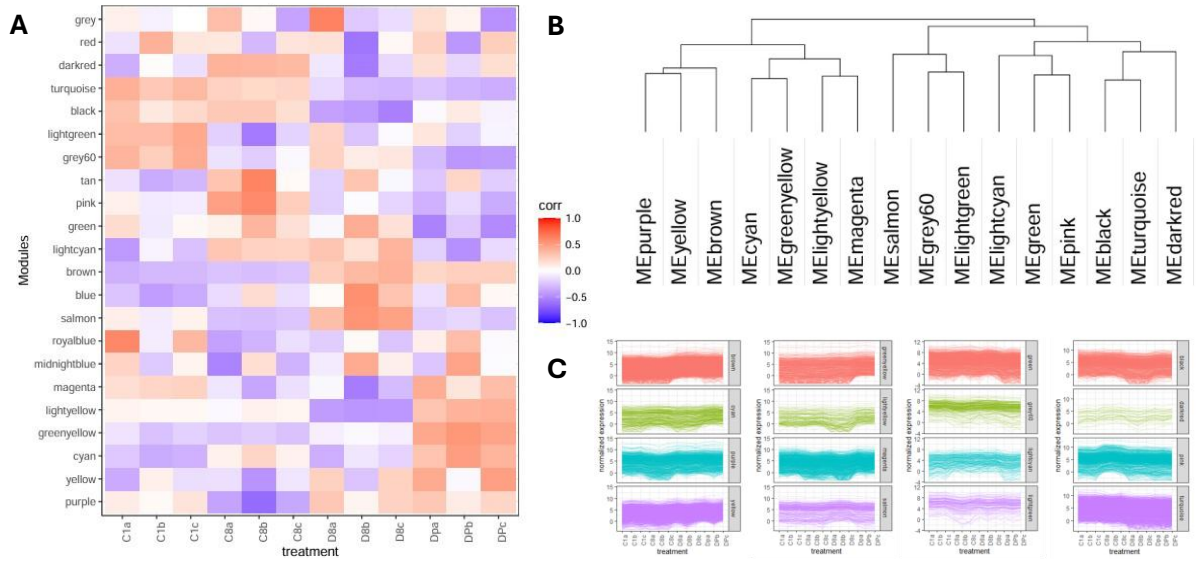


Figure 4.13. Coregulated Modules Identified by WGCNA. A) Module-trait relationships for all 22 coregulated modules based on the correlation between each sample & the eigengene of each module. **B)** Hierarchical clustering by average Euclidean distance for all 16 modules of interest. **C)** Log-normalised CPMs for every gene in each MOI.

From these 22 modules, MOIs were selected based on: i) the strength of module-trait correlation (where | E | > 0.25) and ii) reproducibility between all three biological replicates (std. dev (E) < 0.2). The 16 MOIs that were correlated with the response to PPA during neuronal differentiation were selected for functional annotation **(Figure 4.14A)**. The three largest MOIs (*turquoise*, *brown*, *yellow*) were DE between undifferentiated and differentiated samples, comprising ~ 50% of the genes expressed across all MOIs **(Figure 4.14B),** which is consistent with the PCA presented in **4.3.1.** The ten modules

associated with PPA exposure revealed substantial disruptions to ~ 40% of the neurogenic transcriptome **(Figure 4.14C)** while four modules comprising 10% of expressed genes were associated primarily with serum-depletion **(Figure 4.14D).**

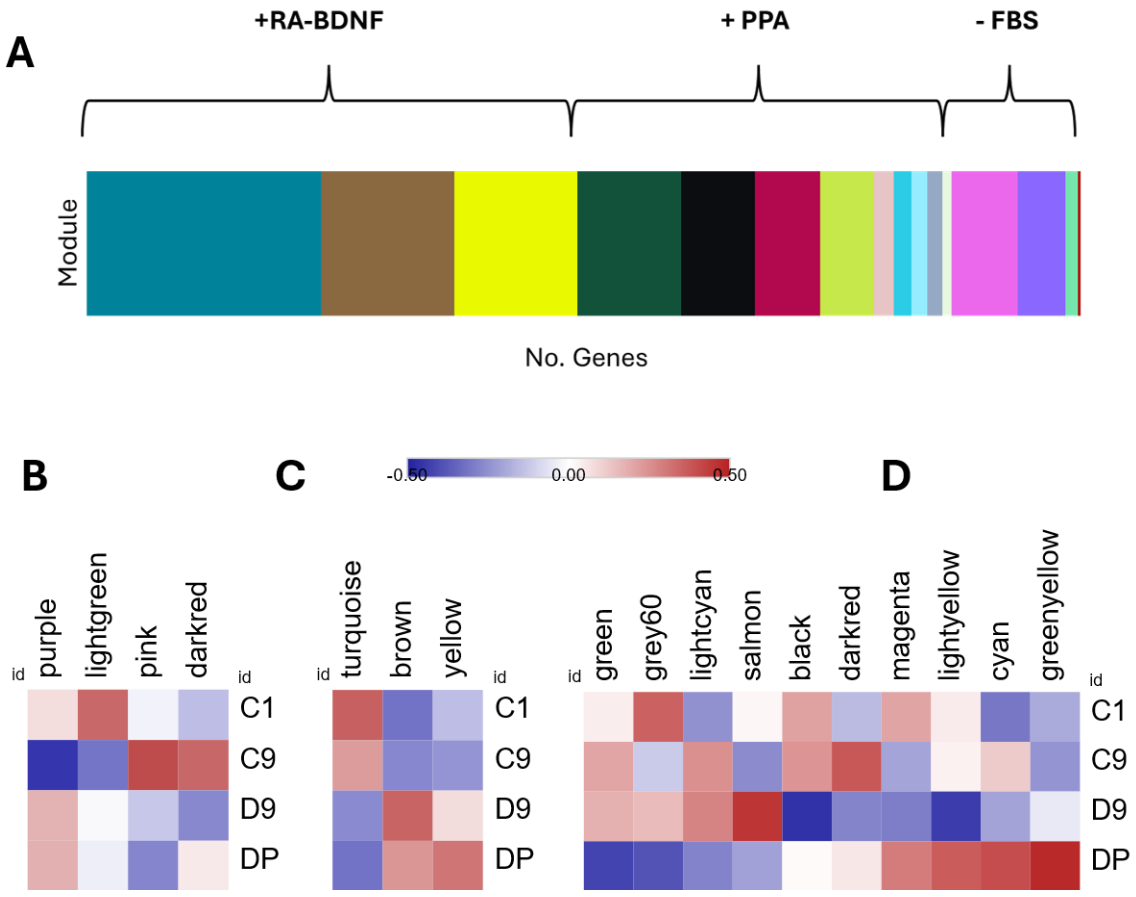


Figure 4.14. Modules of Interest Associated Experimental Conditions. A) Number of genes in each module of interest (MOI) grouped by condition. Module eigengenes are shown for MOIs associated with **B)** Differentiation, **C)** Propionic Acid and **D)** Serum depletion. C1 = undifferentiated controls grown in 15% FBS; C9 = day 9 negative controls maintained at 1% FBS without RA or BDNF; D9 = day 9 positive controls differentiated with RA and BDNF and DP = day 9 neurons differentiated in the presence of 5mM Propionic Acid.

All 16 MOIs were independently annotated **(Table S4.21)** and the top ontologies associated with each condition were summarised **(Figure 4.15; Table S4.22).** This analysis was consistent with the main findings from the pairwise DGE analysis but also revealed novel signatures that distinguished between experimental conditions. Firstly, the modules associated with serum depletion highlighted important distinctions between day 1 and day 9 controls that may explain their differential impact on neurogenic signatures. Day 1 controls displayed the high rates of cell proliferation that are characteristic of undifferentiated progenitors but with an upregulation of adjacent processes associated with cancer cell overgrowth, invasion and metastasis (*lightgreen, purple*). These include cell migration, endosomal recycling, ECM remodelling and angiogenesis driven by TGF-β, NFκβ and cytokine signalling. Day 9 controls suppressed this metastatic signature, but with a clear divergence from the undifferentiated state

marked by an increase in synapse organisation, neurotransmission (*lightcyan*) and stress-responsive signalling (*pink, darkred*). Thus, the RA-BDNF program appears to maintain and repurpose the transcriptional mechanisms that govern ECM dynamics while suppressing the cytotoxic signatures that emerge under serum starvation. Together, all three controls yield insight into the processes that are both facilitated and suppressed by RA-BDNF in the SH-SY5Y system, providing a comprehensive landscape in which to explore neurogenic mechanisms.

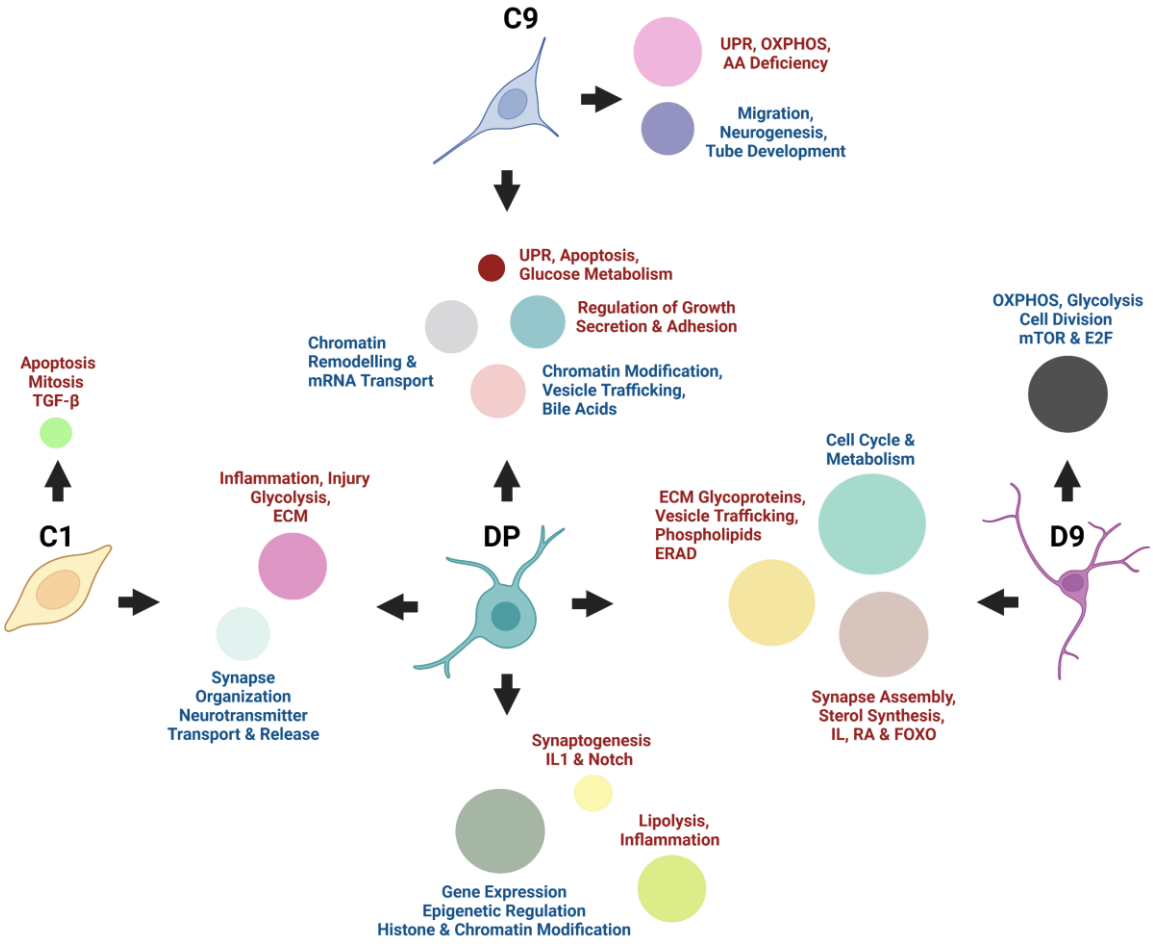


Figure 4.15. Functional Annotations Associated with Modules of Interest. Day 1 controls (C1), Day 9 controls (C9), day 9 differentiated neurons (D9) and neurons exposed to propionic acid (DP) are depicted relative to the up- (red) and down- (blue) regulated modules of interest associated with each condition. Modules are represented by their colour, size (number of genes) and most significantly enriched ontologies.

Indeed, each control yields specific insights into the PPA transcriptome. The neurogenic programme (*turquoise, brown, yellow*) revealed transcriptional hubs involved in cell cycle exit, ECM organisation and synapse assembly that remained largely unperturbed by PPA. However, the similarities between the PPA transcriptome and both day 1 (*lightcyan, magenta*) and day 9 (*grey60, salmon, darkred, cyan*) controls highlighted a shift towards an immature transcriptional landscape under PPA stress. In fact, PPA downregulated four MOIs that were upregulated during differentiation (*green, grey60, lightcyan, salmon*) revealing an inhibition of the neurogenic programme that drives epigenetic regulation,

metabolic remodelling, synaptogenesis and neurotransmission. On the other hand, PPA upregulated four MOIs that were inhibited during neurogenesis (*magenta, lightyellow, cyan, greenyellow*). These modules demonstrate an upregulation of genes involved in ECM assembly, synapse organisation and axon guidance that contradicts, rather than promotes, the neurogenic programme, leading to cytotoxic signatures associated with injury, apoptosis and inflammation.

Notably, PPA suppressed the neurogenic response driven by the two modules that were most strongly inhibited (*black, E= - 0.46*) and activated (*salmon, E = 0.45*) during differentiation. The black module revealed a transcriptional hub governed by Forkhead Box Protein M1 (FOXM1) that controls cell cycle progression via the anaphase promoting complex/ cyclosome (APC/C) and aurora-B kinase (AURKB) **(Figure S4.12A, B).** On the other hand, the salmon module converged on protein-protein interaction networks modulated by sterol regulatory element-binding proteins (SREBPs) **(Figure S4.12C, D),** which couple cholesterol synthesis to vesicle trafficking and secretion to fuel synapse assembly and synaptic vesicle cycling. This is congruent with the functional annotations associated with each module, highlighting central molecular hubs that may underpin PPA-induced disruptions to neuronal proliferation, metabolism and morphology during *in vitro* neurogenesis.

To better characterise the mechanistic relationships that drive the neurotoxic response to PPA, all 16 MOIs were grouped into clusters based on shared functional enrichment signatures **(Figure S4.13).** Iterative clustering identified seven core mechanisms mapped across five overlapping clusters connected by two mechanistic "threads" (**Figure 4.16, Table S4.23).** Here, clusters refer to mechanisms enriched in distinct subsets of MOIs while threads are annotations enriched in at least one MOI across all of the 5 main clusters. Epigenetic mechanisms were enriched across five MOIs governing cell cycle exit, metabolism and morphogenesis (*turquoise, purple, salmon, green, grey60*) while a coordinated remodelling of cell cycle and metabolism was demonstrated by an integrated downregulation of cell division, OXPHOS and glycolysis (*turquoise, lightgreen*). A concurrent shift in lipid utilisation was linked to ECM remodelling and synaptogenesis (*brown, yellow*), while a synergistic upregulation of neurogenesis, tube development and endosomal trafficking (*purple*) converged on the cycles of adhesion and disassembly that couple ECM dynamics to axon guidance and synaptic vesicle recycling. Moreover, an enrichment of immune signalling in both downregulated and upregulated modules suggested a role for NFκβ, cytokine and complement signalling in neuronal survival and maturation.

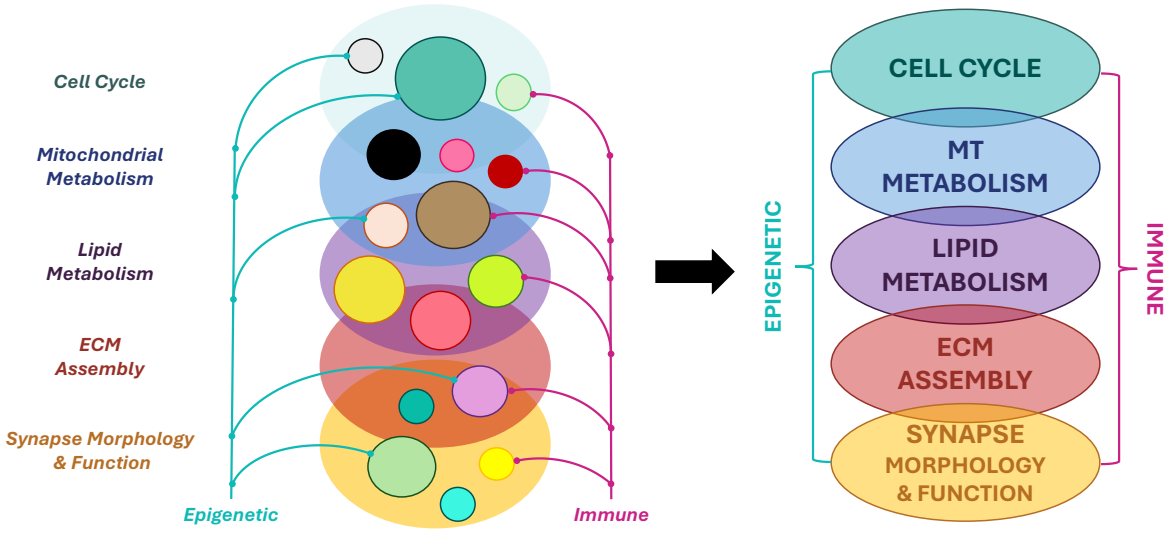


Figure 4.16. Modules of Interest Mapped Across Mechanistic Clusters. Annotating modules of interest (MOIs) using Gene Set Enrichment Analysis (GSEA) identified seven core mechanisms across all 16 MOIs. Modules are depicted according to their name (colour) and size (number of genes per module) and categorised into five mechanistic clusters – namely; the regulation of the cell cycle, mitochondrial metabolism, lipid metabolism, extracellular matrix (ECM) assembly and synapse morphology and function. Clusters overlap at shared modules, which are significantly enriched for both core mechanisms and demonstrate how different clusters are related. All five clusters are regulated by epigenetic mechanisms and converge on the downstream modulation of neuroimmune state.

However, this integrated regulatory network was broadly disrupted under PPA stress. Firstly, PPA suppressed three modules that were enriched for epigenetic regulation and post-transcriptional gene silencing coupled to cell cycle exit and metabolic remodelling (*salmon, grey60, green*). Consequently, PPA disrupted the interdependent relationship between cell proliferation and metabolism. On one hand, PPA induced a coordinated upregulation of cell division, glycolysis and OXPHOS (*black*) while inhibiting the regulation of cell cycle checkpoints that drive cell cycle arrest (*grey60, green*). Concurrently, PPA suppressed the neurogenic signature that couples cholesterol synthesis to endosomal trafficking and vesicle cycling (*salmon*), while altering the synthesis and turnover of essential ECM glycoconjugates and membrane phospholipids (*green-yellow, magenta*). Impairments to neurotransmitter synthesis and synaptic vesicle cycling were associated with disruptions to cholesterol (*salmon*), AA (*lightcyan*) and Ca^{2+} homeostasis (*green, magenta*). At the same time, PPA disturbed interactions between ECM remodelling and synaptogenesis mediated by endocytic recycling, growth cone dynamics, actin filament bundling, neuronal adhesion and junction assembly (*magenta, cyan, lightyellow*). Lastly, disruptions to ECM turnover were linked to signatures associated with wound healing, coagulation and inflammation (*black, greenyellow, magenta, lightyellow*). Together, this framework reveals an interdependent relationship between relationship between metabolic and morphological remodelling underpins in vitro neurogenesis and PPA-associated neurotoxicity **(Figure 4.17).**

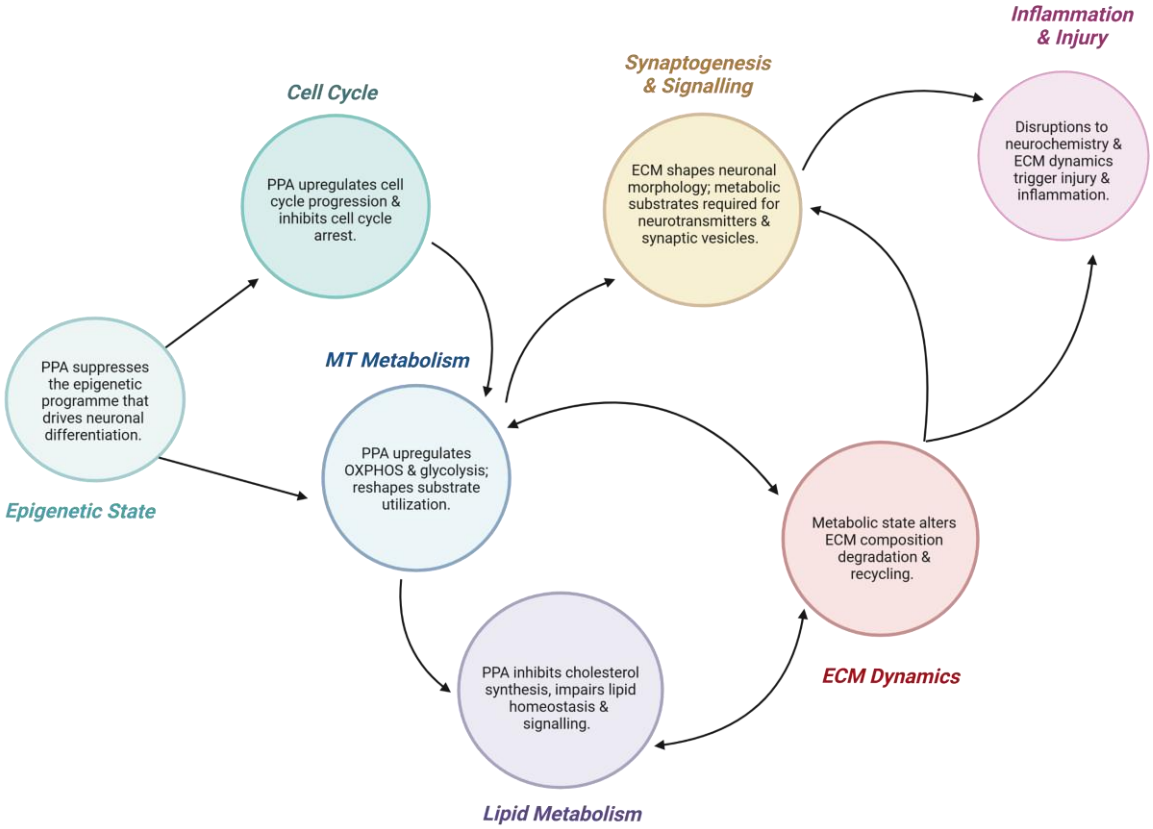


Figure 4.17. A Mechanistic Framework for Propionic Acid-Induced Developmental Neurotoxicity. An overview of the mechanistic relationships between the seven core mechanisms identified across all 16 modules of interest and the disruptions induced by Propionic Acid (PPA). PPA impairs the epigenetic regulation of proliferation and metabolism that drives cell cycle exit and metabolic remodelling to facilitate neuronal commitment. Disruptions to glucose metabolism alter the synthesis of extracellular matrix (ECM) glycoconjugates, while a concurrent shift in lipid utilisation perturbs the synthesis of membrane phospholipids. Impairments to metabolic state influences the synthesis of neurotransmitters and synaptic vesicles, while changes to ECM composition and dynamics impact axon guidance and synaptogenesis. Concurrently, disruptions metabolism, neurochemistry and ECM stability lead to signatures of neuronal injury, coagulation and inflammation.

4.3.4. Ingenuity Pathway Analysis: Upstream Regulators and Downstream Phenotypes

The mechanistic framework proposed by WGCNA highlights broad relationships between biological processes that may influence neuronal morphology and maturation. To further interrogate the causal regulatory networks that drive this response, an integrative assessment of signalling pathways, downstream phenotypes and upstream regulators was conducted using IPA. First, IPA was used to identify significantly enriched pathways in the PPA transcriptome annotated with Z-scores denoting an activation state calculated from a database of experimentally validated causal relationships. This analysis identified 248 significantly enriched biological processes (FDR < 0.05), with 75 pathways assigned $|Z| \geq 2$ **(Table S4.24),** of which 45 passed a threshold of FDR < 0.01 **(Table 4.3).**

Table 4.3. Functional Signatures of Propionic Acid Exposure from Ingenuity Pathway Analysis. Data represent the 45 most significantly enriched (FDR < 0.01; | Z | ≥ 2) pathways among differentially expressed genes in neurons exposed to propionic acid. Pathways are grouped into mechanistic clusters and ranked by FDR-value where downregulated pathways are shown in blue, upregulated pathways in black and pathways assigned | Z | ≥ 3 in bold.

IPA Pathway	Z Score	FDR value
Epigenetic & Transcriptional Regulation		
Generic Transcription Pathway	**-7.61**	**1.67E-06**
Transcriptional regulation by RUNX2	2.32	3.11E-03
Histone Modification Signalling Pathway	**-3.50**	**6.05E-03**
Proliferation & Development		
Eicosanoid Signalling	2.10	3.94E-06
Beta-catenin independent WNT signalling	2.41	1.44E-05
G-Protein Coupled Receptor Signalling	2.19	1.48E-05
PTEN Signalling	-2.19	1.38E-04
Gustation Pathway	2.40	2.25E-03
Human Embryonic Stem Cell Pluripotency	2.72	3.31E-03
Post-translational protein phosphorylation	**3.13**	**9.17E-03**
Metabolism		
CREB Signalling in Neurons	2.77	9.95E-06
Glycosaminoglycan metabolism	**3.00**	**2.82E-05**
ECM Organisation		
Extracellular matrix organisation	**3.67**	**9.01E-08**
L1CAM interactions	2.72	2.14E-07
Neutrophil degranulation	**5.46**	**1.82E-04**
Assembly of collagen fibrils and other multimeric structures	2.52	3.53E-04
Regulation of the EMT by Growth Factors Pathway	2.00	4.36E-04
Integrin cell surface interactions	**3.13**	**5.54E-04**
Sphingosine-1-phosphate Signalling	2.12	1.25E-03
Caveolar-mediated Endocytosis Signalling	2.31	1.71E-03
Leukocyte Extravasation Signalling	2.54	3.04E-03
Sertoli Cell-Sertoli Cell Junction Signalling	2.71	5.45E-03
Antigen Presentation Pathway	**3.46**	**6.00E-03**
GP6 Signalling Pathway	2.35	9.21E-03
Synaptic Assembly & Signalling		
Myelination Signalling Pathway	2.39	3.02E-06
Acetylcholine Receptor Signalling Pathway	2.02	4.19E-06
RHO GTPase cycle	**4.31**	**1.16E-05**
Opioid Signalling	2.04	7.65E-05
Activation of NMDA receptors and postsynaptic events	2.18	1.86E-04
Neuropathic Pain Signalling in Dorsal Horn Neurons	2.20	1.10E-03
Nuclear Cytoskeleton Signalling Pathway	**3.70**	**3.07E-03**

Actin Nucleation by ARP-WASP Complex	2.14	8.03E-03
Nitric Oxide Signalling in the Cardiovascular System	2.24	9.05E-03
Inflammation & Injury		
Pulmonary Fibrosis Idiopathic Signalling Pathway	2.33	1.83E-07
Molecular Mechanisms of Cancer	2.56	1.81E-06
Cardiac Hypertrophy Signalling (Enhanced)	2.53	2.13E-06
Glioblastoma Multiforme Signalling	2.14	1.55E-05
Thrombin Signalling	2.27	1.26E-04
Hepatic Fibrosis Signalling Pathway	**3.91**	**1.54E-04**
eNOS Signalling	2.41	5.35E-04
S100 Family Signalling Pathway	**3.42**	**2.38E-03**
Phagosome Formation	2.33	3.39E-03
Glioma Signalling	2.24	4.35E-03
IL-8 Signalling	2.48	6.14E-03

This analysis validated the trends observed with WGCNA, demonstrating statistically significant perturbations to all of the core mechanistic clusters that emerged in coregulated modules **(Figure 4.18).** Firstly, IPA revealed a suppression of transcriptional regulation and histone modification mediated by cohesin, methyl CpG binding protein 2 (MECP2) and central modulators of chromatin organisation, histone acetylation, DNAm and miRNA processing **(Figure S4.14).** A systemic dysregulation of developmental signalling was demonstrated by significant disruptions to the Wnt, Notch and mTOR pathways that govern NSC fate, and the Shh, PI3K and phospholipase cascades that facilitate morphological remodelling. In line with this, PPA upregulated signatures of pluripotency and mitosis, impaired the regulation of cell cycle checkpoints and suppressed the transcriptional programme that governs energy metabolism. In particular, PPA disrupted the network of RXR, PPAR and CREB transcription factors that remodel glucose and lipid metabolism in response to RA and BDNF, suggesting disruptions to the biochemical crosstalk between neuronal metabolism and development.

Metabolic signatures also demonstrated an upregulation of glucuronate degradation and glycosylation, diverting glucose away from ATP production to fuel the synthesis of ECM glycoconjugates. Systemic perturbations to ECM organisation appeared to be driven by interactions between integrins, collagens and cell adhesion molecules (CAMs), as well as processes involved in cell migration, junction signalling and endocytic trafficking. Congruent impairments to synaptogenesis were mediated by changes to cytoskeletal dynamics (Rho GTPase, PI3K and actin nucleation signalling) and the integrated pathways that govern neurite branching, attraction and repulsion (Wnt/Shh, ROBO-SLIT and ROCK/RhoA). IPA also demonstrated broad disruptions to the synthesis, binding and signalling of monoamine neurotransmitters, revealing signatures of glutamatergic excitotoxicity. Moreover, signatures of neuroinflammation, injury and apoptosis were underpinned by the S100 and thrombin cascades mediated by JAK/STAT, JNK and p38 signalling.

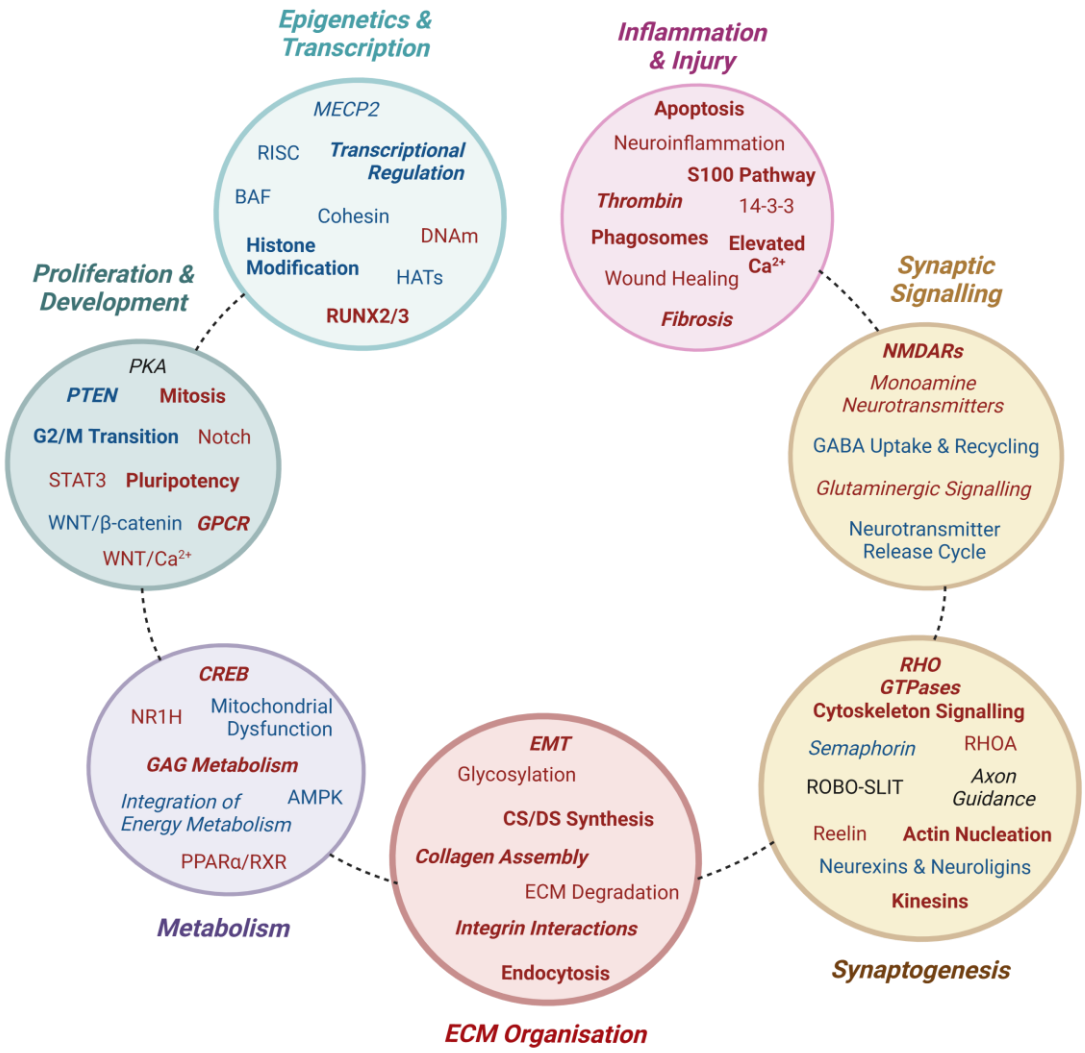


Figure 4.18. Significantly Enriched Pathways Identified with Ingenuity Pathway Analysis. The significantly enriched pathways detailed in Table S4.17 are depicted in mechanistic clusters summarising the top functional annotations associated with Propionic Acid exposure. Upregulated pathways are depicted in red, downregulated pathways in blue and pathways with no assigned Z score in black; FDR < 0.001 are in italics and those with | Z | ≥ 2 are in bold.

Significantly enriched pathways provide valuable insight into molecular players that govern transcriptional responses, but this data can be difficult to interpret with respect to downstream functional implications. Therefore, it is useful to examine whether transcriptional signatures converge on pathological profiles associated with specific disease phenotypes. Ranking significantly enriched IPA disease pathways by p-value and activation score revealed biochemical and phenotypic signatures associated with PA aetiology, including hyperammonaemia, urea cycle dysfunction, seizures and epilepsy **(Table 4.4).** Several other aspects of neuropathology emerged, including an upregulation of neurodegenerative (*cerebral atrophy, paresis*) and neurodevelopmental (*developmental epilepsy, west syndrome, syndactyly*) disorders as well as signs of neuronal injury (*ischaemia, spinocerebellar disease, cerebellar disease*), tumorigenesis and inflammation (*eosinophilic inflammation, sarcoma, carcinoma,*

tumour). Together, these signatures are consistent with a dysregulation of glutamate metabolism and signalling as well as increased oxidative stress, neuroinflammation, proliferation and apoptosis. Here, it is worth noting the significant enrichment of both the ASD (*FDR = 0.001; Z = 1.16*) and Amyotrophic Lateral Sclerosis (*Z = 2.14; FDR = 0.03*) pathways in the PPA transcriptome, both of which reflect an increase in ROS production associated with glutamatergic excitotoxicity and mitochondrial dysfunction. Ultimately, this demonstrates a mechanistic convergence between the processes involved in ASD and those associated with PPA exposure that suggests functional implications for neurodevelopment and function.

Table 4.4. Significantly Enriched Disease Pathways Associated with Propionic Acid. Data represent the top 10 significantly enriched and the 10 most robustly activated disease pathways among genes that were differentially expressed in response to Propionic Acid, ranked by p-value.

Top P-Value		**Top Activation Score**	
Disease Pathway	***P-Value***	***Disease Pathway***	***P-Value***
Hyperammonaemia	1.58E-06	Cerebral Atrophy	3.16E-02
Seizure Disorder	2.51E-06	Angiosarcoma	2.51E-02
Seizures	5.01E-06	Eosinophilic Inflammation	5.01E-02
Urea Cycle Disorder	5.01E-06	Syndromic Infantile Epilepsy	1.58E-03
Syndactyly	2.00E-05	West Syndrome	3.16E-02
Progressive Solid Tumour	2.00E-05	Epileptic Encephalopathy	6.31E-03
Non-small-cell lung carcinoma	5.01E-05	Early-onset Epilepsy	3.16E-02
Non-small-cell adenocarcinoma	6.31E-05	Infantile Epilepsy	1.58E-03
Paresis	7.94E-05	Childhood Epilepsy	1.26E-02
Progression of Carcinoma	7.94E-05	Developmental Epilepsy	1.26E-02

Lastly, transcriptomic data is well-suited to identify causal regulatory networks that drive pathological processes. Therefore, IPA was used to interrogate the upstream transcriptional regulators that shape the PPA transcriptome. Here, IPA identified 131 significantly enriched transcriptional regulators (FDR < 0.001), including 30 genes that passed a threshold of $|Z| \geq 2$ **(Figure 4.19A, B; Table S4.25).** The most significantly enriched regulator was TP53, a master regulator of the intracellular stress response that was activated under PPA stress. The 12 most significantly enriched genes assigned $|Z| \geq 3$ revealed central regulators of development, metabolism and inflammation **(Table 4.5)** where the two most robustly activated regulatory networks were those driven by T-Box Transcription Factor 3 (*TBX3*) and Melanocyte Inducing Transcription Factor (*MTIF*) while the most inhibited networks were regulated by Glioma-Associated Oncogene 1 (*GLI1*) and Transcription Factor 7 (*TCF*). Notably, all four of these genes were DE under PPA exposure and modulate differentiation, proliferation, patterning and survival via TGF-β, mTOR, Shh and Wnt signalling respectively.

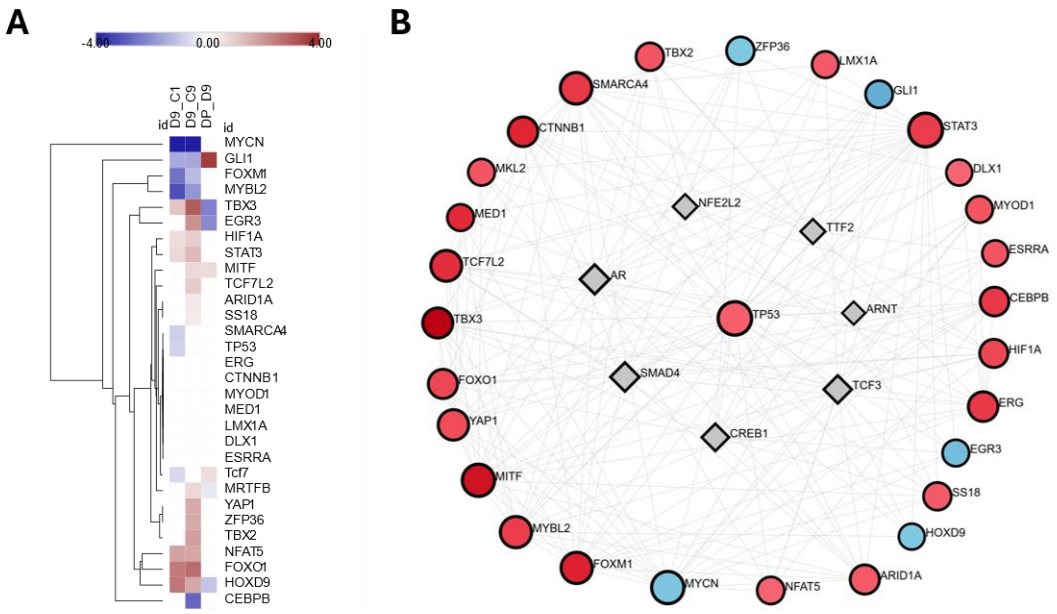


Figure 4.19. Top Transcriptional Regulators in the PPA Transcriptome. **A)** Log Fold Change values showing the differential expression of the 30 most significantly enriched upstream transcriptional regulators (FDR < 0.001, | Z | ≥ 2) between experimental conditions. **B)** All 30 regulators are depicted in a transcription factor – gene interaction network based on the Chea3 database organised in a concentric circle based on the node with the greatest betweenness centrality. Nodes are coloured by the Z score for each regulator where red = activation and blue = inhibition; node sizes reflect the betweenness centrality for each gene.

Table 4.5. Top Transcriptional Regulators in The PPA Transcriptome. Data represent the 12 most significantly enriched (FDR < 0.001; | Z | ≥ 3) upstream transcriptional regulators among differentially expressed genes (DEGs). Activated networks (red) and inhibited networks (blue) are ranked by p-value; those that are also transcriptionally dysregulated by propionic acid are highlighted in bold.

Gene	LogFC	Z	FDR	Function
TBX3	**-2.26**	**5.22**	**2.67E-20**	Regulates Shh, BMP & TGF-β signalling.
ERG		3.13	6.83E-14	Regulates development, proliferation, differentiation, angiogenesis, inflammation & apoptosis.
CTNNB1		3.49	1.79E-13	Acts as a coactivator for TCF/LEF transcription factors in canonical Wnt signalling.
FOXM1		3.69	3.55E-12	Master regulator of cell cycle genes, DNA replication, mitosis and proliferation.
SMARCA4		3.12	7.27E-11	Component of SWI/SNF complex that forms the neural progenitor & neural BAF complexes.
MITF	**0.67**	**4.35**	2.78E-08	Regulates differentiation, proliferation, survival & the response to AA depletion, starvation or stress downstream of mTOR.
TCF7L2		3.29	1.46E-07	Wnt-responsive transcription factor that regulates glucose homeostasis, cell cycle arrest & NSC self-renewal.
STAT3		3.01	3.18E-07	Regulates the G1/S cell cycle transition, cell growth, apoptosis & interleukin signalling.
MED1		3.38	4.22E-05	Mediator protein that bridges gene- specific regulators to basal transcription machinery, controls apoptosis & adipogenesis.
CEBPB		3.05	7.09E-04	Regulates genes involved in adipogenesis, gluconeogenesis & inflammatory responses.
GLI1	**3.59**	**-3.28**	**6.16E-18**	Regulates development & morphogenesis via Shh signalling.
Tcf7	**0.65**	**-3.32**	**3.64E-04**	Activates transcription through Wnt/ β-catenin signalling.

Of the significantly enriched upstream regulators identified by IPA, 30 genes were also transcriptionally dysregulated by PPA, forming a transcription factor network governed by *SMAD3* **(Figure 4.20A, B; Table S4.26).** Of these, PPA reversed the neurogenic profiles of 12 transcription factors associated with NSC self-renewal, pluripotency and proliferation (*SOX2, SALL4*), neuronal differentiation (*POU4F1, EGR3, TSHZ3, MECP2*) and morphogenesis (*GLI1, SMAD3, HOXD9, TBX3*). Interestingly, the DE upstream regulators shown in **Figure 4.16C** included 11 of the central cell fate regulators identified in **4.4.1 (Figure 4.20C, D; Table S4.27)** involved in TGF-β signalling (*TBX3, SMAD3*), Notch signalling (*HES1, NOTCH2*) and neuronal metabolism (*FOXO3*), proliferation (*KLF6, E2F7*) and development (*ETS1, ISL1, HOXD9, EPAS1*). Moreover, 10 DE regulators involved in epigenetic remodelling were found to significantly influence the PPA transcriptome **(Figure 4.20E, F; Table S4.27**), including several genes involved in methylation (*MECP2, PRDM5/8, MBD2*), acetylation (*CREBBP, HDAC4, HDAC3, SIRT1*) and chromatin remodelling (*ASCL1, SMARCA2*). Together, this analysis reveals focal drivers of epigenetic state, pluripotency, metabolism and differentiation that underpin PPA-induced disruptions to neurogenesis.

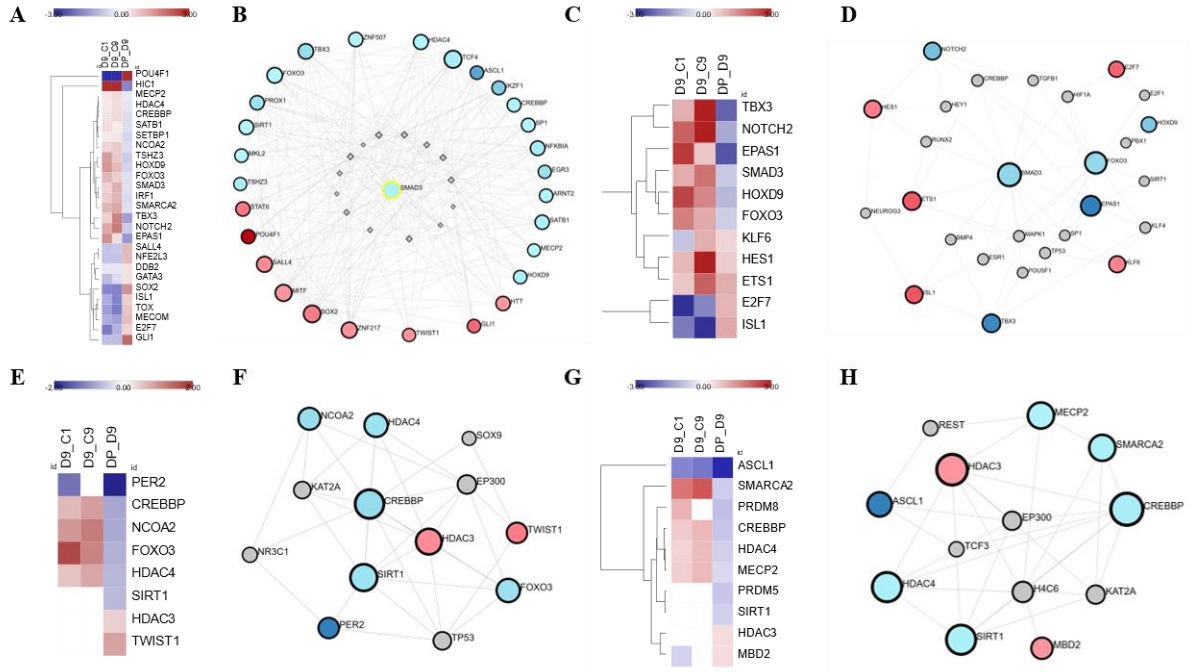


Figure 4.20. Differentially Expressed Regulators in the PPA Transcriptome. **A)** Log Fold Change (FC) values for the top 30 differentially expressed (DE) upstream transcriptional regulators (FDR<0.001) depicted in **B)** a transcription factor – gene regulatory Chea3 network. Nodes are coloured by the LogFC for each gene under PPA stress, where red = upregulation and blue = downregulation. LogFC values and STRING protein-protein interaction networks (confidence ≥ 700) are shown for **C, D)** the 11 cell fate regulators, **E, F)** the eight metabolic genes and **G, H)** the ten epigenetic regulators where input nodes are coloured by the LogFC under PPA stress where red = upregulation and blue = downregulation; node sizes reflect the betweenness centrality for each gene.

Collectively, the upstream regulators identified by IPA implicated processes involved in epigenetic remodelling, proliferation, metabolism, morphogenesis and the intracellular stress response **(Figure**

4.21). Of the eight epigenetic remodellers highlighted in Figure 4.21, four genes either comprise (*SMARCA4, ARID1A, SS18*) or interact with (*IKZF1*) the SWI/SNF neuronal BAF (nBAF) complex that drives neuronal maturation, while *MECP2* and *ASCL1* emerge as critical neurogenic regulators that were suppressed by PPA. A second cluster of regulators governs the interdependent network between Wnt (*CTNNB1, TCF7, TCF7L2*), TGF-β (*TBX3, SMAD2/3, DLX1*), Shh (*GLI1*) and Hippo (*YAP1*) signalling that controls NSC pluripotency, differentiation and morphology. In addition, PPA disrupted central regulators of proliferation (*FOXM1*, *STAT3*), metabolism (*FOXO3, SIRT1, CREBBP*), and survival (*p53, MITF*) with important roles in neurodevelopment and function. Here, *FOXO3* was implicated as an important regulator of both cell fate and metabolism, while *SIRT1, CREBBP, HDAC3* and *HDAC4* were highlighted as focal epigenetic regulators of metabolic state. Ultimately, this analysis is consistent with the significantly enriched biological processes identified with both GSEA and IPA, revealing molecular hubs that may facilitate the mechanistic relationships described with WCNA and validating disruptions to the neurogenic pathways that govern NSC fate.

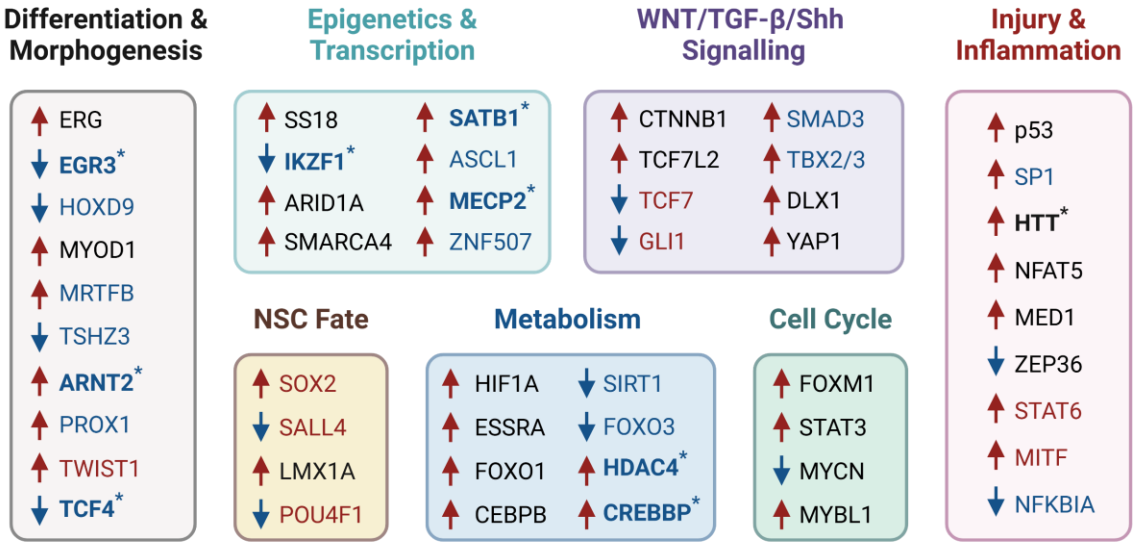


Figure 4.21. Convergent Regulators in the PPA Transcriptome. Data depict the most significantly enriched (FDR < 0.001; | Z | ≥ 2) and differentially expressed (FDR < 0.001; | LogFC | > 0) expressed transcriptional regulators in the PPA Transcriptome. Upregulated genes are shown in red, downregulated genes are shown in blue; nodes represent the activation (red) or inhibition (blue) state of each network and genes in the SFARI database are highlighted in bold.

In its completion, **section 4.3** has presented three untargeted analyses of the PPA transcriptome that converge on common processes associated with PPA-induced neurotoxicity. Pairwise DGE analysis, WGCNA and IPA demonstrated marked impairments to the neurogenic programme that suppressed cell cycle exit, metabolic remodelling, synapse assembly, neurotransmission and epigenetic regulation. Likewise, signatures of neuronal injury, inflammation, glycolysis and ECM organisation were

consistently upregulated in the PPA transcriptome. A more targeted analysis characterised transcriptional hallmarks of metabolic remodelling and developmental neurotoxicity that reshaped substrate utilisation and mitochondrial dynamics, upregulated processes involved in neuronal proliferation, injury and survival and disrupted synaptogenesis, synaptic vesicle cycling and synaptic signalling under PPA stress. An interdependent relationship between epigenetic, metabolic and morphological remodelling emerged in the coregulated modules identified with WGCNA, and IPA tied this response to central epigenetic and transcriptional regulators of NSC fate. Here, disruptions to Notch, Wnt, Shh and TGF-β signalling emerged as focal mechanisms involved in PPA-associated neurotoxicity that contributed to pathological signatures of metabolic, neurodevelopmental and neurodegenerative disease. Together, these mechanistic signatures are consistent with the morphological hallmarks of neurotoxicity presented in Chapter 3 and yield novel insight into the molecular players that drive this response.

4.4. Discussion

This thesis arose from a mechanistic hypothesis based on signatures of mitochondrial dysfunction in molecular ASD datasets. Subsequently, an *in vitro* system was used to study different aspects of this mitochondrial signature in neuronal-like cells, establishing a model for metabolic stress that significantly disrupted neuronal morphology and maturation. Chapter 4 interrogated the mitochondrial dysfunction hypothesis described in Chapter 1 using the *in vitro* system established in Chapters 2 and 3. In this way, Chapter 4 is a culmination of the work presented in this thesis that could highlight novel avenues for future work in both the preclinical and clinical contexts. This chapter presented the first transcriptomic profile for PPA-induced neurotoxicity in the SH-SY5Y system, providing a scoping molecular landscape in which to explore neuropathological mechanisms. Using proliferative controls (day 1), quiescent controls (day 9) and differentiated controls to annotate the PPA transcriptome, global expression profiles revealed distinct signatures associated with serum depletion, differentiation and PPA exposure that reflected the morphological phenotypes characterised in Chapter 3 and highlighted novel aspects of neurogenesis in the SH-SY5Y system.

Serum-depletion upregulated signatures of senescence, starvation and AA deficiency, as well as neurogenic processes involved in cell cycle exit, synaptogenesis and neurotransmission. This data is consistent with the spontaneous emergence of neurite-like processes in negative controls observed in Chapter 3 and reflects previous reports that serum depletion upregulates the expression of neuronal markers and promotes neurite production, elongation and branching in SH-SY5Y cells (Thomson *et al.,* 2022). Interestingly, the transcriptomic signatures presented in this chapter suggest that the neurogenic and neurotoxic responses induced by FBS depletion may be mechanistically intertwined. Serum depletion upregulates transcriptional signatures associated with the UPR, which is known to activate BDNF transcription via X-box-binding protein 1 (XBP1) (Chen *et al.,* 2023). In fact, Saito *et al.,* (2018)

showed that the XBP1 pathway facilitated neurite elongation and branching by upregulating BDNF transcription and TRKβ signalling in primary hippocampal neurons. Moreover, Thomson *et al.,* (2022) demonstrated that serum depletion facilitated the emergence of neuronal-like features by activating the BDNF-TRKβ pathway in SH-SY5Y cells. Thus, the morphological remodelling induced by FBS depletion may be driven by a neuroprotective response that promotes BDNF production under metabolic or proteotoxic stress.

Notably, both day 1 and day 9 controls revealed distinct features of the neurogenic programme. Day 1 controls better reflected the energetic and proliferative nature of undifferentiated progenitors, while signatures isolated using day 9 controls may be confounded by the neurotoxic response to serum depletion that is induced in the absence of neurogenic agents. On the other hand, proliferative controls displayed metastatic signatures associated with cell migration, ECM deposition and cytoskeletal remodelling, which can mask the neurogenic mechanisms that drive ECM assembly and synaptogenesis. Together, day 1 and day 9 controls effectively isolated mechanisms that were both enhanced and suppressed by the RA-BDNF programme that drives *in vitro* neurogenesis. A subset of ~ 3000 neurogenic genes that were DE relative to both day 1 and day 9 controls validated the emergence of a mature neuronal phenotype on a molecular level, demonstrating a decrease in cell proliferation, a remodelling of metabolism and an upregulation of processes involved in synapse assembly and signalling. This is consistent with the morphological changes observed during differentiation – including a significant decrease in cell proliferation and the production and elongation of complex interconnected neurites in mature neurons compared to undifferentiated controls. Ultimately, this data illustrates that the morphological features of neurogenesis observed in Chapter 3 are reflected in underlying transcriptomic signatures. Moreover, this discussion highlights the context-specific utility of both proliferative and quiescent controls to yield insight into molecular mechanisms of differentiation in the SH-SY5Y system.

Using all three controls to annotate the PPA transcriptome revealed marked impairments to neuronal maturation. Pairwise DEG analysis and WGCNA showed that almost 50% of the PPA transcriptome directly counteracted the neurogenic programme, while up to 40% of the neurogenic transcriptome was inhibited under PPA stress. Preliminary GSEA revealed molecular signatures that impaired epigenetic remodelling, cell cycle exit, cholesterol synthesis, synaptogenesis and neurotransmission. A targeted investigation of metabolic signatures showed that PPA perturbed mitochondrial dynamics and reshaped profiles of substrate utilisation involved in the synthesis of ECM glycoconjugates, membrane phospholipids and neurotransmitters. Moreover, PPA impaired validated signatures of *in vitro* neurogenesis, perturbed central mRNA markers associated with developmental neurotoxicity and upregulated signatures associated with proliferation, growth, glycolysis and injury that reflected profiles of acute PPA exposure in the SH-SY5Y model.

Lastly, WGCNA and IPA were used to characterise the mechanistic clusters, signalling networks and upstream regulators that drive pathological responses to PPA stress. Both WGCNA and IPA demonstrated integrated disruptions to epigenetic regulation, proliferation and metabolism, leading to a remodelling of ECM dynamics, neurochemistry and neuroimmune state. IPA revealed a dysregulation of the Wnt, Notch and mTOR pathways that modulate neurogenesis, while an analysis of upstream regulators suggested a role for TP53, TGF-β and Shh signalling in PPA-induced neurotoxicity. Moreover, signatures of metabolic, neurodevelopmental and neurodegenerative disease phenotypes reflected evidence of autotoxicity driven by a dysregulation of GABA/glutamate cycling, tumorigenesis, neuroinflammation and neuronal injury. Together, this analysis demonstrated signatures of developmental delay and neurotoxicity that reflect the disruptions to neuronal morphology and maturation observed in Chapter 3.

The discussion that follows describes the neurotoxic mechanisms in the PPA transcriptome, highlighting central disruptions to the intrinsic and extrinsic factors that modulate stem cell fate. First, emergent signatures of pluripotency are used to explore the epigenetic and transcriptional landscapes that underpin morphological and biochemical hallmarks of neurodevelopmental delay. Subsequently, the coordinated disruptions to proliferation, metabolism and survival are considered with respect to the downstream implications for cell fate and function. Lastly, the implications for synaptogenesis, plasticity and signalling are explored with reference to the mechanistic interface between metabolic and morphological remodelling during neurogenesis. Together, the morphological, molecular and transcriptional signatures of PPA exposure yield novel insights into the relationship between neuronal metabolism and differentiation and highlight new avenues of research into metabolic mechanisms in neurodevelopment and disease.

4.4.1. Transcriptomic Evidence of Epigenetic Reprogramming

The switch from NSC self-renewal to differentiation is driven by an epigenetic shift mediated by distinct chromatin remodelling complexes (CRCs), histone modifying enzymes, DNA methyltransferases and non-coding RNAs (ncRNAs) during different phases of development (Salinas, Connolly and Song, 2020). Chapter 1 emphasised the tight coupling between metabolic and epigenetic remodelling during neurogenesis, proposing that mitochondrial dysfunction may perturb neurodevelopment by disrupting the epigenetic mechanisms that shape the neurogenic transcriptome. Interestingly, the PPA transcriptome presented here reveals marked perturbations to the epigenetic regulation of neurogenesis. A broad suppression of epigenetic and transcriptional regulation was demonstrated with pairwise DGE analysis, while WGCNA showed that PPA inhibited chromatin remodelling, histone modification and post-transcriptional gene silencing. Moreover, IPA demonstrated an inhibition of the cohesin, MECP2 and histone modification pathways, revealing a convergence between significantly enriched epigenetic regulators and downstream signalling pathways modulated by epigenetic state.

Upstream regulators in the PPA transcriptome converged on the ATP-dependent BAF complexes and pioneer transcription factors that reshape chromatin architecture during development. During neurogenesis, the shift from proliferating neuronal progenitors to post-mitotic developing neurons is driven by a switch from the neuronal progenitor BAF-associated complex (npBAF) to the neuronal-specific counterpart (nBAF), underpinned by a shift in BAF subunit composition (Braun *et al.,* 2021). PPA significantly altered the expression of core BAF components (*SMARCB1, PBRM1*), upregulated npBAF components (*ACTL6A)* and downregulated nBAF subunits (*ACTL6B* and *DPF3)*. Moreover, the most substantially inhibited regulator in the PPA transcriptome was Achaete-Scute Family BHLH Transcription Factor 1 (*ASCL1*), a pioneer transcription factor that cooperates with nBAF to shape the neuronal epigenome (Păun *et al.,* 2023), while four of the most significantly enriched upstream regulators were involved in BAF assembly, regulation or function (*SMARCA4, ARID1A, IKZF1, SS18*). Therefore, disruptions to nBAF composition may have functional implications for transcriptional regulation.

Critically, BAF switching is essential to initiate cell cycle exit, differentiation and synaptogenesis and genetic disruptions to BAF subunits are frequently implicated in NDDs (Braun *et al.,* 2021). Indeed, the np/nBAF complexes differentially interact with cell cycle regulators, as well as central effectors of the Notch, Wnt, Shh, Hippo and TGF-β/SMAD pathways that govern pluripotency, differentiation, morphogenesis and patterning (Chmykhalo *et al.,* 2024). Of note, Notch signalling suppresses the expression of nBAF subunits (Zhu *et al.,* 2021), while interactions between nBAF and the Wnt/β-catenin pathway mediate cell cycle arrest, neuronal commitment and mitochondrial reprogramming during differentiation (Wischhof *et al.,* 2022). Thus, the shift in BAF composition under PPA stress not only reflects epigenetic signatures of developmental delay but may provide mechanistic insight into the downstream disruptions to neuronal proliferation, differentiation and metabolism.

In addition to chromatin remodellers that directly change the position of nucleosomes, chromatin architecture can be modified by proteins that add, remove, or bind to epigenetic marks on histone tails or nucleotides (Sánchez-Ramírez *et al.,* 2024). Specific HATs and HDACs govern the spatiotemporal patterns of gene expression that define different stages of development (Park *et al.,* 2022). Undifferentiated neuronal progenitors are marked by high levels of HDACs 1 and 3, while HDACs 2 and 4 are upregulated in mature neurons (Cho and Cavalli, 2014). However, transcriptional signatures showed that PPA significantly downregulated the histone modification pathway and profoundly altered the expression of genes involved in histone acetylation while broadly inhibiting the expression of HATs. Notably, PPA downregulated both *HDAC4* and *SIRT1*, which each play critical roles in synaptogenesis and synaptic plasticity, with protective effects in the context of excitotoxicity and stress-induced apoptosis (Herskovits and Guarente, 2014; Wu *et al.,* 2016; Sild and Booij, 2019). Likewise, PPA decreased the expression of *KAT6A* and *CREBBP*, two neurogenic HATs required for corticogenesis,

neuroplasticity and cognition (Park *et al.,* 2022; Liu *et al.,* 2024) that are causally implicated in NDDs marked by microcephaly and intellectual disability (Wilson, Porter and Garcia, 2022).

Conversely, PPA upregulated both *HDAC1* and *HDAC3*, which are not only associated with NSC pluripotency but are also implicated in neurotoxicity and neurodegeneration. Although HDAC1 is essential for neurodevelopment (Cho and Cavalli, 2014; Jaworska, Ziemka-Nalecz and Zalewska, 2015), a dysregulation of HDAC1 activity is associated with neurodegeneration and neurotoxicity (Bardai *et al.,* 2012). HDAC1 has been shown to drive NSC fate towards gliogenesis (Jacob *et al.,* 2014) and is almost exclusively expressed by glial populations in the mature brain (D'Mello, 2020). On the other hand, HDAC3 promotes NSC self-renewal by inhibiting RA-responsive neuronal genes via the silencing mediator of retinoic acid and thyroid hormone receptor (SMRT) corepressor (Cho and Cavalli, 2014) and suppressing BDNF transcription by binding to the BDNF promoter (Louis Sam Titus *et al.,* 2019). Interestingly, both HDAC1 and HDAC3 have been found to induce cell death in cortical neuronal cultures (Bardai and D'Mello, 2011; Bardai *et al.,* 2012), while interactions between HDAC1 and HDAC3 contribute to neurodegeneration, motor decline, and cognitive and behavioural deficits that are alleviated by selective HDAC1/HDAC3 inhibitors in models of Huntington's disease (D'Mello, 2020). Thus, an upregulation of HDAC1 and HDAC3 reflects a neurotoxic response to PPA that could impact neurodevelopment, identity and survival.

Notably, Chapter 2 considered an interplay between CoA metabolism and histone acetylation that mechanistically couples the metabolic, epigenetic and transcriptomic signatures associated with PPA. The transcriptomic data presented here suggests that disruptions to histone acetylation induced by PPA may have functional consequences for epigenetic remodelling during neurogenesis. Indeed, several lines of evidence suggest that PPA disrupts the expression and activity of HDACs and HATs leading to profound changes in global histone acetylation profiles *in vitro* (Kiefer, Beyer-Sehlmeyer and Pool-Zobel, 2006; Nguyen *et al.,* 2007; Silva *et al.,* 2018; Thomas and Denu, 2021; Ramesh *et al.,* 2023). Recent studies in primary neuronal cultures revealed significant changes to the expression of proteins involved in chromatin remodelling and histone acetylation under PPA stress (Gisevius *et al.,* 2024). Moreover, numerous studies have shown that PPA alters cell identity and differentiation by disrupting histone acetylation patterns, mediated by changes to the activity of p300/CREBBP acetyltransferases (Lagerwaard *et al.,* 2021; Thomas and Denu, 2021; Ramesh *et al.,* 2023), while Thomas and Denu, (2021) showed that this epigenetic remodelling was driven by associated disruptions to acyl CoA metabolism. Thus, the disruptions to chromatin assembly and histone modification in the PPA transcriptome reflect functional impairments to epigenetic remodelling reported in the PPA model.

Notably, the transcriptional signatures associated with PPA exposure highlighted MECP2 as a central orchestrator of the transcriptional and post-transcriptional mechanisms that govern epigenetic state. MECP2 modulates transcription not only in its canonical role as a methyl-binding protein (Carla et al.

2022), but also via interactions with the CCCTC-binding factor and cohesin complexes that drive chromatin remodelling during development (Davis, Onn and Elliott, 2018). In fact, MECP2 also controls post-transcriptional mechanisms that regulate gene expression via interactions with the Drosha and RNA-binding protein complexes that drive miRNA processing and mRNA splicing (Cheng and Qiu, 2014). Notably, MECP2 was identified as one of the top DE upstream regulators in the PPA transcriptome, while IPA demonstrated that PPA significantly inhibited the MECP2 signalling pathway, including central components of the RNA-induced silencing complex (RISC) responsible for miRNA processing (*AGO2/3/4* and *DICER1*). Critically, an upregulation of MECP2 is essential for neuronal maturation, and genetic disruptions to MECP2 are implicated in the monogenic form of ASD known as Rett syndrome (Vuu, Roberts and Rastegar, 2023). Moreover, neurodevelopment is broadly modulated by highly specific and dynamic miRNA profiles that govern BAF-switching (Son and Crabtree, 2014), cell fate decisions, pluripotency, metabolism, development and survival (Singh, 2021; Xuan *et al.,* 2023; Alammari *et al.,* 2024). Indeed, DICER1 is essential for neurodevelopment (Fiorenza and Barco, 2016; Esteves *et al.,* 2020; Guo *et al.,* 2020) while studies in SH-SY5Y cells have shown that suppressing DICER expression impaired RA-BDNF-induced differentiation and promoted cellular senescence (Jauhari *et al.,* 2017). Therefore, the inhibition of both MECP2 and RISC under PPA stress could disrupt both epigenetic and post-transcriptional mechanisms that modulate the neurogenic transcriptome.

Interestingly, the epigenetic regulators implicated in the PPA transcriptome also highlight convergent disruptions to metabolic remodelling. MECP2 functions at the intersection of metabolic state and neurogenesis by directly driving BDNF expression upstream of the mTOR/AMPK axis (Vuu, Roberts and Rastegar, 2023). Indeed, both preclinical and clinical studies of MECP2 deficiency have demonstrated profound disruptions to mitochondrial morphology and dynamics (Shulyakova *et al.,* 2017), mtDNA copy number (Liu *et al.,* 2021), ETC activity (Dave *et al.,* 2019), TCA cycle flux and redox homeostasis (Tomasello *et al.,* 2024) as well as metabolomic (Golubiani *et al.,* 2021), proteomic (Cicaloni *et al.,* 2020) and transcriptomic (Aldosary *et al.,* 2020) signatures of mitochondrial dysfunction. Likewise, *HDAC3*, *HDAC4, SIRT1* and *CREBBP* were implicated as canonical metabolic genes that also served as significantly enriched upstream regulators in the PPA transcriptome. Intriguingly, MECP2 expression is promoted by SIRT1 (D'Angelo *et al.,* 2021), while interactions between MECP2 and CREBBP are critical to remodel glucose and lipid utilisation during neurodevelopment (Vuu, Roberts and Rastegar, 2023), and the MECP2/HDAC3/NCOR1 complex has been implicated as a regulator of energy homeostasis (Kyle *et al.,* 2016), synaptic plasticity and social behaviour (Nott *et al.,* 2016). Moreover, HDAC3, HDAC4 and SIRT1 are independent regulators of energy homeostasis that modulate glucose and lipid utilisation by targeting FOXO transcription factors (Mihaylova and Shaw, 2013; King, Patel and Chandrasekaran, 2021), while CREBBP is a central regulator of mitostasis that coordinates epigenetic and mitochondrial remodelling during neurogenesis (Uittenbogaard, Brantner and Chiaramello, 2018). Together, this data reveals a regulatory hub at the

intersection between epigenetic and metabolic reprogramming during development that is not only transcriptionally disrupted by PPA, but also significantly shapes the PPA transcriptome **(Figure 4.22).** Ultimately, this regulatory hub highlights critical epigenetic regulators involved in crosstalk between metabolic state and neurogenesis that may play a central role in the relationship between mitochondrial dysfunction and neuropathology.

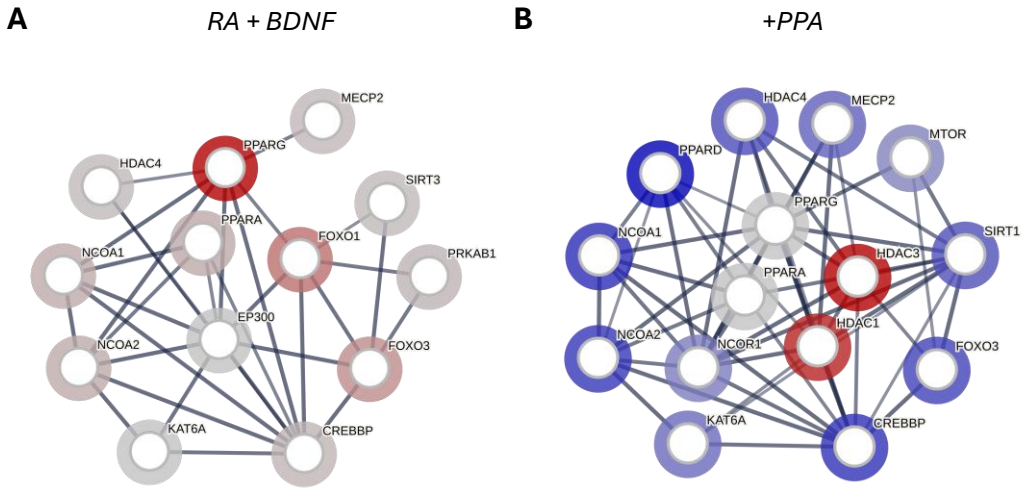


Figure 4.22. Epigenetic Regulators of Metabolic State. Data depict a STRING protein-protein interaction network (confidence ≥ 700) between central metabolic regulators that are **A)** upregulated during differentiation and **B)** disrupted by Propionic Acid; where node halos depict the differential expression induced by PPA relative to differentiated controls (downregulation = dark blue; upregulation = dark red).

Altogether, this discussion proposes systemic impairments to the epigenetic mechanisms that govern neuronal identity, differentiation and metabolism under PPA stress **(Figure 4.23).** Disruptions to BAF switching are marked by a shift towards the npBAF complex associated with NSC pluripotency and proliferation. This is reflected by a broad dysregulation of the epigenetic, transcriptional and post-transcriptional mechanisms that drive neuronal lineage commitment. PPA inhibits the pro-neural pioneer transcription factor ASCL1 that cooperates with nBAF to reshape chromatin architecture and skews the profile of HATs and HDACs associated with NSC self-renewal and differentiation. PPA upregulates HDAC1 and HDAC3, which are hallmarks of stemness, neurodegeneration and neurotoxicity, but suppresses HDAC4, SIRT1, KAT6A and CREBBP, which are critical for neuronal maturation and function. Moreover, PPA inhibits the MECP2 pathway that modulates epigenetic state by controlling chromatin structure, miRNA processing and RNA splicing via interactions with CCTF, cohesin, Drosha and RNA binding proteins. Concurrently, PPA suppresses the RISC complex that governs miRNA profiles and perturbs the regulatory hub between MECP2, SIRT1, CREBBP, HDAC3 and HDAC4 that maintains energy homeostasis and facilitates metabolic reprogramming during development. This data reveals an inhibition of epigenetic remodelling that shapes the PPA transcriptome, leading to an immature epigenetic landscape with the potential to disrupt NSC differentiation, metabolism, morphology and survival.

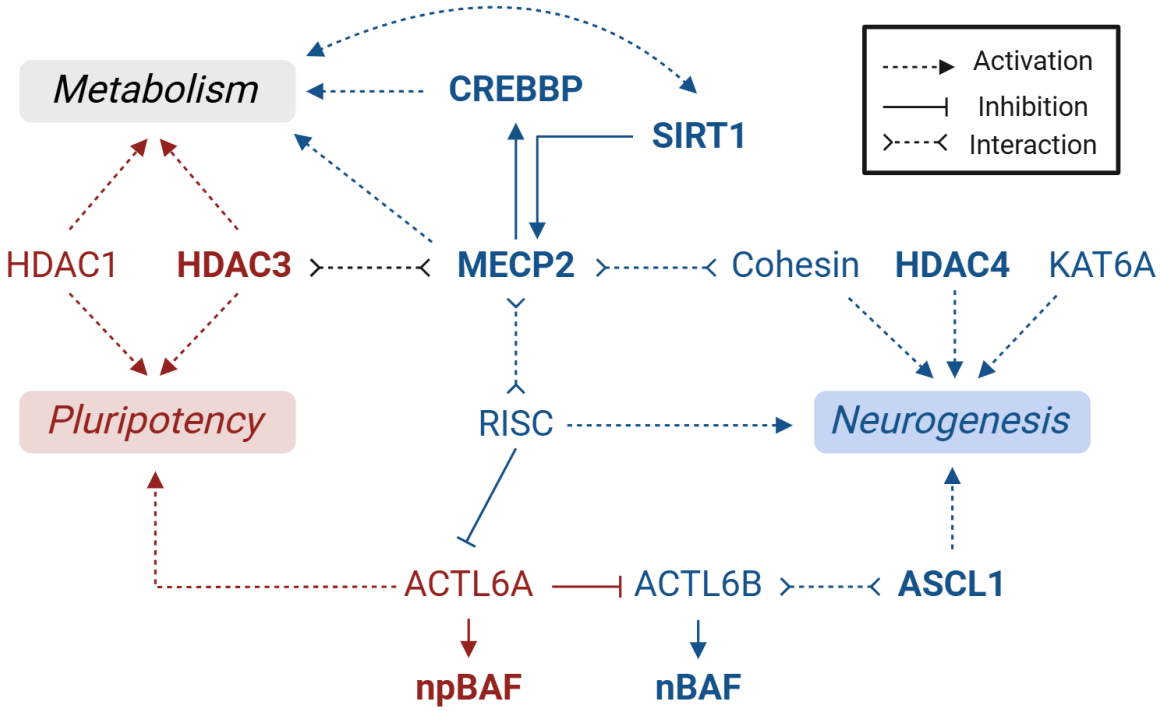


Figure 4.23. Transcriptional Signatures of Epigenetic Remodelling. Propionic Acid (PPA) increased the expression of epigenetic signatures associated with pluripotency, downregulated epigenetic regulators of neurogenesis and perturbed central epigenetic regulators of metabolic state. HDAC1 and HDAC3 interact to drive proliferation and pluripotency. MECP2 is regulated by SIRT1, and directly promotes the expression of CREBBP, forming an epigenetic network that modulates metabolic state. MECP2 also interacts with HDAC3 and cohesin complexes to remodel chromatin structure as well as RNA-binding protein complexes that drive miRNA processing and mRNA splicing. The switch from the npBAF to the nBAF complex is driven by distinct miRNAs that inhibit *ACTL6A,* leading to an upregulation of *ACTL6B*. Interactions between the nBAF and ASCL1 modulate chromatin structure in conjunction with neurogenic HATs like KAT6A and HDACs, like HDAC4. Epigenetic regulators in blue are downregulated by PPA, red denotes upregulation and bold highlights significantly enriched upstream regulators in the PPA transcriptome. ASCL1 = Achaete-Scute complex homolog 1; CREBBP = CREBP binding protein; HDAC = histone deacetylase; KAT6A = lysine acetyltransferase 6A; MECP2 = methyl CpG binding protein 2; npBAF = neuronal progenitor BAF complex; nBAF = neuronal BAF complex; RISC = RNA Induced Silencing Complex; SIRT1 = sirtuin 1.

4.4.2. Intrinsic Signatures of Developmental Delay

The integrated disruptions to epigenetic state induced by PPA could have far-reaching consequences for the complex, dynamic and tightly regulated patterns of gene expression that drive neurogenesis. In fact, transcriptional networks associated with pluripotency were among the most robustly activated pathways in the PPA transcriptome, underpinned by a broad dysregulation of neurogenic signalling. IPA revealed that PPA significantly upregulated Notch signalling, suppressed the Wnt/β-catenin cascade and dysregulated the Wnt/Shh pathway involved in axon guidance. Moreover, the most significantly activated pathways identified by IPA converged on non-canonical Wnt signalling, which was reflected by an activation of downstream effectors involved in PI3K, mTOR and CREB signalling and an inhibition of the negative regulators modulated by AMPK and PTEN. Indeed, canonical effectors of

Notch (*NOTCH2*, *HES1),* Wnt (*CTNNB1*, *TCF7, TCF7L2, TCF4*), Shh (*GLI1*) and TGF-β (*TBX2/3, SMAD3*) signalling emerged as significantly enriched regulators in the PPA transcriptome, several of which were also implicated as central modulators of cell fate (*TBX3, SMAD3, NOTCH2, HES1*). Moreover, targeted overlays validated disruptions to Notch, Wnt, Shh and TGF-β signalling in response to acute PPA exposure (Kim *et al.,* 2019) while neurotoxic signatures in the PPA transcriptome converged on molecular hubs governed by *SMAD3* and *TBX3*.

This data is consistent with several preclinical studies that have revealed disruptions to Notch (Kim *et al.,* 2019), Shh (Rahi *et al.,* 2021), PI3K/mTOR (Aarti Sharma, Bhalla, and Mehan 2022; Abdelli, Samsam, and Naser 2019; Lagod, Abdelli, and Naser 2024) and CREB (MacFabe *et al.,* 2007; Nankova *et al.,* 2014) signalling under PPA stress, but highlights novel disruptions to Wnt/β-catenin and TGF-β signalling that may impair the RA-BDNF neurogenic program. Moreover, aspects of the PPA transcriptome also reflect the reciprocal interplay between neurogenic and metabolic signalling described in Chapter 1. The upregulation of Notch signalling and glycolysis is consistent with an immature metabolic state marked by decreased ETC activity. On the other hand, disruptions to Wnt, AMPK and CREB signalling converge on the relationship between Wnt and mTOR signalling that is governed by mitochondrial function. Thus, the PPA transcriptome reveals a systemic dysregulation of neurogenic pathways that are modulated by metabolic state.

Importantly, *TBX3* and *GLI1* emerged as the top two DE regulators in the PPA transcriptome with essential roles in neurodevelopment. *TBX3* is a transcriptional repressor modulated by Shh, TGF-β and BMP signalling, while *GLI1* is the canonical regulator of Shh signalling that functions as a transcriptional activator for Shh targets but becomes a transcriptional repressor upon proteolytic cleavage (Sigafoos, Paradise and Fernandez-Zapico, 2021). As such, both genes have diverse regulatory roles in stem cell proliferation, lineage commitment, migration, morphogenesis and patterning (Lüdtke *et al.,* 2016; Quarta *et al.,* 2019; Lee *et al.,* 2020; Sigafoos, Paradise and Fernandez-Zapico, 2021). Interestingly, an inverse relationship between gene expression and network activation was observed for both *TBX3* and *GLI1,* which reflects their role as transcriptional repressors. Here, PPA decreased *TBX3* expression 2.3-fold but upregulated TBX3 targets more than 5-fold, suggesting an inhibition of TBX3-dependent transcriptional repression. Conversely, a 3.6-fold increase in *GLI1* expression was associated with a roughly proportional -3.3 inhibition score for GLI1 targets under PPA stress, suggesting that the protein derived from *GLI* mRNA undergoes proteolytic cleavage to produce the GLI repressor. Thus, PPA upregulated the canonical Shh repressor while inhibiting downstream Shh targets, indicating a suppression of Shh signalling that significantly reshapes the neurogenic transcriptome. Notably, the Shh pathway is well known for its critical role in patterning and development, but it also modulates synaptogenesis, neurotransmission, redox homeostasis and neuroimmune state during neurogenesis (Prajapati, Mehan and Khan, 2023). In fact, an inhibition of Shh signalling during neurodevelopment is associated with impaired neurogenesis, excitotoxicity and neuroinflammation and is implicated in a

variety of neurodevelopmental and neurodegenerative disorders, including ASD (Prajapati, Mehan and Khan, 2023). Moreover, *in vivo* studies have found that upregulating Shh signalling mitigates morphological and behavioural impairments induced by PPA (Rahi *et al.,* 2021), demonstrating an important role for Shh signalling in PPA-associated neurotoxicity.

Likewise, disruptions to TGF-β signalling were centrally implicated in the neurotoxic response to PPA. As well as inhibiting the expression of TBX3, PPA significantly downregulated the expression of *SMAD3* - the transcriptional activator primarily responsible for TGF-β dependent transcriptional regulation (Hiew *et al.,* 2021). Interestingly, *SMAD3* emerged as the top hub gene among upstream transcriptional regulators and neurotoxic signatures, while *TBX3* was the top hub gene implicated in both acute and chronic responses to PPA and both *TBX3* and *SMAD3* were top 10 hub genes among central cell fate regulators. Moreover, two of the most significantly activated regulatory networks in the PPA transcriptome were those governed by Distal-Less Homeobox 1 (DLX1) and Yes1 Associated Transcriptional Regulator (YAP1), both of which directly inhibit SMAD3 transcriptional activity (Su, Miao and Guo, 2023). Importantly, TGF- β plays a fundamental role in neurogenic signalling by facilitating crosstalk between the Wnt and mTOR pathways (Vallée *et al.,* 2017). On the other hand, YAP1 functions at the interface between TGF-β and Hippo signalling (Jin *et al.,* 2020), and plays a central role in promoting stemness, proliferation, growth, and apoptosis while inhibiting neuronal differentiation, migration and morphogenesis (Sahu and Mondal, 2021). Collectively, this data suggests that PPA-induced disruptions to neurogenesis may be driven by integrated disruptions to Shh, TGF-β and Hippo signalling facilitated by TBX3, GLI1, SMAD3 and YAP1.

As well as intrinsic disruptions to developmental signalling, PPA may also remodel extrinsic factors that govern neuronal morphogenesis. IPA demonstrated a synergistic activation of the β-catenin-independent and Ca^{2+} -dependent Wnt pathways, as well as GPCR, eicosanoid and gustation signalling. Together, these pathways converge on the PI3K, PLC, PKC and calcineurin cascades that regulate transcription in response to morphogens, neurotrophins, neurotransmitters and attraction/repulsion cues in the ECM. Of note, the BDNF-induced neurogenic programme is driven by RTKs that catalyse PI3K-mTOR, PLC and RAS/RAF signalling (Wang, Kavalali and Monteggia, 2022). Similarly, transmembrane receptors like integrins, syndecans and cadherins mediate interactions between cells in the ECM via PI3K, PLC and JNK signalling (Novoseletskaya, Evdokimov and Efimenko, 2023), while the PI3K, PLC and PKA pathways can also be activated by NMDARs (Lee and Silva, 2009), cytokine receptors (Shao *et al.,* 2022) or FFARs (Falomir-Lockhart *et al.,* 2019) in the plasma membrane. In this way, non-canonical Wnt signalling functions at the interface between extracellular signals and transcriptional regulators that modulate morphogenesis, communication, adaptation and survival (Rosso and Inestrosa, 2013).

Considering the broader transcriptional landscape associated with PPA exposure, the upregulation of non-canonical Wnt signalling may result from glutamatergic excitotoxicity, inflammation, ECM remodelling or FFAR activation. In fact, preclinical studies have demonstrated a central role for FFAR signalling in PPA-induced neurotoxicity. Nankova *et al.,* (2014) previously demonstrated a transcriptional upregulation of cAMP/CREB signalling in PC12 neurons exposed to PPA, proposing that this signature was underpinned by FFAR activation. Studies in hippocampal neurons have shown that PPA impairs dendritic spine density by upregulating ERK/MAPK signalling (Choi *et al.,* 2020), while both *in vitro* and murine models revealed an upregulation of PI3K/AKT signalling in response to PPA driven by the FFAR3-dependent inhibition of PTEN (Abdelli, Samsam and Naser, 2019; Lagod, Abdelli and Naser, 2024). Moreover, the neurochemical and behavioural deficits associated with PPA exposure can be mitigated by targeting CREB (Alhusaini *et al.,* 2020; Khera *et al.,* 2022; Sharma, Bhalla and Mehan, 2022; Kumar *et al.,* 2025), ERK/MAPK (Tiwari *et al.,* 2021) or PI3K/AKT/mTOR (Sharma, Bhalla and Mehan, 2022) signalling *in vivo*. Notably, hyperactive PI3K/AKT/mTOR signalling is a molecular hallmark associated with ASD that impairs synaptogenesis and leads to neuroinflammation, oxidative stress and neurodegeneration (Sharma and Mehan, 2021). Indeed, PI3K/mTOR hyperactivity induced by PTEN deletion is an established model for syndromic ASD, that has been shown to disrupt the migration, differentiation and activation of neurons, astrocytes and microglia, leading to increased synaptic pruning, extreme macrocephaly, neuronal hypertrophy, ectopic axonal projections and ASD-associated behaviours in preclinical models (Kwon *et al.,* 2006; Wen *et al.,* 2013; Sarn *et al.,* 2020). Thus, convergent disruptions to non-canonical Wnt signalling induced by PPA may reflect FFAR activation that drives neurotoxic mechanisms implicated in ASD, with functional consequences for neuronal differentiation and morphogenesis.

Ultimately, this discussion demonstrates a systemic dysregulation of intrinsic and extrinsic regulators of neurodevelopment under PPA stress **(Figure 4.24).** PPA upregulates the Notch pathway that drives pluripotency, inhibits the canonical WNT/β-catenin pathway required for differentiation and broadly dysregulates the non-canonical WNT signalling that regulates transcription in response to extracellular signals. Moreover, PPA suppresses the Shh-GLI pathway that governs polarisation and patterning, inhibits the TGF-β/Smad cascade that drives synaptogenesis and upregulates the Hippo-YAP1 pathway that promotes cell growth, stemness and proliferation. Together, this data demonstrates that the epigenetic signatures associated with pluripotency described in **4.4.1** are reflected by an immature transcriptional landscape that inhibits intrinsic regulators of neurodevelopment, morphology and function.

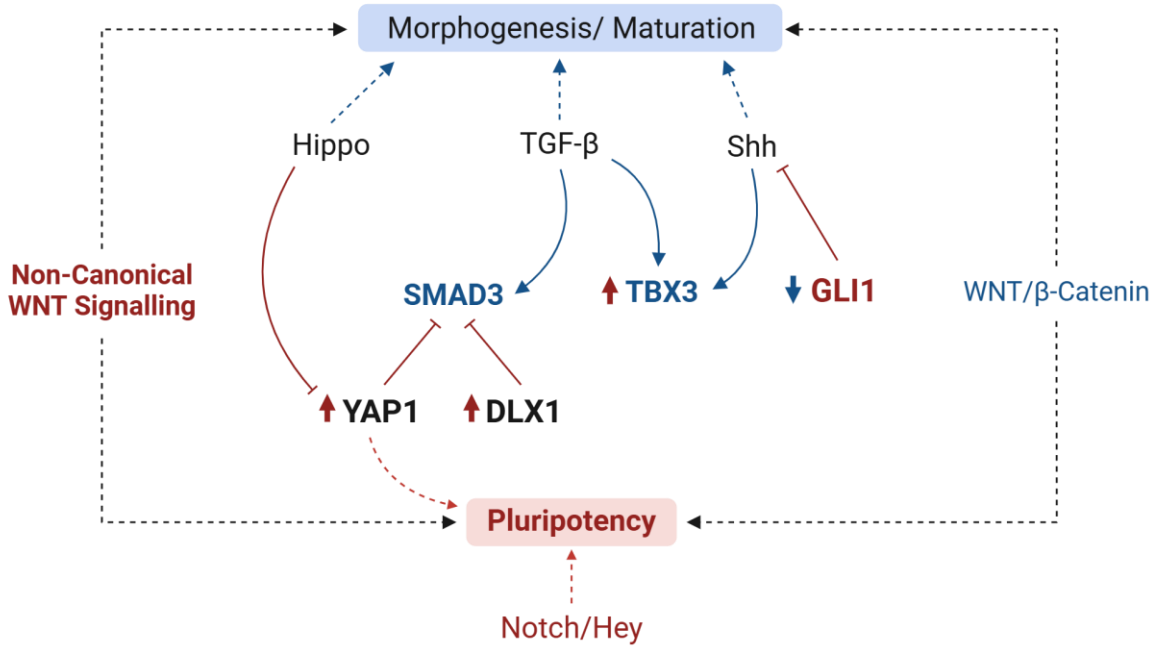


Figure 4.24. Intrinsic Signatures of Developmental Delay. Propionic Acid (PPA) significantly altered signalling pathways and transcriptional networks that regulate proliferation, differentiation and morphogenesis. Notch signalling was significantly upregulated under PPA stress (Notch 1; Z = 1.60, p = 5.52E-03; Notch 3; Z = 1.61; p = 6.23E-03; Hey; Z = 0.85, p = 2.19E-04) along with transcriptional signatures of pluripotency (Z = 2.21, p = 3.31E-03). PPA downregulated the Wnt/β-catenin pathway (Z = -1.73, p = 5.53E-03) and activated non-canonical Wnt signalling (Z = 2.41, p = 1.44E-05). The significant upregulation of GLI1 was accompanied by an inhibition of GLI1 target (Z = -3.28; p = 6.16E-18) while the downregulation of TBX3 was associated with an activation of TBX targets (Z = 5.22, p = 2.67E-20). The decrease in SMAD3 expression was associated with a significant activation of SMAD3 suppressors DLX1 (Z = 2.15, p = 9.19E-05) and YAP1 (Z = 2.61, p = 1.56E-09) in the PPA transcriptome. Together, the significant inhibition of GLI1 targets and the activation of TBX3 targets reflects an inhibition of hedgehog (Shh) signalling while the inhibition of SMAD3 and the activation of DLX1 and YAP1 indicates a suppression of TGF-β and Hippo signalling. Blue denotes downregulation, red denotes upregulation, arrows indicate network activation (red) or inhibition (blue) and bold represents $|Z| \geq 2$. DLX1 - distal-less homeobox 1; GLI1 - glioma-associated oncogene homolog 1; TBX3 - T-Box Transcription Factor 3; SMAD3 - SMAD Family Member 3; YAP1 - yes-associated protein 1.

4.4.3. Integrated Disruptions to Cell Fate and Function

Thus far, the PPA transcriptome has revealed synergistic disruptions to epigenetic and transcriptional remodelling that could have implications for neuronal metabolism and maturation. In fact, functional signatures associated with proliferation, metabolism, apoptosis and inflammation suggest convergent disruptions to neuronal fate and function that could have neurotoxic consequences. Importantly, neurodevelopment is governed by a careful balance between NSC self-renewal, differentiation and programmed cell death that determines the composition, connectivity and plasticity of neuronal networks (Chung and Yu, 2013). Moreover, NSC fate is tightly coupled to metabolic and oxidative state and this relationship is mediated by an interplay between metabolic, neurogenic and stress-responsive signalling (Hwang, Tang and Paik, 2021; Scandella *et al.,* 2023). Notably, the PPA transcriptome revealed a coordinated upregulation of cell cycle progression, glycolysis, and apoptosis, while

integrated disruptions to carbohydrate and lipid utilisation were associated with signatures of neuronal injury, inflammation and excitotoxicity. Together, this illustrates convergent disruptions to NSC homeostasis driven by interdependent networks that govern proliferation, metabolism and survival.

In particular, significantly enriched upstream regulators in the PPA transcriptome converged on interdependent transcriptional networks governed by FOXO3, STAT3 and p53. FOXO3 is an essential regulator of NSC self-renewal, metabolism and differentiation that couples cell cycle exit to metabolic remodelling (Santo and Paik, 2018; Liu *et al.,* 2024). As such, FOXO3 dysregulation is widely implicated in neuropsychiatric and neurodegenerative disorders (Santo and Paik, 2018; Hu *et al.,* 2019; Liu *et al.,* 2024). FOXO3 facilitates cell cycle arrest at the G1/S and G2/M checkpoints by upregulating cell cycle inhibitors (Fasano *et al.,* 2019; Ludikhuize and Rodríguez Colman, 2021) and suppressing the expression of FOXM1, a master cell cycle regulator that drives cell cycle progression (Xue *et al.,* 2010; Fasano *et al.,* 2019). On the other hand, FOXO3 governs mitostasis and substrate utilization by binding directly to mtDNA (Liu *et al.,* 2024) and coordinating with the AMPK, CREB, HIF1α and PPAR axes that shape metabolic state (Fasano *et al.,* 2019). Notably, FOXO3 was one of the most significantly inhibited regulators in the PPA transcriptome that was also implicated as a top hub gene among central cell fate regulators, canonical metabolic genes and neurotoxic signatures. Likewise, WGCNA identified FOXM1 as one of the top regulators of cell cycle progression under PPA stress, while IPA showed that FOXM1 was among the most significantly activated regulators in the PPA transcriptome. Together, this data suggests that the coordinated disruptions to proliferation and metabolism induced by PPA may be driven by a dysregulation of the FOXO3 / FOXM1 cascade.

Indeed, PPA significantly upregulated FOXM1 targets involved in proliferation and mitosis, including the CDKs 1 and 2, Cyclins A, B and D, AURKB, E2F transcription factors and the APC/C that regulates the G1/S and G2/M transitions. Moreover, previous studies have shown that PPA significantly upregulates genes involved in cell cycle progression in murine-derived neuronal cultures (Nankova *et al.,* 2014), while promoting stem cell proliferation in human NSCs (Abdelli, Samsam and Naser, 2019; Yang *et al.,* 2020). Importantly, RA and BDNF mediate cell cycle exit by inhibiting the CDK2/ Cyclin E and the CDK1/Cyclin B complex that drive the G1/S and G2/M transitions respectively (Chen and Ross, 2004; Qiao *et al.,* 2012; Ovejero-Benito and Frade, 2013). Thus, PPA may attenuate the cell cycle exit specifically induced by RA and BDNF in the SH-SY5Y system by disrupting the modulation of G1/S and G/2M checkpoints by FOXO3 and FOXM1 during neurogenesis.

The switch from self-renewal to differentiation substantially alters bioenergetic state while metabolic and redox homeostasis are tightly coupled to NSC fate (Scandella *et al.,* 2023). Accordingly, signatures of proliferation in the PPA transcriptome were associated with a dysregulation of mitochondrial dynamics, morphology and trafficking as well as systemic disruptions to substrate utilisation. In particular, IPA demonstrated a remodelling of the MECP2, AMPK, CREB, HIF-1α and PPAR axes that

coordinate with FOXO3 to shape metabolic state during development. Here, PPA upregulated the CREB pathway governs glucose utilisation, Ca^{2+} homeostasis, mitostasis and neuroplasticity in response to BDNF (Attoff *et al.,* 2020). On the other hand, PPA suppressed the transcriptional program that ties cholesterol synthesis to vesicle transport and secretion via SREBP signalling, which is essential for neurite outgrowth, dendrite complexity, synaptic vesicle cycling and neurotransmission (Chen *et al.,* 2017). Together, this data is consistent with the biochemical signatures of PPA exposure described in Chapter 2, reflecting an erosion of metabolic flexibility and disruptions to the tightly coupled mechanisms that modulate mitostasis and bioenergetic state.

Interestingly, STAT3 also emerged as a central orchestrator of cell cycle progression and metabolism under PPA stress. STAT3 was one of the most significantly activated regulators in the PPA transcriptome, which was reflected by an upregulation of STAT3 signalling and the upstream RAS/RAF, ERK/MAPK, PKA and p38 cascades that comprise the S100, gustation and GPCR pathways. Notably, Chapter 2 discussed several lines of evidence for STAT3 signalling in the response to PPA, highlighting the established role for STAT3 as a focal metabolic regulator (Macias *et al.,* 2014; Yang and Rincon, 2016; Tošić and Frank, 2021) to propose that PPA-induced transcriptional remodelling may be STAT3-dependent. In fact, STAT3 also functions as a central regulator of pluripotency, proliferation, differentiation, inflammation and neuroprotection (Carbognin *et al.,* 2016; Faust and Schafer, 2021; Duan *et al.,* 2024). STAT3 promotes cell cycle progression through the G1/S and G2/M transitions via interactions with E2F, Cyclin B1, p21, MYC and CDKN1A (Hirano, Ishihara and Hibi, 2000; Sun *et al.,* 2019) and plays an essential role in the metabolic remodelling that facilitates neurogenesis (Su *et al.,* 2020). Intriguingly, *in vivo* models have shown that reversing the STAT3 activation induced by PPA mitigates the associated neurochemical, neurophysiological and behavioural deficits (Khera *et al.,* 2022). Thus, STAT3 hyperactivation may underpin the metabolic and neurological disruptions induced by PPA *in vitro*.

Both FOXO3 and STAT3 converge on stress-responsive signalling that regulates proliferation, autophagy and survival in response to starvation, hypoxia, heat shock, DNA damage, inflammation or oxidative stress (Nicolas *et al.,* 2013; Bernardo, Torres and da Silva, 2023). In fact, the coordinated functions of FOXO3 and STAT3 are critical for the regulation of autophagy, regeneration and survival in response to neuronal injury (You *et al.,* 2015; Fasano *et al.,* 2019; Xu *et al.,* 2023). Signatures associated with stress, injury and inflammation were a defining feature of the PPA transcriptome, exemplified by the upregulation of haemostasis, neuroinflammation and apoptosis. Indeed, the most significantly enriched upstream regulator among PPA-associated genes was TP53, which is canonically involved in the response to genotoxic, hypoxic or oxidative stress (Mendrysa, Ghassemifar and Malek, 2011). Interactions between p53 and FOXO3 modulate mitochondrial metabolism, dynamics and turnover in response to oxidative stress (Fasano *et al.,* 2019), while p53 and STAT3 function synergistically to regulate proliferation, autophagy, apoptosis, inflammation and survival (Murase *et*

al., 2012; Pham *et al.,* 2020; Shi and Jiang, 2021). However, p53 signalling also operates as a master regulator of NSC fate that governs diverse regulatory cascades involved in neuronal differentiation and survival (Forsberg and Di Giovanni, 2014).

Firstly, p53 acts as a point of convergence between Wnt and mTOR signalling, which each mediate p53 degradation via independent mechanisms to modulate NSC fate (Licausi and Hartman, 2018; Qin *et al.,* 2018; Sánchez-Alegría *et al.,* 2018). Likewise, cross-talk between p53, Shh and TGF-β signalling is critical to balance NSC proliferation and quiescence (Dupont *et al.,* 2004; Stecca and Ruiz I Altaba, 2009; Ho and Alman, 2010; Kumar *et al.,* 2015) while the p53/Hippo pathway couples SREBP-dependent lipogenesis to cell growth, division and organ morphogenesis (Aylon and Oren, 2016; Raj and Bam, 2019). In fact, several studies have demonstrated that p53 signalling mediates disruptions to NPC self-renewal, neuronal differentiation and gliogenesis in response to mitochondrial dysfunction (Chatoo *et al.,* 2010; Forsberg *et al.,* 2013; Wang *et al.,* 2013), demonstrating a central role for p53 in mitochondrial-induced neurodevelopmental pathology. In this context, the activation of p53 targets in the PPA transcriptome highlights a neurotoxic response to metabolic stress that may orchestrate the associated disruptions to neuronal proliferation, metabolism and maturation.

Collectively, this discussion describes an interplay between cell cycle arrest, metabolic reprogramming and morphological remodelling that converges on stress-responsive signatures in the PPA transcriptome. NSC homeostasis is maintained by a strict balance between self-renewal, quiescence, differentiation and cell death which is critical to establish neuronal architecture. The PPA transcriptome reflected an upregulation of proliferation and glycolysis, significant disruptions to mitochondrial dynamics and substrate utilisation and emergent signatures of apoptosis, injury and inflammation. This was associated with an inhibition of the FOXO3 pathway that attenuates cell cycle progression via FOXM1 and shapes bioenergetic state via interactions with MECP2, AMPK, CREB, HIF1α and PPARs. Concurrently, PPA upregulated STAT3 and p53 targets, which govern pluripotency, proliferation, metabolism and apoptosis in response to injury or inflammation. Thus, PPA-induced disruptions to neurogenesis may be driven by stress-responsive signalling that impairs neuronal maturation, metabolism and survival via an interplay between FOXO3, STAT3 and p53.

4.4.4. The Interface Between Metabolic and Morphological Remodelling

Chapter 2 highlighted that disruptions to glucose utilisation can impact redox homeostasis, neurochemistry and synaptic signalling while lipid metabolism is critical for the development and complexity of neuronal networks. Indeed, the PPA transcriptome reveals an interdependent relationship between neuronal metabolism, structure and function that underpins PPA-induced neurotoxicity. The relationship between neuronal metabolism and morphology is primarily governed by three complex and dynamic structures at the interface between the intracellular and extracellular environment; namely, the ECM, the plasma membrane and the intracellular cytoskeleton. The ECM is a dynamic network of

proteins and carbohydrates that serves as a scaffold between cells in the parenchyma and plays a critical role in neuronal development, elongation, organisation and connectivity (Long and Huttner, 2019). Amounting to 20% of total brain volume, the ECM functions as an important regulator of neuronal proliferation, differentiation, adhesion, migration and survival (Mohan, Edamakanti and Pathak, 2023). In the brain, the ECM is formed from i) a basement membrane of collagen, laminin and fibronectin that constitutes the blood-brain barrier; ii) perineuronal nets between dendrites and cell bodies comprised of fibrous proteins, proteoglycans, glycoproteins and glycosaminoglycans (GAGs); and iii) a porous interstitial matrix of glycoconjugates in between cells in the parenchyma (Shabani *et al.,* 2021).

Importantly, glucose and AAs provide the obligatory substrates for the biomacromolecules that comprise all three layers of the ECM, and the precise composition of the ECM microenvironment is critical to regulate neuronal development, morphology and function (Hayes and Melrose, 2021). Conversely, the molecular and mechanical properties of the ECM profoundly influence intracellular metabolic state and mitochondrial dynamics via the PI3K, ROCK/RhoA, AMPK and TGF-β cascades (Ge *et al.,* 2021; Zhang *et al.,* 2024). The biochemical relationship between ECM mechanics and cholesterol synthesis modulates the composition, viscosity and tension of the plasma membrane (Liao, Li and Liu, 2023), which governs the formation and organisation of nascent synapses (Westra, Gutierrez and MacGillavry, 2021). Likewise, ECM composition is coupled to cytoskeletal remodelling via integrin receptors, which modulate the Rho GTPase and Wnt planar cell polarity (PCP) pathways that shape actomyosin dynamics (Ge *et al.,* 2021). In this way, ECM assembly, organisation and turnover functions at the interface between the metabolic and morphological remodelling that drives neurogenesis **(Figure 4.25).**

ECM integrity relies on a tight balance between stability and plasticity, while the capacity for dynamic remodelling is a defining feature of both the plasma membrane and the intracellular cytoskeleton that is essential for their diverse functions in neurodevelopment, physiology and disease (Di Giaimo *et al.,* 2020). This capacity is largely reliant on the endosomal trafficking system, which facilitates the post-translational processing, assembly, presentation and recycling of ECM biomacromolecules, cytoskeletal proteins and membrane lipids (Steketee and Goldberg, 2012). Endocytic recycling also directly drives neuronal polarisation, elongation and migration through cycles of adhesion and detachment between nascent growth cones (Camblor-Perujo and Kononenko, 2022). Moreover, extracellular vesicles facilitate interactions between cells and the ECM that determine neuronal position, identity and connectivity, while the synthesis, loading, release and recycling of synaptic vesicles is intrinsically coupled to endosomal dynamics (Bahram Sangani *et al.,* 2021). Notably, both endocytic and secretory vesicle trafficking rely on interactions between the cytoskeleton and plasma membrane mediated by Rab GTPases (Di Giaimo *et al.,* 2020). Thus, tightly coupled mechanisms that govern ECM, cytoskeletal and plasma membrane remodelling modulate both the intracellular and extracellular landscapes that shape the developing brain.

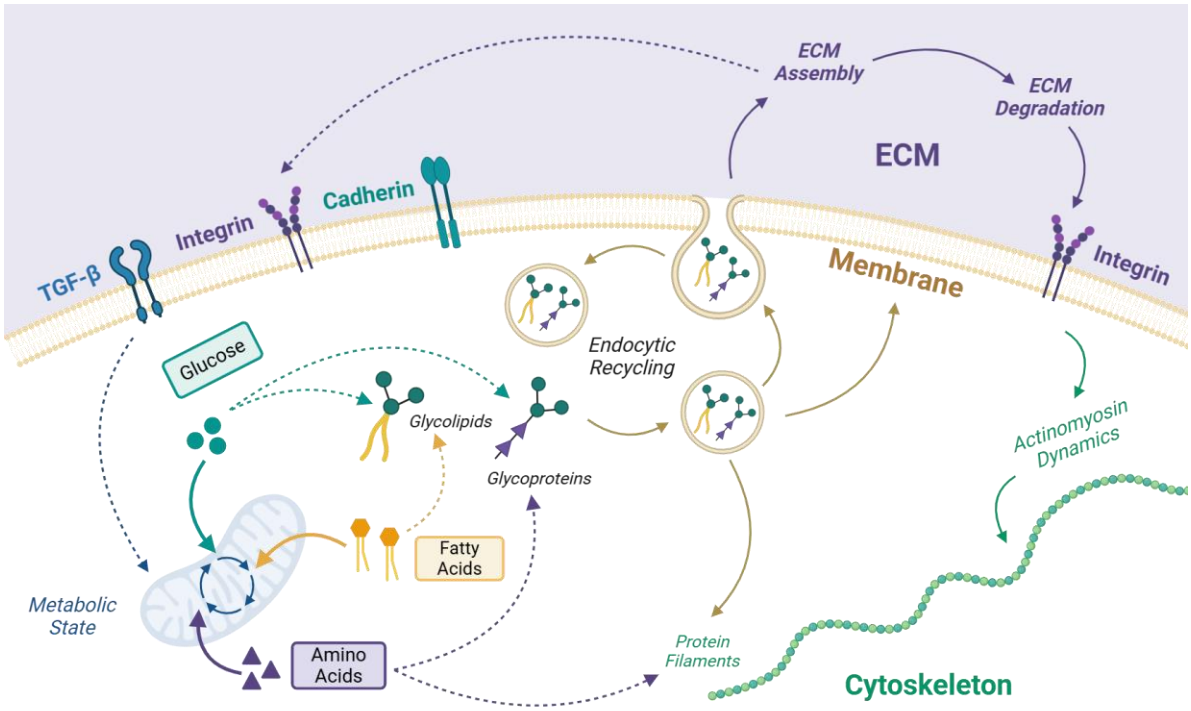


Figure 4.25. The Interplay Between Metabolic and Morphological Remodelling. Neuronal morphology is governed by an interplay between the extracellular matrix (ECM), the plasma membrane and the intracellular cytoskeleton. Distinct profiles of substrate utilisation modulate the balance between energy production and biosynthesis required to produce the glycolipids and glycoproteins that comprise the ECM. The composition, mechanics and plasticity of the ECM regulates intracellular signalling cascades via integrin, TGF-β and E-cadherin receptors, which in turn, modulate neuronal polarisation, actomyosin dynamics and metabolic state. The distribution of attraction and repulsion cues in the ECM determines the balance between synaptic elongation and pruning, while the composition of the plasma membrane and the cytoskeleton determines the structure and stability of axons and synapses. In this way, metabolic reprogramming is coupled to the morphological remodelling that shapes neural architecture during development.

In this context, the disruptions to ECM organisation, cytoskeleton dynamics and endocytic recycling induced by PPA emerge as neurotoxic signatures with profound implications for neuronal morphology and connectivity. Firstly, transcriptional signatures suggested that the perturbations to glucose metabolism significantly altered the synthesis and recycling of the neuronal *glycocalyx*, comprising the proteoglycans, glycoproteins and glycolipids that mediate cell surface interactions with the extracellular environment (Dwyer and Esko, 2016). Pairwise DGE analysis demonstrated a significant upregulation of GAG metabolism that played a central role in determining cell fate, while WGCNA and IPA demonstrated congruent disruptions to glycosylation, glycogen metabolism and GAG homeostasis under PPA stress. Notably, these glycoconjugates exhibit highly specific spatiotemporal expression profiles during development, and disruptions to glycosylation are implicated in a variety of neurodevelopmental and neuropsychiatric disorders, including ASD (Dwyer and Esko, 2016). In fact, *in vivo* models for ASD have demonstrated altered glycosylation patterns across glycoconjugates implicated in ECM remodelling, axon guidance, neuronal injury repair and maturation (Liu *et al.,* 2022).

Chapter 2 described the biochemical landscape of PPA exposure that systemically disrupts glucose utilisation with profound consequences for bioenergetic state. Here, transcriptional signatures indicate a relationship between glucose metabolism and ECM remodelling that could impair synaptogenesis under PPA stress. As well as broadly upregulating the synthesis and turnover of ECM glycoconjugates, PPA significantly upregulated genes involved in the synthesis of chondroitin and dermatan proteoglycans (CS and DSPGs); these function as attraction and repulsion cues in the ECM that modulate the induction, elimination and stabilisation of synapses (Shabani *et al.,* 2021). However, CSPGs inhibit neurite migration, elongation, adhesion and plasticity by disrupting BDNF-Trkβ (Mencio *et al.,* 2021) and ROCK/RhoA signalling *in vitro* (Galindo *et al.,* 2018). Moreover, an overproduction of CSPGs is a response triggered by neuronal injury as part of a neuroinflammatory cascade that drives glial scar formation and astrogliosis (Hayes and Melrose, 2021). Thus, perturbations to the ECM glycocalyx not only have implications for neuronal morphology and maturation but also for the regulation of neuroimmune state under PPA stress.

Importantly, the PPA-induced disruptions to ECM organisation were not limited to its composition. IPA revealed a profound dysregulation of ECM assembly, degradation and recycling underpinned by an upregulation of the endocytic trafficking system. In fact, WGCNA highlighted impairments to synaptic vesicle cycling driven by disruptions to cholesterol metabolism, as well as broad perturbations to the biosynthesis, transport, turnover and signalling of membrane phospholipids. Notably, several studies have found that PPA significantly perturbs neuronal phospholipid profiles and *in vitro* (El Ansary *et al.,* 2013) leading to ASD-associated behaviours *in vivo* (MacFabe *et al.,* 2007). This suggests integrated disruptions to lipid metabolism and ECM dynamics that could impact synaptogenesis by i) changing the composition and plasticity of the plasma membrane; ii) changing the composition of the ECM microenvironment; iii) interfering with intercellular communication driven by synaptic signalling; or iv) disrupting the directional neurite outgrowth that relies on endocytic recycling.

Indeed, signatures associated with ECM organisation were associated with a broad dysregulation of cytoskeletal remodelling and synaptogenesis. IPA found that axon guidance signalling was the most significantly enriched pathway in the PPA transcriptome. PPA significantly upregulated Rho GTPase, kinesin, nuclear cytoskeleton and actin nucleation pathways that modulate the assembly and polymerisation of neurite protrusions in response to RTK, GPCR and integrin signalling (Lei *et al.,* 2016). In conjunction, PPA broadly altered the signalling pathways that govern synaptogenesis, including the ROBO/SLIT, RhoA, semaphorin, netrin and reelin pathways that are well-established regulators of cytoskeletal dynamics (Miller and Suter, 2018). Together, this suggests congruent disruptions to the extracellular and intracellular mechanisms that modulate neuronal morphology, driven by integrated changes to ECM composition and metabolic state.

Notably, this data is consistent with the stunted neuronal morphology induced by PPA in Chapter 3, which was marked by long, flat growth cones without complex neurite processes. Although this study did not evaluate how these morphological perturbations might influence neuronal function, the PPA transcriptome does reflect functional impairments reported in other preclinical models of PPA exposure. Chapter 3 highlighted that PPA exposure consistently perturbs neuronal morphology, ultrastructure, organisation and complexity while promoting neuronal injury and degeneration *in vivo* (Sharma, Rahi and Mehan, 2019; Lobzhanidze *et al.,* 2020; Rahi *et al.,* 2021; Baser, Kesli and Ates, 2023; Zhvania *et al.,* 2024). On the one hand, these morphological disruptions may be associated with the aforementioned impairments to epigenetic remodelling, metabolic state, neurogenic signalling, ECM assembly or synaptogenesis evident in the PPA transcriptome. On the other hand, the PPA transcriptome also revealed an upregulation of processes involved in fibrosis and injury repair – including collagen biosynthesis, polymerisation and degradation, fibrin dissolution, integrin interactions and haemostasis. Haemostasis promotes wound healing by upregulating ECM assembly, coagulation and proliferation in response to interactions between degraded ECM fragments and cell-surface integrins (Sharma, Hill and Schwarzbauer, 2023). However, ongoing cycles of injury and repair can lead to a pathological state known as fibrosis, which profoundly alters the composition and tension of the local ECM (Lu *et al.,* 2011). This not only impacts the modulation of axon guidance and synaptogenesis but also significantly impairs organ function (Mercer and Chambers, 2013).

Many of the neurotoxic consequences associated with CNS fibrosis are driven by the coagulation cascade, which promotes oxidative stress, hypercalcaemia, neuroinflammation, proliferation and neurodegeneration ((Manon-Jensen, Kjeld and Karsdal, 2016). In conjunction, coagulation impairs neurite outgrowth, adhesion, ECM integrity and tube morphogenesis by disrupting VEGF, RHOA, PI3K and PLC signalling (Iannucci, Renehan and Grammas, 2020). Interestingly, these mechanisms reflect the neurotoxic signatures in the PPA transcriptome associated with proliferation, elevated cytosolic Ca^{2+}, glutamatergic signalling and neuroinflammation. Indeed, preclinical models have shown that PPA upregulates NSC proliferation (Abdelli, Samsam and Naser, 2019; Lagod, Abdelli and Naser, 2024), increases intracellular Ca^{2+} and neuronal excitability (Ju *et al.,* 2023) and promotes glutamatergic signalling (El-Ansary *et al.,* 2018; Al-Suwailem *et al.,* 2019; Khera *et al.,* 2022; Alsubaiei *et al.,* 2023), neuroinflammation and gliosis (Choi *et al.,* 2018; Abdelli, Samsam and Naser, 2019; González-Cano *et al.,* 2021; Khera *et al.,* 2022; Baser, Kesli and Ates, 2023; Lagod and Naser, 2023; Erdogan *et al.,* 2024). This data reflects the autotoxic loop described in Chapter 1 as a fundamental mechanism in neuropathology that is thought to contribute to ASD neurophysiology and behaviour. While several authors have proposed a relationship between glutamatergic excitotoxicity and neuroinflammation in PPA-induced neurotoxicity (Shultz and Macfabe, 2014; El-Ansary *et al.,* 2017; Khera *et al.,* 2022), the transcriptomic data presented here illustrates how both of these signatures could be underpinned by changes to metabolic state and ECM composition culminating in fibrosis and haemostasis. Thus, the

PPA transcriptome highlights novel mechanisms that may drive changes to neurophysiology, neurochemistry and neuroimmune state that underpin PPA-induced neurotoxicity *in vivo*.

Ultimately, this discussion reveals a molecular signature that validates and explains the disruptions to neuronal morphology observed in Chapter 3. PPA-induced metabolic remodelling contributes to a systemic dysregulation of ECM dynamics, triggering signalling cascades involved in neuronal injury and neuroinflammation. This disrupts the neurogenic cascades that drive cytoskeletal remodelling and synaptogenesis, interferes with the crosstalk between the intracellular and extracellular environment that shapes neuronal architecture and upregulates excitotoxic signalling associated with neuronal hyperactivity, inflammation and oxidative stress. Moreover, the marked impairments to neuronal morphology in conjunction with the systemic dysregulation of monoamine neurotransmission suggests that PPA could substantially influence neurophysiology and function. In this way, the PPA transcriptome not only reflects impairments to neuronal development and physiology but also highlights significant implications for neuronal signalling and function that may influence behaviour, cognition and communication.

4.5. Summary and Conclusions

This chapter employed RNAseq to investigate the neurotoxic mechanisms that alter neurogenesis under PPA stress. The impairments to neuronal morphology and maturation demonstrated in Chapter 3 were validated by i) transcriptional signatures associated with NSC pluripotency and developmental delay; ii) disruptions to focal regulators of neuronal development and patterning; iii) perturbations to ECM assembly, synaptogenesis and cytoskeletal remodelling; and iv) neuropathological signatures associated with neuronal injury and inflammation. Moreover, this chapter identified core mechanisms that inhibit neurodevelopment under PPA stress by disrupting intrinsic and extrinsic regulators of neuronal cell fate **(Figure 4.26).** The PPA transcriptome suggested a dysregulation of the epigenetic remodelling that drives neuronal differentiation, as well as the transcriptional networks that govern neuronal identity, migration and patterning via Notch, Wnt, Shh, TGF-β and Hippo signalling. In particular, PPA perturbed a regulatory hub at the intersection between epigenetic and metabolic reprogramming, converging on interactions between MECP2, FOXO3 and CREBBP that govern metabolic state. Moreover, TBX3 and GLI1 emerged as focal regulators of the PPA transcriptome implicated in the Shh and TGF-β pathways that govern developmental morphogenesis and cell fate decisions.

Consequently, PPA substantially altered the downstream processes that modulate neuronal fate and function by disrupting an interplay between proliferation, metabolism and survival. Here, impairments to FOXO3 and STAT3 signalling appeared to attenuate neurogenic signatures associated with cell cycle exit and metabolic remodelling under PPA stress. In conjunction, PPA activated stress-responsive pathways governed by p53, leading to signatures associated with neuronal injury, inflammation and

apoptosis. Together, this reflects significant impairments to the processes that modulate neuronal proliferation, differentiation and survival underpinned by changes to metabolic state. In fact, transcriptional signatures suggested a remodelling of substrate utilisation that reshaped the extrinsic landscape of the developing brain. On the one hand, disruptions to glucose utilisation altered the composition of the ECM glycocalyx and perturbed GABA/glutamate cycling. On the other hand, impairments to lipid synthesis, trafficking and degradation perturbed endocytic trafficking, synapse assembly and synaptic vesicle cycling. Moreover, the systemic dysregulation of ECM dynamics disrupted axon guidance signalling, impaired cytoskeletal remodelling and upregulated signatures associated with fibrosis, leading to neuroinflammation and excitotoxicity. Ultimately, this illustrates a neurotoxic feedback loop between intrinsic and extrinsic regulators of neurodevelopment that amplifies disruptions to neuronal morphology and survival under PPA stress.

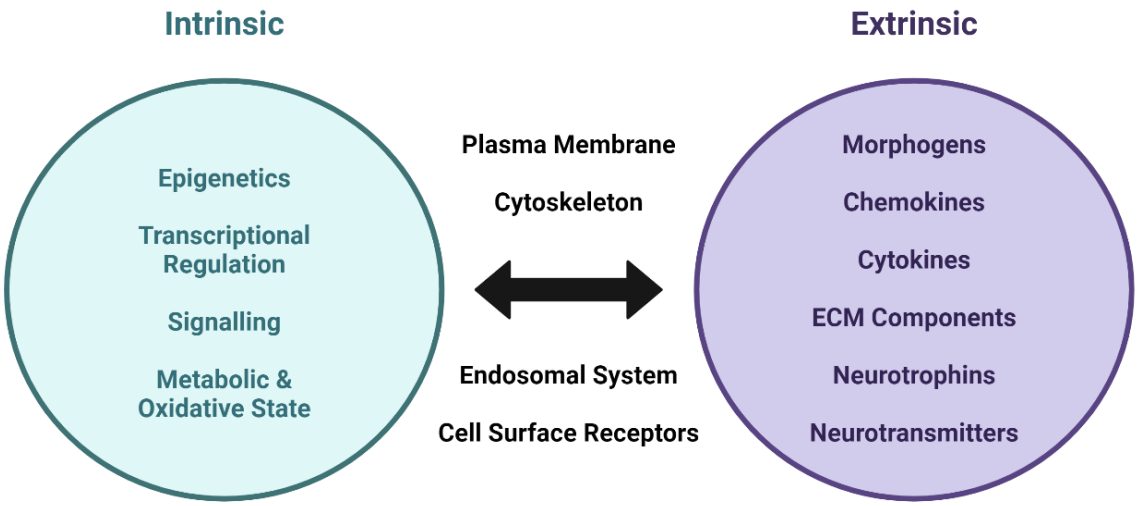


Figure 4.26. Reshaping the Intrinsic and Extrinsic Landscapes of *In Vitro* Neurogenesis. Neurodifferentiation is governed by an interplay between intrinsic and extrinsic factors that shape the neurogenic transcriptome. Propionic Acid (PPA) altered the intrinsic epigenetic and transcriptional regulatory networks that orchestrate the intracellular response to neurogenic signalling pathways. In conjunction, the PPA transcriptome reflected a dysregulation of extracellular matrix (ECM) dynamics and disruptions to the signalling cascades that respond to extrinsic signals like growth factors, morphogens, chemokines and neurotransmitters. Moreover, PPA perturbed processes involved in endosomal trafficking, cytoskeletal remodelling, and plasma membrane plasticity, which function at the interface between the intracellular and extracellular environment to modulate neuronal maturation, synaptogenesis and neurotransmission. Together, PPA appears to reshape both the intrinsic and extrinsic mechanisms that govern neuronal identity, morphology and function during development.

As a transcriptomic dataset derived from a reductionist *in vitro* system, the translatability of this data in a clinical context is inherently limited. The mechanisms highlighted here should be validated in further transcriptomic and proteomic studies to demonstrate functional changes to specific signalling pathways and transcriptional regulators. Moreover, functional studies will be needed to establish how PPA changes metabolic and redox homeostasis, ECM composition, synapse assembly or neurotransmission.

Targeted gene knockdowns could be used to identify necessary and sufficient components of the PPA stress response, while multipotent model systems will be needed to explore how PPA influences the glial functions that shape neuroimmune state. Still, this work has effectively translated the PPA model into an *in vitro* model for neurogenesis to demonstrate and mechanistically characterise PPA-associated neurotoxicity. This chapter has revealed impairments to both intrinsic and extrinsic mechanisms that shape neuronal architecture, and highlighted neurotoxic mechanisms that disrupt neuronal physiology, neurochemistry and neuroimmune homeostasis. Moreover, this work identifies novel target genes that drive the transcriptional response to PPA, highlighting regulatory hubs that mediate crosstalk between metabolism and neurogenesis. Both the *in vitro* model for neurogenesis and the novel transcriptomic dataset developed in this chapter could inform diverse avenues of research into ASD and PPA-induced neurotoxicity. This system can be harnessed to examine novel genes identified in our ongoing cohort work, translating gene association studies into mechanistic studies of neurodevelopment. As our tissue culture capacity expands, this work could play an important role in promoting ASD research in SA and better characterising the unique architecture of NDDs in our population.

Synthesis, Conclusions & Future Directions

This thesis evolved from a growing body of work demonstrating a central role for mitochondrial metabolism in neurodevelopment and disease. Building on molecular signatures of mitochondrial dysfunction in an SA ASD cohort, this thesis examined the mechanistic relationship between neuronal metabolism, morphology and maturation *in vitro.* Chapter 1 described a functional convergence between the metabolic and neurological facets of ASD aetiology that shapes neurodevelopment, physiology and function with direct implications for long-term clinical outcomes. Chapter 2 translated the DNAm signatures in our SA cohort into an *in vitro* model for mitochondrial dysfunction by recapitulating the accumulation of PPA that is associated with a dysregulation of PCCB. Chapter 3 expanded this model in the context of neurogenesis, establishing and characterising a system to study neuronal differentiation *in vitro.* Having demonstrated that PPA induces both mitochondrial dysfunction and developmental neurotoxicity, Chapter 4 examined the transcriptional mechanisms that may disrupt neuronal morphology and maturation under PPA stress. Together, this work provided novel insight into PPA-induced neurotoxicity and highlighted molecular players that underpin the relationship between mitostasis and neurodevelopment. Moreover, this project effectively established a cost-effective, reproducible *in vitro* system to study mitochondrial mechanisms in neuropathology, explore new signatures identified in our cohort or evaluate neuroprotective agents that target mitochondrial function.

Three distinct threads have emerged throughout this thesis, highlighting novel contributions to three ongoing areas of research: i) The SH-SY5Y Model; ii) The PPA Model and iii) Mitochondrial Mechanisms in ASD **(Figure B).** Firstly, this thesis grappled with the utility of reductionist *in vitro* systems to study complex disorders, noting the limited relevance of the neuronally committed SH-SY5Y cell line to understand the highly diverse and interdependent metabolic signatures of different neural subtypes *in vivo.* Nevertheless, the intricate and dynamic mechanisms that govern mitochondrial function are most effectively studied under strictly controlled and reproducible conditions. Given the inaccessible nature of brain tissue, the challenges of ASD cohort recruitment in SA and the resource-constrained context, Chapter 2 introduced the SH-SY5Y model as a cost-effective system in which to ask specific mechanistic questions.

While the SH-SY5Y cell line is widely employed in neurotoxicology and neuropathology research, few authors have considered the cell culture conditions best suited to study metabolic mechanisms in this system. Here, this consideration was addressed by collating and comparing available data from the SH-SY5Y cell line to establish an *in vitro* system that recapitulates a neuronal metabolic profile. Chapter 2 noted that undifferentiated SH-SY5Y cells demonstrate a more oxidative profile than non-neuronal *in vitro* systems but retain a predominantly glycolytic profile under high-glucose conditions. Furthermore, undifferentiated SH-SY5Y cells display an inherently limited mitochondrial capacity that does not reflect the mature neuronal phenotype, as well as an opportunistic metabolic profile that compensates

for mitochondrial dysfunction by enhancing glycolytic flux. Ultimately, this contradicts the oxidative reliance observed in primary neurons which may limit the utility of the undifferentiated phenotype to study mitochondrial dysfunction in neuropathology.

Yet, Chapter 3 noted that more than 75% of respirometric studies in the SH-SY5Y cell line have been conducted using only the undifferentiated phenotype. Moreover, the nature of metabolic remodelling during SH-SY5Y differentiation remains poorly characterised – in fact, no studies have examined how alternative differentiation protocols might influence the metabolic profile of the terminal neuronal phenotype. Based on available respirometric profiles of SH-SY5Y differentiation, Chapter 3 demonstrated divergent metabolic signatures that reflect the emergent and non-emergent properties of SH-SY5Y metabolism. This analysis revealed an intrinsic oxidative shift that increases mitochondrial capacity during SH-SY5Y differentiation. However, differentiation did not inherently reduce glycolytic reliance unless this was enforced with glucose or serum depletion. Importantly, this analysis highlighted that the morphological and molecular markers often used to verify neurodifferentiation *in vitro* may not reflect a mature metabolic profile. In addition, this discussion emphasised a need to consider how basal media, serum supplementation, neurogenic agents and the length of differentiation could differentially influence metabolic state in the SH-SY5Y system.

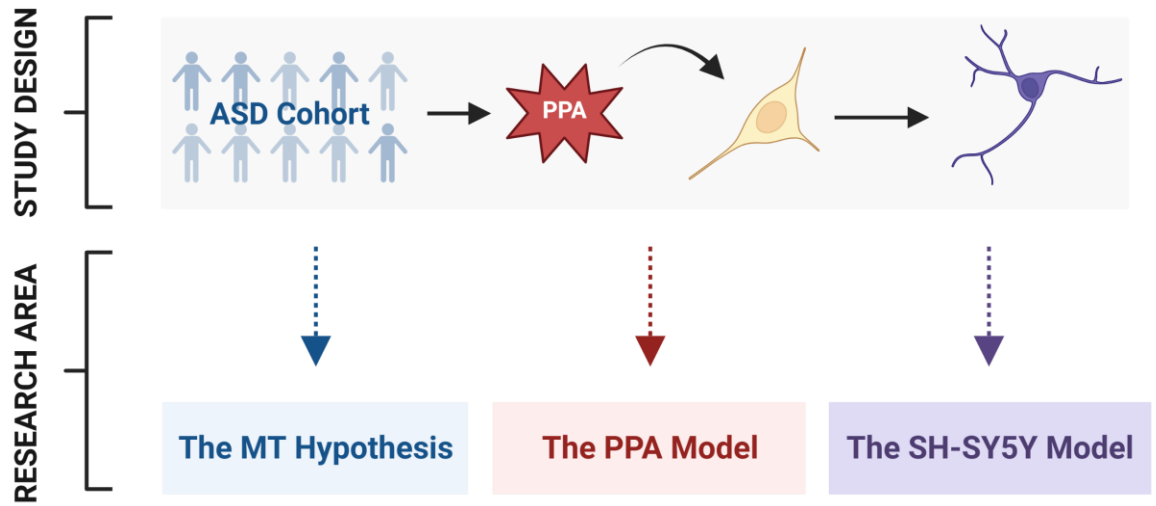


Figure B. Main Considerations and Conclusions Emerging from this Thesis. This study aimed to model signatures of mitochondrial dysfunction observed in an Autism Spectrum Disorder (ASD) cohort in a neuronal-like system. This work provides novel considerations for the use of the SH-SY5Y cell line to study metabolic aspects of neurogenesis and function. Moreover, this study characterised novel features of the propionic acid (PPA) model, demonstrating changes to cell viability, transcription and mitostasis that significantly impaired neurodifferentiation. Here, transcriptomic signatures revealed an interplay between metabolic and morphological remodelling that drives PPA-induced neurotoxicity. Together, this work highlights novel avenues for future research into the mitochondrial component of ASD.

Lastly, Chapter 4 emphasised that *in vitro* studies of neuronal metabolism also need to consider the extent to which metabolic remodelling is reflected in underlying molecular signatures. This chapter

noted a divergence between respirometric, transcriptomic and proteomic profiles of SH-SY5Y differentiation, emphasising that molecular signatures may not always correlate with metabolic activity. Nevertheless, a systemic remodelling of substrate utilisation was indicated on both the transcriptomic and proteomic levels, demonstrating an intrinsic reprogramming of both glucose and lipid metabolism that reflects the shift from NPC self-renewal to differentiation. Both respirometric and proteomic data suggested that BDNF promotes the shift towards an oxidative profile, which is consistent with the mechanisms of action associated with BDNF-induced differentiation. Still, BDNF did not appear to be sufficient to reduce glycolytic reliance under high glucose conditions. Together, this analysis posed an interesting question regarding the relationship between the transcriptional and translational mechanisms that drive metabolic remodelling in the SH-SY5Y model. Moreover, this work reveals a need to better characterise the impact of different neurogenic agents on SH-SY5Y metabolism to identify the conditions best suited to study mitochondrial mechanisms in neurogenesis.

Considering the available literature in its entirety, Chapter 2 established the SH-SY5Y model in the context of oxidative reliance using glucose and serum depletion in conjunction with glutamine and NEAA supplementation. This protocol was able to detect differences in both oxidative and glycolytic metabolism under stress, which is necessary for a comprehensive view of metabolic state. Moreover, undifferentiated cells displayed an oxidative reliance above 90%, which is reminiscent of mature neurons *in vivo*. In Chapter 3, this model was expanded to study neurogenesis *in vitro*. It is widely acknowledged that BDNF is required to promote neurite elongation, branching and survival, but prior data from the SH-SY5Y system suggested that a combined RA-BDNF protocol is better suited than the two-stage approach to model *in vivo* neurodevelopment – particularly for the study of neuropathological mechanisms relevant to ASD aetiology. Moreover, the morphological, molecular and metabolic signatures reported in the literature indicate that SH-SY5Y models of differentiation should combine glucose and serum depletion with both RA and BDNF administration to best recapitulate the metabolic shift that drives neurogenesis.

Accordingly, this study used a nine-day combined RA-BDNF administration protocol in low-serum EMEM: F12 to induce neurodifferentiation. Preliminary live-cell respirometry analysis indicated that this model successfully facilitated an oxidative metabolic shift without enhancing glycolytic activity, which reflects the proteomic and respirometric data previously reported in the same experimental system. Further work will be required to validate and better characterise the metabolic profile associated with this protocol. Nonetheless, this metabolic shift was accompanied by efficient cell cycle exit, successful neurite production, elongation and branching, and an increased β3T: NES ratio that is consistent with neuronal maturation. The decrease in total NES expression as well as the clear shift in NES localisation demonstrated cytoskeletal remodelling in line with expected measures of neuronal differentiation. On the other hand, total β3T expression remained unchanged during neurogenesis,

although β3T area increased significantly, illustrated by the emergence of β3T+ neurite extensions. The dynamic profile of β3T expression during neurogenesis may necessitate the use of an alternative neuronal marker that is absent in undifferentiated cells for future studies. Still, β3T effectively facilitated an analysis of neurite networks to supplement more qualitative assessments of neuron morphology.

Here, image analysis pipelines were successfully established to quantify neurite production, branching and connectivity. However, it remains challenging to develop a fully automated pipeline that correctly distinguishes between neurite processes and cell body outlines. Going forward, advanced techniques using machine learning will be explored as more accurate and objective measures of neurite morphology. Still, the combined manual and autotracing techniques employed here demonstrated consistent and significant increases in neurite abundance, length and complexity which reflected the morphological changes observed with phase contrast microscopy. Indeed, these changes were supported by transcriptomic signatures that revealed an inhibition of proliferation with an upregulation of synaptogenesis, synaptic vesicle cycling and neurotransmitter signalling. Together, this work established a protocol to study SH-SY5Y metabolism in the context of oxidative reliance and developed a differentiation protocol that induced morphological, molecular and metabolic features consistent with *in vivo* neurogenesis.

In this thesis, the SH-SY5Y system described above was harnessed to establish an *in vitro* model for mitochondrial dysfunction marked by changes to mitochondrial dynamics and bioenergetics. It is this work that comprises the second, and most central, thread woven through this thesis pertaining to the PPA model. Chapter 2 introduced PCCB as a DM gene in our ASD cohort at the centre of the methylmalonyl pathway that couples mitochondrial metabolism to DNAm. This chapter described the PPA model that is used to study PCCB dysfunction in preclinical models of PA and is widely employed as an *in vivo* model for ASD. Building on studies that had examined the effect of PPA on cell viability, mitogenesis, mitophagy and apoptosis in the SH-SY5Y cell line, this chapter interrogated mitochondrial dynamics, metabolism and function under PPA stress. This work revealed dose- and time-dependent effects on cell viability in conjunction with mitochondrial membrane depolarisation and a systemic dysregulation of the transcriptional mechanisms that govern mitostasis. Here, PPA significantly perturbed eleven central regulators of mitochondrial metabolism and dynamics, highlighting novel molecular mechanisms associated with PPA-induced mitochondrial dysfunction.

In particular, this chapter identified a potential relationship between PPA and *PCCB* transcription that remains understudied. Accordingly, the transcriptional regulation of *PCCB* in response to metabolic stress presents an important target for future research to understand how the DM of PCCB in our cohort might influence PCCB expression and activity. Chapter 2 also highlighted significant disruptions to genes that drive metabolic remodelling during neurogenesis, which could have functional implications for neurodevelopment. Future work will be required to characterise the mechanisms that drive

transcriptional remodelling under PPA stress, and the downstream changes to protein expression, localisation and activity that impact mitochondrial function. However, the transcriptional impairments to mitostasis were reflected by congruent impairments to mitochondrial morphology and metabolism.

Confocal microscopy demonstrated substantial disruptions to mitochondrial network integrity and turnover, while live-cell respirometry revealed deficits in both oxidative and glycolytic energy production that profoundly remodelled metabolic state. This data highlights a novel feature of PPA-induced metabolic stress, which not only inhibits oxidative respiration but also attenuates the compensatory glycolysis that is typically employed by SH-SY5Y cells in response to mitochondrial dysfunction. Thus, the implications for PPA-associated neurotoxicity extend beyond an energetic deficit; instead encompassing diverse processes involved in synaptogenesis, neurotransmission and redox homeostasis that rely on glycolytic intermediates. Indeed, the broader literature suggests that PPA systemically erodes metabolic flexibility by inhibiting OXPHOS, glycolysis and glutaminolysis. Concurrent impairments to CoA buffering and malonyl CoA synthesis may perturb the balance between FAO and lipogenesis while disrupting the volume, composition, connectivity and integrity of mitochondrial networks. In this context, the coupling between mitochondrial dynamics, morphology and metabolic state is a novel target for future research that could yield insight into the diverse mitochondrial deficits associated with the PPA model.

In Chapters 3 and 4, the PPA model was used to study the relationship between mitochondrial dysfunction and developmental neurotoxicity in the SH-SY5Y system. This work revealed morphological and transcriptional hallmarks of neuronal differentiation that were markedly disrupted by metabolic stress. PPA exposure significantly impaired neurite outgrowth, elongation and connectivity and skewed both the expression and localisation of cytoskeletal markers in differentiated cultures. While total cell counts did not indicate changes to cell proliferation or survival, transcriptomic signatures displayed an upregulation of processes involved in both cell cycle progression and apoptosis. Thus, cell counts may have been confounded by altered rates of both cell division and cell death, which could be better detected by markers of senescence or apoptosis in future studies. The decreased β3T: NES ratio induced by PPA was underpinned by transcriptional signatures of pluripotency, reflected by impairments to epigenetic and neurogenic signalling pathways that facilitate neuronal maturation. Likewise, the decrease in neurite length and complexity was associated with transcriptional disruptions to ECM dynamics, axon guidance and cytoskeletal remodelling, as well as impairments to synaptogenesis, synapse assembly and synaptic signalling. Together, this data illustrates an inhibition of neuronal maturation under PPA stress reflected by morphological hallmarks of neurotoxicity and transcriptional signatures of developmental delay.

Although Chapters 2 and 4 explored fundamentally different paradigms of PPA exposure, it is worth noting that convergent mechanistic signatures emerged across both datasets. The acute mitochondrial

membrane depolarisation coupled with significant cytotoxicity observed in Chapter 2 was associated with an upregulation of apoptotic processes in the PPA transcriptome, pointing to the mPTP-mediated apoptosis frequently reported in the PPA model. Likewise, impairments to mitochondrial network integrity were reflected by transcriptional disruptions to genes involved in mitochondrial metabolism, dynamics and turnover, while the changes to autophagic flux observed in Chapter 2 coincided with a transcriptional upregulation of genes involved in phagosome formation. Moreover, the substantial impairments to metabolic state revealed by live-cell respirometry were associated with a systemic remodelling of substrate utilisation in the PPA transcriptome.

Transcriptomic signatures also converged on molecular mechanisms proposed in Chapter 2 as possible mediators of PPA-induced disruptions to mitostasis. For example, the p38/MAPK and STAT3 cascades highlighted in Chapter 2 as PPA-sensitive transcriptional remodellers were found to be transcriptionally upregulated in Chapter 4. The dysregulation of glucose metabolism described in Chapter 2 was reflected by global disturbances to ECM glycoconjugates and GABA/glutamate cycling in transcriptomic signatures. Concurrently, the transcriptional inhibition of histone acetylation and cholesterol synthesis induced by PPA suggests disruptions to CoA cycling that are widely reported in the PPA model and could broadly impair metabolic flexibility. Indeed, the convergent impairments to metabolic flexibility discussed in Chapter 2 were supported by a coordinated downregulation of central epigenetic regulators of metabolic state, as well as genes involved in the integration of energy metabolism and the response to mitochondrial dysfunction.

Further characterising the PPA transcriptome revealed central mechanisms that may perturb neuronal maturation, with several relevant considerations for ASD aetiology. Firstly, transcriptional signatures highlighted potential disruptions to epigenetic state under PPA stress, driven by impairments to the nBAF, cohesin and MECP2 complexes that facilitate chromatin remodelling. In conjunction, HDAC1 and HDAC3 emerged as possible orchestrators of PPA-induced neurotoxicity, while HDAC4, CREBBP, SIRT1 and MECP2 revealed an epigenetic hub required for metabolic remodelling that was suppressed by PPA. Interestingly, the PPA transcriptome suggests disruptions to epigenetic mechanisms that are sensitive to metabolic and oxidative state; for example, changes to TCA cycle flux may alter the intracellular pools of acetyl CoA, NAD^+, αKG, succinate and fumarate that regulate histone acetylation and methylation patterns. Thus, further investigating the relationship between epigenetic and metabolic state in PPA-associated neurotoxicity may yield mechanistic insight into the link between epigenetic and metabolic mechanisms in ASD that remains largely uncharacterised.

These epigenetic signatures of developmental delay were reflected by a transcriptional upregulation of Notch signalling, proliferation and glycolysis, disruptions to the WNT/β-catenin and PI3K/AKT/mTOR cascades and an inhibition of the Shh and TGF-β pathways responsible for developmental morphogenesis. Notably, Chapter 1 highlighted that both Notch and Wnt signalling are modulated by

energetic, redox and Ca^{2+} homeostasis. Therefore, the upregulation of glycolysis and intracellular Ca^{2+} signalling in the PPA transcriptome coupled with significant disruptions to Notch and Wnt signalling may propose a dysregulation of the relationship between metabolic and neurogenic signalling. In fact, the signatures of PI3K/mTOR activation associated with an inhibition of AMPK and PTEN signalling may suggest perturbations to the biochemical crosstalk between the Wnt and mTOR pathways that are separately implicated in ASD. Moreover, PPA appeared to disrupt the balance between neuronal proliferation, metabolism, differentiation and survival via an interplay between FOXO3, STAT3 and p53. Cumulatively, this data indicates impairments to the epigenetic, metabolic and neurogenic signalling pathways that drive neuronal maturation *in vitro,* highlighting neurotoxic signatures associated with metabolic stress that could yield insight into the mitochondrial component of ASD aetiology.

Lastly, a mechanistic relationship between neuronal metabolism, morphology and maturation emerged in the PPA transcriptome. The transcriptional dysregulation of glucose utilisation was coupled with changes to the ECM glycocalyx while impairments to cholesterol synthesis were associated with disruptions to synaptogenesis and synaptic vesicle cycling. Consequently, PPA systemically disrupted processes involved in ECM assembly, degradation and recycling and perturbed pathways involved in axon guidance, neurotransmitter cycling and synaptic signalling. This was reflected by an upregulation of neuronal injury, coagulation and fibrosis, revealing a neurotoxic cascade that inhibits neuron morphogenesis, plasticity and function. Concurrently, PPA upregulated pathways involved in neuroinflammation and glutamatergic excitotoxicity, which reflects the autotoxic loop described in Chapter 1 as a convergent mechanism in neuropathology. Together, this data validates the disruptions to neuronal morphology described in Chapter 3, highlighting underlying mechanisms that may impair neurodevelopment, integrity and survival. Moreover, this work reveals neurotoxic mechanisms that could influence neurophysiology and function by dysregulating the neuroimmune and neurochemical landscapes of the developing brain.

Altogether, Chapters 3 and 4 successfully translated the PPA model in the context of neuronal differentiation, establishing a model for PPA-induced neurotoxicity that can be harnessed for more targeted studies of neurodevelopment and pathology. This work proposes novel mechanisms by which PPA may alter the intrinsic and extrinsic factors that govern neurodevelopment, driven by an interplay between epigenetic, metabolic and morphological remodelling. Validation studies in the SH-SY5Y cell line will be required to demonstrate changes to protein expression and function that mediate changes to epigenetic, metabolic or neuroimmune state under PPA stress. In particular, the transcriptome presented here highlights several targets for future research that could yield insight into the mitochondrial regulation of neurodevelopment. The interplay between metabolic and morphological remodelling proposed by transcriptomic signatures suggests a role for ECM dynamics in PPA-induced neurotoxicity,

which may provide insight into the neurological components of mitochondrial disease. Moreover, further investigating the coupling between lipid metabolism and synaptic vesicle cycling could illustrate a mechanistic relationship that governs neurophysiology, integrity and function under PPA stress.

As neuronally committed progenitors, SH-SY5Y cells cannot be used to study the balance between neuro- and glio-genesis that plays a critical role in neurodevelopment, nor to examine the interactions between neurons, oligodendrocytes and astrocytes that are fundamental for metabolic, redox and neuroimmune homeostasis *in vivo.* This highlights a need to explore multipotent *in vitro* models to comprehensively understand PPA-associated neurotoxicity and its relevance for ASD aetiology. Thus, ongoing work in our group, beyond the scope of this thesis includes; i) establishing a multipotent NSC model to study different metabolic signatures in neurons and glial cells under PPA stress; ii) developing targeted gene knockdown techniques to examine to study how PCCB deficiency specifically impacts neuronal metabolism and function and iii) expanding our cohort work to include RNA sequencing data that will supplement our DNAm signatures to identify novel features of ASD aetiology in the SA population. Together, the PPA model established in this project can be used to inform more complex *in vitro* systems to study the relationship between metabolic and neuroimmune mechanisms in ASD aetiology, mechanistically characterise novel target genes identified in our cohort and explore the efficacy of targeted mitochondrial interventions to mitigate neurotoxicity. In the long term, better characterising the mitochondrial component of ASD could open an avenue of research into the utility of repurposing mitochondrial biomarkers and therapies to diagnose and mitigate neuro- and psychopathology in this context.

Beyond the *in vitro* context, this thesis also highlighted novel avenues for research into mitochondrial mechanisms in ASD more broadly. Chapter 1 described how mitochondria function at the interface between sociological and biological factors that influence quality of life in ASD. The mitochondrial component of ASD aetiology has become increasingly well-recognised just as the concept of MAL has been established in the scientific literature. However, while environmental factors are known to influence clinical outcomes in ASD, the relationship between ASD and MAL remains unexplored. In particular, MAL proposes a novel mechanism that may contribute to psychopathology in ASD by regulating the molecular components of allostatic load. Considering the mitochondrial component of ASD in a broader socio-economic and psychosocial context highlights the utility of mitochondrial psychobiology to advance ASD research in SA. Indeed, characterising the relationship between ASD aetiology and socio-economic stressors in the SA population could be crucial to identify the factors that determine long-term outcomes. Ultimately, using a biopsychosocial approach to understand internal experiences in ASD highlights the novelty of molecular neuroscience that is informed by participatory research practices and emphasises a need to address both social and biological factors that affect clinical outcomes in ASD.

~ APPENDICES ~

Appendix 1

Table S1.1. ASD Molecular Datasets (Taken from Mahony and O'Ryan, (2021))**.** 19 Proteomic, Transcriptomic and DNA methylation datasets collated for analysis, detailing the tissue type, age and gender for the cohort samples used for each study.

Sample	Reference	Cohort
PROTEOMIC ANALYSIS		
Blood	(Shen *et al.,* 2019)	24M and 6F cases (2–6 yrs); age / gender-matched controls
	(Hewitson *et al.,* 2021)	76M cases and 78 M controls (18 months - 8 yrs)
	(Shen *et al.,* 2018)	24M and 6F cases (2–6 yrs) and age / gender-matched controls
	(Yang *et al.,* 2018)	68 cases (mean 12.4 yrs) and 80 age-matched controls (mean 14.3 yrs)
Brain tissue	(Yao *et al.,* 2021)	79 brain tissue samples from 19 cases (2-56yrs) and 17 controls (16-56yrs)
	(Abraham *et al.,* 2019)	9 cases (2-60 yrs) and 9 age- and gender matched controls (1-60 yrs)
TRANSCRIPTOMIC META-ANALYSIS		
Blood	(Tylee *et al.,* 2017)	626 cases and 447 controls (5 ± 3.8 yrs)
	(Mordaunt *et al.,* 2019)	59 cases, 92 non- typically developing, 120 typically developing controls
	(Gao *et al.,* 2021)	96 cases and 42 controls (2-18 yrs)
	(He *et al.,* 2019)	485 cases and 398 controls
	(He *et al.,* 2019)	109 cases and 129 controls
	(Forés-Martos *et al.,* 2019)	34 cases and 130 controls (mean 20.3 yrs)
	(Rahman *et al.,* 2020)	15 cases and 15 controls
Brain tissue	(Wright *et al.,* 2017)	13 cases (3F, 10M; 4 - 67yrs) and 39 controls (9F, 30M; 2- 69yrs)
	(Yao *et al.,* 2021)	79 brain tissue samples from 19 cases (2-56yrs) and 17 controls (16-56yrs)
	(Ramaswami *et al.,* 2020)	82 and 74 samples from 47 case and 44 control brains (28 +/- 17 yrs)
DNA METHYLATION ANALYSIS		
Blood	(Mordaunt *et al.,* 2020)	112M (56 cases;56 controls), 40F (20 cases, 20 controls)
	(Hu *et al.,* 2020)	21 cases and 21 controls (mean 8.4 yrs)
Brain tissue	(Wong *et al.,* 2019)	43 cases (29. +/-18.9yrs) and 38 controls (48.7+/-8.8 yrs)
	(Ramaswami *et al.,* 2020)	56 and 41 samples from 33 case and 26 control brains (34 +/- 15yrs)
Buccal cells	(Stathopoulos *et al.,* 2020)	48M (32 cases and 16 controls, 6–12 yrs)

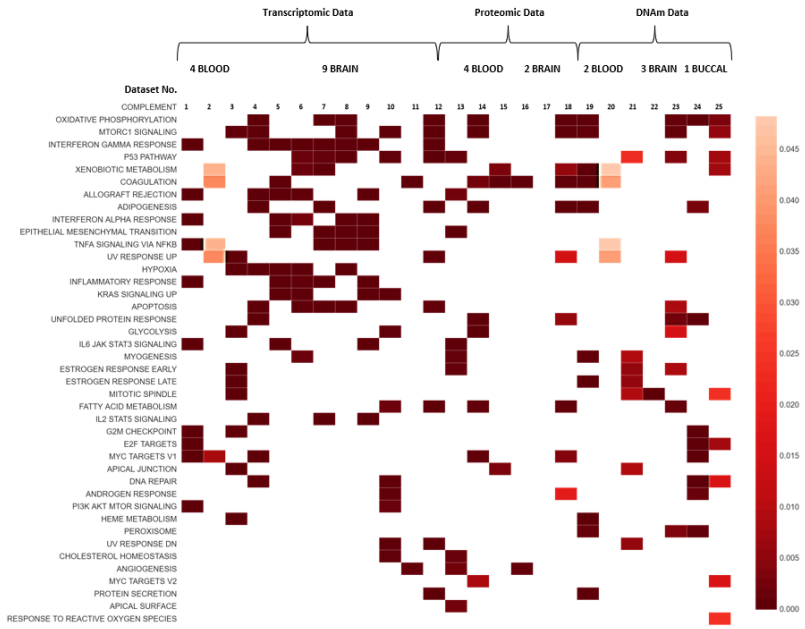


Figure S1.1. Hallmark Enrichment Signatures (Taken from Mahony and O'Ryan, (2021)**).** The top 10 significantly enriched Hallmark canonical pathways in 19 datasets of ASD molecular data where the heatmap represents the FDR value of enrichment.

Table S1.2. An Overview of Hallmark Enrichment Signatures by Tissue Type and Molecular Technique. (Taken from Mahony and O'Ryan, (2021)). Hallmark Enrichment Signatures of 19 ASD molecular datasets are summarised, highlighting canonical pathways that were most consistently implicated in ASD proteomic, transcriptomic, and DNAm datasets from blood and brain tissue. Each independent dataset was annotated with respect to the top ten significantly enriched Hallmark canonical pathways (FDR<0.05); data indicate the number of enrichment signatures implicating each canonical pathway. Pathways in bold = strongly supported using all three molecular approaches: Pathways in italicised = supported by two (of three) molecular datasets. OXPHOS = oxidative phosphorylation; IFN = interferon; EMT = epithelial mesenchymal transition.

Proteomic		**Transcriptomic**		**DNAm**	
Canonical Pathway	**Blood/ Brain**	**Canonical Pathway**	**Blood/ Brain**	**Canonical Pathway**	**Blood/ Brain/ Buccal**
Coagulation	3/2	IFNγ Response	3/6	**OXPHOS**	0/2/1
Complement	3/0	*Complement*	4/4	*P53 Pathway*	1/1/1
OXPHOIS	1/2	**mTORC1**	3/3	Mitotic Spindle	1/1/1
mTORC1	1/2	*P53 Pathway*	2/5	**mTORC1**	0/1/1
Xenobiotic Metabolism	1/2	Allograft Rejection	3/3	*Xenobiotic Metabolism*	1/0/1
Adipogenesis	1/2	IFNα Response	4/4	UV Response Up	1/1/0
Unfolded Protein Response	1/1	TNFa Via NFKB	4/3	*Unfolded Protein Response*	0/2/0
Myogenesis	1/1	Hypoxia	2/3	Estrogen Response Early	1/1/0
Fatty Acid Metabolism	1/1	Inflammatory Response	3/4	E2F Targets	0/1/1
Myc Targets V1	1/1	Apoptosis	3/4	DNA Repair	0/1/1
Angiogenesis	2/0	**OXPHOS**	1/3	Peroxisome	0/2/0
		EMT	1/4		
		KRAS Up	0/4		

Appendix 2

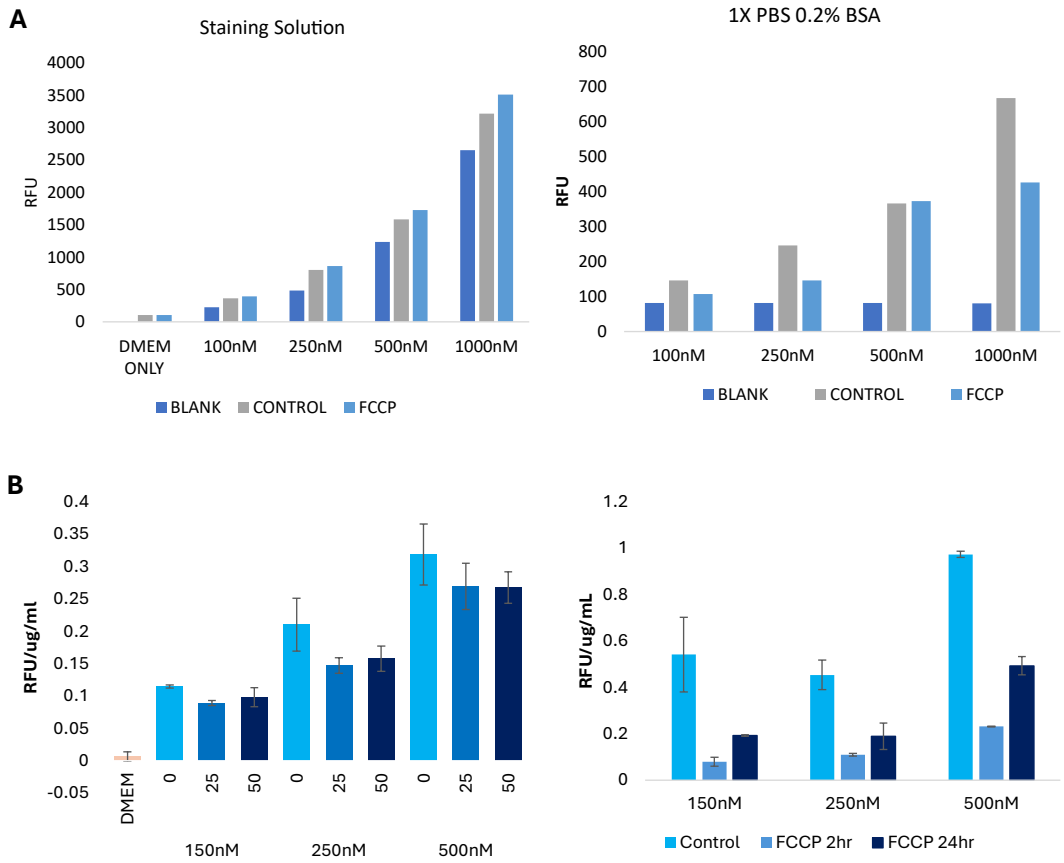


Figure S2.1. Optimisation of TMRE Microplate Assay. Data show A) relative fluorescent units (RFU) for untreated SH-SHY5Y cells stained with 100 – 1000nM TMRE either the staining solution or after a 1X PBS 0.2% BSA wash and B) RFU corrected to total protein content per well for SH-SY5Y cells stained with 150 – 500nM TMRE after no treatment (control), 2 hours and 24 hours of 25µM FCCP treatment.

Table S2.1. Details of RT-qPCR Assays used to measure mtDNA copy number and mRNA expression. F= forward primer; R = reverse primer.

Gene	Primer Sequence	Reference	Master Mix	Cycling Conditions
B2M (DNA)	F: 5'-CCAGCAGAGAATGGAAAGTCAA-3' R: 5'-TCTCTCTCCATTCTTCAGTAAGTCAACT-3'	(Grady *et al.*, 2014)	1µL DNA, 0.5µL F, 0.5µL R	1 x (95°C, 5min); 40 x (95°C, 15s; 60°C, 30s)
ND1	F: 5'-CCCTAAAACCCGCCACATCT-3' R: 5'-GAGCGATGGTGAGAGCTAAGGT-3'			
ND4	F: 5'-CCATTCTCCTCCTATCCCTCAAC-3' R: 5'CACAATCTGATGTTTTGGTTAAACTATATTT-3'			
B2M (RNA)	F: 5'-CCAGCAGAGAATGGAAAGTCAA-3' R: 5'-TCTCTCTCCATTCTTCAGTAAGTCAACT-3'	(Grady *et al.*, 2014)	0.6µL cDNA, 0.75µL F, 0.75µL R	Dependent on GOI

CMYC	F: 5'- ACCACCAGCAGCGACTCTGA-3′ R: 5'- TCCAGCAGAAGGTGATCCAGACT-3′	(Wang *et al.,* 2018)	1µL cDNA, 1µL F, 1µL R	1 x (95°C 60s); 40X (95°C, 10s; 60°C, 30s; 72°C,10s)
NRF1	F: 5'-TTGAGTCTAATCCATCTATCCG-3' R: 5'-TACTTACGCACCACATTCTC-3'	(Pinho *et al.,* 2022)		
Nfe2l2	F: 5'-CAGCGACGGAAAGAGTATGA-3' R: 5'-TGGGCAACCTGGGAGTAG-3'	(Schrier *et al.,* 2022)	0.8µL cDNA, 0.5µL F, 0.5µL R	
TFAM	F: 5'-GTCACTGCCTCATCCACC-3' R: 5'-CCGCCCTATAAGCATCTT-3'	(Ye *et al.,* 2022)		
18S	F: 5'-CCTGGATACCGCAGCTAGGA-3' R: 5'-GCGGCGCAATACGAATGCCCC-3'	(Kang *et al.,* 2018)	1µL cDNA, 1µL F, 1µL R	1 x (95°C, 5min); 35 x (95°C,30s; 60°C, 45s; 72°C, 50s)
PGC1α	F: 5′-CCGAGAATTCATGGAGCAAT -3' R: 5′- TTTCTGTGGGTTTGGTGTGA-3'	(Kim *et al.,* 2019)	0.5µL cDNA, 0.5µL F, 0.5µL R	
DRP1	F: 5'-TCAACCTCCGCGTCTACTC-3' R: 5'-GATCTGGAACTCGATGTCGGG-3'	(Kosmider *et al.,* 2019)	0.8µL cDNA, 0.5µL F, 0.5µL R	1 x (95°C, 60s); 35 x (95°C,15s; 63°C, 30s; 72°C, 10s)
MFN1	F: 5'-GAGGTGCTATCTCGGAGACAC-3' R: 5'-GCCAATCCCACTAGGGAGAAC-3'			
MFN2	F: 5'-TGGCTCAAGACTATAAGCTGCG-3' R: 5'-GAGGACTACTGGAGAAGGGTGG-3'	(Duraisamy, Mohammad and Kowluru, 2019)	0.8µL cDNA, 0.4 µL F, 0.4 µL R	
STOML2	F: 5'-GTGACTCTCGACAATGTAAC-3' R: 5'-TGATCTCATAACGGAGGCAG-3'	(Hu *et al.,* 2018)	0.8 µL cDNA, 0.5 µL F, 0.5µL R	1 x (95°C, 10min); 40 x (95°C, 15s; 62°C, 30s)
OPA1	F: 5'- AGCCTCGCAGGAATTTTTGG-3' R: 5'-AGCCGATCCTAGTATGAGATAGC-3'	(Bean *et al.,* 2021)	0.6 µL cDNA, 0.75 µL F, 0.75 µL R	1 x (95°C, 60s); 40 x (95°C,10s; 60°C, 40s; 72°C, 20s)
PCCB	F: 5'- AGGCAGTCTGTCAGGAGCACAT-3' R: 5'- CCAGAGTCATTCAGCCCAATCAC-3'	Origene, CAT#: HP200504	1 µL cDNA, 0.5 µL F, 0.5 µL R	

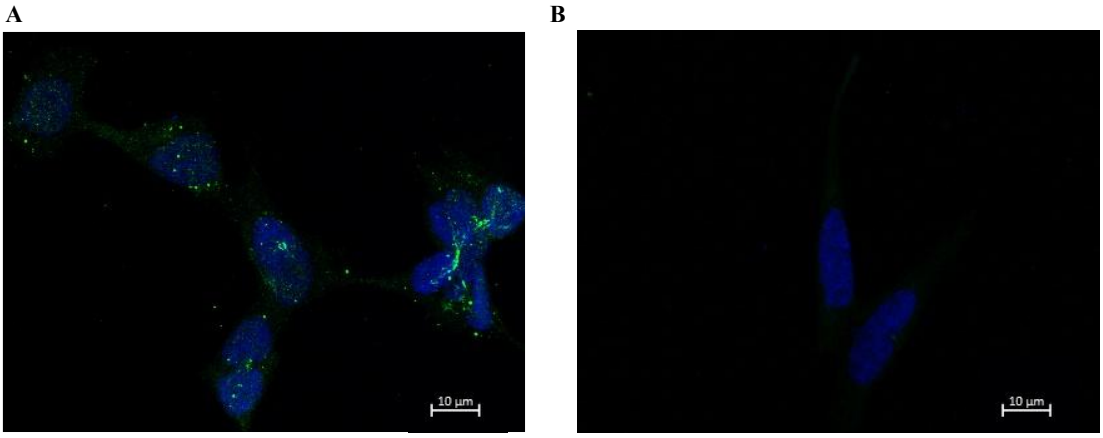


Figure S2.2. Confirmation of LC3β Antibody Specificity. Data shows the maximum intensity projections for untreated SH-SY5Y cells stained with Alexa Flour-488 A) with and B) without 300nM MitoTracker CMX ROS and 1:200 anti-LC3.

Table S2.2. Seahorse XFp Cell Characterisation: Optimisation of Seeding Density

Cell density (x10^3)	Basal OCR [OPT 20-160 pmol/min]	Basal ECAR [OPT 10 - 90 mpH/min]	Min O2 > 40
5	5-7	1-2	YES
7.5	11-12	8 - 14	YES
15	18-24	25-27	YES
30	20-36	9.8-19	YES
45	60-80	28 - 30	YES
50	50-103	27 - 32	NO

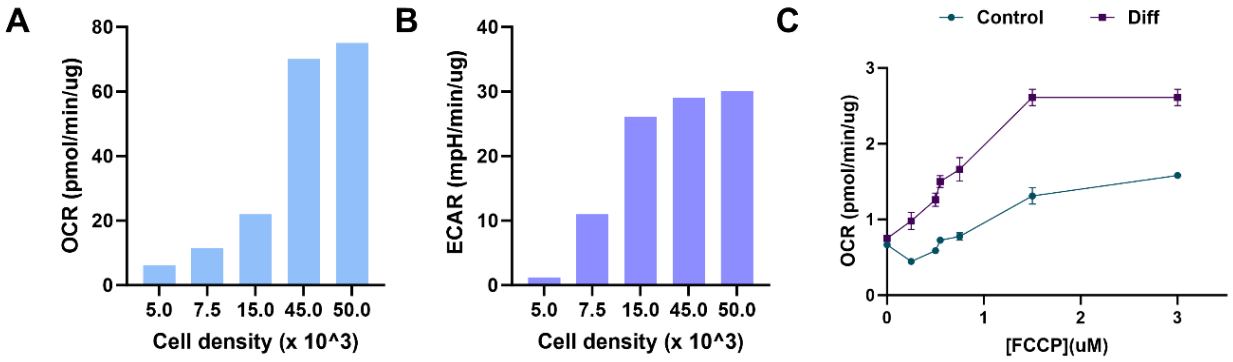


Figure S2.3. Cell characterisation for live cell respirometry. A, B) Basal oxygen consumption rate (OCR) and extracellular acidification rate (ECAR) at different seeding densities. C) FCCP titration.

Table S2.3. Seahorse XFp Protocol for ATP Rate Assay

	Basal	Oligomycin (1.5µM)	Rot/AA (0.5µM)
Number of Cycles	3	3	3
Mix (Mins)	3	3:30	3
Measurement (Mins)	3	3	3
Total Duration (Mins)	**18**	**19:30**	**18**

Table S2.4. Seahorse XFp Protocol for MitoStress Tests

	Basal	Oligomycin (1.5µM)	FCCP (1.5µM)	Rot/AA (0.5µM)
Number of Cycles	3	3	3	3
Mix (Mins)	3	3:30	3:30	3
Measurement (Mins)	3	3	3	3
Total Duration (Mins)	**18**	**19:30**	**19:30**	**18**

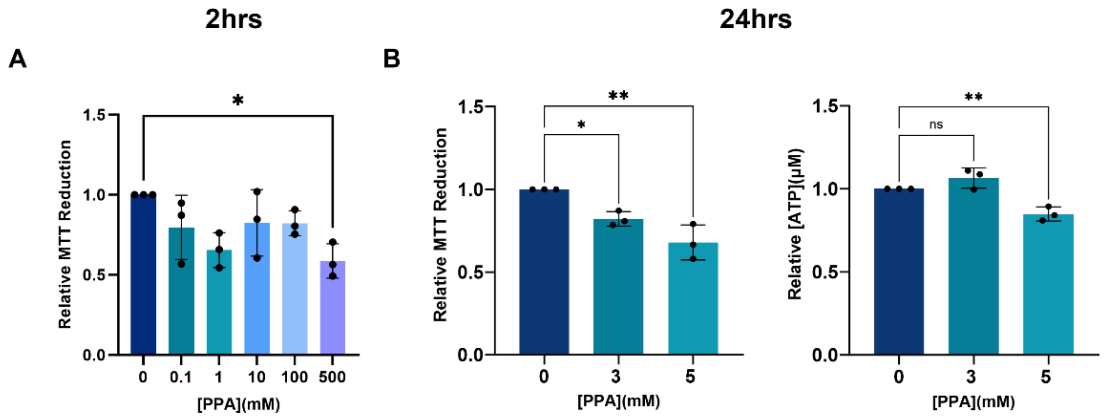


Figure S2.4. Cytotoxicity of Propionic Acid in DMEM: F12. Undifferentiated SH-SY5Y cells were exposed to PPA in DMEM: F12 followed by MTT or ATP assays to establish context-dependent windows of cytotoxicity. **A)** Acute cytotoxicity of 2-hour exposure to pathophysiological concentrations of PPA in DMEM measured by MTT reduction (n=3). **B)** Cell viability of pathological PPA concentrations measured using both MTT reduction and ATP production (n=3). All experiments were conducted in triplicate and cell viability was calculated relative to untreated controls. Data represent mean and standard deviation and significance was determined using one-way ANOVAs and Dunnet's Post-Hoc Comparisons where *p<0.05, **p<0.01, ***p<0.001, and ****p<0.0001.

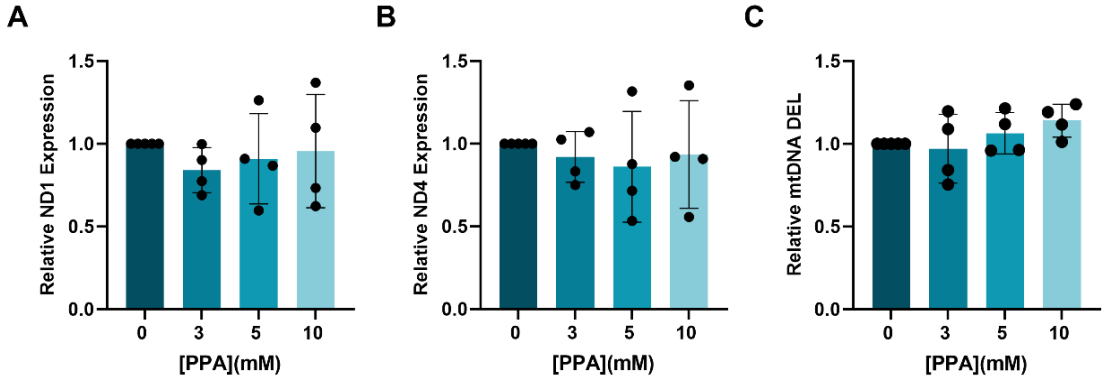


Figure S2.5. Mitochondrial DNA Copy Number and Deletions Under Propionic Acid Stress. RT-qPCR was used to measure **A)** Relative ND1 Copy Number, **B)** Relative ND4 Copy Number and **C)** mtDNA deletions in cells treated with 3,5 and 10mM PPA for 72 hours (n=4). Data represent the fold-change in expression relative to untreated controls according to the ΔΔCT method ($2^{-\Delta\Delta CT}$) (A,B) and the ND4:ND1 ratio (C). Each assay was performed in triplicate and significance was established using one-way ANOVAs with Dunnet's multiple comparisons or Kruskal-Wallis test with Dunn's Post-Hoc Comparisons where *p<0.05, **p<0.01, ***p<0.001, and ****p<0.0001.

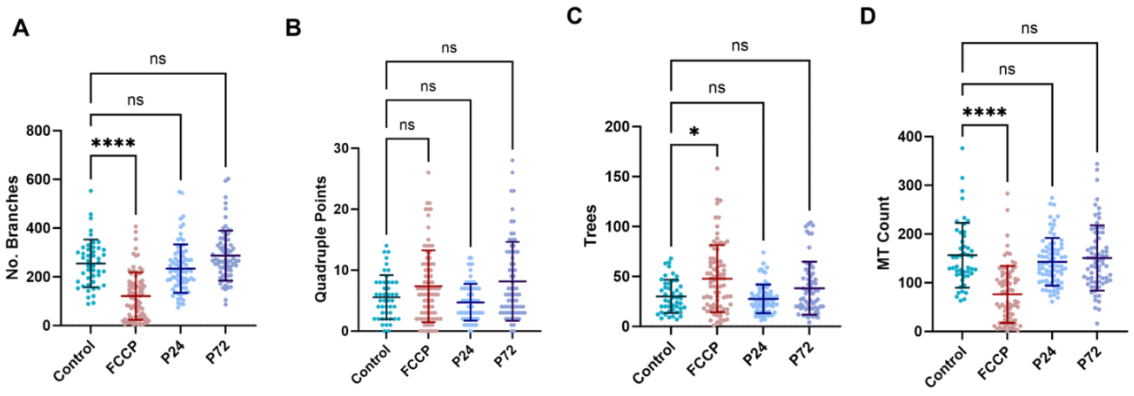


Figure S2.6. Mitochondrial Content and Connectivity. Mitochondrial networks were stained with MitoTracker CMX Ros and 2D and 3D network skeletons were generated from binarised 8-bit masks. Changes in network morphology were quantified by measuring the number of A) total branch points, B) quadruple points C) Trees and D) mitochondria across the mitochondrial network. Data represent 288 cells with 46-86 cells per treatment condition from three independent biological repeats. Data was filtered using the ROUT method to identify outliers before being tested for normality using the Shapiro Wilks test. Significance was evaluated using Kruskal-Wallis test with Dunn's Post-Hoc Comparisons where *p<0.05, **p<0.01, ***p<0.001, and ****p<0.0001.

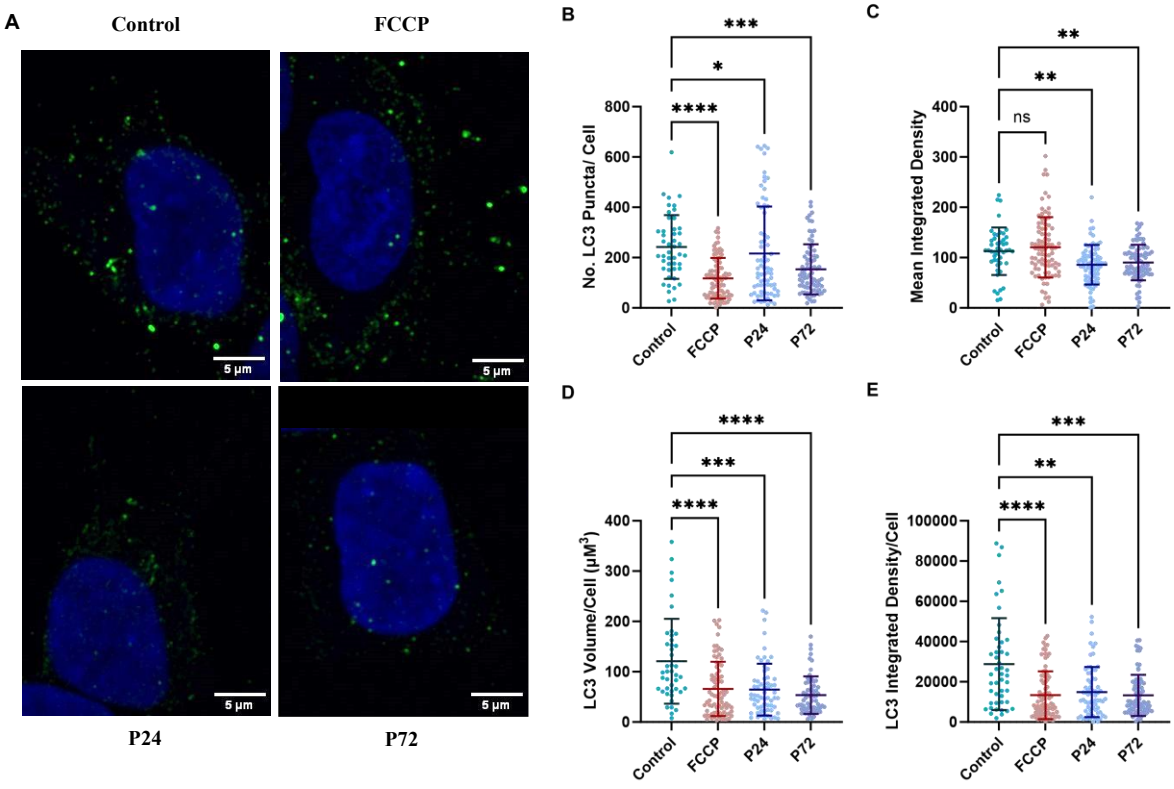


Figure S2.7. Decreased LC3β Expression Under Propionic Acid Stress. A) Representative maximum intensity projections of SH-SY5Y cells stained with LC3 tagged with Alexa-Flour 488 and visualised with a 63X oil DIC objective and an Argon 25mW laser at 488 nm. LC3 puncta were quantified by measuring **B)** Mean Puncta Volume, **C)** Mean Integrated Density, **D)** Total LC3 Volume and **E)** Total Integrated Density per cell. Data represent 288 cells with 46-86 cells per treatment condition from three independent biological repeats. Data was filtered using the ROUT method to identify outliers before being tested for normality using the Shapiro Wilks test. Significance was evaluated using Kruskal-Wallis test with Dunn's Post-Hoc Comparisons where *p<0.05, **p<0.01, ***p<0.001, and ****p<0.0001.

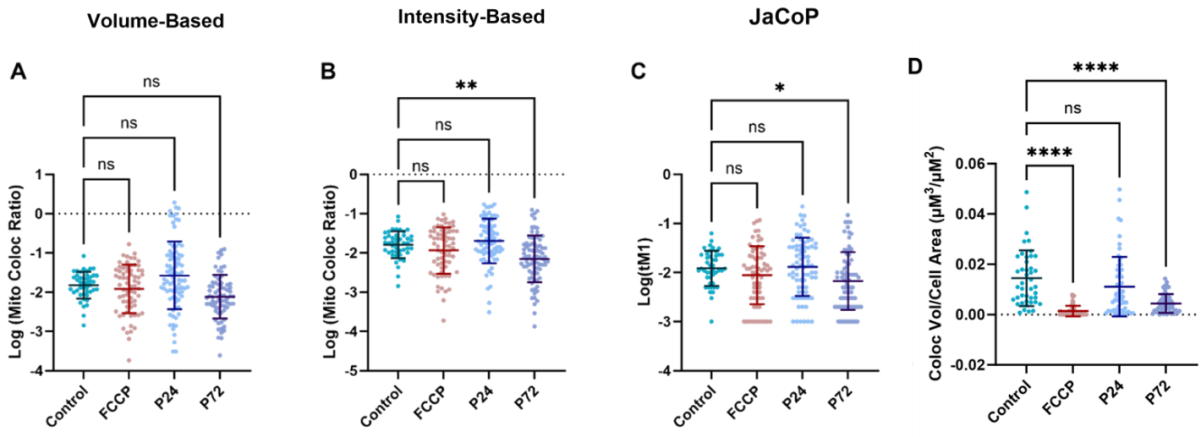


Figure 2.8. Mitochondrial Colocalisation Ratios. A) Volume-based and **B)** Intensity-based colocalisation coefficients measured as the colocalisation ratio across mitochondrial networks. **C)** Manders coefficient calculated from the JaCoP ImageJ plugin. **D)** Total colocalised volume per cell normalised to cell area. Data represent 288 cells with 46-86 cells per treatment condition from three independent biological repeats. Data was log-normalised and filtered using the ROUT method to identify outliers before being tested for normality using the Shapiro Wilks test. Significance was evaluated using Kruskal-Wallis test with Dunn's Post-Hoc Comparisons where *p<0.05, **p<0.01, ***p<0.001, and ****p<0.0001.

Appendix 3

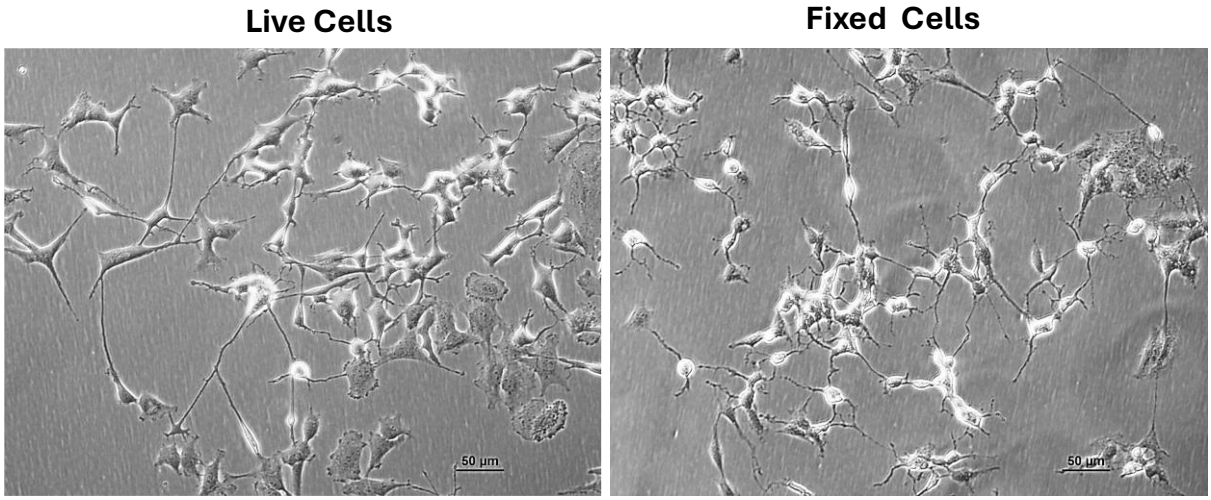


Figure S3.1. The Effect of Fixation on Neurite Morphology. Neurite morphology can be altered both by the adherent cell surface and fixation agents. Phase-contrast images at 20X magnification show clearly visible tubular extensions in both live cell cultures in plastic-bottomed plates and after cell fixation with 4% paraformaldehyde on glass coverslips.

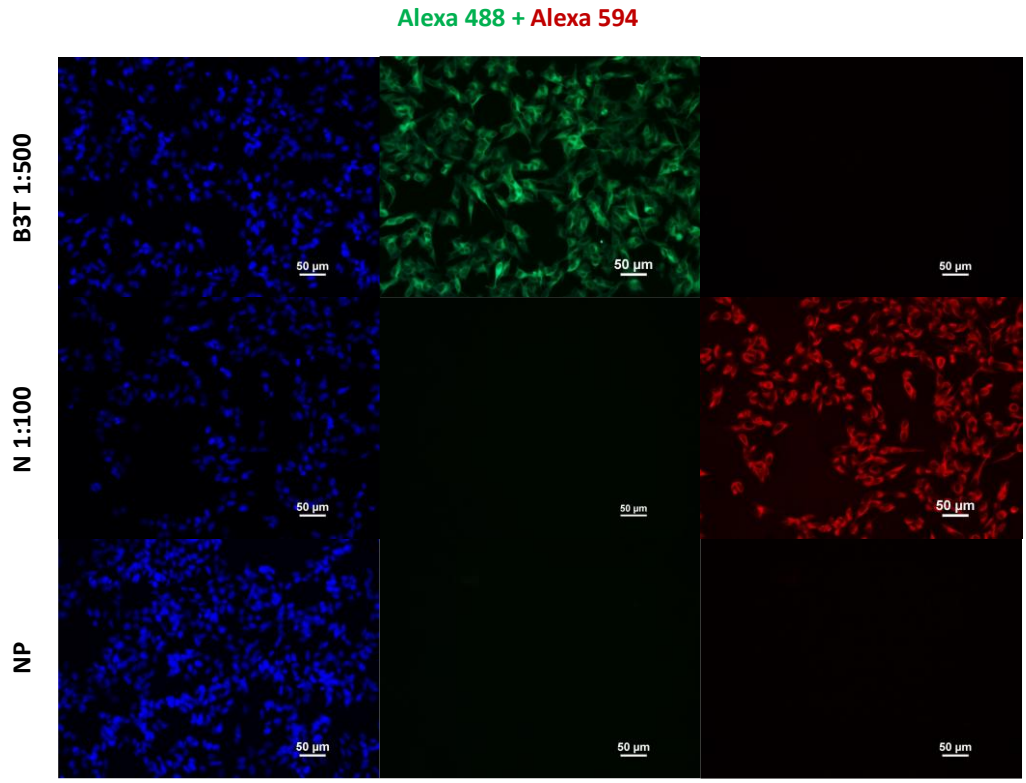


Figure S3.2. Specificity of primary and secondary antibodies. Undifferentiated SH-SY5Y cells were fixed, permeabilised and blocked before being stained with no primary antibody (NP), 1:500 anti-β3T or1:100 anti-NES primary monoclonal antibodies and both anti-mouse alexa-488 and anti-goat alexa-594 at 1:1000 and 2:1000 for 90 minutes before being visualised with a FITC and Texas Red filter. The absence of Alexa-594 signal with anti-β3T only, the absence of Alexa-488 signal with anti-NES only and the absence of both signals with no primary antibody confirms the specificity of secondary antibody binding and reveals no cross-talk between anti-goat and anti-rabbit primary and secondary antibodies.

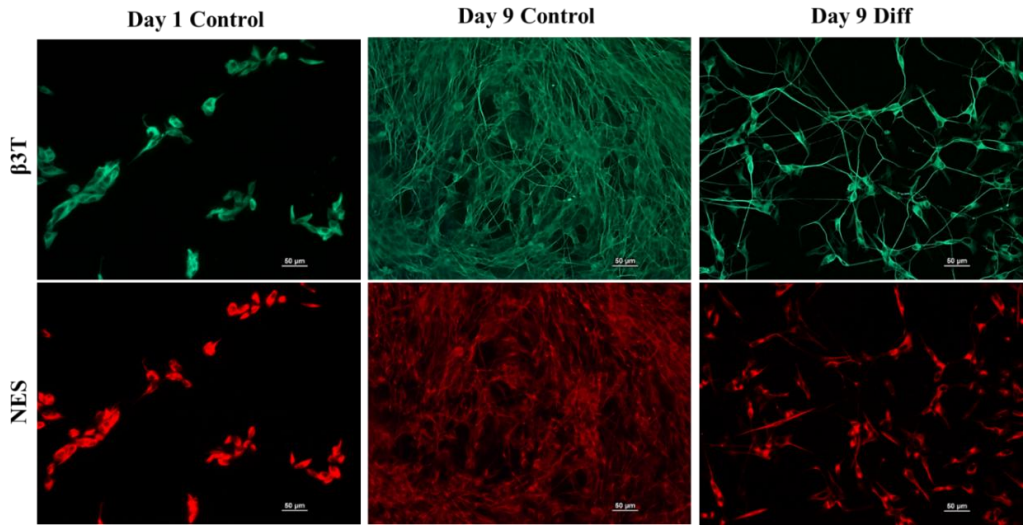


Figure S3.3. The Density of Day 9 Controls Precludes Automated Thresholding and Signal Quantification. SH-SY5Y cells grown in 15% FBS for 24 hours (day 1 controls), maintained at 1% FBS for 9 days (day 9 controls) or differentiated for 9 days with retinoic acid and brain-derived neurotrophic factor (day 9 diff) were stained with β-3-tubulin and Nestin and visualised at 20X magnification. Both day 1 controls and day 9 differentiated samples display clearly segmented cell monolayers while day 9 controls are highly confluent with multiple overlapping cell layers.

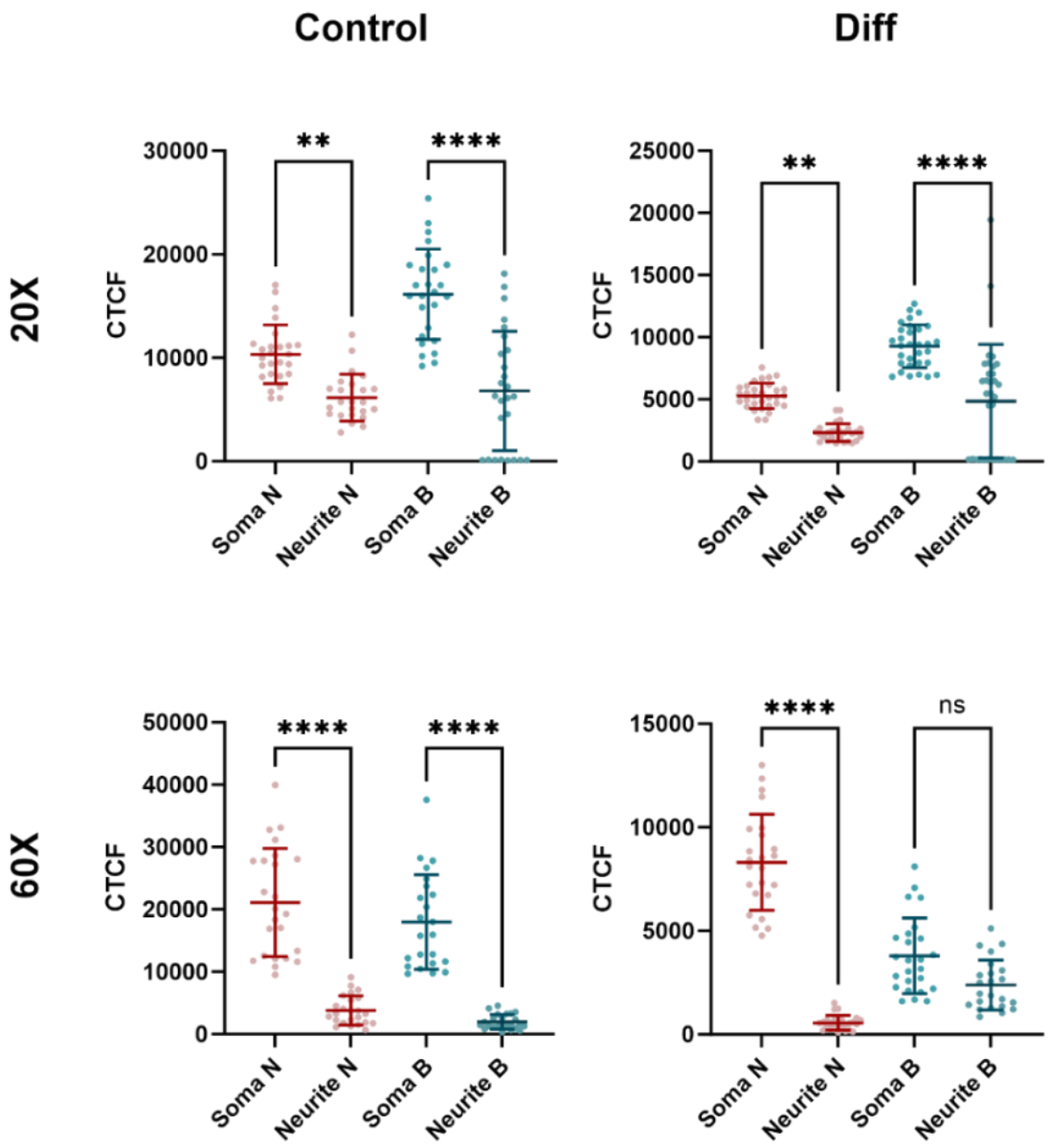


Figure S3.4. β-3-tubulin and Nestin Display a Distinct Intracellular Gradient in SH-SY5Y Cells. Data represent corrected total cell fluorescence (CTCF) for β3T (B) and NES (N) in cell soma and neurites in undifferentiated controls and differentiated neurons at 20X and 60X magnification. Data represent mean and standard deviation, and significance was evaluated using either one-way ANOVAs or Kruskal Wallis Tests with Dunn's Post-Hoc Multiple Comparisons where *p<0.05, **p<0.01, ***p<0.001, and ****p<0.0001.

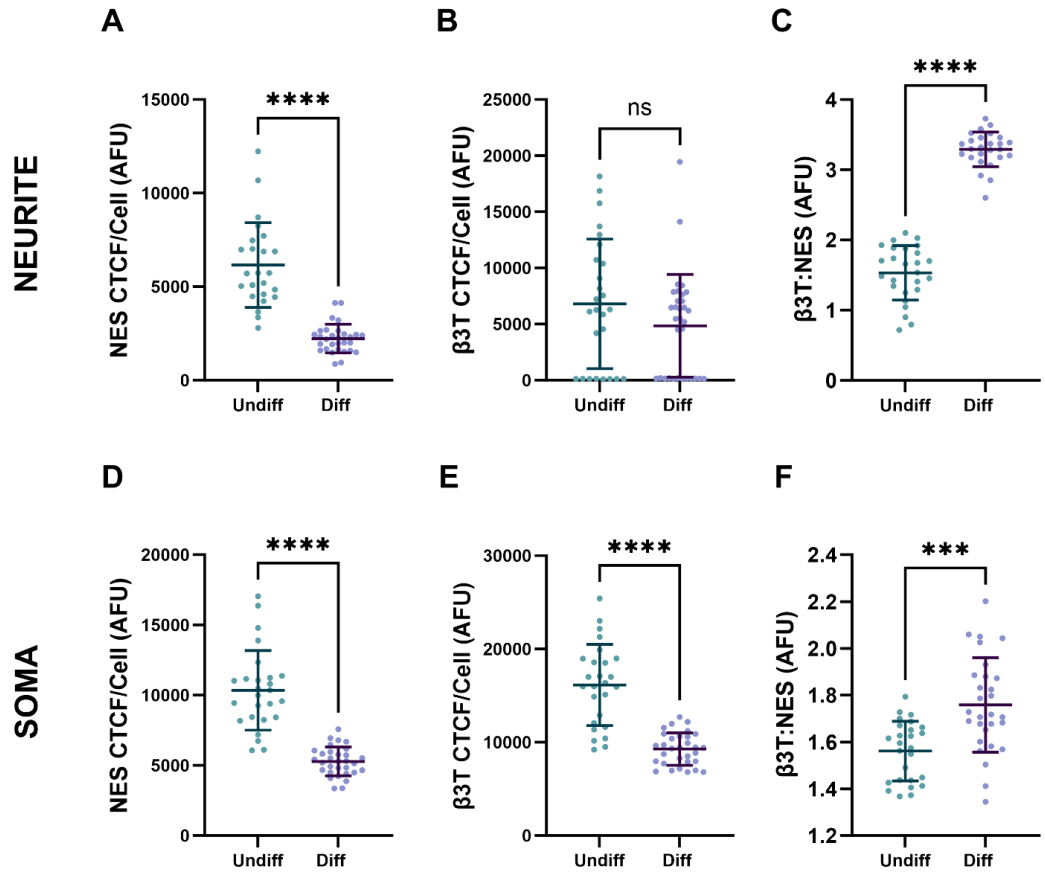


Figure S3.5. Differentiation Alters β-3-Tubulin and Nestin Expression in Cell Soma and Neurites. Undifferentiated SH-SY5Y cells and cells differentiated with retinoic acid and brain-derived neurotrophic factor for nine days were evaluated with immunocytochemistry to measure Nestin, and β-3-Tubulin expression in cell neurites (A-C) and soma (D-F). Samples from three independent biological repeats were imaged across 25-35 ROIs per condition using a Nikon C-HGFIE inverted microscope with a 20X S Plan Flour (NA=0.45) objective equipped with a DS-Fi2 colour camera. Signals were quantified using corrected total cell fluorescence (CTCF) = Integrated Density – (Fluorescence Area X Mean Background Fluorescence) normalised to Dapi count. Data represent mean and standard deviation, where significance was evaluated using either one-way ANOVAs or Kruskal Wallis Tests with Dunn's Post-Hoc Multiple Comparisons and *p<0.05, **p<0.01, ***p<0.001, and ****p<0.0001.

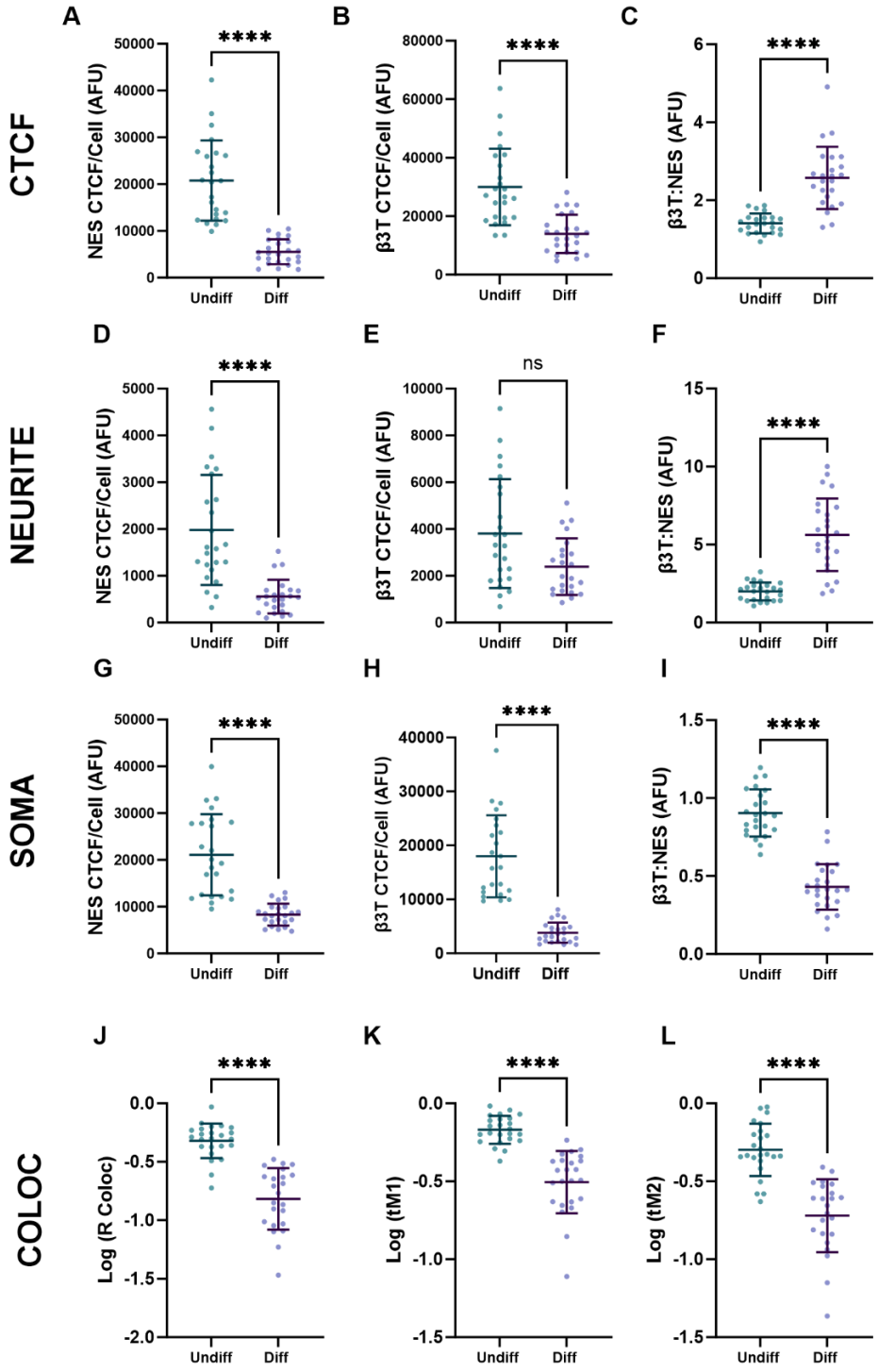


Figure S3.6. Signal Quantification in 60X Images Supports Data from 20X Images. Undifferentiated SH-SY5Y cells and cells differentiated with retinoic acid and brain-derived neurotrophic factor for nine days were evaluated with evaluated with immunocytochemistry to measure Nestin, and β-3-Tubulin expression in total cell area (A-C), cell neurites (D-F) and cell soma (G-I). Samples were imaged across 24-27 ROIs per condition using a Nikon C-HGFIE inverted microscope with an Apo TIRF 60X oil DIC objective (NA=1.49). Signals were quantified using corrected total cell fluorescence (CTCF) = Integrated Density – (Fluorescence Area X Mean Background Fluorescence) normalised to Dapi count. Data represent mean and standard where significance was evaluated using either one-way ANOVAs or Kruskal Wallis Tests with Dunn's Post-Hoc Multiple Comparisons where *p<0.05, **p<0.01, ***p<0.001, and ****p<0.0001.

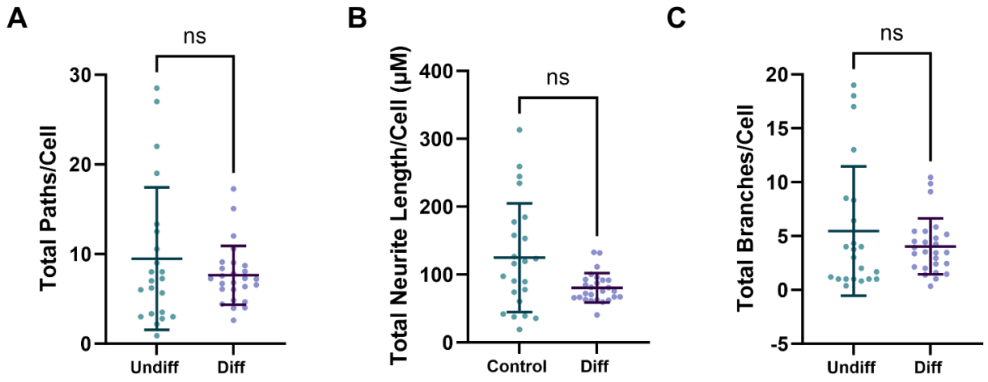


Figure S3.7. Autotracing Does Not Reflect Significant Changes to Neurite Production, Elongation and Branching per Cell. Maximum intensity projections derived from 60X β3T Z-stacks were subject to preprocessing, Gaussian convolution and thresholding to generate binary masks of neurite outlines. Binary masks were autotraced with the Single Neurite Tracer (SNT) Image J plugin to measure **A)** The total number of paths, **B)** Total neurite length and **C)** The total number of branches normalised to cell count per ROI. Data represent mean and standard deviation across 24-27 ROIs per condition from three biological repeats, where significance was evaluated using either one-way ANOVAs or Kruskal Wallis Tests with Dunn's Post-Hoc Multiple Comparisons where *p<0.05, **p<0.01, ***p<0.001, and ****p<0.0001.

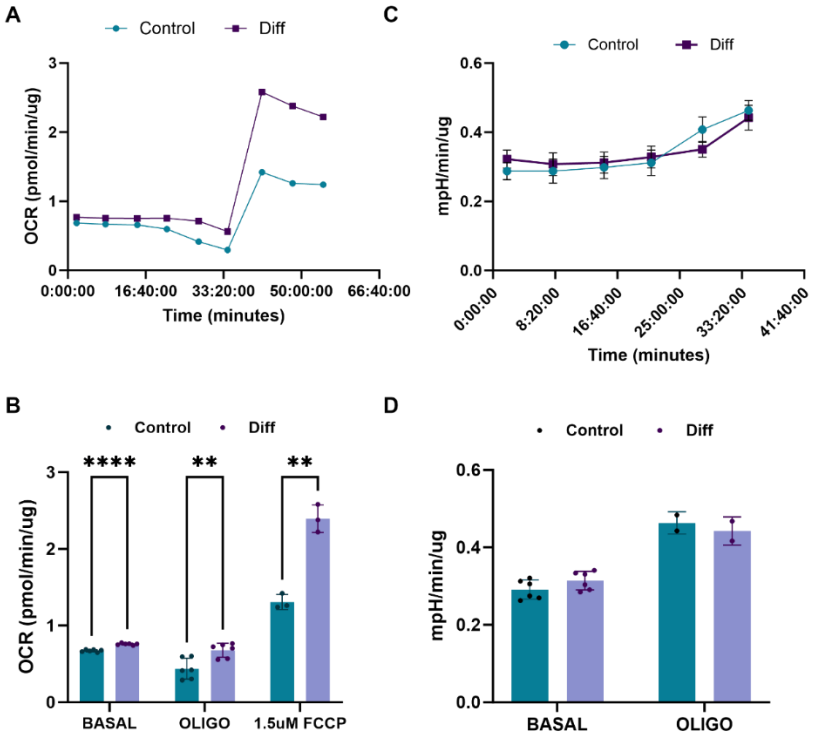


Figure S3.8. Cell Characterisation Assay Reflects a Metabolic Shift During Differentiation. Undifferentiated SH-SY5Y cells in 15% FBS and differentiated cells subject to nine days at 1% FBS + 10uM RA and 50ng/mL BDNF were seeded in 6-well PDL coated XFp miniplates and assessed using the XFp Bioanalyser to evaluate oxygen consumption rate (OCR) (A,B) and extracellular acidification rate (ECAR) (C,D) at basal conditions, following 1.5uM oligomycin and following 1.5uM FCCP injection. Data points represent the mean of three measurements under each condition, across three to six replicates from one biological repeat.

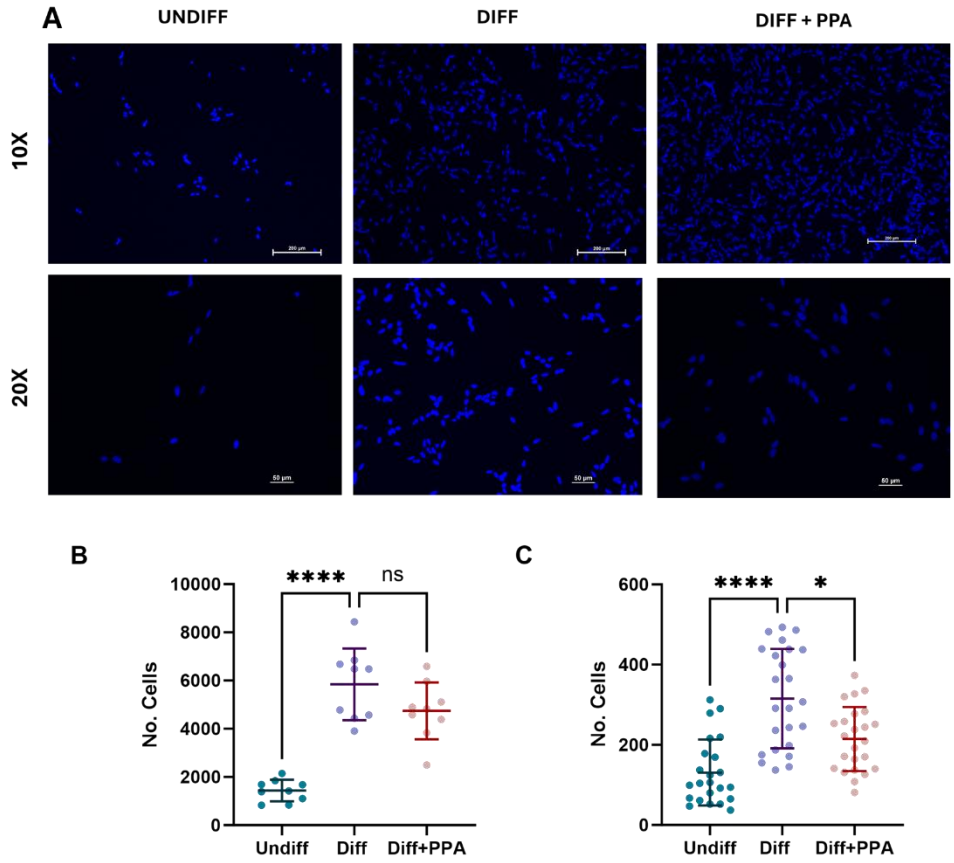


Figure S3.9. Propionic Acid Minimally Influences Cell Count During Differentiation. SH-SY5Y cells were maintained at 15% FBS for 24 hours (C1) or differentiated with 1% FBS + 10uM RA and 50ng/mL BDNF in the absence (D9) or presence of 5mM propionic acid (DP) for 9 days. Cell populations were fixed, permeabilised and stained with 250nM Dapi for 10 minutes before being visualised with a Nikon Ti-E inverted microscope equipped with a CHGFIE Intensilight mercury-fiber illuminator, a Nikon D200 DS-Fi2 colour camera and a DAPI Filter Set #49000 (Ex/Em = 320-380nm/ 435-485nm). A) Representative images of cell populations at 10x and 20x magnification, scale bars = 200µM and 50µM respectively. Image J was used to measure the number of cells across A) 17-24 ROIs per condition from three independent biological repeats at 10X magnification and B) 22-24 ROIs per condition from three independent biological repeats at 20X magnification. Data represent mean and standard deviation and significance was determined using a Kruskal Wallis Test with Dunn's Post-Hoc Multiple Comparisons where *p<0.05, **p<0.01, ***p<0.001, and ****p<0.0001.

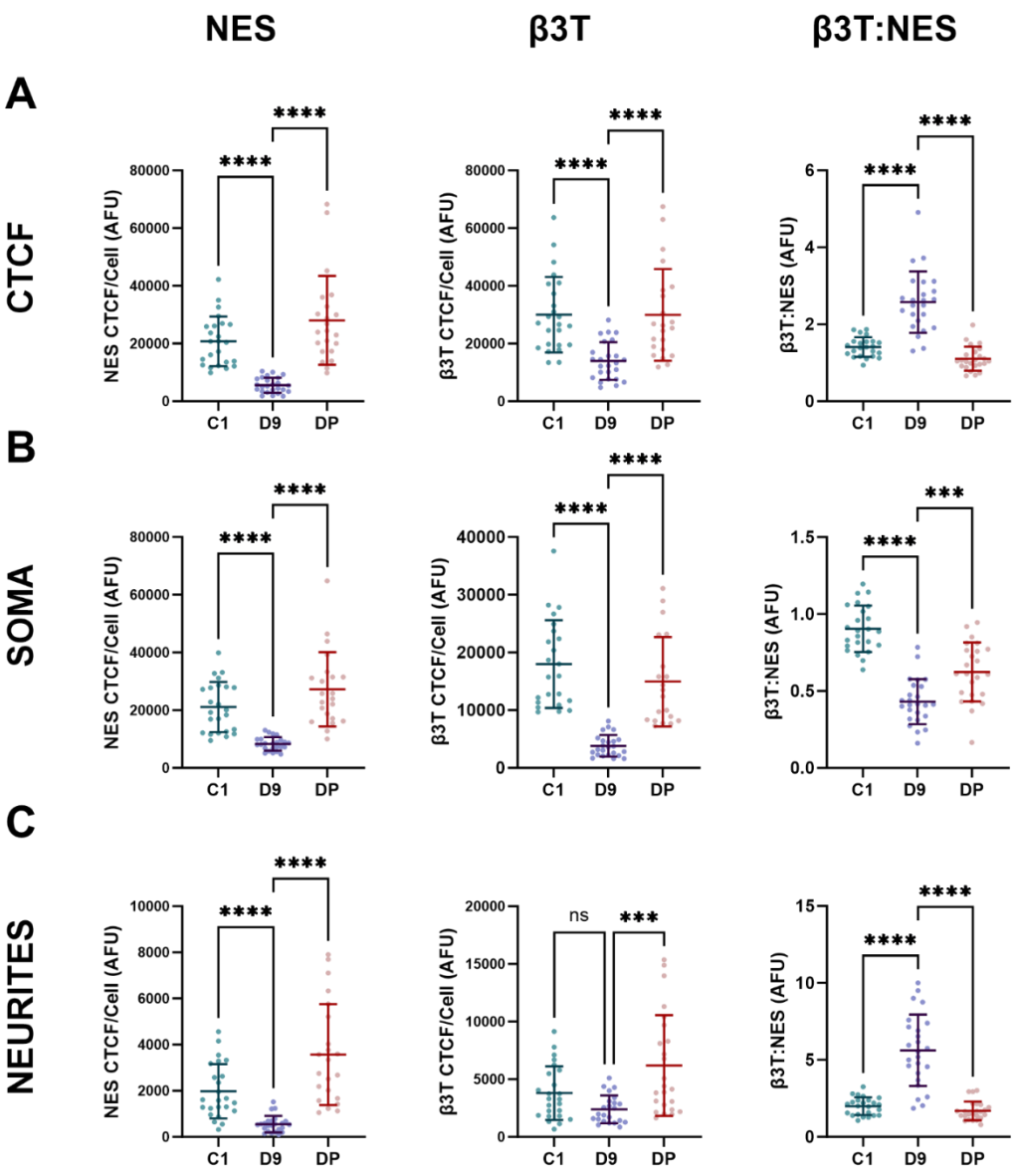


Figure S3.10. Signal Quantification in 60X Images Supports Disruptions to Signal Expression and Localisation Under Propionic Acid Stress. Nestin (NES) and β-3-tubulin (β3T) expression was evaluated in SH-SY5Y cells differentiated with 10μM RA and 50ng/mL BDNF for nine days in the absence (D9) or presence (DP) of 5mM propionic acid (PPA). The corrected total cell fluorescence (CTCF) method was used to measure total NES and β3T expression per cell in **A)** Total Cell Area, **B)** Cell Soma and C**)** Neurite Extensions where CTCF = Integrated Density – (Fluorescence Area X Mean Background Fluorescence) normalised to Dapi count. Data represent mean and standard deviation across 20-25 ROIs per condition from three independent biological repeats, and significance was determined using either one-way ANOVAs or Kruskal Wallis Tests with Dunn's Post-Hoc Multiple Comparisons where *p<0.05, **p<0.01, ***p<0.001, and ****p<0.0001.

Appendix 4

Table S4.1. Manually Curated Metabolic Signatures. Data Show the GO Biological Processes and Reactome Pathways used to Generate Manually Curated Gene Sets Representing Different Metabolic Pathways.

Metabolic Process	Collated Gene Lists
Oxidative Phosphorylation	GO:1903862 positive regulation of OXPHOS; GO:0090324 negative regulation of OXPHOS; GO:0002082_regulation_of_OXPHOS; R-HSA-1406_ pyruvate_ metabolism_ and_TCA; GO:0006119_GO OXPHOS; R-HSA-1428517_TCA_ETC
Mitogenesis	GO:0090298_negative_regulation_of_MTDNA_replication; GO:0090297_positive_regulation _of_MTDNA_replication; GO:0090296_regulation of MTDNA replication; GO:0006264_ MTDNA_replication; R-HSA-1592230_mitochondrial_biogenesis
MT Biosynthesis	GO:1903109_+_regulation_of_MT_transcription; GO:1903108_regulation of MT transcription; GO:0006391_ MT transcription; GO:0070130_-_regulation_of_MT_translation; GO:0070131_+_regulation_of_MT_translation; GO:0070129_regulation_of_MT_translation; GO:0032543_MT_translation; R-HSA-5368287_mitochondrial_translation; GO:0140053_MT_gene_expression
Mt Dynamics	GO:0090258_negative_regulation_of_MT_fission; GO:0090141_positive_regulation _of_MT_fission; GO:0090140_regulation_of_MT_fission; GO:0000266_MT fission; GO:0010637_negative_regulation_of_MT_fusion; GO:0010636_ positive_regulation_ of_MT_fusion; GO:0008053_MT_fusion; GO:0006839_MT_transport
Mitophagy	GO:1905090_negative_regulation_of_mitophagy; GO:1901526_positrive_regulation_ of_mitophagy; GO:0000423_mitophagy; R-HSA-5205647_mitophagy
Calcium	GO:0051560_MT_calcium_homeostasis; R-HSA-8949215__MT_calcium_ion_transport
Glycolysis	GO:0045821_positive regulation of glycolysis; GO:0045820_negative regulation of glycolysis GO:0006110_regulation of gycolytic process; GO:0006096_glycolytic_process; R-HSA-70171_canonical_glycolysis; GO:1905856_negative regulation of pentose-phosphate shunt; GO:1905857_positive regulation of pentose-phosphate shunt; GO:0043456_regulation of pentose-phosphate shunt; GO:0006098_pentose-phosphate shunt; GO:0009052_pentose-phosphate shunt, non-oxidative branch; GO:0009051 pentose-phosphate shunt, oxidative branch; R-HSA-71336_ppp
Gluconeogenesis	GO:0045722_positive regulation of gluconeogenesis; GO:0045721_negative regulation of gluconeogenesis; GO:0006111_regulation of gluconeogenesis; GO:0006094_gluconeogenesis R-HSA-70263_gluconeogenesis
Fatty Acid Oxidation	GO:0032000_positive_regulation_of_bFAO; GO:0031999_negative_regulation_of_bFAO; GO:0046322_negative_regulation_of_FAO; GO:0031998_regulation_of_bFAO; GO:0046320_regulation_of_FAO; GO:0006635_bFAO; GO:0019395_FAO; R-HSA-77289_MT_bFAO
Fatty Acid Elongation	GO:0045723_positive_regulation_of_FA_biosynthesis; GO:0045717_negative_regulation_of_FA_biosynthesis; GO:0042304_regulation_of_FA_biosynthesis; GO:0019367_FA_elongation; GO:0006633_FA_biosynthesis; R-HSA-8978868_FA_metabolism
Lipid Metabolism	GO:0050996_positive_regulation_of_lipid_catabolism; GO:0050995_negative_regulation _of_lipid_catabolism; GO:0016042_lipid_catabolism; GO:0046889_positive_regulation _of_lipid_biosynthesis; GO:0051055_negative_regulation_of_lipid_biosynthesis; GO:0008610_lipid_biosynthesis; R-HSA-556833_metabolism_of_lipids
Amino Acid Metabolism	GO:0009083_BCAA_catabolism; R-HSA-70895_BCAA_catabolism; GO:0006546_AA_ catabolism; GO:0009082_BCAA_biosynthesis; GO:0009449_AA_biosynthesis; R-HSA-71291_AA_and_derivatives_metabolism

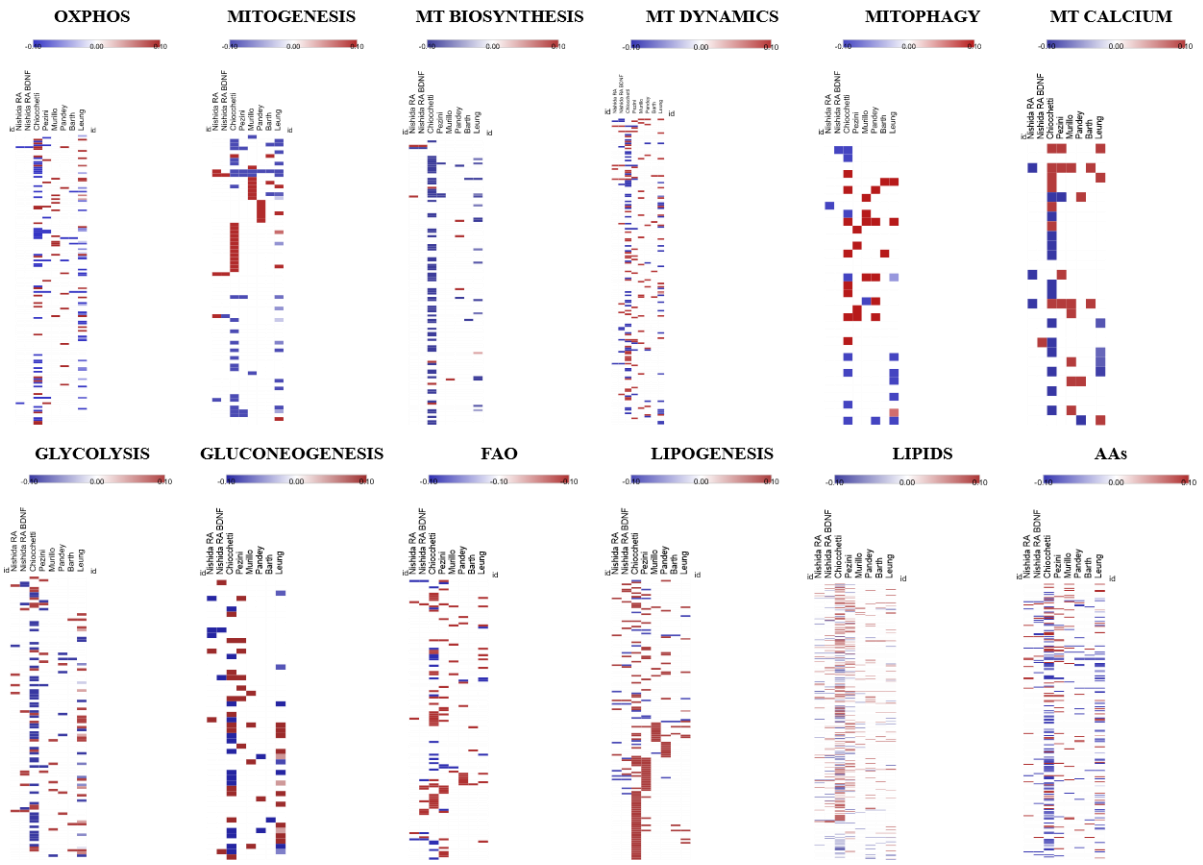


Figure S4.1. Global Expression Profiles of Metabolic Genes in Transcriptomic and Proteomic Profiles of SH-SY5Y Differentiation. Data represent four transcriptomic and four proteomic profile derived from the studies listed in **Table 4.1**, where heatmaps represent log fold change in expression in differentiated samples relative to undifferentiated controls (blue = downregulation, red = upregulation). Each pathway is comprised from the non-redundant gene sets detailed in Table S4.1.

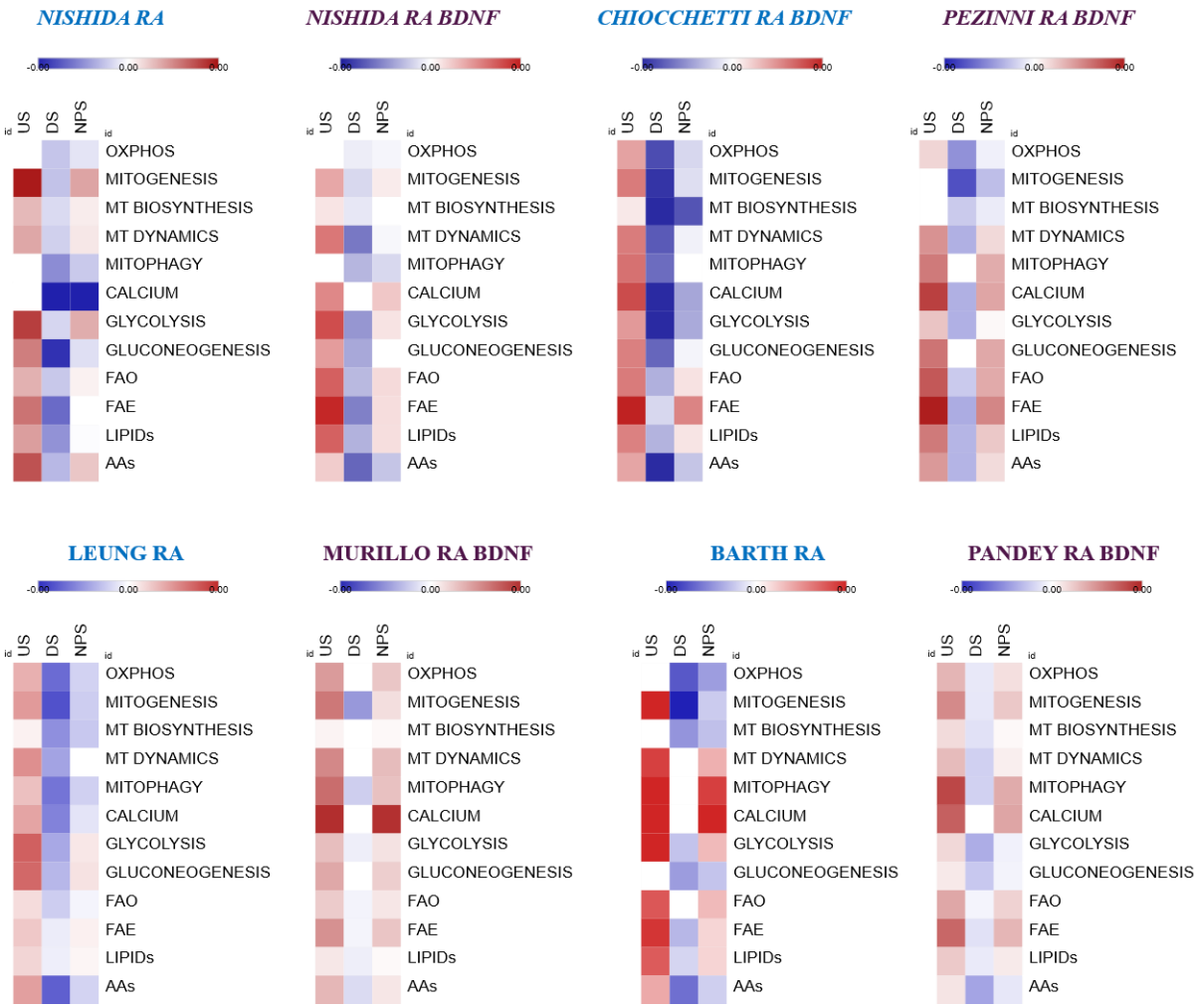


Figure S4.2. Metabolic Signatures of SH-SY5Y Differentiation. Data represent upregulation scores (US), downregulation scores (DS) and net perturbation scores (NPS) for each dataset. Transcriptomic datasets are shown in italics, proteomic datasets are shown in bold, RA only datasets are in blue and RA+BDNF are shown in purple. The NPS is calculated using an approach that is conceptually similar to the Reaction Perturbation Score (RPS) employed by the open-source platform *Biocyc,* which "*aims to measure the extent to which a pathway is up- or down-regulated by averaging the level of deviation from zero … over all the reactions in the pathway*" (Karp *et al.,* 2021). However, because absolute fold differences were not publicly available for every dataset, the NPS used here is a simple way to summarise the metabolic signatures in different molecular datasets by calculating the difference between the fraction of up- or downregulated genes in each pathway corrected for the total number of up- or downregulated genes in each dataset. $US\ or\ DS = \frac{No.of\ up\ or\ downregulated\ genes\ in\ pathway}{(No.of\ up\ or\ downregulated\ genes\ in\ each\ dataset)}$; $NPS = \frac{(Fraction\ of\ Upregulated\ Genes\ per\ Pathway)}{Total\ No.of\ Upregulated\ Genes\ per\ Dataset)} - \frac{(Fraction\ of\ Downregulated\ Genes\ per\ Pathway)}{Total\ No.of\ Downregulated\ Genes\ per\ Dataset)}$. Note: each pathway is governed by interactions between negative and positive regulators, as well as a specific balance of transcripts and proteins that are modulated by post-transcriptional and post-translational mechanisms. Therefore, perturbation scores should not be considered as an absolute measure of pathway activity but rather supplements GSEA as a way to summarise relative expression data across metabolic pathways represented in different molecular datasets.

Table S4.2. Quality Control for RNA Samples used for RNA Sequencing.

Sample ID	Conc. (ng/µl)	260/280 ratio	260/230 ratio	RINe
C1.C1.1	106.5	2.02	1.66	10.0
C1.C8.2	294.9	2.10	2.03	10.0
C1.D8.2	70.4	1.98	1.83	9.8
C1.DP2	64.1	2.01	1.80	9.7
C2.C1.1	262.1	2.10	2.01	9.9
C2.C8.2	393.1	2.00	2.05	9.2
C2.D8.2	96.6	2.06	1.94	9.4
C2.DP1	81.5	2.07	2.07	9.4
C3.C1.1	232.5	2.10	2.06	9.8
C3.C8.2	245.3	2.10	1.94	9.9
C3.D8.1	75.2	2.07	1.89	9.7
C3.DP1	77.7	2.01	1.58	9.6

Table S4.3. RNA Library Quantification and Indexing.

Sample code	Conc. (ng/µL)	Ave Fragment Size (bp)	Index ID	i7 index	i5 index
C1.C1.1	62.0	361	UDP0052	TCTTACATCA	GTGCGTCCTT
C1.C8.2	40.8	358	UDP0053	TTACAATTCC	AGCACATCCT
C1.D8.2	64.5	361	UDP0054	AAGCTTATGC	TTCCGTCGCA
C1.DP2	61.6	398	UDP0055	TATTCCTCAG	CTTAACCACT
C2.C1.1	66.9	385	UDP0056	CTCGTGCGTT	GCCTCGGATA
C2.C8.2	7.9	351	UDP0057	TTAGGATAGA	CGTCGACTGG
C2. D**8.2**	56.3	382	UDP0058	CCGAAGCGAG	TACTAGTCAA
C2.DP1	60.8	376	UDP0059	GGACCAACAG	ATAGACCGTT
C3.C1.1	83.3	370	UDP0060	TTCCAGGTAA	ACAGTTCCAG
C3.C8.2	124.5	366	UDP0061	TGATTAGCCA	AGGCATGTAG
C3. D**8.1**	135.2	382	UDP0062	TAACAGTGTT	GCAAGTCTCA
C3.DP1	156.9	359	UDP0063	ACCGCGCAAT	TTGGCTCCGC
Final Pool	**97.6**	**361**			

Table S4.4. Multi QC Report for RNA Sequencing.

Sample	R	Total # Seqs	Total Bases (Gbp)	Seq length (bp)	% GC	% Duplicates	Deduplicated %	Ave Seq Length (bp)	% Fails
C1-C1-1	1	16475627	1.1	35-68	44	62.16	37.84	67.33	18.18
C1-C1-1	2	16475627	1.1	35-68	44	53.04	46.96	67.33	18.18
C1-C1-1	1	15993971	1	35-68	44	58.64	41.36	67.34	18.18
C1-C1-1	2	15993971	1	35-68	44	50.07	49.93	67.35	18.18
C1-C8-2	1	16358483	1.1	35-68	46	67.16	32.84	67.31	27.27
C1-C8-2	2	16358483	1.1	35-68	46	61.81	38.19	67.3	18.18
C1-C8-2	1	15758718	1	35-68	46	63.59	36.41	67.32	27.27
C1-C8-2	2	15758718	1	35-68	46	58.23	41.77	67.32	18.18
C1-D8-2	1	15084233	1	35-68	46	62.01	37.99	67.26	18.18

C1-D8-2	2	15084233	1	35-68	47	56.69	43.31	67.26	18.18
C1-D8-2	1	14721257	0.99	35-68	46	58.51	41.49	67.28	18.18
C1-D8-2	2	14721257	0.99	35-68	46	53.16	46.84	67.27	18.18
C1-DP2	1	17781539	1.1	35-68	47	66.67	33.33	67.3	27.27
C1-DP2	2	17781539	1.1	35-68	47	60.26	39.74	67.29	27.27
C1-DP2	1	17428954	1.1	35-68	47	63.18	36.82	67.32	27.27
C1-DP2	2	17428954	1.1	35-68	47	57.08	42.92	67.3	27.27
C2-C1-1	1	19675034	1.3	35-68	47	65.37	34.63	67.16	18.18
C2-C1-1	2	19675034	1.3	35-68	47	58.17	41.83	67.16	27.27
C2-C1-1	1	19212921	1.2	35-68	47	62.19	37.81	67.19	18.18
C2-C1-1	2	19212921	1.2	35-68	47	54.84	45.16	67.19	27.27
C2-C8-2	1	57993038	3.8	35-68	43	73.57	26.43	67.12	27.27
C2-C8-2	2	57993038	3.8	35-68	44	67.03	32.97	67.15	27.27
C2-D8-2	1	56565000	3.7	35-68	43	71.59	28.41	67.14	27.27
C2-D8-2	2	56565000	3.7	35-68	44	64.64	35.36	67.17	27.27
C2-D8-2	1	14222064	0.96	35-68	43	56.94	43.06	67.3	18.18
C2-D8-2	2	14222064	0.96	35-68	43	51.56	48.44	67.3	18.18
C2-D8-2	1	13822128	0.93	35-68	43	52.7	47.3	67.32	18.18
C2-D8-2	2	13822128	0.93	35-68	43	47.42	52.58	67.31	9.09
C2-DP1	1	14876113	1	35-68	43	59.07	40.93	67.37	18.18
C2-DP1	2	14876113	1	35-68	44	53.55	46.45	67.35	18.18
C2-DP1	1	14568624	0.98	35-68	43	54.81	45.19	67.38	18.18
C2-DP1	2	14568624	0.98	35-68	44	49.55	50.45	67.36	9.09
C3-C1-1	1	15066399	1	35-68	45	63.88	36.12	67.38	18.18
C3-C1-1	2	15066399	1	35-68	46	55.42	44.58	67.37	18.18
C3-C1-1	1	14738815	0.99	35-68	45	60.4	39.6	67.39	18.18
C3-C1-1	2	14738815	0.99	35-68	46	52.02	47.98	67.38	18.18
C3-C8-2	1	15093302	1	35-68	45	64.5	35.5	67.33	18.18
C3-C8-2	2	15093302	1	35-68	46	57.58	42.42	67.33	18.18
C3-C8-2	1	14766364	0.99	35-68	45	60.76	39.24	67.35	18.18
C3-C8-2	2	14766364	0.99	35-68	46	53.92	46.08	67.34	18.18
C3-D8-1	1	13352393	0.9	35-68	45	58.17	41.83	67.32	18.18
C3-D8-1	2	13352393	0.9	35-68	46	51.61	48.39	67.32	18.18
C3-D8-1	1	13188434	0.89	35-68	45	54.31	45.69	67.34	18.18
C3-D8-1	2	13188434	0.89	35-68	46	47.87	52.13	67.33	9.09
C3-DP1	1	13185544	0.89	35-68	46	56.18	43.82	67.28	18.18
C3-DP1	2	13185544	0.89	35-68	47	53.37	46.63	67.27	27.27
C3-DP1	1	12931293	0.87	35-68	46	52.43	47.57	67.3	18.18
C3-DP1	2	12931293	0.87	35-68	47	49.47	50.53	67.29	18.18

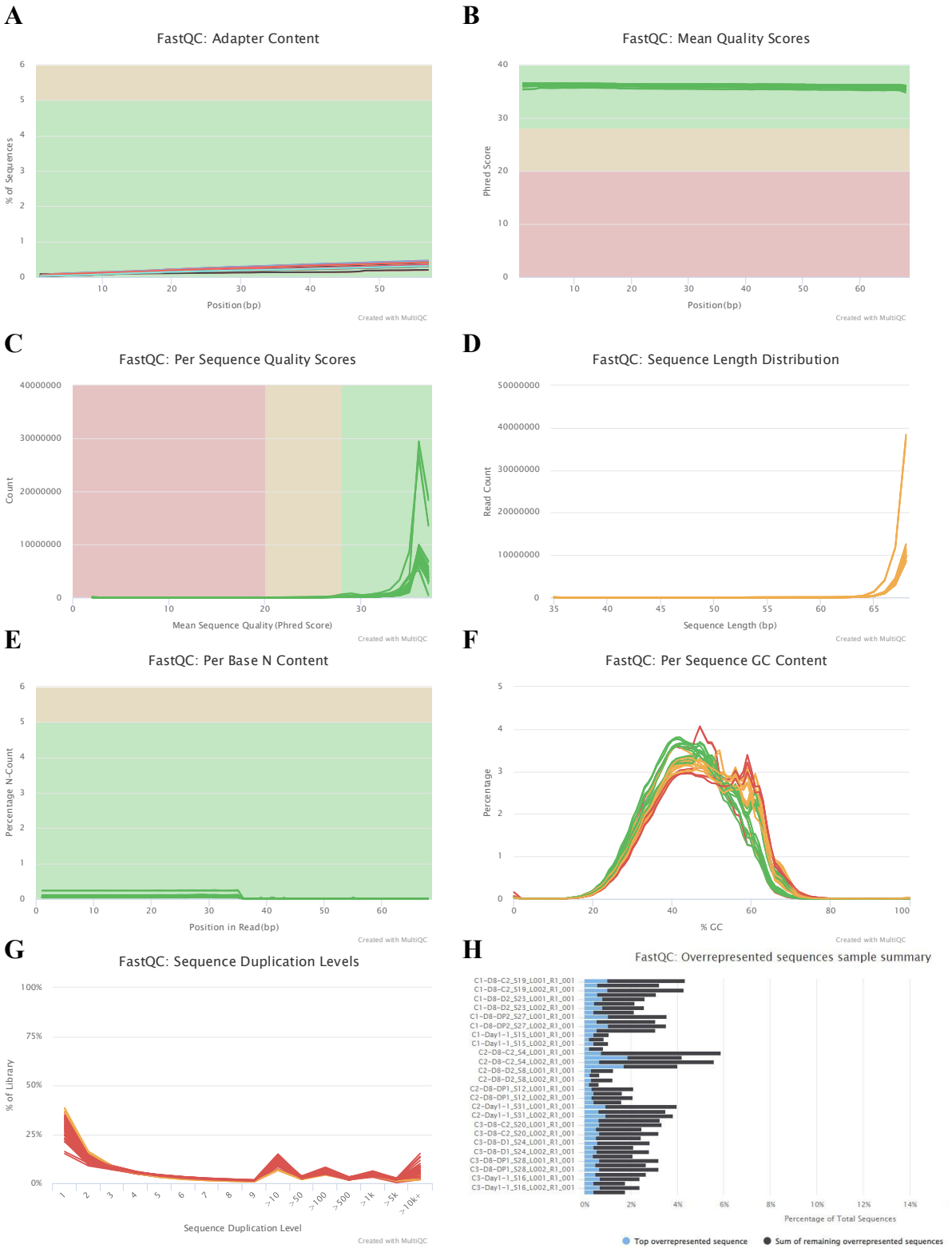


Figure S4.3. FASTQC Analysis for Global RNA Sequencing. A) The cumulative proportion of the library that has detected adapter sequences at each position. **B)** The mean quality value across each base position in the read. **C)** A plot of the total number of reads vs the average quality score over full length of that read. The distribution of average read quality is tightly spread in the upper range of the plot. **D)** The distribution of fragment sizes for each sample. **E)** Per base N content. **F)** Per Sequence GC Content. **G)** The relative level of duplication found for the first 100,000 sequences of each sample. **H)** The number of sequences categorised as overrepresented in each sample.

Table S4.5. Quality Control Parameters for Read Alignment using STAR

Sample	Total Seqs	% Uniquely Mapped	% Unique Genes of Total	% Unique Genes of Mapped	% Multi-Mapped	% Too Many Maps	% Mismatch	% Too Short	% Other Unmapped
C1.C1.1	**32469598**	87.29	64.05	73.38	6.14	0.15	0	6.31	0.12
C1.C8.2	**32117201**	83.25	62.04	74.52	10.16	0.24	0	6.24	0.11
C1. D8.2	**29805490**	84.57	59.57	70.44	8.24	0.17	0	6.88	0.14
C1.DP2	**35210493**	84.59	64.35	76.07	8.7	0.17	0	6.43	0.11
C2.C1.1	**38887955**	82.27	59.67	72.53	9.57	0.18	0	7.82	0.15
C2.C8.2	**1.15E+08**	79.65	50.58	63.51	9.28	0.99	0	9.88	0.2
C2. D8.2	**28044192**	86.68	53.58	61.81	6.05	0.39	0	6.73	0.16
C2.DP1	**29444737**	86.14	54.37	63.11	7.67	0.42	0	5.62	0.14
C3.C1.1	**29805214**	86.67	64.72	74.67	7.72	0.21	0	5.3	0.1
C3.C8.2	**29859666**	85.13	62.58	73.51	9.06	0.17	0	5.56	0.09
C3. D8.1	**26540827**	86.14	56.64	65.76	7.84	0.21	0	5.69	0.12
C3.DP1	**26116837**	85.3	58.83	68.97	8.04	0.16	0	6.37	0.12

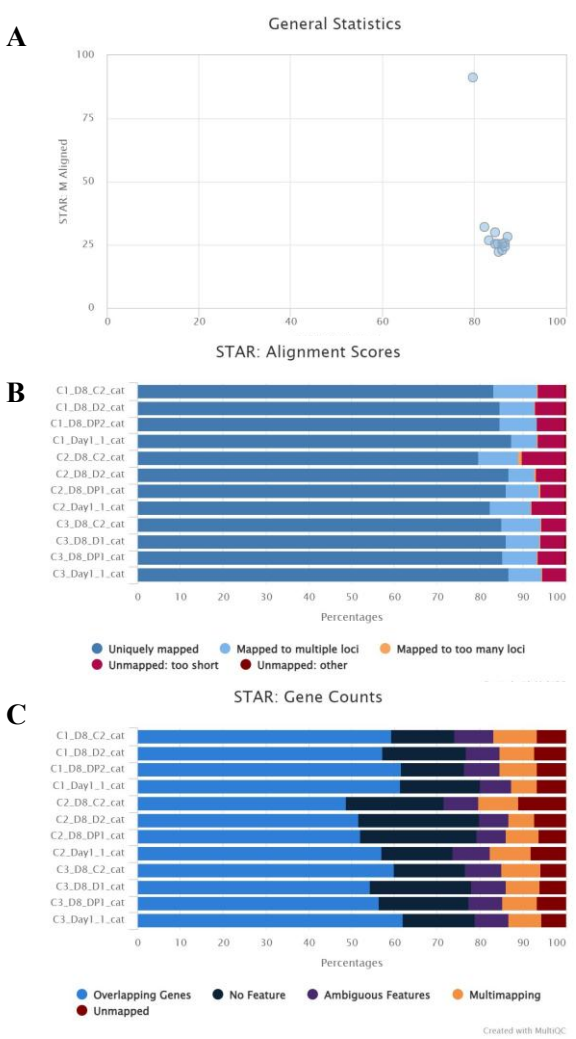


Figure S4.4. A) % uniquely mapped reads vs no. of uniquely mapped reads (in millions) for each sample. **B)** STAR alignment scores for each sample. **C)** STAR gene counts for each sample.

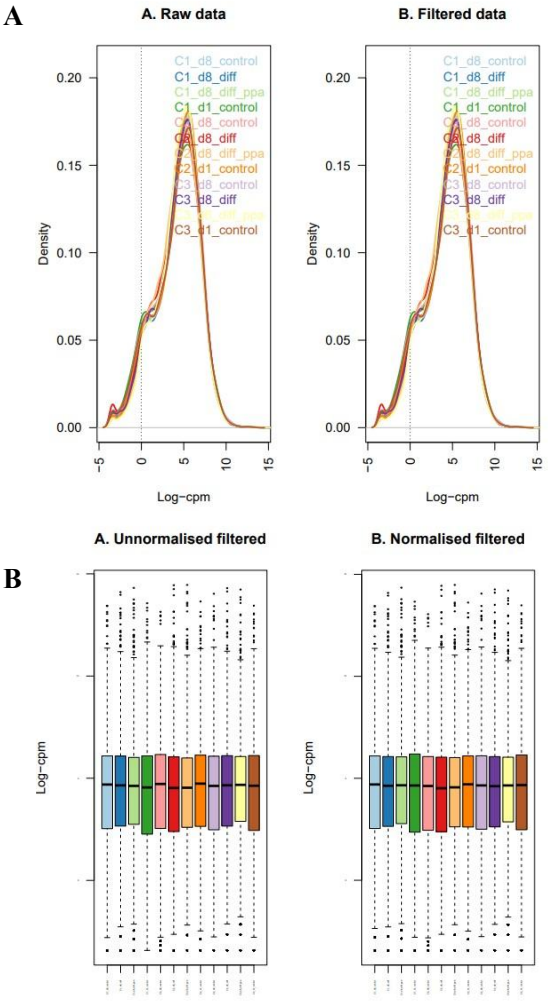


Figure S4.5. Log -normalised gene counts in counts per million (CPM) for all mapped genes **A)** before and **B)** after filtering.

Table S4.6. Identification of Soft-Threshold Used for Weighted Gene Co-expression Network Analysis

Power	SFT.R.sq.	slope	truncated.R.sq.	mean.k.	median.k.	max.k.
1	0.880	4.389	0.993	5686.612	5799.052	7440.289
2	0.690	1.519	0.974	3080.397	3129.940	4923.323
3	0.270	0.523	0.928	1927.119	1928.011	3614.150
4	0.000	0.003	0.886	1310.942	1281.732	2809.489
5	0.170	-0.364	0.878	942.819	898.566	2271.863
6	0.370	-0.610	0.895	705.773	654.148	1886.362
7	0.500	-0.792	0.914	544.630	489.771	1597.384
8	0.580	-0.940	0.917	430.472	375.393	1373.550
9	0.630	-1.052	0.924	346.922	293.812	1195.696
10	0.660	-1.139	0.928	284.136	233.395	1051.458
12	0.720	-1.269	0.943	198.169	153.724	833.010
14	0.740	-1.378	0.947	143.984	105.413	676.796
16	0.770	-1.448	0.953	107.987	74.695	560.657
18	0.790	-1.502	0.963	83.076	54.374	471.698
20	0.800	-1.558	0.964	65.260	40.449	401.927

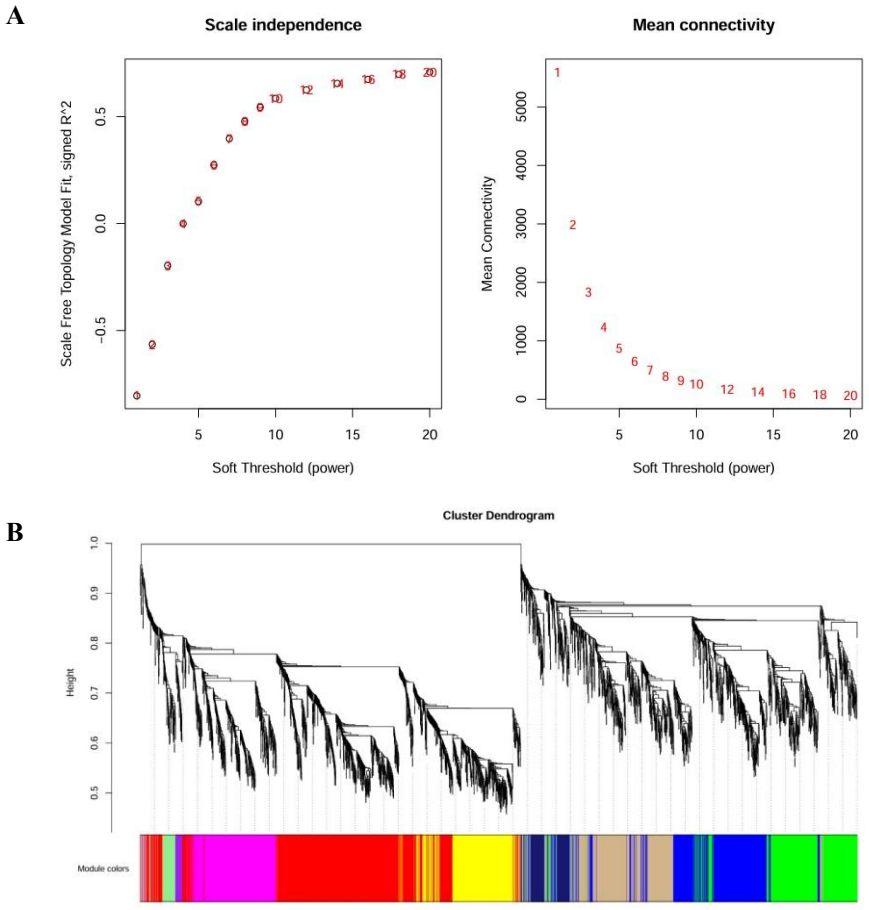


Figure S4.6. Identification of Correlated Modules Using Weighted Gene Co-expression Network Analysis. **A**) Soft-threshold selection for Weighted Gene Co-expression Network Analysis showing scale independence vs mean connectivity. **B)** Gene dendrogram generated using average hierarchical clustering showing coregulated modules determined by the Dynamic Tree Cut after merging based on a dissimilarity threshold of 0.25.

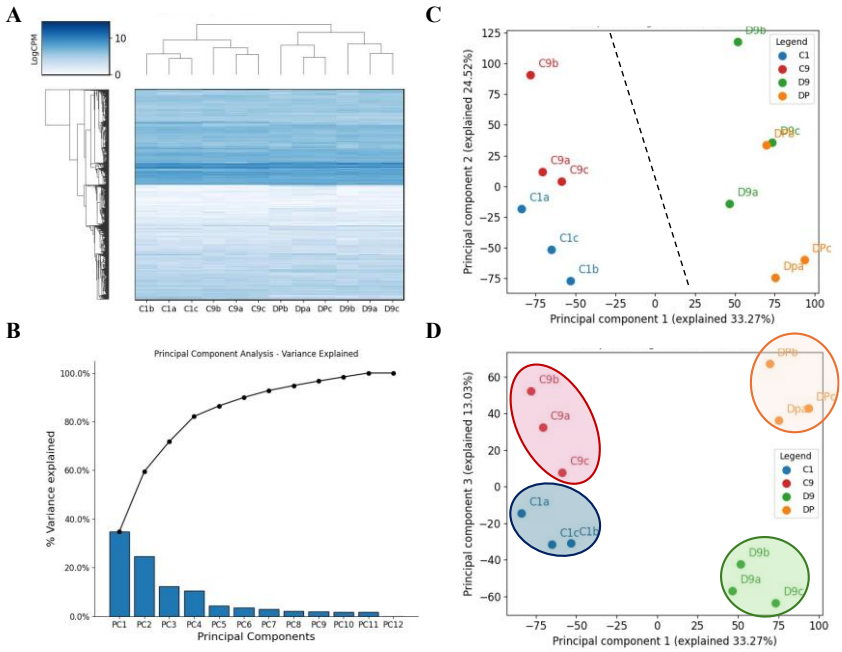


Figure S4.7. Distinct Transcriptomic Signatures Associated with Different Conditions. Neurons exposed to PPA during differentiation (DP) were compared to day 1 undifferentiated controls grown in 15% FBS (C1), day 9 negative controls maintained at 1% FBS without RA or BDNF (C9) and day 9 positive controls differentiated with RA and BDNF (D9). **A)** Hierarchical Clustering by Average Euclidean Distance for all 12 samples based on log-normalised counts per million (CPMs) for all 144555genes retained after filtering. **B)** Scree plot obtained from Principle Component Analysis (PCA) showing the cumulative variance captured by each principle component. Scatter plots show experimental samples plotted against **C)** PC1 and PC2, demonstrating separation between undifferentiated and differentiated samples and **D)** PC1 and PC3, demonstrating clustering within all four experimental conditions.

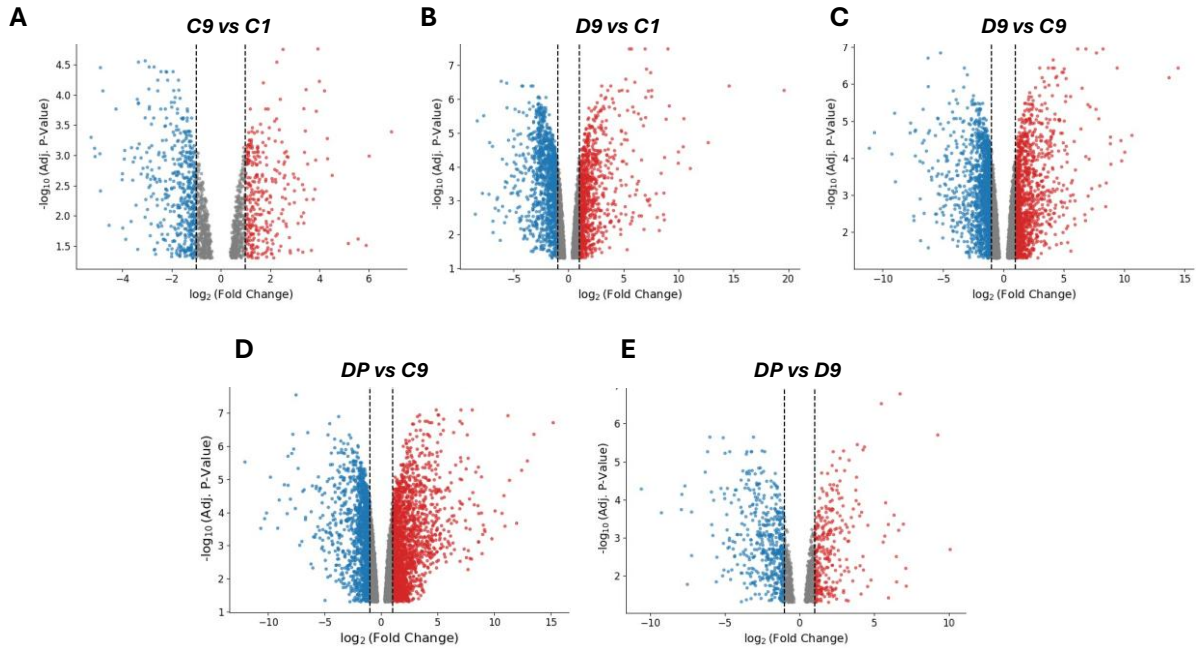


Figure S4.8. Differentially Expressed Genes Identified by QL-F Tests. Data represent volcano plots showing the log fold change and the FDR value for all 9605 unique genes that were differentially expressed between **A)** day 1 controls (C1) and day 9 controls (C9), **B)** Day 9 differentiated samples (D9) and C1, **C)** D9 and C9, **D)** day 9 neurons differentiated with Propionic Acid (DP) and C9 and **E)** DP and D9.

Table S4.7. Signatures of Serum Depletion. Data represent the top 10 hallmark, GO Biological Processes and Reactome Pathways enriched in the genes that were significantly down and up-regulated in serum-depleted controls relative to day 1 undifferentiated controls.

Downregulated Genes					
Hallmark		**GO BP**		**Reactome**	
E2F Targets	5.84E-40	Regulation Of Cell Migration (GO:0030334)	1.69E-12	Cell Cycle, Mitotic R-HSA-69278	1.34E-36
G2-M Checkpoint	5.86E-38	Positive Regulation of Cell Cycle Process (GO:0090068)	3.05E-12	Cell Cycle R-HSA-1640170	2.17E-35
Epithelial Mesenchymal Transition	2.93E-27	Mitotic Sister Chromatid Segregation (GO:0000070)	3.52E-11	Signal Transduction R-HSA-162582	9.48E-25
Mitotic Spindle	6.10E-14	Microtubule Cytoskeleton Organisation Involved in Mitosis (GO:1902850)	6.58E-10	M Phase R-HSA-68886	1.05E-19
Apical Junction	3.53E-10	Positive Regulation of Cell Population Proliferation (GO:0008284)	3.07E-09	Signalling By Rho GTPases R-HSA-194315	1.49E-18
TNF-alpha Signalling via NF-kB	8.91E-09	Mitotic Spindle Organisation (GO:0007052)	3.43E-09	Signalling By Rho GTPases, Miro GTPases and RHOBTB3 R-HSA-9716542	1.77E-18
KRAS Signalling Up	1.65E-08	Sister Chromatid Segregation (GO:0000819)	6.85E-08	Cell Cycle Checkpoints R-HSA-69620	6.97E-18
Inflammatory Response	5.63E-08	Regulation Of Cell Population Proliferation (GO:0042127)	8.86E-08	Mitotic Metaphase and Anaphase R-HSA-2555396	1.16E-16
Hypoxia	2.32E-07	Positive Regulation of Cell Migration (GO:0030335)	1.37E-07	Mitotic Prometaphase R-HSA-68877	1.33E-16
Coagulation	2.32E-07	Positive Regulation of Cellular Process (GO:0048522)	1.62E-07	Mitotic Anaphase R-HSA-68882	3.03E-16
Upregulated Genes					
Unfolded Protein Response	1.03E-03	Cytoplasmic Translation (GO:0002181)	4.26E-30	Response Of EIF2AK4 (GCN2) To Amino Acid Deficiency R-HSA-9633012	3.86E-34
p53 Pathway	1.24E-01	Peptide Biosynthetic Process (GO:0043043)	8.07E-18	Cellular Response to Starvation R-HSA-9711097	4.19E-31
mTORC1 Signalling	3.59E-01	Translation (GO:0006412)	8.13E-16	Eukaryotic Translation Elongation R-HSA-156842	3.65E-30
Pancreas Beta Cells	3.59E-01	Macromolecule Biosynthetic Process (GO:0009059)	5.57E-15	Peptide Chain Elongation R-HSA-156902	3.75E-30
KRAS Signalling Dn	3.72E-01	Gene Expression (GO:0010467)	4.42E-07	Selenocysteine Synthesis R-HSA-2408557	4.94E-30
Hedgehog Signalling	4.23E-01	Calcium Ion-Regulated Exocytosis of Neurotransmitter (GO:0048791)	1.03E-02	Formation Of a Pool of Free 40S Subunits R-HSA-72689	8.64E-30
Hypoxia	7.88E-01	Ribonucleoprotein Complex Biogenesis (GO:0022613)	2.55E-02	Viral mRNA Translation R-HSA-192823	2.50E-29
Inflammatory Response	7.88E-01	Synaptic Vesicle Exocytosis (GO:0016079)	2.55E-02	L13a-mediated Translational Silencing of Ceruloplasmin Expression R-HSA-156827	3.99E-29
Spermatogenesis	8.06E-01	Cellular Response to Acetylcholine (GO:1905145)	3.12E-02	GTP Hydrolysis and Joining Of 60S Ribosomal Subunit R-HSA-72706	6.85E-29
UV Response Dn	8.63E-01	Chemical Synaptic Transmission (GO:0007268)	4.22E-02	Eukaryotic Translation Termination R-HSA-72764	5.70E-28

Table S4.8. The Neurogenic Signature of Serum Depletion. Data represent the top 10 hallmark, GO Biological Processes and Reactome Pathways enriched in the genes that were significantly down and up-regulated in both differentiated neurons and serum-depleted controls relative to day 1 undifferentiated controls.

Downregulated Genes					
Hallmark		**GO BP**		**Reactome**	
E2F Targets	9.61E-62	Mitotic Sister Chromatid Segregation (GO:0000070)	2.38E-18	Cell Cycle, Mitotic R-HSA-69278	2.33E-62
G2-M Checkpoint	5.95E-53	Positive Regulation of Cell Cycle Process (GO:0090068)	2.45E-17	Cell Cycle R-HSA-1640170	8.11E-62
Epithelial Mesenchymal Transition	4.69E-16	Microtubule Cytoskeleton Organisation Involved in Mitosis (GO:1902850)	3.79E-13	M Phase R-HSA-68886	4.00E-36
Mitotic Spindle	1.30E-13	Mitotic Spindle Organisation (GO:0007052)	9.29E-13	Cell Cycle Checkpoints R-HSA-69620	3.38E-31
Myc Targets V1	7.43E-08	Sister Chromatid Segregation (GO:0000819)	1.78E-12	Mitotic Prometaphase R-HSA-68877	4.44E-30
Glycolysis	5.25E-04	Metaphase Plate Congression (GO:0051310)	8.77E-12	Mitotic Metaphase and Anaphase R-HSA-2555396	4.94E-28
Spermatogenesis	5.71E-04	Mitotic Nuclear Division (GO:0140014)	6.81E-11	Mitotic Anaphase R-HSA-68882	2.48E-27
mTORC1 Signalling	5.71E-04	Mitotic Metaphase Plate Congression (GO:0007080)	8.58E-11	Resolution Of Sister Chromatid Cohesion R-HSA-2500257	1.89E-24
Estrogen Response Late	9.14E-04	Positive Regulation of Chromosome Separation (GO:1905820)	2.53E-10	EML4 And NUDC In Mitotic Spindle Formation R-HSA-9648025	3.78E-24
Coagulation	9.68E-04	Negative Regulation of Mitotic Metaphase/Anaphase Transition (GO:0045841)	5.01E-10	RHO GTPases Activate Formins R-HSA-5663220	1.66E-23
Upregulated Genes					
KRAS Signalling Dn	4.53E-01	Phospholipid Homeostasis (GO:0055091)	2.61E-01	Neuronal System R-HSA-112316	4.49E-01
p53 Pathway	5.29E-01	Anterograde Trans-Synaptic Signalling (GO:0098916)	2.61E-01	Potassium Channels R-HSA-1296071	6.14E-01
UV Response Dn	1.00E+00	Chemical Synaptic Transmission (GO:0007268)	2.61E-01	Signalling By Retinoic Acid R-HSA-5362517	6.80E-01
Adipogenesis	1.00E+00	Regulation Of Catecholamine Secretion (GO:0050433)	2.61E-01	Cardiac Conduction R-HSA-5576891	6.80E-01
Androgen Response	1.00E+00	Calcium Ion-Regulated Exocytosis of Neurotransmitter (GO:0048791)	2.61E-01	Stimuli-sensing Channels R-HSA-2672351	6.80E-01
Pperoxisome	1.00E+00	Potassium Ion Transmembrane Transport (GO:0071805)	2.61E-01	Ion Channel Transport R-HSA-983712	6.80E-01
Estrogen Response Early	1.00E+00	Cellular Response to Topologically Incorrect Protein (GO:0035967)	2.61E-01	Macroautophagy R-HSA-1632852	6.80E-01
Hedgehog Signalling	1.00E+00	Cellular Response to Starvation (GO:0009267)	2.61E-01	Regulation Of Insulin Secretion R-HSA-422356	6.80E-01
Inflammatory Response	1.00E+00	Sulfation (GO:0051923)	2.61E-01	BBSome-mediated Cargo-Targeting to Cilium R-HSA-5620922	6.99E-01
Hypoxia	1.00E+00	Autophagy Of Mitochondrion (GO:0000422)	2.61E-01	Inwardly Rectifying K+ Channels R-HSA-1296065	6.99E-01

Table S4.9. Neurotoxic Signatures of Serum Depletion. Data represent the top 10 hallmark, GO Biological Processes and Reactome Pathways enriched in the genes that were significantly differentially expressed in serum-depleted controls but not differentiated neurons relative to day 1 undifferentiated controls.

Downregulated Genes					
Hallmark		**GO BP**		**Reactome**	
Epithelial Mesenchymal Transition	4.90E-07	Regulation Of Cell Migration (GO:0030334)	3.73E-08	Signal Transduction R-HSA-162582	3.04E-06
TNF-alpha Signalling via NF-kB	4.90E-07	Positive Regulation of Cell Migration (GO:0030335)	2.75E-04	Extracellular Matrix Organisation R-HSA-1474244	7.87E-04
Myogenesis	4.52E-06	Positive Regulation of Cell Motility (GO:2000147)	1.31E-03	Cytokine Signalling in Immune System R-HSA-1280215	1.32E-03
Apical Junction	6.09E-06	Positive Regulation of Cellular Process (GO:0048522)	1.31E-03	Interleukin-10 Signalling R-HSA-6783783	1.91E-03
Inflammatory Response	2.76E-05	Regulation Of Cell Junction Assembly (GO:1901888)	2.12E-03	Immune System R-HSA-168256	7.68E-03
Interferon Alpha Response	8.98E-05	Positive Regulation Of NF-kappaB Transcription Factor Activity (GO:0051092)	2.92E-03	Interferon Alpha/Beta Signalling R-HSA-909733	7.68E-03
IL-2/STAT5 Signalling	8.98E-05	Response To Cytokine (GO:0034097)	3.01E-03	Innate Immune System R-HSA-168249	1.75E-02
Estrogen Response Early	8.98E-05	Positive Regulation of Cell Population Proliferation (GO:0008284)	3.01E-03	MyD88 Deficiency (TLR2/4) R-HSA-5602498	1.77E-02
IL-6/JAK/STAT3 Signalling	1.21E-04	Cytokine-Mediated Signalling Pathway (GO:0019221)	3.01E-03	Interferon Signalling R-HSA-913531	1.77E-02
TGF-beta Signalling	4.57E-04	Negative Regulation of Neuron Death (GO:1901215)	3.01E-03	Signalling By Interleukins R-HSA-449147	1.87E-02
Upregulated Genes					
mTORC1 Signalling	1.61E-01	Cytoplasmic Translation (GO:0002181)	2.27E-36	Response Of EIF2AK4 (GCN2) To Amino Acid Deficiency R-HSA-9633012	1.67E-42
Unfolded Protein Response	2.69E-01	Peptide Biosynthetic Process (GO:0043043)	1.98E-25	Peptide Chain Elongation R-HSA-156902	2.18E-40
Spermatogenesis	3.68E-01	Translation (GO:0006412)	9.65E-23	Formation Of a Pool of Free 40S Subunits R-HSA-72689	9.36E-40
p53 Pathway	3.75E-01	Macromolecule Biosynthetic Process (GO:0009059)	3.44E-22	Eukaryotic Translation Elongation R-HSA-156842	1.05E-39
Oxidative Phosphorylation	7.84E-01	Gene Expression (GO:0010467)	7.94E-16	L13a-mediated Translational Silencing of Ceruloplasmin Expression R-HSA-156827	1.24E-38
Hedgehog Signalling	8.88E-01	Ribonucleoprotein Complex Biogenesis (GO:0022613)	7.78E-08	GTP Hydrolysis and Joining Of 60S Ribosomal Subunit R-HSA-72706	1.81E-38
Bile Acid Metabolism	8.88E-01	Ribosome Biogenesis (GO:0042254)	2.65E-06	Viral mRNA Translation R-HSA-192823	1.81E-38
Pancreas Beta Cells	8.88E-01	Ribosomal Small Subunit Biogenesis (GO:0042274)	3.92E-05	Eukaryotic Translation Termination R-HSA-72764	2.84E-38
heme Metabolism	8.88E-01	rRNA Metabolic Process (GO:0016072)	8.17E-03	Selenocysteine Synthesis R-HSA-2408557	2.84E-38
DNA Repair	8.88E-01	Ribosomal Large Subunit Biogenesis (GO:0042273)	8.17E-03	Cellular Response to Starvation R-HSA-9711097	3.50E-38

Table S4.10. The RA-BDNF Neurogenic Programme. Data represent the top 10 hallmark, GO Biological Processes and Reactome Pathways enriched in the genes that were significantly differentially expressed in differentiated neurons relative to both day 1 and day 9 controls.

Downregulated Genes					
Hallmark		**GO BP**		**Reactome**	
Myc Targets V1	6.38E-75	DNA Metabolic Process (GO:0006259)	9.54E-19	Cell Cycle R-HSA-1640170	2.46E-61
E2F Targets	1.25E-63	DNA-templated DNA Replication (GO:0006261)	8.38E-14	Cell Cycle, Mitotic R-HSA-69278	7.00E-54
G2-M Checkpoint	5.72E-47	DNA Replication (GO:0006260)	1.27E-11	Cell Cycle Checkpoints R-HSA-69620	1.20E-40
mTORC1 Signalling	2.78E-20	Positive Regulation of Cell Cycle Process (GO:0090068)	4.36E-11	M Phase R-HSA-68886	1.66E-31
Myc Targets V2	7.54E-14	DNA Repair (GO:0006281)	1.08E-10	Mitotic Metaphase and Anaphase R-HSA-2555396	1.06E-28
Oxidative Phosphorylation	7.87E-13	Double-Strand Break Repair (GO:0006302)	2.60E-09	Mitotic Anaphase R-HSA-68882	3.08E-28
Unfolded Protein Response	9.04E-13	Double-Strand Break Repair Via Homologous Recombination (GO:0000724)	3.11E-09	Resolution Of Sister Chromatid Cohesion R-HSA-2500257	7.88E-23
Estrogen Response Late	3.50E-07	Mitotic Sister Chromatid Segregation (GO:0000070)	3.97E-09	Unattached Kinetochores Signal Amplification Via A MAD2 Inhibitory Signal R-HSA-141444	3.15E-22
Glycolysis	3.50E-07	Cellular Respiration (GO:0045333)	3.61E-07	DNA Replication R-HSA-69306	2.48E-21
Mitotic Spindle	2.08E-04	Negative Regulation of Mitotic Metaphase/Anaphase Transition (GO:0045841)	3.61E-07	EML4 And NUDC In Mitotic Spindle Formation R-HSA-9648025	4.78E-21
Upregulated Genes					
UV Response Dn	1.11E-03	Nervous System Development (GO:0007399)	9.80E-06	Extracellular Matrix Organisation R-HSA-1474244	1.43E-03
Interferon Gamma Response	1.11E-03	Synapse Assembly (GO:0007416)	1.25E-03	Initial Triggering of Complement R-HSA-166663	5.04E-03
Interferon Alpha Response	9.58E-03	Calcium-Dependent Cell-Cell Adhesion Via Plasma Membrane Cell Adhesion Molecules (GO:0016339)	2.64E-03	Complement Cascade R-HSA-166658	1.20E-02
Apical Surface	1.96E-02	Extracellular Matrix Organisation (GO:0030198)	2.35E-02	Regulation Of FOXO Transcriptional Activity by Acetylation R-HSA-9617629	5.73E-02
IL-6/JAK/STAT3 Signalling	1.96E-02	Cell-Cell Adhesion Via Plasma-Membrane Adhesion Molecules (GO:0098742)	2.35E-02	Synthesis Of Bile Acids and Bile Salts R-HSA-192105	9.66E-02
Estrogen Response Early	4.15E-02	Negative Regulation of Wnt Signalling Pathway (GO:0030178)	2.35E-02	Canonical Retinoid Cycle in Rods (Twilight Vision) R-HSA-2453902	9.66E-02
KRAS Signalling Up	4.65E-02	Positive Regulation of Synaptic Transmission (GO:0050806)	3.03E-02	Regulation Of Complement Cascade R-HSA-977606	9.66E-02
Epithelial Mesenchymal Transition	4.95E-02	Quaternary Ammonium Group Transport (GO:0015697)	3.03E-02	Degradation Of Extracellular Matrix R-HSA-1474228	1.03E-01
Coagulation	5.62E-02	Cell Junction Assembly (GO:0034329)	3.27E-02	FOXO-mediated Transcription R-HSA-9614085	1.20E-01
Angiogenesis	6.88E-02	Neuron Projection Guidance (GO:0097485)	3.64E-02	Acyl Chain Remodelling of PE R-HSA-1482839	1.20E-01

Table S4.11. Different Controls Differentially Influence Neurogenic Signatures. Data represent the top 10 GO Biological Processes in the Global Enrich Nets from the genes that were significantly down and up-regulated in differentiated neurons (D9) compared to day 1 proliferative controls (C1) or day 9 serum-depleted controls (C9).

Downregulated Genes					
Hallmark		**GO BP**		**Reactome**	
D9 vs C1					
E2F Targets	9.66E-83	DNA Metabolic Process (GO:0006259)	2.80E-21	Cell Cycle R-HSA-1640170	1.82E-78
Myc Targets V1	1.06E-72	DNA Repair (GO:0006281)	8.61E-14	Cell Cycle, Mitotic R-HSA-69278	4.96E-70
G2-M Checkpoint	6.30E-57	mRNA Splicing, Via Spliceosome (GO:0000398)	3.08E-13	Cell Cycle Checkpoints R-HSA-69620	5.74E-46
mTORC1 Signalling	7.29E-28	mRNA Processing (GO:0006397)	3.69E-12	M Phase R-HSA-68886	3.41E-45
Myc Targets V2	6.30E-18	DNA-templated DNA Replication (GO:0006261)	3.95E-12	Mitotic Metaphase and Anaphase R-HSA-2555396	5.48E-35
Oxidative Phosphorylation	1.11E-11	RNA Splicing, Via Transesterification Reactions with Bulged Adenosine as Nucleophile (GO:0000377)	5.35E-12	Mitotic Anaphase R-HSA-68882	1.33E-34
Unfolded Protein Response	4.40E-11	DNA Replication (GO:0006260)	1.42E-11	Metabolism Of RNA R-HSA-8953854	3.77E-31
Glycolysis	1.42E-10	protein-DNA Complex Assembly (GO:0065004)	2.17E-10	DNA Replication R-HSA-69306	6.05E-27
UV Response Up	3.08E-08	Mitotic Sister Chromatid Segregation (GO:0000070)	2.47E-10	Processing Of Capped Intron-Containing Pre-mRNA R-HSA-72203	7.31E-27
Estrogen Response Late	3.24E-08	Positive Regulation of Cell Cycle Process (GO:0090068)	2.47E-10	Mitotic Prometaphase R-HSA-68877	7.73E-27
D9 vs C9					
Myc Targets V1	3.67E-71	Translation (GO:0006412)	4.05E-39	Translation R-HSA-72766	1.18E-54
E2F Targets	3.50E-45	Cytoplasmic Translation (GO:0002181)	9.29E-31	Cell Cycle R-HSA-1640170	2.31E-46
G2-M Checkpoint	2.93E-33	Peptide Biosynthetic Process (GO:0043043)	8.03E-30	Cell Cycle, Mitotic R-HSA-69278	9.61E-41
mTORC1 Signalling	3.12E-24	Macromolecule Biosynthetic Process (GO:0009059)	1.37E-24	Metabolism Of RNA R-HSA-8953854	9.66E-38
Oxidative Phosphorylation	8.53E-21	Ribonucleoprotein Complex Biogenesis (GO:0022613)	5.49E-24	Cell Cycle Checkpoints R-HSA-69620	1.06E-35
Unfolded Protein Response	2.24E-13	Ribosome Biogenesis (GO:0042254)	1.68E-23	Response Of EIF2AK4 (GCN2) To Amino Acid Deficiency R-HSA-9633012	2.51E-35
Myc Targets V2	8.07E-12	Gene Expression (GO:0010467)	3.32E-22	Cap-dependent Translation Initiation R-HSA-72737	3.78E-35
Glycolysis	1.14E-05	Ribosomal Small Subunit Biogenesis (GO:0042274)	6.59E-14	rRNA Processing in Nucleus and Cytosol R-HSA-8868773	1.22E-34
Estrogen Response Late	3.62E-05	Ribosomal Large Subunit Biogenesis (GO:0042273)	2.19E-12	rRNA Processing R-HSA-72312	5.95E-34
Spermatogenesis	4.33E-05	DNA-templated DNA Replication (GO:0006261)	2.79E-12	L13a-mediated Translational Silencing of Ceruloplasmin Expression R-HSA-156827	6.52E-34

Upregulated Genes					
Hallmark		**GO BP**		**Reactome**	
D9 vs C1					
UV Response Dn	2.41E-01	Nervous System Development (GO:0007399)	2.33E-01	Synthesis Of Bile Acids and Bile Salts R-HSA-192105	1.17E-01
Interferon Gamma Response	3.21E-01	Calcium-Dependent Cell-Cell Adhesion Via Plasma Membrane Cell Adhesion Molecules (GO:0016339)	2.33E-01	Initial Triggering of Complement R-HSA-166663	1.57E-01
TGF-beta Signalling	4.08E-01	Postsynapse Assembly (GO:0099068)	2.33E-01	Bile Acid and Bile Salt Metabolism R-HSA-194068	1.73E-01
Interferon Alpha Response	4.08E-01	Synapse Assembly (GO:0007416)	2.33E-01	Regulation Of FOXO Transcriptional Activity by Acetylation R-HSA-9617629	1.73E-01
IL-6/JAK/STAT3 Signalling	4.08E-01	Neuron Projection Guidance (GO:0097485)	2.49E-01	Complement Cascade R-HSA-166658	2.00E-01
KRAS Signalling Up	4.33E-01	Anterograde Trans-Synaptic Signalling (GO:0098916)	2.49E-01	Generic Transcription Pathway R-HSA-212436	2.00E-01
KRAS Signalling Dn	4.33E-01	Regulation Of Receptor Signalling Pathway Via STAT (GO:1904892)	2.49E-01	Interleukin-21 Signalling R-HSA-9020958	2.00E-01
Apical Surface	4.33E-01	Regulation Of Erythrocyte Differentiation (GO:0045646)	2.49E-01	Interleukin-15 Signalling R-HSA-8983432	2.00E-01
Angiogenesis	4.33E-01	Positive Regulation of Myeloid Cell Differentiation (GO:0045639)	2.49E-01	Potassium Channels R-HSA-1296071	2.41E-01
Coagulation	4.33E-01	Potassium Ion Transmembrane Transport (GO:0071805)	2.49E-01	Interleukin-2 Family Signalling R-HSA-451927	2.54E-01
D9 vs C9					
Interferon Alpha Response	2.06E-11	Nervous System Development (GO:0007399)	4.67E-06	Extracellular Matrix Organisation R-HSA-1474244	4.13E-09
Interferon Gamma Response	3.40E-10	Extracellular Matrix Organisation (GO:0030198)	7.92E-06	Interferon Alpha/Beta Signalling R-HSA-909733	1.17E-05
Epithelial Mesenchymal Transition	2.25E-08	Regulation Of Cell Migration (GO:0030334)	1.24E-04	Degradation Of Extracellular Matrix R-HSA-1474228	2.05E-05
UV Response Dn	5.86E-08	Defense Response to Symbiont (GO:0140546)	1.84E-04	Interferon Gamma Signalling R-HSA-877300	1.40E-04
Coagulation	2.74E-07	Positive Regulation of Nucleic Acid-Templated Transcription (GO:1903508)	2.08E-04	Signal Transduction R-HSA-162582	1.45E-04
TNF-alpha Signalling via NF-kB	9.20E-07	Cellular Response to Cytokine Stimulus (GO:0071345)	2.12E-04	Interleukin-10 Signalling R-HSA-6783783	1.90E-03
Estrogen Response Early	2.37E-06	Negative Regulation of Wnt Signalling Pathway (GO:0030178)	5.06E-04	Signalling By Retinoic Acid R-HSA-5362517	2.73E-03
TGF-beta Signalling	6.23E-06	Positive Regulation of Synaptic Transmission (GO:0050806)	5.54E-04	Regulation Of IGF Transport and Uptake by IGFBPs R-HSA-381426	2.73E-03
IL-6/JAK/STAT3 Signalling	1.29E-05	Negative Regulation of Canonical Wnt Signalling Pathway (GO:0090090)	6.32E-04	Post-translational Protein Phosphorylation R-HSA-8957275	3.06E-03
KRAS Signalling Up	6.39E-05	Regulation Of Inflammatory Response (GO:0050727)	1.00E-03	Interleukin-4 And Interleukin-13 Signalling R-HSA-6785807	3.57E-03

Table S4.12. Functional Signatures of Propionic Acid Stress. Data represent the top 10 hallmark, GO Biological Processes and Reactome Pathways enriched in the genes that were significantly differentially expressed with Propionic Acid Exposure during differentiation.

Downregulated Genes					
Hallmark		**GO BP**		**Reactome**	
Inflammatory Response	2.87E-02	Regulation Of Gene Expression (GO:0010468)	5.78E-07	Generic Transcription Pathway R-HSA-212436	2.01E-04
KRAS Signalling Up	2.44E-01	Regulation Of DNA-templated Transcription (GO:0006355)	3.28E-06	RNA Polymerase II Transcription R-HSA-73857	4.05E-04
UV Response Dn	2.44E-01	Regulation Of Nucleic Acid-Templated Transcription (GO:1903506)	3.94E-06	Gene Expression (Transcription) R-HSA-74160	4.05E-04
TNF-alpha Signalling via NF-kB	2.44E-01	Negative Regulation Of DNA-templated Transcription (GO:0045892)	1.60E-03	Neuronal System R-HSA-112316	1.28E-03
Pancreas Beta Cells	2.78E-01	Chemical Synaptic Transmission (GO:0007268)	8.87E-03	Chromatin Modifying Enzymes R-HSA-3247509	3.99E-02
Hedgehog Signalling	4.06E-01	Regulation Of Hemopoiesis (GO:1903706)	9.26E-03	Synthesis Of Bile Acids and Bile Salts Via 27-Hydroxycholesterol R-HSA-193807	3.99E-02
Notch Signalling	7.45E-01	Anterograde Trans-Synaptic Signalling (GO:0098916)	1.25E-02	RUNX1 Interacts with Co-Factors Whose Precise Effect on RUNX1 Targets Is Not Known R-HSA-8939243	4.83E-02
Estrogen Response Early	9.14E-01	Enzyme-Linked Receptor Protein Signalling Pathway (GO:0007167)	1.43E-02	Serotonin Neurotransmitter Release Cycle R-HSA-181429	6.25E-02
p53 Pathway	9.25E-01	Regulation Of Transcription by RNA Polymerase II (GO:0006357)	3.10E-02	Regulation Of Insulin Secretion R-HSA-422356	6.25E-02
Epithelial Mesenchymal Transition	9.25E-01	Synapse Assembly (GO:0007416)	3.10E-02	NR1H3 And NR1H2 Regulate Gene Expression Linked to Cholesterol Transport and Efflux R-HSA-9029569	6.81E-02
Upregulated Genes					
Epithelial Mesenchymal Transition	1.95E-09	Regulation Of Cell Migration (GO:0030334)	2.69E-07	Hemostasis R-HSA-109582	6.70E-11
Estrogen Response Late	4.80E-07	Extracellular Matrix Organisation (GO:0030198)	2.04E-05	Signal Transduction R-HSA-162582	4.02E-09
Glycolysis	2.18E-05	Axonogenesis (GO:0007409)	2.27E-05	Signalling By GPCR R-HSA-372790	8.74E-09
Estrogen Response Early	2.18E-05	Positive Regulation of Cell Motility (GO:2000147)	4.09E-05	Glycosaminoglycan Metabolism R-HSA-1630316	2.19E-08
KRAS Signalling Up	2.76E-05	Positive Regulation of Cell Migration (GO:0030335)	7.57E-05	Extracellular Matrix Organisation R-HSA-1474244	3.37E-08
Coagulation	5.84E-05	Positive Regulation of T Cell Mediated Cytotoxicity (GO:0001916)	1.42E-04	GPCR Downstream Signalling R-HSA-388396	5.55E-07

Apical Junction	7.79E-05	Regulation Of T Cell Mediated Cytotoxicity (GO:0001914)	1.42E-04	Neurotransmitter Receptors and Postsynaptic Signal Transmission R-HSA-112314	7.73E-07
Hypoxia	7.30E-04	Nervous System Development (GO:0007399)	1.42E-04	Neuronal System R-HSA-112316	1.22E-06
Complement	0.001075	Axon Guidance (GO:0007411)	1.88E-04	GPCR Ligand Binding R-HSA-500792	3.25E-06
Spermatogenesis	0.001707	Antigen Processing and Presentation of Endogenous Peptide Antigen (GO:0002483)	2.74E-04	Muscle Contraction R-HSA-397014	3.83E-06

Table S4.13. Convergent Cell Fate Regulators Perturbed by Propionic Acid. Data represent the top 10 hallmark, GO Biological Processes and Reactome Pathways enriched in the 204 genes that were significantly differentially expressed in all five pairwise comparisons.

Hallmark		GO BP		Reactome	
Coagulation	2.59E-08	G Protein-Coupled Receptor Signalling Pathway, Coupled to Cyclic Nucleotide Second Messenger (GO:0007187)	5.98E-05	Glycosaminoglycan Metabolism R-HSA-1630316	5.04E-03
Epithelial Mesenchymal Transition	6.13E-05	Axon Guidance (GO:0007411)	9.43E-03	Extracellular Matrix Organisation R-HSA-1474244	5.98E-03
UV Response Dn	2.07E-04	Neuron Projection Guidance (GO:0097485)	9.43E-03	Syndecan Interactions R-HSA-3000170	1.64E-02
G2-M Checkpoint	2.07E-04	Axonogenesis (GO:0007409)	9.43E-03	Non-integrin membrane-ECM Interactions R-HSA-3000171	1.64E-02
Hypoxia	2.07E-04	Cellular Response to Acetylcholine (GO:1905145)	2.79E-02	Signal Transduction R-HSA-162582	2.07E-02
Inflammatory Response	5.62E-03	Regulation Of Cell Population Proliferation (GO:0042127)	2.79E-02	Dissolution Of Fibrin Clot R-HSA-75205	2.07E-02
TNF-alpha Signalling via NF-kB	3.55E-02	Heart Development (GO:0007507)	6.08E-02	ECM Proteoglycans R-HSA-3000178	2.07E-02
Apical Junction	3.55E-02	Atrial Septum Development (GO:0003283)	6.08E-02	Class A/1 (Rhodopsin-like Receptors) R-HSA-373076	2.48E-02
Notch Signalling	4.08E-02	Regulation Of Endothelial Cell Migration (GO:0010594)	6.68E-02	Heparan Sulfate/Heparin (HS-GAG) Metabolism R-HSA-1638091	2.48E-02
Complement	4.56E-02	Sensory Perception of Pain (GO:0019233)	7.28E-02	HS-GAG Biosynthesis R-HSA-2022928	2.48E-02

Table S4.14. Top 10 Cell-Fate Regulators Altered by PPA Exposure. Data represent the top ten hub genes with the highest degree of betweenness centrality in the Chea3 transcription factor – gene network for the 204 genes that were significantly differentially expressed in all five pairwise comparisons.

Gene	Log2FC	Betweenness	Function
SMAD3	-0.78	2641.19	Intracellular signal transducer and transcriptional modulator activated by TGF-β and activin type 1 receptor kinases. Binds TRE elements to activate transcription.
FOXO3	-0.71	878.81	Regulates autophagy, apoptosis, mitogenesis & fatty acid metabolism in response to metabolic & oxidative stress.
TBX3	-2.26	820.08	Transcriptional repressor involved in development, patterning, proliferation & senescence by regulating Shh, BMP & TGF-β signalling.
KLF6	0.57	674.45	Kruppel-like transcription factor involved in proliferation, survival, differentiation and adipogenesis.

POU3F2	1.45	656.83	POU-III transcription factor involved in neuronal differentiation.
HES1	0.69	442.48	Transcriptional effector of Notch signalling that regulates NSC self-renewal, pluripotency & neurogenesis.
ST3GAL1	-0.89	340.53	Glycosyltransferase involved in terminal sialylation of glycoproteins & glycolipids.
PLXNA2	1.21	219.55	Plexin-A semaphorin co-receptor involved in axon repulsion, invasive growth and cell migration.
ELK3	0.52	265.29	ETS & TCF transcription factor that is recruited by serum response factor to regulate target genes involved in proliferation, growth, apoptosis, differentiation, cytoskeletal remodelling & morphogenesis.
NRP1	-1.45	239.58	Neuropilin involved in cell survival, migration, the formation of neuronal circuits and axon repulsion/attraction via interactions with vascular endothelial growth factor (VEGF) & semaphorin.

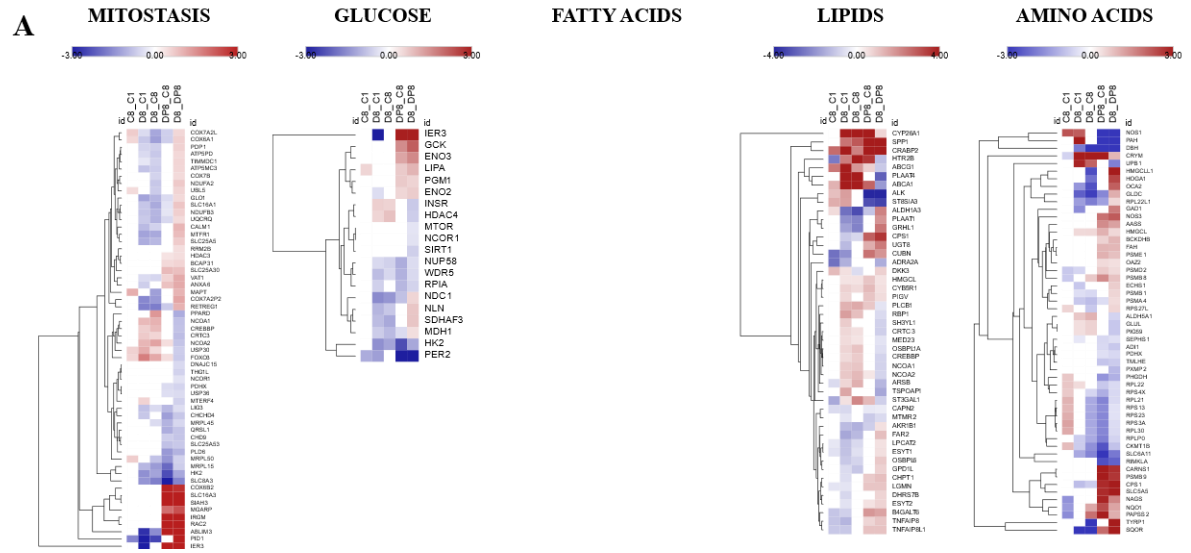


Figure S4.9. Metabolic Signatures of Propionic Acid Exposure. Data represent LogFoldChange Values for Genes Involved in Mitochondrial, Glucose, Lipid and Amino Acid metabolism that are Significantly Differentially Expressed under Propionic Acid (PPA) Stress.

Table S4.15. Canonical Metabolic Genes That Were Substantially Disrupted by Propionic Acid. Data represent the 43 metabolic genes that were most substantially differentially expressed (| LogFC | ≥ 1) in response to Propionic Acid.

Gene	LogFC	Function
	Mitochondrial Metabolism and Dynamics	
RAC2	4.39	Plasma membrane-associated small GTPase that regulates secretion, vesicle transport, phagocytosis, cell polarisation & ROS production.
IRGM	4.03	Regulates selective autophagy via AMPK, including mitophagy by binding to cardiolipin & inducing mitochondrial fission.
SIAH3	3.19	Negative regulator of PRKN translocation to damaged mitochondria by destabilising PINK1.
SLC16A3	3.12	Proton-linked monocarboxylate transporter that mediates lactate efflux from highly glycolytic cells. Also involved in the transport of pyruvate, BCAAs & ketone bodies.
PID1	3.07	Involved in mitochondrion morphogenesis.
COX6B2	2.33	Component of the cytochrome c oxidase, the last enzyme in the mitochondrial ETC.
MGARP	1.2	Plays a role in the trafficking of mitochondria along microtubules to nerve terminals and in the maintenance of mitochondrial abundance & morphology.
VAT1	1.13	Negatively regulates mitochondrial fusion in cooperation with mitofusin proteins.

ANXA6	1.13	Regulates the release of Ca (2+) from intracellular stores.
RETREG1	1.02	Endoplasmic reticulum-anchored autophagy receptor that mediates ER delivery into lysosomes through sequestration into autophagosomes during the ER stress response.
PLD6	-1.01	Phospholipase in the outer mitochondrial membrane protein that plays a key role in mitochondrial fusion & fission.
SLC8A3	-1.63	Sodium/calcium exchanger that mediates Ca (2+) efflux from mitochondria & contributes to mitochondrial Ca (2+) ion homeostasis. Facilitates the decrease in cytoplasmic Ca (2+) after neuronal activation & thereby contributes to synaptic plasticity, learning & memory.
Glycolysis		
IER3	8.96	Central regulator & effector of ERK signalling that plays a role in the response to stress & starvation.
GCK	2.17	Mediates the initial step of glycolysis by converting D-glucose to D-glucose 6-phosphate.
ENO3	1.58	Glycolytic enzyme that converts 2-phosphoglycerate to phosphoenolpyruvate.
HK2	-1.16	Outer mitochondrial membrane protein that couples extramitochondrial glycolysis to intramitochondrial oxidative phosphorylation & plays a key role in maintaining the integrity of the mitochondrial membrane & preventing apoptosis.
Amino Acid Metabolism		
TYRP1	7.51	Hydroxylates tyrosine.
SQOR	5.81	Mitochondrial enzyme that catalyses the conversion of sulphide to persulphides, thereby decreasing toxic concentrations of sulphide.
SLC5A5	4.16	Mediates the transport of chlorate, thiocyanate, nitrate & selenocynate.
CPS1	3.56	Mitochondrial enzyme that catalyses the synthesis of carbamoyl phosphate from ammonia & bicarbonate in the first committed step of the urea cycle.
HMGCLL1	3.37	Enables hydroxymethylglutaryl-CoA lyase activity to produce acetyl-CoA & acetoacetate during ketogenesis.
CARNS1	2.76	Catalyses the synthesis of carnosine & homocarnosine.
PSMB9	2.66	Proteosome subunit that cleaves peptides with Arg, Phe, Tyr, Leu, & Glu.
HOGA1	2.45	Mitochondrial enzyme that catalyses the final step in the metabolic pathway of hydroxyproline, releasing glyoxylate & pyruvate.
NOS3	2.16	Produces NO which acts as a signalling molecular & neurotransmitter.
SLC6A11	-2.01	Sodium-dependent transporter that uptakes GABA to end GABA neurotransmission.
RIMKLA	-2.34	Involved in glutamine family amino acid metabolism.
DBH	-4.16	Catalyses the hydroxylation of dopamine to noradrenaline.
NOS1	-4.35	Produces nitric oxide (NO).
PAH (1)	-6.28	Hydroxylates phenylalanine to tyrosine & is the rate-limiting step in phenylalanine catabolism.
Lipid Metabolism		
CRABP2	4.37	Transports RA to the nucleus, associated with increased circulating LDL cholesterol.
GDPD5	3.20	Glycerophosphocholine phosphodiesterase that mediates the cleavage of glycosylphosphatidylinositol (GPI) anchor of target proteins.
ANXA1 (2)	3.17	Inhibits phospholipase A2, plays a role in the formation of phagosomes & interactions between phagosomes & the actin cytoskeleton.
CYP1A1	2.92	ER protein involved in RA biosynthesis.
UGT8	2.35	Catalyses the transfer of galactose to ceramide during the biosynthesis of galactocerebrosides, which are abundant sphingolipids of the myelin membrane in the CNS.
ALOXE3	2.25	Activates PPARα, oxygenates polyunsaturated fatty acids to produce fatty acid hydroperoxides.
ALDH1A3	2.20	Catalyses the NAD-dependent oxidation of all-trans-retinal to all-trans-retinoate.
CYP2J2	2.16	Cytochrome P450 protein involved in the synthesis of cholesterol & other lipids.
INSIG1	-2.21	Mediates feedback control of cholesterol synthesis by controlling SCAP & HMGCR. Functions by blocking the processing of sterol regulatory element-binding proteins (SREBPs).
PTGIS	-2.86	Cytochrome P450 protein involved in synthesis of cholesterol & other lipids.
PLAAT4	-2.95	RAR receptor, phospholipase & acyltransferase.
ST8SIA3	-3.47	Involved in ganglioside biosynthesis, glycoprotein metabolism & protein sialylation.
ALK	-4.87	Receptor tyrosine kinase that is expressed in specific regions of the CNS & plays an important role in regulating energy balance, lipolysis, apoptosis, proliferation and NFκβ signalling during the genesis & differentiation of the nervous system.

Table S4.16. Metabolic Regulators of Neuronal Stem Cell Fate. Data represent the 14 metabolic genes that were differentially expressed across all five pairwise comparisons where genes implicated in the SFARI database of ASD risk genes are highlighted in red with their SFARI score. Log fold change values represent the differential expression between neurons exposed to propionic acid and differentiated controls, betweenness centrality values are listed for each gene in the transcription factor – gene regulatory network between all 204 genes that were shared across all five pairwise comparisons.

Gene	Log2FC	Betweenness	Function
FOXO3	-0.71	878.81	Regulates autophagy, apoptosis, mitogenesis & fatty acid metabolism in response to metabolic & oxidative stress.
ST3GAL1	-0.89	340.53	Glycosyltransferase involved in terminal sialylation of glycoproteins & glycolipids.
ABCG1	-0.99	82.2	ABC transporter that regulates lipid homeostasis & facilitates cholesterol & phospholipid efflux.
PLD1	1.38	79.69	Phosphatidylcholine-specific phospholipase that hydrolyses phospholipids into fatty acids & other lipophilic molecules. Involved in signal transduction, membrane trafficking, & the regulation of mitosis.
ABCA1	-1.86	56.89	ABC transporter that functions as a cholesterol efflux pump, transporting specific phospholipids from the cytoplasmic to the extracellular leaflet of the plasma membrane.
ALDH1A3 (S)	2.20	54.14	Aldehyde dehydrogenase that oxidises all-trans-retinal to all-trans-retinoate which is a critical lipid for embryonic development.
ANXA1 (2)	3.17	44.95	CAM involved in proliferation, differentiation, polarisation, motility, trafficking, apoptosis and tissue architecture by rearranging the actin cytoskeleton. Binds phospholipids at the plasma membrane, regulates inflammatory signalling & wound healing, inhibits hormone exocytosis & facilitates phagocytosis.
CNR1 (2)	-1.79	40.13	GPCR for endogenous cannabinoids that modulates mitochondrial respiration, SREBF-dependent lipogenesis, cholesterol metabolism & neurotransmission.
COX6A1	0.63	40.11	Terminal enzyme of the mitochondrial ETC.
CRABP2	4.37	21.73	RA binding protein that facilitates RA signalling & nuclear translocation.

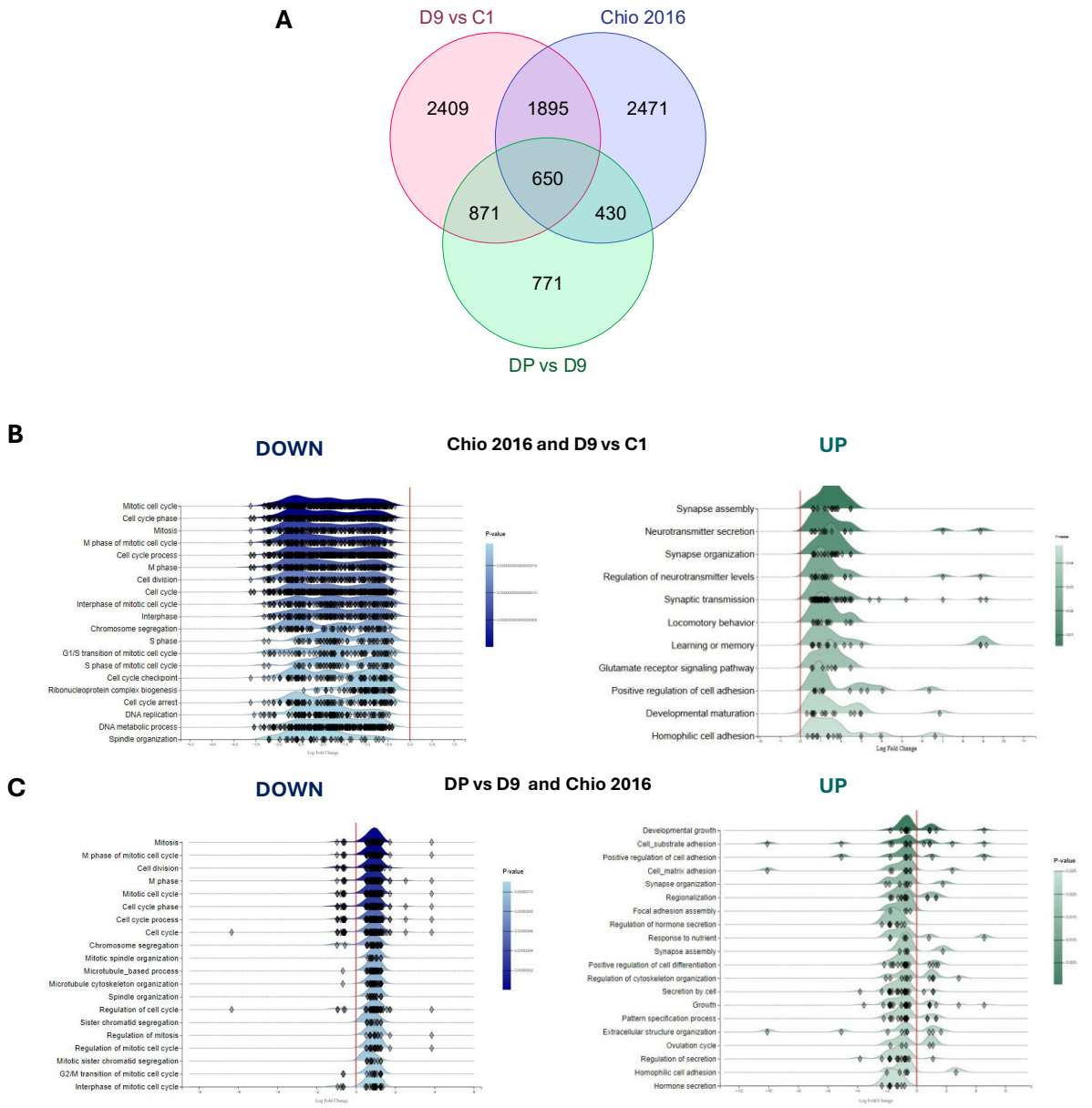


Figure S4.10. Transcriptomic Profiles of Neurogenesis. A) Venn diagram depicting the common differentially expressed genes (DEGs) in day 9 neurons relative to day 1 controls (D9 vs C1), neurons exposed to Propionic Acid (PPA) relative to differentiated controls (DP vs D9) and previous transcriptomic profiles of SH-SY5Y differentiation (Chiocchetti *et al*, 2016). B) Ridgeline plot showing the top 20 enriched GO biological processes in the genes that were differentially expressed during SH-SY5Y differentiation in both this study and the data published by Chiocchetti *et al*, (2016) where DEGs in each pathway are represented by their log fold change in expression induced by differentiation compared to undifferentiated controls. C**)** Ridgeline plot showing the top 20 GO processes among the neurogenic genes disrupted by PPA that were also implicated in the Chiocchetti 2016 transcriptome where DEGs in each pathway are represented by their log fold change in expression induced by PPA compared to differentiated controls.

Table S4.17. Central Cell Fate Regulators in the SH-SY5Y Transcriptome. Data represent the top ten hub genes among the 55 central cell fate regulators validated in the Chiocchetti 2016 transcriptome that were disrupted by Propionic Acid during neurogenesis, where genes are ranked by betweenness centrality in the relevant Chea3 transcription factor – gene regulatory networks.

Gene	Betweenness	LogFC	Function
SMAD3	417.98	-0.78	Intracellular signal transducer and transcriptional modulator activated by TGF-β and activin type 1 receptor kinases. Binds TRE elements to activate transcription.
FOXO3	196.89	-0.71	Regulates autophagy, apoptosis, mitogenesis & fatty acid metabolism in response to metabolic & oxidative stress.
PLXNA2	154.38	1.21	Plexin-A semaphorin co-receptor involved in axon repulsion, invasive growth and cell migration.
POU3F2	106.14	1.45	POU-III transcription factor involved in neuronal differentiation.
EFNB2	131.25	-1.56	Crucial for migration, repulsion and adhesion during neuronal development
DIAPH3	106.46	0.81	Actin nucleation and elongation factor required for the assembly of F-actin structures via Rho GTPAses, mediates cytokinesis, stress fiber formation, transcriptional activation of the serum response factor and regulates cell movement and adhesion.
STC2	93.14	3.76	Secreted glycoprotein that regulates phosphate transport, cell metabolism, or cellular calcium/phosphate homeostasis.
SPATS2L	92.57	-0.63	Enables RNA binding activity.
ECT2	66.25	0.81	Guanine nucleotide exchange factor and transforming protein that is upregulated during DNA synthesis, and G2 and M phases of mitosis. Promotes guanine nucleotide exchange on Rho GTPases, required for signal transduction pathways that regulate cytokinesis, polarity, neurite outgrowth and proliferation.
E2F7	57.24	0.99	Involved in DNA damage response, p53 signalling, angiogenesis, regulation of G1/S phases by repressing classical E2F transcription factors.

Table S4.18. Mechanisms Perturbed by Propionic Acid in both Undifferentiated and Differentiated SH-SY5Y Cells. Data represent the top 10 Hallmark Pathways and GO Biological Processes enriched in the genes disrupted by Propionic Acid during differentiation that were also reported by Kim *et al*, (2019) to be significantly differentially expressed in undifferentiated SH-SY5Y cells exposed to 5mM PPA for 72 hours.

Shared Downregulated Genes			
Hallmark		**GO BP**	
Hedgehog Signalling	0.186307	Nervous System Development (GO:0007399)	0.08956
UV Response Dn	0.199615	Neuron Development (GO:0048666)	0.08956
mTORC1 Signalling	0.308232	Negative Regulation Of DNA-templated Transcription (GO:0045892)	0.08956
Hypoxia	0.53946	Negative Regulation of Steroid Biosynthetic Process (GO:0010894)	0.08956
Glycolysis	0.53946	Central Nervous System Development (GO:0007417)	0.08956
Inflammatory Response	0.53946	Cell Differentiation in Hindbrain (GO:0021533)	0.08956
Myc Targets V2	0.53946	Negative Regulation of Cell Activation (GO:0050866)	0.108326
Protein Secretion	0.53946	Embryonic Cranial Skeleton Morphogenesis (GO:0048701)	0.110307
Androgen Response	0.53946	Cardiac Myofibril Assembly (GO:0055003)	0.112853
Apoptosis	0.53946	Positive Regulation of Mitotic Cell Cycle Phase Transition (GO:1901992)	0.126055
Shared Upregulated Genes			
Epithelial Mesenchymal Transition	3.16E-04	Regulation Of Plasma Membrane Repair (GO:1905684)	0.01439
Hypoxia	4.71E-04	Negative Regulation of Neuron Projection Development (GO:0010977)	0.112542
Estrogen Response Late	4.71E-04	Neuron Migration (GO:0001764)	0.112542

Glycolysis	4.71E-04	Peripheral Nervous System Neuron Development (GO:0048935)	0.236226
KRAS Signalling Up	0.009762	Glycolipid Transport (GO:0046836)	0.236226
Spermatogenesis	0.020279	Protection From Natural Killer Cell Mediated Cytotoxicity (GO:0042270)	0.236226
Myogenesis	0.029764	Cellular Response to Prostaglandin E Stimulus (GO:0071380)	0.239783
UV Response Up	0.029788	Negative Regulation of Growth (GO:0045926)	0.239783
Angiogenesis	0.029788	Generation Of Neurons (GO:0048699)	0.239783
IL-2/STAT5 Signalling	0.070752	Negative Regulation of Fatty Acid Oxidation (GO:0046322)	0.239783

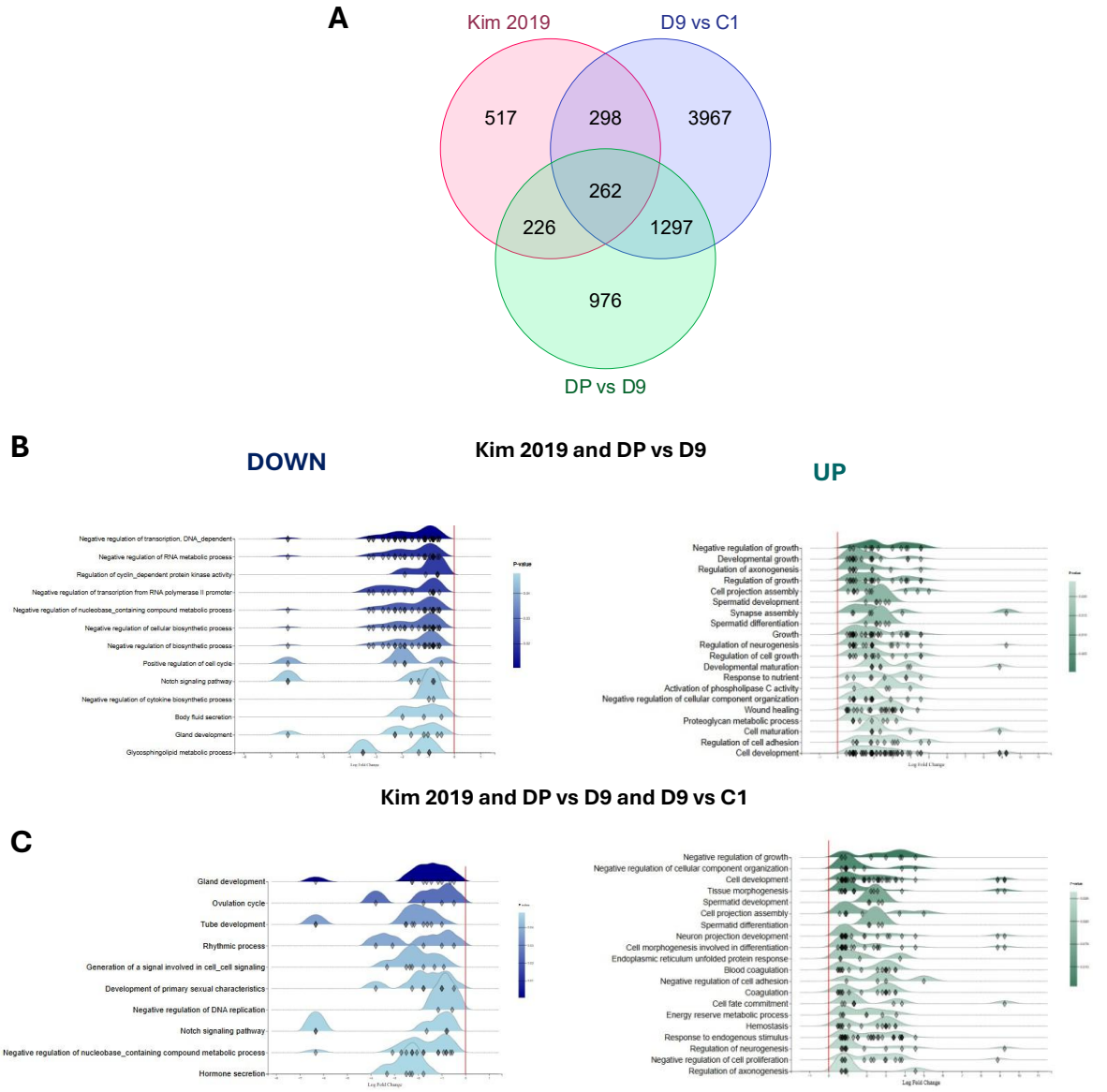


Figure S4.11. Transcriptomic Signatures of Propionic Acid in both Undifferentiated and Differentiated SH-SY5Y Cells. A) Venn diagram depicting significantly differentially expressed genes (DEGs) in day 9 neurons relative to day 1 controls (D9 vs C1), neurons exposed to Propionic Acid (PPA) relative to differentiated controls (DP vs D9) and the DEGs in undifferentiated SH-SY5Y cells exposed to PPA for 4 – 72 hours (S. A. Kim *et al.,* 2019). Ridgeline plots show the top 20 GO processes among B) the genes that were differentially expressed in response to PPA in both undifferentiated and differentiated SH-SY5Y cells that were C) also differentially expressed during neurogenesis where DEGs in each pathway are represented by their log fold change in expression induced by PPA compared to differentiated controls.

Table S4.19. Acute Disruptions to Central Cell Fate Regulators. Data represent the 19 central cell fate regulators that showed congruent responses to Propionic Acid (PPA) in both undifferentiated and differentiated SH-SY5Y cells. Genes are ranked by betweenness centrality in the relevant Chea3 transcription factor – gene regulatory networks; neurogenic genes that were validated in the Chiocchetti 2016 transcriptome are highlighted in bold and genes implicated in the SFARI database are highlighted in red with their associated risk score.

Gene	Betweenness	LogFC	Function
TBX3	103.1	-2.26	Transcriptional repressor involved in development, patterning, proliferation & senescence via interactions with Shh, BMP & TGFβ.
STC2	**93.23**	**3.76**	Secreted glycoprotein that regulates phosphate transport, cell metabolism, or cellular calcium/phosphate homeostasis.
FRMD4A	53.59	-0.62	Scaffolding protein that regulates epithelial cell polarity by connecting ARF6 activation with the PAR3 complex.
S100A10	36.09	7.67	Regulates cell cycle progression and differentiation, regulate ANXA2 phosphorylation.
RERG	**52.29**	**2.23**	Member of the RAS superfamily of GTPases that inhibits cell proliferation and tumour formation.
PPP2R2B	36.33	2.63	One of the four major Ser/Thr phosphatases is implicated in the negative control of cell growth and division. Isoform 2 regulates neuronal survival through the mitochondrial fission and fusion balance.
CHRM3 (2)	28.77	0.78	Cholinergic receptor that modulates PI turnover, adenylate cyclase and potassium channels through the action of G proteins.
SIRPA	22.58	-0.74	Member of the RAS superfamily of GTPases, inhibits cell proliferation and tumour formation
HTRA1	27.63	1.54	Serine protease with a variety of targets, including ECM proteins such as fibronectin and proteoglycans. Regulates angiogenesis, neuronal survival and differentiation through FGF, IGF and TGF-beta signalling.
IQGAP2	22.78	3.21	Interacts with components of the cytoskeleton, with cell adhesion molecules, and with several signalling molecules to regulate cell morphology and motility.
ANXA2	22.24	1.72	Calcium-dependent phospholipid-binding protein that plays a role in the regulation of cellular growth and in signal transduction pathways.
PCDH17	**20.53**	**1.54**	Calcium-dependent CAM involved in the establishment and function of specific cell-cell connections in the brain.
FXYD5	11.02	5.01	Glycoprotein that functions in the up-regulation of chemokine production and is involved in the reduction of cell adhesion via its ability to down-regulate E-cadherin.
SERPINE2	23.77	3.01	Serine protease inhibitor that promotes neurite extension by inhibiting thrombin.
FGFR3	**22.63**	**3.85**	Tyrosine-protein kinase that acts as a cell-surface receptor for fibroblast growth factors and plays an essential role in the regulation of cell proliferation, differentiation, neural outgrowth and apoptosis.
GPC3	6.32	2.73	Cell surface heparan sulfate proteoglycans that negatively regulates Shh signalling, positively regulates Wnt signalling and modulates the effects of growth factors on branching morphogenesis.
SCN9A (2)	3.71	2.11	Mediates the voltage-dependent sodium ion permeability of excitable membranes.
C1QL4	9.27	3.93	Regulates the number of excitatory synapses that are formed on hippocampus neurons, negatively regulates adipogenesis and proliferation, acts upstream to the ERK cascade.
CTSV	**6.26**	**2.35**	Cysteine protease.

Table S4.20. Transcriptomic Signatures of Neurotoxicity. Data represent the 23 mRNA markers for differentiation and developmental toxicity in the SH-SY5Y model that were significantly disrupted by Propionic Acid (PPA). Genes are ranked by differential expression where genes that were downregulated during differentiation but upregulated by PPA are shown in red, genes that were upregulated during differentiation but downregulation by PPA in blue, neurotoxic markers are in bold and SFARI genes are shown in red with their associated risk score.

Gene	LogFC	Function
GABRG3 (2)	**4.18**	Gamma subunit of the heteropentameric ligand-gated chloride channel gated by gamma-aminobutyric acid (GABA).
FGFR4	3.42	Tyrosine kinase for fibroblast growth factors involved in cell proliferation, differentiation, migration, lipid metabolism, bile acid biosynthesis, vitamin D metabolism, glucose uptake, and phosphate homeostasis.
GABRD	3.24	Delta subunit of the heteropentameric ligand-gated chloride channel gated by gamma-aminobutyric acid (GABA).
PGF	2.23	Involved in positive regulation of cell population proliferation, migration & angiogenesis via VEGF.
GAP43	1.71	Crucial for neuronal regeneration after injury, expressed at high levels in neuronal growth cones during development and modulates axonal and dendritic filopodia.
VCAN	**1.64**	Large chondroitin sulfate proteoglycan in the ECM involved in cell adhesion, proliferation, proliferation, migration and angiogenesis.
RGS9	1.18	Inhibits signal transduction by increasing the GTPase activity of G protein alpha subunits thereby driving them into their inactive GDP-bound form.
EGFR	0.83	Transmembrane glycoprotein kinase that upregulates proliferation in response to EGF.
CHRM3 (2)	**0.78**	Cholinergic receptor that modulates PI turnover, adenylate cyclase & potassium channels through GPCRs.
RAPGEF4 (2)	**0.74**	Regulates neurotransmitter receptor localisation to postsynaptic specialisation membrane, postsynapse organisation and exocytosis.
SEMA5A (2)	**-0.87**	Bifunctional axonal guidance cue regulated by sulphated proteoglycans that results in the disassembly of F-actin stress fibres, disruption of focal adhesions & cellular collapse as well as inhibition of cell migration & invasion.
PDGFRA	**-1**	Modulates wound healing, embryonic development, cell proliferation, survival and chemotaxis.
NTNG2 (S)	-1.49	Modulates patterning and neuronal circuit formation, basement membrane assembly; cell morphogenesis, differentiation; and cell projection organisation.
NTRK1 (2)	**-1.49**	Required for neuronal differentiation and lineage specification coupled to the Ras, Cdc42/Rac/RhoG, MAPK, PI3K and PLCgamma signalling pathways.
EFNB2	**-1.56**	Crucial for migration, repulsion and adhesion during neuronal development.
CNR1 (2)	**-1.79**	GPCR for endogenous cannabinoids that modulates mitochondrial respiration, SREBF-dependent lipogenesis, cholesterol metabolism & neurotransmission.
CACNA2D2	**-1.83**	The alpha-2/delta subunit of voltage-dependent calcium channels regulates calcium current density and activation/inactivation kinetics of the calcium channel.

OPRD1	**-1.95**	Intrinsic component of plasma membrane involved in GPCR signalling, response to hypoxia, inhibits neurotransmitter release by reducing calcium ion currents and increasing potassium ion conductance.
GFRA1	**-2.05**	Glial cell line-derived neurotrophic factor receptor that controls neuron survival and differentiation via the RET cascade. Enhances survival and morphological differentiation of dopaminergic neurons and increases their high-affinity dopamine uptake.
KCNJ11	**-2.73**	Potassium channel with a greater tendency to allow potassium to flow into a cell rather than out of a cell.
RYR2	**-2.8**	Cytosolic calcium channel that mediates the release of Ca (2+) from the sarcoplasmic reticulum into the cytosol.
GFRA2	**-3.19**	Receptor for neurturin (NRTN), a growth factor that supports the survival of sympathetic neurons via the RET cascade.
SNCAIP	-3.82	Interacts with alpha-synuclein in neuronal tissue & may play a role in the formation of cytoplasmic inclusions & neurodegeneration. Inhibits the ubiquitin ligase activity of SIAH1 and inhibits proteasomal degradation of target proteins.

Table S4.21. Functional Signatures of Modules of Interest. Data represent the top 10 Hallmark, GO Biological Processes and Reactome Pathways enriched in the 16 Modules of Interest Identified with WGCNA where significant enrichment (FDR <0.05) is indicated in bold.

Hallmark		**GO BP**		**Reactome**	
Pathway	**FDR**	**Pathway**	**FDR**	**Pathway**	**FDR**
TURQUOISE					
Myc Targets V1	**7.52E-62**	DNA Metabolic Process	**9.95E-23**	Cell Cycle R-HSA-1640170	**2.37E-76**
E2F Targets	**4.59E-61**	Ribosome Biogenesis	**2.30E-20**	Cell Cycle, Mitotic R-HSA-69278	**2.29E-63**
G2-M Checkpoint	**3.81E-37**	Ribonucleoprotein Complex Biogenesis	**4.19E-19**	Metabolism Of RNA R-HSA-8953854	**1.36E-62**
Myc Targets V2	**3.82E-25**	mRNA Splicing, Via Spliceosome	**5.04E-19**	M Phase R-HSA-68886	**1.83E-42**
mTORC1 Signalling	**4.47E-13**	DNA Repair	**2.34E-18**	Cell Cycle Checkpoints R-HSA-69620	**3.58E-42**
Oxidative Phosphorylation	**6.47E-07**	mRNA Processing	**1.39E-16**	Processing Of Capped Intron-Containing Pre-mRNA R-HSA-72203	**1.15E-36**
Unfolded Protein Response	**3.34E-06**	RNA Splicing, Via Transesterification Reactions with Bulged Adenosine as Nucleophile	**2.73E-16**	Mitotic Metaphase and Anaphase R-HSA-2555396	**2.44E-28**
DNA Repair	**1.58E-04**	DNA-templated DNA Replication	**7.33E-15**	Mitotic Anaphase R-HSA-68882	**6.43E-28**
UV Response Up	**1.58E-04**	Ribosomal Small Subunit Biogenesis	**1.59E-13**	DNA Repair R-HSA-73894	**5.03E-27**
Glycolysis	**4.60E-03**	protein-RNA Complex Assembly	**4.77E-13**	G2/M Checkpoints R-HSA-69481	**9.78E-26**
BLACK					
Oxidative Phosphorylation	**8.85E-05**	Cellular Respiration	**1.13E-03**	Respiratory Electron Transport, ATP Synthesis by Chemiosmotic Coupling, Heat Production by Uncoupling Proteins R-HSA-163200	**1.85E-04**

mTORC1 Signalling	**1.72E-04**	Mitochondrial ATP Synthesis Coupled Electron Transport	**1.13E-03**	Citric Acid (TCA) Cycle and Respiratory Electron Transport R-HSA-1428517	**2.81E-04**
Estrogen Response Late	**1.72E-04**	Aerobic Electron Transport Chain	**2.65E-03**	Respiratory Electron Transport R-HSA-611105	**3.49E-03**
G2-M Checkpoint	**5.31E-04**	Proton Motive Force-Driven ATP Synthesis	**1.07E-02**	APC/C-mediated Degradation of Cell Cycle Proteins R-HSA-174143	**3.49E-03**
Glycolysis	**5.79E-03**	Energy Derivation by Oxidation of Organic Compounds	**1.12E-02**	Separation Of Sister Chromatids R-HSA-2467813	**3.49E-03**
E2F Targets	**5.79E-03**	Oxidative Phosphorylation	**1.52E-02**	CREB1 Phosphorylation Thru Activation of CaMKII/CaMKK/CaMKIV Cascade R-HSA-442729	**5.13E-03**
Estrogen Response Early	**5.79E-03**	Proton Motive Force-Driven Mitochondrial ATP Synthesis	**4.82E-02**	Regulation Of Ornithine Decarboxylase (ODC) R-HSA-350562	**5.69E-03**
Spermatogenesis	**9.21E-03**	Mitochondrial Electron Transport, Ubiquinol to Cytochrome C	6.79E-02	APC/C: Cdc20 Mediated Degradation of Mitotic Proteins R-HSA-176409	**5.69E-03**
Adipogenesis	6.55E-02	Protein Localisation to Cell Periphery	7.17E-02	Activation Of APC/C And APC/C: Cdc20 Mediated Degradation of Mitotic Proteins R-HSA-176814	**5.93E-03**
Mitotic Spindle	1.42E-01	Regulation Of Protein Catabolic Process	1.19E-01	CaMK IV-mediated Phosphorylation of CREB R-HSA-111932	**6.60E-03**
LIGHT GREEN					
TNF-alpha Signalling via NF-kB	**5.72E-03**	Positive Regulation of Smooth Muscle Cell Proliferation (GO:0048661)	6.72E-02	Nuclear Events (Kinase and Transcription Factor Activation) R-HSA-198725	6.72E-02
TGF-beta Signalling	**2.84E-02**	Embryonic Organ Morphogenesis (GO:0048562)	6.72E-02	NGF-stimulated Transcription R-HSA-9031628	6.72E-02
Apoptosis	**2.84E-02**	Lipid Oxidation (GO:0034440)	1.76E-01	Cytokine Signalling in Immune System R-HSA-1280215	1.76E-01
Epithelial Mesenchymal Transition	5.27E-02	Ventricular Cardiac Muscle Tissue Development (GO:0003229)	1.76E-01	Signalling By Interleukins R-HSA-449147	1.76E-01
Mitotic Spindle	2.85E-01	Actin-Myosin Filament Sliding (GO:0033275)	2.62E-01	Transcriptional Regulation by RUNX2 R-HSA-8878166	2.62E-01
Interferon Alpha Response	2.85E-01	Muscle Filament Sliding (GO:0030049)	2.62E-01	Glycolysis R-HSA-70171	2.62E-01
Androgen Response	2.85E-01	Cellular Response to Transforming Growth Factor Beta Stimulus (GO:0071560)	2.62E-01	Signalling By NTRK1 (TRKA) R-HSA-187037	2.62E-01
IL-2/STAT5 Signalling	2.85E-01	Cardiac Muscle Tissue Morphogenesis (GO:0055008)	2.62E-01	Caspase Activation Via Dependence Receptors in Absence of Ligand R-HSA-418889	2.62E-01
Protein Secretion	2.85E-01	Negative Regulation of Membrane Protein Ectodomain Proteolysis (GO:0051045)	2.62E-01	Regulation Of Glycolysis by Fructose 2,6-Bisphosphate Metabolism R-HSA-9634600	2.62E-01
Reactive Oxygen Species Pathway	2.85E-01	Regulation Of Heart Contraction (GO:0008016)	2.62E-01	Post-translational Protein Phosphorylation R-HSA-8957275	2.62E-01

BROWN					
Interferon Gamma Response	**7.82E-03**	Cellular Response to Type I Interferon (GO:0071357)	5.11E-02	Interleukin-20 Family Signalling R-HSA-8854691	1.71E-01
Interferon Alpha Response	7.00E-02	Memory (GO:0007613)	5.11E-02	Synthesis Of Bile Acids and Bile Salts R-HSA-192105	1.71E-01
UV Response Dn	1.20E-01	Receptor Signalling Pathway Via STAT (GO:0097696)	5.11E-02	Interleukin-9 Signalling R-HSA-8985947	1.71E-01
heme Metabolism	4.42E-01	Cellular Response to Interleukin-2 (GO:0071352)	5.11E-02	RA Biosynthesis Pathway R-HSA-5365859	1.71E-01
IL-6/JAK/STAT3 Signalling	6.95E-01	Cellular Response to Interleukin-9 (GO:0071355)	5.11E-02	Bile Acid and Bile Salt Metabolism R-HSA-194068	1.76E-01
Estrogen Response Early	7.55E-01	Interleukin-2-Mediated Signalling Pathway (GO:0038110)	5.11E-02	Endogenous Sterols R-HSA-211976	1.76E-01
Apical Surface	8.19E-01	Interleukin-9-Mediated Signalling Pathway (GO:0038113)	5.11E-02	Cytochrome P450 - Arranged by Substrate Type R-HSA-211897	1.76E-01
Pancreas Beta Cells	8.95E-01	Negative Regulation of Viral Process (GO:0048525)	5.42E-02	Interferon Alpha/Beta Signalling R-HSA-909733	1.76E-01
Pperoxisome	8.95E-01	Type I Interferon-Mediated Signalling Pathway (GO:0060337)	5.77E-02	Interleukin-21 Signalling R-HSA-9020958	1.76E-01
TNF-alpha Signalling via NF-kB	8.95E-01	Cellular Response to Interleukin-15 (GO:0071350)	5.77E-02	Regulation Of FOXO Transcriptional Activity by Acetylation R-HSA-9617629	1.87E-01
DARK RED					
Unfolded Protein Response	3.52E-01	Response To Gonadotropin (GO:0034698)	1.46E-01	LTC4-CYSLTR Mediated IL4 Production R-HSA-9664535	2.16E-01
Hypoxia	3.52E-01	Regulation Of Glucagon Secretion (GO:0070092)	1.46E-01	Sulphide Oxidation to Sulfate R-HSA-1614517	2.16E-01
p53 Pathway	3.52E-01	Regulation Of Neuron Death (GO:1901214)	1.46E-01	Synthesis Of Leukotrienes (LT) And Eoxins (EX) R-HSA-2142691	2.16E-01
Glycolysis	3.52E-01	Cellular Response to Gonadotropin Stimulus (GO:0071371)	1.46E-01	Anti-inflammatory Response Favouring Leishmania Infection R-HSA-9662851	2.16E-01
mTORC1 Signalling	3.52E-01	Glutathione Catabolic Process (GO:0006751)	1.46E-01	Calcitonin-like Ligand Receptors R-HSA-419812	2.16E-01
		Leukotriene D4 Biosynthetic Process (GO:1901750)	1.46E-01	Aflatoxin Activation and Detoxification R-HSA-5423646	2.16E-01
		Leukotriene D4 Metabolic Process (GO:1901748)	1.46E-01	Glutathione Synthesis and Recycling R-HSA-174403	2.16E-01
		Short-Chain Fatty Acid Catabolic Process (GO:0019626)	1.46E-01	Degradation Of Cysteine and Homocysteine R-HSA-1614558	2.16E-01
		Hepatocyte Differentiation (GO:0070365)	1.46E-01	Reduction Of Cytosolic Ca++ Levels R-HSA-418359	2.16E-01
		Positive Regulation of Protein Localisation to Centrosome (GO:1904781)	1.46E-01	LGI-ADAM Interactions R-HSA-5682910	2.16E-01
PINK					
Unfolded Protein Response	**1.16E-03**	Cytoplasmic Translation (GO:0002181)	**8.25E-36**	Response Of EIF2AK4 (GCN2) To Amino Acid Deficiency R-HSA-9633012	**2.44E-40**
Oxidative Phosphorylation	**1.16E-03**	Translation (GO:0006412)	**1.29E-24**	Eukaryotic Translation Elongation R-HSA-156842	**2.99E-36**

mTORC1 Signalling	**8.55E-03**	Peptide Biosynthetic Process (GO:0043043)	**2.21E-24**	L13a-mediated Translational Silencing of Ceruloplasmin Expression R-HSA-156827	**3.11E-36**
Pancreas Beta Cells	**3.72E-02**	Macromolecule Biosynthetic Process (GO:0009059)	**1.12E-21**	Selenocysteine Synthesis R-HSA-2408557	**3.11E-36**
Myc Targets V1	1.03E-01	Gene Expression (GO:0010467)	**6.47E-16**	Peptide Chain Elongation R-HSA-156902	**3.11E-36**
DNA Repair	4.43E-01	Ribosome Biogenesis (GO:0042254)	**8.10E-07**	GTP Hydrolysis and Joining Of 60S Ribosomal Subunit R-HSA-72706	**3.32E-36**
Allograft Rejection	7.90E-01	Ribonucleoprotein Complex Biogenesis (GO:0022613)	**1.11E-06**	Formation Of a Pool of Free 40S Subunits R-HSA-72689	**2.11E-35**
p53 Pathway	7.90E-01	rRNA Processing (GO:0006364)	**5.83E-04**	Cellular Response to Starvation R-HSA-9711097	**4.74E-35**
Fatty Acid Metabolism	8.96E-01	Ribosomal Small Subunit Biogenesis (GO:0042274)	**7.50E-04**	Cap-dependent Translation Initiation R-HSA-72737	**1.32E-34**
heme Metabolism	8.96E-01	rRNA Metabolic Process (GO:0016072)	**1.10E-03**	Viral mRNA Translation R-HSA-192823	**3.38E-34**
SALMON					
Interferon Alpha Response	9.55E-01	Lytic Vacuole (GO:0000323)	3.34E-01	RHOD GTPase Cycle R-HSA-9013405	7.73E-01
UV Response Dn	9.55E-01	Germ Plasm (GO:0060293)	4.12E-01	Maturation Of Nucleoprotein R-HSA-9683610	7.73E-01
Pperoxisome	9.55E-01	P Granule (GO:0043186)	4.12E-01	Nicotinamide Salvaging R-HSA-197264	7.73E-01
Xenobiotic Metabolism	9.55E-01	Secretory Vesicle (GO:0099503)	4.12E-01	Association Of TriC/CCT With Target Proteins During Biosynthesis R-HSA-390471	7.73E-01
Apical Junction	9.55E-01	Exocytic Vesicle (GO:0070382)	4.12E-01	SUMOylation Of DNA Methylation Proteins R-HSA-4655427	7.73E-01
Pancreas Beta Cells	9.55E-01	Microbody Lumen (GO:0031907)	4.12E-01	Signalling By Cytosolic FGFR1 Fusion Mutants R-HSA-1839117	7.73E-01
Bile Acid Metabolism	9.55E-01	Golgi-associated Vesicle (GO:0005798)	4.12E-01	PI Metabolism R-HSA-1483255	7.73E-01
Coagulation	9.55E-01	Peroxisomal Matrix (GO:0005782)	4.12E-01	SUMOylation Of Transcription Cofactors R-HSA-3899300	7.73E-01
Interferon Gamma Response	9.55E-01	Lysosome (GO:0005764)	4.12E-01	RAC2 GTPase Cycle R-HSA-9013404	7.73E-01
Protein Secretion	9.55E-01	Pi-Body (GO:0071546)	5.07E-01	Chaperonin-mediated Protein Folding R-HSA-390466	7.73E-01
YELLOW					
Apical Junction	**3.64E-04**	Glycoprotein Metabolic Process (GO:0009100)	**9.33E-03**	Glycerophospholipid Biosynthesis R-HSA-1483206	**1.13E-04**
Myogenesis	**5.44E-04**	Protein Localisation (GO:0008104)	**9.33E-03**	Phospholipid Metabolism R-HSA-1483257	**6.28E-04**
Interferon Alpha Response	**4.91E-02**	Macroautophagy (GO:0016236)	**2.45E-02**	Metabolism Of Lipids R-HSA-556833	**9.73E-03**
Interferon Gamma Response	2.97E-01	Regulation Of I-kappaB kinase/NF-kappaB Signalling (GO:0043122)	**2.45E-02**	Post-translational Protein Modification R-HSA-597592	**9.73E-03**
Pperoxisome	2.97E-01	Ubiquitin-Dependent ERAD Pathway (GO:0030433)	**3.10E-02**	Chondroitin Sulfate/Dermatan Sulfate Metabolism R-HSA-1793185	**1.24E-02**
Hedgehog Signalling	4.78E-01	Positive Regulation of Synaptic Transmission (GO:0050806)	**4.34E-02**	Neutrophil Degranulation R-HSA-6798695	**1.24E-02**
Mitotic Spindle	4.78E-01	Lysosomal Transport (GO:0007041)	**4.34E-02**	Rab Regulation of Trafficking R-HSA-9007101	**1.37E-02**

Xenobiotic Metabolism	4.78E-01	Protein Ubiquitination (GO:0016567)	**4.34E-02**	TBC/RABGAPs R-HSA-8854214	**1.37E-02**
Wnt-beta Catenin Signalling	5.12E-01	Organelle Organisation (GO:0006996)	5.31E-02	Diseases Of Glycosylation R-HSA-3781865	**1.37E-02**
p53 Pathway	5.12E-01	Negative Regulation of MiRNA Transcription (GO:1902894)	5.31E-02	Innate Immune System R-HSA-168249	7.66E-02
MAGENTA					
Epithelial Mesenchymal Transition	**1.30E-06**	Homotypic Cell-Cell Adhesion (GO:0034109)	**5.24E-07**	Neutrophil Degranulation R-HSA-6798695	**4.50E-05**
Myogenesis	**4.02E-04**	Platelet Aggregation (GO:0070527)	**4.10E-05**	Hemostasis R-HSA-109582	**4.50E-05**
Apical Junction	**5.20E-04**	Integrin-Mediated Signalling Pathway (GO:0007229)	**2.08E-04**	Extracellular Matrix Organisation R-HSA-1474244	**4.50E-05**
Hypoxia	**2.61E-03**	Positive Regulation of Cell-Substrate Adhesion (GO:0010811)	**3.39E-03**	Immune System R-HSA-168256	**1.09E-03**
Inflammatory Response	**2.61E-03**	Actin Filament Organisation (GO:0007015)	**7.38E-03**	Innate Immune System R-HSA-168249	**1.09E-03**
Glycolysis	**9.03E-03**	Cell-Matrix Adhesion (GO:0007160)	**9.96E-03**	Metabolism Of Carbohydrates R-HSA-71387	**1.09E-03**
Allograft Rejection	**2.38E-02**	Regulation Of Plasma Membrane Repair (GO:1905684)	**1.16E-02**	Post-translational Protein Phosphorylation R-HSA-8957275	**1.09E-03**
Coagulation	**2.38E-02**	Regulation Of Cell Migration (GO:0030334)	**1.16E-02**	Platelet Degranulation R-HSA-114608	**1.60E-03**
p53 Pathway	**2.38E-02**	Positive Regulation of Substrate Adhesion-Dependent Cell Spreading (GO:1900026)	**1.16E-02**	Integrin Cell Surface Interactions R-HSA-216083	**1.60E-03**
Apical Surface	**2.88E-02**	Positive Regulation of Cell Migration (GO:0030335)	**1.94E-02**	Glycosaminoglycan Metabolism R-HSA-1630316	**2.06E-03**
GREENYELLOW					
KRAS Signalling Up	5.14E-01	Positive Regulation of Epithelial Tube Formation (GO:1905278)	5.08E-01	Transport Of Inorganic Cations/Anions and Amino Acids/Oligopeptides R-HSA-425393	4.27E-01
Apical Surface	5.14E-01	Nucleotide-Binding Oligomerisation Domain Containing Signalling Pathway (GO:0070423)	5.08E-01	Phototransduction Cascade R-HSA-2514856	4.27E-01
TGF-beta Signalling	5.14E-01	Axonemal Central Apparatus Assembly (GO:1904158)	5.08E-01	Transport Of Small Molecules R-HSA-382551	4.27E-01
IL-2/STAT5 Signalling	5.14E-01	Neutrophil Extravasation (GO:0072672)	5.08E-01	Keratan Sulfate Degradation R-HSA-2022857	4.41E-01
Angiogenesis	5.14E-01	Metal Ion Transport (GO:0030001)	5.08E-01	Post-translational Modification: Synthesis Of GPI-anchored Proteins R-HSA-163125	4.46E-01
Apoptosis	5.14E-01	Regulation Of Phosphatidylinositol 3-Kinase Signalling (GO:0014066)	5.08E-01	ERBB2 Activates PTK6 Signalling R-HSA-8847993	4.46E-01
Apical Junction	5.14E-01	Tight Junction Assembly (GO:0120192)	5.08E-01	Extrinsic Pathway of Fibrin Clot Formation R-HSA-140834	4.46E-01

Epithelial Mesenchymal Transition	5.14E-01	Regulation Of T Cell Mediated Cytotoxicity (GO:0001914)	5.08E-01	Synthesis Of (16-20)-Hydroxyeicosatetraenoic Acids (HETE) R-HSA-2142816	4.46E-01
Estrogen Response Early	5.14E-01	Regulation Of Cell Migration (GO:0030334)	5.08E-01	SLC-mediated Transmembrane Transport R-HSA-425407	4.46E-01
Fatty Acid Metabolism	5.14E-01	Antigen Processing and Presentation of Endogenous Peptide Antigen (GO:0002483)	5.08E-01	Glycosaminoglycan Metabolism R-HSA-1630316	4.46E-01
PURPLE					
Interferon Gamma Response	**5.51E-07**	Positive Regulation of Cellular Process (GO:0048522)	**3.27E-03**	Signal Transduction R-HSA-162582	**5.93E-04**
Interferon Alpha Response	**5.51E-07**	Response To Cytokine (GO:0034097)	**5.45E-03**	YAP1- And WWTR1 (TAZ)-stimulated Gene Expression R-HSA-2032785	**2.04E-02**
Estrogen Response Early	**9.43E-06**	Positive Regulation Of DNA-binding Transcription Factor Activity (GO:0051091)	**1.55E-02**	Physiological Factors R-HSA-5578768	6.33E-02
IL-6/JAK/STAT3 Signalling	**9.43E-06**	Positive Regulation of Cell Migration (GO:0030335)	**3.47E-02**	Immune System R-HSA-168256	6.33E-02
Epithelial Mesenchymal Transition	**7.56E-05**	Cellular Response to Steroid Hormone Stimulus (GO:0071383)	**3.47E-02**	Interferon Alpha/Beta Signalling R-HSA-909733	6.33E-02
Xenobiotic Metabolism	**3.96E-04**	Response To Type II Interferon (GO:0034341)	**3.47E-02**	TNFs Bind Their Physiological Receptors R-HSA-5669034	6.33E-02
KRAS Signalling Up	**4.33E-04**	Regulation Of Neurogenesis (GO:0050767)	**3.69E-02**	Transcriptional Regulation by MECP2 R-HSA-8986944	6.33E-02
TNF-alpha Signalling via NF-kB	**9.77E-04**	Regulation Of Intrinsic Apoptotic Signalling Pathway in Response to DNA Damage (GO:1902229)	**4.64E-02**	Interferon Gamma Signalling R-HSA-877300	6.33E-02
Coagulation	**1.17E-03**	Cardiac Epithelial to Mesenchymal Transition (GO:0060317)	**4.64E-02**	Intra-Golgi Traffic R-HSA-6811438	6.76E-02
IL-2/STAT5 Signalling	**1.53E-03**	Positive Regulation of Cell Motility (GO:2000147)	**4.64E-02**	COPI-mediated Anterograde Transport R-HSA-6807878	6.76E-02
CYAN					
KRAS Signalling Up	8.16E-01	Positive Regulation of Pathway-Restricted SMAD Protein Phosphorylation (GO:0010862)	4.34E-01	TICAM1-dependent Activation of IRF3/IRF7 R-HSA-9013973	5.15E-01
Inflammatory Response	8.16E-01	Cardiac Muscle Cell-Cardiac Muscle Cell Adhesion (GO:0086042)	4.34E-01	TNFR1-induced Proapoptotic Signalling R-HSA-5357786	5.15E-01
Complement	9.34E-01	Regulation Of Pathway-Restricted SMAD Protein Phosphorylation (GO:0060393)	4.34E-01	TRAF6 Mediated IRF7 Activation R-HSA-933541	5.15E-01
Interferon Alpha Response	9.34E-01	Neuron Projection Extension Involved in Neuron Projection Guidance (GO:1902284)	4.34E-01	GPCR Downstream Signalling R-HSA-388396	5.15E-01
Allograft Rejection	9.34E-01	Axon Extension Involved in Axon Guidance (GO:0048846)	4.34E-01	Tachykinin Receptors Bind Tachykinins R-HSA-380095	5.15E-01

Adipogenesis	9.34E-01	Purine-Containing Compound Metabolic Process (GO:0072521)	4.34E-01	Activation Of IRF3/IRF7 Mediated by TBK1/IKK Epsilon R-HSA-936964	5.15E-01
IL-6/JAK/STAT3 Signalling	9.34E-01	Positive Regulation of Filopodium Assembly (GO:0051491)	4.52E-01	Signalling By GPCR R-HSA-372790	5.15E-01
Fatty Acid Metabolism	9.34E-01	Sympathetic Ganglion Development (GO:0061549)	4.52E-01	Signal Transduction R-HSA-162582	5.15E-01
Xenobiotic Metabolism	9.34E-01	Branching Involved in Ureteric Bud Morphogenesis (GO:0001658)	4.62E-01	FGFR1b Ligand Binding and Activation R-HSA-190370	5.15E-01
Estrogen Response Late	9.34E-01	Ras Protein Signal Transduction (GO:0007265)	4.62E-01	Peptide Hormone Metabolism R-HSA-2980736	5.15E-01
LIGHTYELLOW					
Epithelial Mesenchymal Transition	**2.66E-02**	Synapse Organisation (GO:0050808)	**7.15E-04**	Receptor-type Tyrosine-Protein Phosphatases R-HSA-388844	**1.19E-03**
Wnt-beta Catenin Signalling	4.19E-01	Neuron Projection Morphogenesis (GO:0048812)	**1.18E-03**	Neuronal System R-HSA-112316	1.25E-01
Glycolysis	6.01E-01	Positive Regulation of Interleukin-1 Beta Production (GO:0032731)	**1.07E-02**	DSCAM Interactions R-HSA-376172	1.25E-01
KRAS Signalling Dn	6.01E-01	Positive Regulation of Interleukin-1 Production (GO:0032732)	**1.24E-02**	Signalling By NOTCH1 R-HSA-1980143	1.25E-01
Notch Signalling	6.01E-01	Response To Organophosphorus (GO:0046683)	**1.27E-02**	Protein-protein Interactions at Synapses R-HSA-6794362	1.25E-01
Hedgehog Signalling	6.01E-01	Cell Morphogenesis Involved in Neuron Differentiation (GO:0048667)	**1.60E-02**	ECM Proteoglycans R-HSA-3000178	1.53E-01
KRAS Signalling Up	6.01E-01	Cell Junction Assembly (GO:0034329)	**1.60E-02**	Signalling By NOTCH3 R-HSA-9012852	1.53E-01
Apoptosis	6.01E-01	Regulation Of Interleukin-1 Beta Production (GO:0032651)	**1.60E-02**	Cell Recruitment (Pro-Inflammatory Response) R-HSA-9664424	1.53E-01
UV Response Dn	6.01E-01	Positive Regulation of Cell Junction Assembly (GO:1901890)	**1.74E-02**	Constitutive Signalling by NOTCH1 HD+PEST Domain Mutants R-HSA-2894862	2.33E-01
Myogenesis	6.01E-01	Generation Of Neurons (GO:0048699)	**2.17E-02**	NOTCH4 Intracellular Domain Regulates Transcription R-HSA-9013695	2.33E-01
LIGHT CYAN					
Estrogen Response Late	8.82E-01	Chemical Synaptic Transmission (GO:0007268)	**4.15E-03**	Neuronal System R-HSA-112316	**4.64E-05**
Notch Signalling	8.82E-01	Anterograde Trans-Synaptic Signalling (GO:0098916)	**5.40E-03**	Glutamate Neurotransmitter Release Cycle R-HSA-210500	**5.25E-04**
Hypoxia	8.82E-01	Signal Release from Synapse (GO:0099643)	**6.43E-03**	Neurotransmitter Release Cycle R-HSA-112310	**6.59E-04**
p53 Pathway	8.82E-01	Neurotransmitter Secretion (GO:0007269)	**1.05E-02**	Transmission Across Chemical Synapses R-HSA-112315	**6.59E-04**
Hedgehog Signalling	8.82E-01	Neurotransmitter Transport (GO:0006836)	1.19E-01	Serotonin Neurotransmitter Release Cycle R-HSA-181429	**3.69E-03**
Inflammatory Response	8.82E-01	Regulation Of Chemotaxis (GO:0050920)	1.56E-01	Dopamine Neurotransmitter Release Cycle R-HSA-212676	**7.08E-03**

IL-6/JAK/STAT3 Signalling	8.82E-01	Inhibitory Synapse Assembly (GO:1904862)	1.58E-01	Presynaptic Depolarisation and Calcium Channel Opening R-HSA-112308	**9.63E-03**
heme Metabolism	8.82E-01	Oligosaccharide Catabolic Process (GO:0009313)	1.65E-01	Acetylcholine Neurotransmitter Release Cycle R-HSA-264642	**3.32E-02**
Estrogen Response Early	8.82E-01	Positive Regulation of Calcium Ion-Dependent Exocytosis (GO:0045956)	1.65E-01	Norepinephrine Neurotransmitter Release Cycle R-HSA-181430	**3.32E-02**
Bile Acid Metabolism	8.82E-01	Regulation Of Axon Guidance (GO:1902667)	1.65E-01	Sensory Processing of Sound by Inner Hair Cells of Cochlea R-HSA-9662360	7.62E-02
GREEN					
KRAS Signalling Dn	1.00E+00	Regulation Of Gene Expression (GO:0010468)	**6.71E-06**	Gene Expression (Transcription) R-HSA-74160	**3.67E-05**
Complement	1.00E+00	Regulation Of DNA-templated Transcription (GO:0006355)	**1.91E-04**	RNA Polymerase II Transcription R-HSA-73857	**1.01E-04**
Hedgehog Signalling	1.00E+00	Regulation Of Transcription by RNA Polymerase II (GO:0006357)	**4.34E-04**	Generic Transcription Pathway R-HSA-212436	**3.48E-03**
Pancreas Beta Cells	1.00E+00	Chromatin Remodelling (GO:0006338)	**5.06E-03**	NrCAM Interactions R-HSA-447038	3.03E-01
Apical Surface	1.00E+00	Negative Regulation of Transcription by RNA Polymerase II (GO:0000122)	**7.08E-03**	mRNA 3-End Processing R-HSA-72187	8.05E-01
Spermatogenesis	1.00E+00	Regulation Of Nucleic Acid-Templated Transcription (GO:1903506)	**1.19E-02**	RNA Polymerase II Transcription Termination R-HSA-73856	8.05E-01
Wnt-beta Catenin Signalling	1.00E+00	Negative Regulation Of DNA-templated Transcription (GO:0045892)	5.95E-02	RHOBTB GTPase Cycle R-HSA-9706574	1.00E+00
p53 Pathway	1.00E+00	Positive Regulation of Double-Strand Break Repair (GO:2000781)	1.94E-01	DARPP-32 Events R-HSA-180024	1.00E+00
Notch Signalling	1.00E+00	RNA Metabolic Process (GO:0016070)	2.27E-01	Small Interfering RNA (siRNA) Biogenesis R-HSA-426486	1.00E+00
Inflammatory Response	1.00E+00	Positive Regulation of Calcium Ion Import Across Plasma Membrane (GO:1905665)	5.04E-01	RHOBTB1 GTPase Cycle R-HSA-9013422	1.00E+00
GREY 60					
Inflammatory Response	**7.26E-03**	Regulation Of Transcription by RNA Polymerase II (GO:0006357)	**2.20E-03**	Chromatin Modifying Enzymes R-HSA-3247509	**2.92E-03**
Epithelial Mesenchymal Transition	**8.38E-03**	Chromatin Remodelling (GO:0006338)	**2.20E-03**	Transport Of Mature mRNA Derived from An Intronless Transcript R-HSA-159231	**1.21E-02**
TNF-alpha Signalling via NF-kB	3.66E-01	Regulation Of DNA-templated Transcription (GO:0006355)	**3.72E-03**	RMTs Methylate Histone Arginines R-HSA-3214858	**1.21E-02**
Interferon Gamma Response	4.91E-01	Chromatin Organisation (GO:0006325)	**4.12E-03**	Transport Of Mature mRNAs Derived from Intronless Transcripts R-HSA-159234	**1.21E-02**
Estrogen Response Late	4.91E-01	Regulation Of G0 To G1 Transition (GO:0070316)	**4.20E-03**	Transport Of Mature Transcript to Cytoplasm R-HSA-72202	**2.44E-02**
TGF-beta Signalling	4.91E-01	RNA Export from Nucleus (GO:0006405)	**9.18E-03**	SUMOylation Of Chromatin Organisation Proteins R-HSA-4551638	**2.70E-02**

Estrogen Response Early	4.91E-01	Regulation Of DNA Repair (GO:0006282)	**1.20E-02**	Transport Of SLBP Independent Mature mRNA R-HSA-159227	**3.66E-02**
IL-6/JAK/STAT3 Signalling	4.91E-01	Regulation Of Nucleotide-Excision Repair (GO:2000819)	**2.62E-02**	Transport Of SLBP Dependant Mature mRNA R-HSA-159230	**3.66E-02**
Hypoxia	4.91E-01	mRNA Transport (GO:0051028)	**4.23E-02**	Transport Of Mature mRNA Derived from An Intron-Containing Transcript R-HSA-159236	5.97E-02
Apoptosis	6.57E-01	Positive Regulation of Myoblast Differentiation (GO:0045663)	**4.23E-02**	SUMOylation Of DNA Replication Proteins R-HSA-4615885	6.77E-02

Table S4.22. **Functional Signatures Associate with Modules of Interest.** A summary of the top functional annotations associated with each module of interest derived from enriched Hallmark, Reactome and GO Biological Process Pathways. EMT = epithelial to mesenchymal transition; UPR = unfolded protein response; AA = amino acid; FA = fatty acid; OXPHOS = oxidative phosphorylation; RA = Retinoic Acid; GP = Glycoprotein; GAG = glycosaminoglycan; IL = Interleukin; ER = endoplasmic reticulum; ECM = extracellular matrix; ROS = reactive oxygen species; PI3K = Phosphoinositide 3-kinase.

Expression	MOI	Top Ontologies
FBS-Depletion		
Down	Light Green	Mitosis, Apoptosis, TGF-β & NFκβ
	Purple	Cytokine Response, Migration, Neurogenesis, Endosomal System
Up	Pink	Response to starvation/ AA deficiency, UPR, OXPHOS, Glycolysis
	Lightcyan	Neurotransmitter synthesis, Ca^{2+} signalling, synapse assembly
Differentiation		
Down	Turquoise	Cell Division, Cell Cycle Regulation, OXPHOS, Glycolysis
Up	Brown	IL, NFκβ & FOXO, RA Biosynthesis, Sterol Metabolism, Synaptogenesis
	Yellow	Neurotransmission, Glycosylation, Phospholipid, GP & GAG Metabolism, Vacuole Organisation & Trafficking, ER-Associated Degradation
PPA		
Down in DP, Up in D9	Light Cyan	Neurotransmitter Synthesis & Signalling, Ca^{2+} Signalling, Synapse Organisation
	Salmon	Chromatin Modification, Vesicle Trafficking, Bile Acid Metabolism
Down in DP	Grey60	Chromatin Remodelling, Histone Modification, Regulation of Transcription,
	Green	mRNA Transport & Processing, Regulation of Cell Cycle & Proliferation
Down in D9, not DP	Black	OXPHOS, Glycolysis, mTOR signalling, Cell Cycle, G2M checkpoint, E2F Targets
	Dark Red	Glycolysis, Apoptosis, ROS, HIF-1α, mTORC1
Up in DP	GreenYellow	PI3K Signalling, FA & GAG Metabolism, Lipolysis, Inflammatory Response
	Cyan	Regulation of Cell Growth, Axon Guidance, Hormone Secretion, Protein Folding
Up in DP, Down in D9	Magenta	Injury Repair, Inflammation, Glycolysis, ECM organisation, Integrin Interactions, GAG Metabolism, Migration, Adhesion
	LightYellow	Synapse Assembly & Organisation, IL-1 & Notch signalling

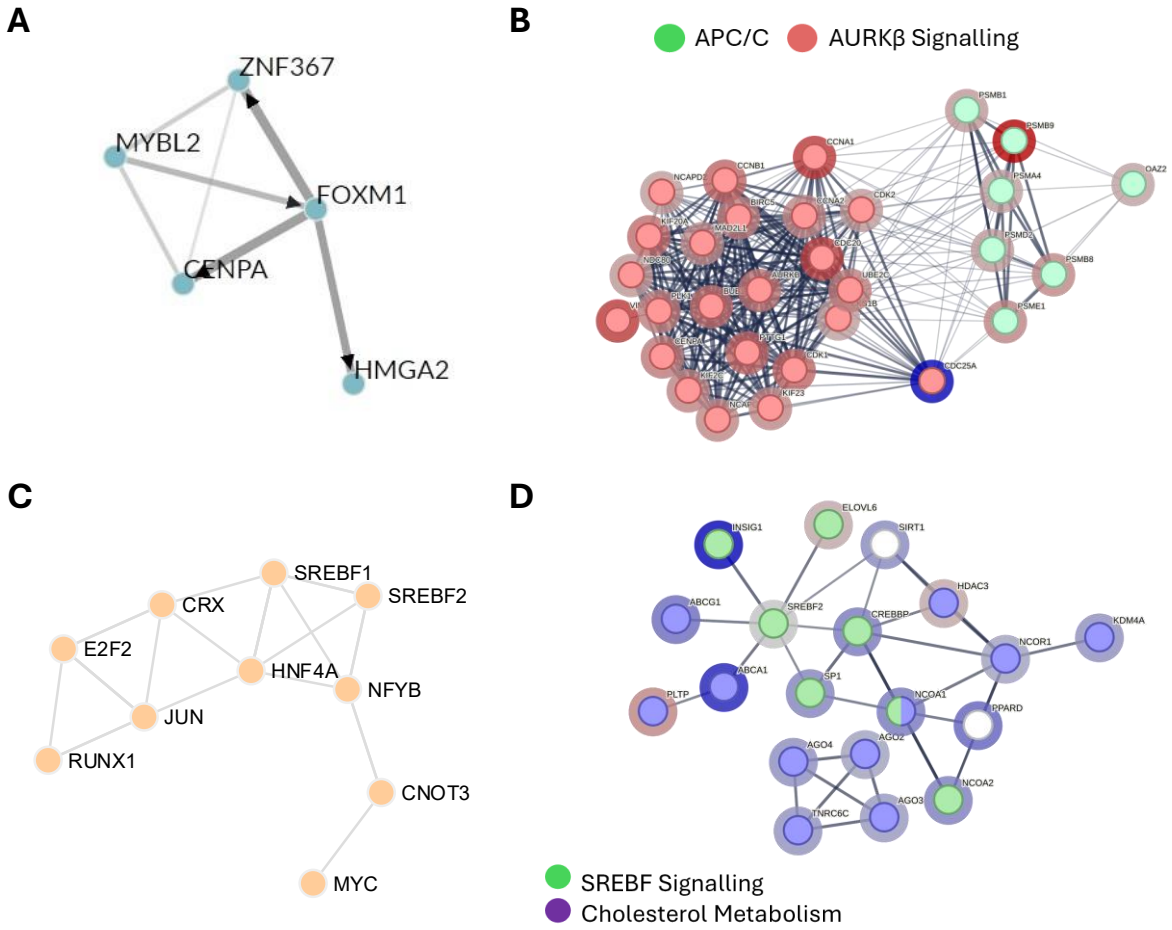


Figure S4.12. Molecular Hubs in Neurogenic Modules. A) Top five significantly enriched upstream transcriptional regulators in the black module that is upregulated by PPA identified by mean rank in the CHEA3 database. **B)** STRING protein-protein interaction (PPI) network between central cell cycle regulators modulated by aurora-β kinase (AURKβ) (green) and the anaphase promoting complex/ cyclosome (APC/C) (green). **C)** Top ten transcription factor PPIs among the significantly differentially expressed genes in the Salmon module. **D)** STRING protein-protein interaction network between SREBF proteins and central regulators of cholesterol metabolism that are dysregulated by PPA. String PPIs were constructed with a confidence threshold of 700; node halos depict the differential expression induced by PPA relative to differentiated controls (downregulation = dark blue; upregulation = dark red) and nodes are coloured according to gene ontology.

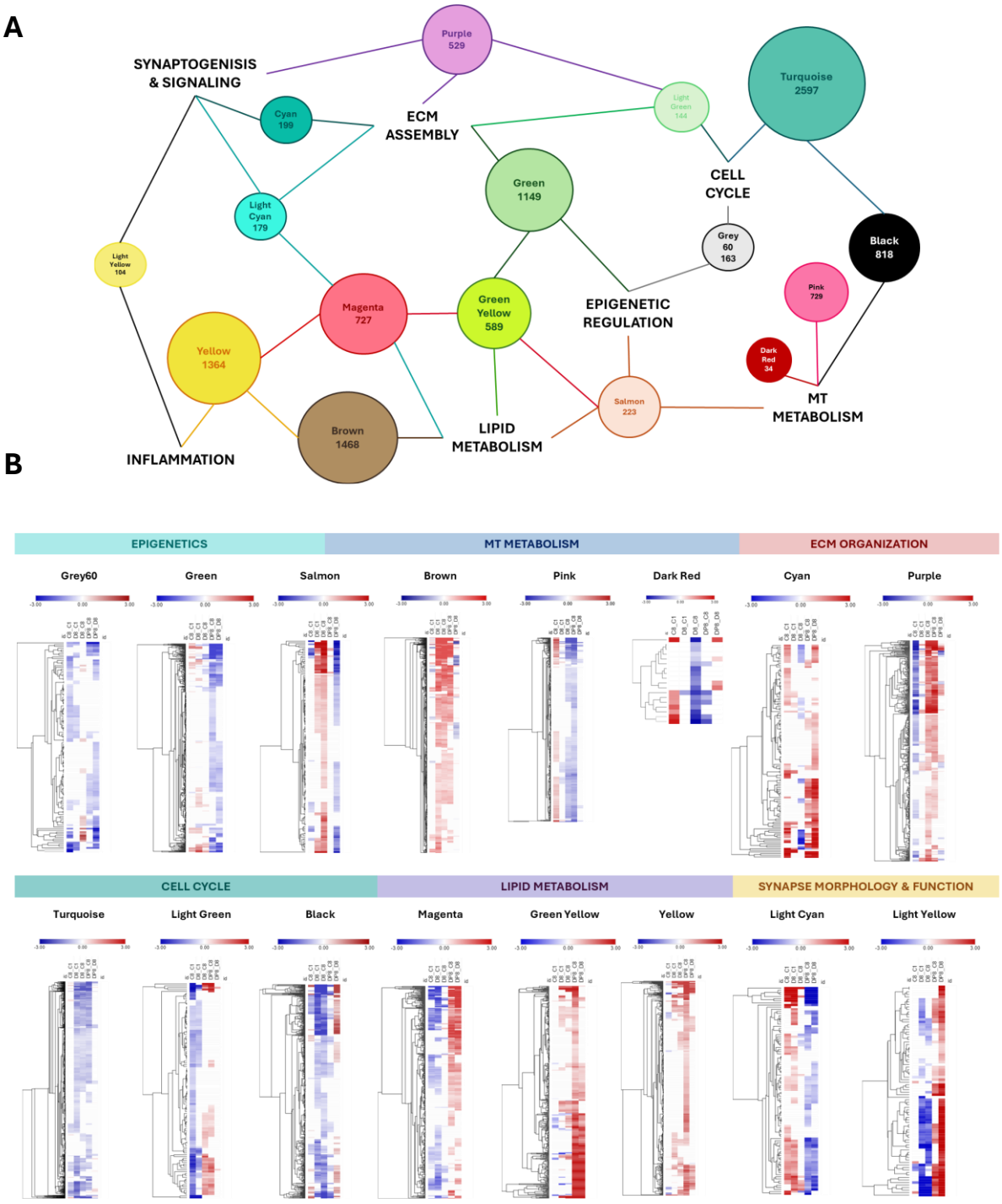


Figure S4.13. 16 Modules of Interest Derived from WGCNA Grouped into Mechanistic Clusters. A) The most significantly enriched function annotations in each MOI depicted according to their colour and size. **B)** Data represent the log fold change for all significantly differentially expressed genes in each module across all five pairwise comparisons.

Table S4.23. Interdependent Mechanisms that Govern Neurogenesis. Data represent the functional annotations associated with the 16 modules of interest identified by WGCNA, categorised by expression profile and mechanism. MT = mitochondrial; UPR = unfolded protein response; AA = amino acid; ETC = Electron Transport Chain; FA = fatty acid; OXPHOS = oxidative phosphorylation; RA = Retinoic Acid; PG = proteoglycan; GAG = glycosaminoglycan; ER = endoplasmic reticulum; ECM = extracellular matrix; PI = Phosphatidylinositol; PL = Phospholipase; APC/C = anaphase promoting complex/ cyclosome; PTMs = post-translational modifications.

			Epigenetics	***Cell Cycle***	***Mitochondrial Metabolism***	***Lipid Metabolism***	***Extracellular Matrix Organisation***	***Synapse Assembly & Signalling***	***Immune & Injury***
Neurogenic Signature	**DOWN**	**Turquoise**	Chromosome Maintenance, Nucleosome Assembly, RNA Metabolism	Cell Cycle Checkpoints, Proliferation, MYC & E2F	OXPHOS & Glycolysis				
		Light Green		Regulation of Mitosis	Glycolysis		TGF-β Signalling		Caspase Activation, Apoptosis, TNFα – NFκβ Signalling
		Pink			OXPHOS, MT Translation & Transport				UPR, Response to Starvation & AA Deficiency
	UP	**Purple**	Regulation by MECP2				Endosomal System, Vesicle Trafficking	Angiogenesis & Tube Development, Neurogenesis, Cell Migration	TNFs, NFκβ, INFs, JAK-STAT, Coagulation Signalling
		Brown			FOXO Activity	RA Metabolism & Signalling, Sterol & Bile Acid Metabolism,		Synapse Assembly & Organisation, Cell Adhesion, Synaptic Signalling	IL6, INF γ, α, β, NFκβ, Complement Cascade
		Yellow			Glycosylation, GAG, PG Metabolism	Phospholipid, Lipoprotein & PIP Metabolism	Vacuole organisation & trafficking, Endocytosis, Autophagy, PTMs	TGF-β, Synapse Transmission	Regulation of NFKβ, IFNα
PPA Signature	**DOWN**	**Green**	Chromatin Modification, CTCF, Transcription, mRNA Processing	G2/M Transition			NrCAM Interactions	Ca^{2+} Import	
		Grey 60	Chromatin Remodelling, mRNA Transport	Regulation of G0/G1 Transition, Regulation of Proliferation & Differentiation					
		Salmon	Chromatin Modification			Cholesterol & PI Metabolism	Endosomal Vesicle Transport, Protein Folding	Vesicle Secretion	
		Light Cyan			AA Transport	Glycosphingolipid metabolism, Ceramide Metabolism		Synapse Assembly & Transmission, Neurotransmitter Release Glutamate, Dopamine, Acetylcholine, Norepinephrine,	
	UP	**Black & Dark Red**		Mitosis, G1/S & G2M checkpoints, APC/C, E2F Targets, mTORC1	TCA Cycle, ETC & OXPHOS, Glycolysis, CREB1				Neurodegeneration, Neuronal Apoptosis, UPR
		Magenta			Carbohydrate metabolism, Glycolysis, GAGs, Glycosylation	Sphingolipid, Cholesterol & FA Metabolism, Adipogenesis	ECM Organisation, Integrin interactions, Cell Migration	Adhesion, Actin Filament Organisation, Axon Guidance, Lamellipodium Assembly	P53, Wound Healing, Elevated Cytosolic Ca^{2+}, Coagulation, Inflammation
		Green Yellow			Nitrogen, Thiamine & Biotin Metabolism	Lipolysis, PL Signalling	Antigen Processing & Presentation		Allograft Rejection, MHCs
		Cyan					Protein Folding, Secretion	Adhesion, Axon Guidance, GPCR Signalling, Secretion	
		Light Yellow					EMT, Protein Secretion	Synapse Organisation & Assembly, Morphogenesis, Neuron Differentiation	IL-1, IL-8, Cytokine Production

Table S4.24. Significantly Enriched IPA Pathways Associated with Propionic Acid. Data represent significantly enriched IPA pathways (FDR < 0.05) among propionic acid-induced differentially expressed genes within pertinent mechanistic clusters ranked by FDR-value. Pathways in bold indicate | Z | ≥ 2, where downregulated pathways are indicated in blue and upregulated pathways in black.

IPA Pathway	Z Score	FDR
EPIGENETIC & TRANSCRIPTIONAL REGULATION		
Generic Transcription Pathway	-7.61	1.67E-06
Transcriptional Regulation by MECP2	-0.63	5.26E-04
Transcriptional regulation by RUNX2	**2.32**	**3.11E-03**
HOTAIR Regulatory Pathway	1.22	3.86E-03
Cohesin Chromatin Regulation Pathway	-0.93	4.43E-03
Histone Modification Signalling Pathway	**-3.50**	**6.05E-03**
Transcriptional Regulatory Network in Embryonic Stem Cells	1.41	7.32E-03
DNA Methylation and Transcriptional Repression Signalling	0.73	2.46E-02
Transcriptional regulation by RUNX3	**2.67**	**3.64E-02**
DEVELOPMENTAL SIGNALLING		
Protein Kinase A Signalling	0.73	1.73E-06
Eicosanoid Signalling	**2.10**	**3.94E-06**
Beta-catenin independent WNT signalling	**2.41**	**1.44E-05**
G-Protein Coupled Receptor Signalling	**2.19**	**1.48E-05**
PTEN Signalling	**-2.19**	**1.38E-04**
HEY1 Signalling Pathway	0.85	2.19E-04
Autism Signalling Pathway	1.60	1.48E-03
Gustation Pathway	**2.40**	**2.25E-03**
WNT/Ca+ pathway	0.24	2.47E-03
Human Embryonic Stem Cell Pluripotency	**2.72**	**3.31E-03**
STAT3 Pathway	1.71	3.35E-03
Signalling by NOTCH1	1.61	5.52E-03
WNT/β-catenin Signalling	-1.73	5.53E-03
Signalling by NOTCH3	1.60	6.23E-03
WNT/SHH Axonal Guidance Signalling Pathway	1.46	6.33E-03
Post-translational protein phosphorylation	**3.13**	**9.17E-03**
RAF/MAP kinase cascade	**3.13**	**1.15E-02**
Notch Signalling	0.00	1.33E-02
mTOR Signalling	0.82	2.04E-02
PI3K/AKT Signalling	0.23	2.10E-02
PIP3 activates AKT signalling	**2.35**	**2.68E-02**
ERK/MAPK Signalling	1.67	3.25E-02
Signalling by NOTCH2	0.33	4.23E-02
CELL CYCLE REGULATION		
Kinetochore Metaphase Signalling Pathway	1.53	1.20E-02
Mitotic Roles of Polo-Like Kinase	1.73	1.38E-02
Cyclins and Cell Cycle Regulation	1.50	1.44E-02
Mitotic Prometaphase	**3.67**	**1.65E-02**
Mitotic Metaphase and Anaphase	**4.11**	**1.98E-02**
Mitotic Telophase/Cytokinesis	0.45	2.13E-02
CDK5 Signalling	1.21	3.26E-02
Regulation of mitotic cell cycle	**4.24**	**3.29E-02**
Cell Cycle: G2/M DNA Damage Checkpoint Regulation	**-2.31**	**3.67E-02**
METABOLISM		
CREB Signalling in Neurons	**2.77**	**9.95E-06**
Glycosaminoglycan metabolism	1.77	2.82E-05
Integration of energy metabolism	-0.63	1.10E-04
Adipogenesis pathway	1.77	6.30E-04

O-linked glycosylation	1.40	3.67E-03
AMPK Signalling	-1.46	5.01E-03
Regulation of IGF transport and uptake by IGFBPs	**2.60**	**1.30E-02**
Xenobiotic Metabolism PXR Signalling Pathway	1.18	1.54E-02
Chondroitin Sulfate Biosynthesis (Late Stages)	**2.50**	**2.32E-02**
D-glucuronate Degradation I		2.66E-02
Xenobiotic Metabolism Signalling	1.18	2.76E-02
Chondroitin Sulfate Biosynthesis	**2.14**	**2.79E-02**
Dermatan Sulfate Biosynthesis (Late Stages)	**2.31**	**3.29E-02**
NR1H2 and NR1H3-mediated signalling	0.58	3.31E-02
Xenobiotic Metabolism CAR Signalling Pathway	1.57	3.37E-02
PPARα/RXRα Activation	1.53	3.39E-02
Superoxide Radicals Degradation		3.40E-02
Dermatan Sulfate Biosynthesis	**2.14**	**3.50E-02**
Mitochondrial Dysfunction	-0.83	4.76E-02
ECM ASSEMBLY & TURNOVER		
Extracellular matrix organisation	**3.67**	**9.01E-08**
L1CAM interactions	**2.72**	**2.14E-07**
Neutrophil degranulation	**5.46**	**1.82E-04**
Assembly of collagen fibrils and other multimeric structures	**2.52**	**3.53E-04**
Regulation of the EMT by Growth Factors Pathway	**2.00**	**4.36E-04**
Integrin cell surface interactions	**3.13**	**5.54E-04**
Collagen biosynthesis and modifying enzymes	1.15	1.11E-03
Sphingosine-1-phosphate Signalling	**2.12**	**1.25E-03**
Caveolar-mediated Endocytosis Signalling	**2.31**	**1.71E-03**
Leukocyte Extravasation Signalling	**2.54**	**3.04E-03**
Sertoli Cell-Sertoli Cell Junction Signalling	**2.71**	**5.45E-03**
Antigen Presentation Pathway	**3.46**	**6.00E-03**
Collagen degradation	1.00	6.09E-03
GP6 Signalling Pathway	**2.35**	**9.21E-03**
Integrin Signalling	**2.20**	**1.15E-02**
Degradation of the extracellular matrix	1.00	1.18E-02
Syndecan interactions	**2.33**	**1.19E-02**
Collagen chain trimerisation	1.16	1.46E-02
MHC class II antigen presentation	**4.20**	**1.56E-02**
Virus Entry via Endocytic Pathways	**2.83**	**2.42E-02**
Cell junction organisation	**2.52**	**2.61E-02**
Glioma Invasiveness Signalling	**2.32**	**2.65E-02**
Dissolution of Fibrin Clot	**2.24**	**4.29E-02**
SYNAPTOGENESIS		
Axonal Guidance Signalling		3.48E-11
Myelination Signalling Pathway	**2.39**	**3.02E-06**
Semaphorin Neuronal Repulsive Signalling Pathway	-1.30	1.12E-05
RHO GTPase cycle	**4.31**	**1.16E-05**
Synaptogenesis Signalling Pathway	0.00	1.57E-05
Actin Cytoskeleton Signalling	1.72	6.31E-05
Nuclear Cytoskeleton Signalling Pathway	**3.70**	**3.07E-03**
Ephrin Receptor Signalling	0.85	3.60E-03
Neuregulin Signalling	1.50	3.66E-03
Actin Nucleation by ARP-WASP Complex	**2.14**	**8.03E-03**
Netrin Signalling	1.22	8.81E-03
ROBO SLIT Signalling Pathway	0.00	9.34E-03
Signalling by ROBO receptors	0.82	1.16E-02
RHO GTPases Activate Formins	**4.43**	**1.52E-02**
Semaphorin interactions	0.26	2.01E-02
RHOA Signalling	1.53	2.31E-02
Kinesins	**3.21**	**2.80E-02**
Smooth Muscle Contraction	**3.32**	**2.83E-02**

EPH-Ephrin signalling	-0.23	3.09E-02
Regulation of Actin-based Motility by Rho	1.81	3.28E-02
Neurexins and neuroligins	-1.39	3.62E-02
fMLP Signalling in Neutrophils	**2.24**	**3.71E-02**
Reelin Signalling in Neurons	1.09	3.73E-02
SYNAPTIC SIGNALLING		
Serotonin Receptor Signalling	1.67	2.30E-06
Acetylcholine Receptor Signalling Pathway	**2.02**	**4.19E-06**
Glutaminergic Receptor Signalling Pathway (Enhanced)	0.97	8.62E-06
Dopamine-DARPP32 Feedback in cAMP Signalling	0.87	1.26E-05
Melatonin Signalling	1.71	4.71E-05
Opioid Signalling	**2.04**	**7.65E-05**
Activation of NMDA receptors and postsynaptic events	**2.18**	**1.86E-04**
GABAergic Receptor Signalling Pathway (Enhanced)	0.00	6.40E-04
Synaptic Long-Term Depression	0.48	7.86E-04
Neuropathic Pain Signalling in Dorsal Horn Neurons	**2.20**	**1.10E-03**
α-Adrenergic Signalling	1.21	1.45E-03
Synaptic Long-Term Potentiation	1.51	2.44E-03
Adrenergic Receptor Signalling Pathway (Enhanced)	-0.48	3.08E-03
Cardiac β-adrenergic Signalling	-0.69	3.08E-03
SNARE Signalling Pathway	-0.19	3.61E-03
GABA Receptor Signalling		4.45E-03
Neurotransmitter release cycle	-1.16	7.26E-03
Oxytocin in Spinal Neurons Signalling Pathway	-0.30	7.73E-03
Nitric Oxide Signalling in the Cardiovascular System	**2.24**	**9.05E-03**
Oxytocin in Brain Signalling Pathway	**2.20**	**1.22E-02**
Orexin Signalling Pathway	1.09	1.55E-02
GABA synthesis, release, reuptake and degradation	-1.89	1.80E-02
Choline Biosynthesis III	-0.45	2.12E-02
GABA receptor activation	1.07	2.56E-02
IMMUNE SIGNALLING		
Thrombin Signalling	**2.27**	**1.26E-04**
CXCR4 Signalling	1.46	1.90E-03
S100 Family Signalling Pathway	**3.42**	**2.38E-03**
IL-15 Production	0.58	3.56E-03
IL-8 Signalling	**2.48**	**6.14E-03**
Neuroinflammation Signalling Pathway	0.49	9.41E-03
Interleukin-4 and Interleukin-13 signalling	**2.40**	**3.66E-02**
fMLP Signalling in Neutrophils	**2.24**	**3.71E-02**
INJURY & STRESS RESPONSIVE SIGNALLING		
Pulmonary Fibrosis Idiopathic Signalling Pathway	**2.33**	**1.83E-07**
Molecular Mechanisms of Cancer	**2.56**	**1.81E-06**
Cardiac Hypertrophy Signalling (Enhanced)	**2.53**	**2.13E-06**
Glioblastoma Multiforme Signalling	**2.14**	**1.55E-05**
ID1 Signalling Pathway	0.89	3.29E-05
Hepatic Fibrosis Signalling Pathway	**3.91**	**1.54E-04**
eNOS Signalling	**2.41**	**5.35E-04**
Wound Healing Signalling Pathway	1.16	1.47E-03
Phagosome Formation	**2.33**	**3.39E-03**
Glioma Signalling	**2.24**	**4.35E-03**
Response to elevated platelet cytosolic Ca^{2+}	**3.78**	**4.49E-03**
14-3-3-mediated Signalling	1.46	9.28E-03
Platelet homeostasis	**2.36**	**2.70E-02**
Amyotrophic Lateral Sclerosis Signalling	**2.14**	**3.44E-02**
Apoptotic execution phase	**2.31**	**4.21E-02**

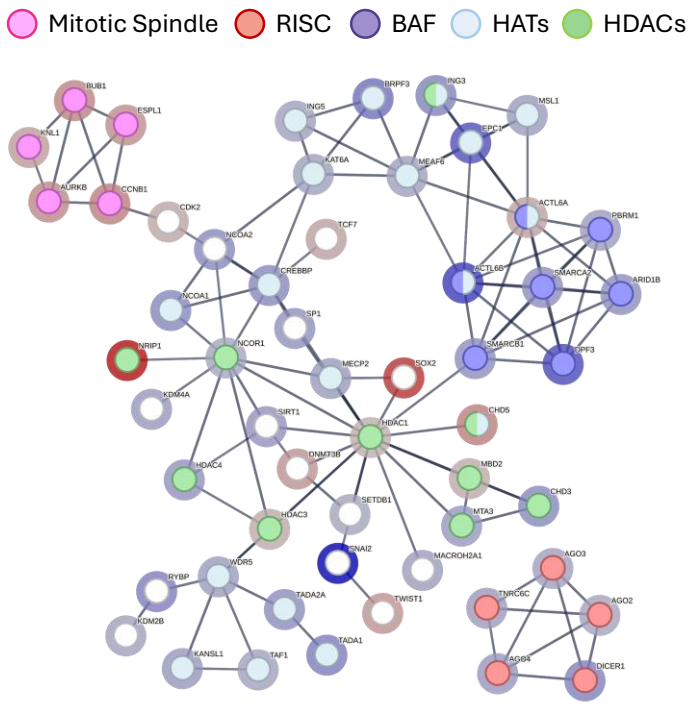


Figure S4.14. Central Regulators of Epigenetic State Disrupted by Propionic Acid. Data depict a STRING protein-protein interaction network between central epigenetic regulators (confidence ≥ 900) identified by Ingenuity Pathway Analysis that are transcriptionally dysregulated by PPA. Node halos depict the differential expression induced by PPA relative to differentiated controls (downregulation = dark blue; upregulation = dark red) and nodes are coloured according to gene ontology; purple = SWI/SNF BAF complex, red = RNA-induced silencing complex (RISC), green = histone deacetylases, light blue = histone acetyltransferases, pink = mitotic spindle components.

Table S4.25. Most Significantly Enriched Transcriptional Regulators in The PPA Transcriptome. Data represent the most significantly enriched (FDR < 0.001; | Z | ≥ 2) upstream transcriptional regulators among propionic acid-induced differentially expressed genes (DEGs) ranked by FDR value. Red denotes activation, blue denotes inhibition, regulators that are among significant DEGs are shown on bold and genes with scores above level 3 in the SFARI database are shown in red.

Regulator	LogFC	Z-score	FDR	Function
TP53		2.26	6.48E-22	Responds to diverse cellular stresses to regulate cell cycle arrest, apoptosis, senescence, DNA repair and metabolism.
TBX3	-2.26	5.22	2.67E-20	Transcriptional repressor involved in development, patterning, proliferation & senescence via interactions with Shh, BMP & TGFβ.
ARID1A		2.38	3.50E-17	Component of SWI/SNF chromatin Remodelling complexes that form nBAF and npBAF complexes.
ERG		3.13	6.83E-14	Key regulator of embryonic development, cell proliferation, differentiation, angiogenesis, inflammation, and apoptosis.
CTNNB1		3.49	1.79E-13	Key downstream component of the canonical Wnt signalling pathway that acts as a coactivator for TCF/LEF transcription factors leading the expression of Wnt responsive genes.
FOXM1		3.69	3.55E-12	Master regulator of cell cycle genes essential for DNA replication, mitosis and proliferation.
SMARCA4		3.12	7.27E-11	Component of SWI/SNF chromatin remodelling complex that forms the neural-progenitor and neural BAF complexes. required for transcriptional activation.
YAP1		2.61	1.56E-09	Central effector of Hippo signalling involved in development, growth, repair, and homeostasis. Modulates anchorage-independent growth, EMT and morphogenesis by regulating the cortical actomyosin network and F-actin polymerisation.
MITF	0.67	4.35	2.78E-08	Regulates cell differentiation, proliferation and survival, involved in the response to amino acid depletion, starvation or stress by acting downstream of MTOR.
HIF1A		2.77	1.27E-07	Master regulator of energy metabolism, angiogenesis and apoptosis.
TCF7L2		3.29	1.46E-07	Wnt-responsive transcription factor that regulates glucose homeostasis, cell cycle arrest and NSC self-renewal. Modulates MYC expression by binding to its promoter.

MYOD1		2.5	1.98E-07	Involved in cell-cycle arrest and differentiation.
STAT3		3.01	3.18E-07	Signal transducer and transcription activator that regulates the G1/S cell cycle transition, cell growth, apoptosis and interleukin signalling.
MRTFB	-0.41	2.4	1.65E-05	Acts as a transcriptional coactivator of serum response factor which controls cell cycle regulation, apoptosis, cell growth, migration, differentiation and morphogenesis.
NFAT5		2.11	3.29E-05	Mediates DNA-damage and immune responses.
MED1		3.38	4.22E-05	Component of the Mediator complex that bridges gene-specific regulatory proteins to the basal RNA polymerase II transcription machinery. Regulates p53-dependent apoptosis and is essential for adipogenesis.
DLX1		2.15	9.19E-05	Inhibits TGF-β1 signalling by interfering with SMAD2/3. Plays a role in patterning, differentiation and survival of inhibitory neurons.
ESRRA		2.41	2.12E-04	Interacts with the PGC-1 family of transcription cofactors to regulate cellular energy production and mitogenesis.
SS18		2.31	2.72E-04	Part of SWI/SNF complex.
TBX2		2.47	3.42E-04	Modulates proliferation, patterning, branching morphogenesis and EMT in response to p38/MAPK, Shh, BMP and TGFβ signalling.
MYBL2		2.97	4.11E-04	Nuclear protein involved in cell cycle progression that regulates survival, proliferation, and differentiation.
FOXO1		2.76	4.54E-04	Master regulator of metabolic homeostasis in response to oxidative stress, modulates glucose/lipid utilisation, autophagy, apoptosis and cell death.
LMX1A		2.33	6.03E-04	Regulates insulin gene transcription and plays a role in the development of dopamine producing neurons during embryogenesis.
CEBPB		3.05	7.09E-04	Regulates expression of genes involved in adipogenesis, gluconeogenesis and inflammatory responses. Plays also a significant role in adipogenesis
GLI1	3.59	-3.28	6.16E-18	Transcriptional activator that regulates CNS development, proliferation & differentiation by mediating Shh signalling.
MYCN		-2.32	1.99E-08	Positively regulates the transcription of MYCNOS in neuroblastoma cells, which regulates stability of MYCN in neuroblastoma cells by inhibiting GSK3B-mediated MYCN phosphorylation.
EGR3	-2.1	-2.63	6.45E-05	Immediate-early growth response gene involved in neuronal growth, migration & development.
Tcf7	0.65	-3.32	3.64E-04	Forms a complex with β-catenin and activates transcription through Wnt signalling. Feedback transcriptional repressor of CTNNB1 and TCF7L2 target genes.
HOXD9	-1.03	-2.23	8.25E-04	Critical for morphogenesis, development & patterning.
ZFP36		-2.29	9.59E-04	Facilitates mRNA decay with RISC complex, regulates translation of MHCs and operates as part of a negative feedback loop to limit the inflammatory response.

Table S4.26. Differentially Expressed Genes Identified as Upstream Transcriptional Regulators. Data represent the 30 genes that were differentially expressed in response to propionic acid and also identified as significantly enriched (FDR<0.001) upstream transcriptional regulators. Activated networks (red) and inhibited networks (blue) are ranked by FDR-value, those that pass a threshold of $|Z| \geq 2$ are highlighted in bold and genes with scores above level 3 in the SFARI database are shown in red.

Gene	Betweenness	LogFC	Z	FDR	Function
SMAD3	85.05	-0.78	0.96	1.23E-04	Intracellular signal transducer and transcriptional modulator activated by TGF-β and activin type 1 receptor kinases. Binds TRE elements to activate transcription.
SOX2	53.06	2.65	1.39	7.80E-07	Forms a trimeric complex with OCT4 to control the expression of genes involved in embryonic development,

					Critical for pluripotency/self-renewal, suppresses neuronal differentiation.
TCF4	50.68	-1.13	-0.11	3.39E-10	Involved in the initiation of neuronal differentiation.
MITF	**41.63**	**0.67**	**4.35**	**2.78E-08**	Regulates cell differentiation, proliferation and survival, involved in the response to amino acid depletion, starvation or stress by acting downstream of MTOR.
FOXO3	31.99	-0.71	-0.81	5.82E-06	Regulates autophagy, apoptosis, mitogenesis & fatty acid metabolism in response to metabolic & oxidative stress.
ZNF217	31.03	0.99	-0.24	4.91E-05	Transcriptional repressor that promotes cell proliferation and antagonises cell death.
POU4F1	20.59	9.25	-0.72	5.97E-06	Regulates the expression of specific genes involved in differentiation and survival within a subset of neuronal lineages. Protects neuronal cells from apoptosis and induces neuronal process outgrowth and the coordinate expression of genes encoding synaptic proteins.
SIRT1	19.52	-0.65	-1.4	8.16E-06	NAD-dependent protein deacetylase that links transcriptional regulation directly to intracellular energetics and participates in the coordination of several separated cellular functions such as cell cycle, response to DNA damage, metabolism, apoptosis and autophagy.
PROX1	15.77	-1.89	0.23	1.88E-04	Transcription factor involved in cell fate determination, embryonic development and neurogenesis. Represses transcription of the retinoid-related orphan receptor RORG, transcriptional activator activity of RORA and RORG, and the expression of RORA/G-target genes.
SALL4	14.64	1.66	-0.53	3.06E-08	Transcription factor with a key role in the maintenance and self-renewal of embryonic and hematopoietic stem cells.
SATB1	11.48	-0.77	0.23	9.83E-04	Transcriptional repressor controlling nuclear and viral gene expression in a phosphorylated and acetylated status-dependent manner.
TBX3	**10.58**	**-2.26**	**5.22**	**2.67E-20**	Transcriptional repressor involved in development, patterning, proliferation & senescence via interactions with Shh, BMP & TGFβ.
GLI1	**8.34**	**3.59**	**-3.28**	**6.16E-18**	Transcriptional activator that regulates CNS development, proliferation & differentiation by mediating Shh signalling.
HDAC4	6.97	-0.66	0.17	4.59E-04	Histone deacetylation gives a tag for epigenetic repression and plays an important role in transcriptional regulation, cell cycle progression and developmental events.
NFKBIA	6.56	-1.21	-0.88	3.38E-08	Inhibits the activity of dimeric NF-kappa-B/REL complexes by trapping REL dimers in the cytoplasm through masking of their nuclear localisation signals. On cellular stimulation by immune and proinflammatory responses, becomes phosphorylated promoting ubiquitination and degradation, enabling the dimeric RELA to translocate to the nucleus and activate transcription.
TSHZ3	4.88	-1.26	-0.26	1.48E-04	Transcriptional repressor involved in neuron developmental processes that functions in association with APBB1, SET and HDAC.s
HTT	4.2	0.42	0.2	1.58E-16	Required for normal development, promotes the formation of autophagic vesicle, involved in microtubule-mediated transport or vesicle function.
ZNF507	3.91	-0.58	1.28	3.14E-04	Predicted to enable DNA binding activity, metal ion binding activity and positive regulation of RNA polymerase II.
SP1	3.8	-0.7	0.99	9.57E-15	Regulates the expression of many genes involved in cell growth, apoptosis, differentiation and immune responses. Highly regulated by post-translational modifications (phosphorylation, SUMOylation, proteolytic cleavage, glycosylation and acetylation).
STAT6	3.72	2.98	1.5	3.81E-04	Involved in IL4- and IL3- mediated signalling.
CREBBP	3.13	-0.81	1.59	5.80E-04	Acetylates histones, giving a specific tag for transcriptional activation. Also acetylates non- histone proteins. Binds specifically to phosphorylated CREB and enhances its transcriptional activity toward cAMP-responsive genes.
TWIST1	2.65	0.87	1.16	7.99E-08	Regulates neural tube closure, limb development, brown fat metabolism, inhibits myogenesis, promotes tumour cell

					invasion and metastasis and represses expression of proinflammatory cytokines.
MECP2	2.61	-0.54	1.21	8.09E-05	Chromosomal protein that binds to methylated DNA. Essential for embryonic development, causes Rett syndrome and cognitive deficits.
ASCL1	2.59	-6.33	1.65	6.14E-07	Transcription factor that plays a key role in neuronal differentiation: acts as a pioneer transcription factor, accessing closed chromatin to allow other factors to bind and activate neural pathways.
IKZF1	2.55	-3.64	-1.34	2.06E-05	Chromatin remodelling gene that interacts with HDACs, NuRD, and BAF and regulates hematopoietic cell differentiation.
HOXD9	**1.68**	**-1.03**	**-2.21**	**8.25E-04**	Critical for morphogenesis, development & patterning.
EGR3	1.45	**-2.1**	**-2.63**	**6.45E-05**	Immediate-early growth response gene involved in neuronal growth, migration & development.
ARNT2	1.44	-0.66	1.41	1.83E-04	Plays a role in the development of the HPA and postnatal brain growth by binding the xenobiotic response element (XRE).
MRTFB	**0.43**	**-0.41**	**2.4**	**1.65E-05**	Acts as a transcriptional coactivator of serum response factor which controls cell cycle regulation, apoptosis, cell growth, migration, differentiation and morphogenesis.

Table S4.27. Central Regulators of Neuronal Identity and Epigenetic State Identified as Significantly Enriched Upstream Transcriptional Regulators. Data represent the central cell fate regulators, epigenetic regulators and canonical metabolic genes that were differentially expressed in response to propionic acid and also identified as significantly enriched (FDR<0.05) upstream transcriptional regulators. Networks in each category are ranked by FDR, those that pass a threshold of $|Z| \geq 2$ are highlighted in bold and genes with scores above level 3 in the SFARI database are shown in red.

Cell Fate Regulators				
Regulator	**LogFC**	**Z**	**FDR**	**Function**
HES1	0.69	-0.22	2.67E-20	Transcriptional effector of Notch signalling that regulates NSC self-renewal, pluripotency & neurogenesis.
NOTCH2	-1.23	0.39	5.82E-06	Functions as a receptor for membrane-bound ligands Jagged-1 (JAG1), Jagged-2 (JAG2) and Delta-1 (DLL1) to regulate cell-fate determination.
TBX3	**-2.26**	**5.22**	**1.23E-04**	Transcriptional repressor involved in development, patterning, proliferation & senescence via interactions with Shh, BMP & TGFβ.
ETS1	1.1	2.57	8.25E-04	Involved in stem cell development, cell senescence and death, and tumorigenesis. Directly controls the expression of cytokine and chemokine genes in a wide variety of different cellular contexts.
EPAS1	-2.47	1.66	1.63E-03	Transcription factor involved in the induction of oxygen regulated genes, binds to HREs in the genome. Modulates angiogenesis and tube development via VEGF.
FOXO3	-0.71	-0.81	2.70E-03	Regulates autophagy, apoptosis, mitogenesis & fatty acid metabolism in response to metabolic & oxidative stress.
ISL1	1.16	-1.03	3.80E-03	Essential for required for motor neuron generation and RGC differentiation.
SMAD3	-0.78	0.96	6.70E-03	Intracellular signal transducer and transcriptional modulator activated by TGF-β and activin type 1 receptor kinases. Binds TRE elements to activate transcription.
HOXD9	-1.03	-2.21	1.19E-02	Critical for morphogenesis, development & patterning.
KLF6	0.57	0.89	2.96E-02	Kruppel-like transcription factor involved in proliferation, survival, differentiation and adipogenesis.
E2F7	0.99		4.56E-02	Involved in DNA damage response, p53 signalling, angiogenesis, regulation of G1/S phases by repressing classical E2F transcription factors.
Epigenetic Regulators				
ASCL1	-6.33	1.65	6.14E-07	Transcription factor that plays a key role in neuronal differentiation: acts as a pioneer transcription factor, accessing closed chromatin to allow other factors to bind and activate neural pathways.
SIRT1	-0.64	-1.40	8.16E-06	NAD-dependent protein deacetylase that links transcriptional regulation directly to intracellular energetics and participates in the coordination of

				several separated cellular functions such as cell cycle, response to DNA damage, metabolism, apoptosis and autophagy.
MECP2	-0.54	1.21	8.09E-05	Chromosomal protein that binds to methylated DNA. Essential for embryonic development, causes Rett syndrome and cognitive deficits.
CREBBP	-0.81	1.59	5.80E-04	Acetylates histones, giving a specific tag for transcriptional activation. Also acetylates non- histone proteins. Binds specifically to phosphorylated CREB and enhances its transcriptional activity toward cAMP-responsive genes.
HDAC4	-0.66	0.17	4.59E-04	Histone deacetylation gives a tag for epigenetic repression and plays an important role in transcriptional regulation, cell cycle progression and developmental events.
PRDM5	-0.79	-1.00	7.99E-03	Represses transcription at least in part by recruitment of the histone methyltransferase EHMT2/G9A and histone deacetylases such as HDAC1. Involved in ECM organisation, cell differentiation, migration, adhesion and cell cycle arrest.
PRDM8	-0.89	1.00	1.10E-02	Histone methyltransferase that predominantly act as a negative regulator of transcription. Forms with BHLHE22 a transcriptional repressor complex controlling genes involved in neural development and neuronal differentiation.
MBD2	0.46	0.80	1.75E-02	Methyl binding protein that recruits histone deacetylases and DNA methyltransferases, acts as a component of the histone deacetylase NuRD complex which participates in the Remodelling of chromatin, as a transcriptional repressor and as a scaffold protein to repress transcription.
SMARCA2	-0.72	0.55	2.07E-02	Part of the large ATP-dependent chromatin Remodelling complex SNF/SWI, which is required for transcriptional activation of genes normally repressed by chromatin.
HDAC3	0.45	0.08	3.77E-02	Histone deacetylation gives a tag for epigenetic repression and plays an important role in transcriptional regulation, cell cycle progression and developmental events.
Metabolic Regulators				
TWIST1	0.87	1.16	3.86E-09	Basic helix-loop-helix (bHLH) transcription factor that plays an important role in embryonic development, neural tube closure, limb development and brown fat metabolism.
NCOA2	-0.79	-1.20	3.71E-03	Transcriptional coactivator for nuclear hormone receptors, including steroid, thyroid, retinoid, and vitamin D receptors involved in energy balance and glucose homeostasis.
PER2	**-3.09**	**-2.42**	**3.68E-02**	Transcriptional repressor that regulates circadian rhythms, fatty acid metabolism, glutamate uptake and inflammatory signalling.
FOXO3	-0.71	-0.81	2.70E-03	Regulates autophagy, apoptosis, mitogenesis & fatty acid metabolism in response to metabolic & oxidative stress.

References

1. Abcam (2016) 'TMRE Mitochondrial Membrane Potential Assay Kit', 113852(August).
2. Abdelli, L.S., Samsam, A. and Naser, S.A. (2019) 'Propionic Acid Induces Gliosis and Neuro-inflammation through Modulation of PTEN/AKT Pathway in Autism Spectrum Disorder', *Scientific Reports*, 9(1), p. 8824. Available at: https://doi.org/10.1038/s41598-019-45348-z.
3. Abily-Donval, L. *et al.* (2017) 'Methylmalonyl-CoA epimerase deficiency mimicking propionic aciduria', *International Journal of Molecular Sciences*, 18(11). Available at: https://doi.org/10.3390/IJMS18112294.
4. Abraham, J., Szoko, N. and Natowicz, M.R. (2019) 'Proteomic Investigations of Autism Spectrum Disorder: Past Findings, Current Challenges, and Future Prospects', *Advances in Experimental Medicine and Biology*, 1118, pp. 235–252. Available at: https://doi.org/10.1007/978-3-030-05542-4_12.
5. Abraham, J.R. *et al.* (2019) 'Proteomic Investigations of Autism Brain Identify Known and Novel Pathogenetic Processes', *Scientific Reports*, 9(1), pp. 1–11. Available at: https://doi.org/10.1038/s41598-019-49533-y.
6. Abubakar, A., Ssewanyana, D. and Newton, C.R. (2016) 'A systematic review of research on autism spectrum disorders in sub-Saharan Africa', *Behavioural Neurology*, 2016. Available at: https://doi.org/10.1155/2016/3501910.
7. Adaniya, S.M. *et al.* (2019) 'Posttranslational modifications of mitochondrial fission and fusion proteins in cardiac physiology and pathophysiology', *American Journal of Physiology - Cell Physiology*. American Physiological Society, pp. C583–C604. Available at: https://doi.org/10.1152/ajpcell.00523.2018.
8. Adler, G.K. *et al.* (2021) 'Acute effects of the food preservative propionic acid on glucose metabolism in humans', *BMJ Open Diabetes Research and Care*, 9(1), p. e002336. Available at: https://doi.org/10.1136/BMJDRC-2021-002336.
9. Afridi, R. *et al.* (2020) 'Metabolic Regulation of Glial Phenotypes: Implications in Neuron–Glia Interactions and Neurological Disorders', *Frontiers in Cellular Neuroscience*, 14, p. 20. Available at: https://doi.org/10.3389/FNCEL.2020.00020/BIBTEX.
10. Agilent Technologies (2021) *Explore Metabolism Where You Couldn 't Before Delivering higher sensitivity using fewer cells with the Agilent XF HS miniplate*.
11. Agorastos, A. *et al.* (2019) 'Developmental trajectories of early life stress and trauma: A narrative review on neurobiological aspects beyond stress system dysregulation', *Frontiers in Psychiatry*, 10(MAR), p. 118. Available at: https://doi.org/10.3389/FPSYT.2019.00118/BIBTEX.
12. Agostini, M. *et al.* (2016) 'Metabolic reprogramming during neuronal differentiation', *Cell Death & Differentiation 2016 23:9*, 23(9), pp. 1502–1514. Available at: https://doi.org/10.1038/cdd.2016.36.
13. Aguilar, K. *et al.* (2024) 'Primary mitochondrial diseases: The intertwined pathophysiology of bioenergetic dysregulation, oxidative stress and neuroinflammation', *European Journal of Clinical Investigation*, 54(7), p. e14217. Available at: https://doi.org/10.1111/ECI.14217.
14. Alagendran, K. *et al.* (2019) 'Cortisol Responsivity to Social Play in Children with Autism: A Systematic Review', *Journal of Occupational Therapy, Schools, and Early Intervention*, 12(4), pp. 427–443. Available at: https://doi.org/10.1080/19411243.2019.1604285.
15. Alammari, F. *et al.* (2024) 'Hidden regulators: the emerging roles of lncRNAs in brain development and disease', *Frontiers in Neuroscience*, 18, p. 1392688. Available at: https://doi.org/10.3389/FNINS.2024.1392688/BIBTEX.
16. Alberti, P. *et al.* (2022) 'Neurons: The Interplay between Cytoskeleton, Ion Channels/Transporters and Mitochondria', *Cells*, 11(16), p. 2499. Available at: https://doi.org/10.3390/CELLS11162499/S1.
17. Al-Daihan, S. and Shafi Bhat, R. (2015) 'Impact of Propionic Acid on Liver Damage in Rats.', *International journal of molecular and cellular medicine*, 4(3), pp. 188–95. Available at: http://www.ncbi.nlm.nih.gov/pubmed/26629488 (Accessed: 5 December 2020).
18. Aldosary, M. *et al.* (2020) 'Rett Syndrome, a Neurodevelopmental Disorder, Whole-Transcriptome, and Mitochondrial Genome Multiomics Analyses Identify Novel Variations and Disease Pathways', *OMICS: A Journal of Integrative Biology*, 24(3), pp. 160–171. Available at: https://doi.org/10.1089/omi.2019.0192.
19. Alfawaz, H.A. *et al.* (2022) 'Protective Effects of Bee Pollen on Multiple Propionic Acid-Induced Biochemical Autistic Features in a Rat Model', *Metabolites 2022, Vol. 12, Page 571*, 12(7), p. 571. Available at: https://doi.org/10.3390/METABO12070571.
20. Alhusaini, A. *et al.* (2020) 'Neuroprotective efficacy of nano-CoQ against propionic acid toxicity in rats: Role of BDNF and CREB protein expressions', *Journal of Biochemical and Molecular Toxicology*, 34(4), p. e22449. Available at: https://doi.org/10.1002/JBT.22449.

21. Alhusaini, A. *et al.* (2022) 'Acetyl-L-carnitine and/or liposomal co-enzyme Q10 prevent propionic acid-induced neurotoxicity by modulating oxidative tissue injury, inflammation, and ALDH1A1-RA-RARα signaling in rats', *Biomedicine & Pharmacotherapy*, 153, p. 113360. Available at: https://doi.org/10.1016/J.BIOPHA.2022.113360.
22. Al-Kafaji, G. *et al.* (2023) 'Mitochondrial DNA copy number in autism spectrum disorder and attention deficit hyperactivity disorder: a systematic review and meta-analysis', *Frontiers in Psychiatry*, 14, p. 1196035. Available at: https://doi.org/10.3389/FPSYT.2023.1196035/BIBTEX.
23. Al-Kafaji, G. and Golbahar, J. (2013) 'High glucose-induced oxidative stress increases the copy number of mitochondrial DNA in human mesangial cells', *BioMed Research International*, 2013. Available at: https://doi.org/10.1155/2013/754946.
24. Allen, J., Caruncho, H.J. and Kalynchuk, L.E. (2021) 'Severe life stress, mitochondrial dysfunction, and depressive behavior: A pathophysiological and therapeutic perspective', *Mitochondrion*, 56, pp. 111–117. Available at: https://doi.org/10.1016/J.MITO.2020.11.010.
25. Alrashidi, H., Eaton, S. and Heales, S. (2021) 'Biochemical characterization of proliferative and differentiated SH-SY5Y cell line as a model for Parkinson's disease', *Neurochemistry International*, 145. Available at: https://doi.org/10.1016/J.NEUINT.2021.105009.
26. Alsubaiei, S.R.M. *et al.* (2023) 'Nutritional Intervention as a Complementary Neuroprotective Approach against Propionic Acid-Induced Neurotoxicity and Associated Biochemical Autistic Features in Rat Pups', *Metabolites 2023, Vol. 13, Page 738*, 13(6), p. 738. Available at: https://doi.org/10.3390/METABO13060738.
27. Al-Suwailem, E. *et al.* (2019) 'Glutamate Signaling Defects in Propionic Acid Orally Administered to Juvenile Rats as an Experimental Animal Model of Autism', *Neurochemical Journal 2019 13:1*, 13(1), pp. 90–98. Available at: https://doi.org/10.1134/S1819712419010021.
28. Álvarez, M. *et al.* (2023) 'Dysregulated Cell Homeostasis and miRNAs in Human iPSC-Derived Cardiomyocytes from a Propionic Acidemia Patient with Cardiomyopathy', *International Journal of Molecular Sciences 2023, Vol. 24, Page 2182*, 24(3), p. 2182. Available at: https://doi.org/10.3390/IJMS24032182.
29. American Psychiatric Association (2022) *Diagnostic and Statistical Manual of Mental Disorders*, *Diagnostic and Statistical Manual of Mental Disorders*. American Psychiatric Association Publishing. Available at: https://doi.org/10.1176/appi.books.9780890425787.
30. Andersen, J. V. *et al.* (2021) 'Glutamate metabolism and recycling at the excitatory synapse in health and neurodegeneration', *Neuropharmacology*, 196, p. 108719. Available at: https://doi.org/10.1016/J.NEUROPHARM.2021.108719.
31. Andrews, S. V. *et al.* (2018) 'Case-control meta-analysis of blood DNA methylation and autism spectrum disorder', *Molecular Autism*, 9(1), pp. 1–11. Available at: https://doi.org/10.1186/S13229-018-0224-6/TABLES/4.
32. Ang, Z. *et al.* (2018) 'FFAR2-FFAR3 receptor heteromerization modulates short-chain fatty acid sensing', *The FASEB Journal*, 32(1), pp. 289–303. Available at: https://doi.org/10.1096/fj.201700252RR.
33. Angelova, P.R. *et al.* (2022) 'Hyperammonaemia induces mitochondrial dysfunction and neuronal cell death', *JHEP Reports*, 4(8). Available at: https://doi.org/10.1016/J.JHEPR.2022.100510.
34. El Ansary, A. *et al.* (2013) 'Neuroprotective effect of creatine against propionic acid toxicity in neuroblastoma SH-SY5Y cells in culture', *African Journal of Biotechnology*, 12(31), pp. 4925–4935. Available at: https://doi.org/10.5897/AJB12.2880.
35. El Ansary, A., Abu Shmais, G. and Al Dbass, A. (2013) 'Neuroprotective effect of creatine against propionic acid toxicity in neuroblastoma SH-SY5Y cells in culture', *African Journal of Biotechnology*, 12(31), pp. 4925–4935. Available at: https://doi.org/10.5897/AJB12.2880.
36. Anzmann, A.F. *et al.* (2019) 'Multi-omics studies in cellular models of methylmalonic acidemia and propionic acidemia reveal dysregulation of serine metabolism', *Biochimica et Biophysica Acta (BBA) - Molecular Basis of Disease*, 1865(12), p. 165538. Available at: https://doi.org/10.1016/J.BBADIS.2019.165538.
37. Aoyama, K. (2021) 'Glutathione in the Brain', *International Journal of Molecular Sciences*, 22(9), p. 22. Available at: https://doi.org/10.3390/IJMS22095010.
38. Araki, T., Ikegaya, Y. and Koyama, R. (2021) 'The effects of microglia- and astrocyte-derived factors on neurogenesis in health and disease', *European Journal of Neuroscience*, 54(5), pp. 5880–5901. Available at: https://doi.org/10.1111/EJN.14969.
39. Arrázola, M.S. *et al.* (2018) 'Mitochondria in Developmental and Adult Neurogenesis', *Neurotoxicity Research 2018 36:2*, 36(2), pp. 257–267. Available at: https://doi.org/10.1007/S12640-018-9942-Y.
40. Arrázola, M.S., Silva-Alvarez, C. and Inestrosa, N.C. (2015) 'How the Wnt signaling pathway protects from neurodegeneration: The mitochondrial scenario', *Frontiers in Cellular Neuroscience*, 9(MAY), p. 128405. Available at: https://doi.org/10.3389/FNCEL.2015.00166/BIBTEX.

41. Ashrafi, G. and Schwarz, T.L. (2012) 'The pathways of mitophagy for quality control and clearance of mitochondria', *Cell Death & Differentiation 2013 20:1*, 20(1), pp. 31–42. Available at: https://doi.org/10.1038/cdd.2012.81.
42. Astakhova, A. *et al.* (2019) 'Inhibitors of Oxidative Phosphorylation Modulate Astrocyte Inflammatory Responses through AMPK-Dependent Ptgs2 mRNA Stabilization', *Cells 2019, Vol. 8, Page 1185*, 8(10), p. 1185. Available at: https://doi.org/10.3390/CELLS8101185.
43. Atilano, S.R. *et al.* (2015) 'Mitochondrial DNA variants can mediate methylation status of inflammation, angiogenesis and signaling genes', *Human Molecular Genetics*, 24(16), pp. 4491–4503. Available at: https://doi.org/10.1093/hmg/ddv173.
44. Attoff, K. *et al.* (2020) 'Acrylamide alters CREB and retinoic acid signalling pathways during differentiation of the human neuroblastoma SH-SY5Y cell line', *Scientific Reports 2020 10:1*, 10(1), pp. 1–15. Available at: https://doi.org/10.1038/s41598-020-73698-6.
45. Avci, C.B. *et al.* (2013) 'Regulation of URG4/URGCP and PPARα gene expressions after retinoic acid treatment in neuroblastoma cells', *Tumor Biology*, 34(6), pp. 3853–3857. Available at: https://doi.org/10.1007/S13277-013-0970-1/FIGURES/2.
46. Averill, L.A. *et al.* (2020) 'Early life stress and glutamate neurotransmission in major depressive disorder', *European Neuropsychopharmacology*, 35, pp. 71–80. Available at: https://doi.org/10.1016/J.EURONEURO.2020.03.015.
47. Aylon, Y. and Oren, M. (2016) 'The Hippo pathway, p53 and cholesterol', *Cell Cycle*, 15(17), pp. 2248–2255. Available at: https://doi.org/10.1080/15384101.2016.1207840.
48. Aytulun, A. and Ünal, D. (2024) 'Neuroinflammation and autism: what have we learned so far?', *International Journal of Developmental Disabilities* [Preprint]. Available at: https://doi.org/10.1080/20473869.2024.2366722.
49. Bae, S.M. and Hong, J.Y. (2018) 'The Wnt Signaling Pathway and Related Therapeutic Drugs in Autism Spectrum Disorder', *Clinical Psychopharmacology and Neuroscience*, 16(2), p. 129. Available at: https://doi.org/10.9758/CPN.2018.16.2.129.
50. Baeker, V. (2013) *Separate Nuclei Tool - ImageJ-macros - MRI's Redmine*. Available at: https://dev.mri.cnrs.fr/projects/imagej-macros/wiki/Separate_Nuclei_Tool (Accessed: 5 May 2024).
51. Bahram Sangani, N. *et al.* (2021) 'The role of Extracellular Vesicles during CNS development', *Progress in Neurobiology*, 205, p. 102124. Available at: https://doi.org/10.1016/J.PNEUROBIO.2021.102124.
52. Bakare, M.O. *et al.* (2022) 'Picture of Autism Spectrum Disorder (ASD) Research in West Africa—A Scoping Review', *Research in Autism Spectrum Disorders*, 90(May 2021), p. 101888. Available at: https://doi.org/10.1016/j.rasd.2021.101888.
53. Bakulski, K.M. *et al.* (2021) 'Autism-Associated DNA Methylation at Birth From Multiple Tissues Is Enriched for Autism Genes in the Early Autism Risk Longitudinal Investigation', *Frontiers in Molecular Neuroscience*, 14, p. 775390. Available at: https://doi.org/10.3389/FNMOL.2021.775390/BIBTEX.
54. Balachandar, V. *et al.* (2020) 'Mitochondrial dysfunction: A hidden trigger of autism?', *Genes & Diseases* [Preprint]. Available at: https://doi.org/10.1016/j.gendis.2020.07.002.
55. Bam, S. *et al.* (2021) 'DNA Methylation of PGC-1α Is Associated With Elevated mtDNA Copy Number and Altered Urinary Metabolites in Autism Spectrum Disorder', *Frontiers in Cell and Developmental Biology*, 9, p. 2024. Available at: https://doi.org/10.3389/fcell.2021.696428.
56. Bamford, R.A. *et al.* (2024) 'CNTN4 modulates neural elongation through interplay with APP', *Open Biology*, 14(5). Available at: https://doi.org/10.1098/RSOB.240018.
57. Banerjee, N. and Adak, P. (2021) 'DNA methylation signatures in autism spectrum disorders', *Nucleus (India)*. Springer, pp. 359–372. Available at: https://doi.org/10.1007/s13237-021-00370-3.
58. Bantle, C.M. *et al.* (2021) 'Mitochondrial Dysfunction in Astrocytes: A Role in Parkinson's Disease?', *Frontiers in Cell and Developmental Biology*, 8, p. 1587. Available at: https://doi.org/10.3389/FCELL.2020.608026/BIBTEX.
59. Baranova, J. *et al.* (2021) 'Autism Spectrum Disorder: Signaling Pathways and Prospective Therapeutic Targets', *Cellular and Molecular Neurobiology*, 41(4), pp. 619–649. Available at: https://doi.org/10.1007/S10571-020-00882-7.
60. Barber, C.N. and Raben, D.M. (2019) 'Lipid metabolism crosstalk in the brain: Glia and neurons', *Frontiers in Cellular Neuroscience*, 13, p. 212. Available at: https://doi.org/10.3389/FNCEL.2019.00212/BIBTEX.
61. Bardai, F.H. *et al.* (2012) 'Histone deacetylase-1 (HDAC1) is a molecular switch between neuronal survival and death', *Journal of Biological Chemistry*, 287(42), pp. 35444–35453. Available at: https://doi.org/10.1074/jbc.M112.394544.

62. Bardai, F.H. and D'Mello, S.R. (2011) 'Selective Toxicity by HDAC3 in Neurons: Regulation by Akt and GSK3β', *Journal of Neuroscience*, 31(5), pp. 1746–1751. Available at: https://doi.org/10.1523/JNEUROSCI.5704-10.2011.
63. Barth, M. *et al.* (2022) 'Quantitative proteomics and in-cell cross-linking reveal cellular reorganisation during early neuronal differentiation of SH-SY5Y cells', *Communications Biology*, 5(1), p. 551. Available at: https://doi.org/10.1038/s42003-022-03478-7.
64. Baser, S., Kesli, R. and Ates, M.B. (2023) 'Evaluation of Microglia Activation Neuroinflammation and Neuronal Loss Presence in Experimentally Generated Rat Autism Model with Propionic Acid'. Available at: https://doi.org/10.54289/JPBT2300102.
65. Baum, T. and Gama, V. (2021) 'Dynamic properties of mitochondria during human corticogenesis', *Development (Cambridge)*, 148(4). Available at: https://doi.org/10.1242/DEV.194183/237449.
66. Bautista, S.J. *et al.* (2018) 'mTOR complex 1 controls the nuclear localization and function of glycogen synthase kinase 3β', *Journal of Biological Chemistry*, 293(38), pp. 14723–14739. Available at: https://doi.org/10.1074/JBC.RA118.002800.
67. Bayeva, N., Coll, E. and Piskareva, O. (2021) 'Differentiating Neuroblastoma: A Systematic Review of the Retinoic Acid, Its Derivatives, and Synergistic Interactions', *Journal of Personalized Medicine 2021, Vol. 11, Page 211*, 11(3), p. 211. Available at: https://doi.org/10.3390/JPM11030211.
68. Bean, C. *et al.* (2021) 'The mitochondrial protein Opa1 promotes adipocyte browning that is dependent on urea cycle metabolites', *Nature Metabolism 2021 3:12*, 3(12), pp. 1633–1647. Available at: https://doi.org/10.1038/s42255-021-00497-2.
69. Beckervordersandforth, R. (2017) 'Mitochondrial Metabolism-Mediated Regulation of Adult Neurogenesis', *Brain Plasticity*, 3(1), pp. 73–87. Available at: https://doi.org/10.3233/bpl-170044.
70. Bejoy, J. *et al.* (2020) 'Wnt-Notch Signaling Interactions During Neural and Astroglial Patterning of Human Stem Cells', *Tissue Engineering. Part A*, 26(7–8), p. 419. Available at: https://doi.org/10.1089/TEN.TEA.2019.0202.
71. Bell, E. *et al.* (2013) 'Cell Survival Signalling through PPARδ and Arachidonic Acid Metabolites in Neuroblastoma', *PLOS ONE*, 8(7), p. e68859. Available at: https://doi.org/10.1371/JOURNAL.PONE.0068859.
72. Bell, M. and Zempel, H. (2021) 'SH-SY5Y-derived neurons: a human neuronal model system for investigating TAU sorting and neuronal subtype-specific TAU vulnerability', *Reviews in the neurosciences*, 33(1), pp. 1–15. Available at: https://doi.org/10.1515/REVNEURO-2020-0152.
73. Bell, N. *et al.* (2013) 'Store-operated Ca2+ entry in proliferating and retinoic acid-differentiated N- and S-type neuroblastoma cells', *Biochimica et Biophysica Acta - Molecular Cell Research*, 1833(3), pp. 643–651. Available at: https://doi.org/10.1016/J.BBAMCR.2012.11.025.
74. Bellizzi, D. *et al.* (2012) 'Global DNA methylation levels are modulated by mitochondrial DNA variants', *Epigenomics*, 4(1), pp. 17–27. Available at: https://doi.org/10.2217/epi.11.109.
75. Belmonte-Mateos, C. and Pujades, C. (2022) 'From Cell States to Cell Fates: How Cell Proliferation and Neuronal Differentiation Are Coordinated During Embryonic Development', *Frontiers in Neuroscience*, 15, p. 781160. Available at: https://doi.org/10.3389/FNINS.2021.781160/BIBTEX.
76. Bengoa-Vergniory, N. and Kypta, R.M. (2015) 'Canonical and noncanonical Wnt signaling in neural stem/progenitor cells', *Cellular and Molecular Life Sciences 2015 72:21*, 72(21), pp. 4157–4172. Available at: https://doi.org/10.1007/S00018-015-2028-6.
77. Ben-Shachar, D. (2017) 'Mitochondrial multifaceted dysfunction in schizophrenia; complex I as a possible pathological target', *Schizophrenia research*, 187, pp. 3–10. Available at: https://doi.org/10.1016/J.SCHRES.2016.10.022.
78. Ben-Shachar, D. (2020) 'The bimodal mechanism of interaction between dopamine and mitochondria as reflected in Parkinson's disease and in schizophrenia', *Journal of Neural Transmission*, 127(2), pp. 159–168. Available at: https://doi.org/10.1007/s00702-019-02120-x.
79. Ben-Shachar, D. and Ene, H.M. (2018) 'Mitochondrial Targeted Therapies: Where Do We Stand in Mental Disorders?', *Biological Psychiatry*, 83(9), pp. 770–779. Available at: https://doi.org/10.1016/J.BIOPSYCH.2017.08.007.
80. Berardelli, I. *et al.* (2020) 'The Involvement of Hypothalamus–Pituitary–Adrenal (HPA) Axis in Suicide Risk', *Brain Sciences 2020, Vol. 10, Page 653*, 10(9), p. 653. Available at: https://doi.org/10.3390/BRAINSCI10090653.
81. Berenguer, M *et al.* (2022) 'Retinoic acid, RARs and early development', *Journal of Molecular Endocrinology*, 69(4), pp. T59–T67. Available at: https://doi.org/10.1530/JME-22-0041.
82. Berezhnov, A. V. *et al.* (2016) 'Intracellular pH Modulates Autophagy and Mitophagy', *The Journal of Biological Chemistry*, 291(16), p. 8701. Available at: https://doi.org/10.1074/JBC.M115.691774.

83. Bernal, A. and Arranz, L. (2018) 'Nestin-expressing progenitor cells: function, identity and therapeutic implications', *Cellular and Molecular Life Sciences: CMLS*, 75(12), p. 2177. Available at: https://doi.org/10.1007/S00018-018-2794-Z.
84. Bernardo, V.S., Torres, F.F. and da Silva, D.G.H. (2023) 'FoxO3 and oxidative stress: a multifaceted role in cellular adaptation', *Journal of Molecular Medicine 2023 101:1*, 101(1), pp. 83–99. Available at: https://doi.org/10.1007/S00109-022-02281-5.
85. Bernier, L.-P., York, E.M. and MacVicar, B.A. (2020) 'Immunometabolism in the Brain: How Metabolism Shapes Microglial Function', *Trends in Neurosciences*, 43(11), pp. 854–869. Available at: https://doi.org/10.1016/j.tins.2020.08.008.
86. Bernkopf, D.B. and Behrens, J. (2018) 'Feedback regulation of mitochondrial homeostasis via Wnt/β-catenin signaling', *Molecular & Cellular Oncology*, 5(3). Available at: https://doi.org/10.1080/23723556.2018.1458015.
87. Beurel, E., Toups, M. and Nemeroff, C.B. (2020) 'The Bidirectional Relationship of Depression and Inflammation: Double Trouble', *Neuron*. Cell Press, pp. 234–256. Available at: https://doi.org/10.1016/j.neuron.2020.06.002.
88. Beveridge, N.J. *et al.* (2009) 'Down-regulation of miR-17 family expression in response to retinoic acid induced neuronal differentiation', *Cellular Signalling*, 21(12), pp. 1837–1845. Available at: https://doi.org/10.1016/j.cellsig.2009.07.019.
89. Bhattacharya, A. *et al.* (2024) 'Neuroendocrine and cellular mechanisms in stress resilience: From hormonal influence in the CNS to mitochondrial dysfunction and oxidative stress', *Journal of Cellular and Molecular Medicine*, 28(7), p. e18220. Available at: https://doi.org/10.1111/JCMM.18220.
90. Bi, P. and Kuang, S. (2015) 'Notch signaling as a novel regulator of metabolism', *Trends in Endocrinology and Metabolism*, 26(5), pp. 248–255. Available at: https://doi.org/10.1016/J.TEM.2015.02.006/ASSET/D7B06B95-9C67-41AB-B801-F316FD8A633F/MAIN.ASSETS/GR3.JPG.
91. Bilotta, A.J. *et al.* (2021) 'Propionate Enhances Cell Speed and Persistence to Promote Intestinal Epithelial Turnover and Repair', *Cellular and Molecular Gastroenterology and Hepatology*, 11(4), pp. 1023–1044. Available at: https://doi.org/10.1016/J.JCMGH.2020.11.011.
92. Bjørklund, G., Meguid, N.A., *et al.* (2020) 'Oxidative Stress in Autism Spectrum Disorder', *Molecular Neurobiology*, 57(5), pp. 2314–2332. Available at: https://doi.org/10.1007/s12035-019-01742-2.
93. Bjørklund, G., Tinkov, A.A., *et al.* (2020) 'The role of glutathione redox imbalance in autism spectrum disorder: A review', *Free Radical Biology and Medicine*, 160, pp. 149–162. Available at: https://doi.org/10.1016/j.freeradbiomed.2020.07.017.
94. Bjørklund, G. *et al.* (2021) 'The impact of glutathione metabolism in autism spectrum disorder', *Pharmacological Research*, 166, p. 105437. Available at: https://doi.org/10.1016/j.phrs.2021.105437.
95. van der Bliek, A.M., Shen, Q. and Kawajiri, S. (2013) 'Mechanisms of Mitochondrial Fission and Fusion', *Cold Spring Harbor Perspectives in Biology*, 5(6). Available at: https://doi.org/10.1101/CSHPERSPECT.A011072.
96. Blum, K. *et al.* (2024) 'Dopamine Dysregulation in Reward and Autism Spectrum Disorder', *Brain Sciences 2024, Vol. 14, Page 733*, 14(7), p. 733. Available at: https://doi.org/10.3390/BRAINSCI14070733.
97. Boeck, C. *et al.* (2016) 'Inflammation in adult women with a history of child maltreatment: The involvement of mitochondrial alterations and oxidative stress', *Mitochondrion*, 30, pp. 197–207. Available at: https://doi.org/10.1016/J.MITO.2016.08.006.
98. Boksha, I.S. *et al.* (2021) 'Protein Phosphorylation Signaling Cascades in Autism: The Role of mTOR Pathway', *Biochemistry (Moscow) 2021 86:5*, 86(5), pp. 577–596. Available at: https://doi.org/10.1134/S0006297921050072.
99. Bolte, S. and Cordelières, F.P. (2006) 'A guided tour into subcellular colocalization analysis in light microscopy', *Journal of Microscopy*, 224(3), pp. 213–232. Available at: https://doi.org/10.1111/J.1365-2818.2006.01706.X.
100. Bonapersona, V., Joëls, M. and Sarabdjitsingh, R.A. (2018) 'Effects of early life stress on biochemical indicators of the dopaminergic system: A 3 level meta-analysis of rodent studies', *Neuroscience & Biobehavioral Reviews*, 95, pp. 1–16. Available at: https://doi.org/10.1016/j.neubiorev.2018.09.003.
101. Bonzano, S. *et al.* (2024) 'Mitochondrial regulation of adult hippocampal neurogenesis: Insights into neurological function and neurodevelopmental disorders', *Neurobiology of Disease*, 199, p. 106604. Available at: https://doi.org/10.1016/J.NBD.2024.106604.
102. Bott, C.J. *et al.* (2019) 'Nestin in immature embryonic neurons affects axon growth cone morphology and Semaphorin3a sensitivity', *Molecular Biology of the Cell*, 30(10), p. 1214. Available at: https://doi.org/10.1091/MBC.E18-06-0361.

103. Bou Najm, D., Alame, S. and Takash Chamoun, W. (2024) 'Unraveling the Role of Wnt Signaling Pathway in the Pathogenesis of Autism Spectrum Disorder (ASD): A Systematic Review', *Molecular Neurobiology*, pp. 1–22. Available at: https://doi.org/10.1007/S12035-024-04558-X/TABLES/2.
104. Bovio, F. *et al.* (2021) 'Cadmium promotes glycolysis upregulation and glutamine dependency in human neuronal cells', *Neurochemistry International*, 149, p. 105144. Available at: https://doi.org/10.1016/J.NEUINT.2021.105144.
105. Bowers, M. *et al.* (2020) 'FASN-Dependent Lipid Metabolism Links Neurogenic Stem/Progenitor Cell Activity to Learning and Memory Deficits', *Cell Stem Cell*, 27(1), pp. 98-109.e11. Available at: https://doi.org/10.1016/j.stem.2020.04.002.
106. Bradshaw, T.Y. *et al.* (2016) 'A reduction in Drp1-mediated fission compromises mitochondrial health in autosomal recessive spastic ataxia of Charlevoix Saguenay', *Human molecular genetics*, 25(15), pp. 3232–3244. Available at: https://doi.org/10.1093/HMG/DDW173.
107. Braun, S.M.G. *et al.* (2021) 'BAF subunit switching regulates chromatin accessibility to control cell cycle exit in the developing mammalian cortex', *Genes & Development*, 35(5–6), pp. 335–353. Available at: https://doi.org/10.1101/GAD.342345.120.
108. Brondani, M. *et al.* (2023) 'Mitochondrial dysfunction, oxidative stress, ER stress and mitochondria-ER crosstalk alterations in a chemical rat model of Huntington's disease: Potential benefits of bezafibrate', *Toxicology Letters*, 381, pp. 48–59. Available at: https://doi.org/10.1016/J.TOXLET.2023.04.011.
109. Brown, M., Worrell, C. and Pariante, C.M. (2021) 'Inflammation and early life stress: An updated review of childhood trauma and inflammatory markers in adulthood', *Pharmacology Biochemistry and Behavior*, 211, p. 173291. Available at: https://doi.org/10.1016/J.PBB.2021.173291.
110. Brunetti, D. *et al.* (2021) 'Mitochondria in Neurogenesis: Implications for Mitochondrial Diseases', *Stem Cells*, 39(10), pp. 1289–1297. Available at: https://doi.org/10.1002/STEM.3425.
111. Buchanan, E. *et al.* (2023) 'Propionic acid induces alterations in mitochondrial morphology and dynamics in SH-SY5Y cells', *Scientific reports*, 13(1), p. 13248. Available at: https://doi.org/10.1038/s41598-023-40130-8.
112. Burbulla, L.F. *et al.* (2017) 'Dopamine oxidation mediates mitochondrial and lysosomal dysfunction in Parkinson's disease', *Science*, 357(6357), pp. 1255–1261. Available at: https://doi.org/10.1126/science.aam9080.
113. Burgueño, A.L. *et al.* (2013) 'Maternal high-fat intake during pregnancy programs metabolic-syndrome-related phenotypes through liver mitochondrial DNA copy number and transcriptional activity of liver PPARGC1A', *Journal of Nutritional Biochemistry*, 24(1), pp. 6–13. Available at: https://doi.org/10.1016/j.jnutbio.2011.12.008.
114. Buttiglione, M. *et al.* (2007) 'Behaviour of SH-SY5Y neuroblastoma cell line grown in different media and on different chemically modified substrates', *Biomaterials*, 28(19), pp. 2932–2945. Available at: https://doi.org/10.1016/J.BIOMATERIALS.2007.02.022.
115. Cage, E. and Troxell-Whitman, Z. (2019) 'Understanding the Reasons, Contexts and Costs of Camouflaging for Autistic Adults', *Journal of Autism and Developmental Disorders*, 49(5), pp. 1899–1911. Available at: https://doi.org/10.1007/S10803-018-03878-X/TABLES/5.
116. Cai, C. *et al.* (2021) 'c-Myc regulates neural stem cell quiescence and activation by coordinating the cell cycle and mitochondrial remodeling', *Signal Transduction and Targeted Therapy*, 6(1), p. 306. Available at: https://doi.org/10.1038/s41392-021-00664-7.
117. Cai, N. *et al.* (2015) 'Molecular signatures of major depression', *Current Biology*, 25(9), pp. 1146–1156. Available at: https://doi.org/10.1016/J.CUB.2015.03.008/ATTACHMENT/01352182-1850-4C0A-96D7-E14947BC4160/MMC1.PDF.
118. Calì, C. *et al.* (2024) 'Metabolic Reprogramming of Astrocytes in Pathological Conditions: Implications for Neurodegenerative Diseases', *International Journal of Molecular Sciences 2024, Vol. 25, Page 8922*, 25(16), p. 8922. Available at: https://doi.org/10.3390/IJMS25168922.
119. Camblor-Perujo, S. and Kononenko, N.L. (2022) 'Brain-specific functions of the endocytic machinery', *The FEBS Journal*, 289(8), pp. 2219–2246. Available at: https://doi.org/10.1111/FEBS.15897.
120. Campbell, G., Licht-Mayer, S. and Mahad, D. (2019) 'Targeting mitochondria to protect axons in progressive MS', *Neuroscience Letters*, 710, p. 134258. Available at: https://doi.org/10.1016/J.NEULET.2019.05.012.
121. Campos Cogo, S. *et al.* (2020) 'An overview of neuroblastoma cell lineage phenotypes and in vitro models', *Experimental biology and medicine (Maywood, N.J.)*, 245(18), pp. 1637–1647. Available at: https://doi.org/10.1177/1535370220949237.
122. Campos, J.C., Bozi, L.H.M. and Ferreira, J.C.B. (2022) 'Mitochondrial Biogenesis and Dynamics in Health and Disease', *Essential Aspects of Immunometabolism in Health and Disease*, pp. 31–51. Available at: https://doi.org/10.1007/978-3-030-86684-6_3.

123. Cantando, I. *et al.* (2024) 'Metabolic dynamics in astrocytes and microglia during post-natal development and their implications for autism spectrum disorders', *Frontiers in Cellular Neuroscience*, 18, p. 1354259. Available at: https://doi.org/10.3389/FNCEL.2024.1354259/BIBTEX.
124. Caracci, M.O. *et al.* (2021) 'Wnt/β-Catenin-Dependent Transcription in Autism Spectrum Disorders', *Frontiers in Molecular Neuroscience*, 14, p. 764756. Available at: https://doi.org/10.3389/FNMOL.2021.764756/BIBTEX.
125. Caracci, M.O., Avila, M.E. and De Ferrari, G. V. (2016) 'Synaptic Wnt/GSK3 β Signaling Hub in Autism', *Neural Plasticity*, 2016. Available at: https://doi.org/10.1155/2016/9603751.
126. Carbognin, E. *et al.* (2016) 'Stat3 promotes mitochondrial transcription and oxidative respiration during maintenance and induction of naive pluripotency', *The EMBO Journal*, 35(6), pp. 618–634. Available at: https://doi.org/10.15252/EMBJ.201592629/SUPPL_FILE/EMBJ201592629-SUP-0004-SDATAAPPENDIX.ZIP.
127. Cardanho-Ramos, C. and Morais, V.A. (2021) 'Mitochondrial Biogenesis in Neurons: How and Where', *International Journal of Molecular Sciences 2021, Vol. 22, Page 13059*, 22(23), p. 13059. Available at: https://doi.org/10.3390/IJMS222313059.
128. Carla, L.S. *et al.* (2022) 'The Role of MeCP2 in Regulating Synaptic Plasticity in the Context of Stress and Depression', pp. 1–17.
129. Casanova, M.F. *et al.* (2020) 'Editorial: Secondary vs. Idiopathic Autism', *Frontiers in Psychiatry*. Frontiers Media S.A., p. 522652. Available at: https://doi.org/10.3389/fpsyt.2020.00297.
130. Cassidy, S. *et al.* (2014) 'Suicidal ideation and suicide plans or attempts in adults with Asperger's syndrome attending a specialist diagnostic clinic: a clinical cohort study', *The Lancet Psychiatry*, 1(2), pp. 142–147. Available at: https://doi.org/10.1016/S2215-0366(14)70248-2.
131. Cassidy, S.A. *et al.* (2020) 'Is Camouflaging Autistic Traits Associated with Suicidal Thoughts and Behaviours? Expanding the Interpersonal Psychological Theory of Suicide in an Undergraduate Student Sample', *Journal of Autism and Developmental Disorders*, 50(10), pp. 3638–3648. Available at: https://doi.org/10.1007/S10803-019-04323-3/FIGURES/1.
132. Castelbaum, L. *et al.* (2019) 'On the Nature of Monozygotic Twin Concordance and Discordance for Autistic Trait Severity: A Quantitative Analysis', *Behavior Genetics*, 50(4), p. 263. Available at: https://doi.org/10.1007/S10519-019-09987-2.
133. Castellani, C.A. *et al.* (2020) *Thinking outside the nucleus: Mitochondrial DNA copy number in health and disease*, *Mitochondrion*. Elsevier. Available at: https://doi.org/10.1016/j.mito.2020.06.004.
134. Castora, F.J. (2019) 'Mitochondrial function and abnormalities implicated in the pathogenesis of ASD', *Progress in Neuro-Psychopharmacology and Biological Psychiatry*, 92, pp. 83–108. Available at: https://doi.org/10.1016/J.PNPBP.2018.12.015.
135. Castro-Portuguez, R. and Sutphin, G.L. (2020) 'Kynurenine pathway, NAD+ synthesis, and mitochondrial function: Targeting tryptophan metabolism to promote longevity and healthspan', *Experimental Gerontology*, 132, p. 110841. Available at: https://doi.org/10.1016/j.exger.2020.110841.
136. Catale, C. *et al.* (2022) 'Early Life Social Stress Causes Sex- and Region-Dependent Dopaminergic Changes that Are Prevented by Minocycline', *Molecular Neurobiology*, 59(6), pp. 3913–3932. Available at: https://doi.org/10.1007/s12035-022-02830-6.
137. Catanesi, M. *et al.* (2021) 'L-methionine protects against oxidative stress and mitochondrial dysfunction in an in vitro model of parkinson's disease', *Antioxidants*, 10(9), p. 1467. Available at: https://doi.org/10.3390/ANTIOX10091467/S1.
138. Cavalcanti-de-Albuquerque, J.P. *et al.* (2021) 'Coupling of GABA Metabolism to Mitochondrial Glucose Phosphorylation', *Neurochemical Research*, pp. 1–11. Available at: https://doi.org/10.1007/S11064-021-03463-2/FIGURES/4.
139. Ceruso, A. *et al.* (2020) 'Alterations of the HPA Axis Observed in Patients with Major Depressive Disorder and Their Relation to Early Life Stress: A Systematic Review', *Neuropsychobiology*, 79(6), pp. 417–427. Available at: https://doi.org/10.1159/000506484.
140. Chakraborty, P. and Mukherjee, C. (2024) 'The interplay of metabolic and epigenetic players in disease development', *Biochemical and Biophysical Research Communications*, 734, p. 150621. Available at: https://doi.org/10.1016/J.BBRC.2024.150621.
141. Chandler, R.J. *et al.* (2011) 'Adeno-associated virus serotype 8 gene transfer rescues a neonatal lethal murine model of propionic acidemia', *Human Gene Therapy*, 22(4), pp. 477–481. Available at: https://doi.org/10.1089/HUM.2010.164.

142. Chang, P. *et al.* (2023) 'BNP protects against diabetic cardiomyopathy by promoting Opa1-mediated mitochondrial fusion via activating the PKG-STAT3 pathway', *Redox biology*, 62. Available at: https://doi.org/10.1016/J.REDOX.2023.102702.
143. Chapman, K.A. *et al.* (2016) 'Recapitulation of metabolic defects in a model of propionic acidemia using patient-derived primary hepatocytes', *Molecular Genetics and Metabolism* [Preprint]. Available at: https://doi.org/10.1016/j.ymgme.2015.12.008.
144. Chapman, K.A. *et al.* (2018) 'Propionyl-CoA carboxylase pcca-1 and pccb-1 gene deletions in Caenorhabditis elegans globally impair mitochondrial energy metabolism', *Journal of Inherited Metabolic Disease* [Preprint]. Available at: https://doi.org/10.1007/s10545-017-0111-x.
145. Chatoo, W. *et al.* (2010) 'Bmi1 distinguishes immature retinal progenitor/stem cells from the main progenitor cell population and is required for normal retinal development', *Stem Cells*, 28(8), pp. 1412–1423. Available at: https://doi.org/10.1002/stem.462.
146. Chaudhry, A., Shi, R. and Luciani, D.S. (2020) 'A pipeline for multidimensional confocal analysis of mitochondrial morphology, function, and dynamics in pancreatic β-cells', *American Journal of Physiology-Endocrinology and Metabolism*, 318(2), pp. E87–E101. Available at: https://doi.org/10.1152/ajpendo.00457.2019.
147. Chausse, B., Kakimoto, P.A. and Kann, O. (2021) 'Microglia and lipids: how metabolism controls brain innate immunity', *Seminars in Cell & Developmental Biology*, 112, pp. 137–144. Available at: https://doi.org/10.1016/j.semcdb.2020.08.001.
148. Chen, B. *et al.* (2022) 'Cortical myelination in toddlers and preschoolers with autism spectrum disorder', *Developmental Neurobiology*, 82(3), pp. 261–274. Available at: https://doi.org/10.1002/DNEU.22874.
149. Chen, H. *et al.* (2003) 'Mitofusins Mfn1 and Mfn2 coordinately regulate mitochondrial fusion and are essential for embryonic development', *Journal of Cell Biology*, 160(2), pp. 189–200. Available at: https://doi.org/10.1083/JCB.200211046/VIDEO-3.
150. Chen, H. *et al.* (2023) 'Neurodevelopmental effects of maternal folic acid supplementation: a systematic review and meta-analysis', *Critical Reviews in Food Science and Nutrition*, 63(19), pp. 3771–3787. Available at: https://doi.org/10.1080/10408398.2021.1993781.
151. Chen, J. and Park, J.M. (2022) 'Assessing Pyruvate Carboxylase Flux as a Mechanistic Biological Marker in Fasting', pp. 429–443. Available at: https://doi.org/10.1007/978-3-031-07389-2_27.
152. Chen, L. *et al.* (2021) 'Oxidative stress marker aberrations in children with autism spectrum disorder: a systematic review and meta-analysis of 87 studies (N = 9109)', *Translational Psychiatry 2021 11:1*, 11(1), pp. 1–10. Available at: https://doi.org/10.1038/s41398-020-01135-3.
153. Chen, L. *et al.* (2022) 'PGC-1α-Mediated Mitochondrial Quality Control: Molecular Mechanisms and Implications for Heart Failure', *Frontiers in Cell and Developmental Biology*, 10, p. 871357. Available at: https://doi.org/10.3389/FCELL.2022.871357/BIBTEX.
154. Chen, N. *et al.* (2024) 'Brain short chain fatty acids induce ACSS2 to ameliorate depressive-like behavior via PPARγ-TPH2 axis', *Research* [Preprint]. Available at: https://doi.org/10.34133/research.0400.
155. Chen, Q. and Ross, A.C. (2004) 'Retinoic acid regulates cell cycle progression and cell differentiation in human monocytic THP-1 cells', *Experimental Cell Research*, 297(1), pp. 68–81. Available at: https://doi.org/10.1016/J.YEXCR.2004.02.017.
156. Chen, S. *et al.* (2015) 'Elevated mitochondrial DNA copy number in peripheral blood cells is associated with childhood autism', *BMC Psychiatry*, 15(1), p. 50. Available at: https://doi.org/10.1186/s12888-015-0432-y.
157. Chen, W., Zhao, H. and Li, Y. (2023) 'Mitochondrial dynamics in health and disease: mechanisms and potential targets', *Signal Transduction and Targeted Therapy 2023 8:1*, 8(1), pp. 1–25. Available at: https://doi.org/10.1038/s41392-023-01547-9.
158. Chen, X. *et al.* (2023) 'Endoplasmic reticulum stress: molecular mechanism and therapeutic targets', *Signal Transduction and Targeted Therapy 2023 8:1*, 8(1), pp. 1–40. Available at: https://doi.org/10.1038/s41392-023-01570-w.
159. Chen, Y. *et al.* (2017) 'Neuronal Activity-Induced Sterol Regulatory Element Binding Protein-1 (SREBP1) is Disrupted in Dysbindin-Null Mice—Potential Link to Cognitive Impairment in Schizophrenia', *Molecular Neurobiology*, 54(3), pp. 1699–1709. Available at: https://doi.org/10.1007/S12035-016-9773-X/FIGURES/7.
160. Chen, Y., Lun, A.T.L. and Smyth, G.K. (2016) 'From reads to genes to pathways: differential expression analysis of RNA-Seq experiments using Rsubread and the edgeR quasi-likelihood pipeline', *F1000Research*, 5. Available at: https://doi.org/10.12688/F1000RESEARCH.8987.2.
161. Cheng, N., Rho, J.M. and Masino, S.A. (2017) 'Metabolic dysfunction underlying autism spectrum disorder and potential treatment approaches', *Frontiers in Molecular Neuroscience*, 10, p. 230528. Available at: https://doi.org/10.3389/FNMOL.2017.00034/BIBTEX.

162. Cheng, T.L. and Qiu, Z. (2014) 'MeCP2: Multifaceted roles in gene regulation and neural development', *Neuroscience Bulletin*, 30(4), pp. 601–609. Available at: https://doi.org/10.1007/s12264-014-1452-6.
163. Cheroni, C., Caporale, N. and Testa, G. (2020) 'Autism spectrum disorder at the crossroad between genes and environment: Contributions, convergences, and interactions in ASD developmental pathophysiology', *Molecular Autism*. BioMed Central Ltd, p. 69. Available at: https://doi.org/10.1186/s13229-020-00370-1.
164. Cherry, A.D. and Piantadosi, C.A. (2015) 'Regulation of Mitochondrial Biogenesis and Its Intersection with Inflammatory Responses', *Antioxidants and Redox Signaling*, 22(12), pp. 965–976. Available at: https://doi.org/10.1089/ars.2014.6200.
165. Chiang, M.C. *et al.* (2013) 'PPARγ regulates the mitochondrial dysfunction in human neural stem cells with tumor necrosis factor alpha', *Neuroscience*, 229, pp. 118–129. Available at: https://doi.org/10.1016/J.NEUROSCIENCE.2012.11.003.
166. Chiapperino, L. and Hens, K. (2023) 'How to talk about autism: reconciling genomics and neurodiversity', *Nature Medicine 2023 29:7*, 29(7), pp. 1607–1608. Available at: https://doi.org/10.1038/s41591-023-02403-7.
167. Chiocchetti, A.G. *et al.* (2016) 'Transcriptomic signatures of neuronal differentiation and their association with risk genes for autism spectrum and related neuropsychiatric disorders', *Translational Psychiatry*, 6(8), pp. e864–e864. Available at: https://doi.org/10.1038/tp.2016.119.
168. Chmykhalo, V.K. *et al.* (2024) 'SWI/SNF Complex Connects Signaling and Epigenetic State in Cells of Nervous System', *Molecular Neurobiology 2024*, pp. 1–22. Available at: https://doi.org/10.1007/S12035-024-04355-6.
169. Cho, Y. and Cavalli, V. (2014) 'HDAC signaling in neuronal development and axon regeneration', *Current opinion in neurobiology*, 0, p. 118. Available at: https://doi.org/10.1016/J.CONB.2014.03.008.
170. Choi, G.E. *et al.* (2021) 'BNIP3L/NIX-mediated mitophagy protects against glucocorticoid-induced synapse defects', *Nature Communications*, 12(1). Available at: https://doi.org/10.1038/S41467-020-20679-Y.
171. Choi, G.E. and Han, H.J. (2021) 'Glucocorticoid impairs mitochondrial quality control in neurons', *Neurobiology of Disease*, 152, p. 105301. Available at: https://doi.org/10.1016/j.nbd.2021.105301.
172. Choi, H. *et al.* (2020) 'Propionic acid induces dendritic spine loss by MAPK/ERK signaling and dysregulation of autophagic flux', *Molecular Brain*, 13(1), p. 86. Available at: https://doi.org/10.1186/s13041-020-00626-0.
173. Choi, J., Lee, S., Won, J., Jin, Y., Hong, Yunkyung, Hur, T.Y., *et al.* (2018) 'Pathophysiological and neurobehavioral characteristics of a propionic acid-mediated autism-like rat model', *PLoS ONE*, 13(2). Available at: https://doi.org/10.1371/journal.pone.0192925.
174. Choi, J., Lee, S., Won, J., Jin, Y., Hong, Yunkyung, Hur, T.-Y., *et al.* (2018) 'Pathophysiological and neurobehavioral characteristics of a propionic acid-mediated autism-like rat model', *PLOS ONE*. Edited by J. Homberg, 13(2), p. e0192925. Available at: https://doi.org/10.1371/journal.pone.0192925.
175. Choi, L. and An, J.-Y. (2021) 'Genetic architecture of autism spectrum disorder: Lessons from large-scale genomic studies', *Neuroscience & Biobehavioral Reviews*, 128, pp. 244–257. Available at: https://doi.org/10.1016/j.neubiorev.2021.06.028.
176. Choubey, V., Zeb, A. and Kaasik, A. (2022) 'Molecular Mechanisms and Regulation of Mammalian Mitophagy', *Cells*, 11(1). Available at: https://doi.org/10.3390/CELLS11010038.
177. Chown, N. and Beardon, L. (2017) 'Theoretical Models and Autism', *Encyclopedia of Autism Spectrum Disorders*, pp. 1–7. Available at: https://doi.org/10.1007/978-1-4614-6435-8_102171-1.
178. Christie, D.A. *et al.* (2011) 'Stomatin-Like Protein 2 Binds Cardiolipin and Regulates Mitochondrial Biogenesis and Function', *Molecular and Cellular Biology*, 31(18), pp. 3845–3856. Available at: https://doi.org/10.1128/mcb.05393-11.
179. Chung, J.K. *et al.* (2019) 'Investigation of mitochondrial DNA copy number in patients with major depressive disorder', *Psychiatry Research*, 282. Available at: https://doi.org/10.1016/j.psychres.2019.112616.
180. Chung, K.M. and Yu, S.W. (2013) 'Interplay between autophagy and programmed cell death in mammalian neural stem cells', *BMB Reports*, 46(8), p. 383. Available at: https://doi.org/10.5483/BMBREP.2013.46.8.164.
181. Cicaloni, V. *et al.* (2020) 'Proteomic profiling reveals mitochondrial alterations in Rett syndrome', *Free Radical Biology and Medicine*, 155, pp. 37–48. Available at: https://doi.org/10.1016/j.freeradbiomed.2020.05.014.
182. Ciernia, A.V. and LaSalle, J. (2016) 'The landscape of DNA methylation amid a perfect storm of autism aetiologies', *Nature Reviews Neuroscience*, 17(7), pp. 411–423. Available at: https://doi.org/10.1038/nrn.2016.41.
183. Cigliano, A. *et al.* (2017) 'Deregulated c-Myc requires a functional HSF1 for experimental and human hepatocarcinogenesis', *Oncotarget*, 8(53), p. 90638. Available at: https://doi.org/10.18632/ONCOTARGET.21469.
184. Citrigno, L. *et al.* (2020) 'The Mitochondrial Dysfunction Hypothesis in Autism Spectrum Disorders: Current Status and Future Perspectives', *International Journal of Molecular Sciences*, 21(16), p. 5785. Available at: https://doi.org/10.3390/ijms21165785.

185. Coelho, P. *et al.* (2022) 'Mitochondrial function and dynamics in neural stem cells and neurogenesis: Implications for neurodegenerative diseases', *Ageing Research Reviews*, 80, p. 101667. Available at: https://doi.org/10.1016/j.arr.2022.101667.
186. Colina, C., Puhl, H.L. and Ikeda, S.R. (2018) 'Selective tracking of FFAR3-expressing neurons supports receptor coupling to N-type calcium channels in mouse sympathetic neurons', *Scientific Reports 2018 8:1*, 8(1), pp. 1–14. Available at: https://doi.org/10.1038/s41598-018-35690-z.
187. Collado, M.S. *et al.* (2020) 'Biochemical and anaplerotic applications of in vitro models of propionic acidemia and methylmalonic acidemia using patient-derived primary hepatocytes', *Molecular Genetics and Metabolism*, 130(3), pp. 183–196. Available at: https://doi.org/10.1016/J.YMGME.2020.05.003.
188. Conn, K.J. *et al.* (2003) 'cDNA Microarray Analysis of Changes in Gene Expression Associated with MPP+ Toxicity in SH-SY5Y Cells', *Neurochemical Research*, 28(12), pp. 1873–1881. Available at: https://doi.org/10.1023/A:1026179926780.
189. Connolly, N.M.C. *et al.* (2017) 'Guidelines on experimental methods to assess mitochondrial dysfunction in cellular models of neurodegenerative diseases', *Cell Death & Differentiation 2017 25:3*, 25(3), pp. 542–572. Available at: https://doi.org/10.1038/s41418-017-0020-4.
190. Cook, J. *et al.* (2021) 'Camouflaging in autism: A systematic review', *Clinical Psychology Review*, 89, p. 102080. Available at: https://doi.org/10.1016/J.CPR.2021.102080.
191. Coppedè, F. (2021) 'One-carbon epigenetics and redox biology of neurodegeneration', *Free Radical Biology and Medicine*, 170, pp. 19–33. Available at: https://doi.org/10.1016/j.freeradbiomed.2020.12.002.
192. Coppedè, F. (2024) 'Mitochondrial DNA methylation and mitochondria-related epigenetics in neurodegeneration', *Neural Regeneration Research*, 19(2), pp. 405–406. Available at: https://doi.org/10.4103/1673-5374.379045.
193. Corbett, B.A. and Schupp, C.W. (2014) 'The cortisol awakening response (CAR) in male children with autism spectrum disorder', *Hormones and Behavior*, 65(4), pp. 345–350. Available at: https://doi.org/10.1016/J.YHBEH.2014.01.012.
194. Corbett, B.A. and Simon, D. (2014) 'Adolescence, Stress and Cortisol in Autism Spectrum Disorders', *OA autism*, 1(1), p. 2. Available at: https://doi.org/10.13172/2052-7810-1-1-348.
195. Cordelières, F.P. and Zhang, C. (2020) '3D Quantitative Colocalisation Analysis', pp. 33–66. Available at: https://doi.org/10.1007/978-3-030-22386-1_3.
196. Corley, M.J. *et al.* (2019) 'Epigenetic Delay in the Neurodevelopmental Trajectory of DNA Methylation States in Autism Spectrum Disorders', *Frontiers in Genetics*, 10, p. 907. Available at: https://doi.org/10.3389/fgene.2019.00907.
197. Corona, J.C. and Duchen, M.R. (2016) 'PPARγ as a therapeutic target to rescue mitochondrial function in neurological disease', *Free Radical Biology and Medicine*, 100, pp. 153–163. Available at: https://doi.org/10.1016/J.FREERADBIOMED.2016.06.023.
198. Cortés-Pereira, E. *et al.* (2019) 'Differential Association of Mitochondrial DNA Haplogroups J and H With the Methylation Status of Articular Cartilage: Potential Role in Apoptosis and Metabolic and Developmental Processes', *Arthritis and Rheumatology*, 71(7), pp. 1191–1200. Available at: https://doi.org/10.1002/art.40857.
199. Costa, A.P., Loor, C. and Steffgen, G. (2020) 'Suicidality in adults with autism spectrum disorder: The role of depressive symptomatology, alexithymia, and antidepressants.', *Journal of Autism and Developmental Disorders*, 50(10), pp. 3585–3597. Available at: https://doi.org/10.1007/S10803-020-04433-3.
200. Da Costa, R.T. *et al.* (2021) 'Methylmalonic Acid Compromises Respiration and Reduces the Expression of Differentiation Markers of SH-SY5Y Human Neuroblastoma Cells', *ACS Chemical Neuroscience*, 12(14), pp. 2608–2618. Available at: https://doi.org/10.1021/acschemneuro.1c00119.
201. Cowan, M., Petri, W.A. and Jr. (2018) 'Microglia: Immune Regulators of Neurodevelopment', *Frontiers in Immunology*, 9(NOV), p. 2576. Available at: https://doi.org/10.3389/FIMMU.2018.02576.
202. Cui, P. *et al.* (2021) 'HIF-1α Affects the Neural Stem Cell Differentiation of Human Induced Pluripotent Stem Cells via MFN2-Mediated Wnt/β-Catenin Signaling', *Frontiers in Cell and Developmental Biology*, 9, p. 671704. Available at: https://doi.org/10.3389/fcell.2021.671704.
203. Curpan, A.S., Luca, A.C. and Ciobica, A. (2021) 'Potential Novel Therapies for Neurodevelopmental Diseases Targeting Oxidative Stress', *Oxidative Medicine and Cellular Longevity*, 2021. Available at: https://doi.org/10.1155/2021/6640206.
204. Czarny, P. *et al.* (2020) 'Mitochondrial DNA copy number, damage, repair and degradation in depressive disorder', *World Journal of Biological Psychiatry*, 21(2), pp. 91–101. Available at: https://doi.org/10.1080/15622975.2019.1588993.

205. Czumaj, A. *et al.* (2020) 'The Pathophysiological Role of CoA', *International Journal of Molecular Sciences*, 21(23), pp. 1–30. Available at: https://doi.org/10.3390/IJMS21239057.
206. Dagda, R.K. *et al.* (2009) 'Loss of PINK1 function promotes mitophagy through effects on oxidative stress and mitochondrial fission', *Journal of Biological Chemistry*, 284(20), pp. 13843–13855. Available at: https://doi.org/10.1074/jbc.M808515200.
207. Dagda, R.K. and Rice, M. (2017) 'Protocols for assessing mitophagy in neuronal cell lines and primary neurons', *Neuromethods*, 123, p. 249. Available at: https://doi.org/10.1007/978-1-4939-6890-9_13.
208. Dai, H. *et al.* (2015) 'PINK1/Parkin-mediated mitophagy alleviates chlorpyrifos-induced apoptosis in SH-SY5Y cells', *Toxicology*, 334, pp. 72–80. Available at: https://doi.org/10.1016/J.TOX.2015.06.003.
209. D'Aloia, A. *et al.* (2024) 'A new advanced cellular model of functional cholinergic-like neurons developed by reprogramming the human SH-SY5Y neuroblastoma cell line', *Cell Death Discovery 2024 10:1*, 10(1), pp. 1–16. Available at: https://doi.org/10.1038/s41420-023-01790-7.
210. D'Andrea, L. *et al.* (2024) 'Glucose-derived glutamate drives neuronal terminal differentiation in vitro', *EMBO Reports*, 25(3), p. 991. Available at: https://doi.org/10.1038/S44319-023-00048-8.
211. D'Angelo, B. *et al.* (2011) 'Signal transduction pathways involved in PPARβ/δ-induced neuronal differentiation', *Journal of Cellular Physiology*, 226(8), pp. 2170–2180. Available at: https://doi.org/10.1002/JCP.22552.
212. D'Angelo, M. *et al.* (2018) 'PPARs and Energy Metabolism Adaptation during Neurogenesis and Neuronal Maturation', *International Journal of Molecular Sciences*, 19(7), p. 1869. Available at: https://doi.org/10.3390/ijms19071869.
213. D'Angelo, S. *et al.* (2021) 'Sirt1 Activity in the Brain: Simultaneous Effects on Energy Homeostasis and Reproduction', *International Journal of Environmental Research and Public Health*, 18(3), pp. 1–17. Available at: https://doi.org/10.3390/IJERPH18031243.
214. Daniels, T.E., Olsen, E.M. and Tyrka, A.R. (2020) 'Stress and Psychiatric Disorders: The Role of Mitochondria', *Annual Review of Clinical Psychology*. Annual Reviews, pp. 165–186. Available at: https://doi.org/10.1146/annurev-clinpsy-082719-104030.
215. Das, E. and Bhattacharyya, N.P. (2014) 'MicroRNA-432 contributes to dopamine cocktail and retinoic acid induced differentiation of human neuroblastoma cells by targeting NESTIN and RCOR1 genes', *FEBS Letters*, 588(9), pp. 1706–1714. Available at: https://doi.org/10.1016/j.febslet.2014.03.015.
216. Dave, A. *et al.* (2019) 'Mitochondrial Electron Transport Chain Complex Dysfunction in MeCP2 Knock-Down Astrocytes: Protective Effects of Quercetin Hydrate', *Journal of Molecular Neuroscience*, 67(1), pp. 16–27. Available at: https://doi.org/10.1007/s12031-018-1197-9.
217. Davis, L., Onn, I. and Elliott, E. (2018) 'The emerging roles for the chromatin structure regulators CTCF and cohesin in neurodevelopment and behavior', *Cellular and Molecular Life Sciences*, 75(7), pp. 1205–1214. Available at: https://doi.org/10.1007/S00018-017-2706-7/TABLES/2.
218. Delgado-Deida, Y., Alula, K.M. and Theiss, A.L. (2020) 'The influence of mitochondrial-directed regulation of Wnt signaling on tumorigenesis', *Gastroenterology Report*, 8(3), pp. 215–223. Available at: https://doi.org/10.1093/GASTRO/GOAA025.
219. Delhey, L.M. *et al.* (2017) 'The Effect of Mitochondrial Supplements on Mitochondrial Activity in Children with Autism Spectrum Disorder.', *Journal of clinical medicine*, 6(2). Available at: https://doi.org/10.3390/jcm6020018.
220. Dempster, K.S. *et al.* (2021) 'Linking the hemodynamic consequences of adverse childhood experiences to an altered HPA axis and acute stress response', *Brain, Behavior, and Immunity*, 93, pp. 254–263. Available at: https://doi.org/10.1016/j.bbi.2020.12.018.
221. Deng, Y. *et al.* (2024) 'The Notch1/Hes1 pathway regulates Neuregulin 1/ErbB4 and participates in microglial activation in rats with VPA-induced autism', *Progress in Neuro-Psychopharmacology and Biological Psychiatry*, 131, p. 110947. Available at: https://doi.org/10.1016/J.PNPBP.2024.110947.
222. DeRosse, P. and Barber, A.D. (2021) 'Overlapping Neurobiological Substrates for Early-Life Stress and Resilience to Psychosis', *Biological Psychiatry: Cognitive Neuroscience and Neuroimaging*, 6(2), pp. 144–153. Available at: https://doi.org/10.1016/J.BPSC.2020.09.003.
223. Desai, M. *et al.* (2019) 'Programmed Epigenetic DNA Methylation-Mediated Reduced Neuroprogenitor Cell Proliferation and Differentiation in Small-for-Gestational-Age Offspring', *Neuroscience*, 412, pp. 60–71. Available at: https://doi.org/10.1016/J.NEUROSCIENCE.2019.05.044.
224. Deth, R. *et al.* (2008) 'How environmental and genetic factors combine to cause autism: A redox/methylation hypothesis', *NeuroToxicology*, 29(1), pp. 190–201. Available at: https://doi.org/10.1016/j.neuro.2007.09.010.
225. Deutschmann, A.U., Kirkland, J.M. and Briand, L.A. (2021) 'Adolescent social isolation induced alterations in nucleus accumbens glutamate signalling', *Addiction Biology*, p. e13077. Available at: https://doi.org/10.1111/ADB.13077.

226. Dieckmann, C.L. (2024) 'A hub for regulation of mitochondrial metabolism: Fatty acid and lipoic acid biosynthesis', *IUBMB Life*, 76(6), pp. 332–344. Available at: https://doi.org/10.1002/IUB.2802.
227. Dieter, F., Esselun, C. and Eckert, G.P. (2022) 'Redox Active α-Lipoic Acid Differentially Improves Mitochondrial Dysfunction in a Cellular Model of Alzheimer and Its Control Cells', *International Journal of Molecular Sciences 2022, Vol. 23, Page 9186*, 23(16), p. 9186. Available at: https://doi.org/10.3390/IJMS23169186.
228. D'Mello, S.R. (2020) 'Histone deacetylase-3: Friend and foe of the brain', *Experimental Biology and Medicine*, 245(13), p. 1130. Available at: https://doi.org/10.1177/1535370220928278.
229. Dobin, A. *et al.* (2013) 'STAR: ultrafast universal RNA-seq aligner', *Bioinformatics (Oxford, England)*, 29(1), pp. 15–21. Available at: https://doi.org/10.1093/BIOINFORMATICS/BTS635.
230. Dong, Y. *et al.* (2020) 'Regulation of cancer cell metabolism: oncogenic MYC in the driver's seat', *Signal Transduction and Targeted Therapy 2020 5:1*, 5(1), pp. 1–11. Available at: https://doi.org/10.1038/s41392-020-00235-2.
231. Doyle, N. (2020) 'Neurodiversity at work: A biopsychosocial model and the impact on working adults', *British Medical Bulletin*, 135(1), pp. 108–125. Available at: https://doi.org/10.1093/bmb/ldaa021.
232. Dravid, A. *et al.* (2021) 'Optimised techniques for high-throughput screening of differentiated SH-SY5Y cells and application for neurite outgrowth assays', *Scientific Reports*, 11(1), pp. 1–15. Available at: https://doi.org/10.1038/s41598-021-03442-1.
233. Dravid, A., Raos, B. and Svirskis, D. (2021) 'Differentiated SH-SY5Y Cells for High-Throughput Screening in a 96-Well Plate Format : Protocol Optimisation and Application for Neurite Outgrowth Assays', pp. 0–22.
234. Du, J. *et al.* (2009) 'Dynamic regulation of mitochondrial function by glucocorticoids', *Proceedings of the National Academy of Sciences of the United States of America*, 106(9), pp. 3543–3548. Available at: https://doi.org/10.1073/PNAS.0812671106.
235. Duan, Q. *et al.* (2024) 'Stat3 Has a Different Role in Axon Growth During Development Than It Does in Axon Regeneration After Injury', *Molecular Neurobiology*, 61(3), pp. 1753–1768. Available at: https://doi.org/10.1007/S12035-023-03644-W/FIGURES/7.
236. Duarte, F. V., Ciampi, D. and Duarte, C.B. (2023) 'Mitochondria as central hubs in synaptic modulation', *Cellular and Molecular Life Sciences 2023 80:6*, 80(6), pp. 1–21. Available at: https://doi.org/10.1007/S00018-023-04814-8.
237. Ducray, A.D. *et al.* (2017) 'Effects of silica nanoparticle exposure on mitochondrial function during neuronal differentiation', *Journal of Nanobiotechnology*, 15(1), pp. 1–14. Available at: https://doi.org/10.1186/S12951-017-0284-3/FIGURES/7.
238. Ducray, A.D. *et al.* (2020) 'Quantitative Characterization of Phenotypical Markers After Differentiation of SH-SY5Y Cells', *CNS & neurological disorders drug targets*, 19(8), pp. 618–629. Available at: https://doi.org/10.2174/1871527319666200708132716.
239. Duffney, L.J. *et al.* (2018) 'Epigenetics and autism spectrum disorder: A report of an autism case with mutation in H1 linker histone HIST1H1E and literature review', *American Journal of Medical Genetics Part B: Neuropsychiatric Genetics*, 177(4), pp. 426–433. Available at: https://doi.org/10.1002/ajmg.b.32631.
240. Duly, A.M.P. *et al.* (2022) 'βIII-Tubulin Gene Regulation in Health and Disease', *Frontiers in Cell and Developmental Biology*, 10. Available at: https://doi.org/10.3389/FCELL.2022.851542.
241. Dupont, S. *et al.* (2004) 'Convergence of p53 and TGF-beta signaling networks', *Cancer Letters*, 213(2), pp. 129–138. Available at: https://doi.org/10.1016/j.canlet.2004.06.008.
242. Duraisamy, A.J., Mohammad, G. and Kowluru, R.A. (2019) 'Mitochondrial fusion and maintenance of mitochondrial homeostasis in diabetic retinopathy', *Biochimica et Biophysica Acta (BBA) - Molecular Basis of Disease*, 1865(6), pp. 1617–1626. Available at: https://doi.org/10.1016/J.BBADIS.2019.03.013.
243. Dutcher, E.G. *et al.* (2020) 'Early-life stress and inflammation: A systematic review of a key experimental approach in rodents.', *Brain and neuroscience advances*, 4, p. 2398212820978049. Available at: https://doi.org/10.1177/2398212820978049.
244. Dwane, S., Durack, E. and Kiely, P.A. (2013) 'Optimising parameters for the differentiation of SH-SY5Y cells to study cell adhesion and cell migration', *BMC Research Notes*, 6(1), pp. 1–11. Available at: https://doi.org/10.1186/1756-0500-6-366/FIGURES/6.
245. Dwyer, C.A. and Esko, J.D. (2016) 'Glycan susceptibility factors in autism spectrum disorders', *Molecular aspects of medicine*, 51, p. 104. Available at: https://doi.org/10.1016/J.MAM.2016.07.001.
246. Ebrahimi-Fakhari, D. *et al.* (2016) 'Impaired Mitochondrial Dynamics and Mitophagy in Neuronal Models of Tuberous Sclerosis Complex', *Cell Reports* [Preprint]. Available at: https://doi.org/10.1016/j.celrep.2016.09.054.

247. Edmiston, E.K., Blain, S.D. and Corbett, B.A. (2017) 'Salivary cortisol and behavioral response to social evaluative threat in adolescents with autism spectrum disorder', *Autism Research*, 10(2), pp. 346–358. Available at: https://doi.org/10.1002/AUR.1660.
248. Edmonson, C., Ziats, M.N. and Rennert, O.M. (2014) 'Altered glial marker expression in autistic post-mortem prefrontal cortex and cerebellum', *Molecular Autism*, 5(1), p. 3. Available at: https://doi.org/10.1186/2040-2392-5-3.
249. El-Ansary, A. *et al.* (2017) 'Glutamate excitotoxicity induced by orally administered propionic acid, a short chain fatty acid can be ameliorated by bee pollen', *Lipids in Health and Disease*, 16(1), pp. 1–9. Available at: https://doi.org/10.1186/S12944-017-0485-7/TABLES/3.
250. El-Ansary, A. *et al.* (2018) 'Probiotic treatment reduces the autistic-like excitation/inhibition imbalance in juvenile hamsters induced by orally administered propionic acid and clindamycin', *Metabolic Brain Disease*, 33(4), pp. 1155–1164. Available at: https://doi.org/10.1007/S11011-018-0212-8/TABLES/4.
251. El-Ansary, A.K., Al-Daihan, S.K. and El-Gezeery, A.R. (2011) 'On the protective effect of omega-3 against propionic acid-induced neurotoxicity in rat pups', *Lipids in Health and Disease*, 10(1), pp. 1–10. Available at: https://doi.org/10.1186/1476-511X-10-142/FIGURES/7.
252. El-Ansary, A.K., Bacha, A. Ben and Kotb, M. (2012) 'Etiology of autistic features: the persisting neurotoxic effects of propionic acid', *Journal of Neuroinflammation*, 9(1), p. 661. Available at: https://doi.org/10.1186/1742-2094-9-74.
253. Elgamal, M.A. *et al.* (2023) 'Mechanisms of Valproic acid-Induced Autism: Canonical Wnt-β- Catenin Pathway', *Records of Pharmaceutical and Biomedical Sciences*, 7(3), pp. 51–62. Available at: https://doi.org/10.21608/RPBS.2023.189540.1205.
254. Encinas, M. *et al.* (2000) 'Sequential treatment of SH-SY5Y cells with retinoic acid and brain-derived neurotrophic factor gives rise to fully differentiated, neurotrophic factor-dependent, human neuron-like cells', *Journal of Neurochemistry*, 75(3), pp. 991–1003. Available at: https://doi.org/10.1046/j.1471-4159.2000.0750991.x.
255. Erdogan, M.A. *et al.* (2024) 'Amelioration of propionic acid-induced autism-like behaviors in rats by fenofibrate: A focus on reduction of brain galectin-3 levels', *International Journal of Developmental Neuroscience*, 84(8), pp. 977–990. Available at: https://doi.org/10.1002/JDN.10393.
256. Esposito, D. *et al.* (2024) 'A Systematic Review on Autism and Hyperserotonemia: State-of-the-Art, Limitations, and Future Directions', *Brain Sciences*, 14(5), p. 481. Available at: https://doi.org/10.3390/BRAINSCI14050481/S1.
257. Esteves, M. *et al.* (2020) 'New insights into the regulatory roles of microRNAs in adult neurogenesis', *Current Opinion in Pharmacology*, 50, pp. 38–45. Available at: https://doi.org/10.1016/J.COPH.2019.11.003.
258. Etyemez, S. *et al.* (2020) 'Higher prevalence of mood disorders in admitted patients with autism', *Neurology, Psychiatry and Brain Research*, 37, pp. 87–90. Available at: https://doi.org/10.1016/J.NPBR.2020.06.007.
259. Evanson, N.K. and Herman, J.P. (2015) 'Role of Paraventricular Nucleus Glutamate Signaling in Regulation of HPA Axis Stress Responses', *Interdisciplinary Information Sciences*, 21(3), pp. 253–260. Available at: https://doi.org/10.4036/IIS.2015.B.10.
260. Evers, K. *et al.* (2021) 'How well are DSM-5 diagnostic criteria for ASD represented in standardized diagnostic instruments?', *European Child and Adolescent Psychiatry*, 30(1), pp. 75–87. Available at: https://doi.org/10.1007/S00787-020-01481-Z/TABLES/3.
261. Ewald, J. *et al.* (2023) 'Using ExpressAnalyst for Comprehensive Gene Expression Analysis in Model and Non-Model Organisms', *Current Protocols*, 3(11), p. e922. Available at: https://doi.org/10.1002/CPZ1.922.
262. Ewels, P. *et al.* (2016) 'MultiQC: summarize analysis results for multiple tools and samples in a single report', *Bioinformatics (Oxford, England)*, 32(19), pp. 3047–3048. Available at: https://doi.org/10.1093/BIOINFORMATICS/BTW354.
263. F. C. Lopes, A. (2020) 'Mitochondrial metabolism and DNA methylation: a review of the interaction between two genomes', *Clinical Epigenetics*. BioMed Central Ltd, pp. 1–13. Available at: https://doi.org/10.1186/s13148-020-00976-5.
264. Fadó, R., Rodríguez-Rodríguez, R. and Casals, N. (2021) 'The return of malonyl-CoA to the brain: Cognition and other stories', *Progress in Lipid Research*, 81. Available at: https://doi.org/10.1016/J.PLIPRES.2020.101071.
265. Fairley, L.H., Wong, J.H. and Barron, A.M. (2021) 'Mitochondrial Regulation of Microglial Immunometabolism in Alzheimer's Disease', *Frontiers in Immunology*, 12. Available at: https://doi.org/10.3389/FIMMU.2021.624538.

266. Falomir-Lockhart, L.J. *et al.* (2019) 'Fatty acid signaling mechanisms in neural cells: Fatty acid receptors', *Frontiers in Cellular Neuroscience*, 13, p. 448584. Available at: https://doi.org/10.3389/FNCEL.2019.00162/BIBTEX.
267. Fan, R. *et al.* (2022) 'Stomatin-like protein-2 attenuates macrophage pyroptosis and H9c2 cells apoptosis by protecting mitochondrial function', *Biochemical and Biophysical Research Communications*, 636, pp. 112–120. Available at: https://doi.org/10.1016/J.BBRC.2022.10.047.
268. Fanibunda, S.E. *et al.* (2019) 'Serotonin regulates mitochondrial biogenesis and function in rodent cortical neurons via the 5-HT2A receptor and SIRT1–PGC-1α axis', *Proceedings of the National Academy of Sciences of the United States of America*, 166(22), pp. 11028–11037. Available at: https://www.eurekalert.org/multimedia/565359 (Accessed: 12 August 2020).
269. Farina, A.R. *et al.* (2018) 'TrkAIII signals endoplasmic reticulum stress to the mitochondria in neuroblastoma cells, resulting in glycolytic metabolic adaptation', *Oncotarget*, 9(9), p. 8368. Available at: https://doi.org/10.18632/ONCOTARGET.23618.
270. Fasano, C. *et al.* (2019) 'FOXO3a from the Nucleus to the Mitochondria: A Round Trip in Cellular Stress Response', *Cells 2019, Vol. 8, Page 1110*, 8(9), p. 1110. Available at: https://doi.org/10.3390/CELLS8091110.
271. Fasano, C.A. *et al.* (2009) 'Bmi-1 cooperates with Foxgl to maintain neural stem cell self-renewal in the forebrain', *Genes and Development*, 23(5), pp. 561–574. Available at: https://doi.org/10.1101/gad.1743709.
272. Faust, T.E. and Schafer, D.P. (2021) 'IL-6 boosts synaptogenesis STAT!', *Immunity*, 54(11), pp. 2444–2446. Available at: https://doi.org/10.1016/J.IMMUNI.2021.10.010.
273. Fawal, M.A. *et al.* (2018) 'Cross Talk between One-Carbon Metabolism, Eph Signaling, and Histone Methylation Promotes Neural Stem Cell Differentiation', *Cell Reports*, 23(10), pp. 2864-2873.e7. Available at: https://doi.org/10.1016/j.celrep.2018.05.005.
274. Feles, S. *et al.* (2022) 'Streamlining Culture Conditions for the Neuroblastoma Cell Line SH-SY5Y: A Prerequisite for Functional Studies', *Methods and Protocols 2022, Vol. 5, Page 58*, 5(4), p. 58. Available at: https://doi.org/10.3390/MPS5040058.
275. Feng, B., Wang, R. and Sheng, S.L. (2006) 'Mimic model of nerve cells in the study of neurodegenerative disease: Origin, characteristics and application of human neuroblastoma cell line SH-SY5Y', *Chinese Journal of Clinical Rehabilitation*, 10(6), pp. 121–123.
276. Ferger, A.I. *et al.* (2010) 'Effects of mitochondrial dysfunction on the immunological properties of microglia', *Journal of Neuroinflammation*, 7(1), pp. 1–10. Available at: https://doi.org/10.1186/1742-2094-7-45/FIGURES/7.
277. Fernandez-Marcos, P.J. and Auwerx, J. (2011) 'Regulation of PGC-1α, a nodal regulator of mitochondrial biogenesis', *The American Journal of Clinical Nutrition*, 93(4), p. 884S. Available at: https://doi.org/10.3945/AJCN.110.001917.
278. Ferreira, G.C. and McKenna, M.C. (2017) 'l-Carnitine and Acetyl-l-carnitine Roles and Neuroprotection in Developing Brain', *Neurochemical Research 2017 42:6*, 42(6), pp. 1661–1675. Available at: https://doi.org/10.1007/S11064-017-2288-7.
279. Fetit, R. *et al.* (2021) 'The neuropathology of autism: A systematic review of post-mortem studies of autism and related disorders', *Neuroscience & Biobehavioral Reviews*, 129, pp. 35–62. Available at: https://doi.org/10.1016/J.NEUBIOREV.2021.07.014.
280. Fiebig, C. *et al.* (2019) 'Mitochondrial Dysfunction in Astrocytes Impairs the Generation of Reactive Astrocytes and Enhances Neuronal Cell Death in the Cortex Upon Photothrombotic Lesion', *Frontiers in Molecular Neuroscience*, 12, p. 40. Available at: https://doi.org/10.3389/fnmol.2019.00040.
281. Filippone, A. *et al.* (2020) 'Protective effect of sodium propionate in Aβ1-42 -induced neurotoxicity and spinal cord trauma', *Neuropharmacology*, 166(August 2019), p. 107977. Available at: https://doi.org/10.1016/j.neuropharm.2020.107977.
282. Filippone, A. *et al.* (2022) 'Sodium Propionate Contributes to Tumor Cell Growth Inhibition through PPAR-γ Signaling', *Cancers 2023, Vol. 15, Page 217*, 15(1), p. 217. Available at: https://doi.org/10.3390/CANCERS15010217.
283. Filograna, R. *et al.* (2015) 'Analysis of the catecholaminergic phenotype in human SH-SY5Y and BE(2)-M17 neuroblastoma cell lines upon differentiation', *PLoS ONE*, 10(8). Available at: https://doi.org/10.1371/JOURNAL.PONE.0136769.
284. Filonenko, V. and Gout, I. (2023) 'Discovery and functional characterisation of protein CoAlation and the antioxidant function of coenzyme A', *BBA Advances*, 3, p. 100075. Available at: https://doi.org/10.1016/J.BBADVA.2023.100075.

285. Finsterwald, C. and Alberini, C.M. (2014) 'Stress and glucocorticoid receptor-dependent mechanisms in long-term memory: from adaptive responses to psychopathologies', *Neurobiology of learning and memory*, 0, p. 17. Available at: https://doi.org/10.1016/J.NLM.2013.09.017.
286. Fiorenza, A. and Barco, A. (2016) 'Role of Dicer and the miRNA system in neuronal plasticity and brain function', *Neurobiology of Learning and Memory*, 135, pp. 3–12. Available at: https://doi.org/10.1016/J.NLM.2016.05.001.
287. Fix, D.K. *et al.* (2019) 'Regulation of Skeletal Muscle DRP-1 and FIS-1 Protein Expression by IL-6 Signaling', *Oxidative Medicine and Cellular Longevity*, 2019. Available at: https://doi.org/10.1155/2019/8908457.
288. Fletcher-Watson, S. *et al.* (2019) 'Making the future together: Shaping autism research through meaningful participation', *Autism : the international journal of research and practice*, 23(4), pp. 943–953. Available at: https://doi.org/10.1177/1362361318786721.
289. Fogelman, N. and Canli, T. (2019) 'Early life stress, physiology, and genetics: A review', *Frontiers in Psychology*, 10(JULY), p. 1668. Available at: https://doi.org/10.3389/FPSYG.2019.01668/BIBTEX.
290. Forés-Martos, J. *et al.* (2019) 'Transcriptomic metaanalyses of autistic brains reveals shared gene expression and biological pathway abnormalities with cancer', *Molecular Autism*, 10(1), p. 17. Available at: https://doi.org/10.1186/s13229-019-0262-8.
291. Forsberg, K. *et al.* (2013) 'The Tumor Suppressor p53 Fine-Tunes Reactive Oxygen Species Levels and Neurogenesis via PI3 Kinase Signaling', *The Journal of Neuroscience*, 33(36). Available at: https://doi.org/10.1523/JNEUROSCI.1056-13.2013.
292. Forsberg, K. and Di Giovanni, S. (2014) 'Cross talk between cellular redox status, metabolism, and p53 in neural stem cell biology', *Neuroscientist*, 20(4), pp. 326–342. Available at: https://doi.org/10.1177/1073858413514634/ASSET/IMAGES/LARGE/10.1177_1073858413514634-FIG4.JPEG.
293. Forster, J.I. *et al.* (2016) 'Characterization of Differentiated SH-SY5Y as Neuronal Screening Model Reveals Increased Oxidative Vulnerability', *SLAS Discovery*, 21(5), pp. 496–509. Available at: https://doi.org/10.1177/1087057115625190.
294. Foster, D.W. (2012) 'Malonyl-CoA: The regulator of fatty acid synthesis and oxidation', *Journal of Clinical Investigation*. American Society for Clinical Investigation, pp. 1958–1959. Available at: https://doi.org/10.1172/JCI63967.
295. Franz, L. *et al.* (2017) 'Autism spectrum disorder in sub-saharan africa: A comprehensive scoping review', *Autism Research*, 10(5), pp. 723–749. Available at: https://doi.org/10.1002/aur.1766.
296. Freemerman, A.J. *et al.* (2014) 'Metabolic reprogramming of macrophages: Glucose transporter 1 (GLUT1)-mediated glucose metabolism drives a proinflammatory phenotype', *Journal of Biological Chemistry*, 289(11), pp. 7884–7896. Available at: https://doi.org/10.1074/JBC.M113.522037/ATTACHMENT/3E25BABB-19E7-4212-A90A-55F44762AD61/MMC1.ZIP.
297. Frickel, E. *et al.* (2023) 'Molecular Autism Research in Africa: Emerging Themes and Prevailing Disparities', *Review Journal of Autism and Developmental Disorders*. Springer, pp. 1–17. Available at: https://doi.org/10.1007/s40489-023-00415-0.
298. Frustaci, A. *et al.* (2012) 'Oxidative stress-related biomarkers in autism: systematic review and meta-analyses', *Free radical biology & medicine*, 52(10), pp. 2128–2141. Available at: https://doi.org/10.1016/J.FREERADBIOMED.2012.03.011.
299. Frye, -L R ; *et al.* (2023) 'The Rationale for Vitamin, Mineral, and Cofactor Treatment in the Precision Medical Care of Autism Spectrum Disorder', *Journal of Personalized Medicine 2023, Vol. 13, Page 252*, 13(2), p. 252. Available at: https://doi.org/10.3390/JPM13020252.
300. Frye, R.E. *et al.* (2015) 'Gastrointestinal dysfunction in autism spectrum disorder: the role of the mitochondria and the enteric microbiome', *Microbial Ecology in Health & Disease*, 26(0). Available at: https://doi.org/10.3402/mehd.v26.27458.
301. Frye, R.E. (2020) 'Mitochondrial Dysfunction in Autism Spectrum Disorder: Unique Abnormalities and Targeted Treatments', *Seminars in Pediatric Neurology*, 35, p. 100829. Available at: https://doi.org/10.1016/j.spen.2020.100829.
302. Frye, R.E. *et al.* (2021) 'Mitochondrial morphology is associated with respiratory chain uncoupling in autism spectrum disorder', *Translational Psychiatry*, 11(1), p. 527. Available at: https://doi.org/10.1038/S41398-021-01647-6.
303. Frye, R.E. *et al.* (2024) 'Biomarkers of mitochondrial dysfunction in autism spectrum disorder: A systematic review and meta-analysis', *Neurobiology of Disease*, 197, p. 106520. Available at: https://doi.org/10.1016/j.nbd.2024.106520.

304. Frye, R.E., Slattery, J.C. and Quadros, E. V. (2017) 'Folate metabolism abnormalities in autism: Potential biomarkers', *Biomarkers in Medicine*, 11(8), pp. 687–699. Available at: https://doi.org/10.2217/BMM-2017-0109/ASSET/IMAGES/LARGE/FIGURE4.JPEG.
305. Furtado, M. and Katzman, M.A. (2015) 'Examining the role of neuroinflammation in major depression', *Psychiatry Research*, 229(1–2), pp. 27–36. Available at: https://doi.org/10.1016/J.PSYCHRES.2015.06.009.
306. Galindo, L.T. *et al.* (2018) 'Chondroitin Sulfate Impairs Neural Stem Cell Migration Through ROCK Activation', *Molecular Neurobiology*, 55(4), pp. 3185–3195. Available at: https://doi.org/10.1007/S12035-017-0565-8/FIGURES/5.
307. Galvez-Contreras, A.Y. *et al.* (2020) 'Role of Oligodendrocytes and Myelin in the Pathophysiology of Autism Spectrum Disorder', *Brain Sciences 2020, Vol. 10, Page 951*, 10(12), p. 951. Available at: https://doi.org/10.3390/BRAINSCI10120951.
308. Ganesan, H. *et al.* (2019) 'mTOR signalling pathway - A root cause for idiopathic autism?', *BMB Reports*, 52(7). Available at: /pmc/articles/PMC6675248/ (Accessed: 26 July 2021).
309. Gao, H. *et al.* (2021) 'Integrated Systems Analysis Explores Dysfunctional Molecular Modules and Regulatory Factors in Children with Autism Spectrum Disorder', *Journal of molecular neuroscience : MN*, 71(2), pp. 358–368. Available at: https://doi.org/10.1007/S12031-020-01658-W.
310. Gao, J. *et al.* (2018) 'S-Adenosyl Methionine and Transmethylation Pathways in Neuropsychiatric Diseases Throughout Life', *Neurotherapeutics*, 15(1), pp. 156–175. Available at: https://doi.org/10.1007/S13311-017-0593-0.
311. Gao, W. *et al.* (2021) 'Propionate alleviates palmitic acid–induced endoplasmic reticulum stress by enhancing autophagy in calf hepatic cells', *Journal of Dairy Science*, 104(8), pp. 9316–9326. Available at: https://doi.org/10.3168/JDS.2020-19969.
312. García-Ortiz, M.V. *et al.* (2021) 'Analysis of Global and Local DNA Methylation Patterns in Blood Samples of Patients With Autism Spectrum Disorder', *Frontiers in Pediatrics*, 9, p. 685310. Available at: https://doi.org/10.3389/FPED.2021.685310/BIBTEX.
313. Gardner, A. and Boles, R.G. (2011) 'Beyond the serotonin hypothesis: Mitochondria, inflammation and neurodegeneration in major depression and affective spectrum disorders', *Progress in Neuro-Psychopharmacology and Biological Psychiatry*, 35(3), pp. 730–743. Available at: https://doi.org/10.1016/j.pnpbp.2010.07.030.
314. Garone, C., De Giorgio, F. and Carli, S. (2024) 'Mitochondrial metabolism in neural stem cells and implications for neurodevelopmental and neurodegenerative diseases', *Journal of Translational Medicine 2024 22:1*, 22(1), pp. 1–18. Available at: https://doi.org/10.1186/S12967-024-05041-W.
315. Garrido-Torres, N. *et al.* (2023) 'miRNAs as biomarkers of autism spectrum disorder: a systematic review and meta-analysis', *European Child and Adolescent Psychiatry*, 33(9), pp. 2957–2990. Available at: https://doi.org/10.1007/S00787-023-02138-3/TABLES/4.
316. Ge, H. *et al.* (2021) 'Extracellular Matrix Stiffness: New Areas Affecting Cell Metabolism', *Frontiers in Oncology*, 11. Available at: https://doi.org/10.3389/FONC.2021.631991.
317. Ge, S. *et al.* (2024) 'Unveiling the neuroprotection effects of Volvalerenic acid A: Mitochondrial fusion induction via IDO1-mediated Stat3-Opa1 signaling pathway', *Phytomedicine*, 129, p. 155555. Available at: https://doi.org/10.1016/j.phymed.2024.155555.
318. Geoghegan, F. *et al.* (2017) 'Direct effects of phenformin on metabolism/bioenergetics and viability of SH-SY5Y neuroblastoma cells', *Oncology Letters*, 14(5), pp. 6298–6306. Available at: https://doi.org/10.3892/ol.2017.6929.
319. Getachew, B. *et al.* (2020) 'Butyrate Protects Against Salsolinol-Induced Toxicity in SH-SY5Y Cells: Implication for Parkinson's Disease', *Neurotoxicity Research*, 38(3), pp. 596–602. Available at: https://doi.org/10.1007/S12640-020-00238-5/FIGURES/4.
320. Gevi, F., Belardo, A. and Zolla, L. (2020) 'A metabolomics approach to investigate urine levels of neurotransmitters and related metabolites in autistic children', *Biochimica et Biophysica Acta - Molecular Basis of Disease*, 1866(10), p. 165859. Available at: https://doi.org/10.1016/j.bbadis.2020.165859.
321. Ghafouri-Fard, S. *et al.* (2023) 'A Review on the Role of Genetic Mutations in the Autism Spectrum Disorder', *Molecular Neurobiology*, 60(9), pp. 5256–5272. Available at: https://doi.org/10.1007/S12035-023-03405-9/TABLES/6.
322. Ghani, M. *et al.* (2024) 'Stable knockdown of Drp1 improves retinoic acid-BDNF-induced neuronal differentiation through global transcriptomic changes and results in reduced phosphorylation of ERK1/2 independently of DUSP1 and 6', *Frontiers in Cell and Developmental Biology*, 12, p. 1342741. Available at: https://doi.org/10.3389/FCELL.2024.1342741/BIBTEX.

323. Ghasemi, M. *et al.* (2021) 'The mtt assay: Utility, limitations, pitfalls, and interpretation in bulk and single-cell analysis', *International Journal of Molecular Sciences*, 22(23). Available at: https://doi.org/10.3390/IJMS222312827/S1.
324. Gholamalizadeh, H. *et al.* (2024) 'DNA Methylation in Autism Spectrum Disorders: Biomarker or Pharmacological Target?', *Brain Sciences*, 14(8). Available at: https://doi.org/10.3390/BRAINSCI14080737.
325. Giacomello, M. *et al.* (2020) 'The cell biology of mitochondrial membrane dynamics', *Nature Reviews Molecular Cell Biology 2020 21:4*, 21(4), pp. 204–224. Available at: https://doi.org/10.1038/s41580-020-0210-7.
326. Di Giacomo, E. *et al.* (2017) 'Roles of PPAR transcription factors in the energetic metabolic switch occurring during adult neurogenesis', *Cell Cycle*, 16(1), pp. 59–72. Available at: https://doi.org/10.1080/15384101.2016.1252881.
327. Di Giaimo, R. *et al.* (2020) 'Cross Talk at the Cytoskeleton–Plasma Membrane Interface: Impact on Neuronal Morphology and Functions', *International Journal of Molecular Sciences 2020, Vol. 21, Page 9133*, 21(23), p. 9133. Available at: https://doi.org/10.3390/IJMS21239133.
328. Giménez-Palomo, A. *et al.* (2021) 'The Role of Mitochondria in Mood Disorders: From Physiology to Pathophysiology and to Treatment', *Frontiers in Psychiatry*, 12, p. 546801. Available at: https://doi.org/10.3389/FPSYT.2021.546801/BIBTEX.
329. Gimeno-Bayón, J. *et al.* (2014) 'Glucose pathways adaptation supports acquisition of activated microglia phenotype', *Journal of Neuroscience Research*, 92(6), pp. 723–731. Available at: https://doi.org/10.1002/JNR.23356.
330. Gimsa, U. *et al.* (2009) 'Behavior and stress reactivity in mouse strains with mitochondrial DNA variations', *Annals of the New York Academy of Sciences*, 1153, pp. 131–138. Available at: https://doi.org/10.1111/J.1749-6632.2008.03960.X.
331. Ginsberg, M.R. *et al.* (2012) 'Brain Transcriptional and Epigenetic Associations with Autism', *PLoS ONE*, 7(9). Available at: https://doi.org/10.1371/journal.pone.0044736.
332. Gisevius, B. *et al.* (2024) 'Propionic acid promotes neurite recovery in damaged multiple sclerosis neurons', *Brain Communications*, 6(3). Available at: https://doi.org/10.1093/BRAINCOMMS/FCAE182.
333. Giulivi, C. *et al.* (2010) 'Mitochondrial dysfunction in autism', *JAMA - Journal of the American Medical Association*, 304(21), pp. 2389–2396. Available at: https://doi.org/10.1001/jama.2010.1706.
334. Gkini, V. and Namba, T. (2023) 'Glutaminolysis and the Control of Neural Progenitors in Neocortical Development and Evolution', *The Neuroscientist*, 29(2), p. 177. Available at: https://doi.org/10.1177/10738584211069060.
335. Gładysz, D., Krzywdzińska, A. and Hozyasz, K.K. (2018) 'Immune Abnormalities in Autism Spectrum Disorder—Could They Hold Promise for Causative Treatment?', *Molecular Neurobiology*. Humana Press Inc., pp. 6387–6435. Available at: https://doi.org/10.1007/s12035-017-0822-x.
336. Gleyzer, N. and Scarpulla, R.C. (2016) 'Concerted action of PGC-1-related coactivator (PRC) and c-MYC in the stress response to mitochondrial dysfunction', *Journal of Biological Chemistry*, 291(49), pp. 25529–25541. Available at: https://doi.org/10.1074/jbc.M116.719682.
337. Glinton, K.E. and Elsea, S.H. (2019) 'Untargeted Metabolomics for Autism Spectrum Disorders: Current Status and Future Directions', *Frontiers in Psychiatry*. Frontiers Media S.A. Available at: https://doi.org/10.3389/fpsyt.2019.00647.
338. Goglia, I. *et al.* (2024) 'Fusion–fission–mitophagy cycling and metabolic reprogramming coordinate nerve growth factor (NGF)-dependent neuronal differentiation', *The FEBS Journal*, 291(13), pp. 2811–2835. Available at: https://doi.org/10.1111/FEBS.17083.
339. Gogvadze, V., Zhivotovsky, B. and Orrenius, S. (2010) 'The Warburg effect and mitochondrial stability in cancer cells', *Molecular Aspects of Medicine*, 31(1), pp. 60–74. Available at: https://doi.org/10.1016/J.MAM.2009.12.004.
340. Goicoechea, L. *et al.* (2024) 'S-Adenosyl-l-methionine restores brain mitochondrial membrane fluidity and GSH content improving Niemann-Pick type C disease', *Redox Biology*, 72, p. 103150. Available at: https://doi.org/10.1016/J.REDOX.2024.103150.
341. Goldie, B.J., Barnett, M.M. and Cairns, M.J. (2014) 'BDNF and the maturation of posttranscriptional regulatory networks in human SH-SY5Y neuroblast differentiation', *Frontiers in Cellular Neuroscience*, 8(OCT), p. 325. Available at: https://doi.org/https://doi.org/10.3389/fncel.2014.00325.
342. Golovina, E. *et al.* (2021) 'Understanding the impact of SNPs associated with autism spectrum disorder on biological pathways in the human fetal and adult cortex', *Scientific Reports 2021 11:1*, 11(1), pp. 1–15. Available at: https://doi.org/10.1038/s41598-021-95447-z.

343. Golubiani, G. *et al.* (2021) 'Metabolomic Fingerprint of Mecp2-Deficient Mouse Cortex: Evidence for a Pronounced Multi-Facetted Metabolic Component in Rett Syndrome', *Cells*, 10(9), p. 2494. Available at: https://doi.org/10.3390/cells10092494.
344. Golzio, C. and Katsanis, N. (2016) 'Mitochondrial copy number as a biomarker for autism?', *Pediatrics*. American Academy of Pediatrics. Available at: https://doi.org/10.1542/peds.2016-0049.
345. Gómez-Sánchez, R. *et al.* (2014) 'Mitochondrial impairment increases FL-PINK1 levels by calcium-dependent gene expression', *Neurobiology of Disease*, 62(100), pp. 426–440. Available at: https://doi.org/10.1016/j.nbd.2013.10.021.
346. González-Cano, S.I. *et al.* (2021) 'Prenatal exposure to propionic acid induces altered locomotion and reactive astrogliosis in male rats', *Journal of Chemical Neuroanatomy*, 117, p. 102011. Available at: https://doi.org/10.1016/J.JCHEMNEU.2021.102011.
347. González-Pardo, H. *et al.* (2020) 'Sex-Specific Effects of Early Life Stress on Brain Mitochondrial Function, Monoamine Levels and Neuroinflammation', *Brain Sciences 2020, Vol. 10, Page 447*, 10(7), p. 447. Available at: https://doi.org/10.3390/BRAINSCI10070447.
348. Gorospe, C.M. *et al.* (2023) 'Mitochondrial membrane potential acts as a retrograde signal to regulate cell cycle progression', *Life Science Alliance*, 6(12). Available at: https://doi.org/10.26508/LSA.202302091.
349. Gout, I. (2018) 'Coenzyme A, protein CoAlation and redox regulation in mammalian cells', *Biochemical Society Transactions*, 46(3), pp. 721–728. Available at: https://doi.org/10.1042/BST20170506.
350. Graciarena, M. *et al.* (2019) 'Hypomyelination and oligodendroglial alterations in a mouse model of autism spectrum disorder', *Frontiers in Cellular Neuroscience*, 12, p. 423518. Available at: https://doi.org/10.3389/FNCEL.2018.00517/BIBTEX.
351. Grady, J.P. *et al.* (2014) 'Accurate measurement of mitochondrial DNA deletion level and copy number differences in human skeletal muscle', *PLoS ONE*, 9(12). Available at: https://doi.org/10.1371/journal.pone.0114462.
352. Graham, J. and Train, T.L. (2017) 'Measuring Nestin Expression in RA-BDNF Differentiated SH-SY5Y Human Neuroblastoma Cells by Flow Cytometry', *The FASEB Journal*, 31(S1), pp. 936.14-936.14. Available at: https://doi.org/10.1096/fasebj.31.1_supplement.936.14.
353. Graves, J.A. *et al.* (2012) 'Mitochondrial structure, function and dynamics are temporally controlled by c-Myc', *PLoS ONE*, 7(5). Available at: https://doi.org/10.1371/journal.pone.0037699.
354. Gregory, S.G. *et al.* (2009) 'Genomic and epigenetic evidence for oxytocin receptor deficiency in autism', *BMC Medicine*, 7(1), p. 62. Available at: https://doi.org/10.1186/1741-7015-7-62.
355. Grevengoed, T.J., Klett, E.L. and Coleman, R.A. (2014) 'Acyl-CoA Metabolism and Partitioning', *Annual review of nutrition*, 34, p. 1. Available at: https://doi.org/10.1146/ANNUREV-NUTR-071813-105541.
356. Griffiths, K.K. and Levy, R.J. (2017) 'Evidence of Mitochondrial Dysfunction in Autism: Biochemical Links, Genetic-Based Associations, and Non-Energy-Related Mechanisms', *Oxidative medicine and cellular longevity*, 2017. Available at: https://doi.org/10.1155/2017/4314025.
357. Griffiths, S. *et al.* (2019) 'The Vulnerability Experiences Quotient (VEQ): A Study of Vulnerability, Mental Health and Life Satisfaction in Autistic Adults', *Autism Research*, 12(10), pp. 1516–1528. Available at: https://doi.org/10.1002/AUR.2162.
358. Gu, F. *et al.* (2013) 'Alterations in mitochondrial DNA copy number and the activities of electron transport chain complexes and pyruvate dehydrogenase in the frontal cortex from subjects with autism', *Translational Psychiatry 2013 3:9*, 3(9), pp. e299–e299. Available at: https://doi.org/10.1038/tp.2013.68.
359. Gu, X. *et al.* (2017) 'SAMTOR is an S-adenosylmethionine sensor for the mTORC1 pathway', *Science*, 358(6364), pp. 813–818. Available at: https://doi.org/10.1126/SCIENCE.AAO3265/SUPPL_FILE/AAO3265_GU_SM.PDF.
360. de Guia, R.M. (2020) 'Stress, glucocorticoid signaling pathway, and metabolic disorders', *Diabetes & Metabolic Syndrome: Clinical Research & Reviews*, 14(5), pp. 1273–1280. Available at: https://doi.org/10.1016/J.DSX.2020.06.038.
361. Guidi, J. *et al.* (2021) 'Allostatic Load and Its Impact on Health: A Systematic Review', *Psychotherapy and Psychosomatics*, 90(1), pp. 11–27. Available at: https://doi.org/10.1159/000510696.
362. Gulati, S. *et al.* (2024) 'Transmethylation and Oxidative Biomarkers in Children with Autism Spectrum Disorder: A Cross Sectional Study', *Journal of Autism and Developmental Disorders*, pp. 1–9. Available at: https://doi.org/10.1007/S10803-024-06542-9/TABLES/4.
363. Guler, J.L. *et al.* (2008) 'Mitochondrial fatty acid synthesis is required for normal mitochondrial morphology and function in Trypanosoma brucei', *Molecular Microbiology*, 67(5), pp. 1125–1142. Available at: https://doi.org/10.1111/J.1365-2958.2008.06112.X.

364. Gulyaeva, N. V. (2021) 'Glucocorticoid Regulation of the Glutamatergic Synapse: Mechanisms of Stress-Dependent Neuroplasticity', *Journal of Evolutionary Biochemistry and Physiology 2021 57:3*, 57(3), pp. 564–576. Available at: https://doi.org/10.1134/S0022093021030091.
365. Guo, C. hong *et al.* (2020) 'Development and characterization of an inducible Dicer conditional knockout mouse model of Parkinson's disease: validation of the antiparkinsonian effects of a sigma-1 receptor agonist and dihydromyricetin', *Acta Pharmacologica Sinica 2020 41:4*, 41(4), pp. 499–507. Available at: https://doi.org/10.1038/s41401-020-0379-5.
366. Guzenko, V. V. *et al.* (2024) 'Acetylation of c-Myc at Lysine 148 Protects Neurons After Ischemia', *NeuroMolecular Medicine*, 26(1), pp. 1–17. Available at: https://doi.org/10.1007/S12017-024-08777-2/FIGURES/5.
367. Hadwin, J.A. *et al.* (2019) 'Cortisol awakening response in children and adolescents with autism spectrum disorder: a systematic review and meta-analysis', *Evidence-Based Mental Health*, 22(3), pp. 118–124. Available at: https://doi.org/10.1136/EBMENTAL-2019-300098.
368. Hájek, P., Chomyn, A. and Attardi, G. (2007) 'Identification of a novel mitochondrial complex containing mitofusin 2 and stomatin-like protein', *Journal of Biological Chemistry*, 282(8), pp. 5670–5681. Available at: https://doi.org/10.1074/jbc.M608168200.
369. Halvorsen, O. and Skrede, S. (1982) 'Regulation of the biosynthesis of CoA at the level of pantothenate kinase', *European journal of biochemistry*, 124(1), pp. 211–215. Available at: https://doi.org/10.1111/J.1432-1033.1982.TB05927.X.
370. Han, K. *et al.* (2024) 'Propionate functions as a feeding state–dependent regulatory metabolite to counter proinflammatory signaling linked to nutrient load and obesity', *Journal of Leukocyte Biology*, 115(4), pp. 738–749. Available at: https://doi.org/10.1093/JLEUKO/QIAE006.
371. Han, S. *et al.* (2021) 'The role of mitophagy in the regulation of mitochondrial energetic status in neurons', *Autophagy*, 17(12), pp. 4182–4201. Available at: https://doi.org/10.1080/15548627.2021.1907167.
372. Hanaford, A. and Johnson, S.C. (2022) 'The immune system as a driver of mitochondrial disease pathogenesis: a review of evidence', *Orphanet Journal of Rare Diseases 2022 17:1*, 17(1), pp. 1–12. Available at: https://doi.org/10.1186/S13023-022-02495-3.
373. Harry, G.J. *et al.* (2020) 'An association between mitochondria and microglia effector function: what do we think we know?', *Neuroimmunology and Neuroinflammation*, 7(2), pp. 150–165. Available at: https://doi.org/10.20517/2347-8659.2020.07.
374. Haslinger, D. *et al.* (2018) 'Loss of the Chr16p11.2 ASD candidate gene QPRT leads to aberrant neuronal differentiation in the SH-SY5Y neuronal cell model 06 Biological Sciences 0604 Genetics', *Molecular Autism*, 9(1), pp. 1–17. Available at: https://doi.org/10.1186/S13229-018-0239-Z/FIGURES/3.
375. Hassan, H. *et al.* (2021) 'A link between mitochondrial dysregulation and idiopathic autism spectrum disorder (Asd): Alterations in mitochondrial respiratory capacity and membrane potential', *Current Issues in Molecular Biology*, 43(3), pp. 2238–2252. Available at: https://doi.org/10.3390/cimb43030157.
376. Havdahl, A. *et al.* (2021) 'Genetic contributions to autism spectrum disorder', *Psychological Medicine*, 51(13), pp. 2260–2273. Available at: https://doi.org/10.1017/S0033291721000192.
377. Havranek, T., Bacova, Z. and Bakos, J. (2024) 'Oxytocin, GABA, and dopamine interplay in autism', *Endocrine Regulations*, 58(1), pp. 105–114. Available at: https://doi.org/10.2478/ENR-2024-0012.
378. Hayes, A.J. and Melrose, J. (2021) 'Neural Tissue Homeostasis and Repair Is Regulated via CS and DS Proteoglycan Motifs', *Frontiers in Cell and Developmental Biology*, 9, p. 696640. Available at: https://doi.org/10.3389/FCELL.2021.696640/BIBTEX.
379. He, W. *et al.* (2021) 'Metabolic perturbations mediated by propionyl-CoA accumulation in organs of mouse model of propionic acidemia', *Molecular Genetics and Metabolism*, 134(3), pp. 257–266. Available at: https://doi.org/10.1016/J.YMGME.2021.09.009.
380. He, Y. *et al.* (2017) 'Blockade of cyclophilin D rescues dexamethasone-induced oxidative stress in gingival tissue', *PLOS ONE*, 12(3), p. e0173270. Available at: https://doi.org/10.1371/JOURNAL.PONE.0173270.
381. He, Y. *et al.* (2019) 'An integrated transcriptomic analysis of autism spectrum disorder', *Scientific Reports*, 9(1), pp. 1–9. Available at: https://doi.org/10.1038/s41598-019-48160-x.
382. He, Y. *et al.* (2023) 'Luteoloside Induces G0/G1 Phase Arrest of Neuroblastoma Cells by Targeting p38 MAPK', *Molecules*, 28(4), p. 1748. Available at: https://doi.org/10.3390/MOLECULES28041748/S1.
383. Herskovits, A.Z. and Guarente, L. (2014) 'SIRT1 in neurodevelopment and brain senescence', *Neuron*, 81(3), p. 471. Available at: https://doi.org/10.1016/J.NEURON.2014.01.028.

384. Herzig, S. and Shaw, R.J. (2017) 'AMPK: guardian of metabolism and mitochondrial homeostasis', *Nature Reviews Molecular Cell Biology 2017 19:2*, 19(2), pp. 121–135. Available at: https://doi.org/10.1038/nrm.2017.95.
385. Hewitson, L. *et al.* (2021) 'Blood biomarker discovery for autism spectrum disorder: A proteomic analysis', *PLOS ONE*. Edited by S.H. Fatemi, 16(2), p. e0246581. Available at: https://doi.org/10.1371/journal.pone.0246581.
386. Hiew, L.F. *et al.* (2021) 'TGF-β/Smad Signalling in Neurogenesis: Implications for Neuropsychiatric Diseases', *Cells 2021, Vol. 10, Page 1382*, 10(6), p. 1382. Available at: https://doi.org/10.3390/CELLS10061382.
387. Higashimura, Y. *et al.* (2015) 'Propionate promotes fatty acid oxidation through the up-regulation of peroxisome proliferator-activated receptor α in intestinal epithelial cells', *Journal of Nutritional Science and Vitaminology*, 61(6), pp. 511–515. Available at: https://doi.org/10.3177/jnsv.61.511.
388. Hinojosa, M.G. *et al.* (2023) 'Evaluation of mRNA markers in differentiating human SH-SY5Y cells for estimation of developmental neurotoxicity', *NeuroToxicology*, 97(May), pp. 65–77. Available at: https://doi.org/10.1016/j.neuro.2023.05.011.
389. Hirano, T., Ishihara, K. and Hibi, M. (2000) 'Roles of STAT3 in mediating the cell growth, differentiation and survival signals relayed through the IL-6 family of cytokine receptors', *Oncogene 2000 19:21*, 19(21), pp. 2548–2556. Available at: https://doi.org/10.1038/sj.onc.1203551.
390. Ho, A. *et al.* (2022) 'Clinical Discordance in Monozygotic Twins With Autism Spectrum Disorder', *Cureus*, 14(5), p. e24813. Available at: https://doi.org/10.7759/CUREUS.24813.
391. Ho, L. and Alman, B. (2010) 'Protecting the hedgerow: p53 and hedgehog pathway interactions', *Cell Cycle*, 9(3), pp. 506–511. Available at: https://doi.org/10.4161/CC.9.3.10552.
392. Ho, L.K.H. *et al.* (2020) 'Gut microbiota changes in children with autism spectrum disorder: A systematic review', *Gut Pathogens*, 12(1), pp. 1–18. Available at: https://doi.org/10.1186/S13099-020-0346-1/TABLES/5.
393. Hoffmann, A. and Spengler, D. (2018) 'The mitochondrion as potential interface in early-life stress brain programming', *Frontiers in Behavioral Neuroscience*, 12. Available at: https://doi.org/10.3389/FNBEH.2018.00306.
394. Hoffmann, L.F. *et al.* (2023) 'Neural regeneration research model to be explored: SH-SY5Y human neuroblastoma cells', *Neural Regeneration Research*, 18(6), pp. 1265–1266. Available at: https://doi.org/10.4103/1673-5374.358621.
395. Hollestein, V. *et al.* (2023) 'Excitatory/inhibitory imbalance in autism: the role of glutamate and GABA gene-sets in symptoms and cortical brain structure', *Translational Psychiatry 2023 13:1*, 13(1), pp. 1–9. Available at: https://doi.org/10.1038/s41398-023-02317-5.
396. Hou, Y. *et al.* (2012) 'Mitochondrial superoxide production negatively regulates neural progenitor proliferation and cerebral cortical development', 30(11), pp. 2535–2547. Available at: http://doi.wiley.com/10.1002/stem.1213 (Accessed: 28 February 2020).
397. Howe, S.J. *et al.* (2020) 'Suicidality Among Children and Youth With and Without Autism Spectrum Disorder: A Systematic Review of Existing Risk Assessment Tools', *Journal of Autism and Developmental Disorders*, 50(10), pp. 3462–3476. Available at: https://doi.org/10.1007/S10803-020-04394-7/TABLES/5.
398. Hoxha, B. *et al.* (2021) 'Folic Acid and Autism: A Systematic Review of the Current State of Knowledge', *Cells 2021, Vol. 10, Page 1976*, 10(8), p. 1976. Available at: https://doi.org/10.3390/CELLS10081976.
399. Hromadkova, L. *et al.* (2020) 'Brain-derived neurotrophic factor (BDNF) promotes molecular polarization and differentiation of immature neuroblastoma cells into definitive neurons', *Biochimica et biophysica acta. Molecular cell research*, 1867(9). Available at: https://doi.org/10.1016/J.BBAMCR.2020.118737.
400. Hu, G. *et al.* (2018) 'Stomatin-like protein 2 inhibits cisplatin-induced apoptosis through MEK/ERK signaling and the mitochondrial apoptosis pathway in cervical cancer cells', *Cancer Science*, 109(5), pp. 1357–1368. Available at: https://doi.org/10.1111/CAS.13563.
401. Hu, L. *et al.* (2024) 'Mfn2/Hsc70 Complex Mediates the Formation of Mitochondria-Lipid Droplets Membrane Contact and Regulates Myocardial Lipid Metabolism', *Advanced Science*, 11(14), p. 2307749. Available at: https://doi.org/10.1002/ADVS.202307749.
402. Hu, M. *et al.* (2018) 'Propionate protects haloperidol-induced neurite lesions mediated by neuropeptide Y', *Frontiers in Neuroscience*, 12(OCT). Available at: https://doi.org/10.3389/FNINS.2018.00743.
403. Hu, T. *et al.* (2020) 'The Gut Microbiota and Oxidative Stress in Autism Spectrum Disorders (ASD)', *Oxidative Medicine and Cellular Longevity*. Edited by K. Abo-el-Sooud, 2020, pp. 1–13. Available at: https://doi.org/10.1155/2020/8396708.
404. Hu, V.W. *et al.* (2020) 'Altered DNA methylation in a severe subtype of idiopathic autism: Evidence for sex differences in affected metabolic pathways', *Autism*, p. 136236132097108. Available at: https://doi.org/10.1177/1362361320971085.

405. Hu, V.W. *et al.* (2021) 'Altered DNA methylation in a severe subtype of idiopathic autism: Evidence for sex differences in affected metabolic pathways', *Autism : the international journal of research and practice*, 25(4), pp. 887–910. Available at: https://doi.org/10.1177/1362361320971085.
406. Hu, W. *et al.* (2019) 'Roles of forkhead box O (FoxO) transcription factors in neurodegenerative diseases: A panoramic view', *Progress in Neurobiology*, 181, p. 101645. Available at: https://doi.org/10.1016/J.PNEUROBIO.2019.101645.
407. Hu, Y. *et al.* (2021) 'Stomatin-Like Protein-2: A Potential Target to Treat Mitochondrial Cardiomyopathy', *Heart, lung & circulation*, 30(10), pp. 1449–1455. Available at: https://doi.org/10.1016/J.HLC.2021.05.074.
408. Huang, D. *et al.* (2023) 'Dlk1 maintains adult mice long-term HSCs by activating Notch signaling to restrict mitochondrial metabolism', *Experimental Hematology and Oncology*, 12(1), pp. 1–16. Available at: https://doi.org/10.1186/S40164-022-00369-9/FIGURES/6.
409. Huang, T.T., Zou, Y. and Corniola, R. (2012) 'Oxidative stress and adult neurogenesis-Effects of radiation and superoxide dismutase deficiency', *Seminars in Cell and Developmental Biology*. Elsevier Ltd, pp. 738–744. Available at: https://doi.org/10.1016/j.semcdb.2012.04.003.
410. Hughes, H.K., R.J.Moreno and Ashwood, P. (2023) 'Innate immune dysfunction and neuroinflammation in autism spectrum disorder (ASD)', *Brain, Behavior, and Immunity*, 108, pp. 245–254. Available at: https://doi.org/10.1016/J.BBI.2022.12.001.
411. Hull, L., Petrides, K. V. and Mandy, W. (2020) 'The Female Autism Phenotype and Camouflaging: a Narrative Review', *Review Journal of Autism and Developmental Disorders*, 7(4), pp. 306–317. Available at: https://doi.org/10.1007/S40489-020-00197-9/TABLES/1.
412. Hurlbut, G.D. *et al.* (2007) 'Crossing paths with Notch in the hyper-network', *Current Opinion in Cell Biology*, 19(2), pp. 166–175. Available at: https://doi.org/10.1016/J.CEB.2007.02.012.
413. Hwang, I., Tang, D. and Paik, J. (2021) 'Oxidative stress sensing and response in neural stem cell fate', *Free Radical Biology and Medicine*, 169, pp. 74–83. Available at: https://doi.org/10.1016/j.freeradbiomed.2021.03.043.
414. Hyer, M.M. *et al.* (2021) 'Chronic adolescent stress causes sustained impairment of cognitive flexibility and hippocampal synaptic strength in female rats', *Neurobiology of Stress*, 14, p. 100303. Available at: https://doi.org/10.1016/J.YNSTR.2021.100303.
415. Hynds, D.A.L. and Snow, D.M. (2001) 'Fibronectin and laminin elicit differential behaviors from SH-SY5Y growth cones contacting inhibitory chondroitin sulfate proteoglycans', *Journal of Neuroscience Research*, 66(4), pp. 630–642. Available at: https://doi.org/10.1002/JNR.10020.
416. Iakoucheva, L.M., Muotri, A.R. and Sebat, J. (2019) 'Getting to the Cores of Autism', *Cell*. Cell Press, pp. 1287–1298. Available at: https://doi.org/10.1016/j.cell.2019.07.037.
417. Iannucci, J., Renehan, W. and Grammas, P. (2020) 'Thrombin, a Mediator of Coagulation, Inflammation, and Neurotoxicity at the Neurovascular Interface: Implications for Alzheimer's Disease', *Frontiers in Neuroscience*, 14. Available at: https://doi.org/10.3389/FNINS.2020.00762.
418. Iannucci, L.F. *et al.* (2016) 'Short chain fatty acids induce UCP2-mediated autophagy in hepatic cells', *Biochemical and Biophysical Research Communications*, 480(3), pp. 461–467. Available at: https://doi.org/10.1016/j.bbrc.2016.10.072.
419. Iglesias–vázquez, L. *et al.* (2020) 'Composition of Gut Microbiota in Children with Autism Spectrum Disorder: A Systematic Review and Meta-Analysis', *Nutrients 2020, Vol. 12, Page 792*, 12(3), p. 792. Available at: https://doi.org/10.3390/NU12030792.
420. Ikeda, Y. *et al.* (2015) 'Molecular Mechanisms Mediating Mitochondrial Dynamics and Mitophagy and Their Functional Roles in the Cardiovascular System', *Journal of molecular and cellular cardiology*, 0, p. 116. Available at: https://doi.org/10.1016/J.YJMCC.2014.09.019.
421. Ikon, N. and Ryan, R.O. (2017) 'Cardiolipin and mitochondrial cristae organization', *Biochimica et Biophysica Acta (BBA) - Biomembranes*, 1859(6), pp. 1156–1163. Available at: https://doi.org/10.1016/J.BBAMEM.2017.03.013.
422. Indika, N.L.R. *et al.* (2021) 'Sulfur amino acid metabolism and related metabotypes of autism spectrum disorder: A review of biochemical evidence for a hypothesis', *Biochimie*. Elsevier, pp. 143–157. Available at: https://doi.org/10.1016/j.biochi.2021.02.018.
423. Indika, N.-L.R. *et al.* (2023) 'Metabolic Approaches to the Treatment of Autism Spectrum Disorders', *Neurobiology of Autism Spectrum Disorders*, pp. 291–312. Available at: https://doi.org/10.1007/978-3-031-42383-3_14.

424. Ioghen, O.C., Ceafalan, L.C. and Popescu, B.O. (2023) 'SH-SY5Y Cell Line In Vitro Models for Parkinson Disease Research—Old Practice for New Trends', *Journal of Integrative Neuroscience*, 22(1), p. 20. Available at: https://doi.org/10.31083/j.jin2201020.
425. Ishihara, N. *et al.* (2009) 'Mitochondrial fission factor Drp1 is essential for embryonic development and synapse formation in mice', *Nature Cell Biology 2009 11:8*, 11(8), pp. 958–966. Available at: https://doi.org/10.1038/ncb1907.
426. Iskusnykh, I.Y., Zakharova, A.A. and Pathak, D. (2022) 'Glutathione in Brain Disorders and Aging', pp. 1–13.
427. Ito, Kyoko *et al.* (2016) 'Self-renewal of a purified Tie2+ hematopoietic stem cell population relies on mitochondrial clearance', *Science*, 354(6316), pp. 1156–1160. Available at: https://doi.org/10.1126/SCIENCE.AAF5530/SUPPL_FILE/ITO.SM.PDF.
428. Iwata, R., Casimir, P. and Vanderhaeghen, P. (2020) 'Mitochondrial dynamics in postmitotic cells regulate neurogenesis', *Science*, 369(6505), pp. 858–862. Available at: https://doi.org/10.1126/science.aba9760.
429. Iwata, R. and Vanderhaeghen, P. (2021) 'Regulatory roles of mitochondria and metabolism in neurogenesis', *Current Opinion in Neurobiology*, 69, pp. 231–240. Available at: https://doi.org/10.1016/j.conb.2021.05.003.
430. Jacob, C. *et al.* (2014) 'HDAC1 and HDAC2 Control the Specification of Neural Crest Cells into Peripheral Glia', *Journal of Neuroscience*, 34(17), pp. 6112–6122. Available at: https://doi.org/10.1523/JNEUROSCI.5212-13.2014.
431. James, S.J. *et al.* (2004) 'Metabolic biomarkers of increased oxidative stress and impaired methylation capacity in children with autism', *The American journal of clinical nutrition*, 80(6), pp. 1611–1617. Available at: https://doi.org/10.1093/AJCN/80.6.1611.
432. James, S.J. *et al.* (2009) 'Cellular and mitochondrial glutathione redox imbalance in lymphoblastoid cells derived from children with autism', *The FASEB Journal*, 23(8), pp. 2374–2383. Available at: https://doi.org/10.1096/fj.08-128926.
433. Jang, E.H., Lee, J.H. and Kim, S.A. (2021) 'Acute valproate exposure induces mitochondrial biogenesis and autophagy with foxo3a modulation in sh-sy5y cells', *Cells*, 10(10). Available at: https://doi.org/10.3390/CELLS10102522/S1.
434. Jaszczyk, A. and Juszczak, G.R. (2021) 'Glucocorticoids, metabolism and brain activity', *Neuroscience & Biobehavioral Reviews*, 126, pp. 113–145. Available at: https://doi.org/10.1016/J.NEUBIOREV.2021.03.007.
435. Jauhari, A. *et al.* (2017) 'Differentiation Induces Dramatic Changes in miRNA Profile, Where Loss of Dicer Diverts Differentiating SH-SY5Y Cells Toward Senescence', *Molecular Neurobiology*, 54(7), pp. 4986–4995. Available at: https://doi.org/10.1007/s12035-016-0042-9.
436. Jaworska, J., Ziemka-Nalecz, M. and Zalewska, T. (2015) 'Histone deacetylases 1 and 2 are required for brain development', *International Journal of Developmental Biology*, 59(4–6), pp. 171–177. Available at: https://doi.org/10.1387/IJDB.150071TZ.
437. Jeon, H. *et al.* (2022) 'Restoration of Cathepsin D Level via L-Serine Attenuates PPA-Induced Lysosomal Dysfunction in Neuronal Cells', *International Journal of Molecular Sciences*, 23(18), p. 10613. Available at: https://doi.org/10.3390/IJMS231810613/S1.
438. Jeste, S.S. and Geschwind, D.H. (2016) 'Clinical trials for neurodevelopmental disorders: At a therapeutic frontier', *Science Translational Medicine*, 8(321). Available at: https://doi.org/10.1126/SCITRANSLMED.AAD9874.
439. Jia, T. *et al.* (2019) 'Epigenome-wide meta-analysis of blood DNA methylation and its association with subcortical volumes: findings from the ENIGMA Epigenetics Working Group', *Molecular Psychiatry 2019 26:8*, 26(8), pp. 3884–3895. Available at: https://doi.org/10.1038/s41380-019-0605-z.
440. Jia, Z. *et al.* (2022) 'ACSS3 in brown fat drives propionate catabolism and its deficiency leads to autophagy and systemic metabolic dysfunction', *Clinical and Translational Medicine*, 12(2), p. e665. Available at: https://doi.org/10.1002/CTM2.665.
441. Jiang, L. *et al.* (2020) 'Dual mRNA therapy restores metabolic function in long-term studies in mice with propionic acidemia', *Nature Communications*, 11(1). Available at: https://doi.org/10.1038/S41467-020-19156-3.
442. Jiao, A. *et al.* (2021) 'Sodium acetate, propionate, and butyrate reduce fat accumulation in mice via modulating appetite and relevant genes', *Nutrition*, 87–88, p. 111198. Available at: https://doi.org/10.1016/J.NUT.2021.111198.
443. Jin, J. *et al.* (2020) 'The Effects of YAP and Its Related Mechanisms in Central Nervous System Diseases', *Frontiers in Neuroscience*, 14. Available at: https://doi.org/10.3389/FNINS.2020.00595.
444. Jin, Z. *et al.* (2009) 'Different transcription factors regulate nestin gene expression during P19 cell neural differentiation and central nervous system development', *Journal of Biological Chemistry*, 284(12), pp. 8160–8173. Available at: https://doi.org/10.1074/jbc.M805632200.

445. Johnson, B.B. *et al.* (2022) 'Modelling metabolic shifts during cardiomyocyte differentiation, iron deficiency and transferrin rescue using human pluripotent stem cells', *Metabolites*, 12(1), p. 9. Available at: https://doi.org/10.3390/METABO12010009/S1.
446. Johnson, S.C. *et al.* (2013) 'mTOR Inhibition Alleviates Mitochondrial Disease in a Mouse Model of Leigh Syndrome', *Science*, 342(6165), pp. 1524–1528. Available at: https://doi.org/10.1126/SCIENCE.1244360.
447. Jones, C.M., Merrick, M.T. and Houry, D.E. (2020) 'Identifying and Preventing Adverse Childhood Experiences: Implications for Clinical Practice', *JAMA*, 323(1), pp. 25–26. Available at: https://doi.org/10.1001/JAMA.2019.18499.
448. Jones, E. *et al.* (2017) 'A threshold of transmembrane potential is required for mitochondrial dynamic balance mediated by DRP1 and OMA1', *Cellular and Molecular Life Sciences*, 74(7), pp. 1347–1363. Available at: https://doi.org/10.1007/S00018-016-2421-9/FIGURES/6.
449. Joon, P., Kumar, A. and Parle, M. (2023) 'The Resemblance between the Propionic Acid Rodent Model of Autism and Autism Spectrum Disorder', *Journal of Psychiatry and Neurochemistry Research*, 1(3), pp. 1–8. Available at: www.mkscienceset.com (Accessed: 24 May 2024).
450. Jornayvaz, F.R. and Shulman, G.I. (2010) 'Regulation of mitochondrial biogenesis', *Essays in biochemistry*, 47, pp. 69–84. Available at: https://doi.org/10.1042/BSE0470069.
451. Joshi, A.U. *et al.* (2019) 'Fragmented mitochondria released from microglia trigger A1 astrocytic response and propagate inflammatory neurodegeneration', *Nature Neuroscience 2019 22:10*, 22(10), pp. 1635–1648. Available at: https://doi.org/10.1038/s41593-019-0486-0.
452. Ju, Y. *et al.* (2023) 'Dual-parameter cell biosensor for real-time monitoring of effects of propionic acid on neurons', *Biosensors and Bioelectronics*, 229, p. 115227. Available at: https://doi.org/10.1016/j.bios.2023.115227.
453. Jung, M. *et al.* (2020) 'Correlative Light and Transmission Electron Microscopy Showed Details of Mitophagy by Mitochondria Quality Control in Propionic Acid Treated SH-SY5Y Cell', *Materials 2020, Vol. 13, Page 4336*, 13(19), p. 4336. Available at: https://doi.org/10.3390/MA13194336.
454. Juster, R.P. *et al.* (2016) 'Allostatic load and comorbidities: A mitochondrial, epigenetic, and evolutionary perspective', *Development and Psychopathology*, 28(4pt1), pp. 1117–1146. Available at: https://doi.org/10.1017/S0954579416000730.
455. Kang, Y. *et al.* (2018) 'Evaluation of reference genes for gene expression studies in mouse and N2a cell ischemic stroke models using quantitative real-time PCR', *BMC Neuroscience*, 19(1), pp. 1–11. Available at: https://doi.org/10.1186/S12868-018-0403-6/FIGURES/6.
456. Karp, P.D. *et al.* (2021) 'Pathway Tools version 23.0 update: software for pathway/genome informatics and systems biology', *Briefings in Bioinformatics*, 22(1), p. 109. Available at: https://doi.org/10.1093/BIB/BBZ104.
457. Kasahara, A. and Scorrano, L. (2014) 'Mitochondria: from cell death executioners to regulators of cell differentiation', *Trends in Cell Biology*, 24(12), pp. 761–770. Available at: https://doi.org/10.1016/J.TCB.2014.08.005.
458. Kasahara, E. and Inoue, M. (2015) 'Cross-talk between HPA-axis-increased glucocorticoids and mitochondrial stress determines immune responses and clinical manifestations of patients with sepsis', *Redox Report*, 20(1), pp. 1–10. Available at: https://doi.org/10.1179/1351000214Y.0000000107.
459. Kawada, K., Kuramoto, N. and Mimori, S. (2020) 'Possibility that the Onset of Autism Spectrum Disorder is Induced by Failure of the Glutamine-Glutamate Cycle', *Current Molecular Pharmacology*, 13. Available at: https://doi.org/10.2174/1874467213666200319125109.
460. Kaya, Z.B. *et al.* (2024) 'Optimizing SH-SY5Y cell culture: exploring the beneficial effects of an alternative media supplement on cell proliferation and viability', *Scientific Reports 2024 14:1*, 14(1), pp. 1–11. Available at: https://doi.org/10.1038/s41598-024-55516-5.
461. Keil, K.P. and Lein, P.J. (2016) 'DNA methylation: a mechanism linking environmental chemical exposures to risk of autism spectrum disorders?', *Environmental Epigenetics*, 2(1), p. dvv012. Available at: https://doi.org/10.1093/eep/dvv012.
462. Kelson, T.L., Ohura, T. and Kraus, J.P. (1996) 'Chaperonin-mediated Assembly of Wild-Type and Mutant Subunits of Human Propionyl-CoA Carboxylase Expressed in Escherichia Coli', *Human Molecular Genetics*, 5(3), pp. 331–337. Available at: https://doi.org/10.1093/HMG/5.3.331.
463. Kereszturi, É. (2023) 'Diversity and Classification of Genetic Variations in Autism Spectrum Disorder', *International Journal of Molecular Sciences 2023, Vol. 24, Page 16768*, 24(23), p. 16768. Available at: https://doi.org/10.3390/IJMS242316768.

464. Khacho, M. *et al.* (2016) 'Mitochondrial Dynamics Impacts Stem Cell Identity and Fate Decisions by Regulating a Nuclear Transcriptional Program', *Cell Stem Cell*, 19(2), pp. 232–247. Available at: https://doi.org/10.1016/j.stem.2016.04.015.
465. Khacho, M. and Slack, R.S. (2018) 'Mitochondrial dynamics in the regulation of neurogenesis: From development to the adult brain', *Developmental Dynamics*, 247(1), pp. 47–53. Available at: https://doi.org/10.1002/DVDY.24538.
466. Khalil, S.R. *et al.* (2015) 'Apitoxin protects rat pups brain from propionic acid-induced oxidative stress: The expression pattern of Bcl-2 and Caspase-3 apoptotic genes', *NeuroToxicology*, 49, pp. 121–131. Available at: https://doi.org/10.1016/J.NEURO.2015.05.011.
467. Khaliulin, I., Hamoudi, W. and Amal, H. (2024) 'The multifaceted role of mitochondria in autism spectrum disorder', *Molecular Psychiatry 2024*, pp. 1–22. Available at: https://doi.org/10.1038/s41380-024-02725-z.
468. Khanbabaei, M. *et al.* (2019) 'Precocious myelination in a mouse model of autism', *Translational Psychiatry 2019 9:1*, 9(1), pp. 1–14. Available at: https://doi.org/10.1038/s41398-019-0590-7.
469. Khelfaoui, H., Ibaceta-Gonzalez, C. and Angulo, M.C. (2024) 'Functional myelin in cognition and neurodevelopmental disorders', *Cellular and Molecular Life Sciences 2024 81:1*, 81(1), pp. 1–14. Available at: https://doi.org/10.1007/S00018-024-05222-2.
470. Khemakhem, A.M. *et al.* (2017) 'Novel biomarkers of metabolic dysfunction is autism spectrum disorder: potential for biological diagnostic markers', *Metabolic Brain Disease*, 32(6), pp. 1983–1997. Available at: https://doi.org/10.1007/s11011-017-0085-2.
471. Khera, R., Mehan, S., Bhalla, S., *et al.* (2022) 'Guggulsterone Mediated JAK/STAT and PPAR-Gamma Modulation Prevents Neurobehavioral and Neurochemical Abnormalities in Propionic Acid-Induced Experimental Model of Autism', *Molecules*, 27(3). Available at: https://doi.org/10.3390/molecules27030889.
472. Khera, R., Mehan, S., Kumar, S., *et al.* (2022) 'Role of JAK-STAT and PPAR-Gamma Signalling Modulators in the Prevention of Autism and Neurological Dysfunctions', *Molecular Neurobiology* [Preprint], (0123456789). Available at: https://doi.org/10.1007/s12035-022-02819-1.
473. Khogeer, A.A.; *et al.* (2022) 'The Role of Genetics, Epigenetics, and the Environment in ASD: A Mini Review', *Epigenomes 2022, Vol. 6, Page 15*, 6(2), p. 15. Available at: https://doi.org/10.3390/EPIGENOMES6020015.
474. Kiefer, J., Beyer-Sehlmeyer, G. and Pool-Zobel, B.L. (2006) 'Mixtures of SCFA, composed according to physiologically available concentrations in the gut lumen, modulate histone acetylation in human HT29 colon cancer cells', *British Journal of Nutrition*, 96(5), pp. 803–810. Available at: https://doi.org/10.1017/BJN20061948.
475. Kim, J. *et al.* (2015) 'High-capacity glycolytic and mitochondrial oxidative metabolisms mediate the growth ability of glioblastoma', *International journal of oncology*, 47(3), pp. 1009–1016. Available at: https://doi.org/10.3892/IJO.2015.3101.
476. Kim, J.I. *et al.* (2019) 'Peripheral Mitochondrial DNA Copy Number is Increased in Korean Attention-Deficit Hyperactivity Disorder Patients', *Frontiers in Psychiatry*, 10. Available at: https://doi.org/10.3389/fpsyt.2019.00506.
477. Kim, S.A. *et al.* (2019) 'Propionic acid induces mitochondrial dysfunction and affects gene expression for mitochondria biogenesis and neuronal differentiation in SH-SY5Y cell line', *NeuroToxicology*, 75, pp. 116–122. Available at: https://doi.org/10.1016/j.neuro.2019.09.009.
478. Kim, Y. *et al.* (2019) 'Mitochondria, Metabolism, and Redox Mechanisms in Psychiatric Disorders', *https://home.liebertpub.com/ars*, 31(4), pp. 275–317. Available at: https://doi.org/10.1089/ARS.2018.7606.
479. King, J., Patel, M. and Chandrasekaran, S. (2021) 'Metabolism, HDACs, and HDAC Inhibitors: A Systems Biology Perspective', *Metabolites 2021, Vol. 11, Page 792*, 11(11), p. 792. Available at: https://doi.org/10.3390/METABO11110792.
480. Klein, I.L. *et al.* (2021) 'Cognitive functioning and mental health in mitochondrial disease: A systematic scoping review', *Neuroscience & Biobehavioral Reviews*, 125, pp. 57–77. Available at: https://doi.org/10.1016/J.NEUBIOREV.2021.02.004.
481. Kloypan, C. *et al.* (2015) 'LINE-1 hypomethylation induced by reactive oxygen species is mediated via depletion of S-adenosylmethionine', *Cell Biochemistry and Function*, 33(6), pp. 375–384. Available at: https://doi.org/10.1002/CBF.3124.
482. Knobloch, M. *et al.* (2013) 'Metabolic control of adult neural stem cell activity by Fasn-dependent lipogenesis', *Nature*, 493(7431), pp. 226–230. Available at: https://doi.org/10.1038/nature11689.
483. Knobloch, M. *et al.* (2017) 'A Fatty Acid Oxidation-Dependent Metabolic Shift Regulates Adult Neural Stem Cell Activity', *Cell Reports*, 20(9), pp. 2144–2155. Available at: https://doi.org/10.1016/j.celrep.2017.08.029.

484. Ko, J. *et al.* (2016) 'PPAR-γ activation attenuates deltamethrin-induced apoptosis by regulating cytosolic PINK1 and inhibiting mitochondrial dysfunction', *Toxicology Letters*, 260, pp. 8–17. Available at: https://doi.org/10.1016/J.TOXLET.2016.08.016.
485. Kokkinopoulou, I. and Moutsatsou, P. (2021) 'Mitochondrial Glucocorticoid Receptors and Their Actions', *International Journal of Molecular Sciences 2021, Vol. 22, Page 6054*, 22(11), p. 6054. Available at: https://doi.org/10.3390/IJMS22116054.
486. Kõlves, K. *et al.* (2021) 'Assessment of Suicidal Behaviors Among Individuals With Autism Spectrum Disorder in Denmark', *JAMA network open*, 4(1), p. e2033565. Available at: https://doi.org/10.1001/jamanetworkopen.2020.33565.
487. Kondadi, A.K. and Reichert, A.S. (2024) 'Mitochondrial Dynamics at Different Levels: From Cristae Dynamics to Interorganellar Cross Talk', *Annual Review of Biophysics*, 53(1), pp. 147–168. Available at: https://doi.org/10.1146/ANNUREV-BIOPHYS-030822-020736/CITE/REFWORKS.
488. Konopelski Snavely, S.E. *et al.* (2023) 'Non-canonical WNT5A-ROR signaling: New perspectives on an ancient developmental pathway', *Current topics in developmental biology*, 153, pp. 195–227. Available at: https://doi.org/10.1016/BS.CTDB.2023.01.009.
489. Kopinski, P.K. *et al.* (2019) 'Regulation of nuclear epigenome by mitochondrial DNA heteroplasmy', *Proceedings of the National Academy of Sciences of the United States of America*, 116(32), pp. 16028–16035. Available at: https://doi.org/10.1073/pnas.1906896116.
490. Korecka, J.A. *et al.* (2013) 'Phenotypic Characterization of Retinoic Acid Differentiated SH-SY5Y Cells by Transcriptional Profiling', *PLOS ONE*, 8(5), p. e63862. Available at: https://doi.org/10.1371/JOURNAL.PONE.0063862.
491. Korteling, D. *et al.* (2022) 'Untargeted metabolic analysis in dried blood spots reveals metabolic signature in 22q11.2 deletion syndrome', *Translational Psychiatry 2022 12:1*, 12(1), pp. 1–7. Available at: https://doi.org/10.1038/s41398-022-01859-4.
492. Kosmider, B. *et al.* (2019) 'Mitochondrial dysfunction in human primary alveolar type II cells in emphysema', *EBioMedicine*, 46, p. 305. Available at: https://doi.org/10.1016/J.EBIOM.2019.07.063.
493. Kovalevich, J. and Langford, D. (2013) 'Considerations for the use of SH-SY5Y neuroblastoma cells in neurobiology', *Methods in Molecular Biology*, 1078, pp. 9–21. Available at: https://doi.org/10.1007/978-1-62703-640-5_2.
494. Kovalevich, J., Santerre, M. and Langford, D. (2021) 'Considerations for the Use of SH-SY5Y Neuroblastoma Cells in Neurobiology', in *Methods in Molecular Biology*. Humana Press Inc., pp. 9–23. Available at: https://doi.org/10.1007/978-1-0716-1437-2_2.
495. Kowiański, P. *et al.* (2017) 'BDNF: A Key Factor with Multipotent Impact on Brain Signaling and Synaptic Plasticity', *Cellular and Molecular Neurobiology 2017 38:3*, 38(3), pp. 579–593. Available at: https://doi.org/10.1007/S10571-017-0510-4.
496. Kraan, C.M. *et al.* (2020) 'DNA Methylation at Birth Predicts Intellectual Functioning and Autism Features in Children with Fragile X Syndrome', *International Journal of Molecular Sciences 2020, Vol. 21, Page 7735*, 21(20), p. 7735. Available at: https://doi.org/10.3390/IJMS21207735.
497. Krishna, A. *et al.* (2014) 'Systems genomics evaluation of the SH-SY5Y neuroblastoma cell line as a model for Parkinson's disease', *BMC Genomics*, 15(1), p. 1154. Available at: https://doi.org/10.1186/1471-2164-15-1154.
498. Kronenberger, L. *et al.* (2024) 'Metabolic Profiling of SH-SY5Y and Neuro2A Cells in Relation to Fetal Calf Serum (FCS) Concentration in Culture Media', *Metabolites*, 14(4), p. 188. Available at: https://doi.org/10.3390/METABO14040188/S1.
499. Kubota, T. and Mochizuki, K. (2016) 'Epigenetic Effect of Environmental Factors on Autism Spectrum Disorders', *International Journal of Environmental Research and Public Health 2016, Vol. 13, Page 504*, 13(5), p. 504. Available at: https://doi.org/10.3390/IJERPH13050504.
500. Kuenzel, E. *et al.* (2021) 'Early adversity and positive parenting: Association with cognitive outcomes in children with autism spectrum disorder', *Autism Research* [Preprint]. Available at: https://doi.org/10.1002/AUR.2613.
501. Kühnen, P. *et al.* (2016) 'Interindividual Variation in DNA Methylation at a Putative POMC Metastable Epiallele Is Associated with Obesity', *Cell Metabolism*, 24(3), pp. 502–509. Available at: https://doi.org/10.1016/j.cmet.2016.08.001.
502. Kuleshov, M. V. *et al.* (2016) 'Enrichr: a comprehensive gene set enrichment analysis web server 2016 update', *Nucleic acids research*, 44(W1), pp. W90–W97. Available at: https://doi.org/10.1093/nar/gkw377.
503. Kumar, M. *et al.* (2025) 'Therapeutic efficacy of Genistein in activation of neuronal AC/cAMP/CREB/PKA and mitochondrial ETC-Complex pathways in experimental model of autism: Evidence from CSF, blood plasma and brain analysis', *Brain Research*, 1846, p. 149251. Available at: https://doi.org/10.1016/j.brainres.2024.149251.

504. Kumar, P. *et al.* (2015) 'Impaired TGF-β induced growth inhibition contributes to the increased proliferation rate of neural stem cells harboring mutant p53', *American Journal of Cancer Research*, 5(11), p. 3436. Available at: /pmc/articles/PMC4697689/ (Accessed: 8 October 2024).
505. Kunkel, G.H., Chaturvedi, P. and Tyagi, S.C. (2016) 'Mitochondrial pathways to cardiac recovery: TFAM', *Heart Failure Reviews 2016 21:5*, 21(5), pp. 499–517. Available at: https://doi.org/10.1007/S10741-016-9561-8.
506. Kursu, V.A.S. *et al.* (2013) 'Defects in mitochondrial fatty acid synthesis result in failure of multiple aspects of mitochondrial biogenesis in Saccharomyces cerevisiae', *Molecular Microbiology*, 90(4), pp. 824–840. Available at: https://doi.org/10.1111/MMI.12402/SUPPINFO.
507. Kwan, V., Unda, B.K. and Singh, K.K. (2016) 'Wnt signaling networks in autism spectrum disorder and intellectual disability', *Journal of Neurodevelopmental Disorders*, 8(1). Available at: https://doi.org/10.1186/S11689-016-9176-3.
508. Kwon, C.H. *et al.* (2006) 'Pten Regulates Neuronal Arborization and Social Interaction in Mice', *Neuron*, 50(3), pp. 377–388. Available at: https://doi.org/10.1016/j.neuron.2006.03.023.
509. Kyle, S.M. *et al.* (2016) 'MeCP2 co-ordinates liver lipid metabolism with the NCoR1/HDAC3 corepressor complex', *Human Molecular Genetics*, 25(14), pp. 3029–3041. Available at: https://doi.org/10.1093/HMG/DDW156.
510. de la Bâtie, C.D. *et al.* (2018) 'Autism spectrum disorders in propionic acidemia patients', *Journal of Inherited Metabolic Disease*, 41(4), pp. 623–629. Available at: https://doi.org/10.1007/S10545-017-0070-2/TABLES/1.
511. Lacombe, A. and Scorrano, L. (2024) 'The interplay between mitochondrial dynamics and autophagy: From a key homeostatic mechanism to a driver of pathology', *Seminars in Cell & Developmental Biology*, 161–162, pp. 1–19. Available at: https://doi.org/10.1016/J.SEMCDB.2024.02.001.
512. Ladd-Acosta, C. *et al.* (2014) 'Common DNA methylation alterations in multiple brain regions in autism', *Molecular Psychiatry*, 19(8), pp. 862–871. Available at: https://doi.org/10.1038/mp.2013.114.
513. Lagerwaard, B. *et al.* (2021) 'Propionate hampers differentiation and modifies histone propionylation and acetylation in skeletal muscle cells', *Mechanisms of Ageing and Development*, 196, p. 111495. Available at: https://doi.org/10.1016/J.MAD.2021.111495.
514. Lagod, P.P., Abdelli, L.S. and Naser, S.A. (2024) 'An In Vivo Model of Propionic Acid-Rich Diet-Induced Gliosis and Neuro-Inflammation in Mice (FVB/N-Tg(GFAPGFP)14Mes/J): A Potential Link to Autism Spectrum Disorder', *International Journal of Molecular Sciences 2024, Vol. 25, Page 8093*, 25(15), p. 8093. Available at: https://doi.org/10.3390/IJMS25158093.
515. Lagod, P.P. and Naser, S.A. (2023) 'The Role of Short-Chain Fatty Acids and Altered Microbiota Composition in Autism Spectrum Disorder: A Comprehensive Literature Review', *International Journal of Molecular Sciences 2023, Vol. 24, Page 17432*, 24(24), p. 17432. Available at: https://doi.org/10.3390/IJMS242417432.
516. Lähdepuro, A. *et al.* (2019) 'The Impact of Early Life Stress on Anxiety Symptoms in Late Adulthood', *Scientific Reports 2019 9:1*, 9(1), pp. 1–13. Available at: https://doi.org/10.1038/s41598-019-40698-0.
517. Lake, N.J. *et al.* (2015) 'Leigh SyndromeNeuropathology and Pathogenesis', *Journal of Neuropathology & Experimental Neurology*, 74(6), pp. 482–492. Available at: https://doi.org/10.1097/NEN.0000000000000195.
518. Lampada, A. and Taylor, V. (2023) 'Notch signaling as a master regulator of adult neurogenesis', *Frontiers in Neuroscience*, 17, p. 1179011. Available at: https://doi.org/10.3389/FNINS.2023.1179011/BIBTEX.
519. Landry, T. and Huang, H. (2021) 'Mini review: The relationship between energy status and adult hippocampal neurogenesis', *Neuroscience Letters*, 765, p. 136261. Available at: https://doi.org/10.1016/J.NEULET.2021.136261.
520. Langerscheidt, F., Bell-Simons, M. and Zempel, H. (2024) 'Differentiating SH-SY5Y Cells into Polarized Human Neurons for Studying Endogenous and Exogenous Tau Trafficking: Four Protocols to Obtain Neurons with Noradrenergic, Dopaminergic, and Cholinergic Properties', *Methods in Molecular Biology*, 2754, pp. 521–532. Available at: https://doi.org/10.1007/978-1-0716-3629-9_30.
521. Langfelder, P. and Horvath, S. (2008) 'WGCNA: An R package for weighted correlation network analysis', *BMC Bioinformatics*, 9(1), pp. 1–13. Available at: https://doi.org/10.1186/1471-2105-9-559/FIGURES/4.
522. Lapp, H.E., Bartlett, A.A. and Hunter, R.G. (2019) 'Stress and glucocorticoid receptor regulation of mitochondrial gene expression', *Journal of Molecular Endocrinology*, 62(2), pp. R121–R128. Available at: https://doi.org/10.1530/JME-18-0152.
523. Lauro, C. and Limatola, C. (2020) 'Metabolic Reprograming of Microglia in the Regulation of the Innate Inflammatory Response', *Frontiers in Immunology*, 0, p. 493. Available at: https://doi.org/10.3389/FIMMU.2020.00493.

524. Lawana, V. *et al.* (2020) 'Neuromelanin formation exacerbates HAA-induced mitochondrial toxicity and mitophagy impairments', *NeuroToxicology*, 81, pp. 147–160. Available at: https://doi.org/10.1016/J.NEURO.2020.10.005.
525. Leadbitter, K. *et al.* (2021) 'Autistic Self-Advocacy and the Neurodiversity Movement: Implications for Autism Early Intervention Research and Practice', *Frontiers in Psychology*, 12, p. 782. Available at: https://doi.org/10.3389/FPSYG.2021.635690/BIBTEX.
526. Lee, D.H., Kim, M.T. and Han, J.H. (2024) 'GPR41 and GPR43: From development to metabolic regulation', *Biomedicine & Pharmacotherapy*, 175, p. 116735. Available at: https://doi.org/10.1016/J.BIOPHA.2024.116735.
527. Lee, E.C. and Hu, V.W. (2020) 'Phenotypic subtyping and re-analysis of existing methylation data from autistic probands in simplex families reveal ASD subtype-associated differentially methylated genes and biological functions', *International Journal of Molecular Sciences*, 21(18), pp. 1–23. Available at: https://doi.org/10.3390/ijms21186877.
528. Lee, H. *et al.* (2019) 'Constitutional mislocalization of Pten drives precocious maturation in oligodendrocytes and aberrant myelination in model of autism spectrum disorder', *Translational Psychiatry 2019 9:1*, 9(1), pp. 1–12. Available at: https://doi.org/10.1038/s41398-018-0364-7.
529. Lee, S.R. *et al.* (2013) 'Glucocorticoids and their receptors: Insights into specific roles in mitochondria', *Progress in Biophysics and Molecular Biology*, 112(1–2), pp. 44–54. Available at: https://doi.org/10.1016/j.pbiomolbio.2013.04.001.
530. Lee, Y., Cho, J.H., *et al.* (2019) 'Neuroprotective effects of MHY908, a PPAR α/γ dual agonist, in a MPTP-induced Parkinson's disease model', *Brain Research*, 1704, pp. 47–58. Available at: https://doi.org/10.1016/J.BRAINRES.2018.09.036.
531. Lee, Y., Lee, S., *et al.* (2019) 'Significant roles of neuroinflammation in Parkinson's disease: therapeutic targets for PD prevention', *Archives of Pharmacal Research 2019 42:5*, 42(5), pp. 416–425. Available at: https://doi.org/10.1007/S12272-019-01133-0.
532. Lee, Y.S. and Silva, A.J. (2009) 'The molecular and cellular biology of enhanced cognition', *Nature Reviews Neuroscience*, 10(2), pp. 126–140. Available at: https://doi.org/10.1038/NRN2572.
533. Lee, Y.Y. *et al.* (2020) 'Bcl-2 Overexpression Induces Neurite Outgrowth via the Bmp4/Tbx3/NeuroD1 Cascade in H19-7 Cells', *Cellular and Molecular Neurobiology*, 40(1), pp. 153–166. Available at: https://doi.org/10.1007/S10571-019-00732-1/FIGURES/6.
534. Lei, W. *et al.* (2016) 'Actin Cytoskeleton in Dendritic Spine Development and Plasticity', *Current opinion in neurobiology*, 39, p. 86. Available at: https://doi.org/10.1016/J.CONB.2016.04.010.
535. LeMoult, J. *et al.* (2020) 'Meta-analysis: Exposure to Early Life Stress and Risk for Depression in Childhood and Adolescence', *Journal of the American Academy of Child & Adolescent Psychiatry*, 59(7), pp. 842–855. Available at: https://doi.org/10.1016/j.jaac.2019.10.011.
536. Leung, T.C.N. *et al.* (2024) 'Temporal Quantitative Proteomic and Phosphoproteomic Profiling of SH-SY5Y and IMR-32 Neuroblastoma Cells during All-Trans-Retinoic Acid-Induced Neuronal Differentiation', *International Journal of Molecular Sciences*, 25(2), p. 1047. Available at: https://doi.org/10.3390/IJMS25021047/S1.
537. Lezi, E. and Swerdlow, R.H. (2016) 'Lactate's effect on human neuroblastoma cell bioenergetic fluxes', *Biochemical pharmacology*, 99, pp. 88–100. Available at: https://doi.org/10.1016/J.BCP.2015.11.002.
538. Li, B. *et al.* (2022) 'Emerging methods for and novel insights gained by absolute quantification of mitochondrial DNA copy number and its clinical applications', *Pharmacology and Therapeutics*. Pergamon, p. 107995. Available at: https://doi.org/10.1016/j.pharmthera.2021.107995.
539. Li, D. *et al.* (2020) 'Metabolic Enhancement of Glycolysis and Mitochondrial Respiration Are Essential for Neuronal Differentiation', *Cellular Reprogramming*, 22(6), pp. 291–299. Available at: https://doi.org/10.1089/CELL.2020.0034/ASSET/IMAGES/LARGE/CELL.2020.0034_FIGURE5.JPEG.
540. Li, H. *et al.* (2023) 'Neurons require glucose uptake and glycolysis in vivo', *Cell Reports*, 42(4), p. 112335. Available at: https://doi.org/10.1016/J.CELREP.2023.112335.
541. Li, J. *et al.* (2023) 'Phosphatidylethanolamine N-methyltransferase: from Functions to Diseases', *Aging and Disease*, 14(3), p. 879. Available at: https://doi.org/10.14336/AD.2022.1025.
542. Li, Y. *et al.* (2017) 'Regulating the balance between the kynurenine and serotonin pathways of tryptophan metabolism', *The FEBS Journal*, 284(6), pp. 948–966. Available at: https://doi.org/10.1111/FEBS.14026.
543. Li, Y. *et al.* (2023) 'The Notch1/Hes1 signaling pathway affects autophagy by adjusting DNA methyltransferases expression in a valproic acid-induced autism spectrum disorder model', *Neuropharmacology*, 239, p. 109682. Available at: https://doi.org/10.1016/J.NEUROPHARM.2023.109682.

544. Liang, J. *et al.* (2015) 'Myristoylation confers noncanonical AMPK functions in autophagy selectivity and mitochondrial surveillance', *Nature Communications 2015 6:1*, 6(1), pp. 1–14. Available at: https://doi.org/10.1038/ncomms8926.
545. Liao, X., Yang, J., *et al.* (2020) 'Microglia mediated neuroinflammation in autism spectrum disorder', *Journal of Psychiatric Research*, 130, pp. 167–176. Available at: https://doi.org/10.1016/j.jpsychires.2020.07.013.
546. Liao, X., Liu, Y., *et al.* (2020) 'Postmortem Studies of Neuroinflammation in Autism Spectrum Disorder: a Systematic Review', *Molecular Neurobiology*. Springer, pp. 3424–3438. Available at: https://doi.org/10.1007/s12035-020-01976-5.
547. Liao, X., Li, X. and Liu, R. (2023) 'Extracellular-matrix mechanics regulate cellular metabolism: A ninja warrior behind mechano-chemo signaling crosstalk', *Reviews in Endocrine and Metabolic Disorders*, 24(2), pp. 207–220. Available at: https://doi.org/10.1007/S11154-022-09768-Z/FIGURES/4.
548. Licausi, F. and Hartman, N.W. (2018) 'Role of mTOR complexes in neurogenesis', *International Journal of Molecular Sciences*. MDPI AG. Available at: https://doi.org/10.3390/ijms19051544.
549. Liddelow, S.A., Marsh, S.E. and Stevens, B. (2020) 'Microglia and Astrocytes in Disease: Dynamic Duo or Partners in Crime?', *Trends in Immunology*, 41(9), pp. 820–835. Available at: https://doi.org/10.1016/j.it.2020.07.006.
550. Lin, N. *et al.* (2014) 'Homocysteine induces cytotoxicity and proliferation inhibition in neural stem cells via DNA methylation in vitro', *The FEBS Journal*, 281(8), pp. 2088–2096. Available at: https://doi.org/10.1111/FEBS.12764.
551. Lin, X. *et al.* (2022) 'The role of microbiota in autism spectrum disorder: A bibliometric analysis based on original articles', *Frontiers in Psychiatry*, 13, p. 976827. Available at: https://doi.org/10.3389/FPSYT.2022.976827/BIBTEX.
552. Lintas, C. (2019) 'Linking genetics to epigenetics: The role of folate and folate-related pathways in neurodevelopmental disorders', *Clinical Genetics*, 95(2), pp. 241–252. Available at: https://doi.org/10.1111/CGE.13421.
553. Liu, C. *et al.* (2019) 'Testosterone Deficiency Caused by Castration Modulates Mitochondrial Biogenesis Through the AR/PGC1α/TFAM Pathway', *Frontiers in Genetics*, 10(MAY), p. 505. Available at: https://doi.org/10.3389/fgene.2019.00505.
554. Liu, F. *et al.* (2019) 'Altered composition and function of intestinal microbiota in autism spectrum disorders: a systematic review', *Translational Psychiatry 2019 9:1*, 9(1), pp. 1–13. Available at: https://doi.org/10.1038/s41398-019-0389-6.
555. Liu, J. *et al.* (2009) 'Bmi1 regulates mitochondrial function and the DNA damage response pathway', *Nature*, 459(7245), pp. 387–392. Available at: https://doi.org/10.1038/nature08040.
556. Liu, J. *et al.* (2022) 'Wnt/β-catenin signalling: function, biological mechanisms, and therapeutic opportunities', *Signal Transduction and Targeted Therapy 2021 7:1*, 7(1), pp. 1–23. Available at: https://doi.org/10.1038/s41392-021-00762-6.
557. Liu, Q. *et al.* (2020) 'Stomatin-like Protein 2 Promotes Tumor Cell Survival by Activating the JAK2-STAT3-PIM1 Pathway, Suggesting a Novel Therapy in CRC', *Molecular Therapy Oncolytics*, 17, pp. 169–179. Available at: https://doi.org/10.1016/j.omto.2020.03.010.
558. Liu, Q.Q. *et al.* (2024) 'The role of Foxo3a in neuron-mediated cognitive impairment', *Frontiers in Molecular Neuroscience*, 17, p. 1424561. Available at: https://doi.org/10.3389/FNMOL.2024.1424561/BIBTEX.
559. Liu, S. *et al.* (2021) 'Mitochondrial DNA Copy Number in Rett Syndrome Caused by MECP2 Variants', *The Journal of Pediatrics* [Preprint]. Available at: https://doi.org/10.1016/J.JPEDS.2021.09.052.
560. Liu, X. *et al.* (2024) 'Mitochondria as a sensor, a central hub and a biological clock in psychological stress-accelerated aging', *Ageing Research Reviews*, 93, p. 102145. Available at: https://doi.org/10.1016/J.ARR.2023.102145.
561. Liu, Y. *et al.* (2022) 'Altered expression of glycan patterns and glycan-related genes in the medial prefrontal cortex of the valproic acid rat model of autism', *Frontiers in Cellular Neuroscience*, 16, p. 1057857. Available at: https://doi.org/10.3389/FNCEL.2022.1057857/BIBTEX.
562. Liu, Y. *et al.* (2024) 'KAT6A deficiency impairs cognitive functions through suppressing RSPO2/Wnt signaling in hippocampal CA3', *Science Advances*, 10(20). Available at: https://doi.org/10.1126/SCIADV.ADM9326/SUPPL_FILE/SCIADV.ADM9326_SM.PDF.
563. Liu, Y.K. *et al.* (2021) 'Association of neonatal blood levels of brain-derived neurotrophic factor with development of autism spectrum disorder: a systematic review and meta-analysis', *World Journal of Pediatrics*, 17(2), pp. 164–170. Available at: https://doi.org/10.1007/S12519-021-00415-2/FIGURES/3.

564. Livak, K.J. and Schmittgen, T.D. (2001) 'Analysis of relative gene expression data using real-time quantitative PCR and the 2(-Delta Delta C(T)) Method', *Methods (San Diego, Calif.)*, 25(4), pp. 402–408. Available at: https://doi.org/10.1006/METH.2001.1262.
565. Lively, S. and Schlichter, L.C. (2018) 'Microglia responses to pro-inflammatory stimuli (LPS, IFNγ+TNFα) and reprogramming by resolving cytokines (IL-4, IL-10)', *Frontiers in Cellular Neuroscience*, 12. Available at: https://doi.org/10.3389/fncel.2018.00215.
566. Lobzhanidze, G. *et al.* (2020) 'Behavioural and brain ultrastructural changes following the systemic administration of propionic acid in adolescent male rats. Further development of a rodent model of autism', *International Journal of Developmental Neuroscience*, 80(2), pp. 139–156. Available at: https://doi.org/10.1002/JDN.10011.
567. Lombard, J. (1998) 'Autism: a mitochondrial disorder?', *Medical Hypotheses*, 50(6), pp. 497–500. Available at: https://doi.org/10.1016/S0306-9877(98)90270-5.
568. Lombardo, M. V. and Mandelli, V. (2022) 'Rethinking Our Concepts and Assumptions About Autism', *Frontiers in Psychiatry*, 0, p. 1184. Available at: https://doi.org/10.3389/FPSYT.2022.903489.
569. Long, K.R. and Huttner, W.B. (2019) 'How the extracellular matrix shapes neural development', *Royal Society Open Biology*, 9(1). Available at: https://doi.org/10.1098/RSOB.180216.
570. Longair, M.H., Baker, D.A. and Armstrong, J.D. (2011) 'Simple Neurite Tracer: open source software for reconstruction, visualization and analysis of neuronal processes', *Bioinformatics*, 27(17), pp. 2453–2454. Available at: https://doi.org/10.1093/BIOINFORMATICS/BTR390.
571. Longhitano, L. *et al.* (2023) '(+)-Lipoic Acid Reduces Lipotoxicity and Regulates Mitochondrial Homeostasis and Energy Balance in an In Vitro Model of Liver Steatosis', *International Journal of Molecular Sciences*, 24(19), p. 14491. Available at: https://doi.org/10.3390/IJMS241914491/S1.
572. Lopes, F.M. *et al.* (2010) 'Comparison between proliferative and neuron-like SH-SY5Y cells as an in vitro model for Parkinson disease studies', *Brain Research*, 1337, pp. 85–94. Available at: https://doi.org/10.1016/j.brainres.2010.03.102.
573. Lopez, S.A. and Flagel, S.B. (2020) 'A proposed role for glucocorticoids in mediating dopamine-dependent cue-reward learning', *https://doi.org/10.1080/10253890.2020.1768240*, 24(2), pp. 154–167. Available at: https://doi.org/10.1080/10253890.2020.1768240.
574. Lopez-Suarez, L. *et al.* (2022) 'The SH-SY5Y human neuroblastoma cell line, a relevant in vitro cell model for investigating neurotoxicology in human: Focus on organic pollutants', *NeuroToxicology*, 92, pp. 131–155. Available at: https://doi.org/10.1016/J.NEURO.2022.07.008.
575. López-Tobón, A. *et al.* (2019) 'Human Cortical Organoids Expose a Differential Function of GSK3 on Cortical Neurogenesis', *Stem Cell Reports*, 13(5), pp. 847–861. Available at: https://doi.org/10.1016/j.stemcr.2019.09.005.
576. Di Loreto, S. *et al.* (2007) 'PPARβ agonists trigger neuronal differentiation in the human neuroblastoma cell line SH-SY5Y', *Journal of Cellular Physiology*, 211(3), pp. 837–847. Available at: https://doi.org/10.1002/JCP.20996.
577. Loth, E., Murphy, D.G. and Spooren, W. (2016) 'Defining precision medicine approaches to autism spectrum disorders: Concepts and challenges', *Frontiers in Psychiatry*, 7(NOV), p. 188. Available at: https://doi.org/10.3389/FPSYT.2016.00188/BIBTEX.
578. Louis Sam Titus, A.S.C. *et al.* (2019) 'The Bdnf and Npas4 genes are targets of HDAC3-mediated transcriptional repression', *BMC Neuroscience*, 20(1). Available at: https://doi.org/10.1186/S12868-019-0546-0.
579. Loving, B.A. and Bruce, K.D. (2020) 'Lipid and Lipoprotein Metabolism in Microglia', *Frontiers in Physiology*, 0, p. 393. Available at: https://doi.org/10.3389/FPHYS.2020.00393.
580. Lozoya, O.A. *et al.* (2018) 'Mitochondrial nicotinamide adenine dinucleotide reduced (NADH) oxidation links the tricarboxylic acid (TCA) cycle with methionine metabolism and nuclear DNA methylation', *PLOS Biology*. Edited by R. Tian, 16(4), p. e2005707. Available at: https://doi.org/10.1371/journal.pbio.2005707.
581. Lu, J. *et al.* (2013) 'Effect of cholinergic signaling on neuronal cell bioenergetics', *Journal of Alzheimer's disease : JAD*, 33(4), pp. 1135–1146. Available at: https://doi.org/10.3233/JAD-2012-121822.
582. Lu, P. *et al.* (2011) 'Extracellular Matrix Degradation and Remodeling in Development and Disease', *Cold Spring Harbor Perspectives in Biology*, 3(12). Available at: https://doi.org/10.1101/CSHPERSPECT.A005058.
583. Luan, Yi *et al.* (2021) 'Structure and Function of Mitochondria-Associated Endoplasmic Reticulum Membranes (MAMs) and Their Role in Cardiovascular Diseases', *Oxidative Medicine and Cellular Longevity*, 2021. Available at: https://doi.org/10.1155/2021/4578809.
584. Ludikhuize, M.C. and Rodríguez Colman, M.J. (2021) 'Metabolic Regulation of Stem Cells and Differentiation: A Forkhead Box O Transcription Factor Perspective', *Antioxidants and Redox Signaling*, 34(13), pp. 1004–1024. Available at: https://doi.org/10.1089/ARS.2020.8126/ASSET/IMAGES/ARS.2020.8126_FIGURE6.JPG.

585. Lüdtke, T.H. *et al.* (2016) 'Tbx2 and Tbx3 Act Downstream of Shh to Maintain Canonical Wnt Signaling during Branching Morphogenesis of the Murine Lung', *Developmental Cell*, 39(2), pp. 239–253. Available at: https://doi.org/10.1016/J.DEVCEL.2016.08.007.
586. Luo, X. *et al.* (2019) 'Posttranslational regulation of PGC-1α and its implication in cancer metabolism', *International Journal of Cancer*, 145(6), p. 1475. Available at: https://doi.org/10.1002/IJC.32253.
587. Luo, Y. and Wang, Z. (2024) 'The Impact of Microglia on Neurodevelopment and Brain Function in Autism', *Biomedicines 2024, Vol. 12, Page 210*, 12(1), p. 210. Available at: https://doi.org/10.3390/BIOMEDICINES12010210.
588. Lurie, D.I. (2018) 'An Integrative Approach to Neuroinflammation in Psychiatric disorders and Neuropathic Pain.', *Journal of experimental neuroscience*, 12, p. 1179069518793639. Available at: https://doi.org/10.1177/1179069518793639.
589. Lv, S. yang *et al.* (2022) 'Review of lipoic acid: From a clinical therapeutic agent to various emerging biomaterials', *International Journal of Pharmaceutics*, 627, p. 122201. Available at: https://doi.org/10.1016/J.IJPHARM.2022.122201.
590. Ly, C.H., Lynch, G.S. and Ryall, J.G. (2020) 'A Metabolic Roadmap for Somatic Stem Cell Fate', *Cell Metabolism*, 31(6), pp. 1052–1067. Available at: https://doi.org/10.1016/J.CMET.2020.04.022.
591. Ma, L., Han, T. and Zhan, Y.A. (2024) 'Mechanism and role of mitophagy in the development of severe infection', *Cell Death Discovery 2024 10:1*, 10(1), pp. 1–13. Available at: https://doi.org/10.1038/s41420-024-01844-4.
592. Ma, X. and Wang, Q. (2022) 'Short-Chain Fatty Acids Attenuate Renal Fibrosis and Enhance Autophagy of Renal Tubular Cells in Diabetic Mice Through the HDAC2/ULK1 Axis', *Endocrinology and Metabolism*, 37(3), p. 432. Available at: https://doi.org/10.3803/ENM.2021.1336.
593. MacFabe, D.F. *et al.* (2007) 'Neurobiological effects of intraventricular propionic acid in rats: possible role of short chain fatty acids on the pathogenesis and characteristics of autism spectrum disorders', *Behavioural brain research*, 176(1), pp. 149–169. Available at: https://doi.org/10.1016/J.BBR.2006.07.025.
594. Macias, E. *et al.* (2014) 'Stat3 binds to mitochondrial DNA and regulates mitochondrial gene expression in keratinocytes', *The Journal of investigative dermatology*, 134(7), p. 1971. Available at: https://doi.org/10.1038/JID.2014.68.
595. Maffezzini, C. *et al.* (2020) 'Metabolic regulation of neurodifferentiation in the adult brain', *Cellular and Molecular Life Sciences*. Springer, pp. 2483–2496. Available at: https://doi.org/10.1007/s00018-019-03430-9.
596. Magdalon, J. *et al.* (2020) 'Complement System in Brain Architecture and Neurodevelopmental Disorders', *Frontiers in Neuroscience*, 0, p. 23. Available at: https://doi.org/10.3389/FNINS.2020.00023.
597. Mahony, C. and O'Ryan, C. (2021) 'Convergent canonical pathways in autism spectrum disorder from proteomic, transcriptomic and DNA methylation data', *International Journal of Molecular Sciences*, p. 10757. Available at: https://doi.org/10.3390/ijms221910757.
598. Mahony, C. and O'Ryan, C. (2022) 'A molecular framework for autistic experiences: Mitochondrial allostatic load as a mediator between autism and psychopathology', *Frontiers in Psychiatry*, 13, p. 2677. Available at: https://doi.org/10.3389/fpsyt.2022.985713.
599. Majcher-Maślanka, I. *et al.* (2017) 'The effects of early-life stress on dopamine system function in adolescent female rats', *International Journal of Developmental Neuroscience*, 57, pp. 24–33. Available at: https://doi.org/10.1016/J.IJDEVNEU.2017.01.001.
600. Makris, G. *et al.* (2021) 'Stress System Activation in Children and Adolescents With Autism Spectrum Disorder', *Frontiers in Neuroscience*, 15. Available at: https://doi.org/10.3389/FNINS.2021.756628.
601. Makris, G., Eleftheriades, A. and Pervanidou, P. (2022) 'Early Life Stress, Hormones, and Neurodevelopmental Disorders', *Hormone Research in Paediatrics*, pp. 1–8. Available at: https://doi.org/10.1159/000523942.
602. Maldonado, C., Vázquez, M. and Fagiolino, P. (2020) 'Potential Therapeutic Role of Carnitine and Acetylcarnitine in Neurological Disorders', *Current Pharmaceutical Design*, 26(12), pp. 1277–1285. Available at: https://doi.org/10.2174/1381612826666200212114038.
603. Malinovskaya, N.A. *et al.* (2018) 'Early Life Stress: Consequences for the Development of the Brain', *Neuroscience and Behavioral Physiology 2018 48:2*, 48(2), pp. 233–250. Available at: https://doi.org/10.1007/S11055-018-0557-9.
604. von der Malsburg, A. *et al.* (2023) 'Structural mechanism of mitochondrial membrane remodelling by human OPA1', *Nature 2023 620:7976*, 620(7976), pp. 1101–1108. Available at: https://doi.org/10.1038/s41586-023-06441-6.
605. Maly, I. V., Morales, M.J. and Pletnikov, M. V. (2021) 'Astrocyte Bioenergetics and Major Psychiatric Disorders', pp. 173–227. Available at: https://doi.org/10.1007/978-3-030-77375-5_9.

606. Manivasagam, T. *et al.* (2020) 'Role of Oxidative Stress and Antioxidants in Autism', *Advances in Neurobiology*, 24, pp. 193–206. Available at: https://doi.org/10.1007/978-3-030-30402-7_7.
607. Manoli, D.S. and State, M.W. (2021) 'Autism spectrum disorder genetics and the search for pathological mechanisms', *American Journal of Psychiatry*. American Psychiatric Association, pp. 30–38. Available at: https://doi.org/10.1176/appi.ajp.2020.20111608.
608. Manon-Jensen, T., Kjeld, N.G. and Karsdal, M.A. (2016) 'Collagen-mediated hemostasis', *Journal of Thrombosis and Haemostasis*, 14(3), pp. 438–448. Available at: https://doi.org/10.1111/JTH.13249.
609. Marchuk, H., Wang, Y., Ladd, Z.A., Chen, X. and Zhang, G.-F. (2023) 'Pathophysiological mechanisms of complications associated with propionic acidemia', *Pharmacology & Therapeutics*, 249, p. 108501. Available at: https://doi.org/10.1016/j.pharmthera.2023.108501.
610. Marchuk, H., Wang, Y., Ladd, Z.A., Chen, X. and Zhang, G.F. (2023) 'Pathophysiological mechanisms of complications associated with propionic acidemia', *Pharmacology & Therapeutics*, 249, p. 108501. Available at: https://doi.org/10.1016/J.PHARMTHERA.2023.108501.
611. Marotta, R. *et al.* (2020) 'The Neurochemistry of Autism', *Brain Sciences*, 10(3), pp. 1–18. Available at: https://doi.org/10.3390/brainsci10030163.
612. Martin, E.R., Gandawijaya, J. and Oguro-Ando, A. (2022) 'A novel method for generating glutamatergic SH-SY5Y neuron-like cells utilizing B-27 supplement', *Frontiers in Pharmacology*, 13, p. 943627. Available at: https://doi.org/10.3389/FPHAR.2022.943627/FULL.
613. Martin, H. *et al.* (2024) 'Review: Dopamine, Serotonin, and the Translational Neuroscience of Aggression in Autism Spectrum Disorder', *JAACAP Open* [Preprint]. Available at: https://doi.org/10.1016/J.JAACOP.2024.01.010.
614. Martin, S.A. *et al.* (2018) 'GSK3β Regulates Brain Energy Metabolism', *Cell Reports*, 23(7), pp. 1922-1931.e4. Available at: https://doi.org/10.1016/J.CELREP.2018.04.045.
615. Martínez-Palma, L. *et al.* (2019) 'Mitochondrial Modulation by Dichloroacetate Reduces Toxicity of Aberrant Glial Cells and Gliosis in the SOD1G93A Rat Model of Amyotrophic Lateral Sclerosis', *Neurotherapeutics*, 16(1), pp. 203–215. Available at: https://doi.org/10.1007/S13311-018-0659-7.
616. Martorana, F. *et al.* (2018) 'Differentiation by nerve growth factor (NGF) involves mechanisms of crosstalk between energy homeostasis and mitochondrial remodeling', *Cell Death & Disease 2018 9:3*, 9(3), pp. 1–16. Available at: https://doi.org/10.1038/s41419-018-0429-9.
617. Masini, E. *et al.* (2020) 'An Overview of the Main Genetic, Epigenetic and Environmental Factors Involved in Autism Spectrum Disorder Focusing on Synaptic Activity', *International Journal of Molecular Sciences*, 21(21), p. 8290. Available at: https://doi.org/10.3390/ijms21218290.
618. Masser, D.R. *et al.* (2016) 'Loss of the antioxidant enzyme CuZnSOD (Sod1) mimics an age-related increase in absolute mitochondrial DNA copy number in the skeletal muscle', *Age*, 38(4), pp. 323–333. Available at: https://doi.org/10.1007/s11357-016-9930-1.
619. Massrali, A. *et al.* (2019) 'Integrated genetic and methylomic analyses identify shared biology between autism and autistic traits', *Molecular Autism*, 10(1), p. 31. Available at: https://doi.org/10.1186/s13229-019-0279-z.
620. Mathew, S. and Joy, K.P. (2019) 'Monosodium Glutamate Triggers Neuroendocrine Stress Axis Leading to Apoptosis and Neural Progenitor Cell Activation', *The FASEB Journal*, 33(S1), pp. 554.1-554.1. Available at: https://doi.org/10.1096/FASEBJ.2019.33.1_SUPPLEMENT.554.1.
621. Matilainen, O., Quirós, P.M. and Auwerx, J. (2017) 'Mitochondria and Epigenetics – Crosstalk in Homeostasis and Stress', *Trends in Cell Biology*, 27(6), pp. 453–463. Available at: https://doi.org/10.1016/J.TCB.2017.02.004/ATTACHMENT/16FC8124-B18A-47FC-B21C-8E29EB1D97BA/MMC1.PDF.
622. Matrella, M.L. *et al.* (2024) 'High OXPHOS efficiency in RA-FUdr-differentiated SH-SY5Y cells: involvement of cAMP signalling and respiratory supercomplexes', *Scientific Reports 2024 14:1*, 14(1), pp. 1–18. Available at: https://doi.org/10.1038/s41598-024-57613-x.
623. May, K.S. and Den Hartigh, L.J. (2021) 'Modulation of Adipocyte Metabolism by Microbial Short-Chain Fatty Acids', *Nutrients 2021, Vol. 13, Page 3666*, 13(10), p. 3666. Available at: https://doi.org/10.3390/NU13103666.
624. Mayorga-Weber, G., Rivera, F.J. and Castro, M.A. (2022) 'Neuron-glia (mis)interactions in brain energy metabolism during aging', *Journal of Neuroscience Research* [Preprint]. Available at: https://doi.org/10.1002/JNR.25015.
625. McAvoy, K. and Kawamata, H. (2019) 'Glial mitochondrial function and dysfunction in health and neurodegeneration', *Molecular and Cellular Neuroscience*, 101, p. 103417. Available at: https://doi.org/10.1016/J.MCN.2019.103417.

626. McCracken, J.T. *et al.* (2021) 'Drug development for Autism Spectrum Disorder (ASD): Progress, challenges, and future directions', *European Neuropsychopharmacology*, 48, pp. 3–31. Available at: https://doi.org/10.1016/J.EURONEURO.2021.05.010.
627. Mehan, S. *et al.* (2020) 'Adenylate cyclase activator forskolin alleviates intracerebroventricular propionic acid-induced mitochondrial dysfunction of autistic rats', *Neural Regeneration Research*, 15(6), pp. 1140–1149. Available at: https://doi.org/10.4103/1673-5374.270316.
628. Meijering, E. *et al.* (2004) 'Design and Validation of a Tool for Neurite Tracing and Analysis in Fluorescence Microscopy Images', *Cytometry Part A*, 58(2), pp. 167–176. Available at: https://doi.org/10.1002/CYTO.A.20022.
629. Meiliana, A., Dewi, N.M. and Wijaya, A. (2021) 'Mitochondria: Master Regulator of Metabolism, Homeostasis, Stress, Aging and Epigenetics', *The Indonesian Biomedical Journal*, 13(3), pp. 221–41. Available at: https://doi.org/10.18585/INABJ.V13I3.1616.
630. Mekori-Domachevsky, E., Segal-Gavish, H. and Gross, R. (2019) 'Neuroinflammation and neuroprotection in schizophrenia and autism spectrum disorder', in *Neuroprotection in Autism, Schizophrenia and Alzheimer's disease*. Elsevier, pp. 101–122. Available at: https://doi.org/10.1016/B978-0-12-814037-6.00011-2.
631. Melchinger, P. and Garcia, B.M. (2023) 'Mitochondria are midfield players in steroid synthesis', *The International Journal of Biochemistry & Cell Biology*, 160, p. 106431. Available at: https://doi.org/10.1016/J.BIOCEL.2023.106431.
632. Melnyk, S. *et al.* (2012) 'Metabolic imbalance associated with methylation dysregulation and oxidative damage in children with autism', *Journal of Autism and Developmental Disorders*, 42(3), pp. 367–377. Available at: https://doi.org/10.1007/s10803-011-1260-7.
633. Mencio, C.P. *et al.* (2021) 'The Role of Chondroitin Sulfate Proteoglycans in Nervous System Development', *Journal of Histochemistry and Cytochemistry*, 69(1), p. 61. Available at: https://doi.org/10.1369/0022155420959147.
634. Mendrysa, S.M., Ghassemifar, S. and Malek, R. (2011) 'p53 in the CNS: Perspectives on Development, Stem Cells, and Cancer', *Genes & Cancer*, 2(4), p. 431. Available at: https://doi.org/10.1177/1947601911409736.
635. Mercatelli, D. *et al.* (2021) 'The transcriptome of sh-sy5y at single-cell resolution: A cite-seq data analysis workflow', *Methods and Protocols*, 4(2). Available at: https://doi.org/10.3390/mps4020028.
636. Mercer, P.F. and Chambers, R.C. (2013) 'Coagulation and coagulation signalling in fibrosis', *Biochimica et Biophysica Acta (BBA) - Molecular Basis of Disease*, 1832(7), pp. 1018–1027. Available at: https://doi.org/10.1016/J.BBADIS.2012.12.013.
637. Meyer, N. and Rinholm, J.E. (2021) 'Mitochondria in Myelinating Oligodendrocytes: Slow and Out of Breath?', *Metabolites 2021, Vol. 11, Page 359*, 11(6), p. 359. Available at: https://doi.org/10.3390/METABO11060359.
638. Michelhaugh, S.K., Guastella, A.R. and Mittal, S. (2015) 'Chapter 1: Overview of the kynurenine pathway of tryptophan metabolism', in *Targeting the Broadly Pathogenic Kynurenine Pathway*. Springer, Cham, pp. 3–9. Available at: https://doi.org/10.1007/978-3-319-11870-3_1.
639. Miglio, G., Rosa, A.C., *et al.* (2009) 'PPARγ stimulation promotes mitochondrial biogenesis and prevents glucose deprivation-induced neuronal cell loss', *Neurochemistry International*, 55(7), pp. 496–504. Available at: https://doi.org/10.1016/J.NEUINT.2009.05.001.
640. Miglio, G., Rattazzi, L., *et al.* (2009) 'PPARγ stimulation promotes neurite outgrowth in SH-SY5Y human neuroblastoma cells', *Neuroscience Letters*, 454(2), pp. 134–138. Available at: https://doi.org/10.1016/J.NEULET.2009.03.014.
641. Mihaylova, M.M. and Shaw, R.J. (2013) 'Metabolic reprogramming by class I and II histone deacetylases', *Trends in Endocrinology & Metabolism*, 24(1), pp. 48–57. Available at: https://doi.org/10.1016/J.TEM.2012.09.003.
642. Miller, K.E. and Suter, D.M. (2018) 'An integrated cytoskeletal model of neurite outgrowth', *Frontiers in Cellular Neuroscience*, 12. Available at: https://doi.org/10.3389/FNCEL.2018.00447.
643. Miller, K.N., Clark, J.P. and Anderson, R.M. (2019) 'Mitochondrial regulator PGC-1a—Modulating the modulator', *Current Opinion in Endocrine and Metabolic Research*, 5, pp. 37–44. Available at: https://doi.org/10.1016/j.coemr.2019.02.002.
644. Minghetti, L. *et al.* (2014) 'Nonenzymatic oxygenated metabolites of α-linolenic acid B1- and L1-phytoprostanes protect immature neurons from oxidant injury and promote differentiation of oligodendrocyte progenitors through PPAR-γ activation', *Free Radical Biology and Medicine*, 73, pp. 41–50. Available at: https://doi.org/10.1016/J.FREERADBIOMED.2014.04.025.
645. Mira, R.G. and Cerpa, W. (2020) 'Building a Bridge Between NMDAR-Mediated Excitotoxicity and Mitochondrial Dysfunction in Chronic and Acute Diseases', *Cellular and Molecular Neurobiology 2020 41:7*, 41(7), pp. 1413–1430. Available at: https://doi.org/10.1007/S10571-020-00924-0.

646. Mirza, R. and Sharma, B. (2018) 'Selective modulator of peroxisome proliferator-activated receptor-α protects propionic acid induced autism-like phenotypes in rats', *Life Sciences*, 214, pp. 106–117. Available at: https://doi.org/10.1016/J.LFS.2018.10.045.
647. Mirza, R. and Sharma, B. (2019) 'A selective peroxisome proliferator-activated receptor-γ agonist benefited propionic acid induced autism-like behavioral phenotypes in rats by attenuation of neuroinflammation and oxidative stress', *Chemico-Biological Interactions*, 311, p. 108758. Available at: https://doi.org/10.1016/J.CBI.2019.108758.
648. Mishra, A. *et al.* (2019) 'Dopamine receptor activation mitigates mitochondrial dysfunction and oxidative stress to enhance dopaminergic neurogenesis in 6-OHDA lesioned rats: A role of Wnt signalling', *Neurochemistry International*, 129, p. 104463. Available at: https://doi.org/10.1016/J.NEUINT.2019.104463.
649. Mitsopoulos, P. *et al.* (2015) 'Stomatin-like protein 2 is required for in vivo mitochondrial respiratory chain supercomplex formation and optimal cell function', *Molecular and cellular biology*, 35(10), pp. 1838–1847. Available at: https://doi.org/10.1128/MCB.00047-15.
650. Mocayar Marón, F.J. *et al.* (2019) 'Hypertension linked to allostatic load: from psychosocial stress to inflammation and mitochondrial dysfunction', *Stress*, 22(2), pp. 169–181. Available at: https://doi.org/10.1080/10253890.2018.1542683.
651. Mohammed Izham, A. *et al.* (2018) 'The Effect of DMEM and DMEM: F12 Culture Media on the Growth of SH-SY5Y Cells', *Life Sciences, Medicine and Biomedicine*, 2(3), p. 23. Available at: https://doi.org/10.28916/LSMB.2.3.2018.23.
652. Mohan, V., Edamakanti, C.R. and Pathak, A. (2023) 'Editorial: Role of extracellular matrix in neurodevelopment and neurodegeneration', *Frontiers in Cellular Neuroscience*, 17. Available at: https://doi.org/10.3389/FNCEL.2023.1135555.
653. Molina-Carballo, A., Jerez-Calero, A.E. and Muñoz-Hoyos, A. (2020) 'Possible Protective Role of Melatonin in Pediatric Infectious Diseases and Neurodevelopmental Pathologies', *Journal of Child Science*, 10(01), pp. e104–e109. Available at: https://doi.org/10.1055/s-0040-1716713.
654. Monné, M. *et al.* (2022) 'Mitochondrial transport and metabolism of the major methyl donor and versatile cofactor S-adenosylmethionine, and related diseases: A review†', *IUBMB Life*, 74(7), pp. 573–591. Available at: https://doi.org/10.1002/IUB.2658.
655. Montanari, M. *et al.* (2022) 'Autism Spectrum Disorder: Focus on Glutamatergic Neurotransmission', *International Journal of Molecular Sciences 2022, Vol. 23, Page 3861*, 23(7), p. 3861. Available at: https://doi.org/10.3390/IJMS23073861.
656. Mora-Romero, B. *et al.* (2024) 'Microglia mitochondrial complex I deficiency during development induces glial dysfunction and early lethality', *Nature Metabolism 2024 6:8*, 6(8), pp. 1479–1491. Available at: https://doi.org/10.1038/s42255-024-01081-0.
657. Morciano, G. *et al.* (2021) 'Mitochondrial OMA1 and OPA1 as Gatekeepers of Organellar Structure/Function and Cellular Stress Response.', *Frontiers in Cell and Developmental Biology*, 9, pp. 626117–626117. Available at: https://doi.org/10.3389/FCELL.2021.626117.
658. Mordaunt, C.E. *et al.* (2019) 'A meta-analysis of two high-risk prospective cohort studies reveals autism-specific transcriptional changes to chromatin, autoimmune, and environmental response genes in umbilical cord blood', *Molecular Autism*, 10(1), pp. 1–21. Available at: https://doi.org/10.1186/s13229-019-0287-z.
659. Mordaunt, C.E. *et al.* (2020) 'Cord blood DNA methylome in newborns later diagnosed with autism spectrum disorder reflects early dysregulation of neurodevelopmental and X-linked genes', *Genome Medicine 2020 12:1*, 12(1), pp. 1–25. Available at: https://doi.org/10.1186/S13073-020-00785-8.
660. Morgan, J.T. *et al.* (2010) 'Microglial activation and increased microglial density observed in the dorsolateral prefrontal cortex in autism', *Biological psychiatry*, 68(4), pp. 368–376. Available at: https://doi.org/10.1016/J.BIOPSYCH.2010.05.024.
661. Morrish, F. and Hockenbery, D. (2014) 'MYC and mitochondrial biogenesis.', *Cold Spring Harbor perspectives in medicine*, 4(5), p. 24789872. Available at: https://doi.org/10.1101/cshperspect.a014225.
662. Moseley, R.L. *et al.* (2024) 'Lifetime stressor exposure is related to suicidality in autistic adults: A multinational study', *https://doi.org/10.1177/13623613241299872* [Preprint]. Available at: https://doi.org/10.1177/13623613241299872.
663. Mosienko, V., Teschemacher, A.G. and Kasparov, S. (2015) 'Is L-lactate a novel signaling molecule in the brain?', *Journal of Cerebral Blood Flow and Metabolism*. Nature Publishing Group, pp. 1069–1075. Available at: https://doi.org/10.1038/jcbfm.2015.77.

664. Mposhi, A. and Turner, J.D. (2023) 'How can early life adversity still exert an effect decades later? A question of timing, tissues and mechanisms', *Frontiers in Immunology*, 14, p. 1215544. Available at: https://doi.org/10.3389/FIMMU.2023.1215544/BIBTEX.
665. Mulligan, K.A. and Cheyette, B.N.R. (2016) 'Neurodevelopmental Perspectives on Wnt Signaling in Psychiatry', *Molecular Neuropsychiatry*, 2(4), pp. 219–246. Available at: https://doi.org/10.1159/000453266.
666. Murase, S. *et al.* (2012) 'Loss of Signal Transducer and Activator of Transcription 3 (STAT3) Signaling during Elevated Activity Causes Vulnerability in Hippocampal Neurons', *Journal of Neuroscience*, 32(44), pp. 15511–15520. Available at: https://doi.org/10.1523/JNEUROSCI.2940-12.2012.
667. Murillo, J.R. *et al.* (2017) 'Quantitative proteomic analysis identifies proteins and pathways related to neuronal development in differentiated SH-SY5Y neuroblastoma cells', *EuPA Open Proteomics*, 16, p. 1. Available at: https://doi.org/10.1016/J.EUPROT.2017.06.001.
668. Muro, S. *et al.* (2001) 'Effect of PCCB Gene Mutations on the Heteromeric and Homomeric Assembly of Propionyl-CoA Carboxylase', *Molecular Genetics and Metabolism*, 74(4), pp. 476–483. Available at: https://doi.org/10.1006/MGME.2001.3254.
669. Murtaza, N. *et al.* (2022) 'Neuron-specific protein network mapping of autism risk genes identifies shared biological mechanisms and disease-relevant pathologies', *Cell Reports*, 41(8). Available at: https://doi.org/10.1016/J.CELREP.2022.111678.
670. Muscatello, R.A. *et al.* (2020) 'Exploring Key Physiological System Profiles at Rest and the Association with Depressive Symptoms in Autism Spectrum Disorder', *Journal of Autism and Developmental Disorders*, 51(1), pp. 15–29. Available at: https://doi.org/10.1007/S10803-020-04516-1/FIGURES/3.
671. Muscatello, R.A. and Corbett, B.A. (2018) 'Comparing the effects of age, pubertal development, and symptom profile on cortisol rhythm in children and adolescents with autism spectrum disorder', *Autism Research*, 11(1), pp. 110–120. Available at: https://doi.org/10.1002/AUR.1879.
672. Nabi, S.U. *et al.* (2022) 'Treatment of Autism Spectrum Disorders by Mitochondrial-targeted Drug: Future of Neurological Diseases Therapeutics', *Current Neuropharmacology*, 21(5), pp. 1042–1064. Available at: https://doi.org/10.2174/1570159X21666221121095618/CITE/REFWORKS.
673. Nagarajan, R.P. *et al.* (2006) 'Reduced MeCP2 expression is frequent in autism frontal cortex and correlates with aberrant MECP2 promoter methylation', *Epigenetics*, 1(4), pp. 172–182. Available at: https://doi.org/10.4161/epi.1.4.3514.
674. Naia, L. *et al.* (2021) 'Neuronal cell-based high-throughput screen for enhancers of mitochondrial function reveals luteolin as a modulator of mitochondria-endoplasmic reticulum coupling', *BMC biology*, 19(1). Available at: https://doi.org/10.1186/S12915-021-00979-5.
675. Nan, J. *et al.* (2017) 'TNFR2 Stimulation Promotes Mitochondrial Fusion via Stat3- and NF-kB-Dependent Activation of OPA1 Expression', *Circulation Research*, 121(4), pp. 392–410. Available at: https://doi.org/10.1161/CIRCRESAHA.117.311143/-/DC1.
676. Nangdev, P. *et al.* (2024) 'Exploring the Neurogenetic Landscape of Autism Spectrum Disorder: The Role of Brain-Derived Neurotrophic Factor (BDNF) Gene in the Complex Web of Neurodevelopment', *Journal of Health and Rehabilitation Research*, 4(2), pp. 233–238. Available at: https://doi.org/10.61919/JHRR.V4I2.792.
677. Nankova, B.B. *et al.* (2014) 'Enteric Bacterial Metabolites Propionic and Butyric Acid Modulate Gene Expression, Including CREB-Dependent Catecholaminergic Neurotransmission, in PC12 Cells - Possible Relevance to Autism Spectrum Disorders', *PLoS ONE*. Edited by Y. Tsuji, 9(8), p. e103740. Available at: https://doi.org/10.1371/journal.pone.0103740.
678. Nettis, M.A. and Pariante, C.M. (2020) 'Is there neuroinflammation in depression? Understanding the link between the brain and the peripheral immune system in depression', *International Review of Neurobiology*, 152, pp. 23–40. Available at: https://doi.org/10.1016/BS.IRN.2019.12.004.
679. Ngo, J. *et al.* (2023) ' Mitochondrial morphology controls fatty acid utilization by changing CPT1 sensitivity to malonyl-CoA ', *The EMBO Journal*, 42(11). Available at: https://doi.org/10.15252/EMBJ.2022111901/SUPPL_FILE/EMBJ2022111901-SUP-0003-TABLEEV2.PDF.
680. Nguyen, A. *et al.* (2010) 'Global methylation profiling of lymphoblastoid cell lines reveals epigenetic contributions to autism spectrum disorders and a novel autism candidate gene, RORA, whose protein product is reduced in autistic brain', *The FASEB Journal*, 24(8), pp. 3036–3051. Available at: https://doi.org/10.1096/FJ.10-154484.
681. Nguyen, N.H.T. *et al.* (2007) 'Propionate increases neuronal histone acetylation, but is metabolized oxidatively by glia. Relevance for propionic acidemia', *Journal of Neurochemistry* [Preprint]. Available at: https://doi.org/10.1111/j.1471-4159.2006.04397.x.

682. Ni, P., Ma, Y. and Chung, S. (2022) 'Mitochondrial dysfunction in psychiatric disorders', *Schizophrenia Research* [Preprint]. Available at: https://doi.org/10.1016/J.SCHRES.2022.08.027.
683. Nicolas, C.S. *et al.* (2013) 'The role of JAK-STAT signaling within the CNS', *JAK-STAT*, 2(1), p. e22925. Available at: https://doi.org/10.4161/JKST.22925.
684. von Niederhäusern, N. *et al.* (2019) 'Effects of radiofrequency electromagnetic field exposure on neuronal differentiation and mitochondrial function in SH-SY5Y cells', *Toxicology in Vitro*, 61, p. 104609. Available at: https://doi.org/10.1016/j.tiv.2019.104609.
685. Nisar, S. *et al.* (2022) 'Genetics of glutamate and its receptors in autism spectrum disorder', *Molecular Psychiatry 2022*, pp. 1–13. Available at: https://doi.org/10.1038/s41380-022-01506-w.
686. Nishida, Y. *et al.* (2008) 'Identification and classification of genes regulated by phosphatidylinositol 3-kinase- and TRKB-mediated signalling pathways during neuronal differentiation in two subtypes of the human neuroblastoma cell line SH-SY5Y', *BMC research notes*, 1. Available at: https://doi.org/10.1186/1756-0500-1-95.
687. Notarangelo, F.M. and Pocivavsek, A. (2017) 'Elevated kynurenine pathway metabolism during neurodevelopment: Implications for brain and behavior', *Neuropharmacology*. Elsevier Ltd, pp. 275–285. Available at: https://doi.org/10.1016/j.neuropharm.2016.03.001.
688. Nott, A. *et al.* (2016) 'Histone deacetylase 3 associates with MeCP2 to regulate FOXO and social behavior', *Nature neuroscience*, 19(11), pp. 1497–1505. Available at: https://doi.org/10.1038/NN.4347.
689. Novoseletskaya, E.S., Evdokimov, P.V. and Efimenko, A.Y. (2023) 'Extracellular matrix-induced signaling pathways in mesenchymal stem/stromal cells', *Cell Communication and Signaling*, 21(1), pp. 1–20. Available at: https://doi.org/10.1186/S12964-023-01252-8/FIGURES/5.
690. Nowinski, S.M. *et al.* (2020) 'Mitochondrial fatty acid synthesis coordinates oxidative metabolism in mammalian mitochondria', *eLife*, 9, pp. 1–35. Available at: https://doi.org/10.7554/ELIFE.58041.
691. Nyirenda, M.J. (2016) 'Non-communicable diseases in sub-Saharan Africa: understanding the drivers of the epidemic to inform intervention strategies', *International health*, 8(3), pp. 157–158. Available at: https://doi.org/10.1093/INTHEALTH/IHW021.
692. Oakley, B., Loth, E. and Murphy, D.G. (2021) 'Autism and mood disorders', *International Review of Psychiatry*. Taylor & Francis, pp. 280–299. Available at: https://doi.org/10.1080/09540261.2021.1872506.
693. Ogawa, S. *et al.* (2017) 'Associations of acute and chronic stress hormones with cognitive functions in autism spectrum disorder', *Neuroscience*, 343, pp. 229–239. Available at: https://doi.org/10.1016/J.NEUROSCIENCE.2016.12.003.
694. Ohta, K. ichi *et al.* (2020) 'The effects of early life stress on the excitatory/inhibitory balance of the medial prefrontal cortex', *Behavioural Brain Research*, 379, p. 112306. Available at: https://doi.org/10.1016/J.BBR.2019.112306.
695. Okada, N. *et al.* (2021) 'Reduced mitochondrial complex II activity enhances cell death via intracellular reactive oxygen species in STHdhQ111 striatal neurons with mutant huntingtin', *Journal of Pharmacological Sciences*, 147(4), pp. 367–375. Available at: https://doi.org/10.1016/J.JPHS.2021.09.001.
696. O'Neill Sarah, Irani Julia, Fodjo Siewe Nelson Joseph, Nono Denis, Abbo Catherine, Sato Yasuaki, Mugarura Augustine, Dolo Housseini, Ronse Maya, N.K.A. and C.R. (2019) 'SH SY5Y human neuroblastoma cell line : in vitro cell model of dopaminergic neurons in Parkinson's diseas', *medical Association publishing house*, pp. 35–44.
697. Orhon, I. and Reggiori, F. (2017) 'Assays to Monitor Autophagy Progression in Cell Cultures', *Cells 2017, Vol. 6, Page 20*, 6(3), p. 20. Available at: https://doi.org/10.3390/CELLS6030020.
698. Ornoy, A. *et al.* (2019) 'S-adenosyl methionine prevents ASD like behaviors triggered by early postnatal valproic acid exposure in very young mice', *Neurotoxicology and Teratology*, 71, pp. 64–74. Available at: https://doi.org/10.1016/J.NTT.2018.01.005.
699. Ornoy, A. *et al.* (2023) 'Gender specific neurobehavioral and gene expression changes in a valproic acid (VPA)–induced mouse model of autistic like behavior and correction by S-adenosylmethionine (SAMe)', *Sex, Gender, and Epigenetics: From Molecule to Bedside*, pp. 163–180. Available at: https://doi.org/10.1016/B978-0-12-823937-7.00024-9.
700. Ostendorf, F. *et al.* (2020) 'Propionic Acid and Fasudil as Treatment against Rotenone Toxicity in an In Vitro Model of Parkinson's Disease', *Molecules 2020, Vol. 25, Page 2502*, 25(11), p. 2502. Available at: https://doi.org/10.3390/MOLECULES25112502.
701. Oswald, L.M. *et al.* (2014) 'History of childhood adversity is positively associated with ventral striatal dopamine responses to amphetamine', *Psychopharmacology*, 231(12), pp. 2417–2433. Available at: https://doi.org/10.1007/S00213-013-3407-Z/FIGURES/5.

702. Ovejero-Benito, M.C. and Frade, J.M. (2013) 'Brain-derived neurotrophic factor-dependent cdk1 inhibition prevents G2/M progression in differentiating tetraploid neurons', *PloS one*, 8(5). Available at: https://doi.org/10.1371/JOURNAL.PONE.0064890.
703. ÖZ, A. (2019) 'Experimental cell culture models for investigating neurodegenerative diseases', *Journal of Cellular Neuroscience and Oxidative Stress*, 11(2), pp. 835–851. Available at: https://doi.org/10.37212/jcnos.683400.
704. Özar, T. *et al.* (2024) 'HN1 is a novel dedifferentiation factor involved in regulating the cell cycle and microtubules in SH-SY5Y neuroblastoma cells', *Journal of Cellular Biochemistry* [Preprint]. Available at: https://doi.org/10.1002/JCB.30569.
705. Ozgen, S. *et al.* (2022) 'Significance of mitochondrial activity in neurogenesis and neurodegenerative diseases', *Neural Regeneration Research*, 17(4), pp. 741–747. Available at: https://doi.org/10.4103/1673-5374.322429.
706. Pace, T.W.W. and Miller, A.H. (2009) 'Cytokines and Glucocorticoid Receptor Signaling: Relevance to Major Depression', *Annals of the New York Academy of Sciences*, 1179, p. 86. Available at: https://doi.org/10.1111/J.1749-6632.2009.04984.X.
707. Pahlman, S. *et al.* (1990) 'Human neuroblastoma cells in culture: A model for neuronal cell differentiation and function', in *Acta Physiologica Scandinavica, Supplement*, pp. 25–37. Available at: https://pubmed.ncbi.nlm.nih.gov/2267941/ (Accessed: 5 August 2022).
708. Pandey, A. *et al.* (2022) 'Studies on Regulation of Global Protein Profile and Cellular Bioenergetics of Differentiating SH-SY5Y Cells', *Molecular Neurobiology*, 59(3), pp. 1799–1818. Available at: https://doi.org/10.1007/s12035-021-02667-5.
709. Pangrazzi, L., Balasco, L. and Bozzi, Y. (2020) 'Oxidative Stress and Immune System Dysfunction in Autism Spectrum Disorders', *International Journal of Molecular Sciences 2020, Vol. 21, Page 3293*, 21(9), p. 3293. Available at: https://doi.org/10.3390/IJMS21093293.
710. Pani, G. *et al.* (2014) 'MorphoNeuroNet: An automated method for dense neurite network analysis', *Cytometry Part A*, 85(2), pp. 188–199. Available at: https://doi.org/10.1002/CYTO.A.22408.
711. Papadopoli, D., Pollak, M. and Topisirovic, I. (2021) 'The role of GSK3 in metabolic pathway perturbations in cancer', *Biochimica et Biophysica Acta (BBA) - Molecular Cell Research*, 1868(8), p. 119059. Available at: https://doi.org/10.1016/J.BBAMCR.2021.119059.
712. Papageorgiou, M.P. and Filiou, M.D. (2024) 'Mitochondrial dynamics and psychiatric disorders: The missing link', *Neuroscience & Biobehavioral Reviews*, 165, p. 105837. Available at: https://doi.org/10.1016/J.NEUBIOREV.2024.105837.
713. Parganlija, D. *et al.* (2014) 'Loss of PINK1 Impairs Stress-Induced Autophagy and Cell Survival', *PLOS ONE*, 9(4), p. e95288. Available at: https://doi.org/10.1371/JOURNAL.PONE.0095288.
714. Park, H.S. *et al.* (2020) 'Sodium propionate exerts anticancer effect in mice bearing breast cancer cell xenograft by regulating JAK2/STAT3/ROS/p38 MAPK signaling', *Acta Pharmacologica Sinica 2020 42:8*, 42(8), pp. 1311–1323. Available at: https://doi.org/10.1038/s41401-020-00522-2.
715. Park, J. *et al.* (2013) 'Mitochondrial dynamics modulate the expression of pro-inflammatory mediators in microglial cells', *Journal of Neurochemistry*, 127(2), pp. 221–232. Available at: https://doi.org/10.1111/JNC.12361.
716. Park, J. *et al.* (2022) 'The role of histone modifications: from neurodevelopment to neurodiseases', *Signal Transduction and Targeted Therapy 2022 7:1*, 7(1), pp. 1–23. Available at: https://doi.org/10.1038/s41392-022-01078-9.
717. Park, K.C. *et al.* (2020) 'Cardiac Complications of Propionic and Other Inherited Organic Acidemias', *Frontiers in Cardiovascular Medicine*, 7, p. 617451. Available at: https://doi.org/10.3389/FCVM.2020.617451/BIBTEX.
718. Park, K.C. *et al.* (2023) 'Disrupted propionate metabolism evokes transcriptional changes in the heart by increasing histone acetylation and propionylation', *Nature Cardiovascular Research 2023 2:12*, 2(12), pp. 1221–1245. Available at: https://doi.org/10.1038/s44161-023-00365-0.
719. Park, S.J. *et al.* (2015) 'Heterogeneous nuclear ribonucleoprotein A1 post-transcriptionally regulates Drp1 expression in neuroblastoma cells', *Biochimica et Biophysica Acta (BBA) - Gene Regulatory Mechanisms*, 1849(12), pp. 1423–1431. Available at: https://doi.org/10.1016/J.BBAGRM.2015.10.017.
720. Patergnani, S. *et al.* (2021) 'Methods to Monitor Mitophagy and Mitochondrial Quality: Implications in Cancer, Neurodegeneration, and Cardiovascular Diseases', *Methods in Molecular Biology*, 2310, pp. 113–159. Available at: https://doi.org/10.1007/978-1-0716-1433-4_9/FIGURES/12.
721. Păun, O. *et al.* (2023) 'Pioneer factor ASCL1 cooperates with the mSWI/SNF complex at distal regulatory elements to regulate human neural differentiation', *Genes and Development*, 37(5–6), pp. 218–242. Available at: https://doi.org/10.1101/GAD.350269.122/-/DC1.

722. Pavăl, D. (2023) 'The dopamine hypothesis of autism spectrum disorder: A comprehensive analysis of the evidence', *International Review of Neurobiology*, 173, pp. 1–42. Available at: https://doi.org/10.1016/BS.IRN.2023.08.009.
723. Pecorelli, A. *et al.* (2020) 'Alterations of mitochondrial bioenergetics, dynamics, and morphology support the theory of oxidative damage involvement in autism spectrum disorder', *FASEB Journal*, 34(5), pp. 6521–6538. Available at: https://doi.org/10.1096/fj.201902677R.
724. Pérez-Cerdá, C. *et al.* (2003) 'Functional analysis of PCCB mutations causing propionic acidemia based on expression studies in deficient human skin fibroblasts', *Biochimica et Biophysica Acta (BBA) - Molecular Basis of Disease*, 1638(1), pp. 43–49. Available at: https://doi.org/10.1016/S0925-4439(03)00039-5.
725. Pérez-Hernández, C.A. *et al.* (2022) 'Mitochondrial Ultrastructure and Activity Are Differentially Regulated by Glycolysis-, Krebs Cycle-, and Microbiota-Derived Metabolites in Monocytes', *Biology 2022, Vol. 11, Page 1132*, 11(8), p. 1132. Available at: https://doi.org/10.3390/BIOLOGY11081132.
726. Pérez-Rodríguez, D.R., Blanco-Luquin, I. and Mendioroz, M. (2021) 'The Participation of Microglia in Neurogenesis: A Review', *Brain Sciences 2021, Vol. 11, Page 658*, 11(5), p. 658. Available at: https://doi.org/10.3390/BRAINSCI11050658.
727. Pernas, L. and Scorrano, L. (2016) 'Mito-Morphosis: Mitochondrial Fusion, Fission, and Cristae Remodeling as Key Mediators of Cellular Function', *Annual Review of Physiology*, 78(Volume 78, 2016), pp. 505–531. Available at: https://doi.org/10.1146/ANNUREV-PHYSIOL-021115-105011/1.
728. Perry, R.J. *et al.* (2016) 'Propionate increases hepatic pyruvate cycling and anaplerosis and alters mitochondrial metabolism', *Journal of Biological Chemistry*, 291(23), pp. 12161–12170. Available at: https://doi.org/10.1074/jbc.M116.720631.
729. Perry, S.W. *et al.* (2011) 'Mitochondrial membrane potential probes and the proton gradient: a practical usage guide', *BioTechniques*, 50(2), p. 98. Available at: https://doi.org/10.2144/000113610.
730. Petrelli, F., Pucci, L. and Bezzi, P. (2016) 'Astrocytes and microglia and their potential link with autism spectrum disorders', *Frontiers in Cellular Neuroscience*, 10(FEB). Available at: https://doi.org/10.3389/fncel.2016.00021.
731. Petrolini, V., Rodríguez-Armendariz, E. and Vicente, A. (2023) 'Autistic camouflaging across the spectrum', *New Ideas in Psychology*, 68. Available at: https://doi.org/10.1016/J.NEWIDEAPSYCH.2022.100992.
732. Pezzini, F. *et al.* (2017) 'Transcriptomic Profiling Discloses Molecular and Cellular Events Related to Neuronal Differentiation in SH-SY5Y Neuroblastoma Cells', *Cellular and Molecular Neurobiology*, 37(4), pp. 665–682. Available at: https://doi.org/10.1007/S10571-016-0403-Y/FIGURES/7.
733. Pham, C.H. *et al.* (2021) 'Anticancer Effects of Propionic Acid Inducing Cell Death in Cervical Cancer Cells', *Molecules*, 26(16). Available at: https://doi.org/10.3390/MOLECULES26164951.
734. Pham, T.H. *et al.* (2020) 'STAT3 and p53: Dual Target for Cancer Therapy', *Biomedicines*, 8(12), pp. 1–24. Available at: https://doi.org/10.3390/BIOMEDICINES8120637.
735. Piazza, A., Carlone, R. and Spencer, G.E. (2024) 'Non-canonical retinoid signaling in neural development, regeneration and synaptic function', *Frontiers in Molecular Neuroscience*, 17, p. 1371135. Available at: https://doi.org/10.3389/FNMOL.2024.1371135/BIBTEX.
736. Picard, M. *et al.* (2015) 'Mitochondrial functions modulate neuroendocrine, metabolic, inflammatory, and transcriptional responses to acute psychological stress', *Proceedings of the National Academy of Sciences of the United States of America*, 112(48), pp. E6614–E6623. Available at: https://doi.org/10.1073/PNAS.1515733112.
737. Picard, M. *et al.* (2018) 'An energetic view of stress: Focus on mitochondria', *Frontiers in Neuroendocrinology*, 49, pp. 72–85. Available at: https://doi.org/10.1016/J.YFRNE.2018.01.001.
738. Picard, M., Juster, R.-P. and McEwen, B.S. (2014) 'Mitochondrial allostatic load puts the "gluc" back in glucocorticoids', *Nature Reviews Endocrinology*, 10(5), pp. 303–310. Available at: https://doi.org/10.1038/nrendo.2014.22.
739. Picard, M. and McEwen, B.S. (2018a) 'Psychological Stress and Mitochondria: A Conceptual Framework', *Psychosomatic medicine*, 80(2), p. 126. Available at: https://doi.org/10.1097/PSY.0000000000000544.
740. Picard, M. and McEwen, B.S. (2018b) 'Psychological Stress and Mitochondria: A Systematic Review', *Psychosomatic medicine*, 80(2), p. 141. Available at: https://doi.org/10.1097/PSY.0000000000000545.
741. Picard, M., Trumpff, C. and Burelle, Y. (2019) 'Mitochondrial psychobiology: foundations and applications', *Current Opinion in Behavioral Sciences*, 28, pp. 142–151. Available at: https://doi.org/10.1016/j.cobeha.2019.04.015.
742. Picard, M., Wallace, D.C. and Burelle, Y. (2016) 'The rise of mitochondria in medicine', *Mitochondrion*, 30, pp. 105–116. Available at: https://doi.org/10.1016/J.MITO.2016.07.003.

743. Picca, A. and Lezza, A.M.S. (2015) 'Regulation of mitochondrial biogenesis through TFAM–mitochondrial DNA interactions: Useful insights from aging and calorie restriction studies', *Mitochondrion*, 25, pp. 67–75. Available at: https://doi.org/10.1016/J.MITO.2015.10.001.
744. Pinho, S.A. *et al.* (2022) 'Mitochondrial and metabolic remodelling in human skin fibroblasts in response to glucose availability', *The FEBS journal*, 289(17), pp. 5198–5217. Available at: https://doi.org/10.1111/FEBS.16413.
745. Pintacuda, G. *et al.* (2023) 'Protein interaction studies in human induced neurons indicate convergent biology underlying autism spectrum disorders', *Cell Genomics*, 3(3). Available at: https://doi.org/10.1016/J.XGEN.2022.100250/ASSET/B9DF9A32-ED35-4C2C-8FDC-BAB123AEE811/MAIN.ASSETS/GR4_LRG.JPG.
746. Piras, C. *et al.* (2022) 'Alteration of the Intestinal Permeability Are Reflected by Changes in the Urine Metabolome of Young Autistic Children : Preliminary Results'.
747. Polat, T. *et al.* (2024) 'Autism spectrum disorder (ASD) diagnosis: A biochemical investigation into the diagnostic utility of S-adenosylmethionine (SAM), S-adenosylhomocysteine (SAH) levels and the SAM/SAH ratio', *Research in Autism Spectrum Disorders*, 117, p. 102464. Available at: https://doi.org/10.1016/J.RASD.2024.102464.
748. Pompili, M. *et al.* (2010) 'The hypothalamic-pituitary-adrenal axis and serotonin abnormalities: a selective overview for the implications of suicide prevention', *European Archives of Psychiatry and Clinical Neuroscience 2010 260:8*, 260(8), pp. 583–600. Available at: https://doi.org/10.1007/S00406-010-0108-Z.
749. Pradhan, P. *et al.* (2020) 'Enhanced accumulation of reduced glutathione by Scopoletin improves survivability of dopaminergic neurons in Parkinson's model', *Cell Death & Disease 2020 11:9*, 11(9), pp. 1–11. Available at: https://doi.org/10.1038/s41419-020-02942-8.
750. Prado, A. *et al.* (2015) 'A trivalent approach for determining in vitro toxicology: Examination of oxime K027', *Journal of Applied Toxicology*, 35(2), pp. 219–227. Available at: https://doi.org/10.1002/jat.3013.
751. Prajapati, A., Mehan, S. and Khan, Z. (2023) 'The role of Smo-Shh/Gli signaling activation in the prevention of neurological and ageing disorders', *Biogerontology*, 24(4), pp. 493–531. Available at: https://doi.org/10.1007/S10522-023-10034-1/TABLES/2.
752. Prasad, R. *et al.* (2014) 'Oxidative stress and adrenocortical insufficiency', *Journal of Endocrinology*, 221(3), pp. R63–R73. Available at: https://doi.org/10.1530/JOE-13-0346.
753. Prieto, J. *et al.* (2018) 'MYC Induces a Hybrid Energetics Program Early in Cell Reprogramming', *Stem Cell Reports*, 11(6), pp. 1479–1492. Available at: https://doi.org/10.1016/j.stemcr.2018.10.018.
754. Prosperi, M. *et al.* (2022) 'Interventions on Microbiota: Where Do We Stand on a Gut–Brain Link in Autism? A Systematic Review', *Nutrients 2022, Vol. 14, Page 462*, 14(3), p. 462. Available at: https://doi.org/10.3390/NU14030462.
755. Prozorovski, T. *et al.* (2015) 'Redox-regulated fate of neural stem progenitor cells', *Biochimica et Biophysica Acta (BBA) - General Subjects*, 1850(8), pp. 1543–1554. Available at: https://doi.org/10.1016/j.bbagen.2015.01.022.
756. Pruessner, J.C. *et al.* (2004) 'Dopamine Release in Response to a Psychological Stress in Humans and Its Relationship to Early Life Maternal Care: A Positron Emission Tomography Study Using [11C]Raclopride', *Journal of Neuroscience*, 24(11), pp. 2825–2831. Available at: https://doi.org/10.1523/JNEUROSCI.3422-03.2004.
757. Qiao, J. *et al.* (2012) 'PI3K/AKT AND ERK REGULATE RETINOIC ACID-INDUCED NEUROBLASTOMA CELLULAR DIFFERENTIATION', *Biochemical and biophysical research communications*, 424(3), p. 421. Available at: https://doi.org/10.1016/J.BBRC.2012.06.125.
758. Qin, C. *et al.* (2022) 'STOML2 Restricts Mitophagy and Increases Chemosensitivity in Pancreatic Cancer through Stabilizing PARL-induced PINK1 degradation'. Available at: https://doi.org/10.21203/RS.3.RS-1952708/V1.
759. Qin, J.-J. *et al.* (2018) 'Inhibiting β-Catenin by β-Carboline-Type MDM2 Inhibitor for Pancreatic Cancer Therapy', *Frontiers in Pharmacology*, 9(JAN), p. 5. Available at: https://doi.org/10.3389/FPHAR.2018.00005.
760. Qin, L., Dai, X. and Yin, Y. (2016) 'Valproic acid exposure sequentially activates Wnt and mTOR pathways in rats', *Molecular and Cellular Neuroscience*, 75, pp. 27–35. Available at: https://doi.org/10.1016/j.mcn.2016.06.004.
761. Qu, H. *et al.* (2019) 'STOML2 as a novel prognostic biomarker modulates cell proliferation, motility and chemo-sensitivity via IL6-Stat3 pathway in head and neck squamous cell carcinoma', *American Journal of Translational Research*, 11(2), p. 683. Available at: /pmc/articles/PMC6413287/ (Accessed: 16 June 2024).
762. Quarta, C. *et al.* (2019) 'Functional identity of hypothalamic melanocortin neurons depends on Tbx3', *Nature Metabolism*, 1(2), pp. 222–235. Available at: https://doi.org/10.1038/s42255-018-0028-1.

763. Quintana-Cabrera, R. and Scorrano, L. (2023) 'Determinants and outcomes of mitochondrial dynamics', *Molecular Cell*, 83(6), pp. 857–876. Available at: https://doi.org/10.1016/J.MOLCEL.2023.02.012.
764. Quiros, P.M. *et al.* (2017) 'Analysis of mtDNA/nDNA Ratio in Mice', *Current Protocols in Mouse Biology*, 7(1), pp. 47–54. Available at: https://doi.org/10.1002/cpmo.21.
765. Rabaneda, L.G. *et al.* (2016) 'Altered regulation of the Spry2/Dyrk1A/PP2A triad by homocysteine impairs neural progenitor cell proliferation', *Biochimica et Biophysica Acta (BBA) - Molecular Cell Research*, 1863(12), pp. 3015–3026. Available at: https://doi.org/10.1016/J.BBAMCR.2016.09.018.
766. Radogna, F. *et al.* (2021) 'Assessment of Mitochondrial Cell Metabolism by Respiratory Chain Electron Flow Assays', *Methods in Molecular Biology*, 2276, pp. 129–141. Available at: https://doi.org/10.1007/978-1-0716-1266-8_9/FIGURES/5.
767. Rahi, S. *et al.* (2021) 'Smo-Shh signaling activator purmorphamine ameliorates neurobehavioral, molecular, and morphological alterations in an intracerebroventricular propionic acid-induced experimental model of autism', *Human and Experimental Toxicology*, 40(11), pp. 1880–1898. Available at: https://doi.org/10.1177/09603271211013456/ASSET/IMAGES/10.1177_09603271211013456-IMG1.PNG.
768. Rahman, M.H. and Suk, K. (2020) 'Mitochondrial Dynamics and Bioenergetic Alteration During Inflammatory Activation of Astrocytes', *Frontiers in Aging Neuroscience*. Frontiers Media S.A., p. 459. Available at: https://doi.org/10.3389/fnagi.2020.614410.
769. Rahman, M.R. *et al.* (2020) 'Comprehensive analysis of rna-seq gene expression profiling of brain transcriptomes reveals novel genes, regulators, and pathways in autism spectrum disorder', *Brain Sciences*, 10(10), pp. 1–16. Available at: https://doi.org/10.3390/brainsci10100747.
770. Raj, N. and Bam, R. (2019) 'Reciprocal Crosstalk Between YAP1/Hippo Pathway and the p53 Family Proteins: Mechanisms and Outcomes in Cancer', *Frontiers in Cell and Developmental Biology*, 7, p. 458337. Available at: https://doi.org/10.3389/FCELL.2019.00159/BIBTEX.
771. Ramaswami, G. *et al.* (2020) 'Integrative genomics identifies a convergent molecular subtype that links epigenomic with transcriptomic differences in autism', *Nature Communications*, 11(1), pp. 1–14. Available at: https://doi.org/10.1038/s41467-020-18526-1.
772. Ramesh, V. *et al.* (2023) 'Propionate reinforces epithelial identity and reduces aggressiveness of lung carcinoma', *EMBO molecular medicine*, 15(12). Available at: https://doi.org/10.15252/EMMM.202317836.
773. Rangasamy, S., D'Mello, S.R. and Narayanan, V. (2013) 'Epigenetics, Autism Spectrum, and Neurodevelopmental Disorders', *Neurotherapeutics*, 10(4), pp. 742–756. Available at: https://doi.org/10.1007/S13311-013-0227-0.
774. Razazan, A. *et al.* (2021) 'Activation of Microbiota Sensing – Free Fatty Acid Receptor 2 Signaling Ameliorates Amyloid-β Induced Neurotoxicity by Modulating Proteolysis-Senescence Axis', *Frontiers in Aging Neuroscience*, 13, p. 735933. Available at: https://doi.org/10.3389/FNAGI.2021.735933/BIBTEX.
775. Razi, B. *et al.* (2020) 'Association between MTHFR gene polymorphism and susceptibility to autism spectrum disorders: Systematic review and meta-analysis', *Research in Autism Spectrum Disorders*, 70, p. 101473. Available at: https://doi.org/10.1016/J.RASD.2019.101473.
776. Redmann, M. *et al.* (2018) 'Methods for assessing mitochondrial quality control mechanisms and cellular consequences in cell culture', *Redox Biology*, 17, pp. 59–69. Available at: https://www.sciencedirect.com/science/article/pii/S2213231718301307 (Accessed: 20 June 2019).
777. Revuelta, M. *et al.* (2020) 'Glial Factors Regulating White Matter Development and Pathologies of the Cerebellum', *Neurochemical Research*, 45(3), pp. 643–655. Available at: https://doi.org/10.1007/s11064-020-02961-z.
778. Rharass, T. *et al.* (2014) 'Ca2+-mediated mitochondrial reactive oxygen species metabolism augments Wnt/β-catenin pathway activation to facilitate cell differentiation', *The Journal of biological chemistry*, 289(40), pp. 27937–27951. Available at: https://doi.org/10.1074/JBC.M114.573519.
779. Ribeiro, M.F. *et al.* (2020) 'Diet-dependent gut microbiota impacts on adult neurogenesis through mitochondrial stress modulation', *Brain Communications*, 2(2). Available at: https://doi.org/10.1093/BRAINCOMMS/FCAA165.
780. Ridout, K.K., Khan, M. and Ridout, S.J. (2018) 'Adverse Childhood Experiences Run Deep: Toxic Early Life Stress, Telomeres, and Mitochondrial DNA Copy Number, the Biological Markers of Cumulative Stress', *BioEssays*, 40(9), p. 1800077. Available at: https://doi.org/10.1002/BIES.201800077.
781. Riegerová, P. *et al.* (2021) 'Expression and Localization of AβPP in SH-SY5Y Cells Depends on Differentiation State', *Journal of Alzheimer's Disease*, 82(2), pp. 485–491. Available at: https://doi.org/10.3233/JAD-201409.

782. Ristori, M.V. *et al.* (2020) 'Proteomics and Metabolomics Approaches towards a Functional Insight onto AUTISM Spectrum Disorders: Phenotype Stratification and Biomarker Discovery', *International Journal of Molecular Sciences 2020, Vol. 21, Page 6274*, 21(17), p. 6274. Available at: https://doi.org/10.3390/IJMS21176274.
783. Roberts, R.F. *et al.* (2016) 'Defending the mitochondria: The pathways of mitophagy and mitochondrial-derived vesicles', *The International Journal of Biochemistry & Cell Biology*, 79, pp. 427–436. Available at: https://doi.org/10.1016/J.BIOCEL.2016.07.020.
784. Rodnyy, A.Y. *et al.* (2024) 'The brain serotonin system in autism', *Reviews in the Neurosciences*, 35(1), pp. 1–20. Available at: https://doi.org/10.1515/REVNEURO-2023-0055/XML.
785. Rodrigues, D.C. *et al.* (2020) 'Methylglyoxal couples metabolic and translational control of Notch signalling in mammalian neural stem cells', *Nature Communications 2020 11:1*, 11(1), pp. 1–13. Available at: https://doi.org/10.1038/s41467-020-15941-2.
786. Roginski, A.C. *et al.* (2020) 'Disturbance of bioenergetics and calcium homeostasis provoked by metabolites accumulating in propionic acidemia in heart mitochondria of developing rats', *Biochimica et Biophysica Acta (BBA) - Molecular Basis of Disease*, 1866(5), p. 165682. Available at: https://doi.org/10.1016/J.BBADIS.2020.165682.
787. Rose, J. *et al.* (2017) 'Mitochondrial dysfunction in glial cells: Implications for neuronal homeostasis and survival', *Toxicology*, 391, pp. 109–115. Available at: /pmc/articles/PMC5681369/?report=abstract (Accessed: 19 August 2020).
788. Rose, S. *et al.* (2018) 'Clinical and Molecular Characteristics of Mitochondrial Dysfunction in Autism Spectrum Disorder', *Molecular Diagnosis and Therapy*. Springer International Publishing, pp. 571–593. Available at: https://doi.org/10.1007/s40291-018-0352-x.
789. Rosen, N.E., Lord, C. and Volkmar, F.R. (2021) 'The Diagnosis of Autism: From Kanner to DSM-III to DSM-5 and Beyond', *Journal of Autism and Developmental Disorders 2021 51:12*, 51(12), pp. 4253–4270. Available at: https://doi.org/10.1007/S10803-021-04904-1.
790. Rossignol and Frye (2021a) 'Cerebral folate deficiency, folate receptor alpha autoantibodies and leucovorin (Folinic acid) treatment in autism spectrum disorders: A systematic review and meta-analysis', *Journal of Personalized Medicine*, 11(11), p. 1141. Available at: https://doi.org/10.3390/JPM11111141/S1.
791. Rossignol and Frye (2021b) 'The effectiveness of cobalamin (B12) treatment for autism spectrum disorder: A systematic review and meta-analysis', *Journal of Personalized Medicine*, 11(8), p. 784. Available at: https://doi.org/10.3390/JPM11080784/S1.
792. Rosso, S.B. and Inestrosa, N.C. (2013) 'WNT signaling in neuronal maturation and synaptogenesis', *Frontiers in Cellular Neuroscience*, 7(JUNE). Available at: https://doi.org/10.3389/FNCEL.2013.00103.
793. Rothfuss, O., Gasser, T. and Patenge, N. (2010) 'Analysis of differential DNA damage in the mitochondrial genome employing a semi-long run real-time PCR approach', *Nucleic Acids Research*, 38(4), pp. e24–e24. Available at: https://doi.org/10.1093/nar/gkp1082.
794. Sabnis, H.S., Somasagara, R.R. and Bunting, K.D. (2017) 'Targeting MYC Dependence by Metabolic Inhibitors in Cancer', *Genes 2017, Vol. 8, Page 114*, 8(4), p. 114. Available at: https://doi.org/10.3390/GENES8040114.
795. Sabouny, R. and Shutt, T.E. (2021) 'The role of mitochondrial dynamics in mtDNA maintenance', *Journal of Cell Science*, 134(24). Available at: https://doi.org/10.1242/jcs.258944.
796. Şahin, M. *et al.* (2021) 'Transformation of SH-SY5Y cell line into neuron-like cells: Investigation of electrophysiological and biomechanical changes', *Neuroscience Letters*, 745. Available at: https://doi.org/10.1016/J.NEULET.2021.135628.
797. Sahle, B.W. *et al.* (2021) 'The association between adverse childhood experiences and common mental disorders and suicidality: an umbrella review of systematic reviews and meta-analyses', *European Child and Adolescent Psychiatry*, 1, pp. 1–11. Available at: https://doi.org/10.1007/S00787-021-01745-2/TABLES/3.
798. Sahu, M.R. and Mondal, A.C. (2021) 'Neuronal Hippo signaling: From development to diseases', *Developmental Neurobiology*, 81(2), pp. 92–109. Available at: https://doi.org/10.1002/DNEU.22796.
799. Saikachain, N. *et al.* (2023) 'Neuroprotective effect of short-chain fatty acids against oxidative stress-induced SH-SY5Y injury via GPR43-dependent pathway', *Journal of Neurochemistry*, 166(2), pp. 201–214. Available at: https://doi.org/10.1111/JNC.15827.
800. Saito, A. *et al.* (2018) 'Neuronal activity-dependent local activation of dendritic unfolded protein response promotes expression of brain-derived neurotrophic factor in cell soma', *Journal of Neurochemistry*, 144(1), p. 35. Available at: https://doi.org/10.1111/JNC.14221.
801. Sakagami, H. *et al.* (2017) 'Re-evaluation of Culture Condition of PC12 and SH-SY5Y Cells Based on Growth Rate and Amino Acid Consumption.', *In Vivo*, 31(6), pp. 1089–1095. Available at: https://doi.org/10.21873/INVIVO.11174.

802. Sakuma, T. *et al.* (2024) 'Monocarboxylate Transporters 1 and 2 Are Responsible for L-Lactate Uptake in Differentiated Human Neuroblastoma SH-SY5Y Cells', *Biological and Pharmaceutical Bulletin*, 47(4), pp. 764–770. Available at: https://doi.org/10.1248/BPB.B23-00860.
803. Salinas, R.D., Connolly, D.R. and Song, H. (2020) 'Epigenetics in Neurodevelopment', *Neuropathology and applied neurobiology*, 46(1), p. 6. Available at: https://doi.org/10.1111/NAN.12608.
804. Samadi, S.A. (2022) 'Overview of Services for Autism Spectrum Disorders (ASD) in Low- and Middle-Income Countries (LMICs) and among Immigrants and Minority Groups in High-Income Countries (HICs)', *Brain Sciences 2022, Vol. 12, Page 1682*, 12(12), p. 1682. Available at: https://doi.org/10.3390/BRAINSCI12121682.
805. Sampaio, A.C. *et al.* (2021) 'Association of the Maternal Folic Acid Supplementation with the Autism Spectrum Disorder: A Systematic Review', *Revista Brasileira de Ginecologia e Obstetricia*, 43(10), pp. 775–781. Available at: https://doi.org/10.1055/S-0041-1736298/ID/JR200415-20/BIB.
806. Sánchez-Alegría, K. *et al.* (2018) 'PI3K signaling in neurons: A central node for the control of multiple functions', *International Journal of Molecular Sciences*. MDPI AG. Available at: https://doi.org/10.3390/ijms19123725.
807. Sánchez-Mendoza, E.H. *et al.* (2017) 'Vesicular glutamate transporters play a role in neuronal differentiation of cultured SVZ-derived neural precursor cells', *PLOS ONE*, 12(5), p. e0177069. Available at: https://doi.org/10.1371/JOURNAL.PONE.0177069.
808. Sánchez-Ramírez, E. *et al.* (2024) 'Emerging Functional Connections Between Metabolism and Epigenetic Remodeling in Neural Differentiation', *Molecular Neurobiology 2024*, 61(9), pp. 1–20. Available at: https://doi.org/10.1007/S12035-024-04006-W.
809. Santo, E.E. and Paik, J. (2018) 'FOXO in Neural Cells and Diseases of the Nervous System', *Current topics in developmental biology*, 127, p. 105. Available at: https://doi.org/10.1016/BS.CTDB.2017.10.002.
810. dos Santos, M.G., Gomes, J.R. and Costa, M.D.M. (2023) 'Methods used to achieve different levels of the neuronal differentiation process in SH-SY5Y and Neuro2a cell lines: An integrative review', *Cell Biology International*, 47(12), pp. 1883–1894. Available at: https://doi.org/10.1002/CBIN.12093.
811. Sanz-Martos, A.B. *et al.* (2022) 'Butyric Acid Precursor Tributyrin Modulates Hippocampal Synaptic Plasticity and Prevents Spatial Memory Deficits: Role of PPARγ and AMPK', *International Journal of Neuropsychopharmacology*, 25(6), pp. 498–511. Available at: https://doi.org/10.1093/IJNP/PYAC015.
812. Sarkanen, J.R. *et al.* (2007) 'Cholesterol supports the retinoic acid-induced synaptic vesicle formation in differentiating human SH-SY5Y neuroblastoma cells', *Journal of Neurochemistry*, 102(6), pp. 1941–1952. Available at: https://doi.org/10.1111/J.1471-4159.2007.04676.X.
813. Sarn, N. *et al.* (2020) 'Cytoplasmic-predominant Pten increases microglial activation and synaptic pruning in a murine model with autism-like phenotype', *Molecular Psychiatry*, pp. 1–14. Available at: https://doi.org/10.1038/s41380-020-0681-0.
814. Sato, K. (2015) 'Effects of Microglia on Neurogenesis', *GLIA*. John Wiley and Sons Inc., pp. 1394–1405. Available at: https://doi.org/10.1002/glia.22858.
815. Savino, R. *et al.* (2020) 'Analyzing the Potential Biological Determinants of Autism Spectrum Disorder: From Neuroinflammation to the Kynurenine Pathway', *Brain Sciences 2020, Vol. 10, Page 631*, 10(9), p. 631. Available at: https://doi.org/10.3390/BRAINSCI10090631.
816. Sbrini, G. *et al.* (2020) 'The Absence of Serotonin in the Brain Alters Acute Stress Responsiveness by Interfering With the Genomic Function of the Glucocorticoid Receptors', *Frontiers in Cellular Neuroscience*, 14, p. 128. Available at: https://doi.org/10.3389/FNCEL.2020.00128/BIBTEX.
817. Scandella, V. *et al.* (2023) 'Neural stem cell metabolism revisited: a critical role for mitochondria', *Trends in Endocrinology and Metabolism*, 34(8), pp. 446–461. Available at: https://doi.org/10.1016/J.TEM.2023.05.008/ASSET/93B12B05-8908-4DA2-8B3B-36051EE6B182/MAIN.ASSETS/GR3.JPG.
818. Scarpa, A. *et al.* (2021) 'Enhancing Flexibility: A Biosocial Model for Resilience to Adversity in Youth With Autism', *SAGE Open*, 11(3). Available at: https://doi.org/10.1177/21582440211037997.
819. Schafer, D.P. *et al.* (2012) 'Microglia Sculpt Postnatal Neural Circuits in an Activity and Complement-Dependent Manner', *Neuron*, 74(4), pp. 691–705. Available at: https://doi.org/10.1016/J.NEURON.2012.03.026.
820. Schneeberger, M. *et al.* (2013) 'Mitofusin 2 in POMC neurons connects ER stress with leptin resistance and energy imbalance', *Cell*, 155(1), pp. 172–187. Available at: https://doi.org/10.1016/j.cell.2013.09.003.
821. Schneider, L. *et al.* (2011) 'Differentiation of SH-SY5Y cells to a neuronal phenotype changes cellular bioenergetics and the response to oxidative stress', *Free Radical Biology and Medicine*, 51(11), pp. 2007–2017. Available at: https://doi.org/10.1016/j.freeradbiomed.2011.08.030.
822. Scholpa, N.E. *et al.* (2018) '5-HT1F receptor-mediated mitochondrial biogenesis for the treatment of Parkinson's disease', *British Journal of Pharmacology*, 175(2), pp. 348–358. Available at: https://doi.org/10.1111/BPH.14076.

823. Schrier, M.S. *et al.* (2022) 'Decreased cortical Nrf2 gene expression in autism and its relationship to thiol and cobalamin status', *Biochimie*, 192, pp. 1–12. Available at: https://doi.org/10.1016/J.BIOCHI.2021.09.006.
824. Schroeder, J.H. *et al.* (2014) 'Shedding light on a pervasive problem: A review of research on bullying experiences among children with autism spectrum disorders', *Journal of Autism and Developmental Disorders*, 44(7), pp. 1520–1534. Available at: https://doi.org/10.1007/S10803-013-2011-8/TABLES/1.
825. Schubert-Bast, S. *et al.* (2019) 'The role of mTOR inhibitors in preventing epileptogenesis in patients with TSC: Current evidence and future perspectives', *Epilepsy & Behavior*, 91, pp. 94–98. Available at: https://doi.org/10.1016/J.YEBEH.2018.05.039.
826. Schumann, A. *et al.* (2021) 'Mitochondrial damage in renal epithelial cells is potentiated by protein exposure in propionic aciduria', *Journal of Inherited Metabolic Disease*, 44(6), pp. 1330–1342. Available at: https://doi.org/10.1002/JIMD.12419.
827. Scola, G. *et al.* (2014) 'Lithium reduces the effects of rotenone-induced complex i dysfunction on DNA methylation and hydroxymethylation in rat cortical primary neurons', *Psychopharmacology*, 231(21), pp. 4189–4198. Available at: https://doi.org/10.1007/s00213-014-3565-7.
828. Scuderi, C. *et al.* (2014) 'Palmitoylethanolamide controls reactive gliosis and exerts neuroprotective functions in a rat model of Alzheimer's disease', *Cell Death & Disease 2014 5:9*, 5(9), pp. e1419–e1419. Available at: https://doi.org/10.1038/cddis.2014.376.
829. Sealey, L.A. *et al.* (2016) 'Environmental factors in the development of autism spectrum disorders', *Environment International*, 88, pp. 288–298. Available at: https://doi.org/10.1016/J.ENVINT.2015.12.021.
830. Sedlak, T.W. *et al.* (2019) 'The glutathione cycle shapes synaptic glutamate activity', *Proceedings of the National Academy of Sciences of the United States of America*, 116(7), pp. 2701–2706. Available at: https://doi.org/10.1073/PNAS.1817885116/-/DCSUPPLEMENTAL.
831. Selamet, E. and Usta, M.B. (2023) 'Mitochondrial Dysfunction and mTOR in Autism Spectrum Disorders', *Current Approaches in Psychiatry*, 15(4), pp. 697–704. Available at: https://doi.org/10.18863/PGY.1205786.
832. Serdar, B. *et al.* (2020) 'Comparison of medium supplements in terms of the effects on the differentiation of SH-SY5Y human neuroblastoma cell line', *Neurological Sciences and Neurophysiology*, 37(2), p. 82. Available at: https://doi.org/10.4103/NSN.NSN_15_20.
833. Serdar, B.S. *et al.* (2018) 'Which Medium and Ingredients Provide Better Morphological Differentiation of SH-SY5Y Cells?', *Proceedings 2018, Vol. 2, Page 1577*, 2(25), p. 1577. Available at: https://doi.org/10.3390/PROCEEDINGS2251577.
834. Sestan, N. and State, M.W. (2018) 'Lost in Translation: Traversing the Complex Path from Genomics to Therapeutics in Autism Spectrum Disorder', *Neuron*, 100(2), pp. 406–423. Available at: https://doi.org/10.1016/J.NEURON.2018.10.015.
835. Shabani, Z. *et al.* (2021) 'Modulatory properties of extracellular matrix glycosaminoglycans and proteoglycans on neural stem cells behavior: Highlights on regenerative potential and bioactivity', *International Journal of Biological Macromolecules*, 171, pp. 366–381. Available at: https://doi.org/10.1016/j.ijbiomac.2021.01.006.
836. Shao, F. *et al.* (2022) 'Microglia and Neuroinflammation: Crucial Pathological Mechanisms in Traumatic Brain Injury-Induced Neurodegeneration', *Frontiers in Aging Neuroscience*, 14, p. 825086. Available at: https://doi.org/10.3389/FNAGI.2022.825086/BIBTEX.
837. Sharma, A., Bhalla, S. and Mehan, S. (2022) 'PI3K/AKT/mTOR signalling inhibitor chrysophanol ameliorates neurobehavioural and neurochemical defects in propionic acid-induced experimental model of autism in adult rats', *Metabolic Brain Disease 2022 37:6*, 37(6), pp. 1909–1929. Available at: https://doi.org/10.1007/S11011-022-01026-0.
838. Sharma, A., Hill, K.E. and Schwarzbauer, J.E. (2023) 'Extracellular matrix composition affects outgrowth of dendrites and dendritic spines on cortical neurons', *Frontiers in Cellular Neuroscience*, 17, p. 1177663. Available at: https://doi.org/10.3389/fncel.2023.1177663.
839. Sharma, A. and Mehan, S. (2021) 'Targeting PI3K-AKT/mTOR signaling in the prevention of autism', *Neurochemistry International*, 147, p. 105067. Available at: https://doi.org/10.1016/J.NEUINT.2021.105067.
840. Sharma, R., Rahi, S. and Mehan, S. (2019) 'Neuroprotective potential of solanesol in intracerebroventricular propionic acid induced experimental model of autism: Insights from behavioral and biochemical evidence', *Toxicology Reports*, 6, pp. 1164–1175. Available at: https://doi.org/10.1016/j.toxrep.2019.10.019.
841. Sharpley, C.F. *et al.* (2017) 'Is daily replication necessary when sampling cortisol concentrations in association studies of children with autism spectrum disorder? A systematic review and discussion paper', *Reviews in the Neurosciences*. Walter de Gruyter GmbH, pp. 103–111. Available at: https://doi.org/10.1515/revneuro-2016-0037.

842. Shchelochkov, O.A. *et al.* (2024) 'Intellectual disability and autism in propionic acidemia: a biomarker-behavioral investigation implicating dysregulated mitochondrial biology', *Molecular Psychiatry*, 29(4), pp. 974–981. Available at: https://doi.org/10.1038/s41380-023-02385-5.
843. Sheloukhova, L. and Watanabe, H. (2024) 'Evolution of glial cells: a non-bilaterian perspective', *Neural Development 2024 19:1*, 19(1), pp. 1–20. Available at: https://doi.org/10.1186/S13064-024-00184-4.
844. Shen, L. *et al.* (2018) 'iTRAQ-Based Proteomic Analysis Reveals Protein Profile in Plasma from Children with Autism', *PROTEOMICS - Clinical Applications*, 12(3), p. 1700085. Available at: https://doi.org/10.1002/prca.201700085.
845. Shen, L., Zhao, Y., *et al.* (2019) 'Advances in Biomarker Studies in Autism Spectrum Disorders', *Advances in Experimental Medicine and Biology*, 1118, pp. 207–233. Available at: https://doi.org/10.1007/978-3-030-05542-4_11.
846. Shen, L., Feng, C., *et al.* (2019) 'Proteomics Study of Peripheral Blood Mononuclear Cells (PBMCs) in Autistic Children', *Frontiers in Cellular Neuroscience*, 13, p. 105. Available at: https://doi.org/10.3389/fncel.2019.00105.
847. Sherry, E.B., Lee, P. and Choi, I.Y. (2015) 'In Vivo NMR Studies of the Brain with Hereditary or Acquired Metabolic Disorders', *Neurochemical Research 2015 40:12*, 40(12), pp. 2647–2685. Available at: https://doi.org/10.1007/S11064-015-1772-1.
848. Sheth, C., McGlade, E. and Yurgelun-Todd, D. (2017) 'Chronic Stress in Adolescents and Its Neurobiological and Psychopathological Consequences: An RDoC Perspective', *Chronic Stress*, 1. Available at: https://doi.org/10.1177/2470547017715645.
849. Shi, D. and Jiang, P. (2021) 'A Different Facet of p53 Function: Regulation of Immunity and Inflammation During Tumor Development', *Frontiers in Cell and Developmental Biology*, 9. Available at: https://doi.org/10.3389/FCELL.2021.762651.
850. Shi, L. and Tu, B.P. (2015) 'Acetyl-CoA and the Regulation of Metabolism: Mechanisms and Consequences', *Current opinion in cell biology*, 33, p. 125. Available at: https://doi.org/10.1016/J.CEB.2015.02.003.
851. Shipley, M.M., Mangold, C.A. and Szpara, M.L. (2016) 'Differentiation of the SH-SY5Y Human Neuroblastoma Cell Line', *J. Vis. Exp*, (108), p. 53193. Available at: https://doi.org/10.3791/53193.
852. Shiraki, N. *et al.* (2014) 'Methionine metabolism regulates maintenance and differentiation of human pluripotent stem cells', *Cell Metabolism*, 19(5), pp. 780–794. Available at: https://doi.org/10.1016/j.cmet.2014.03.017.
853. Shpyleva, S. *et al.* (2014) 'Cerebellar oxidative DNA damage and altered DNA methylation in the BTBR T+tf/J mouse model of autism and similarities with human post mortem cerebellum', *PLoS ONE*, 9(11). Available at: https://doi.org/10.1371/journal.pone.0113712.
854. Shulha, H.P. *et al.* (2012) 'Epigenetic Signatures of Autism: Trimethylated H3K4 Landscapes in Prefrontal Neurons', *Archives of General Psychiatry*, 69(3), pp. 314–324. Available at: https://doi.org/10.1001/ARCHGENPSYCHIATRY.2011.151.
855. Shultz, S.R. *et al.* (2008) 'Intracerebroventricular injection of propionic acid, an enteric bacterial metabolic end-product, impairs social behavior in the rat: Implications for an animal model of autism', *Neuropharmacology*, 54(6), pp. 901–911. Available at: https://doi.org/10.1016/j.neuropharm.2008.01.013.
856. Shultz, S.R. and Macfabe, D.F. (2014) 'Propionic Acid Animal Model of Autism', *Comprehensive Guide to Autism* [Preprint], (October). Available at: https://doi.org/10.1007/978-1-4614-4788-7.
857. Shulyakova, N. *et al.* (2017) 'Mitochondrial Dysfunction in the Pathogenesis of Rett Syndrome: Implications for Mitochondria-Targeted Therapies', *Frontiers in Cellular Neuroscience*, 11, p. 58. Available at: https://doi.org/10.3389/FNCEL.2017.00058.
858. Shyh-Chang, N. *et al.* (2013) 'Influence of threonine metabolism on S-adenosylmethionine and histone methylation', *Science*, 339(6116), pp. 222–226. Available at: https://doi.org/10.1126/SCIENCE.1226603/SUPPL_FILE/SHYH-CHANG.SM.REVISED-JEC.PDF.
859. Shyh-Chang, N. and Ng, H.H. (2017) 'The metabolic programming of stem cells', *Genes and Development*. Cold Spring Harbor Laboratory Press, pp. 336–346. Available at: https://doi.org/10.1101/gad.293167.116.
860. Siddiqui, M.F., Elwell, C. and Johnson, M.H. (2016) 'Mitochondrial Dysfunction in Autism Spectrum Disorders', *Autism-Open Access*, 6(4). Available at: https://doi.org/10.4172/2165-7890.1000190.
861. Sigafoos, A.N., Paradise, B.D. and Fernandez-Zapico, M.E. (2021) 'Hedgehog/GLI Signaling Pathway: Transduction, Regulation, and Implications for Disease', *Cancers*, 13(14). Available at: https://doi.org/10.3390/CANCERS13143410.
862. Sild, M. and Booij, L. (2019) 'Histone deacetylase 4 (HDAC4): a new player in anorexia nervosa?', *Molecular Psychiatry 2019 24:10*, 24(10), pp. 1425–1434. Available at: https://doi.org/10.1038/s41380-019-0366-8.

863. Silva, L.G. *et al.* (2018) 'Sodium propionate and sodium butyrate effects on histone deacetylase (HDAC) activity, histone acetylation, and inflammatory gene expression in bovine mammary epithelial cells', *Journal of Animal Science*, 96(12), pp. 5244–5252. Available at: https://doi.org/10.1093/JAS/SKY373.
864. Silva, R.C. *et al.* (2021) 'Biological correlates of early life stressful events in major depressive disorder', *Psychoneuroendocrinology*, 125, p. 105103. Available at: https://doi.org/10.1016/J.PSYNEUEN.2020.105103.
865. Simões, R.F. *et al.* (2021) 'Refinement of a differentiation protocol using neuroblastoma SH-SY5Y cells for use in neurotoxicology research', *Food and Chemical Toxicology*, 149, p. 111967. Available at: https://doi.org/10.1016/J.FCT.2021.111967.
866. Simões, R.F. *et al.* (2022) 'Evaluation of 6-Hydroxydopamine and Rotenone In Vitro Neurotoxicity on Differentiated SH-SY5Y Cells Using Applied Computational Statistics', *International Journal of Molecular Sciences*, 23(6), p. 3009. Available at: https://doi.org/10.3390/IJMS23063009/S1.
867. Singh, K.K. and Tsai, L.H. (2010) 'MicroTUB(B3)ules and Brain Development', *Cell*, 140(1), pp. 30–32. Available at: https://doi.org/10.1016/j.cell.2009.12.038.
868. Singh, S. *et al.* (2018) 'Axin-2 knockdown promote mitochondrial biogenesis and dopaminergic neurogenesis by regulating Wnt/β-catenin signaling in rat model of Parkinson's disease', *Free Radical Biology and Medicine*, 129, pp. 73–87. Available at: https://doi.org/10.1016/J.FREERADBIOMED.2018.08.033.
869. Singh, S., Somvanshi, R.K. and Kumar, U. (2022) 'Somatostatin-Mediated Regulation of Retinoic Acid-Induced Differentiation of SH-SY5Y Cells: Neurotransmitters Phenotype Characterization', *Biomedicines*, 10(2), p. 337. Available at: https://doi.org/10.3390/biomedicines10020337.
870. Singh, V. (2021) 'Intracellular metabolic reprogramming mediated by micro-RNAs in differentiating and proliferating cells under non-diseased conditions', *Molecular Biology Reports*, 48(12), pp. 8123–8140. Available at: https://doi.org/10.1007/S11033-021-06769-0/TABLES/4.
871. Singhal, N.K. *et al.* (2015) 'Changes in Methionine Metabolism and Histone H3 Trimethylation Are Linked to Mitochondrial Defects in Multiple Sclerosis', *Journal of Neuroscience*, 35(45), pp. 15170–15186. Available at: https://doi.org/10.1523/JNEUROSCI.4349-14.2015.
872. Singletary, W.M. (2015) 'An integrative model of autism spectrum disorder: ASD as a neurobiological disorder of experienced environmental deprivation, early life stress and allostatic overload', *Neuropsychoanalysis*. Routledge, pp. 81–119. Available at: https://doi.org/10.1080/15294145.2015.1092334.
873. Siu, M.T. *et al.* (2019) 'Functional DNA methylation signatures for autism spectrum disorder genomic risk loci: 16p11.2 deletions and CHD8 variants', *Clinical Epigenetics*, 11(1), p. 103. Available at: https://doi.org/10.1186/s13148-019-0684-3.
874. Siu, M.T. and Weksberg, R. (2017) 'Epigenetics of Autism Spectrum Disorder', in *Advances in Experimental Medicine and Biology*. Springer New York LLC, pp. 63–90. Available at: https://doi.org/10.1007/978-3-319-53889-1_4.
875. Smerker, H. (2014) 'Weaning and Adaptation of SH-SY5Y Cells to Low Glucose Media for Manganese Exposure Studies'.
876. Smith, A. and Donley, E. (2022) 'A metabolomics approach to parsing the heterogeneity of autism identifies complex dysregulations of cellular bioenergetics', pp. 1–22.
877. Smith, A.M. *et al.* (2020) 'A Metabolomics Approach to Screening for Autism Risk in the Children's Autism Metabolome Project', *Autism Research*, p. aur.2330. Available at: https://doi.org/10.1002/aur.2330.
878. Smith, I.C. and White, S.W. (2020) 'Socio-emotional determinants of depressive symptoms in adolescents and adults with autism spectrum disorder: A systematic review', *Autism*. SAGE PublicationsSage UK: London, England, pp. 995–1010. Available at: https://doi.org/10.1177/1362361320908101.
879. Sofroniew, M. V. (2020) 'Astrocyte Reactivity: Subtypes, States, and Functions in CNS Innate Immunity', *Trends in Immunology*, 41(9), pp. 758–770. Available at: https://doi.org/10.1016/J.IT.2020.07.004.
880. Son, E.Y. and Crabtree, G.R. (2014) 'The role of BAF (mSWI/SNF) complexes in mammalian neural development', *American Journal of Medical Genetics Part C: Seminars in Medical Genetics*, 166(3), pp. 333–349. Available at: https://doi.org/10.1002/AJMG.C.31416.
881. Sotolongo, K., Ghiso, J. and Rostagno, A. (2020) 'Nrf2 activation through the PI3K/GSK-3 axis protects neuronal cells from Aβ-mediated oxidative and metabolic damage', *Alzheimer's Research & Therapy 2020 12:1*, 12(1), pp. 1–22. Available at: https://doi.org/10.1186/S13195-019-0578-9.
882. Spangsberg Petersen, U.S. *et al.* (2024) 'Regulating PCCA gene expression by modulation of pseudoexon splicing patterns to rescue enzyme activity in propionic acidemia', *Molecular Therapy - Nucleic Acids*, 35(1), p. 102101. Available at: https://doi.org/10.1016/J.OMTN.2023.102101.

883. Sperber, H. *et al.* (2015) 'The metabolome regulates the epigenetic landscape during naive-to-primed human embryonic stem cell transition', *Nature Cell Biology 2015 17:12*, 17(12), pp. 1523–1535. Available at: https://doi.org/10.1038/ncb3264.
884. Spratt, E.G. *et al.* (2012) 'Enhanced cortisol response to stress in children in autism', *Journal of Autism and Developmental Disorders*, 42(1), pp. 75–81. Available at: https://doi.org/10.1007/S10803-011-1214-0/FIGURES/2.
885. Stathopoulos, S. *et al.* (2020) 'DNA Methylation Associated with Mitochondrial Dysfunction in a South African Autism Spectrum Disorder Cohort', *Autism Research*, 13(7), pp. 1079–1093. Available at: https://doi.org/10.1002/aur.2310.
886. Stauffer, W., Sheng, H. and Lim, H.N. (2018) 'EzColocalization: An ImageJ plugin for visualizing and measuring colocalization in cells and organisms', *Scientific Reports 2018 8:1*, 8(1), pp. 1–13. Available at: https://doi.org/10.1038/s41598-018-33592-8.
887. Stecca, B. and Ruiz I Altaba, A. (2009) 'A GLI1-p53 inhibitory loop controls neural stem cell and tumour cell numbers', *EMBO Journal*, 28(6), pp. 663–676. Available at: https://doi.org/10.1038/EMBOJ.2009.16/SUPPL_FILE/EMBJ200916-SUP-0010.PDF.
888. Steinberg, F. and Rucker, R.B. (2005) 'The water-soluble vitamins', in *Handbook of Food Science, Technology, and Engineering - 4 Volume Set*, pp. 171–188. Available at: https://doi.org/10.5005/jp/books/11556_7.
889. Steketee, M.B. and Goldberg, J.L. (2012) 'Signaling Endosomes and Growth Cone Motility in Axon Regeneration', in *International Review of Neurobiology*. Academic Press, pp. 35–73. Available at: https://doi.org/10.1016/B978-0-12-407178-0.00003-X.
890. Stern, J. and Wilcox, A.H. (1994) 'Inherited and Acquired Mental Deficiency', *Scientific Foundations of Biochemistry in Clinical Practice*, pp. 253–291. Available at: https://doi.org/10.1016/B978-0-7506-0167-2.50021-2.
891. Stoccoro, A. *et al.* (2023) 'DNA Methylation Biomarkers for Young Children with Idiopathic Autism Spectrum Disorder: A Systematic Review', *International Journal of Molecular Sciences 2023, Vol. 24, Page 9138*, 24(11), p. 9138. Available at: https://doi.org/10.3390/IJMS24119138.
892. Su, C., Miao, J. and Guo, J. (2023) 'The relationship between TGF-β1 and cognitive function in the brain', *Brain Research Bulletin*, 205, p. 110820. Available at: https://doi.org/10.1016/j.brainresbull.2023.110820.
893. Su, Y. *et al.* (2020) 'STAT3 Regulates Mouse Neural Progenitor Proliferation and Differentiation by Promoting Mitochondrial Metabolism', *Frontiers in Cell and Developmental Biology*, 8, p. 530807. Available at: https://doi.org/10.3389/fcell.2020.00362.
894. Su, Y.Y. *et al.* (2022) 'Specific and cumulative lifetime stressors in the aetiology of major depression: A longitudinal community-based population study', *Epidemiology and Psychiatric Sciences*, 31, p. e3. Available at: https://doi.org/10.1017/S2045796021000779.
895. Subramanian, C. *et al.* (2021) 'Pantothenate kinase activation relieves coenzyme A sequestration and improves mitochondrial function in mice with propionic acidemia', *Science Translational Medicine*, 13(611), p. 5965. Available at: https://doi.org/10.1126/SCITRANSLMED.ABF5965/SUPPL_FILE/SCITRANSLMED.ABF5965_DATA_FILE_S1.ZIP.
896. Subramanian, C. *et al.* (2023) 'Relief of CoA sequestration and restoration of mitochondrial function in a mouse model of propionic acidemia', *Journal of Inherited Metabolic Disease*, 46(1), pp. 28–42. Available at: https://doi.org/10.1002/JIMD.12570.
897. Sugama, S. and Kakinuma, Y. (2020) 'Stress and brain immunity: Microglial homeostasis through hypothalamus-pituitary-adrenal gland axis and sympathetic nervous system', *Brain, Behavior, & Immunity - Health*, 7, p. 100111. Available at: https://doi.org/10.1016/J.BBIH.2020.100111.
898. Sun, J. *et al.* (2019) 'E2F is required for STAT3-mediated upregulation of cyclin B1 and Cdc2 expressions and contributes to G2–M phase transition', *Acta Biochimica et Biophysica Sinica*, 51(3), pp. 313–322. Available at: https://doi.org/10.1093/ABBS/GMY174.
899. Sun, J. *et al.* (2023) 'Decreased propionyl-CoA metabolism facilitates metabolic reprogramming and promotes hepatocellular carcinoma', *Journal of Hepatology*, 78(3), pp. 627–642. Available at: https://doi.org/10.1016/J.JHEP.2022.11.017.
900. Sun, L. *et al.* (2022) 'Genome-wide DNA methylation profiles of autism spectrum disorder', *Psychiatric Genetics*, 32(4), pp. 131–145. Available at: https://doi.org/10.1097/YPG.0000000000000314.
901. Sun, W. *et al.* (2016) 'Histone Acetylome-wide Association Study of Autism Spectrum Disorder', *Cell*, 167(5), pp. 1385-1397.e11. Available at: https://doi.org/10.1016/J.CELL.2016.10.031/ATTACHMENT/409140FC-5B1D-41AE-81F9-240B582DE803/MMC7.XLSX.

902. Superti, F. and Russo, R. (2024) ‘Alpha-Lipoic Acid: Biological Mechanisms and Health Benefits’, *Antioxidants 2024, Vol. 13, Page 1228*, 13(10), p. 1228. Available at: https://doi.org/10.3390/ANTIOX13101228.
903. Suzuki, K. *et al.* (2013) ‘Microglial Activation in Young Adults With Autism Spectrum Disorder’, *JAMA Psychiatry*, 70(1), pp. 49–58. Available at: https://doi.org/10.1001/JAMAPSYCHIATRY.2013.272.
904. Swerdlow, R.H. *et al.* (2013) ‘Glycolysis–respiration relationships in a neuroblastoma cell line’, *Biochimica et Biophysica Acta (BBA) - General Subjects*, 1830(4), pp. 2891–2898. Available at: https://doi.org/10.1016/J.BBAGEN.2013.01.002.
905. Sylla, S. *et al.* (2020) ‘Therapeutic Effects of Magnesium Biotinate on Propionic Acid-Induced Autistic Features in Rats’, *The FASEB Journal*, 34(S1), pp. 1–1. Available at: https://doi.org/10.1096/fasebj.2020.34.s1.09493.
906. Szwed, A., Kim, E. and Jacinto, E. (2021) ‘REGULATION AND METABOLIC FUNCTIONS OF mTORC1 AND mTORC2’, *Physiological Reviews*, 101(3), pp. 1371–1426. Available at: https://doi.org/10.1152/PHYSREV.00026.2020/ASSET/IMAGES/LARGE/PHYSREV.00026.2020_F008.JPEG.
907. Szychowski, K.A. and Skóra, B. (2023) ‘The elastin-derived peptide (VGVAPG) activates autophagy in neuroblastoma (SH-SY5Y) cells via peroxisome proliferator-activated receptor gamma (PPARγ)’, *Molecular and Cellular Neuroscience*, 127, p. 103902. Available at: https://doi.org/10.1016/J.MCN.2023.103902.
908. Tan, M.A., Zakharova, E. and An, S.S.A. (2021) ‘Diaportheone A Analogues Instigate a Neuroprotective Effect by Protecting Neuroblastoma SH-SY5Y Cells from Oxidative Stress’, *Biology 2021, Vol. 10, Page 199*, 10(3), p. 199. Available at: https://doi.org/10.3390/BIOLOGY10030199.
909. Tang, Y. *et al.* (2011) ‘Short-chain fatty acids induced autophagy serves as an adaptive strategy for retarding mitochondria-mediated apoptotic cell death’, *Cell Death and Differentiation*, 18(4), p. 602. Available at: https://doi.org/10.1038/CDD.2010.117.
910. Tang, Y. and Le, W. (2016) ‘Differential Roles of M1 and M2 Microglia in Neurodegenerative Diseases’, *Molecular neurobiology*, 53(2), pp. 1181–1194. Available at: https://doi.org/10.1007/S12035-014-9070-5.
911. Targum, S.D. and Nemeroff, C.B. (2019) ‘The Effect of Early Life Stress on Adult Psychiatric Disorders.’, *Innovations in clinical neuroscience*, 1 January, pp. 35–37. Available at: /pmc/articles/PMC6450674/ (Accessed: 6 February 2022).
912. Taudt, A. *et al.* (2017) ‘Histone propionylation is a mark of active chromatin’, *Nature Structural & Molecular Biology*, 24(12), p. 1048. Available at: https://doi.org/10.1038/nsmb.3490.
913. Tay, E.X.Y., Chia, K. and Ong, D.S.T. (2021) ‘Epigenetic plasticity and redox regulation of neural stem cell state and fate’, *Free Radical Biology and Medicine*, 170, pp. 116–130. Available at: https://doi.org/10.1016/J.FREERADBIOMED.2021.02.030.
914. Taylor, J.L. and Corbett, B.A. (2014) ‘A review of rhythm and responsiveness of cortisol in individuals with autism spectrum disorders’, *Psychoneuroendocrinology*, 49(1), pp. 207–228. Available at: https://doi.org/10.1016/j.psyneuen.2014.07.015.
915. Teppola, H. *et al.* (2016) ‘Morphological Differentiation Towards Neuronal Phenotype of SH-SY5Y Neuroblastoma Cells by Estradiol, Retinoic Acid and Cholesterol’, *Neurochemical Research*, 41(4), p. 731. Available at: https://doi.org/10.1007/S11064-015-1743-6.
916. Tetreault, N.A. *et al.* (2012) ‘Microglia in the cerebral cortex in autism’, *Journal of Autism and Developmental Disorders*, 42(12), pp. 2569–2584. Available at: https://doi.org/10.1007/S10803-012-1513-0/TABLES/4.
917. Theeuwes, W.F. *et al.* (2020) ‘Regulation of PGC-1α expression by a GSK-3β-TFEB signaling axis in skeletal muscle’, *Biochimica et Biophysica Acta (BBA) - Molecular Cell Research*, 1867(2), p. 118610. Available at: https://doi.org/10.1016/J.BBAMCR.2019.118610.
918. Thomas, S.D. *et al.* (2023) ‘mTOR Signaling Disruption and Its Association with the Development of Autism Spectrum Disorder’, *Molecules 2023, Vol. 28, Page 1889*, 28(4), p. 1889. Available at: https://doi.org/10.3390/MOLECULES28041889.
919. Thomas, S.P. and Denu, J.M. (2021) ‘Short-chain fatty acids activate acetyltransferase p300’, *eLife*, 10. Available at: https://doi.org/10.7554/eLife.72171.
920. Thomson, A.C. *et al.* (2022) ‘The Effects of Serum Removal on Gene Expression and Morphological Plasticity Markers in Differentiated SH-SY5Y Cells’, *Cellular and Molecular Neurobiology*, 42(6), pp. 1829–1839. Available at: https://doi.org/10.1007/S10571-021-01062-X/FIGURES/6.
921. Thorsen, M. (2020) ‘Oxidative stress, metabolic and mitochondrial abnormalities associated with autism spectrum disorder’, in *Progress in Molecular Biology and Translational Science*. Elsevier B.V., pp. 331–354. Available at: https://doi.org/10.1016/bs.pmbts.2020.04.018.
922. Tian, J., Du, E. and Guo, L. (2023) ‘Mitochondrial Interaction with Serotonin in Neurobiology and Its Implication in Alzheimer’s Disease’, *Journal of Alzheimer’s Disease Reports*, 7(1), pp. 1165–1177. Available at: https://doi.org/10.3233/ADR-230070.

923. Tick, B. *et al.* (2016) 'Heritability of autism spectrum disorders: a meta-analysis of twin studies', *Journal of Child Psychology and Psychiatry*, 57(5), pp. 585–595. Available at: https://doi.org/10.1111/JCPP.12499.
924. Tien, P.C. *et al.* (2023) 'Notch signaling regulates a metabolic switch through inhibiting PGC-1α and mitochondrial biogenesis in dedifferentiated liposarcoma', *Oncogene 2023 42:34*, 42(34), pp. 2521–2535. Available at: https://doi.org/10.1038/s41388-023-02768-6.
925. Tirosh, A. *et al.* (2019) 'The short-chain fatty acid propionate increases glucagon and FABP4 production, impairing insulin action in mice and humans', *Science Translational Medicine*, 11(489). Available at: https://doi.org/10.1126/SCITRANSLMED.AAV0120/SUPPL_FILE/AAV0120_SM.PDF.
926. Tisato, V. *et al.* (2021) 'Genetics and Epigenetics of One-Carbon Metabolism Pathway in Autism Spectrum Disorder: A Sex-Specific Brain Epigenome?', *Genes 2021, Vol. 12, Page 782*, 12(5), p. 782. Available at: https://doi.org/10.3390/GENES12050782.
927. Tiwari, A. *et al.* (2021) 'Neuroprotective Effect of α-Mangostin in Ameliorating Propionic Acid-Induced Experimental Model of Autism in Wistar Rats', *Brain Sciences 2021, Vol. 11, Page 288*, 11(3), p. 288. Available at: https://doi.org/10.3390/BRAINSCI11030288.
928. Toleikis, A. *et al.* (2020) 'Fatty Acid Oxidation and Mitochondrial Morphology Changes as Key Modulators of the Affinity for ADP in Rat Heart Mitochondria', *Cells 2020, Vol. 9, Page 340*, 9(2), p. 340. Available at: https://doi.org/10.3390/CELLS9020340.
929. Tolomeo, M. and Cascio, A. (2021) 'The Multifaced Role of STAT3 in Cancer and Its Implication for Anticancer Therapy', *International Journal of Molecular Sciences 2021, Vol. 22, Page 603*, 22(2), p. 603. Available at: https://doi.org/10.3390/IJMS22020603.
930. Tomarken, A.J., Han, G.T. and Corbett, B.A. (2015) 'Temporal patterns, heterogeneity, and stability of diurnal cortisol rhythms in children with autism spectrum disorder', *Psychoneuroendocrinology*, 62, pp. 217–226. Available at: https://doi.org/10.1016/J.PSYNEUEN.2015.08.016.
931. Tomasello, D.L. *et al.* (2024) 'Mitochondrial dysfunction and increased reactive oxygen species production in MECP2 mutant astrocytes and their impact on neurons', *Scientific Reports 2024 14:1*, 14(1), pp. 1–27. Available at: https://doi.org/10.1038/s41598-024-71040-y.
932. Tome, M.E. *et al.* (2012) 'Mitochondria are the primary source of the H 2O 2 signal for glucocorticoid-induced apoptosis of lymphoma cells', *Experimental and Therapeutic Medicine*, 4(2), pp. 237–242. Available at: https://doi.org/10.3892/ETM.2012.595/HTML.
933. Tordjman, S. *et al.* (2014) 'Altered circadian patterns of salivary cortisol in low-functioning children and adolescents with autism', *Psychoneuroendocrinology*, 50, pp. 227–245. Available at: https://doi.org/10.1016/j.psyneuen.2014.08.010.
934. Tošić, I. and Frank, D.A. (2021) 'STAT3 as a mediator of oncogenic cellular metabolism: Pathogenic and therapeutic implications', *Neoplasia*, 23(12), pp. 1167–1178. Available at: https://doi.org/10.1016/J.NEO.2021.10.003.
935. Tracey, T.J. *et al.* (2018) 'Neuronal Lipid Metabolism: Multiple Pathways Driving Functional Outcomes in Health and Disease', *Frontiers in Molecular Neuroscience*, 11. Available at: https://doi.org/10.3389/FNMOL.2018.00010.
936. Trefely, S. *et al.* (2020) 'Compartmentalised acyl-CoA metabolism and roles in chromatin regulation', *Molecular Metabolism*, 38, p. 100941. Available at: https://doi.org/10.1016/J.MOLMET.2020.01.005.
937. Tremblay, M.W. and Jiang, Y.H. (2019) 'DNA methylation and susceptibility to autism spectrum disorder', *Annual Review of Medicine*, pp. 151–166. Available at: https://doi.org/10.1146/annurev-med-120417-091431.
938. Tripodi, F. *et al.* (2018) 'Methionine supplementation stimulates mitochondrial respiration', *Biochimica et Biophysica Acta (BBA) - Molecular Cell Research*, 1865(12), pp. 1901–1913. Available at: https://doi.org/10.1016/J.BBAMCR.2018.09.007.
939. Troubat, R. *et al.* (2021) 'Neuroinflammation and depression: A review', *European Journal of Neuroscience*, 53(1), pp. 151–171. Available at: https://doi.org/10.1111/EJN.14720.
940. Trundle, G. *et al.* (2022) 'Prevalence of Victimisation in Autistic Individuals: A Systematic Review and Meta-Analysis', *Trauma, Violence, and Abuse*. SAGE PublicationsSage CA: Los Angeles, CA, p. 152483802210936. Available at: https://doi.org/10.1177/15248380221093689.
941. Tsai, C.Y. *et al.* (2023) 'GSKIP modulates cell aggregation through EMT/MET signaling rather than differentiation in SH-SY5Y human neuroblastoma cells', *Journal of Cell Communication and Signaling*, 17(3), pp. 1039–1054. Available at: https://doi.org/10.1007/S12079-023-00752-Z/FIGURES/7.
942. Tseng, C.E.J. *et al.* (2022) 'Epigenetics of Autism Spectrum Disorder: Histone Deacetylases', *Biological Psychiatry*, 91(11), pp. 922–933. Available at: https://doi.org/10.1016/J.BIOPSYCH.2021.11.021.

943. Tylee, D.S. *et al.* (2017) 'Blood transcriptomic comparison of individuals with and without autism spectrum disorder: A combined-samples mega-analysis', *American Journal of Medical Genetics, Part B: Neuropsychiatric Genetics*, 174(3), pp. 181–201. Available at: https://doi.org/10.1002/ajmg.b.32511.
944. Tyrka, A.R. *et al.* (2016) 'Alterations of Mitochondrial DNA Copy Number and Telomere Length With Early Adversity and Psychopathology', *Biological Psychiatry*, 79(2), pp. 78–86. Available at: https://doi.org/10.1016/J.BIOPSYCH.2014.12.025.
945. Uittenbogaard, M., Brantner, C.A. and Chiaramello, A. (2018) 'Epigenetic modifiers promote mitochondrial biogenesis and oxidative metabolism leading to enhanced differentiation of neuroprogenitor cells', *Cell Death and Disease*, 9(3). Available at: https://doi.org/10.1038/s41419-018-0396-1.
946. Ul Fatima, N. and Ananthanarayanan, V. (2023) 'Mitochondrial movers and shapers: Recent insights into regulators of fission, fusion and transport', *Current Opinion in Cell Biology*, 80, p. 102150. Available at: https://doi.org/10.1016/J.CEB.2022.102150.
947. Un, Z. *et al.* (2022) 'Urinary metabolomics using gas chromatography-mass spectrometry: potential biomarkers for autism spectrum disorder', *BMC Neurology 2022 22:1*, 22(1), pp. 1–8. Available at: https://doi.org/10.1186/S12883-022-02630-4.
948. Underwood, M.D. *et al.* (2018) 'Serotonin receptors and suicide, major depression, alcohol use disorder and reported early life adversity', *Translational Psychiatry 2018 8:1*, 8(1), pp. 1–15. Available at: https://doi.org/10.1038/s41398-018-0309-1.
949. Unruh, K.E., Bodfish, J.W. and Gotham, K.O. (2020) 'Adults with Autism and Adults with Depression Show Similar Attentional Biases to Social-Affective Images', *Journal of Autism and Developmental Disorders*, 50(7), pp. 2336–2347. Available at: https://doi.org/10.1007/s10803-018-3627-5.
950. Unsicker, C. *et al.* (2021) 'SHANK2 mutations impair apoptosis, proliferation and neurite outgrowth during early neuronal differentiation in SH-SY5Y cells', *Scientific Reports 2021 11:1*, 11(1), pp. 1–15. Available at: https://doi.org/10.1038/s41598-021-81241-4.
951. Upadhyay, J. *et al.* (2021) 'Dysregulation of Multiple Signaling Neurodevelopmental Pathways during Embryogenesis: A Possible Cause of Autism Spectrum Disorder', *Cells 2021, Vol. 10, Page 958*, 10(4), p. 958. Available at: https://doi.org/10.3390/CELLS10040958.
952. Usui, N., Kobayashi, H. and Shimada, S. (2023) 'Neuroinflammation and Oxidative Stress in the Pathogenesis of Autism Spectrum Disorder', *International Journal of Molecular Sciences 2023, Vol. 24, Page 5487*, 24(6), p. 5487. Available at: https://doi.org/10.3390/IJMS24065487.
953. Vacharasin, J.M. *et al.* (2024) 'Neuroimmune mechanisms in autism etiology - untangling a complex problem using human cellular models', *Oxford Open Neuroscience*, 3. Available at: https://doi.org/10.1093/OONS/KVAE003.
954. Valente, A.J. *et al.* (2017) 'A simple ImageJ macro tool for analyzing mitochondrial network morphology in mammalian cell culture', *Acta Histochemica*, 119(3), pp. 315–326. Available at: https://doi.org/10.1016/j.acthis.2017.03.001.
955. Vallée, A. *et al.* (2017) 'Interactions between TGF-β1, canonical WNT/β-catenin pathway and PPAR γ in radiation-induced fibrosis', *Oncotarget*, 8(52), pp. 90579–90604. Available at: https://doi.org/10.18632/oncotarget.21234.
956. Vallée, A. *et al.* (2018) 'Opposite Interplay Between the Canonical WNT/β-Catenin Pathway and PPAR Gamma: A Potential Therapeutic Target in Gliomas', *Neuroscience bulletin*, 34(3), pp. 573–588. Available at: https://doi.org/10.1007/S12264-018-0219-5.
957. Vallée, A., Lecarpentier, Y. and Vallée, J.N. (2021) 'The Key Role of the WNT/β-Catenin Pathway in Metabolic Reprogramming in Cancers under Normoxic Conditions', *Cancers 2021, Vol. 13, Page 5557*, 13(21), p. 5557. Available at: https://doi.org/10.3390/CANCERS13215557.
958. Vallée, A., Vallée, J.-N.N. and Lecarpentier, Y. (2019) 'PPARγ agonists: potential treatment for autism spectrum disorder by inhibiting the canonical WNT/β-catenin pathway', *Molecular Psychiatry*, 24(5), pp. 643–652. Available at: https://doi.org/10.1038/s41380-018-0131-4.
959. Vantaggiato, C. *et al.* (2019) 'The fine tuning of drp1-dependent mitochondrial remodeling and autophagy controls neuronal differentiation', *Frontiers in Cellular Neuroscience*, 13, p. 424888. Available at: https://doi.org/10.3389/FNCEL.2019.00120/BIBTEX.
960. Vargas, D.L. *et al.* (2005) 'Neuroglial activation and neuroinflammation in the brain of patients with autism', *Annals of Neurology*, 57(1), pp. 67–81. Available at: https://doi.org/10.1002/ANA.20315.
961. Varma, M., Bhandari, R. and Kuhad, A. (2024) 'Repurposing Niclosamide as a plausible neurotherapeutic in autism spectrum disorders, targeting mitochondrial dysfunction: a strong hypothesis', *Metabolic Brain Disease*, 39(3), pp. 387–401. Available at: https://doi.org/10.1007/S11011-023-01247-X/FIGURES/5.

962. Vasu, M.M. *et al.* (2019) 'microRNAs in Autism Spectrum Disorders', *Current Pharmaceutical Design*, 25(41), pp. 4368–4378. Available at: https://doi.org/10.2174/1381612825666191105120901.
963. Vella, S. *et al.* (2016) 'PPAR Gamma in Neuroblastoma: The Translational Perspectives of Hypoglycemic Drugs', *PPAR Research*, 2016(1), p. 3038164. Available at: https://doi.org/10.1155/2016/3038164.
964. Venkatraman, K. *et al.* (2023) 'Cristae formation is a mechanical buckling event controlled by the inner mitochondrial membrane lipidome', *The EMBO Journal*, 42(24). Available at: https://doi.org/10.15252/EMBJ.2023114054.
965. Verkhratsky, A., Rodríguez, J.J. and Parpura, V. (2013) 'Astroglia in neurological diseases', *Future Neurology*. NIH Public Access, pp. 149–158. Available at: https://doi.org/10.2217/fnl.12.90.
966. Vicente-Gutierrez, C. *et al.* (2019) 'Astrocytic mitochondrial ROS modulate brain metabolism and mouse behaviour', *Nature Metabolism 2019 1:2*, 1(2), pp. 201–211. Available at: https://doi.org/10.1038/s42255-018-0031-6.
967. Virmani, M.A. and Cirulli, M. (2022) 'The Role of L-Carnitine in Mitochondria, Prevention of Metabolic Inflexibility and Disease Initiation', *International Journal of Molecular Sciences*. Multidisciplinary Digital Publishing Institute, p. 2717. Available at: https://doi.org/10.3390/ijms23052717.
968. Volobouеva, L.A. *et al.* (2013) 'Inflammatory response of microglial BV-2 cells includes a glycolytic shift and is modulated by mitochondrial glucose-regulated protein 75/mortalin', *FEBS Letters*, 587(6), pp. 756–762. Available at: https://doi.org/10.1016/J.FEBSLET.2013.01.067.
969. Vorstman, J.A.S. *et al.* (2017) 'Autism genetics: opportunities and challenges for clinical translation', *Nature Reviews Genetics 2017 18:6*, 18(6), pp. 362–376. Available at: https://doi.org/10.1038/nrg.2017.4.
970. de Vries, P. (2023) 'What kind of autism research should we do, and where should we do it?', *Spectrum* [Preprint]. Available at: https://doi.org/10.53053/ncpf9992.
971. De Vries, P.J. (2016) 'Thinking globally to meet local needs: Autism spectrum disorders in Africa and other low-resource environments', *Current Opinion in Neurology*, pp. 130–136. Available at: https://doi.org/10.1097/WCO.0000000000000297.
972. Vulin, I. *et al.* (2022) 'Assessment of caffeine neurotoxicity using novel biomarkers of neural function in SH-SY5Y cells – Is there a need for environmental concern?', *Chemico-Biological Interactions*, 365, p. 110082. Available at: https://doi.org/10.1016/J.CBI.2022.110082.
973. Vuu, Y.M., Roberts, C.T. and Rastegar, M. (2023) 'MeCP2 Is an Epigenetic Factor That Links DNA Methylation with Brain Metabolism', *International Journal of Molecular Sciences*, 24(4). Available at: https://doi.org/10.3390/IJMS24044218.
974. Wai, T. and Langer, T. (2016) 'Mitochondrial Dynamics and Metabolic Regulation', *Trends in Endocrinology and Metabolism*, 27(2), pp. 105–117. Available at: https://doi.org/10.1016/j.tem.2015.12.001.
975. Wajner, M., Vargas, C.R. and Amaral, A.U. (2020) 'Disruption of mitochondrial functions and oxidative stress contribute to neurologic dysfunction in organic acidurias', *Archives of Biochemistry and Biophysics*, 696, p. 108646. Available at: https://doi.org/10.1016/J.ABB.2020.108646.
976. Wakabayashi, J. *et al.* (2009) 'The dynamin-related GTPase Drp1 is required for embryonic and brain development in mice', *Journal of Cell Biology*, 186(6), pp. 805–816. Available at: https://doi.org/10.1083/JCB.200903065.
977. Wakabayashi, N. *et al.* (2014) 'Notch-Nrf2 Axis: Regulation of Nrf2 Gene Expression and Cytoprotection by Notch Signaling', *Molecular and Cellular Biology*, 34(4), pp. 653–663. Available at: https://doi.org/10.1128/mcb.01408-13.
978. Wang, C. *et al.* (2013) 'FIP200 is required for maintenance and differentiation of postnatal neural stem cells', *Nature Neuroscience*, 16(5), pp. 532–542. Available at: https://doi.org/10.1038/nn.3365.
979. Wang, C.S., Kavalali, E.T. and Monteggia, L.M. (2022) 'BDNF signaling in context: From synaptic regulation to psychiatric disorders', *Cell*, 185(1), pp. 62–76. Available at: https://doi.org/10.1016/J.CELL.2021.12.003.
980. Wang, G.Y. *et al.* (2023) 'Propionate promotes gluconeogenesis by regulating mechanistic target of rapamycin (mTOR) pathway in calf hepatocytes', *Animal Nutrition*, 15, p. 88. Available at: https://doi.org/10.1016/J.ANINU.2023.07.001.
981. Wang, H. *et al.* (2021) 'Decreased mitochondrial DNA copy number in nerve cells and the hippocampus during nicotine exposure is mediated by autophagy', *Ecotoxicology and Environmental Safety*, 226, p. 112831. Available at: https://doi.org/10.1016/J.ECOENV.2021.112831.
982. Wang, H. *et al.* (2024) 'Mitochondrial dynamics and mitochondrial autophagy: Molecular structure, orchestrating mechanism and related disorders', *Mitochondrion*, 75, p. 101847. Available at: https://doi.org/10.1016/J.MITO.2024.101847.

983. Wang, J. *et al.* (2018) 'GSK-3β inhibitor alsterpaullone attenuates MPP+-induced cell damage in a c-Myc-dependent manner in SH-SY5Y cells', *Frontiers in Cellular Neuroscience*, 12, p. 399933. Available at: https://doi.org/10.3389/FNCEL.2018.00283/BIBTEX.
984. Wang, L. *et al.* (2021) 'Altered Metabolic Characteristics in Plasma of Young Boys with Autism Spectrum Disorder', *Journal of Autism and Developmental Disorders 2021*, pp. 1–11. Available at: https://doi.org/10.1007/S10803-021-05364-3.
985. Wang, N. and Tian, B. (2021) 'Brain-derived neurotrophic factor in autoimmune inflammatory diseases (Review)', *Experimental and Therapeutic Medicine*, 22(5). Available at: https://doi.org/10.3892/etm.2021.10727.
986. Wang, Q. *et al.* (2022) 'Regulation of the kynurenine/serotonin pathway by berberine and the underlying effect in the hippocampus of the chronic unpredictable mild stress mice', *Behavioural Brain Research*, 422, p. 113764. Available at: https://doi.org/10.1016/j.bbr.2022.113764.
987. Wang, S. *et al.* (2022) 'Abnormal transcriptome-wide DNA demethylation induced by folate deficiency causes neural tube defects', *Frontiers in Genetics*, 13, p. 987210. Available at: https://doi.org/10.3389/FGENE.2022.987210/BIBTEX.
988. Wang, X. *et al.* (2022) 'Propionate alleviates fatty acid–induced mitochondrial dysfunction, oxidative stress, and apoptosis by upregulating PPARG coactivator 1 alpha in hepatocytes', *Journal of Dairy Science*, 105(5), pp. 4581–4592. Available at: https://doi.org/10.3168/jds.2021-21198.
989. Wang, Y. *et al.* (2018) 'Propionate-induced changes in cardiac metabolism, notably CoA trapping, are not altered by l-carnitine', *American journal of physiology. Endocrinology and metabolism*, 315(4), pp. E622–E633. Available at: https://doi.org/10.1152/AJPENDO.00081.2018.
990. Wang, Y.M. *et al.* (2021) 'Critical role of dysfunctional mitochondria and defective mitophagy in autism spectrum disorders', *Brain Research Bulletin*, 168, pp. 138–145. Available at: https://doi.org/10.1016/J.BRAINRESBULL.2020.12.022.
991. Warrier, V. and Baron-Cohen, S. (2021) 'Childhood trauma, life-time self-harm, and suicidal behaviour and ideation are associated with polygenic scores for autism', *Molecular Psychiatry*, 26(5), pp. 1670–1684. Available at: https://doi.org/10.1038/s41380-019-0550-x.
992. Waseem, M. *et al.* (2017) 'Melatonin pre-treatment mitigates SHSY-5Y cells against oxaliplatin induced mitochondrial stress and apoptotic cell death', *PLOS ONE*, 12(7), p. e0180953. Available at: https://doi.org/10.1371/JOURNAL.PONE.0180953.
993. Wasner, K. *et al.* (2022) 'Parkin Deficiency Impairs Mitochondrial DNA Dynamics and Propagates Inflammation', *Movement Disorders*, 37(7), pp. 1405–1415. Available at: https://doi.org/10.1002/MDS.29025.
994. Watanabe, K., Yamaji, R. and Ohtsuki, T. (2018) 'MicroRNA-664a-5p promotes neuronal differentiation of SH-SY5Y cells', *Genes to Cells*, 23(3), pp. 225–233. Available at: https://doi.org/10.1111/GTC.12559.
995. Waye, M.M.Y. and Cheng, H.Y. (2018) 'Genetics and epigenetics of autism: A Review', *Psychiatry and Clinical Neurosciences*. Blackwell Publishing, pp. 228–244. Available at: https://doi.org/10.1111/pcn.12606.
996. Weber, G., Lea, M.A. and Stamm, N.B. (1967) 'Inhibition of pyruvate kinase and glucokinase by acetyl CoA and inhibition of glucokinase by phosphoenolpyruvate', *Life Sciences*, 6(22), pp. 2441–2452. Available at: https://doi.org/10.1016/0024-3205(67)90071-9.
997. Wegiel, Jarek *et al.* (2024) 'Contribution of the serotonergic system to developmental brain abnormalities in autism spectrum disorder', *Autism Research*, 17(7), pp. 1300–1321. Available at: https://doi.org/10.1002/AUR.3123.
998. Wei, H. *et al.* (2016) 'Redox/methylation mediated abnormal DNA methylation as regulators of ambient fine particulate matter-induced neurodevelopment related impairment in human neuronal cells', *Scientific Reports 2016 6:1*, 6(1), pp. 1–13. Available at: https://doi.org/10.1038/srep33402.
999. Wei, Y. *et al.* (2024) 'Propionate promotes ferroptosis and apoptosis through mitophagy and ACSL4-mediated ferroptosis elicits anti-leukemia immunity', *Free Radical Biology and Medicine*, 213, pp. 36–51. Available at: https://doi.org/10.1016/J.FREERADBIOMED.2024.01.005.
1000. Weinstein-Fudim, L. *et al.* (2019) 'Gender Related Changes in Gene Expression Induced by Valproic Acid in A Mouse Model of Autism and the Correction by S-adenosyl Methionine. Does It Explain the Gender Differences in Autistic Like Behavior?', *International Journal of Molecular Sciences*, 20(21), p. 5278. Available at: https://doi.org/10.3390/ijms20215278.
1001. Weinstein-Fudim, L. *et al.* (2020) 'Prenatal S-Adenosine Methionine (SAMe) Induces Changes in Gene Expression in the Brain of Newborn Mice That Are Prevented by Co-Administration of Valproic Acid (VPA)', *International Journal of Molecular Sciences 2020, Vol. 21, Page 2834*, 21(8), p. 2834. Available at: https://doi.org/10.3390/IJMS21082834.

1002. Wen, Y. *et al.* (2013) 'Astroglial PTEN loss disrupts neuronal lamination by dysregulating radial glia-guided neuronal migration', *Aging and Disease*, 4(3), pp. 113–126.
1003. Weng, R. *et al.* (2015) 'Metabolomics Approach Reveals Integrated Metabolic Network Associated with Serotonin Deficiency', *Scientific Reports 2015 5:1*, 5(1), pp. 1–13. Available at: https://doi.org/10.1038/srep11864.
1004. Weng, R. *et al.* (2016) 'Lipidomic profiling of tryptophan hydroxylase 2 knockout mice reveals novel lipid biomarkers associated with serotonin deficiency', *Analytical and bioanalytical chemistry*, 408(11), pp. 2963–2973. Available at: https://doi.org/10.1007/S00216-015-9256-3.
1005. Wenham, C. *et al.* (2021) 'Measuring health science research and development in Africa: mapping the available data', *Health research policy and systems*, 19(1). Available at: https://doi.org/10.1186/S12961-021-00778-Y.
1006. Westra, M., Gutierrez, Y. and MacGillavry, H.D. (2021) 'Contribution of Membrane Lipids to Postsynaptic Protein Organization', *Frontiers in Synaptic Neuroscience*, 13, p. 790773. Available at: https://doi.org/10.3389/FNSYN.2021.790773/BIBTEX.
1007. Whiteley, P., Carr, K. and Shattock, P. (2021) 'Research, Clinical, and Sociological Aspects of Autism', *Frontiers in Psychiatry*, 12, p. 560. Available at: https://doi.org/10.3389/fpsyt.2021.481546.
1008. Wiese, M. and Bannister, A.J. (2020) 'Two genomes, one cell: Mitochondrial-nuclear coordination via epigenetic pathways', *Molecular Metabolism*, 38, p. 100942. Available at: https://doi.org/10.1016/J.MOLMET.2020.01.006.
1009. Wilkins, H.M. *et al.* (2016) 'Oxaloacetate enhances neuronal cell bioenergetic fluxes and infrastructure', *Journal of Neurochemistry*, 137(1), pp. 76–87. Available at: https://doi.org/10.1111/JNC.13545.
1010. Wilson, K.A. *et al.* (2017) 'Inter-relations between 3-hydroxypropionate and propionate metabolism in rat liver: Relevance to disorders of propionyl-CoA metabolism', *American Journal of Physiology - Endocrinology and Metabolism*, 313(4), pp. E413–E428. Available at: https://doi.org/10.1152/AJPENDO.00105.2017/ASSET/IMAGES/LARGE/ZH10081777740011.JPEG.
1011. Wilson, K.D., Porter, E.G. and Garcia, B.A. (2022) 'Reprogramming of the epigenome in neurodevelopmental disorders', *Critical Reviews in Biochemistry and Molecular Biology*, 57(1), pp. 73–112. Available at: https://doi.org/10.1080/10409238.2021.1979457.
1012. Winanto *et al.* (2020) 'Organoid cultures of MELAS neural cells reveal hyperactive Notch signaling that impacts neurodevelopment', *Cell Death and Disease*, 11(3), pp. 1–8. Available at: https://doi.org/10.1038/s41419-020-2383-6.
1013. Winden, K.D., Ebrahimi-Fakhari, D. and Sahin, M. (2018) 'Abnormal mTOR Activation in Autism', *Annual Review of Neuroscience*, 41(Volume 41, 2018), pp. 1–23. Available at: https://doi.org/10.1146/ANNUREV-NEURO-080317-061747/CITE/REFWORKS.
1014. Wischhof, L. *et al.* (2022) ' BCL7A -containing SWI/SNF/BAF complexes modulate mitochondrial bioenergetics during neural progenitor differentiation ', *The EMBO Journal*, 41(23). Available at: https://doi.org/10.15252/EMBJ.2022110595/SUPPL_FILE/EMBJ2022110595-SUP-0004-SDATAEV.ZIP.
1015. Wiśniowiecka-Kowalnik, B. and Nowakowska, B.A. (2019) 'Genetics and epigenetics of autism spectrum disorder—current evidence in the field', *Journal of Applied Genetics*. Springer Verlag, pp. 37–47. Available at: https://doi.org/10.1007/s13353-018-00480-w.
1016. Witters, P. *et al.* (2016) 'Autism in patients with propionic acidemia', *Molecular Genetics and Metabolism*, 119(4), pp. 317–321. Available at: https://doi.org/10.1016/j.ymgme.2016.10.009.
1017. Wolfe, A.D. *et al.* (2024) 'Local and dynamic regulation of neuronal glycolysis in vivo', *Proceedings of the National Academy of Sciences of the United States of America*, 121(3), p. e2314699121. Available at: https://doi.org/10.1073/PNAS.2314699121/SUPPL_FILE/PNAS.2314699121.SM02.MP4.
1018. Wong, C.C.Y. *et al.* (2014) 'Methylomic analysis of monozygotic twins discordant for autism spectrum disorder and related behavioural traits', *Molecular Psychiatry*, 19(4), pp. 495–503. Available at: https://doi.org/10.1038/mp.2013.41.
1019. Wong, C.C.Y. *et al.* (2019) 'Genome-wide DNA methylation profiling identifies convergent molecular signatures associated with idiopathic and syndromic autism in post-mortem human brain tissue', *Human Molecular Genetics*, 28(13), pp. 2201–2211. Available at: https://doi.org/10.1093/hmg/ddz052.
1020. Wong, K.Y. *et al.* (2020) 'Relationships between Mitochondrial Dysfunction and Neurotransmission Failure in Alzheimer's Disease', *Aging and disease*, 11(5), p. 1291. Available at: https://doi.org/10.14336/AD.2019.1125.

1021. Wongkittichote, P., Ah Mew, N. and Chapman, K.A. (2017) 'Propionyl-CoA carboxylase – A review', *Molecular Genetics and Metabolism*, 122(4), pp. 145–152. Available at: https://doi.org/10.1016/J.YMGME.2017.10.002.
1022. Wright, C. *et al.* (2017) 'Altered expression of histamine signaling genes in autism spectrum disorder', *Translational Psychiatry*, 7(5), p. e1126. Available at: https://doi.org/10.1038/tp.2017.87.
1023. Wu, Y. *et al.* (2016) 'Aberrant expression of histone deacetylases 4 in cognitive disorders: Molecular mechanisms and a potential target', *Frontiers in Molecular Neuroscience*, 9(NOV2016), p. 225008. Available at: https://doi.org/10.3389/FNMOL.2016.00114/BIBTEX.
1024. Xavier Santos, J., Rasga, C. and Moura Vicente, A. (200AD) *Exposure to Xenobiotics and Gene-Environment Interactions in Autism Spectrum Disorder: A Systematic Review*. IntechOpen. Available at: https://doi.org/10.5772/INTECHOPEN.95758.
1025. Xiao, Y. *et al.* (2019) 'Different influences on mitochondrial function, oxidative stress and cytotoxicity of antibiotics on primary human neuron and cell lines', *Journal of Biochemical and Molecular Toxicology*, 33(4), pp. 1–7. Available at: https://doi.org/10.1002/jbt.22277.
1026. Xicoy, H., Wieringa, B. and Martens, G.J.M. (2017) 'The SH-SY5Y cell line in Parkinson's disease research: a systematic review', *Molecular Neurodegeneration*, 12(1), pp. 1–11. Available at: https://doi.org/10.1186/s13024-017-0149-0.
1027. Xie, H.R., Hu, L. Sen and Li, G.Y. (2010) 'SH-SY5Y human neuroblastoma cell line: In vitro cell model of dopaminergic neurons in Parkinson's disease', *Chinese Medical Journal*, 123(8), pp. 1086–1092. Available at: https://doi.org/10.3760/CMA.J.ISSN.0366-6999.2010.08.021.
1028. Xie, K. (2018) 'Dietary micronutrients enhance neural differentiation through the modulation of cellular metabolism'. Available at: https://researchspace.auckland.ac.nz/handle/2292/44271 (Accessed: 28 May 2024).
1029. Xie, N. *et al.* (2020) 'NAD+ metabolism: pathophysiologic mechanisms and therapeutic potential', *Signal Transduction and Targeted Therapy 2020 5:1*, 5(1), pp. 1–37. Available at: https://doi.org/10.1038/s41392-020-00311-7.
1030. Xu, H. *et al.* (2015) 'Inhibition of Wnt/β-catenin signal is alleviated reactive gliosis in rats with hydrocephalus', *Child's Nervous System*, 31(2), pp. 227–234. Available at: https://doi.org/10.1007/s00381-014-2613-2.
1031. Xu, H. *et al.* (2021) 'mPFC GABAergic transmission mediated the role of BDNF signaling in cognitive impairment but not anxiety induced by adolescent social stress', *Neuropharmacology*, 184, p. 108412. Available at: https://doi.org/10.1016/j.neuropharm.2020.108412.
1032. Xu, S. *et al.* (2021) 'Role of Mitochondria in Neurodegenerative Diseases: From an Epigenetic Perspective', *Frontiers in Cell and Developmental Biology*, 9, p. 688789. Available at: https://doi.org/10.3389/FCELL.2021.688789/BIBTEX.
1033. Xu, S. *et al.* (2023) 'Calycosin alleviates cerebral ischemia/reperfusion injury by repressing autophagy via STAT3/FOXO3a signaling pathway', *Phytomedicine*, 115, p. 154845. Available at: https://doi.org/10.1016/J.PHYMED.2023.154845.
1034. Xu, Y. xin *et al.* (2022) 'The food preservative sodium propionate induces hyperglycaemic state and neurological disorder in zebrafish', *Neurotoxicology and Teratology*, 93, p. 107123. Available at: https://doi.org/10.1016/J.NTT.2022.107123.
1035. Xuan, C. *et al.* (2023) 'Regulation of LncRNAs and microRNAs in neuronal development and disease', *PeerJ*, 11. Available at: https://doi.org/10.7717/PEERJ.15197.
1036. Xue, L. *et al.* (2010) 'FoxM1, a forkhead transcription factor is a master cell cycle regulator for mouse mature T cells but not double positive thymocytes', *PloS one*, 5(2). Available at: https://doi.org/10.1371/JOURNAL.PONE.0009229.
1037. Xun, Z. *et al.* (2012) 'Retinoic acid-induced differentiation increases the rate of oxygen consumption and enhances the spare respiratory capacity of mitochondria in SH-SY5Y cells', *Mechanisms of Ageing and Development*, 133(4), p. 176. Available at: https://doi.org/10.1016/J.MAD.2012.01.008.
1038. Yabut, J.M. *et al.* (2019) 'Emerging Roles for Serotonin in Regulating Metabolism: New Implications for an Ancient Molecule', *Endocrine Reviews*, 40(4), pp. 1092–1107. Available at: https://doi.org/10.1210/ER.2018-00283.
1039. Yang, H.N. *et al.* (2016) 'A new method to effectively and rapidly generate neurons from SH-SY5Y cells', *Neuroscience Letters*, 610, pp. 43–47. Available at: https://doi.org/10.1016/j.neulet.2015.10.047.
1040. Yang, J. *et al.* (2018) 'Peptidome Analysis Reveals Novel Serum Biomarkers for Children with Autism Spectrum Disorder in China', *PROTEOMICS - Clinical Applications*, 12(5), p. 1700164. Available at: https://doi.org/10.1002/prca.201700164.

1041. Yang, L. *et al.* (2021) 'Aconitine induces mitochondrial energy metabolism dysfunction through inhibition of AMPK signaling and interference with mitochondrial dynamics in SH-SY5Y cells', *Toxicology Letters*, 347, pp. 36–44. Available at: https://doi.org/10.1016/J.TOXLET.2021.04.020.
1042. Yang, R. and Rincon, M. (2016) 'Mitochondrial Stat3, the Need for Design Thinking', *International Journal of Biological Sciences*, 12(5), pp. 532–544. Available at: https://doi.org/10.7150/IJBS.15153.
1043. Yang, S. *et al.* (2021) 'Microglia reprogram metabolic profiles for phenotype and function changes in central nervous system', *Neurobiology of Disease*, 152, p. 105290. Available at: https://doi.org/10.1016/J.NBD.2021.105290.
1044. Yang, T. *et al.* (2020) 'Propionic acid abrogates the deleterious effects of cerebral ischemic reperfusion injury through nuclear factor-κb signaling in mice', *Pharmacognosy Magazine*, 16(67), p. 177. Available at: https://doi.org/10.4103/pm.pm_306_19.
1045. Yao, F. *et al.* (2021) 'Protein Biomarkers of Autism Spectrum Disorder Identified by Computational and Experimental Methods', *Frontiers in Psychiatry*, 12(February), pp. 1–13. Available at: https://doi.org/10.3389/fpsyt.2021.554621.
1046. Yasuda, Y. *et al.* (2022) 'Genetics of autism spectrum disorders and future direction', *Journal of Human Genetics 2022 68:3*, 68(3), pp. 193–197. Available at: https://doi.org/10.1038/s10038-022-01076-3.
1047. Ye, J. *et al.* (2016) 'Electron transport chain inhibitors induce microglia activation through enhancing mitochondrial reactive oxygen species production', *Experimental Cell Research*, 340(2), pp. 315–326. Available at: https://doi.org/10.1016/J.YEXCR.2015.10.026.
1048. Ye, P. *et al.* (2022) 'BMAL1 regulates mitochondrial homeostasis in renal ischaemia-reperfusion injury by mediating the SIRT1/PGC-1α axis', *Journal of Cellular and Molecular Medicine*, 26(7), pp. 1994–2009. Available at: https://doi.org/10.1111/JCMM.17223.
1049. Yeo, H. *et al.* (2013) 'FoxO3 coordinates metabolic pathways to maintain redox balance in neural stem cells', *The EMBO Journal*, 32(19), p. 2589. Available at: https://doi.org/10.1038/EMBOJ.2013.186.
1050. Yoo, H.J., Park, M. and Kim, S.A. (2017) 'Difference in mitochondrial DNA copy number in peripheral blood cells between probands with autism spectrum disorders and their unaffected siblings', *World Journal of Biological Psychiatry*, 18(2), pp. 151–156. Available at: https://doi.org/10.1080/15622975.2016.1234069.
1051. You, L. *et al.* (2015) 'The role of STAT3 in autophagy', *Autophagy*, 11(5), pp. 729–739. Available at: https://doi.org/10.1080/15548627.2015.1017192.
1052. Youle, R.J. and Van Der Bliek, A.M. (2012) 'Mitochondrial fission, fusion, and stress', *Science*, 337(6098), pp. 1062–1065. Available at: https://doi.org/10.1126/SCIENCE.1219855/ASSET/C3B6BC71-F565-4092-BCAA-4AFD65982687/ASSETS/GRAPHIC/337_1062_F3.JPEG.
1053. Young, N. and Findling, R.L. (2015) 'An update on pharmacotherapy for autism spectrum disorder in children and adolescents', *Current Opinion in Psychiatry*, 28(2), pp. 91–101. Available at: https://doi.org/10.1097/YCO.0000000000000132.
1054. Yu, J. *et al.* (2024) 'Metabolic and proteostatic differences in quiescent and active neural stem cells', *Neural Regeneration Research*, 19(1), pp. 43–48. Available at: https://doi.org/10.4103/1673-5374.375306.
1055. Yu, M. *et al.* (2014) 'Folic acid stimulation of neural stem cell proliferation is associated with altered methylation profile of PI3K/Akt/CREB', *The Journal of Nutritional Biochemistry*, 25(4), pp. 496–502. Available at: https://doi.org/10.1016/J.JNUTBIO.2013.12.010.
1056. Yu, Q. *et al.* (2024) 'Alleviative effects of the parthenolide derivative ACT001 on insulin resistance induced by sodium propionate combined with a high-fat diet and its potential mechanisms', *European Journal of Pharmacology*, 971, p. 176529. Available at: https://doi.org/10.1016/J.EJPHAR.2024.176529.
1057. Yu, Y. *et al.* (2023) 'α-Lipoic acid improves mitochondrial biogenesis and dynamics by enhancing antioxidant and inhibiting Wnt/Ca2+ pathway to relieve fluoride-induced hepatotoxic injury', *Chemico-biological interactions*, 385. Available at: https://doi.org/10.1016/J.CBI.2023.110719.
1058. Zandona, A. *et al.* (2021) 'Activation of (un)regulated cell death as a new perspective for bispyridinium and imidazolium oximes', *Archives of Toxicology*, 95(8), pp. 2737–2754. Available at: https://doi.org/10.1007/S00204-021-03098-W/TABLES/6.
1059. Zanon, A. *et al.* (2024) 'Intracellular delivery of Parkin-RING0-based fragments corrects Parkin-induced mitochondrial dysfunction through interaction with SLP-2', *Journal of Translational Medicine*, 22(1). Available at: https://doi.org/10.1186/s12967-024-04850-3.
1060. Zarrabi, A.J. *et al.* (2017) 'Hypoxia-induced Suppression of c-Myc by HIF-2α in Human Pulmonary Endothelial Cells Attenuates TFAM Expression', *Cellular signalling*, 38, p. 230. Available at: https://doi.org/10.1016/J.CELLSIG.2017.07.008.

1061. Zeidán-Chuliá, F. *et al.* (2014) 'Altered expression of Alzheimer's disease-related genes in the cerebellum of autistic patients: a model for disrupted brain connectome and therapy.', *Cell death & disease*, 5(5), pp. e1250–e1250. Available at: https://doi.org/10.1038/cddis.2014.227.
1062. Zeng, Y. *et al.* (2019) 'Impaired mitochondrial fusion and oxidative phosphorylation triggered by high glucose is mediated by tom22 in endothelial cells', *Oxidative Medicine and Cellular Longevity*, 2019. Available at: https://doi.org/10.1155/2019/4508762.
1063. Zengeler, K.E. and Lukens, J.R. (2021) 'Innate immunity at the crossroads of healthy brain maturation and neurodevelopmental disorders', *Nature Reviews Immunology 2021 21:7*, 21(7), pp. 454–468. Available at: https://doi.org/10.1038/s41577-020-00487-7.
1064. Zhan, K. *et al.* (2020) 'Propionate enhances the expression of key genes involved in the gluconeogenic pathway in bovine intestinal epithelial cells', *Journal of dairy science*, 103(6), pp. 5514–5524. Available at: https://doi.org/10.3168/JDS.2019-17309.
1065. Zhang, B. and Horvath, S. (2005) 'A general framework for weighted gene co-expression network analysis', *Statistical applications in genetics and molecular biology*, 4(1). Available at: https://doi.org/10.2202/1544-6115.1128.
1066. Zhang, H. *et al.* (2021) 'Expression of STOML2 promotes proliferation and glycolysis of multiple myeloma cells via upregulating PAI-1', *Journal of Orthopaedic Surgery and Research*, 16(1), pp. 1–9. Available at: https://doi.org/10.1186/s13018-021-02819-2.
1067. Zhang, Han *et al.* (2024) 'STAT3 phosphorylation at Tyr705 affects DRP1 (dynamin-related protein 1) controlled-mitochondrial fission during the development of apoptotic-resistance in pulmonary arterial endothelial cells', *Genes and Genomics*, pp. 1–12. Available at: https://doi.org/10.1007/S13258-024-01522-W/FIGURES/6.
1068. Zhang, Hanlin *et al.* (2024) 'The extracellular matrix integrates mitochondrial homeostasis', *Cell*, 187(16), pp. 4289-4304.e26. Available at: https://doi.org/10.1016/j.cell.2024.05.057.
1069. Zhang, J. *et al.* (2022) 'Alpha-Lipoic Acid Attenuates MPTP/MPP+-Induced Neurotoxicity: Roles of SIRT1-Dependent PGC-1α Signaling Pathways', *Neurotoxicity Research*, 40(2), pp. 410–419. Available at: https://doi.org/10.1007/S12640-022-00479-6/FIGURES/5.
1070. Zhang, L., Zhang, J. and You, Z. (2018) 'Switching of the microglial activation phenotype is a possible treatment for depression disorder', *Frontiers in Cellular Neuroscience*, 12, p. 306. Available at: https://doi.org/10.3389/FNCEL.2018.00306/BIBTEX.
1071. Zhang, S. *et al.* (2021) 'Glucose metabolic crosstalk and regulation in brain function and diseases', *Progress in neurobiology*, 204, p. 102089. Available at: https://doi.org/10.1016/J.PNEUROBIO.2021.102089.
1072. Zhang, T., Gygi, S.P. and Paulo, J.A. (2021) 'Temporal Proteomic Profiling of SH-SY5Y Differentiation with Retinoic Acid Using FAIMS and Real-Time Searching', *Journal of Proteome Research*, 20(1), pp. 704–714. Available at: https://doi.org/10.1021/acs.jproteome.0c00614.
1073. Zhang, W. *et al.* (2019) 'An Underlying Mechanism of Dual Wnt Inhibition and AMPK Activation: Mitochondrial Uncouplers Masquerading as Wnt Inhibitors', *Journal of Medicinal Chemistry*, 62(24), pp. 11348–11358. Available at: https://doi.org/10.1021/ACS.JMEDCHEM.9B01685/SUPPL_FILE/JM9B01685_SI_002.CSV.
1074. Zhang, W. *et al.* (2023) 'Human forebrain organoid-based multi-omics analyses of PCCB as a schizophrenia associated gene linked to GABAergic pathways', *Nature Communications 2023 14:1*, 14(1), pp. 1–13. Available at: https://doi.org/10.1038/s41467-023-40861-2.
1075. Zhang, X.C. *et al.* (2019) 'Autism spectrum disorders: autistic phenotypes and complicated mechanisms', *World Journal of Pediatrics*. Institute of Pediatrics of Zhejiang University, pp. 17–25. Available at: https://doi.org/10.1007/s12519-018-0210-2.
1076. Zhang, Y.H., Wang, T., Li, Y.F., Deng, Y.N., He, X.L., *et al.* (2023) 'N-acetylcysteine improves autism-like behavior by recovering autophagic deficiency and decreasing Notch-1/Hes-1 pathway activity', *https://doi.org/10.1177/15353702231179924*, 248(11), pp. 966–978. Available at: https://doi.org/10.1177/15353702231179924.
1077. Zhang, Y.H., Wang, T., Li, Y.F., Deng, Y.N. and Shen, F.G. (2023) 'Roles of the Notch signaling pathway and microglia in autism', *Behavioural Brain Research*, 437, p. 114131. Available at: https://doi.org/10.1016/J.BBR.2022.114131.
1078. Zhang, Z. *et al.* (2019) 'MFN1-dependent alteration of mitochondrial dynamics drives hepatocellular carcinoma metastasis by glucose metabolic reprogramming', *British Journal of Cancer 2019 122:2*, 122(2), pp. 209–220. Available at: https://doi.org/10.1038/s41416-019-0658-4.

1079. Zhang, Z. *et al.* (2022) 'Hippocampal Mitochondrial Transplantation Alleviates Age-Associated Cognitive Decline via Enhancing Wnt Signaling and Neurogenesis', *Computational Intelligence and Neuroscience*, 2022(1), p. 9325302. Available at: https://doi.org/10.1155/2022/9325302.
1080. Zhao, S. *et al.* (2018) 'Evaluation of two main RNA-seq approaches for gene quantification in clinical RNA sequencing: PolyA+ selection versus rRNA depletion', *Scientific Reports*, 8(1), p. 4781. Available at: https://doi.org/10.1038/s41598-018-23226-4.
1081. Zhao, Y. *et al.* (2018) 'GPR43 mediates microbiota metabolite SCFA regulation of antimicrobial peptide expression in intestinal epithelial cells via activation of mTOR and STAT3', *Mucosal Immunology*, 11(3), pp. 752–762. Available at: https://doi.org/10.1038/MI.2017.118.
1082. Zheng, X. *et al.* (2016) 'Metabolic reprogramming during neuronal differentiation from aerobic glycolysis to neuronal oxidative phosphorylation', *eLife*, 5(JUN2016). Available at: https://doi.org/10.7554/eLife.13374.
1083. Zheng, Y. *et al.* (2021) 'STOML2 potentiates metastasis of hepatocellular carcinoma by promoting PINK1-mediated mitophagy and regulates sensitivity to lenvatinib', *Journal of Hematology & Oncology*, 14(1), p. 16. Available at: https://doi.org/10.1186/s13045-020-01029-3.
1084. Zheng, Z. *et al.* (2016) 'Blood Glutamate Levels in Autism Spectrum Disorder: A Systematic Review and Meta-Analysis', *PLOS ONE*, 11(7), p. e0158688. Available at: https://doi.org/10.1371/JOURNAL.PONE.0158688.
1085. Zhou, H. *et al.* (2018) 'Melatonin inhibits rotenone-induced SH-SY5Y cell death via the downregulation of Dynamin-Related Protein 1 expression', *European Journal of Pharmacology*, 819, pp. 58–67. Available at: https://doi.org/10.1016/J.EJPHAR.2017.11.040.
1086. Zhou, J. *et al.* (2022) 'A feedback loop engaging propionate catabolism intermediates controls mitochondrial morphology', *Nature Cell Biology 2022 24:4*, 24(4), pp. 526–537. Available at: https://doi.org/10.1038/s41556-022-00883-2.
1087. Zhu, D., Li, X. and Tian, Y. (2022) 'Mitochondrial-to-nuclear communication in aging: an epigenetic perspective', *Trends in Biochemical Sciences* [Preprint]. Available at: https://doi.org/10.1016/J.TIBS.2022.03.008.
1088. Zhu, M., Li, W.W. and Lu, C.Z. (2014) 'Histone Decacetylase Inhibitors Prevent Mitochondrial Fragmentation and Elicit Early Neuroprotection against MPP+', *CNS Neuroscience & Therapeutics*, 20(4), pp. 308–316. Available at: https://doi.org/10.1111/CNS.12217.
1089. Zhu, Y. *et al.* (2021) 'Smarcd1 Inhibits the Malignant Phenotypes of Human Glioblastoma Cells via Crosstalk with Notch1', *Molecular neurobiology*, 58(4), pp. 1438–1452. Available at: https://doi.org/10.1007/S12035-020-02190-Z.
1090. Zhvania, M.G. *et al.* (2024) 'Propionic acid affects the synaptic architecture of rat hippocampus and prefrontal cortex', *Micron*, 181, p. 103624. Available at: https://doi.org/10.1016/J.MICRON.2024.103624.
1091. Žigman, T. *et al.* (2021) 'Inborn Errors of Metabolism Associated With Autism Spectrum Disorders: Approaches to Intervention', *Frontiers in Neuroscience*, 15, pp. 0–11. Available at: https://doi.org/10.3389/fnins.2021.673600.
1092. Zimmermann, A. *et al.* (2024) 'Metabolic control of mitophagy', *European Journal of Clinical Investigation*, 54(4), p. e14138. Available at: https://doi.org/10.1111/ECI.14138.
1093. Zitkovsky, E.K., Daniels, T.E. and Tyrka, A.R. (2021) 'Mitochondria and early-life adversity', *Mitochondrion*, 57, pp. 213–221. Available at: https://doi.org/10.1016/J.MITO.2021.01.005.